Online ISSN：2186-490X
Print ISSN：1346-4272

地質調査研究報告

BULLETIN OF THE GEOLOGICAL SURVEY OF JAPAN

Vol. 71　No. 4　2020

Special Issue:
Scientific results from InterRad XV in Niigata 2017 (Proceedings)

産総研　地質調査総合センター

令和2年

表紙の写真

InterRad XV の集合写真

InterRad XV（国際放散虫研究者協会第 15 回会議）の開会式で撮影された全参加者の集合写真（2017 年 10 月 23 日，新潟大学中央図書館ライブラリーホール）．世界 16 カ国（オーストラリア，中国，フランス，ドイツ，インドネシア，イタリア，日本，韓国，モンゴル，フィリピン，ロシア，スロベニア，スペイン，スイス，トルコ，アメリカ）から総勢 187 名の参加があった．1980 年代から，産総研地質調査総合センターはナショナルセンターとして日本国内の放散虫研究を支援してきており，2017 年 10 月 20 日～11 月 1 日に開催された InterRad XV を共催した．

（写真：InterRad XV in Niigata 2017, 文：中江　訓）

Cover Photo

Group photograph of InterRad XV

Group photograph of the all participants in the opening ceremony of InterRad XV (15th meeting of the International Association of Radiolarists) taken at the Library Hall in the Central Library of Niigata University on 23 October, 2017. A total of 187 participants from 16 countries (Australia, China, France, Germany, Indonesia, Italy, Japan, Korea, Mongolia, the Philippines, Russia, Slovenia, Spain, Switzerland, Turkey and the United States of America) attended the conference. Since 1980s, the Geological Survey of Japan has been supporting radiolarian studies in Japan as a national center of geological research and thus co-hosted InterRad XV which was organized from 20 October to 1 November 2017.

(Photograph by InterRad XV in Niigata 2017, Caption by NAKAE Satoshi)

地質調査研究報告

BULLETIN OF THE GEOLOGICAL SURVEY OF JAPAN

Vol. 71 No. 4 2020

Special Issue : Scientific results from InterRad XV in Niigata 2017 (Proceedings)

Preface

GSJ Bulletin Special Issue: Scientific results from InterRad XV in Niigata 2017 (Proceedings)
NAKAE Satoshi and UCHINO Takayuki ……… 235

Frontispiece

Radiolarian-inspired art design: Simplification and identification
ITO Tsuyoshi, MORIA, YOKOYAMA Hayato, ISHIWATA Sayaka and MATSUOKA Atsushi ……… 239

Radiolarian biochronological study:
Article

Early Oxfordian radiolarians from the ammonite-bearing Fludergraben section (Northern Calcareous Alps, Austria)
SUZUKI Hisashi and GAWLICK Hans-Jürgen ……… 243

Middle Jurassic radiolarians from the ammonite bearing Toyora Group, Yamaguchi Prefecture, Southwest Japan
NISHIZONO Yukihisa and YONEMITSU Isao ……… 281

Report

Radiolarian age of Triassic striped chert within the Jurassic accretionary complex of the Ashio terrane in the Ashikaga area, Tochigi Prefecture, central Japan
ITO Tsuyoshi ……… 297

Radiolarian fauna related to Jurassic accretionary tectonics in Japan:
Article

Late Jurassic radiolarians from mudstone near the U–Pb-dated sandstone of the North Kitakami Belt in the northeastern Shimokita Peninsula, Tohoku, Japan
UCHINO Takayuki and SUZUKI Noritoshi ……… 313

Isotopic analyses for paleoceanic environmental study:
Article

SIMS analysis of Si isotope for radiolarian test in Mesozoic bedded chert, Inuyama, central Japan
Maximilien BÔLE, IKEDA Masayuki, Peter O. BAUMGARTNER, HORI S. Rie and Anne-Sophie BOUVIER ……… 331

Oxygen isotope analysis of Mesozoic radiolarites using SIMS
Maximilien BÔLE, IKEDA Masayuki, Peter O. BAUMGARTNER, HORI S. Rie, Anne-Sophie BOUVIER and Duje KUKOČ ……… 355

Bibliographic lists related to radiolarian studies by GSJ:
Note and Comment

Radiolarian research by the Geological Survey of Japan, AIST, with bibliographic lists from 1950 to 2019
ITO Tsuyoshi, NAKAE Satoshi and ITAKI Takuya ……… 395

Bulletin of the Geological Survey of Japan, vol. 71 (4), p. 235–237, 2020

Preface

GSJ Bulletin Special Issue: Scientific results from InterRad XV in Niigata 2017 (Proceedings)

NAKAE Satoshi[1,*] and UCHINO Takayuki[1]

Keywords: radiolaria, biostratigraphy, paleoceanology, geology, tectonics, InterRad.

InterRad is an international association of radiolarists, and is a non-profit organization that promotes research on all aspects of radiolarian biology, ecology, taxonomy, evolution, paleobiology, paleoecology, paleobiogeography and biostratigraphy. Since 1978, with the aim of providing an opportunity to exchange ideas for understanding all aspects of radiolarian-related topics beyond the radiolarian society, InterRad has convened conferences regularly every three years in which a wide range of research papers have been presented. The 15th meeting of the International Association of Radiolarists (InterRad XV) was held mainly in Niigata, Japan from 20 October to 1 November 2017, co-hosted by the Geological Society of Japan, the Palaeontological Society of Japan, the Society of Science on Form, Japan, and the Geological Survey of Japan, AIST (National Institute of Advanced Industrial Science and Technology). A total of 187 participants from 16 countries (Australia, China, France, Germany, Indonesia, Italy, Japan, Korea, Mongolia, the Philippines, Russia, Slovenia, Spain, Switzerland, Turkey and the United States of America) attended the conference. The next meeting (InterRad XVI), once decided during the business meeting to be held in Ljubljana, Slovenia in September of this year, is postponed until September 2021 due to the COVID-19 pandemic.

The scientific sessions, held at Niigata University on 23–27 October, focused on the five thematic topics (1–5) devoted as a special symposium reflecting the prevailing research directions and provided other eight general themes (6–13) to wide range of radiolarian studies. They are (1) Paleoceanography of Tethys and Panthalassa (chairs: S. Takahashi and P. O. Baumgartner), (2) Cenozoic paleoceanography in marginal seas (chairs: T. Itaki, Y. Okazaki and R. W. Jordan), (3) Biology and paleobiology of shelled Protista (chairs: K. Kimoto and F. Not), (4) An interface between function and evolution (chairs: Y. Tokuda and Y. Shiino), (5) Jurassic–Cretaceous boundary (chairs: A. Matsuoka and G. Li), (6) Insightful studies for radiolarians (chairs: Y. Aita and J. Rogers), (7) Biosiliceous records (chairs: J. Rogers and Y. Aita), (8) Modern oceanography (chairs: S. R. Hori and K. Kuwahara), (9) Paleobiogeography (chairs: K. Kuwahara and S. R. Hori), (10) Evolution and diversity (chairs: W. H. He and M. Chiari), (11) Biostratigraphy (chairs: M. Chiari and W. H. He), (12) Tibetan tectonics (chairs: T. Danelian and H. Luo) and (13) European tectonics (Chairs: H. Luo and T. Danelian). These sessions attracted 128 papers including oral and poster presentations and the abstracts were published as the Volume 40 of *Radiolaria*, the formal newsletter of InterRad.

The proceedings of the InterRad XV have been separately published as the special issues of *Island Arc* (Sashida *et al.*, 2019), *Paleontological Research* (Matsuoka *et al.*, 2019) and *Revue de Micropaléontologie*. This time the special issue of the *Bulletin of the Geological Survey of Japan* (this issue) is newly released to give representative research topics discussed at the InterRad XV as well as some later invited articles (five research articles, one report paper and one note and comment, together with Frontispiece, are included).

Radiolarian biochronological study:

Suzuki and Gawlick (2020) describe a well-preserved radiolarian fauna from bedded radiolarites of the Fludergraben section in the Northern Calcareous Alps, Austria. These radiolarites deposited just above the Klaus Formation dated by ammonites at latest Callovian or the Callovian–Oxfordian boundary, thus this fauna is undoubtedly assigned to the early Oxfordian age. New index species including *Kilinora spiralis*, *Fultacapsa sphaerica*, *Protunuma japonicus* and *Pseudoeucyrtis reticularis*, which were first appeared in the early Oxfordian, can be distinguished from long-lasting radiolarian species coming from the Callovian. The authors discuss these results and redefined the *Williriedellum dierschei* Zone (lower–middle Oxfordian), which was previously ranked as a subzone in the *Zhamoidellum ovum* Zone, on the basis of the new index species. These new findings fill a gap

[1] AIST, Geological Survey of Japan, Research Institute of Geology and Geoinformation
[*] Corresponding author: NAKAE, S., Central 7, 1-1-1 Higashi, Tsukuba, Ibaraki 305-8567, Japan. Email: nakae-satoshi@aist.go.jp

in the definition of the Oxfordian by radiolarians and result in a better resolution of the radiolarian biostratigraphy.

Nishizono and Yonemitsu (2020) report the first discovery of radiolarian fauna from seven localities of the uppermost Toyora Group, which is one of the representative Lower to Middle Jurassic strata in Japan and is famous for containing abundant ammonoid. The radiolarian faunas consist of representative species of the *Transhsuum hisuikyoense* and *Striatojaponocapsa plicarum* zones, which have formerly been correlated to the Aalenian–Bajocian and the lower Bathonian respectively. The authors point out that this age-assignment is slightly older than the age determined by previously reported ammonoids and inoceramids.

Ito (2020) first compiled the classification of intra-formational structures of striped chert observed in the Jurassic accretionary complexes in the Inner Zone of Southwest Japan, and their radiolarian ages. Furthermore, the author examined the relation between the type of striped chert and the age at four sections in Ashikaga and Sano cities of Tochigi Prefecture, Japan, and consequently summarizes the striped chert might be useful as an alternative age index for the Triassic at least for present four sections.

Radiolarian fauna related to Jurassic accretionary tectonics in Japan:

Uchino and Suzuki (2020) demonstrate the geological map, lithology and radiolarian age of accretionary complexes in the North Kitakami Belt in the northeastern Shimokita Peninsula, Tohoku, Japan. The authors extracted radiolarian fossils such as *Eucyrtidiellum* cf. *pyramis* from mudstone near the previously U–Pb dated sandstone and indicate that it is the Kimmeridgian as well as the depositional age of the sandstone. This radiolarian age proves that the accretionary complex in the peninsula is tectono-stratigraphically divided into the Late Jurassic and the Early Cretaceous units. They also illustrate the revised schematic compilation diagram of the ages and lithostratigraphic columns among the North Kitakami Belt.

Isotopic analyses for paleoceanic environmental study:

Bôle *et al.* (2020a, b) conducted isotopic analyses by respectively measuring δ^{30}Si and δ^{18}O of radiolarian tests for understanding the global silica cycle and paleoceanographic environment. Bôle *et al.* (2020a) measured δ^{30}Si of the Mesozoic radiolarian molds in the Inuyama section, central Japan by SIMS, indicating that the range of δ^{30}Si (-0.3 to 2 ‰) is consistent with that of modern and the Cenozoic ones, and that the 10-Myr scale trend of δ^{30}Si of the Mesozoic radiolarian molds from 250 Ma to 180 Ma is overall out-of-phase relation with biogenic silica (BSi) burial flux. This relation contradicts with the interpretation of δ^{30}Si as a productivity proxy. Bôle *et al.* (2020b) also measured δ^{18}O of Mesozoic radiolarian molds from Japan, Italy, Switzerland and Romania by SIMS. The result shows that the range from 19.8 to 35.8 ‰ is consistent with that of modern and the Cenozoic radiolarian tests from deep-sea cores of the equatorial Pacific. A slightly positive excursion during the Early–Middle Triassic, a high plateau in the Late Triassic, a negative excursion in the Early Jurassic, a slightly positive excursion in the Middle Jurassic and a few low values for the Cretaceous are recognized, although the Early Jurassic negative excursion is not consistent with δ^{18}O trend of less-diagenetic low–Mg calcite shells in shallow marine Tethys. This phenomenon implies a potential preservation of an environmental component even after the diagenesis of biogenic silica.

Bibliographic lists related to radiolarian studies by GSJ:

Ito *et al.* (2020) made a large effort to compile previous radiolarian-related publications by the Geological Survey of Japan, including geological maps, bulletins, cruise reports and newsletters with bibliographic lists from 1950 to 2019. The compilation effort aims to provide bibliographic lists related to radiolarians for future reference.

Since 1980s, the Geological Survey of Japan has been supporting and leading the radiolarian studies in Japan as a national center of geological research (see Ito *et al.*, 2020), and the consequent editing and publishing of this special issue under co-hosting InerRad XV are another form of the supporting. We believe that the articles in the issue will contribute to and profoundly affect future radiolarian researches not only by themselves but also in collaborating with other fields of geological sciences.

Acknowledgements: We express our appreciation to all the authors for their contribution to the current advances in radiolarian studies on biostratigraphy, paleoceanology and tectonic interpretation, and also acknowledge the great efforts contributed by all of the reviewers in providing valuable comments and suggestions, which have improved the quality of the articles in this special issue. We are grateful to the Editor-in-Chief, Dr. SUZUKI Atsushi and the editorial board members of the Bulletin, who support us during the editing process. In addition to the above, as both a member of the organizing committee and the guest editors, we specially thank the Geological Survey of Japan for co-hosting InterRad XV.

References

Bôle, M., Ikeda, M., Baumgartner, P. O., Hori, S. R. and Bouvier, A.-S. (2020a) SIMS analysis of Si isotope for radiolarian test in Mesozoic bedded chert, Inuyama, central Japan. *Bulletin of the Geological Survey of Japan*, **71**, 331–353.

Bôle, M., Ikeda, M., Baumgartner, P. O., Hori, S. R., Bouvier, A.-S. and Duje Kukoč (2020b) Oxygen isotope analysis of Mesozoic radiolarites using SIMS. *Bulletin of the Geological Survey of Japan*, **71**, 355–393.

Ito, T. (2020) Radiolarian age of Triassic striped chert within the Jurassic accretionary complex of the Ashio terrane in the Ashikaga area, Tochigi Prefecture, central Japan. *Bulletin of the Geological Survey of Japan*, **71**, 297–312.

Ito, T., Nakae, S. and Itaki, T. (2020) Radiolarian research by the Geological Survey of Japan, AIST, with bibliographic lists from 1950 to 2019. *Bulletin of the Geological Survey of Japan*, **71**, 395–437.

Matsuoka, A., Kurihara, K., Kamata, Y. and Takemura, A. (2019) Preface: The 15th meeting of the International Association of Radiolarists (InterRad XV), 20 October–1 November, 2017, Niigata, Japan. *Paleontological Research,* **23**, doi:10.2517/2019PR014.

Nishizono, Y. and Yonemitsu, I. (2020) Middle Jurassic radiolarians from the ammonite-bearing Toyora Group, Yamaguchi Prefecture, Southwest Japan. *Bulletin of the Geological Survey of Japan*, **71**, 281–296.

Sashida, K., Matsuoka, A., Kagan, T. U. and Ishida, K. (2019) Thematic section: Proceedings of InterRad XV. *Island Arc*, doi:10.1111/iar.12309.

Suzuki, H. and Gawlick, H.-J. (2020) Early Oxfordian radiolarians from the ammonite-bearing Fludergraben section (Northern Calcareous Alps, Austria). *Bulletin of the Geological Survey of Japan*, **71**, 243–280.

Uchino, T. and Suzuki, N. (2020) Late Jurassic radiolarians from mudstone near the U–Pb-dated sandstone of the North Kitakami Belt in the northeastern Shimokita Peninsula, Tohoku, Japan. *Bulletin of the Geological Survey of Japan*, **71**, 313–330.

15th InterRad Niigata 2017

Guest Editors:
NAKAE Satoshi
(Executive member of Organizing Committee for InterRad XV in Niigata)
UCHINO Takayuki

Recieved October 1, 2020
Accepted October 9, 2020

Bulletin of the Geological Survey of Japan, vol. 71 (4), p. 239–242, 2020

Frontispiece

Radiolarian-inspired art design: Simplification and identification

ITO Tsuyoshi[1,*], MORIA[2], YOKOYAMA Hayato[3],
ISHIWATA Sayaka[4] and MATSUOKA Atsushi[5]

The makeup of a certain organism has been applied to human design activities, including architecture and art. Radiolaria, a type of holoplanktonic protozoa, contain siliceous shells that develop into various forms. Several artists have become interested in geometrically complex structures of radiolarians, and have created works of the art based on radiolarians (e.g. Hart, 1998, 2000; Morgante, 2017; Vones, 2018). These artificial expressions are diverse, ranging from the realistic to the abstract, and have been applied to several materials, such as the simplified image (Fig. 1A), silver model (Fig. 1B) and bead model (Figs. 1C, D). De Wever (2016) and Jungck *et al.* (2019) introduced several reproductions and architectural designs that were inspired by radiolarians. Nagai and Shiraki (2017a, b) reported on hand-sized realistic radiolarian models as an educational tool, which were either made in Europe or the United States from the late 19th century.

When an abstraction inspired by real organisms is created, the original forms are often simplified. Some scientific information is therefore lost. However, the simplified images of radiolarians illustrated by Moria (Fig. 1A)

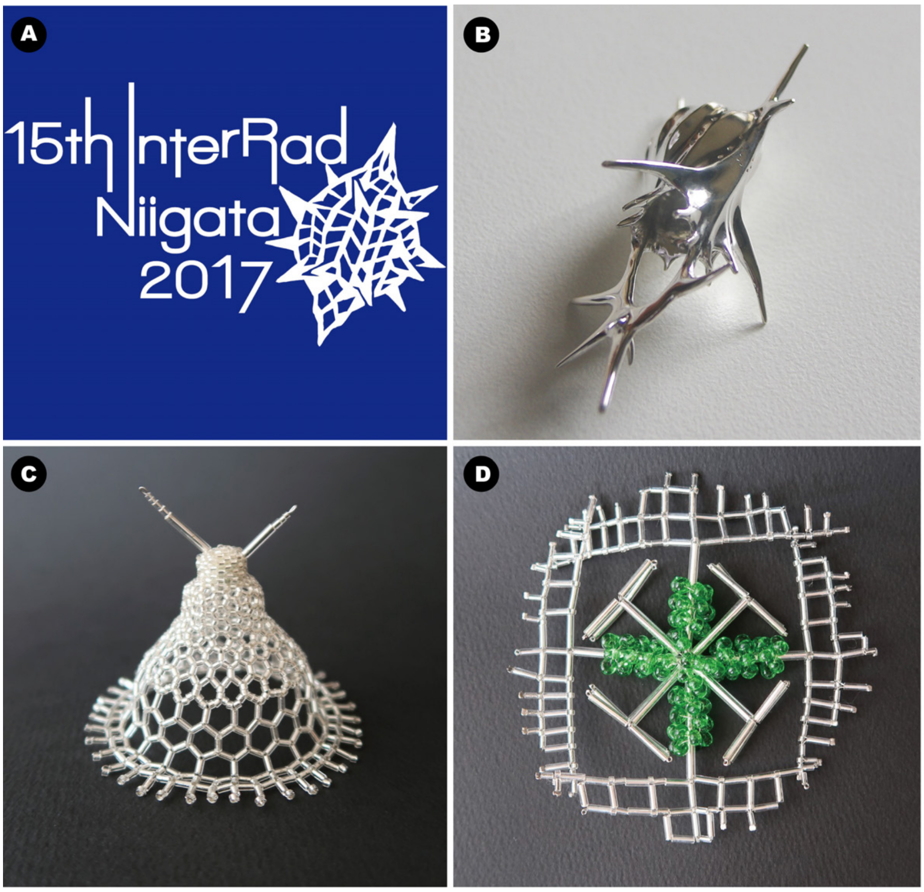

Fig. 1 Radiolarian-inspired artwork. A: Logo for InterRad XV in Niigata 2017 including simplified image of *Unuma echinatus* Ichikawa and Yao (created by Moria). B: Silver model of *Holoeciscus renzae* Schwartzapfel and Holdsworth, Devonian radiolaria (created by Yokoyama H.). C: Bead model of *Cycladophora pliocenica* (Hays), Neogene radiolaria (created by Ishiwata S.). D: Bead model of *Lithoptera muelleri* Haeckel, recent radiolaria (created by Ishiwata S.).

[1] AIST, Geological Survey of Japan, Research Institute of Geology and Geoinformation
[2] Aqua-plant, Kiryu City, Gunma, Japan. http://aqua-plant.net/
[3] RC GEAR, Nakamura-kita, Nerima City, Tokyo, Japan. http://www.rcgear.jp/
[4] Misoraya, Yokosuka City, Kanagawa, Japan
[5] Faculty of Science, Niigata University, Niigata 950-2181, Japan
[*] Corresponding author: ITO, T., Central 7, 1-1-1 Higashi, Tsukuba, Ibaraki 305-8567, Japan. Email: ito-t@aist.go.jp

have retained this scientific information, which is identifiable at the species level. In other words, Moria's simplified images were drawn through science-based selective simplification. Meanwhile, the radiolarian silver models created by Yokoyama, H. (Fig. 1B) were precisely-reproduced to retain as much of the original scientific information as possible. The bead models created by S. Ishiwata (Figs. 1C, D) were modified from original species under the limit of the materials, i.e. the models are composed of rod-shaped beads. Green beads of the model (Fig. 1D) expressed symbiotic algae of *Lithoptera muelleri* Haeckel.

Indeed, selective simplification is also important when conducting scientific activities (e.g. creating accurate sketches and schematic models). As such, this study discusses case examples of art designs that were inspired by both organisms and science-based simplification. Here, we introduce simplified images and precisely reproduced silver models involving two radiolarian species (i.e. *Unuma echinatus* and *Neoalbaillella pseudogrypus*).

Unuma echinatus Ichikawa and Yao

The Middle Jurassic *Unuma echinatus* Ichikawa and Yao was a symbolic radiolaria at InterRad XV in Niigata 2017 (the 15th Meeting of the International Association of Radiolarists). That is, the InterRad XV logo implemented this species into its design (Fig. 1A), which was used in the meeting's publication materials (e.g. Matsuoka and Ito, 2017; Ito *et al.*, 2017).

Ichikawa and Yao (1976) described this species as *Unuma* (*Spinunuma*) *echinatus* (Fig. 2A). Subsequent studies have generally not used the subgenus *Spinunuma*. Thus, the subgeneric diagnosis is currently an essential descriptor for this species. The diagnosis is as follows: "*Unuma* with well-developed apical horn, numerous stout

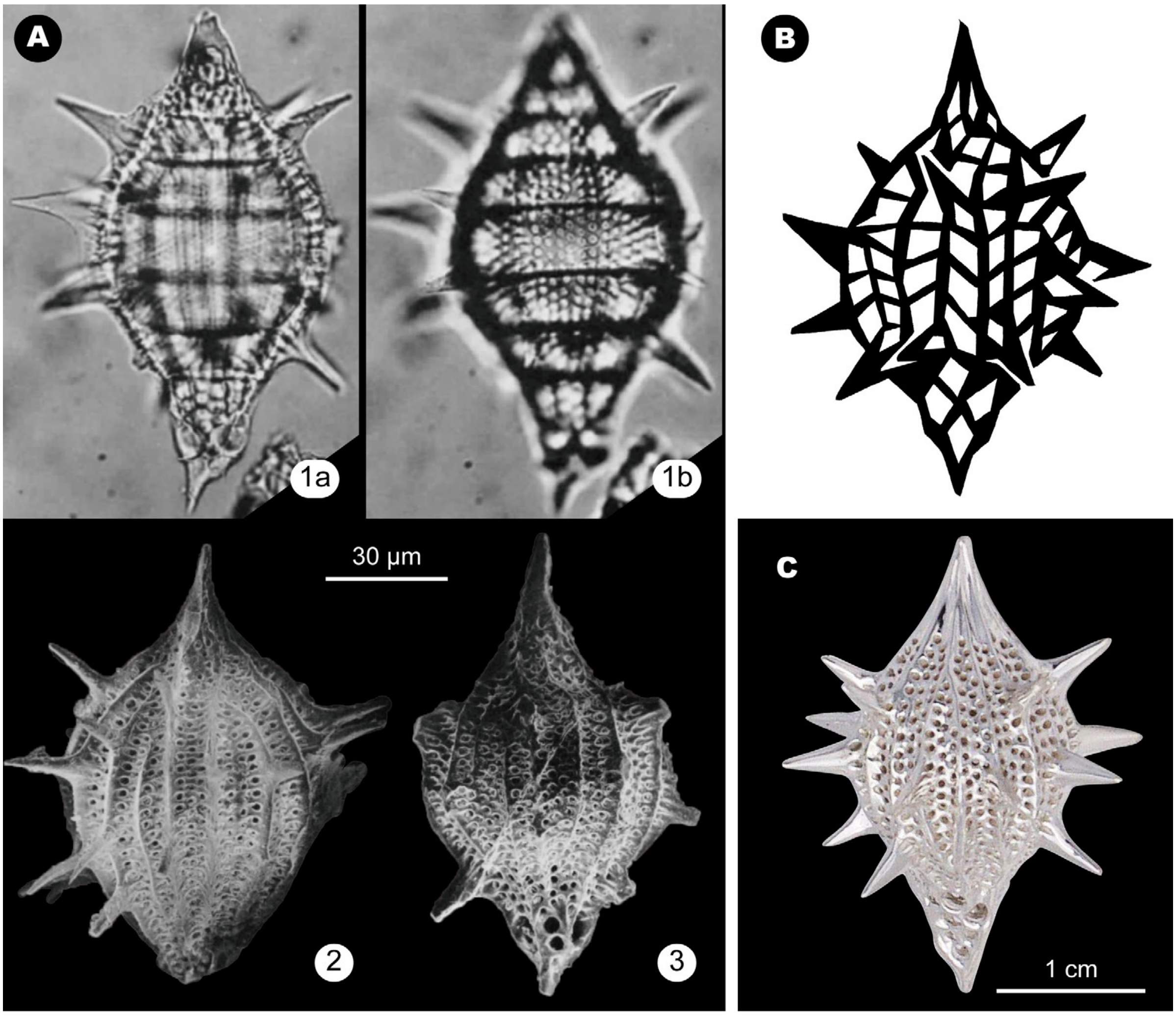

Fig. 2 *Unuma echinatus* Ichikawa and Yao. A: Reprinted type specimens from Ichikawa and Yao (1976). (1) Transmitted photomicrographs of holotype. (2) Scanning electron microscopy (SEM) image of paratype. (3) SEM image of paratype. B: Simplified image illustrated by Moria. C: Silver model created by H. Yokoyama.

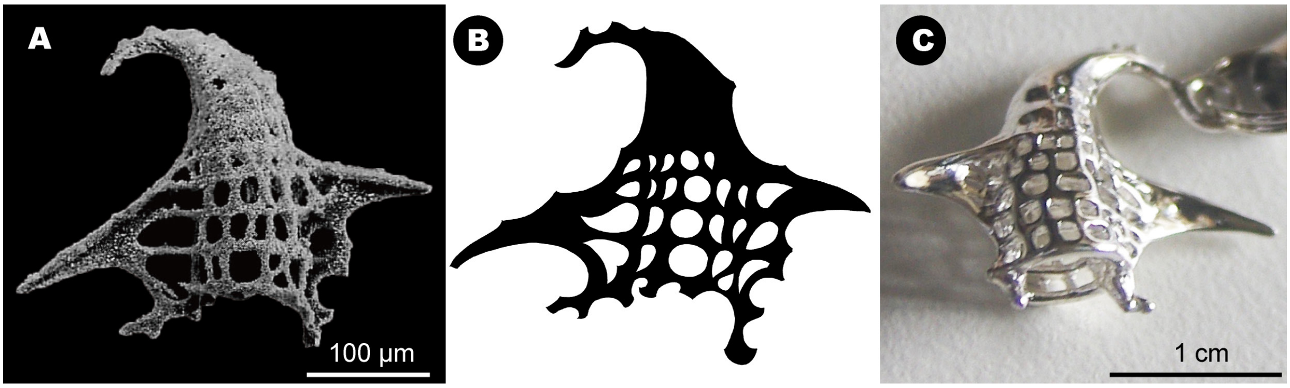

Fig. 3 *Neoalbaillella pseudogrypus* Sashida and Tonishi. A: Reprinted type specimen (SEM image of holotype) from Sashida and Tonishi (1988). B: Simplified image illustrated by Moria. C: Silver model created by H. Yokoyama.

radial spines, and distinct basal spine." The silver model reproduced the diagnosis (Fig. 2C). The simplified image of *U. echinatus* (Fig. 2B) reflects this diagnosis as well, i.e. it contains a well-developed apical horn, numerous stout radial spines and a distinct basal spine. However, some points have been modified to differ from the original characteristics. For example, the surface pores of these specimens are small and circular (Figs. 2A, 2C), while those of the simplified image are large and polygonal (Fig. 2B).

***Neoalbaillella pseudogrypus* Sashida and Tonishi**

The diagnosis of the late Permian radiolaria *Neoalbaillella pseudogrypus* Sashida and Tonishi is "*Neoalbaillella* containing a bilaterally symmetrical shell with strongly curved apical cone and cylindrical pseudoabdomen having 3 to 4 horizontal rows of large square to rectangular windows" (Fig. 3A) (Sashida and Tonishi, 1988). The silver model reproduced the diagnosis as well (Fig. 3C). There are a few similar species, including *Neoalbaillella grypus* Ishiga, Kito and Imoto. However, *N. grypus* has a long pseudoabdomen (Ishiga *et al.*, 1982).

The simplified image of *N. pseudogrypus* (Fig. 3B) possesses the above characteristics (i.e. a strongly curved apical cone and cylindrical pseudoabdomen having 3 to 4 horizontal rows of large square to rectangular windows). However, the surface pores of these specimens and the silver model are grid-like (Figs. 3A, 3C), while those of the simplified images are circular and teardrop-shaped (Fig. 3B).

As is the case in *U. echinatus*, the shape of the surface pores of *N. pseudogrypus* differs between the original specimens and the simplified image. The simplified image of *U. echinatus* has polygonal pores (Fig. 2B) although the original specimens possess circular ones (Fig. 2A), i.e. the surface pores of the simplified image are more angular than those of the original specimens. Contrastively, the simplified image of *N. pseudogrypus* expressed more circular pores (Fig. 3B) compared to the original specimens (Fig. 3A).

Acknowledgments

This study's radiolarian photomicrograph reprints were permitted for use by Prof. SASHIDA Katsuo (University of Tsukuba), Palaeontological Society of Japan and the Micropaleontology Press. The authors are most grateful to Dr. UCHINO Takayuki (Geological Survey of Japan, AIST) for the careful review and constructive comments on the manuscript.

References

De Wever, P. (2016) partie D Architectes, bâtisseurs et marqueurs du temps. *In* De Wever, P., ed., *Merveilleux microfossiles: Bâtisseurs, chronomètres, architects*. Biotope Editions, Méze, France, 177–251. (in French).

Hart, G.W. (1998) Icosahedral constructions. *In* Sarhangi, R., ed. *Bridges: Mathematical Connections in Art, Music, and Science; Conference Proceedings*, 195–202.

Hart, G.W. (2000) Reticulated geodesic constructions. *Computers & Graphics*, **24**, 907–910.

Ichikawa, K. and Yao, A. (1976) Two new genera of Mesozoic cyrtoid radiolarians from Japan. *In* Takayanagi, Y. and Saito, T., eds. *Progress in Micropaleontology, Special Publication*, Micropaleontology Press, The American Museum of Natural History, New York, 110–117.

Ishiga, H., Kito, T. and Imoto N. (1982) Late Permian radiolarian assemblages in the Tamba district and an adjacent area, southwest Japan. *Earth Science (Chikyu Kagaku)*, **36**, 10–22.

Ito, T., Yoshino, T., Itaki, T., Nishizono, Y. and Matsuoka, A., eds. (2017) Abstracts of InterRad XV in Niigata 2017. *Radiolaria*, **40**, 324p.

Jungck, J.R., Wagner, R., van Loo, D., Grossman, B., Khiripet, N., Khiripet, J., Khantuwan, W. and Hagan, M. (2019) Art Forms in Nature: radiolaria from Haeckel and Blaschka to 3D nanotomography, quantitative image analysis, evolution, and contemporary art. *Theory in Biosciences*, **138**, 159–187.

Matsuoka, A. and Ito, T., eds. (2017) *Excursion Guide of InterRad XV in Niigata 2017. Science Reports of Niigata University (Geology)*, no. 32 (supplement), 136p.

Morgante, A. (2017) Radiolaria pavilion. *In* Glynn, R. and Sheil, B., eds. *Fabricate 2011: Making Digital Architecture*, UCL Press, London, 231–234.

Nagai, H. and Shiraki, K. (2017a) Radiolarian models existed at the end of 19 century (Meiji period) in Japan. *Bulletin of the Nagoya University Museum*, no. 32, 41–46. (in Japanese with English abstract).

Nagai, H. and Shiraki, K. (2017b) Japanese radiolarian study and education in the 19th century. *Abstracts of InterRad XV in Niigata 2017. Radiolaria*, **40**, 262–263.

Sashida, K. and Tonishi, K. (1988) Additional note on the Upper Permian radiolarian fauna from Itsukaichi, western part of Tokyo Prefecture, central Japan. *Transactions and Proceedings of the Palaeontological Society of Japan, New Series*, no. 151, 523–542.

Vones, K. (2018) Materials libraries - A jeweler's perspective. *The Journal of Jewellery Research*, **1**, 34–50.

Recieved January 7, 2019
Accepted March 12, 2020
Published on-line June 12, 2020

Bulletin of the Geological Survey of Japan, vol. 71 (4), p. 243–280, 2020

Article

Early Oxfordian radiolarians from the ammonite-bearing Fludergraben section (Northern Calcareous Alps, Austria)

SUZUKI Hisashi[1,*] and GAWLICK Hans-Jürgen[2]

SUZUKI Hisashi and GAWLICK Hans-Jürgen (2020) Early Oxfordian radiolarians from the ammonite-bearing Fludergraben section (Northern Calcareous Alps, Austria). *Bulletin of the Geological Survey of Japan*, vol. 71(4), p. 243–280, 8 figs, 3 plates, 2 appendicies.

Abstract: A well-preserved and relatively rich radiolarian fauna is described from red to grey bedded radiolarites of the Fludergraben section in the Northern Calcareous Alps, Austria. These radiolarites were deposited just above the Klaus Formation, dated by ammonites as latest Callovian or the Callovian/Oxfordian boundary. The radiolarian fauna is therefore of an early Oxfordian age undoubtedly. Among long-lasting radiolarian species coming from the Callovian, we can distinguish some species that appeared in early Oxfordian time: *Kilinora spiralis*, *Fultacapsa sphaerica*, *Protunuma japonicus*, *Pseudoeucyrtis reticularis*. We discuss these results in the light of existing radiolarian zonations for the middle Callovian to Oxfordian, and redefined the *Williriedellum dierschei* Zone (lower-middle Oxfordian), which was previously ranked as subzone in the *Zhamoidellum ovum* Zone, on the basis of the new index species. These new findings fill a gap in the definition of the Oxfordian by radiolarians and result in a better resolution of the radiolarian biostratigraphy.

In the chapter of systematic part, we describe 37 genera, 67 species and 2 subspecies including diagnosis emendations of 2 genera (*Loopus* and *Pseudodictyomitra*) and 1 species (*Protunuma japonicus*). The type species of the genus *Loopus* is examined and redesignated.

Keywords: Western Tethys, biostratigraphy, radiolarians, Oxfordian, Fludergraben section, Northern Calcareous Alps

1. Introduction

The existing Middle to Late Jurassic radiolarian zonations (e.g. Pessagno *et al.*, 1993 for western North America; Matsuoka, 1995 for Japan and western Circum-Pacific region; Baumgartner *et al.*, 1995b; Beccaro, 2004, 2006; Suzuki and Gawlick, 2003a for Tethyan and central Atlantic regions) have been controversially discussed and several attempts were made to refine the stratigraphic ranges of radiolarian taxa (O'Dogherty *et al.*, 2011, 2017). However, until today most radiolarian workers dealing with the Tethyan/Atlantic region have still used in general the Unitary Association Zonation of Baumgartner *et al.* (1995b) without or with only moderate modifications of the age ranges of several radiolarian species. The biostratigraphic resolution of Middle to Late Jurassic radiolarians is not high and the existing biostratigraphic radiolarian zones exhibit relatively long-time duration. A main problem for a stable and precise radiolarian zonation with a much better biostratigraphic resolution is the worldwide scarcity of radiolaria-bearing sedimentary rocks in sections, where radiolarian associations can be correlated with other organisms, especially ammonoids.

In the Western Tethyan realm, and also in the Northern Calcareous Alps, radiolarian assemblages of the Callovian–Oxfordian contain species with relatively long biostratigraphic age ranges. Therefore, in most cases it cannot be decided, if a radiolarian assemblage is of Callovian or Oxfordian age, by use of the present radiolarian zonations.

Radiolarian species, which mark the beginning of the Oxfordian, are practically not known, because no successions, where radiolarian associations can be correlated with uppermost Callovian/lowermost Oxfordian ammonoids, have been worldwide known. In the radiolarian biozonation by Baumgartner *et al.* (1995b) the time span from middle Callovian to early Oxfordian is united in one radiolarian zone as the Unitary

[1] Otani University, Koyama-Kamifusa-cho, Kita-ku, Kyoto 603-8143, Japan

[2] University of Leoben, Department of Applied Geosciences and Geophysics, Petroleum Geology, Peter-Tunner Strasse 5, 8700 Leoben, Austria

[*] Corresponding author: SUZUKI, H., Email:hsuzuki@res.otani.ac.jp

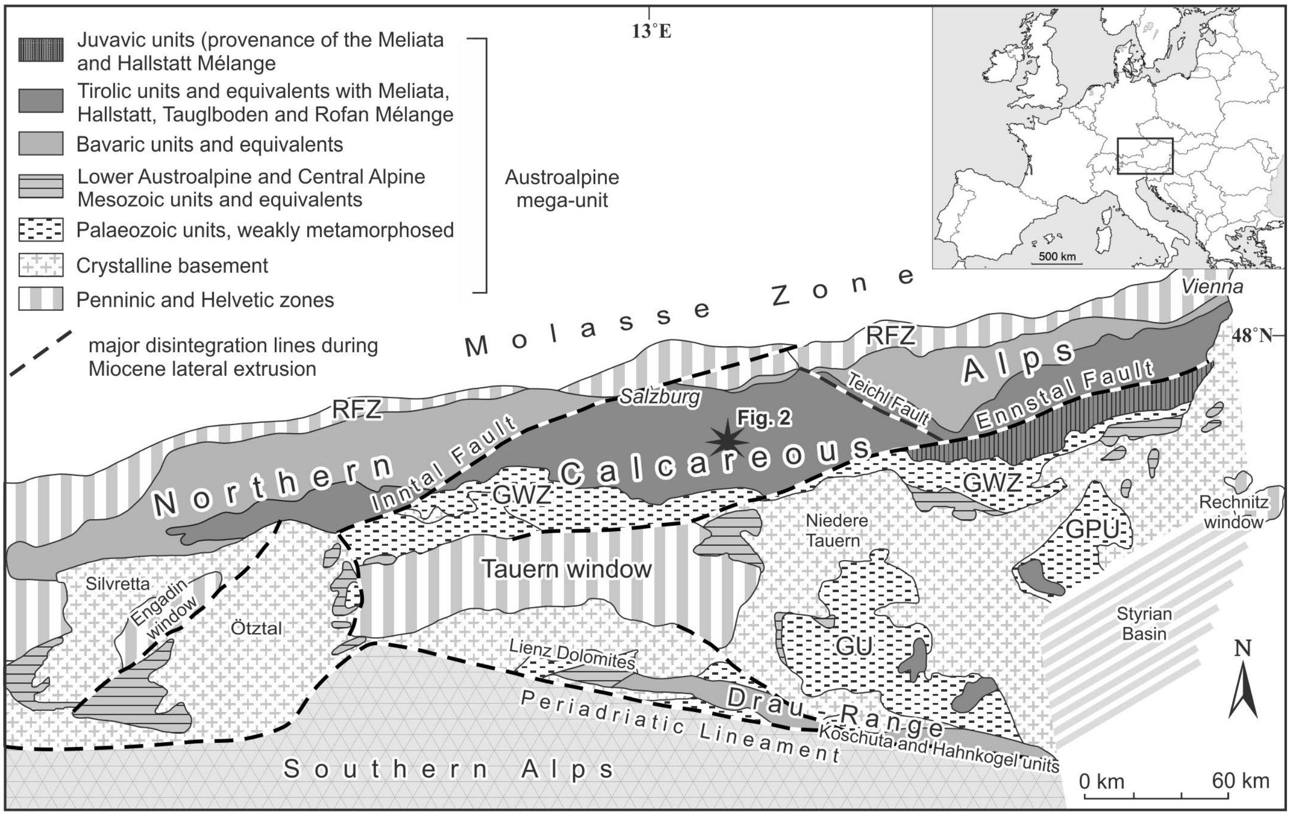

Fig. 1 Schematic tectonic map of the Eastern Alps (Tollmann, 1977; Frisch and Gawlick, 2003) and geographic position of the study area in the Northern Calcareous Alps. GPU: Graz Palaeozoic Unit, GU: Gurktal Unit, GWZ: Greywacke Zone, RFZ: Rhenodanubian Flysch Zone.

Association Zone 8. A more precise radiolarian zonation for the time around the Callovian/Oxfordian boundary is therefore highly needed. We analysed well-preserved Oxfordian radiolarian faunas from the base of a 900 m thick radiolarite succession (Gawlick *et al.*, 2007) in the Northern Calcareous Alps, i.e. the Fludergraben section near Altaussee, Austria (Figs. 1, 2). In the lowermost part of the section, red nodular limestones of the Klaus Formation were formed in the Middle Jurassic to the latest Callovian or to the Callovian/Oxfordian boundary, as proven by the following ammonites (Mandl, 1982): *Euaspidoceras* sp., *Holcophylloceras zignodianum* and fragments of ?*Nebrodites* sp. Therefore, the radiolarite succession of the Fludergraben section provides the best opportunity to search for early Oxfordian marker of radiolarian species. Beside this, the age range of several radiolarian species occurring in these radiolarites must be prolonged, if they are so far known only from lower levels than the Oxfordian. In this paper we present the early Oxfordian radiolarian fauna, which helps to refine the radiolarian zonation for the Callovian and Oxfordian.

2. Geologic setting

The studied Fludergraben section is located in the Fludergraben valley in the central Northern Calcareous Alps, southeast of Salzburg (Figs. 1, 2). The section belongs to the lowermost part of the Tauglboden Formation that overlies the Klaus Formation (Fig. 3). The Klaus Formation consists of red nodular limestone yielding ammonites of the latest Callovian to the Callovian/Oxfordian boundary. The Oxfordian to Tithonian Tauglboden Formation consists of up to 900 m thick grey to black siliceous to radiolaritic rocks (radiolarite) with intercalated simultaneous mass transport deposits (Gawlick and Frisch, 2003; Gawlick *et al.*, 2009). The base of the Tauglboden Formation starts with a red radiolarite followed by a grey to black radiolarite. The basal red radiolarite is up to 3 m thick and this part is distinguished from the main part of the Tauglboden Formation as the Fludergraben Member (Fig. 3a; Gawlick *et al.*, 2009). The sedimentary succession of the Tauglboden Formation was deposited in a trench-like foreland basin (Tauglboden Basin: Diersche, 1980) in front of a propagating nappe stack formed in Oxfordian time (Fig. 3b; Missoni and Gawlick, 2011; Gawlick and Missoni, 2019 and references therein). During the Middle to early Late Jurassic, the former passive continental margin of the Neo-Tethys attained a lower plate position due to ongoing ophiolite obduction. In the course of the ongoing ophiolite obduction, the former (Triassic–Middle Jurassic) outer passive margin became imbricated and a thin-skinned orogen was formed. In front of the

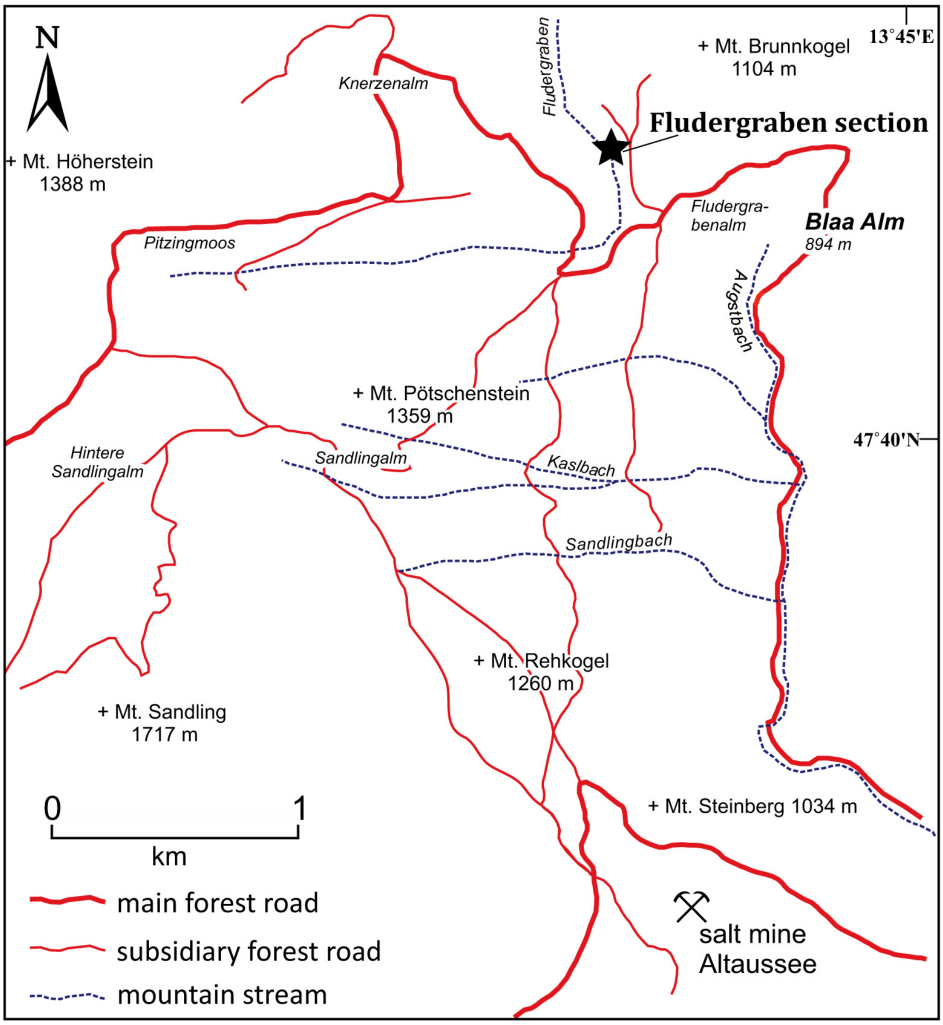

Fig. 2 Geographic position of the Fludergraben section (indicated by a star symbol) in the area of salt mine Altaussee–Mt. Sandling–Mt. Höherstein–Blaa Alm.

northwestward propagation thrust belt (nappe stack), the deep-water trench-like foreland basins were formed and incorporated into the thrust belt. In the early Oxfordian, the thrust belt reached the area of the Tauglboden Basin. Rapid deepening resulted first in the shift from carbonate to radiolarite deposition and later in deposition of mass transport deposits with its source in the adjacent nappe front (Trattberg Rise: Fig. 3b) (Gawlick and Missoni, 2019). A well-preserved section of the Tauglboden Formation is located in the Salzkammergut area, east of Salzburg.

3. Studied section and samples

The Fludergraben section in the Fludergraben valley (Fig. 2) consists of radiolarite, i.e. siliceous sedimentary rocks consisting of radiolarians. Radiolarite deposition of the Fludergraben section started almost instantaneously from the red nodular limestone containing ammonites (Fig. 4). The ammonite-bearing horizon of the uppermost Klaus Formation is only 10 cm below occurrence of the first radiolarite bed. A short-lasting stratigraphic gap on top of the ammonite-bearing layer cannot be excluded because of the bad preservation of the ammonites without their original shells. This indicates that there was an enough time to solve ammonite shells. However, because a serious hardground is not detectable, long-lasting subsolution can be excluded.

The lowermost bed of the radiolarite sequence is originally a *Bositra*-radiolarian-bearing siliceous limestone (Fig. 5a), later completely silicified (sample D1051). The following red radiolarite is well-bedded. The thickness of each bed is 3–10 cm, in some cases intercalated by up to 5 mm-thick reddish siliceous claystones (Diersche, 1980). The radiolarite is completely silicified, but the preservation of the radiolarians is in cases rather good. The microfacies show bioturbated radiolarian wackestones to packstones (Fig. 5b, 5c). All radiolarite beds of up to 10 cm thickness are massive and without sedimentary lamination, as well visible in the higher part of the Tauglboden Formation

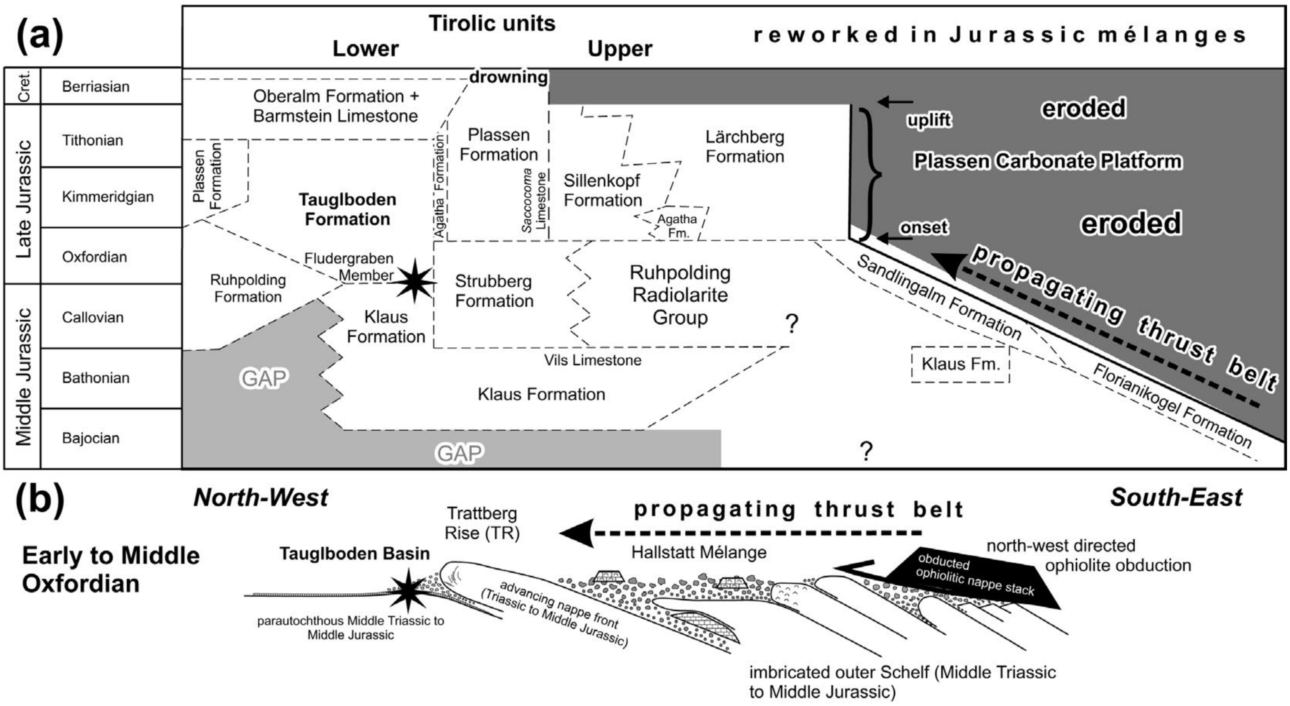

Fig. 3 (a) Simplified Middle to Late Jurassic stratigraphic table of the central Northern Calcareous Alps with an overview of common formation names after Gawlick *et al.* (2009) and stratigraphic and palaeotectonic position of the studied Fludergraben section (indicated by a star symbol). Cret.: Cretaceous, Fm.: Formation. (b) Early to Middle Oxfordian geodynamic reconstruction of the Northern Calcareous Alps according to Missoni and Gawlick (2011) and Gawlick and Missoni (2019). Due to ophiolite obduction since Middle Jurassic time the former northwestern passive continental margin attained a lower plate position and a thin-skinned orogen was formed. The Tauglboden Basin was generated in front of the propagating thrust belt (indicated by a star symbol).

(Gawlick *et al.*, 2012).

From the red radiolarites of the Fludergraben section, six radiolaria-bearing samples were collected in the first one metre just above the red condensed limestones with the ammonite horizon. The six samples are in ascending order as follows (Fig. 4): D1051, D1023, D1024, D1052, EW146, D1025.

4. Radiolarian fauna of the Fludergraben section

We have detected radiolarian species in all six samples with the methods of diluted hydrofluoric acid for decomposition and of hydrogen peroxide for residue cleaning. Their preservation is in some cases very poor, but also moderate to well-preserved radiolarians could be isolated. The radiolarian assemblages from all six samples are listed here, and are depicted in Plates 1–3.

D1051: *Archaeodictyomitra apiarium* (Rüst, 1885), *Williriedellum dierschei* Suzuki and Gawlick, 2004, *Striatojaponocapsa* sp.

D1023: *Acanthocircus* cf. *suboblongus* (Yao, 1972), *Archaeospongoprunum* cf. *elegans* Wu, 1993, *Tritrabs* cf. *exotica* (Pessagno, 1977a), *Archaeodictyomitra apiarium* (Rüst, 1885), *Archaeodictyomitra mirabilis* Aita, 1987, *Archaeodictyomitra rigida* Pessagno, 1977a, *Cinguloturris carpatica* Dumitrica, 1982, *Eucyrtidiellum circumperforatum* Chiari, Marcucci and Prela, 2002, *Eucyrtidiellum ptyctum* (Riedel and Sanfilippo, 1974), *Fultacapsa sphaerica* (Ozvoldova, 1988), *Gongylothorax favosus favosus* Dumitrica, 1970, *Helvetocapsa matsuokai* (Sashida, 1999), *Hsuum brevicostatum* (Ozvoldova, 1975), *Hsuum maxwelli* Pessagno, 1977a, *Loopus doliolum* Dumitrica, 1997, *Neorelumbra skenderbegi* Chiari, Marcucci and Prela, 2002, *Parahsuum* sp. S sensu Matsuoka, 1986, *Protunuma japonicus* Matsuoka and Yao, 1985, *Pseudodictyomitra primitiva* Matsuoka and Yao, 1985, *Stichocapsa cicciona* Chiari, Marcucci and Prela, 2002, *Stichocapsa robusta* Matsuoka, 1984, *Stichomitra annibill* Kocher, 1981, *Striatojaponocapsa synconexa* O'Dogherty *et al.*, 2006, *Kilinora* cf. *spiralis* (Matsuoka, 1982), *Tricolocapsa tetragona* Matsuoka, 1983, *Tricolocapsa undulata* (Heitzer, 1930), *Takemuraella hexagonata* (Heitzer, 1930), *Takemuraella hungarica* (Kozur, 1985), *Unuma gordus* Hull, 1997, *Williriedellum dierschei* Suzuki and Gawlick, 2004, *Zhamoidellum ovum* Dumitrica, 1970, *Zhamoidellum ventricosum* Dumitrica, 1970.

D1024: *Archaeospongoprunum* cf. *elegans* Wu, 1993, *Cinguloturris carpatica* Dumitrica, 1982, *Cyrtocapsa* sp. B, *Dictyomitrella kamoensis* Mizutani and Kido, 1983, *Eucyrtidiellum nodosum* Wakita, 1988, *Eucyrtidiellum ptyctum* (Riedel and Sanfilippo, 1974), *Eucyrtidiellum*

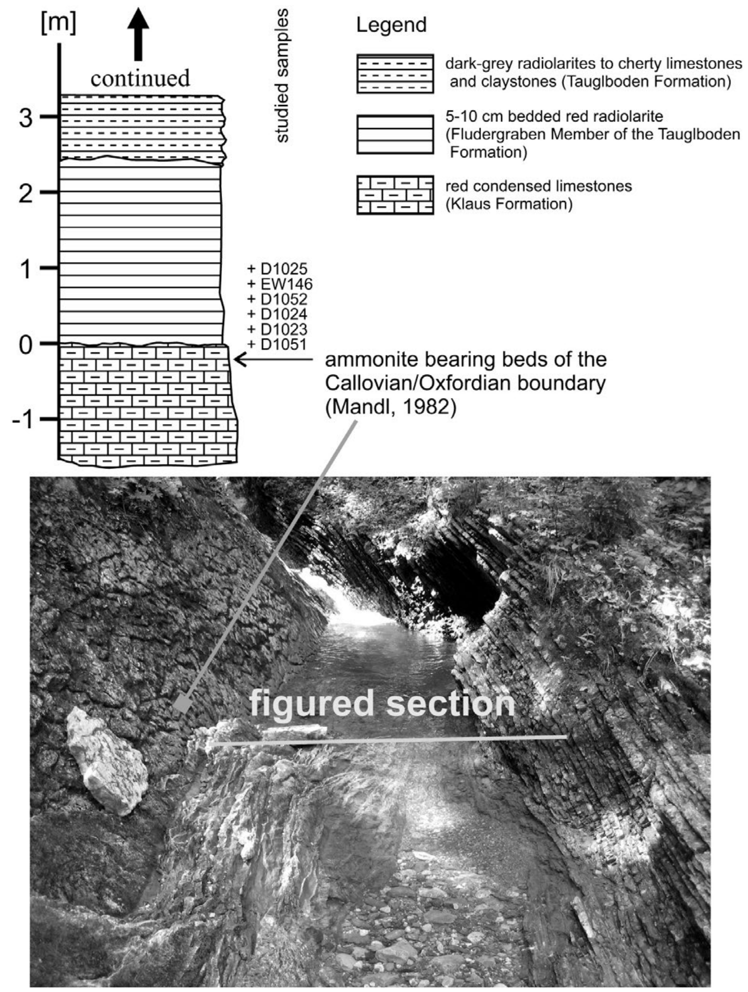

Fig. 4 Columnar section and photo show the lowermost part of the Fludergraben Member and position of studied samples.

unumaense (Yao, 1979), *Gongylothorax favosus favosus* Dumitrica, 1970, *Hsuum maxwelli* Pessagno, 1977a, *Loopus doliolum* Dumitrica, 1997, *Parahsuum* sp. S sensu Matsuoka, 1986, *Protunuma lanosus* Ozvoldova, 1996, *Striatojaponocapsa conexa* (Matsuoka, 1983), *Striatojaponocapsa riri* O'Dogherty *et al.*, 2006, *Striatojaponocapsa synconexa* O'Dogherty *et al.*, 2006, *Tricolocapsa tetragona* Matsuoka, 1983, *Unuma typicus* Ichikawa and Yao, 1976, *Williriedellum crystallinum* Dumitrica, 1970, *Williriedellum dierschei* Suzuki and Gawlick, 2004, *Williriedellum marcucciae* Cortese, 1993, *Zhamoidellum ovum* Dumitrica, 1970.

D1052: *Tritrabs exotica* (Pessagno, 1977a), *Cinguloturris carpatica* Dumitrica, 1982, *Dictyomitrella kamoensis* Mizutani and Kido, 1983, *Eucyrtidiellum circumperforatum* Chiari, Marcucci and Prela, 2002, *Eucyrtidiellum nodosum* Wakita, 1988, *Eucyrtidiellum ptyctum* (Riedel and Sanfilippo, 1974), *Gongylothorax favosus oviformis* Suzuki and Gawlick, 2009, *Hsuum brevicostatum* (Ozvoldova, 1975), *Hsuum maxwelli* Pessagno, 1977a, *Loopus doliolum* Dumitrica, 1997, *Parahsuum* sp. S sensu Matsuoka, 1986, *Podobursa nodosa* (Chiari, Marcucci and Prela, 2002), *Pseudodictyomitra primitiva* Matsuoka and Yao, 1985, *Pseudoeucyrtis reticularis* Matsuoka and Yao, 1985, *Ristola altissima* (Rüst, 1885), *Stichocapsa robusta* Matsuoka, 1984, *Stichomitra annibill* Kocher, 1981, *Stichomitra* sp. A sensu Baumgartner *et al.*, 1995a, *Striatojaponocapsa conexa* (Matsuoka, 1983), *Striatojaponocapsa naradaniensis* (Matsuoka, 1984), *Striatojaponocapsa riri* O'Dogherty *et al.*, 2006, *Striatojaponocapsa synconexa* O'Dogherty *et al.*, 2006, *Tetracapsa* sp. A sensu Suzuki and Gawlick, 2003b, *Tricolocapsa undulata* (Heitzer, 1930), *Unuma gordus* Hull, 1997, *Williriedellum carpathicum* Dumitrica, 1970, *Williriedellum crystallinum* Dumitrica, 1970, *Williriedellum dierschei* Suzuki and Gawlick, 2004, *Williriedellum marcucciae* Cortese, 1993, *Williriedellum sujkowskii* Widz and De Wever, 1993, *Zhamoidellum ovum* Dumitrica, 1970.

EW146: *Archaeospongoprunum* cf. *imlayi* Pessagno, 1977a, *Archaeodictyomitra minoensis* (Mizutani, 1981), *Cinguloturris carpatica* Dumitrica, 1982, *Cinguloturris*

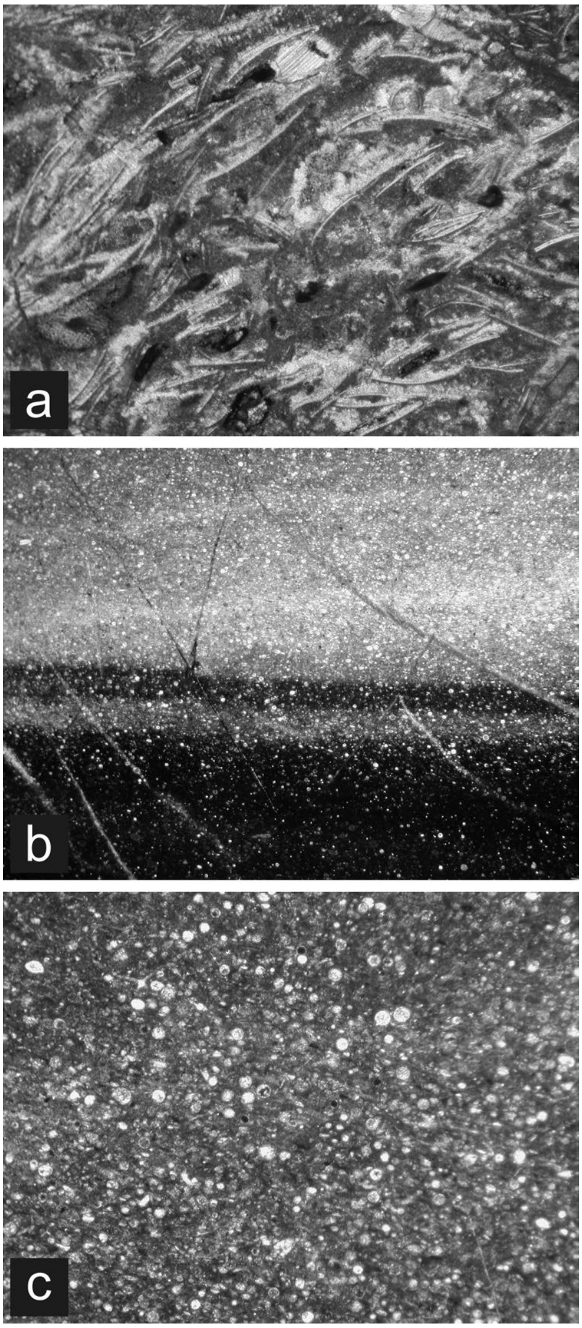

Fig. 5 Microfacies of the slightly siliceous red *Bositra*-bearing nodular limestone and the overlying red radiolarite of the Fludergraben section. (a) *Bositra* shells together with some crinoids and reworked hardground clasts. Width of the photo 0.5 cm. Sample D1051. (b) Red radiolarite above the red nodular limestone. Layered grey-red to red radiolarian wackestone to radiolarian packstone. In the basal radiolarian wackestone the radiolarians are well-preserved, in the upper radiolarian packstone the preservation of the radiolarians is moderate due to intense silicification. Width of the photo 1.4 cm. Sample D1052. (c) Magnification of (b), upper part. The most radiolarians in this bioturbated red radiolarite are recrystallized and only some radiolarians are well-preserved. Width of the photo 0.5 cm.

primorika Kemkin and Taketani, 2004, *Dictyomitrella* cf. *kamoensis* Mizutani and Kido, 1983, *Eucyrtidiellum nodosum* Wakita, 1988, *Eucyrtidiellum* cf. *unumaense* (Yao, 1979), *Hsuum baloghi* Grill and Kozur, 1986, *Hsuum* cf. *brevicostatum* (Ozvoldova, 1975), *Hsuum maxwelli* Pessagno, 1977a, *Parvicingula spinata* Vinassa, 1899, *Tricolocapsa undulata* (Heitzer, 1930), *Takemuraella hungarica* (Kozur, 1985), *Williriedellum carpathicum* Dumitrica, 1970.

D1025: *Archaeospongoprunum* cf. *elegans* Wu, 1993, *Archaeodictyomitra sixi* Yang, 1993, *Spongotripus* sp. D sensu Suzuki and Gawlick, 2003b, *Archaeodictyomitra mirabilis* Aita, 1987, *Archaeodictyomitra patricki*, Kocher, 1981, *Cinguloturris carpatica* Dumitrica, 1982, *Droltus galerus* Suzuki, 1995b, *Eucyrtidiellum nodosum* Wakita, 1988, *Eucyrtidiellum unumaense* (Yao, 1979), *Gongylothorax favosus favosus* Dumitrica, 1970, *Gongylothorax favosus oviformis* Suzuki and Gawlick, 2009, *Gongylothorax* sp. C sensu Suzuki and Gawlick, 2003b, *Helvetocapsa matsuokai* (Sashida, 1999), *Japonocapsa fusiformis* (Yao, 1979), *Praewilliriedellum* aff. *spinosum* Kozur, 1984, *Protunuma fusiformis* Ichikawa and Yao, 1976, *Pseudodictyomitra primitiva* Matsuoka and Yao, 1985, *Saitoum pagei* Pessagno, 1977a, *Stichocapsa robusta* Matsuoka, 1984, *Japonocapsa tegiminis* (Yao, 1979), *Stichomitra annibill* Kocher, 1981, *Striatojaponocapsa naradaniensis* (Matsuoka, 1984), *Striatojaponocapsa synconexa* O'Dogherty *et al.*, 2006, *Stylocapsa oblongula* Kocher, 1981, *Tetracapsa* sp. A sensu Suzuki and Gawlick, 2003b, *Tricolocapsa undulata* (Heitzer, 1930), *Takemuraella hexagonata* (Heitzer, 1930), *Unuma typicus* Ichikawa and Yao, 1976, *Williriedellum dierschei* Suzuki and Gawlick, 2004, *Williriedellum marcucciae* Cortese, 1993, *Williriedellum* sp. C sensu Gawlick *et al.*, 2018, *Zhamoidellum ovum* Dumitrica, 1970.

5. Systematic part

We describe radiolarian species from the Fludergraben section systematically. Radiolarian taxonomic classification shown here is in principle based on Takemura (1986), Suzuki *et al.* (2002), Suzuki and Gawlick (2003b) and Suzuki and Gawlick (2009). The familial classification of Nassellaria of these publications considers the cephalic skeletal elements which construct the fundamental structure of nassellarians (e.g. Takemura, 1986).

In the synonym lists, we use following mark and abbreviations. Astarisk: first description of taxon name, aff.: affinis, cf.: confer, non: not, pt.: partial.

Subclass **RADIOLARIA** Müller, 1858

Order **POLYCYSTIDA** Ehrenberg, 1839; emend. Riedel, 1967b

Suborder **ENTACTINARIA** Kozur and Mostler, 1982

Family **SATURNALIDAE** Deflandre, 1953

Genus ***Acanthocircus*** Squinabol, 1903; emend. Donofrio and Mostler, 1978

Type species: ***Acanthocircus irregularis*** Squinabol, 1903 (Campbell, 1954)

Acanthocircus* cf. *suboblongus (Yao, 1972)
(Plate 1, fig. 14)
cf. *1972 *Spongosaturnalis*? *suboblongus* – Yao, p. 29, pl. 3, figs. 1–6, pl. 10, figs. 3a–3c.
Remarks: Only one part of the ring of this species preserved, so that we identify here with "cf."

Suborder **SPUMELLARIA** Ehrenberg, 1876

Family **SPONGULIDAE** Haeckel, 1862

Genus ***Archaeospongoprunum*** Pessagno, 1973; emend. Kozur and Mostler, 1981

Type species: ***Archaeospongoprunum venadoensis*** Pessagno, 1973

Archaeospongoprunum* cf. *elegans, Wu, 1993
(Plate 1, fig. 3; Plate 2, fig. 1; Plate3, fig. 21)
cf. 1930 *Ellipsoxiphus asper* Rüst – Heitzer, p. 389, pl. 27, fig. 17.
cf.*1993 *Archaeospongoprunum elegans* – Wu, p. 118, pl. 1, figs. 5, 7, 23.

Archaeospongoprunum* cf. *imlayi Pessagno, 1977a
(Plate 3, fig. 8)
cf.*1977a *Archaeospongoprunum imlayi* – Pessagno, p. 73, pl. 3, figs. 2–4; ? pl. 3, fig. 1.
cf. 2003b *Archaeospongoprunum imlayi* Pessagno – Suzuki and Gawlick, p. 171, fig. 5.6; fig. 6.9. (detailed synonymy until 2003)

Genus ***Spongotripus*** Haeckel, 1881

Type species: ***Spongotripus pauper*** Rüst, 1888 (Kiessling, 1999)

***Spongotripus* sp. D** sensu Suzuki and Gawlick, 2003b
(Plate 3, fig. 22)
*2003b *Spongotripus* sp. D – Suzuki and Gawlick, p. 172, fig. 5.7.
2018 *Spongotripus* sp. D sensu Suzuki and Gawlick – Gawlick *et al.*, fig. 18.29.

Family **HAGIASTRIDAE** Riedel, 1971; emend. Baumgartner, 1980

Genus ***Tritrabs*** Baumgartner, 1980

Type species: ***Paronaella*? *casmaliaensis*** Pessagno, 1977a

Tritrabs exotica Pessagno, 1977a
(Plate 1, fig. 8; Plate 2, fig. 22)
*1977a *Paronaella*? *exotica* – Pessagno, p. 70, pl. 1, figs. 12, 13.
1980 *Tritrabs exotica* (Pessagno) – Baumgartner, p. 294, pl. 4, fig. 16.
1995a *Tritrabs exotica* (Pessagno) – Baumgartner *et al.*, p. 608, pl. 3119, figs. 1–3.
2006 *Tritrabs exotica* (Pessagno) – O'Dogherty *et al.*, p. 472, pl. 11, fig. 38.
2013 *Tritrabs exotica* (Pessagno) – Krische *et al.*, pl. 3, fig. 18.

Suborder **NASSELLARIA** Ehrenberg, 1876

Family **POULPIDAE** De Wever, 1981

Genus ***Saitoum*** Pessagno, 1977a

Type species: ***Saitoum pagei*** Pessagno, 1977a

Saitoum pagei Pessagno, 1977a
(Plate 3, fig. 18)
*1977a *Saitoum pagei* – Pessagno, p. 98, pl. 12, figs. 11–14.
2003b *Saitoum pagei* Pessagno – Suzuki and Gawlick, p. 175, fig. 5.38.
2018 *Saitoum pagei* Pessagno – Gawlick *et al.*, fig. 12.18.

Family **THEOPERIDAE** Haeckel, 1881; emend. Takemura, 1986

Genus ***Cinguloturris*** Dumitrica, 1982

Type species: ***Cinguloturris carpatica*** Dumitrica, 1982

Cinguloturris carpatica Dumitrica, 1982
(Plate 1, fig. 15; Plate 2, fig. 3; Plate 3, figs. 6, 9)
*1982 *Cinguloturris carpatica* – Dumitrica in Dumitrica and Mello, p. 23, pl. 4, figs. 7–11.
1994 *Cinguloturris carpatica* Dumitrica – Ishida, fig. 3.2.
2003b *Cinguloturris carpatica* Dumitrica – Suzuki and Gawlick, p. 189, fig. 5.28; fig. 6.50. (detailed synonymy between 1994 and 2003)
2003 *Cinguloturris carpatica* Dumitrica – Wegerer *et al.*, fig. 7.13; fig. 11.5.
2006 *Cinguloturris carpatica* Dumitrica – Auer *et al.*, fig. 6.9.
2007 *Cinguloturris carpatica* Dumitrica – Auer *et al.*, fig. 6.14.
2009 *Cinguloturris carpatica* Dumitrica – Suzuki and Gawlick, p. 167, fig. 5.2; fig. 6.1A, 6.1B.
Remarks: *Cinguloturris carpatica* has tiny circular dents on the solid horizontal ridges of each post-thoracic segment.

Cinguloturris primorika Kemkin and Taketani, 2004
(Plate 3, fig. 10)
2001 *Cinguloturris* cf. *cylindra* Kemkin and Rudenko – Missoni *et al.*, fig. 3.9.
*2004 *Cinguloturris primorika* – Kemkin and Taketani, p. 333, fig. 4.1–4.3.
2006 *Cinguloturris* cf. *cylindra* Kemkin and Rudenko – Gawlick *et al.*, fig. 8a.8.
2009 *Cinguloturris primorika* Kemkin and Taketani – Suzuki and Gawlick, p. 167, fig. 5.3A, 5.3B.
2011 *Cinguloturris primorika* Kemkin and Taketani – Gawlick *et al.*, fig. 3.11.
Remarks: *Cinguloturris primorika* has short costae- or node-like structures on the solid horizontal ridges of each post-thoracic segment, which are not arranged regularly.

Genus ***Parahsuum*** Yao, 1982

Type species: ***Parahsuum simplum*** Yao, 1982

Parahsuum sp. S sensu Matsuoka, 1986
(Plate 1, fig. 7; Plate 2, figs. 2, 24)
*1986 *Parahsuum* sp. S – Matsuoka, pl. 2, fig. 13; pl. 3, fig. 14.
pt. 1995a *Parahsuum* sp. S – Baumgartner *et al.*, p. 384, pl. 3240, figs. 2, 4, 5; non pl. 3240, figs. 1, 3 [= *Parahsuum carpathicum* Widz and De Wever, 1993].
2003b *Parahsuum* sp. S sensu Matsuoka – Suzuki and Gawlick, p. 182, fig. 6.70. (detailed synonymy between 1994 and 2002)
2004 *Parahsuum*? sp. – Ishida, fig. 7.4.
2009 *Parahsuum* sp. S sensu Matsuoka – Suzuki and Gawlick, p. 167, fig. 5.5.
Remarks: *Parahsuum* sp. S has a short conical test and a slender, short apical horn.

Genus ***Hsuum*** Pessagno, 1977a

Type species: ***Hsuum cuestaensis*** Pessagno, 1977a

Hsuum brevicostatum (Ozvoldova, 1975)
(Plate 1, fig. 12; Plate 2, fig. 37)
*1975 *Lithostrobus brevicostatus* – Ozvoldova, p. 84, pl. 102, fig. 1.
1994 *Transhsuum brevicostatum* (Ožvoldová) gr. – Goričan, p. 91, pl. 18, figs. 6–8. (detailed synonymy until 1993)
2003b *Hsuum brevicostatum* (Ozvoldova) – Suzuki and Gawlick, p. 184; fig. 5.33; fig. 6.62. (detailed synonymy between 1994 and 2002)
2004 *Hsuum brevicostatum* (Ozvoldova) – Gawlick *et al.*, fig. 3a.11.
2004 *Hsuum brevicostatum* (Ozvoldova) – Ishida, fig. 7.2; fig. 8.8.
2005 *Hsuum brevicostatum* (Ozvoldova) – Missoni *et al.*, fig. 10.16.
2006 *Hsuum brevicostatum* (Ozvoldova) – Gawlick *et al.*, fig. 8.18; fig. 9.15.
2009 *Hsuum brevicostatum* (Ozvoldova) – Suzuki and Gawlick, p. 168, fig. 5.6.
2014 *Hsuum brevicostatum* (Ozvoldova) – Suzuki *et al.*, p. 11, pl. 4, fig. 11.

Hsuum maxwelli Pessagno, 1977a
(Plate 1, fig. 4; Plate 2, fig. 15)
*1977a *Hsuum maxwelli* – Pessagno, p. 81, pl. 7, figs. 14–16.
1994 *Transhsuum maxwelli* (Pessagno) gr. – Goričan, p. 92, pl. 18, figs. 1–4. (detailed synonymy until 1993)
2003b *Hsuum maxwelli* Pessagno –Suzuki and Gawlick, p. 183, fig. 5.32; fig. 6.64. (detailed synonymy between 1994 and 2002)
2004 *Hsuum maxwelli* Pessagno – Gawlick *et al.*, fig. 3b.26.
2004 *Hsuum maxwelli* Pessagno – Ishida, fig. 7.1; fig. 8.7.
2005 *Hsuum maxwelli* Pessagno – Missoni *et al.*, fig. 7.11; fig. 13.3.
2006 *Hsuum maxwelli* Pessagno – Gawlick *et al.*, fig. 8b.19; fig. 9a.16.
2009 *Hsuum maxwelli* Pessagno – Suzuki and Gawlick, p. 168, fig. 5.7.
2018 *Hsuum maxwelli* Pessagno – Gawlick *et al.*, fig. 12.11; fig. 18.11.

Hsuum baloghi Grill and Kozur, 1986
(Plate 3, fig. 7)
*1986 *Hsuum baloghi* – Grill and Kozur, p. 254, pl. 3, figs. 3–6.
2003b *Hsuum baloghi* Grill and Kozur – Suzuki and Gawlick, p. 182, fig. 5.31.
Remarks: *Hsuum baloghi* has weakly developed longitudinal costae on the post-abdominal segments. In case of *Hsuum maxwelli*, longitudinal costae are strongly developed.

Genus ***Dictyomitrella*** Haeckel, 1887

Type species: ***Eucyrtidium articulatum*** Ehrenberg, 1876 (Campbell, 1954)

Dictyomitrella kamoensis Mizutani and Kido, 1983
(Plate 2, fig. 4; Plate 3, figs. 5, 15)
*1983 *Dictyomitrella*? *kamoensis* – Mizutani and Kido, p. 258, pl. 53, figs. 2–4b.
1994 *Dictyomitrella*? *kamoensis* Mizutani and Kido – Goričan, p. 66, pl. 24, fig. 1. (detailed synonymy until 1993)
2003b *Dictyomitrella kamoensis* Mizutani and Kido – Suzuki and Gawlick, p. 188, fig. 6.49. (detailed synonymy between 1994 and 2002)
2015 *Dictyomitrella*? *kamoensis* Mizutani and Kido – Ishida, pl. 4, figs. 37–42; pl. 11, figs. 1–5.
2018 *Dictyomitrella kamoensis* Mizutani and Kido – Gawlick *et al.*, fig. 12.5.

Genus ***Archaeodictyomitra*** Pessagno, 1976

Type species: ***Archaeodictyomitra squinaboli*** Pessagno, 1976

Archaeodictyomitra apiarium (Rüst, 1885)
(Plate 1, figs. 2, 11)
*1885 *Litocampium apiarium* – Rüst, p. 314, pl. 39, fig. 8.
1977b *Archaeodictyomitra apiara* (Rüst) – Pessagno, p. 41, pl. 6, figs. 6, 14.
1981 *Archaeodictyomitra apiarium* (Rüst) – Kocher, p. 56, pl. 12, fig. 13.
1985 *Archaeodictyomitra apiara* (Rüst) – Matsuoka and Yao, pl. 2, fig. 4.
1999 *Archaeodictyomitra apiarium* (Rüst) – Gawlick and Suzuki, fig. 12.4.
2004 *Archaeodictyomitra apiarium* (Rüst) – Ishida, fig. 10.7.
2004 *Archaeodictyomitra apiarium* (Rüst) – Gawlick *et al.*, fig. 3a.10.
2014 *Archaeodictyomitra apiarium* (Rüst) – Suzuki *et al.*, p. 10, pl. 4, fig. 10; pl. 5, fig. 10.
2020 *Archaeodictyomitra apiarium* (Rüst) – Suzuki *et al.*, p. 107, fig. 3.5.

Archaeodictyomitra minoensis (Mizutani, 1981)
(Plate 3, fig. 11)
*1981 *Pseudodictyomitra minoensis* – Mizutani, p. 178, pl. 58, fig. 4; pl. 63, figs. 9, 10.
1985 *Archaeodictyomitra minoensis* (Mizutani) – Matsuoka and Yao, pl. 2, fig. 5.
1999 *Archaeodictyomitra minoensis* (Mizutani) – Gawlick and Suzuki, fig. 12.2.
1999 *Archaeodictyomitra minoensis* (Mizutani) – Gawlick *et al.*, fig. 8.5.
2006 *Archaeodictyomitra minoensis* (Mizutani) – Auer *et al.*, fig. 6.3.
2009 *Archaeodictyomitra minoensis* (Mizutani) – Auer *et al.*, fig. 9.4.

Archaeodictyomitra mirabilis Aita, 1987
(Plate 1, fig. 17; Plate 3, fig. 20)
*1987 *Archaeodictyomitra*? *mirabilis* – Aita, p. 71, pl. 1, figs. 14a, 14b; pl. 9, figs. 7, 8.
1995a *Archaeodictyomitra*? *mirabilis* Aita – Baumgartner *et al.*, p. 104, pl. 3236, figs. 1–4.
2001 *Archaeodictyomitra*? *mirabilis* Aita – Nishizono, pl. 2, fig. 2.
2003b *Archaeodictyomitra mirabilis* Aita – Suzuki and Gawlick, p. 178, fig. 6.21.
2009 *Archaeodictyomitra mirabilis* Aita – Auer *et al.*, fig. 11.1.

Archaeodictyomitra patricki Kocher, 1981
(Plate 3, fig. 23)
* 1981 *Archaeodictyomitra patricki* – Kocher, p. 57, pl. 12, figs. 14–17.
1997 *Archaeodictyomitra* sp. – Suzuki and Nakae, pl. 1, fig. 7.
2003b *Archaeodictyomitra patricki* Kocher – Suzuki and Gawlick, p. 178, fig. 5.19. (detailed synonymy until 2002)

Archaeodictyomitra rigida Pessagno, 1977a
(Plate 1, fig. 10)
*1977a *Archaeodictyomitra rigida* – Pessagno, p. 81, pl. 7, figs. 10, 11.
2003b *Archaeodictyomitra rigida* Pessagno – Suzuki and Gawlick, p. 179, fig. 5.18; fig. 6.20. (detailed synonymy until 2002)
2004 *Archaeodictyomitra rigida* Pessagno – Gawlick *et al.*, fig. 3b.17.
2004 *Archaeodictyomitra* sp. – Ishida, fig. 7.8; fig. 10.10.
2005 *Archaeodictyomitra rigida* Pessagno – Missoni *et al.*, fig. 7.9; fig. 10.9
2006 *Archaeodictyomitra rigida* Pessagno – Gawlick *et al.*, fig. 8.3; fig. 9.4.
2006 *Archaeodictyomitra rigida* Pessagno – Auer *et al.*, fig. 6.4.
2007 *Archaeodictyomitra rigida* Pessagno – Auer *et al.*, fig. 6.10.
2009 *Archaeodictyomitra rigida* Pessagno – Suzuki and Gawlick, fig. 5.9.

Archaeodictyomitra sixi Yang, 1993
(Plate 3, fig. 50)
*1993 *Archaeodictyomitra sixi* – Yang, p. 122, pl. 19, figs. 3, 19; pl. 20, figs. 9, 10, 19.
2003b *Archaeodictyomitra sixi* Yang – Suzuki and Gawlick, p. 180, fig. 5.17; fig. 6.23. (detailed synonymy until 2003)
2007 *Archaeodictyomitra sixi* Yang – Auer *et al.*, fig. 6.11.
2007 *Archaeodictyomitra sixi* Yang – Gawlick *et al.*, fig. 17.5.
2010 *Archaeodictyomitra sixi* Yang – Gawlick *et al.*, fig. 22.2.
2011 *Archaeodictyomitra sixi* Yang – Gawlick *et al.*, fig. 1.6; fig. 2.5.

Genus ***Neorelumbra*** Kiessling, 1995

Type species: ***Neorelumbra tippitae*** Kiessling, 1995

Neorelumbra skenderbegi Chiari, Marcucci and Prela, 2002
(Plate 1, fig. 9)
*2002 *Neorelumbra skenderbegi*. – Chiari *et al.*, p. 68, pl. 1, figs. 14–21.
2003b *Neorelumbra skenderbegi* Chiari, Marcucci and Prela – Suzuki and Gawlick, p. 190, fig. 6.32. (detailed synonymy until 2002)
2007 *Neorelumbra skenderbegi* Chiari, Marcucci and Prela – Auer *et al.*, fig. 6.48.
2009 *Neorelumbra skenderbegi* Chiari, Marcucci and Prela – Suzuki and Gawlick, p. 169, fig. 5.11.

2011 *Neorelumbra skenderbegi* Chiari, Marcucci and Prela – Gawlick *et al.*, fig. 2.23.

Genus ***Parvicingula*** Pessagno, 1977a

Type species: ***Parvicingula santabarbaraensis*** Pessagno, 1977a

Parvicingula spinata Vinassa, 1899
(Plate 3, fig. 13)
*1899 *Lithocampe spinata* – Vinassa, p. 237, pl. 2, fig. 40.
1995a *Parvicingula*? *spinata* (Vinassa) – Baumgartner *et al.*, p. 412, pl. 3187, figs. 1–3.
2003b *Parvicingula spinata* (Vinassa) – Suzuki and Gawlick, p. 187, fig. 5.34. (detailed synonymy until 2002)
2007 *Parvicingula spinata* (Vinassa) – Auer *et al.*, fig. 6.56.
2014 *Parvicingula spinata* (Vinassa) – Suzuki *et al.*, p. 13, pl. 4, fig. 9.

Genus ***Loopus*** Yang, 1993; emend. herein

*1993 *Loopus* – Yang, p. 123.
1997 *Loopus* Yang – Dumitrica *et al.*, p. 30.
2003b *Loopus* Yang – Suzuki and Gawlick, p. 185.
2009 *Loopus* Yang – Suzuki and Gawlick, p. 170.
Type species: ***Loopus doliolum*** Dumitrica, 1997 (redesignation herein)
Emended diagnosis: Conical to subcylindrical multicyrtid test, in case more or less constricted in distal portion. Cephalis with or without horn. Each segment of abdomen and postabdominal chambers is divided by single transverse row of pores. Boundary of each segment is constricted or not. Rims of pores extend on to the surface of each chamber to make short discontinuous costae. Each costa is usually not highly reliefed and sometimes no costae are developed on the surface of chambers. In the latter case, test surface is smooth.
Remarks: *Pseudodictyomitra primitiva*, the type species of the genus *Loopus* Yang, 1993, should be attributed to the genus *Pseudodictyomitra*, to which Matsuoka and Yao (1985) assigned the species in their original description. Dumitrica *et al.* (1997) stated that fine bifurcating costae just above single row of pores on each segment is too detailed structure to be of a generic diagnosis. We agree with the opinion of Dumitrica *et al.* (1997), and the genus *Loopus* is used in the sense of Dumitrica *et al.* (1997), namely single row of pores on each segment with or without short costae that are not bifurcate above each pore. In these generic features, we redesignate the type speies here, *Loopus doliolum* Dumitrica, 1997.

Loopus doliolum Dumitrica, 1997
(Plate 1, fig. 5; Plate 2, fig. 29)
1982 *Dictyomitra* sp. C – Yao *et al.*, pl. 4, fig. 28.
*1997 *Loopus doliolum* – Dumitrica in Dumitrica *et al.*, p. 30, pl. 5, figs. 3, 5, 14.
2003b *Loopus doliolum* Dumitrica – Suzuki and Gawlick, p. 186, fig. 6.92, 6.93. (detailed synonymy until 2002)
2004 *Loopus nudus* (Schaaf) – Ishida, fig. 8.4; fig. 10.3.
2009 *Loopus doliolum* Dumitrica – Suzuki and Gawlick, p. 170, fig. 6.5.
2011 *Loopus doliolum* Dumitrica – Gawlick *et al.*, fig. 3.24.
2014 *Loopus doliolum* Dumitrica – Suzuki *et al.*, p. 12, pl. 5, fig. 11.
Remarks: *Loopus doliolum* differs from *Pseudodictyomitra primitiva* in having no distinct short costae or very weak short costae, which don't bifurcate just above pores on each segment.

Genus ***Pseudodictyomitra*** Pessagno, 1977b; emend. herein

Type species: ***Pseudodictyomitra pentacolaensis*** Pessagno, 1977b
Emended diagnosis: Multicyrtid test is conical or subcylindrical, in case more or less constricted in distal portion. Cephalis with or without horn. Thorax or abdomen and postabdominal chambers are divided each other by single or double transverse row of pores. In case of single pore rows, imperforate circular dents are arranged below perforate pore rows. Boundary of each postabdominal segment is constricted or not. On the surface of each chamber short discontinuous costae are developed. Each costa is bifurcating downwards to form a rim of pores. Such bifurcating structure is not conspicuous, when chamber surface has robust costae or no costae and smooth.
Remarks: After the original generic definition of Pessagno (1977b) *Pseudodictyomitra* has two transvers rows of primary pores. But many species which can be attributed to the genus *Pesudodictyomitra* has single row of pores with imperforate circular dents. Such character is visible in such species as *Pseudodictyomitra venusta* (Chiari *et al.*, 1997) [as *Cinguloturris*? *venusta*], *Pseudodictyomitra primitiva* Matsuoka and Yao, 1985, *Pseudodictyomitra conicostriata* Dumitrica, 1997, *Pseudodictyomitra lilyae* (Tan, 1927) in sense of Dumitrica *et al.* (1997) etc. Therefore, we change the type species of the genus *Loopus* from *Pseudodictyomitra primitiva* to *Loopus doliolum* (see remarks of the genus *Loopus*).

Pseudodictyomitra primitiva Matsuoka and Yao, 1985
(Plate 1, fig. 6; Plate 2, fig. 38; Plate 3, fig. 19)
*1985 *Pseudodictyomitra primitiva* – Matsuoka and Yao, p. 131, pl. 1, figs. 1–6; pl. 3, figs. 1–4.
1996 *Pseudodictyomitra primitiva* Matsuoka and Yao – Nishizono, pl. 29, figs. 16–19.
2001 *Loopus primitivus* (Matsuoka and Yao) – Nishizono, pl. 2, fig. 10.
2002 *Loopus primitivus* (Matsuoka and Yao) – Hori *et al.*, pl. 11, fig. 25.
2004 *Loopus primitivus* (Matsuoka and Yao) – Ishida and

Kozai, fig. 6.5, 6.9, 6.10.
2004 *Loopus primitivus* (Matsuoka and Yao) – Kozai *et al.*, fig. 7.13, 7.14.
2007 *Pseudodictyomitra primitiva* Matsuoka and Yao – Auer *et al.*, fig. 6.65.
2011 *Pseudodictyomitra primitiva* Matsuoka and Yao – Gawlick *et al.*, fig. 3.29.
2014 *Pseudodictyomitra primitiva* Matsuoka and Yao – Suzuki *et al.*, p. 11, pl. 5, fig. 1.
Remarks: We place this species not in the genus *Loopus*, but in the genus *Pseudodictyomitra*, as mentioned above.

Genus ***Pseudoeucyrtis*** Pessagno, 1977b

Type species: ***Eucyrtis? zhamoidai*** Foreman, 1973

Pseudoeucyrtis reticularis Matsuoka and Yao, 1985
(Plate 2, fig. 18)
*1985 *Pseudoeucyrtis reticularis* – Matsuoka and Yao, p. 132, pl. 1, figs. 16–21; pl. 3, figs. 14–17.
2001 *Pseudoeucyrtis reticularis* Matsuoka and Yao – Missoni *et al.*, fig. 3.12.
2007 *Pseudoeucyrtis reticularis* Matsuoka and Yao – Gawlick *et al.*, fig. 19.31.

Genus ***Ristola*** Pessagno and Whalen, 1982; emend. Baumgartner, 1984

Type species: ***Parvicingula? procera*** Pessagno, 1977a

Ristola altissima (Rüst, 1885)
(Plate 2, fig. 17)
*1885 *Lithocampe altissima* – Rüst, p. 315, pl. 40, fig. 2.
1984 *Ristola altissima* (Rüst) – Baumgartner, p. 783, pl. 8, figs. 3, 4, 9.
2001 *Ristola altissima* (Rüst) – Missoni *et al.*, p. 783, fig. 3.1.
2001 *Ristola altissima* (Rüst) – Nishizono, pl. 3, fig. 9.
2015 *Ristola altissima* (Rüst) – Ishida, pl. 5, figs. 17, 18.

Family **AMPHIPYNDACIDAE** Riedel, 1967a

Genus ***Takemuraella*** O'Dogherty, Goričan and Gawlick, 2017

non 1974 *Triversus* – Sher, p. 323. (Nematoda)
1986 *Triversus* – Takemura, p. 62.
2003b *Triversus* Takemura – Suzuki and Gawlick, p. 194.
*2017 *Takemuraella* – O'Dogherty, Goričan and Gawlick, p. 57.
Type species: ***Triversus japonicus*** Takemura, 1986
Remarks: O'Dogherty *et al.* (2017) pointed out that the genus name "*Triversus*" is preoccupied by the nematoid genus *Triversus* Sher, and they renamed *Takemuraella*.

Takemuraella hungarica (Kozur, 1985)
(Plate 1, fig. 16; Plate 3, fig. 12)
*1985 *Eoxitus hungaricus* – Kozur, p. 216, figs. 1a, 1b, 1d, 1e.
1986 *Triversus spinifer* – Takemura, p. 63, pl. 10, figs. 21–23; pl. 11, figs. 1, 2.
1995a *Parvicingula dhimenaensis* ssp. A – Baumgartner *et al.*, p. 406, pl. 4071, figs. 1–4.
2003b *Triversus hungaricus* (Kozur) – Suzuki and Gawlick, p. 195, fig. 60.58–60.60. (detailed synonymy until 2002)
pt. 2004 *Parvicingula dhimenaensis* Baumgartner – Ishida, fig. 7.9, 7.10; fig. 8.20; non fig. 10.13 [= *Parvicingula dhimenaensis* Baumgartner].
2007 *Triversus hungaricus* (Kozur) – Gawlick *et al.*, fig. 7.10; fig. 8.26; fig. 18.7.
2009 *Triversus hungaricus* (Kozur) – Suzuki and Gawlick, p. 170, fig. 5.14; fig. 6.6–6.8.

Takemuraella hexagonata (Heitzer, 1930)
(Plate 1, fig. 18; Plate 3, figs. 28, 29)
*1930 *Cyrtocalpis hexagonata* – Heitzer, p. 391, pl. 28, fig. 26.
1986 *Pseudodictyomitrella hexagonata* (Heitzer) – Grill and Kozur, pl. 4, figs. 2, 4.
2003b *Triversus hexagonatus* (Heitzer) – Suzuki and Gawlick, p. 194, fig. 5.48; fig. 6.61. (detailed synonymy until 2002)
2004 *Parvicingula* sp. – Ishida, fig. 7.13; non 12.20.
2005 *Triversus hexagonatus* (Heitzer) – Suzuki and Kuwahara, p. 50, pl. 1, fig. 8.
2006 *Triversus hexagonatus* (Heitzer) – Gawlick *et al.*, fig. 8c.40; fig. 9b.20.
2006 *Triversus hexagonatus* (Heitzer) – Auer *et al.*, fig. 6.48.
2009 *Triversus hexagonatus* (Heitzer) – Suzuki and Gawlick, p. 170, fig. 5.15; fig. 6.11A, 6.11B.
2009 *Stichomitra*? spp. – Ishida *et al.*, fig. 6.12, 6.13.
2011 *Triversus hexagonatus* (Heitzer) – Gawlick *et al.*, fig. 1.24; fig. 3.38.

Genus ***Stichomitra*** Cayeux, 1897

Type species: ***Stichomitra bertrandi*** Cayeux, 1897. The type species was subsequently designated by O'Dogherty (1994).

Stichomitra annibill Kocher, 1981; emend. Suzuki and Gawlick, 2003b
(Plate 1, fig. 13; Plate 2, figs. 19, 25; Plate 3, fig. 24)
*1981 *Stichomitra annibill* – Kocher, p. 96, pl. 16, figs. 24–26.
1987 *Stichomitra*? *tairai* – Aita, p. 72, pl. 3, figs. 7–9; pl. 10, figs. 3, 4.
1997 *Xitus singularis* – Hull, p. 138, pl. 47, figs. 1, 7, 20.
1999 *Xitus reticulatus* – Hori, p. 76, fig. 7.1–7.5.
1999 *Xitus singularis* Hull – Hori, p. 76, fig. 7.6.
2003a *Stichomitra annibill* Kocher – Suzuki and Gawlick, p. 119, pl. 1, fig. 14.
2003b *Stichomitra annibill* Kocher – Suzuki and Gawlick,

p. 192, fig. 6.35, 6.36. (detailed synonymy until 2002)
2004 *Xitus spicularius* (Aliev) – Ishida, fig. 7.19; fig. 8.25.
2004 *Xitus* sp. – Ishida, fig. 8.26; ? fig. 7.18.
2005 *Stichomitra annibill* Kocher – Missoni *et al.*, fig. 13.4.
2006 *Stichomitra annibill* Kocher – Gawlick *et al.*, fig. 8b.30.
2006 *Stichomitra annibill* Kocher – Auer *et al.*, fig. 6.37.
2009 *Stichomitra annibill* Kocher – Suzuki and Gawlick, p. 176, fig. 5.16; fig. 6.16A, 6.16B.
2011 *Stichomitra annibill* Kocher – Gawlick *et al.*, fig. 3.32.
2014 *Stichomitra annibill* Kocher – Suzuki *et al.*, p. 15, pl. 5, figs. 5, 9.
2015 *Stichomitra annibill* Kocher – Ishida, pl. 10, figs. 30–36.

***Stichomitra* sp. A** sensu Baumgartner *et al.*, 1995a
(Plate 2, fig. 34)
*1995a *Stichomitra* sp. A – Baumgartner *et al.*, p. 528, pl. 3192, figs. 1–3.

Genus ***Unuma*** Ichikawa and Yao, 1976

Type species: ***Unuma typicus*** Ichikawa and Yao, 1976

Unuma typicus Ichikawa and Yao, 1976
(Plate 2, fig. 6)
*1976 *Unuma* (*Unuma*) *typicus* – Ichikawa and Yao, p. 112, pl. 1, figs. 1–3.
1994 *Unuma typicus* Ichikawa and Yao – Goričan, p. 96, pl. 10, fig. 13.
1995a *Unuma typicus* Ichikawa and Yao – Baumgartner *et al.*, p. 622, pl. 4059, figs. 1, 2. (detailed synonymy until 1991)
2009 *Unuma typicus* Ichikawa and Yao – Suzuki and Gawlick, p. 177, fig. 5.19.
cf. 2016 *Unuma* cf. *typicus* Ichikawa and Yao – Suzuki and Nakai, pl. 1, figs. 4a, 4b.

Unuma gordus Hull, 1997
(Plate 1, fig. 29; Plate 2, fig. 41)
*1997 *Unuma gorda* – Hull, p. 172, pl. 43, figs. 9, 11, 12.
2003b *Unuma gorda* Hull – Suzuki and Gawlick, p. 198, fig. 5.36; fig. 6.68. (detailed synonymy until 2002)
2007 *Unuma gorda* Hull – Gawlick *et al.*, fig. 7.21; fig. 8.44; fig. 17.30; fig. 18.13.
2009 *Unuma gordus* Hull – Suzuki and Gawlick, p. 177, fig. 6.2A, 6.2B.

Genus ***Protunuma*** Ichikawa and Yao, 1976

Type species: ***Protunuma fusiformis*** Ichikawa and Yao, 1976

Protunuma fusiformis Ichikawa and Yao, 1976
(Plate 3, fig. 27)
*1976 *Protunuma fusiformis* – Ichikawa and Yao, p. 116, pl. 2, figs. 1–4b.

Protunuma lanosus Ozvoldova, 1996
(Plate 2, fig. 8)
*1996 ?*Protunuma lanosus* – Ožvoldová in Sykora and Ozvoldova, p. 23, pl. 2, fig. 13; pl. 3, figs. 1–6.
2003a *Protunuma lanosus* Ozvoldova – Suzuki and Gawlick, p. 119, pl. 1, fig. 12.
2007 *Protunuma lanosus* Ozvoldova – Gawlick *et al.*, fig. 7.12.

Protunuma japonicus Matsuoka and Yao, 1985; emend. herein
(Plate 1, fig. 30)
non 1930 *Cenellipsis multicostatus* – Heitzer, p. 388, pl. 17, fig. 13.
*1985 *Protunuma japonicus* – Matsuoka and Yao, p. 130, pl. 1, figs. 11–15; pl. 3, figs. 6–9.
2001 *Protunuma japonicus* Matsuoka and Yao – Wegerer *et al.*, fig. 4b.16; fig. 5.11.
2007 *Protunuma multicostatus* (Heitzer) – Gawlick *et al.*, fig. 7.13; ? fig. 19.30.
2011 *Protunuma multicostatus* (Heitzer) – Gawlick *et al.*, fig. 3.28; ? fig. 2.28.
2013 *Protunuma multicostatus* (Heitzer) – Krische *et al.*, pl. 3, fig. 6.
non 2015 *Protunuma japonicus* Matsuoka and Yao – Ishida, pl. 3, fig. 16; pl. 8, fig. 15 [= *Protunuma multicostatus*].

Emended diagnosis: *Protunuma* species, which possesses not only two, but also three or four rows of pores between neighbouring two longitudinal plicae.

Remarks: Suzuki and Gawlick (2003b) regarded *Protunuma japonicus* as a younger synonym of *Protunuma multicostatus* (Heitzer, 1930) (= *Cenellipsis multicostatus*). If we follow the original description of Matsuoka and Yao (1985) "Two to four rows of pores present between neighbouring two longitudinal plicae", namely including a specimen having "only two rows of pores between neighbouring two longitudinal plicae", *Protunuma japonicus* should be a younger synonym of *Protunuma multicostatus* (Heitzer). Our careful observation of specimens of *Protunuma multicostatus* clarifies that it has only two rows of pores between neighbouring two longitudinal plicae (Fig. 6a). If a specimen having three rows of pores between two longitudinal plicae even in one portion, it should be *Protunuma japonicus* (Fig. 6b; Plate 1, fig. 30). Therefore, we separate *Protunuma japonicus* from the previously synonymized "*Protunuma multicostatus*".

Genus ***Podobursa*** Wisniowski, 1889; emend. Foreman, 1973

Type species: ***Podobursa dunikowskii*** Wisniowski, 1889. Monotype.

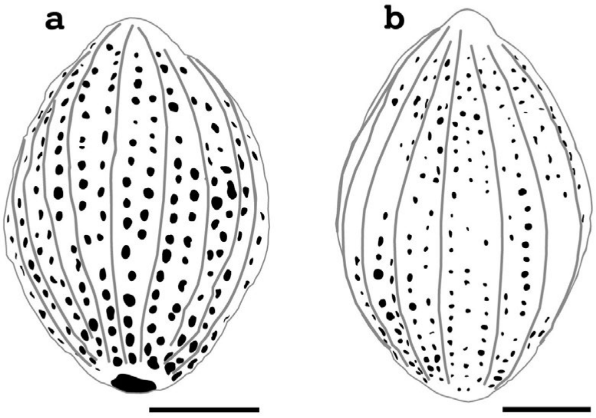

Fig. 6 Sketches of two *Protumuna* species. a: *Protunuma multicostatus* (Heitzer, 1930), from the Brielgraben section, b: *Protunuma japonicus* Matsuoka and Yao, 1985, from the Fludergraben section (Plate 1, fig. 30). *Protunuma japonicus* differs from *P. multicostatus* in having not only two, but also three longitudinal pore rows. Each scale bar is 30 μm.

Podobursa nodosa (Chiari, Marcucci and Prela, 2002)
(Plate 2, fig. 31)
1997 *Podobursa*? sp. B. – Hull, p. 108, pl. 43, figs. 5, 18, 19.
*2002 *Williriedellum nodosum* – Chiari *et al.*, p. 84, pl. 5, figs. 15–19.
2009 *Podobursa nodosa* (Chiari, Marcucci and Prela) – Suzuki and Gawlick, p. 178, fig. 5.20, 5.21.

Genus ***Droltus*** Pessagno and Whalen, 1982

Type species: ***Droltus lyellensis*** Pessagno and Whalen, 1982.
Remarks: Suzuki *et al.* (2002) demonstrated a VB (branch of vertical spine) ring as the cephalic skeletal elements in their specimen of *Droltus hecatensis* Pessagno and Whalen. We, therefore, classify the genus *Droltus* into the family Amphipyndacidae.

Droltus galerus Suzuki, 1995b
(Plate 3, fig. 49)
1995a *Droltus* sp. – Suzuki, fig. 4.15.
*1995b *Droltus galerus* – Suzuki, p. 284, fig. 5.5–5.7; fig. 7.1a, 7.1b.
2006 *Droltus galerus* Suzuki – Auer *et al.*, fig. 6.11.
2007 *Droltus galerus* Suzuki – Auer *et al.*, fig. 6.17.
2009 *Droltus galerus* Suzuki – Suzuki and Gawlick, p. 177, fig. 6.3A–6.4B.
Remarks: Our specimen from the Fludergraben section exhibits sharp pointed cephalis rather than rounded one that seen in type specimens from the Lower Jurassic chert in the Umenoki Unit of Shikoku, Japan (Suzuki, 1995b).

Family **WILLIRIEDELLIDAE** Dumitrica, 1970

Genus ***Williriedellum*** Dumitrica, 1970

Type species: ***Williriedellum crystallinum*** Dumitrica, 1970

Williriedellum crystallinum Dumitrica, 1970
(Plate 2, figs. 16, 36)
*1970 *Williriedellum crystallinum* – Dumitrica, p. 69, pl. 10, figs. 60a–60c, 62, 63.
1994 *Williriedellum crystallinum* Dumitrica – Goričan, p. 96, pl. 12, figs. 1, 2a–2c. (detailed synonymy until 1993)
2003b *Williriedellum crystallinum* Dumitrica – Suzuki and Gawlick, p. 199, fig. 6.76.
2005 *Williriedellum crystallinum* Dumitrica – Missoni *et al.*, fig. 7.23.
2006 *Williriedellum crystallinum* Dumitrica – Gawlick *et al.*, fig. 8c.41.
2006 *Williriedellum crystallinum* Dumitrica – Auer *et al.*, fig. 6.51.
2009 *Williriedellum crystallinum* Dumitrica – Suzuki and Gawlick, p. 178, fig. 5.24.
2011 *Williriedellum crystallinum* Dumitrica – Gawlick *et al.*, fig. 1.26; fig. 2.36; fig. 3.40.

Williriedellum sujkowskii Widz and De Wever, 1993
(Plate 2, fig. 32)
*1993 *Williriedellum sujkowskii* – Widz and De Wever, p. 88, pl. 2, figs. 7–10.
2007 *Williriedellum sujkowskii* Widz and De Wever – Auer *et al.*, fig. 6.123.
2010 *Williriedellum sujkowskii* Widz and De Wever – Gawlick *et al.*, fig. 27.22.
2011 *Williriedellum sujkowskii* Widz and De Wever – Gawlick *et al.*, fig. 1.27; fig. 3.42.

Williriedellum carpathicum Dumitrica, 1970
(Plate 2, fig. 20; Plate 3, fig. 16)
*1970 *Williriedellum carpathicum* – Dumitrica, p. 70, pl. 9, figs. 56a, 56b, 57–59; pl. 10, fig. 61.
2003b *Williriedellum carpathicum* Dumitrica – Suzuki and Gawlick, p. 200, fig. 6.74. (detailed synonymy until 2003)
2004 *Tricolocapsa yaoi* Matsuoka – Ishida, fig. 8.33.
2007 *Williriedellum carpathicum* Dumitrica – Auer *et al.*, fig. 6.120.
2010 *Williriedellum carpathicum* Dumitrica – Gawlick *et al.*, fig. 16A.8; fig. 16B.13; fig. 19.43; fig. 22.6; fig. 50.3.
2011 *Williriedellum carpathicum* Dumitrica – Gawlick *et al.*, fig. 1.25; fig. 3.39.
2015 *Williriedellum* sp. 2 – Ishida, pl. 6, fig. 50.

Williriedellum marcucciae Cortese, 1993
(Plate 2, fig. 10; Plate 3, fig. 44)
1983 *Williriedellum* sp. A gr. – Matsuoka, p. 23, pl. 4, figs. 1–3; pl. 8, figs. 11–15.

*1993 *Williriedellum marcuccii* – Cortese, p. 180, pl. 7, figs. 6, 7.
1994 *Williriedellum* sp. A sensu Matsuoka – Goričan, p. 96, pl. 12, figs. 9a–9c, 10a–10c, 11a, 11b. (detailed synonymy until 1993)
2003b *Williriedellum* sp. A sensu Matsuoka – Suzuki and Gawlick, p. 201, fig. 6.77. (detailed synonymy between 1994 and 2003)
2004 *Williriedellum* sp. A sensu Matsuoka – Gawlick *et al.*, fig. 3b.19.
2005 *Williriedellum* sp. A sensu Matsuoka – Missoni *et al.*, fig. 7.25.
2006 *Williriedellum* sp. A sensu Matsuoka – Auer *et al.*, fig. 6.53.
2006 *Williriedellum* sp. A sensu Matsuoka – Gawlick *et al.*, fig. 8c.43; fig. 9b.24.
2009 *Williriedellum marcucciae* Cortese – Suzuki and Gawlick, p. 179, fig. 5.25; fig. 6.49A, 6.49B.
2015 *Williriedellum marcucciae* Cortese – Ishida, pl. 1, figs. 51, 52; pl. 6, figs. 46–48.
2016 *Williriedellum marcucciae* Cortese – Suzuki and Nakai, pl. 1, figs. 1a, 1b
2018 *Williriedellum marcucciae* Cortese – Gawlick *et al.*, fig. 14.10; fig. 18.39.

Williriedellum dierschei Suzuki and Gawlick, 2004
(Plate 1, figs. 1, 27; Plate 2, figs. 12, 30; Plate 3, fig. 45)
*2004 *Williriedellum dierschei* – Suzuki and Gawlick in Gawlick *et al.*, p. 311, fig. 4.1–4.6. (detailed synonymy until 2001)
2005 *Williriedellum dierschei* Suzuki and Gawlick – Missoni *et al.*, fig. 7.24; fig. 10.35.
2005 *Williriedellum dierschei* Suzuki and Gawlick – Suzuki and Kuwahara, p. 52, pl. 1, figs. 18, 19.
2006 *Williriedellum dierschei* Suzuki and Gawlick – Auer *et al.*, fig. 6.52.
2006 *Williriedellum dierschei* Suzuki and Gawlick – Gawlick *et al.*, fig. 9b.23.
2009 *Williriedellum dierschei* Suzuki and Gawlick – Suzuki and Gawlick, p. 179, fig. 5.27A, 5.27B, 5.28; fig. 6.48A, 6.48B.
2015 *Williriedellum dierschei* Suzuki and Gawlick – Ishida, pl. 1, figs. 47, 48; pl. 6, figs. 43–45.
2018 *Williriedellum dierschei* Suzuki and Gawlick – Gawlick *et al.*, fig. 14.9; fig. 18.37; cf. fig. 25.4.

***Williriedellum* sp. C** sensu Gawlick *et al.*, 2018
(Plate 3, fig. 43)
1992 *Tricolocapsa* sp. A – Ozvoldova, p. 115, pl. 2, figs. 6, 7.
2007 *Tricolocapsa* sp. A sensu Ozvoldova – Auer *et al.*, fig. 6.109.
*2018 *Williriedellum* sp. C – Gawlick *et al.*, fig. 18.40.
Remarks: Depicted specimen exhibits a three-chambered test with a large globose abdomen, which possesses a projected short tube-like aperture on its base. Somewhat large pores are scattered on a smooth surfaced abdomen.

Genus ***Praewilliriedellum*** Kozur, 1984

Type species: ***Praewilliriedellum cephalospinosum*** Kozur, 1984
Remarks: Kozur (1984) mentioned that the thorax of this genus is not or very slightly depressed into the abdomen, although the genus is classified into the family Williriedellidae by Kozur (1984). If the thorax is not depressed into the abdomen commonly, this genus should be classified into the family Arcanicapsidae.

Praewilliriedellum* aff. *spinosum Kozur, 1984
(Plate 3, fig. 46)
aff. *1984 *Praewilliriedellum spinosum* – Kozur, p. 52, pl. 1, figs. 1–3.
Remarks: Our specimens from the Fludergraben section have a slightly elongated test in comparison with the type specimens depicted by Kozur (1984). Thus, we describe here as *Praewilliriedellum* aff. *spinosum*.

Genus ***Zhamoidellum*** Dumitrica, 1970

Type species: ***Zhamoidellum ventricosum*** Dumitrica, 1970

Zhamoidellum ventricosum Dumitrica, 1970
(Plate 1, fig. 25)
*1970 *Zhamoidellum ventricosum* – Dumitrica, p. 79, pl. 9, figs. 55a, 55b.
2003b *Zhamoidellum ventricosum* Dumitrica – Suzuki and Gawlick, p. 202, fig. 6.57. (detailed synonymy until 2002)
2005 *Zhamoidellum ventricosum* Dumitrica – Missoni *et al.*, fig. 13.6.
2006 *Zhamoidellum ventricosum* Dumitrica – Auer *et al.*, fig. 6.57.
2009 *Zhamoidellum ventricosum* Dumitrica – Suzuki and Gawlick, p. 179, fig. 5.29.
2018 *Zhamoidellum ventricosum* Dumitrica – Gawlick *et al.*, fig. 18.41.
Remarks: A depicted specimen shows lager pores and pore frames on globous abdomen than those of other specimens showed previously.

Zhamoidellum ovum Dumitrica, 1970
(Plate 1, fig. 20; Plate 2, figs. 13, 35; Plate 3, fig. 26)
*1970 *Zhamoidellum ovum* – Dumitrica, p. 79, pl. 9, figs. 52a, 52b, 53, 54.
1994 *Zhamoidellum ovum* Dumitrica – Goričan, p. 97, pl. 13, figs. 3–7. (detailed synonymy until 1993)
2003b *Zhamoidellum ovum* Dumitrica – Suzuki and Gawlick, p. 203, fig. 6.56.
2004b *Zhamoidellum ovum* Dumitrica – Suzuki *et al.*, p. 385, fig. 5.3. (detailed synonymy between 1994 and 2003)
2004 *Zhamoidellum ovum* Dumitrica – Gawlick *et al.*, fig. 3b.27.
2004 *Zhamoidellum ovum* Dumitrica – Ishida, fig. 8.32;

fig. 10.22.
2005 *Zhamoidellum ovum* Dumitrica – Missoni *et al.*, fig. 7.28; fig. 13.7.
2006 *Zhamoidellum ovum* Dumitrica – Auer *et al.*, fig. 6.56.
2006 *Zhamoidellum ovum* Dumitrica – Gawlick *et al.*, fig. 8c.45.
2009 *Zhamoidellum ovum* Dumitrica – Suzuki and Gawlick, p. 179, fig. 5.30A, 5.30B; fig. 6.33A, 6.33B.
2009 *Williriedellum yaoi* (Kozur) – Ishida *et al.*, fig. 6.2.
2011 *Zhamoidellum ovum* Dumitrica – Gawlick *et al.*, fig. 1.28; fig. 2.39; fig. 3.45.
2014 *Zhamoidellum ovum* Dumitrica – Suzuki *et al.*, p. 16, pl. 4, fig. 2; pl. 5, fig. 16.
2015 *Zhamoidellum ovum* Dumitrica – Ishida, pl. 1, fig. 62; pl. 6, figs. 59, 60.

Family **ARCANICAPSIDAE** Takemura, 1986

Genus ***Stylocapsa*** Principi, 1909; emend. Tan, 1927

Type species: ***Stylocapsa exagonata*** Principi, 1909

Stylocapsa oblongula Kocher, 1980
(Plate 3, fig. 34)
* 1980 *Stylocapsa oblongula* – Kocher in Baumgartner *et al.*, p. 62, pl. 6, fig. 1.
2001 *Stylocapsa oblongula* Kocher – Suzuki *et al.*, fig. 5.10.
2001 *Stylocapsa oblongula* Kocher – Wegerer *et al.*, fig. 4a.18; fig. 6.3.
2007 *Stylocapsa oblongula* Kocher – Auer *et al.*, fig. 6.86.
2015 *Kilinora*? *oblongula* (Kocher) – Ishida, pl. 1, figs. 7, 8.

Genus ***Kilinora*** Hull, 1997

Type species: ***Stylocapsa? spiralis*** Matsuoka, 1982
Remarks: We agree with the establishment of the genus *Kilinora* by Hull (1997), to separate the species having a thorax with costae ornamentation from that with a latticed thorax.

Kilinora* cf. *spiralis (Matsuoka, 1982)
(Plate 1, fig. 31)
cf. *1982 *Stylocapsa*? *spiralis* – Matsuoka, p. 77, pl. 3, figs. 1–8.
Remarks: Our single specimen is poorly preserved and only a part of peculiar ornamentation, i.e. oblique plicae, can be observed.

Genus ***Gongylothorax*** Foreman, 1968; emend. Dumitrica, 1970

Type species: ***Dicolocapsa verbeeki*** Tan, 1927. Suzuki and Gawlick (2003b) discussed in detail.

Gongylothorax favosus Dumitrica, 1970
Remarks: *Gongylothorax favosus* is subdivided into two subspecies, namely the nominate subspecies *Gongylothorax favosus favosus* Dumitrica and the subspecies *Gongylothorax favosus oviformis* Suzuki and Gawlick.

Gongylothorax favosus favosus Dumitrica, 1970
(Plate 1, fig. 26; Plate 2, figs. 7, 28; Plate 3, fig. 35)
*1970 *Gongylothorax favosus* – Dumitrica, p. 56, pl. 1, figs. 1a–1c, 2.
1994 *Gongylothorax favosus* Dumitrica – Ishida, fig. 3.5.
2003a *Gongylothorax favosus* Dumitrica – Suzuki and Gawlick, p. 119, pl. 1, fig. 13.
2003b *Gongylothorax favosus* Dumitrica – Suzuki and Gawlick, p. 205, fig. 6.96. (detailed synonymy until 2002)
2005 *Gongylothorax favosus* Dumitrica – Missoni *et al.*, fig. 7.30; fig. 13.8.
2006 *Gongylothorax favosus* Dumitrica – Auer *et al.*, fig. 6.17.
2006 *Gongylothorax favosus* Dumitrica – Gawlick *et al.*, fig. 8a.16; fig. 9a.13.
2009 *Gongylothorax favosus favosus* Dumitrica – Suzuki and Gawlick, p. 180, fig. 5.31A–5.31C, 5.32A, 5.32B; fig. 6.21A, 6.21B.
2009 *Gongylothorax favosus* Dumitrica – Ishida *et al.*, fig. 6.9, 6.10.
2014 *Gongylothorax favosus favosus* Dumitrica – Suzuki *et al.*, p. 17, pl. 4, fig. 8; pl. 5, fig. 14.
Remarks: *Gongylothorax favosus favosus* differs from *Gongylothorax favosus oviformis* in having a spherical thorax with a depressed cephalis.

Gongylothorax favosus oviformis Suzuki and Gawlick, 2009
(Plate 2, fig. 23; Plate 3, fig. 36)
1994 *Gongylothorax* aff. *favosus* Dumitrica – Goričan, p. 70, pl. 13, figs. 9a–9c, 11a–11c. (detailed synonymy until 1993)
cf. 2005 *Gongylothorax* aff. *favosus* Dumitrica – Suzuki and Kuwahara, p. 55, pl. 2, figs. 9, 10. (detailed synonymy between 1994 and 2004)
2006 *Gongylothorax* aff. *favosus* Dumitrica – Gawlick *et al.*, fig. 8a.17; fig. 9a.12.
*2009 *Gongylothorax favosus oviformis* – Suzuki and Gawlick, p. 180, fig. 5.33A–5.34C; fig. 6.22A–6.26B.
Remarks: *Gongylothorax favosus oviformis* differs from *Gongylothorax favosus favosus* in having an elliptical test outline with a not so depressed cephalis. In case of *Gongylothorax favosus oviformis*, penta- or hexagonal pore frames become lager down to thoracic base.

***Gongylothorax* sp. C** sensu Suzuki and Gawlick, 2003b
(Plate 3, fig. 42)
1997 *Gongylothorax siphonofer* Dumitrica – Yao, pl. 9, fig. 417.
*2003b *Gongylothorax* sp. C – Suzuki and Gawlick, p. 206, fig. 6.98.

2009 *Gongylothorax* sp. C sensu Suzuki and Gawlick– Suzuki and Gawlick, p. 181, fig. 5.35, 5.36.
2016 *Gongylothorax* sp. C sensu Suzuki and Gawlick – Gawlick *et al.*, fig. 11g.

Remarks: Our single specimen possesses a projected tube-like aperture on a base of bulbous thorax, on which somewhat lager pores are more sparsely distributed in comparison with the materials from north side of Mt. Loser (Suzuki and Gawlick, 2003b) and Hallstatt salt mine (Suzuki and Gawlick, 2009).

Genus ***Tricolocapsa*** Haeckel, 1881

Type species: ***Tricolocapsa theophrasti*** Haeckel, 1887

Tricolocapsa tetragona Matsuoka, 1983
(Plate 1, fig. 32; Plate 2, fig. 9)
*1983 *Tricolocapsa tetragona* – Matsuoka, p. 22, pl. 3, figs. 8–12; pl. 8, figs. 4–10.
cf. 1994 *Tricolocapsa* cf. *tetragona* Matsuoka – Ishida, fig. 3.13.
1994 *Tricolocapsa tetragona* Matsuoka – Goričan, p. 94, pl. 13, figs. 8, 10. (detailed synonymy until 1993)
1999 *Tricolocapsa tetragona* Matsuoka – Wegerer *et al.*, fig. 5.1.
2007 *Tricolocapsa tetragona* Matsuoka – Gawlick *et al.*, fig. 18.40.
2009 *Tricolocapsa tetragona* Matsuoka – Suzuki and Gawlick, p. 183, fig. 5.43.
2010 *Tricolocapsa tetragona* Matsuoka – Gawlick *et al.*, fig. 19.40; fig. 27.19.
2011 *Tricolocapsa tetragona* Matsuoka – Gawlick *et al.*, fig. 3.36.

Tricolocapsa undulata (Heitzer, 1930)
(Plate 1, fig. 22; Plate 2, fig. 27; Plate 3, figs. 17, 33)
*1930 *Lithobotrys undulata* – Heitzer, p. 390, pl. 28, fig. 22.
1987 *Sethocapsa funatoensis* – Aita, p. 73, pl. 2, figs. 6a–b, 7a–b; pl. 9, figs. 14, 15.
1987 *Sethocapsa yahazuensis* – Aita, p. 73, pl. 2, figs. 8a–b, 9a–b; pl. 9, figs. 16, 17.
1993 *Tricolocapsa undulata* (Heitzer) – Ozvoldova and Faupl, pl. 3, fig. 12.
2005 *Tricolocapsa undulata* (Heitzer) – Suzuki and Kuwahara, p. 59, pl. 2, fig. 3. (detailed synonymy until 2004)
2005 *Tricolocapsa undulata* (Heitzer) – Missoni *et al.*, fig. 7.37; fig. 10.45.
2006 *Tricolocapsa undulata* (Heitzer) – Auer *et al.*, fig. 6.44.
2006 *Tricolocapsa undulata* (Heitzer) – Gawlick *et al.*, fig. 8c.36; fig. 9b.21.
2009 *Tricolocapsa undulata* (Heitzer) – Suzuki and Gawlick, p. 183, fig. 5.44A, 5.44B, 5.45A, 5.45B; fig. 6.18A, 6.18B, 6.19A, 6.19B.
2011 *Tricolocapsa undulata* (Heitzer) – Gawlick *et al.*, fig. 2.34; fig. 3.37.
2015 *Zhamoidellum undulata* (Heitzer) – Ishida, pl. 1, figs. 55–59; pl. 6, figs. 52–55.

Remarks: We integrate two species of Aita (1987), i.e. *Sethocapsa funatoensis* and *Sethocapsa yahazuensis*, into *Tricolocapsa undulata* (Heitzer, 1930) as younger synonyms (see Suzuki and Gawlick, 2003b; Suzuki and Kuwahara, 2005).

Genus ***Striatojaponocapsa*** Kozur, 1984

Type species: ***Tricolocapsa plicarum*** Yao, 1979

Striatojaponocapsa conexa (Matsuoka, 1983)
(Plate 2, fig. 39; Plate 3, fig. 31)
*1983 *Tricolocapsa conexa* – Matsuoka, p. 20, pl. 3, figs. 3–7; pl. 7, figs. 11–14.
1994 *Tricolocapsa conexa* Matsuoka – Goričan, p. 94, pl. 11, figs. 7a–b, 8, 9, 10a–b. (detailed synonymy until 1993)
1997 *Striatojaponicapsa conexa* (Matsuoka) – Hull, p. 166, pl. 37, fig. 20.
2003b *Tricolocapsa conexa* Matsuoka – Suzuki and Gawlick, p. 208, fig. 5.42; fig. 6.43–6.45.
2005 *Tricolocapsa conexa* Matsuoka – Missoni *et al.*, fig. 10.44.
2007 *Striatojaponocapsa conexa* (Matsuoka) – Hatakeda *et al.*, p. 54, pl. 2, figs. 1–10.
2009 *Striatojaponocapsa conexa* (Matsuoka) – Suzuki and Gawlick, p. 182, fig. 5.40; fig. 6.32A, 6.32B.
2015 *Striatojaponocapsa conexa* (Matsuoka) – Ishida, pl. 1, figs. 16–19; pl. 6, figs. 21–25.

Striatojaponocapsa riri O'Dogherty, Goričan and Dumitrica, 2006
(Plate 2, figs. 11, 40)
1994 *Tricolocapsa* sp. A – Goričan, p. 9, pl. 11, figs. 11–13.
*2006 *Striatojaponocapsa riri* – O'Dogherty, Goričan and Dumitrica, p. 447, pl. 8, figs. 14, 15.
2007 *Striatojaponocapsa riri* O'Dogherty, Goričan and Dumitrica – Hatakeda *et al.*, p. 55, pl. 2, figs. 11–20.
2007 *Tricolocapsa* sp. A sensu Goričan – Auer *et al.*, fig. 6.108.
2015 *Striatojaponocapsa riri* O'Dogherty, Goričan and Dumitrica – Ishida, pl. 1, figs. 20–24; pl. 6, figs. 26–32.

Striatojaponocapsa synconexa O'Dogherty, Goričan and Dumitrica, 2006
(Plate 1, fig. 24; Plate 2, fig. 33; Plate 3, fig. 30)
*2006 *Striatojaponocapsa synconexa* – O'Dogherty, Goričan and Dumitrica, p. 447, pl. 10, figs. 9–17. (Detailed synonymy)
2007 *Striatojaponocapsa synconexa* O'Dogherty, Goričan and Dumitrica – Hatakeda *et al.*, p. 54, pl. 1, figs. 11–20.
2015 *Striatojaponocapsa synconexa* O'Dogherty, Goričan and Dumitrica – Ishida, pl. 1, figs. 13–15; pl. 6, figs.

19, 20.

Striatojaponocapsa naradaniensis (Matsuoka, 1984)
(Plate 2, fig. 21; Plate 3, fig. 40)
*1984 *Stichocapsa naradaniensis* – Matsuoka, p. 145, pl. 1, figs. 1–5; pl. 2, figs. 1–6.
1994 *Stichocapsa naradaniensis* Matsuoka – Goričan, p. 88, pl. 11, fig. 6. (detailed synonymy until 1993)
2003b *Stichocapsa naradaniensis* Matsuoka – Suzuki and Gawlick, p. 213, fig. 6.53, 6.54a, 6.54b. (detailed synonymy between 1994 and 2002)
2005 *Stichocapsa naradaniensis* Matsuoka – Missoni *et al.*, fig. 7.43; fig. 10.55; fig. 13.12.
2009 *Stichocapsa naradaniensis* Matsuoka – Suzuki and Gawlick, p. 186, fig. 5.57A, 5.57B, 5.58; fig. 6.38A, 6.38B, 6.42A, 6.42B.
2009 *Stichocapsa naradaniensis* Matsuoka – Ishida *et al.*, fig. 6.3; fig. 7.9.

Genus ***Japonocapsa*** Kozur, 1984

Type species: ***Tricolocapsa fusiformis*** Yao, 1979

Japonocapsa fusiformis (Yao, 1979)
(Plate 3, figs. 47, 48)
*1979 *Tricolocapsa*? *fusiformis* – Yao, p. 33, pl. 4, figs. 12–18; pl. 5, figs. 1–4.
1994 *Tricolocapsa*? *fusiformis* Yao – Goričan, p. 94, pl. 9, fig. 14. (detailed synonymy until 1993)
2009 *Tricolocapsa fusiformis* Yao – Suzuki and Gawlick, p. 183, fig. 5.41, 5.42A, 5.42B, 5.57A, 5.57B; fig. 6.13A, 6.13B, 6.14, 6.17.
Remarks: In case of depicted specimens, a basal dish-like appendage is torn off.

Japonocapsa tegiminis (Yao, 1979)
(Plate 3, fig. 41)
*1979 *Stichocapsa tegiminis* – Yao, p. 34, pl. 5, figs. 5–13.
2002 *Stichocapsa tegiminis* Yao – Nakae, fig. 3m.
2009 *Stichocapsa tegiminis* Yao – Suzuki and Gawlick, p. 186, fig. 5.55A, 5.55B.
2018 *Stichocapsa tegiminis* Yao – Gawlick *et al.*, fig. 12.24.
Remarks: *Japonocapsa tegiminis* differs from *Japonocapsa fusiformis* in having four chambers (exclusive of an appendage). A depicted specimen has a wide basal dish-like appendage.

Genus ***Tetracapsa*** Haeckel, 1881

*1881 *Tetracapsa* – Haeckel, p. 438.
pt. 1887 *Stichocapsa* – Haeckel, p. 1515.
pt. 1981 *Tetracapsa* Haeckel – Petrushevskaya, p. 185.
1993 *Tetracapsa* Haeckel – Widz and De Wever, p. 86.
2003b *Tetracapsa* Haeckel – Suzuki and Gawlick, p. 211.
2004b *Tetracapsa* Haeckel – Suzuki *et al.*, p. 387.
2014 *Tetracapsa* Haeckel – Suzuki *et al.*, p. 18.
Type species: ***Tetracapsa pilula*** Rüst, 1885. This type species was subsequently designated by Campbell (1954) (Petrushevskaya, 1981).
Remarks: Morphotypes having latticed four-chambered test with closed base appeared frequently in Middle and Late Jurassic time. These morphotypes have been described under the genus *Sethocapsa* or *Stichocapsa*. However, their four-chambered feature is conspicuous to separate from two-chambered *Sethocapsa* and five- or more chambered *Stichocapsa*.

***Tetracapsa* sp. A** sensu Suzuki and Gawlick, 2003b
(Plate 3, figs. 1, 32)
1997 *Stichocapsa* sp. A sensu Matsuoka and Yao – Suzuki and Nakae, pl. 2, fig. 11.
2001 *Stichocapsa* sp. A sensu Matsuoka and Yao – Miyamoto *et al.*, pl. 7, fig. 8.
2002 *Arcanicapsa* sp. 2 – Hori *et al.*, pl. 8, fig. 24.
*2003b *Tetracapsa* sp. A – Suzuki and Gawlick, p. 211, fig. 5.24.
2004b *Tetracapsa* sp. A – Suzuki *et al.*, p. 387, fig. 5.1a, 5.1b.
2007 *Tetracapsa* sp. A sensu Suzuki and Gawlick – Auer *et al.*, fig. 6.92.
2009 *Tetracapsa* sp. A sensu Suzuki and Gawlick – Suzuki and Gawlick, p. 185, fig. 6.37A, 6.37B.

Genus ***Stichocapsa*** Haeckel, 1881

Type species: ***Stichocapsa jaspidea*** Rüst, 1885 (Campbell, 1954)

Stichocapsa cicciona Chiari, Marcucci and Prela, 2002
(Plate 1, fig. 28)
*2002 *Stichocapsa cicciona* – Chiari *et al.*, p. 76, pl. 3, figs. 8–12.
2007 *Stichocapsa cicciona* Chiari, Marcucci and Prela – Auer *et al.*, fig. 6.78.
2011 *Stichocapsa cicciona* Chiari, Marcucci and Prela – Gawlick *et al.*, fig. 3.31.
Remarks: This species has a test with a wide basal aperture, so that its generic attribution to the genus *Stichocapsa*, which has a closed base, is questionable. Here we tentatively attribute the species to the genus *Stichocapsa*.

Stichocapsa robusta Matsuoka, 1984
(Plate 1, fig. 23; Plate 2, fig. 26; Plate 3, fig. 25)
*1984 *Stichocapsa robusta* – Matsuoka, p. 146, pl. 1, figs. 6–13; pl. 2, figs. 7–12.
2007 *Stichocapsa robusta* Matsuoka – Auer *et al.*, fig. 6.81.

Genus ***Cyrtocapsa*** Haeckel, 1881

Type species: ***Cyrtocapsa ovalis*** Rüst, 1885

***Cyrtocapsa* sp. B**
(Plate 2, fig. 14)
2003 *Cyrtocapsa* sp. – Wegerer *et al.*, fig. 9.18.

Remarks: Four or five chambered tests with a robust horn. Proximal three or four segments make a conical portion, and a final segment exhibits a globous ball-form with larger pores than those of conical portion.

Genus ***Fultacapsa*** Ozvoldova, 1997

Type species: ***Acotripus sphericus*** Ozvoldova, 1988

Fultacapsa sphaerica (Ozvoldova, 1988)
(Plate 1, fig. 21)
* 1988 *Acotripus sphericus* – Ozvoldova, p. 376, pl. 5, figs. 1–5, 7.
1997 *Fultacapsa sphaerica* (Ozvoldova) – Ozvoldova and Frantova, p. 59, pl. 5, figs. 1, 2.
cf. 2003b *Acotripus* cf. *sphaericus* Ozvoldova – Suzuki and Gawlick, p. 191, fig. 5.29.
2010 *Fultacapsa sphaerica* (Ozvoldova) – Gawlick *et al.*, fig. 37B.1.
Remarks: A specimen from the Fludergraben section differs from specimens of Ozvoldova (1988) and Ozvoldova and Frantova (1997) in having weak constriction between a proximal part and a last globous segment.

Genus ***Helvetocapsa*** O'Dogherty, Goričan and Dumitrica, 2006

Type species: ***Tricolocapsa matsuokai*** Sashida, 1999

Helvetocapsa matsuokai (Sashida, 1999); emend. Suzuki and Gawlick, 2009
(Plate 1, fig. 19; Plate 3, fig. 39)
1930 *Cenellipsis* aff. *perspicua* Rüst – Heitzer, p. 388, pl. 27, fig. 11.
*1999 *Tricolocapsa matsuokai* – Sashida in Sashida *et al.*, p. 566, pl. 1, figs. 4, 5.
2003b *Tricolocapsa matsuokai* Sashida – Suzuki and Gawlick, p. 209, fig. 6.38. (detailed synonymy until 2002)
2006 *Helvetocapsa matsuokai* (Sashida) – O'Dogherty *et al.*, p. 452, pl. 7, figs. 19–24.
2009 *Helvetocapsa matsuokai* (Sashida) – Suzuki and Gawlick, p. 187, fig. 5.61A, 5.61B; fig. 6.40, 6.46A, 6.46B.
2018 *Helvetocapsa matsuokai* (Sashida) – Gawlick *et al.*, fig. 14.3.
Remarks: Sashida *et al.* (1999) described this species for the first time under the genus *Tricolocapsa*, a three-chamberd genus. O'Dogherty *et al.* (2006) erected a new genus *Helvetocapsa* and attributed this species to their new genus, although the number of the segments of this species were not observed. Suzuki and Gawlick (2009) observed the inner structure of it with a transmitted light microscope and clarified that *Helvetocapsa matsuokai* has five segments.

Family **EUCYRTIDIELLIDAE** Takemura, 1986

Genus ***Eucyrtidiellum*** Baumgartner, 1984

Type species: ***Eucyrtidium? unumaensis*** Yao, 1979

Eucyrtidiellum circumperforatum Chiari, Marcucci and Prela, 2002
(Plate 1, fig. 33; Plate 3, fig. 3)
*2002 *Eucyrtidiellum*? *circumperforatum* – Chiari *et al.*, p. 65, pl. 1, figs. 2–9.
2007 *Eucyrtidiellum circumperforatum* Chiari, Marcucci and Prela – Auer *et al.*, fig. 6.22.
2007 *Eucyrtidiellum circumperforatum* Chiari, Marcucci and Prela – Gawlick *et al.*, fig. 8.12.
2009 *Eucyrtidiellum circumperforatum* Chiari, Marcucci and Prela – Suzuki and Gawlick, p. 189, fig. 5.64.

Eucyrtidiellum unumaense (Yao, 1979)
(Plate 1, figs. 35, 36; Plate 3, figs. 14, 37)
*1979 *Eucyrtidium*? *unumaensis* – Yao, p. 39, pl. 9, figs. 1–11.
1994 *Eucyrtidiellum unumaense* (Yao) – Goričan, p. 69, pl. 9, figs. 5, 6. (detailed synonymy until 1993)
2003a *Eucyrtidiellum unumaense* (Yao) – Suzuki and Gawlick, p. 119, pl. 1, fig. 9.
2003b *Eucyrtidiellum unumaense* (Yao) – Suzuki and Gawlick, p. 215, fig. 5.21. (detailed synonymy between 1994 and 2002)
2005 *Eucyrtidiellum unumaense* ssp. (Yao) – Missoni *et al.*, fig. 10.62.
2006 *Eucyrtidiellum unumaense* ssp. (Yao) – Gawlick *et al.*, fig. 8a.14; fig. 9a.8.
2009 *Eucyrtidiellum unumaense* (Yao) – Suzuki and Gawlick, p. 188, fig. 5.62.
Remarks: *Eucyrtidiellum unumaense* is subdivided into the three subspecies, i.e. *E. unumaense unumaense* Yao, *E. unumaense dentatum* Baumgartner and *E. unumaense pustulatum* Baumgartner (Baumgartner *et al.*, 1995a; Suzuki and Gawlick, 2003b). Because our specimens possess not so conspicuous features of ornamentation on upper abdomen surface to identify subspecies, we describe them only as *Eucyrtidiellum unumaense*.

Eucyrtidiellum ptyctum (Riedel and Sanfilippo, 1974)
(Plate 1, fig. 34; Plate 3, fig. 4)
*1974 *Eucyrtidium ptyctum* – Riedel and Sanfilippo, p. 778, pl. 5, fig. 7; pl. 12, fig. 14; non pl. 12, fig. 15.
2003b *Eucyrtidiellum ptyctum* (Riedel and Sanfilippo) – Suzuki and Gawlick, p. 218, fig. 6.26, 6.27. (detailed synonymy between 1998 and 2002)
2005 *Eucyrtidiellum ptyctum* (Riedel and Sanfilippo) – Suzuki and Kuwahara, p. 65, pl. 2, fig. 17.
2005 *Eucyrtidiellum ptyctum* (Riedel and Sanfilippo) – Missoni *et al.*, fig. 7.48; fig. 10.61; fig. 13.5.
2006 *Eucyrtidiellum ptyctum* (Riedel and Sanfilippo) – Gawlick *et al.*, fig. 8.10; fig. 9.7.
2006 *Eucyrtidiellum ptyctum* (Riedel and Sanfilippo) – Auer *et al.*, fig. 6.14.

2009 *Eucyrtidiellum ptyctum* (Riedel and Sanfilippo) – Suzuki and Gawlick, p. 188, fig. 5.63.
2014 *Eucyrtidiellum ptyctum* (Riedel and Sanfilippo) – Suzuki *et al.*, p. 19, pl. 5. fig. 4.
2018 *Eucyrtidiellum ptyctum* (Riedel and Sanfilippo) – Gawlick *et al.*, fig. 14.12.

Eucyrtidiellum nodosum Wakita, 1988
(Plate 2, fig. 5; Plate 3, figs. 2, 38)
*1988 *Eucyrtidiellum nodosum* – Wakita, p. 408, pl. 4, fig. 29; pl. 5, fig. 16.
2001 *Eucyrtidiellum nodosum* Wakita – Nishizono, pl. 2, fig. 8.
2003b *Eucyrtidiellum nodosum* Wakita – Suzuki and Gawlick, p. 217, fig. 6.30. (detailed synonymy between 1994 and 2003)
2007 *Eucyrtidiellum nodosum* Wakita – Auer *et al.*, fig. 6.23.
2009 *Eucyrtidiellum nodosum* Wakita – Auer *et al.*, fig. 9.22; cf. fig. 13.3.

6. Discussion – Radiolarian zonation for the lower Oxfordian and correlation

Because radiolarian fauna from the lower Oxfordian that is calibrated by ammonite has hitherto not known all over the world, the Fludergraben fauna is a key for understanding Oxfordian marker species of radiolarians. Previously proposed radiolarian zonations have a relatively long-lasting period for the Callovian and Oxfordian. For example, the U. A. Zone 8 of Baumgartner *et al.* (1995b) ranges in age from middle Callovian to early Oxfordian. Thus, we can distinguish the Oxfordian radiolarian fauna from the Callovian one to make a comparison of faunal contents between Callovian and Oxfordian. In this chapter we discuss the first appearance horizons of possible marker species for the lower Oxfordian with descriptions of the middle and upper Callovian sections in the Northern Calcareous Alps.

6. 1 Radiolarians from the middle Callovian Brielgraben section

In the Brielgraben section of the Northern Calcareous Alps, the Klaus Formation yields middle Callovian ammonites (Krystyn, 1971) from strata that underlie a radiolarite succession. We have detected radiolarians from the radiolarite of the Brielgraben section, which are partly listed in Suzuki and Gawlick (2006, 2009). We show the revised inventory of radiolarians from the sample BT1 in the appendix 1.

6. 2 Radiolarians from the lower part of the Knallalm-Neualm section – upper Callovian

From the lower part of the Knallalm-Neualm section, Auer *et al.* (2007) reported radiolarian assemblages containing *Williriedellum carpathicum* from the samples MR149 and MR175. Gawlick *et al.* (2009) invented a new subzone of the *Zhamoidellum ovum* Zone, i.e. the *Williriedellum carpathicum* Subzone, based on the lower part of the Knallalm-Neualm section that is situated below the *Kilinora spiralis*-bearing radiolarite. If the first appearance horizon of *Kilinora spiralis* can be placed in the lowermost Oxfordian, the *Williriedellum carpathicum* Subzone is correlated to the upper Callovian (see discussion in the section 6. 4). We show the lists of radiolarian species from samples MR149 and MR175 in the appendix 2 (Auer *et al.*, 2007).

6. 3 Marker species for the base of Oxfordian

To compare the above-mentioned radiolarian faunas from the middle and upper Callovian with the Fludergraben fauna, it should be made clear what are the marker species for the base of Oxfordian (Fig. 7). We choose four species, i.e. *Kilinora spiralis* (Matsuoka), *Fultacapsa sphaerica* (Ozvoldova), *Protunuma japonicus* Matsuoka and Yao and *Pseudoeucyrtis reticularis* Matsuoka and Yao. *Kilinora spiralis* occurs, however, very rare in the Northern Calcareous Alps. From the Fludergraben section, we found a single specimen from the sample D1023, identified as *Kilinora* cf. *spiralis*. It is poorly preserved, and its surface ornamentation is ambiguous (Plate 1, fig. 31). Other three marker species, *Fultacapsa sphaerica* (Ozvoldova), *Protunuma japonicus* Matsuoka and Yao and *Pseudoeucyrtis reticularis* Matsuoka and Yao, also occur as a single specimen, respectively. *Pseudodictyomitra primitiva* Matsuoka and Yao has also potential to be a marker, but a forerunner occurrence is known from the upper Callovian of the Knallalm-Neualm section (Auer *et al.*, 2007). In the following three sections, we discuss ranges of these species in detail.

6. 4 Stratigraphic range of *Kilinora spiralis* — lower Oxfordian to lower Kimmeridgian

There is stratigraphical discrepancy of the first appearance horizon of *Kilinora spiralis* between Matsuoka (1995) and Baumgartner and Matsuoka (1995) (*Stylocapsa*? *spiralis* in their publications), although both used the same marker species of calcareous nannoplankton, *Stephanolithion hexum* Rood and Barnars, 1972, as discussed in Suzuki *et al.* (2004a). Matsuoka (1995) placed the first appearance horizon of *Kilinora spiralis* to the upper Callovian, based on the last occurrence of *Stephanolithion hexum* in the core 124 of the Site 534 in the Blake Bahama Basin (DSDP Leg 76). The last occurrence horizon of *Stephanolithion hexum*, which is correlated to the boundary between the middle and upper Callovian with the calibration of magnetostratigraphy (Roth, 1983), lies just above the first appearance horizon of *Kilinora spiralis* (Baumgartner and Matsuoka, 1995). On the other side, Baumgartner and Matsuoka (1995) reinterpreted the horizon of the last occurrence of *Stephanolithion hexum* in the core as a preservational bias, and its horizon was correlated to the upper Bathonian to lower Callovian (U. A. Zone 7) on the basis of a radiolarian age assignment. This is a circular

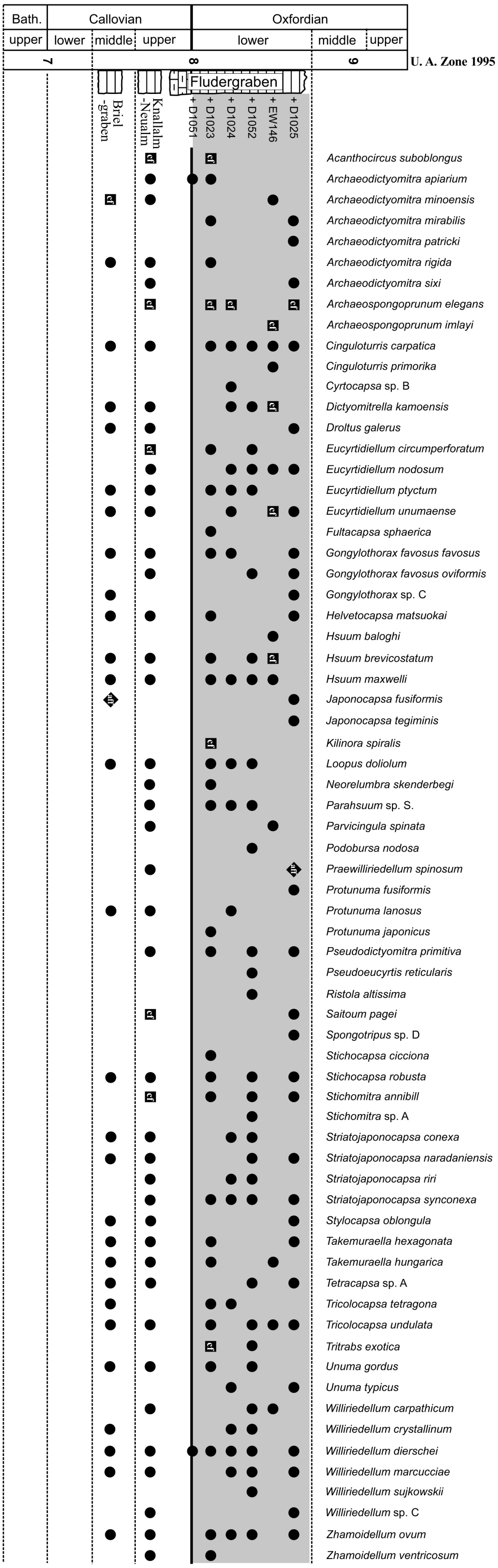

Fig. 7 Stratigraphic distributions of radiolarian species occurring in the lower Oxfordian Fludergraben section with the occurrences in the upper Callovian Knallalm-Neualm section (Auer *et al.*, 2007) and middle Callovian Brielgraben section (Suzuki and Gawlick, 2009 and unpublished data). Bath.: Bathonian, U. A. Zone 1995: Unitary Association Zones by Baumgartner *et al.* (1995b).

argument, because the radiolarian assemblage was used for the radiolarian age calibration. Of course, it is very difficult to determine the last occurrence horizon, if it is really the last occurrence or not, due to preservational condition like dissolution. Our data from the Northern Calcareous Alps support the interpretation of Matsuoka (1995). *Kilinora* cf. *spiralis* occurs in the early Oxfordian Fludergraben section, but not in the Brielgraben section of the middle Callovian (Suzuki and Gawlick, 2009 and data herein). Furthermore, Medd (1982) reported *Stephanolithion hexum* from the lower Oxfordian and also from the Kimmeridgian sporadically. This report suggests that the last occurrence horizon of *Stephanolithion hexum* extends into the lower Oxfordian or higher. In this context, the first appearance horizon of *Kilinora spiralis* can also be shifted upwards around the boundary between Callovian and Oxfordian as demonstrated in the Fludergraben section.

On the other hand, the last occurrence horizon of *Kilinora spiralis* is demonstrated in the Kurisaka Formation of eastern Shikoku, Japan, with the correlation of the ammonite zonation (Ishida *et al.*, 2009). *Kilinora spilaris* occurs in the horizon just below the first appearance horizon of the ammonite *Ataxioceras* (*Ataxioceras*) *kurisakaense* Kobayashi and Fukuda, 1947, indicating a lower Kimmeridgian horizon (Sato *et al.*, 2008).

Consequently, *Kilinora spiralis* occurs in the range from the boundary between Callovian and Oxfordian to the lower Kimmeridgian. Thus, the U. A. Zone 6 (middle Bathonian) to 7 (late Bathonian–early Callovian) attributed to the range of *Kilinora spiralis* by Baumgartner *et al.* (1995b) is too old to be used anymore.

6. 5 Stratigraphic range of *Fultacapsa sphaerica*

Fultacapsa sphaerica was first described by Ozvoldova (1988) as *Acotripus spherica* from the Pienniny Klippen Belt of West Carpatians (Turá Lúka, northeast Slovakia). Although her age determination was based only on radiolarian association, a *Fultacapsa sphaerica*-bearing sample (TL-2) yields also *Podocapsa amphitreptera* Foreman, an index species of Kimmeridgian. Ozvoldova and Frantova (1997) reported *Fultacapsa sphaerica* from a sample bearing also *Podocapsa amphitreptera* Foreman (SJP-4) from the Pieniny Klippen Belt of West Carpathians, and also from another sample (Ps-14) dated only by radiolarians as late Oxfordian–early Kimmeridgian, i.e. the U. A. Zone 10 of Baumgartner *et al.* (1995b). In the Northern Calcareous Alps *Fultacapsa sphaerica* occurs not frequently, but until now we have detected it only from the Oxfordian to Kimmeridgian.

6. 6 First appearance horizon of *Protunuma japonicus*, *Pseudoeucyrtis reticularis* and *Pseudodictyomitra primitiva*

Protunuma japonicus, *Pseudoeucyrtis reticularis* and *Pseudodictyomitra primitiva* were first described from the Torinosu Group of the Island Shikoku and Kii-Yura areas, Southwest Japan (Matsuoka and Yao, 1985). Matsuoka and Yao (1985) inferred the age of the *Pseudodictyomitra primitiva–Pseudodictyomitra* sp. A assemblage to the Tithonian, and this assemblage acts as the type of the *Pseudodictyomitra primitiva* Zone in Japan. According to Matsuoka (1995) the *Pseudodictyomitra primitiva* Zone is defined as the zone between the last occurrence horizon of *Hsuum maxwelli* and the first occurrence horizon of *Pseudodictyomitra carpatica*. Our early Oxfordian samples yield *Hsuum maxwelli* commonly, so that the correlation of our samples to the *Pseudodictyomitra primitiva* Zone of Japan cannot be made. However, some constituents of the *Pseudodictyomitra primitiva–Pseudodictyomitra* sp. A assemblage can be found in our samples, i.e. *Pseudodictyomitra primitiva*, *Pseudoeucyrtis reticularis*, *Protunuma japonicus*, *Archaeodictyomitra apiarium*, *Archaeodictyomitra minoensis*, *Cingulоturris carpatica*, *Eucyrtidiellum ptyctum* and *Zhamoidellum ovum* (= *Tricolocapsa* sp. A). Thus, the *Pseudodictyomitra primitiva–Pseudodictyomitra* sp. A assemblage contains many species determined in the Fludergraben fauna. It should pay attention that the first appearance horizon of *Pseudodictyomitra primitiva* is in the upper Callovian, as demonstrated in Fig. 7. Important is the absence of *Hsuum maxwelli* as the criterion, whether a radiolarian assemblage is attributed to the *Pseudodictyomitra primitiva* Zone or not. As *Protunuma japonicus* and *Pseudoeucyrtis reticularis* were found in our Fludergraben samples, these two species appeared already in early Oxfordian time.

6. 7 Shift of some radiolarian age ranges

Stratigraphic ranges of several species of the Fludergraben fauna, which are so far known in the Callovian or lower, have to be prolonged into the lower Oxfordian. These species are as follows (with previous age assignment).

Dictyomitrella kamoensis (U. A. Zone 3–7: Baumgartner *et al.*, 1995b)
Eucyrtidiellum circumperforatum (U. A. Zone 5–7: Chiari *et al.*, 2002)
Helvetocapsa matsuokai (*Striatojaponocapsa plicarum* Zone – upper Bajocian-lower Bathonian: Sashida *et al.*, 1999; U. A. Zone 6: O'Dogherty *et al.*, 2006)
Hsuum baloghi (lower *Unuma echinatus* Zone – Aalenian to lower Bajocian: Grill and Kozur, 1986)
Japonocapsa fusiformis (U. A. Zone 3–5: Baumgartner *et al.*, 1995b)
Neorelumbra skenderbegi (U. A. Zone 5–7: Chiari *et al.* 2002)
Protunuma fusiformis (Bajocian: Yao, 1997)
Protunuma lanosus (Callovian: Suzuki and Gawlick, 2003a)
Stichocapsa cicciona (U. A. Zone 5–7: Chiari *et al.* 2002)
Stichocapsa robusta (U. A. Zone 5–7: Baumgartner *et al.*, 1995b)
Japonocapsa tegiminis (Bajocian: Yao, 1979, 1997)
Tricolocapsa tetragona (upper *Striatojaponocapsa plicarum* Zone to lower *Striatojaponocapsa conexa* Zone – Bathonian: Matsuoka, 1995)
Unuma gordus (as *Unuma* sp. A, U. A. Zone 4–6: Baumgartner *et al.*, 1995b)
Unuma typicus (Bajocian: Yao, 1997; Callovian: Suzuki and Gawlick, 2009)

Among them we make comments on two important species, i.e. *Protunuma lanosus* and *Tricolocapsa tetragona*. *Protunuma lanosus*, which is the index species of the Callovian *Protunuma lanosus* Subzone of the *Zhamoidellum ovum* Zone of Suzuki and Gawlick (2003a), extends its range upwards into the Oxfordian. Consequently, the previous definition of the base of the *Williriedellum dierschei* Subzone, the last occurrence horizon of *Protunuma lanosus*, has to be changed. Another important species is *Tricolocapsa tetragona*, which was considered having a short stratigraphic range within the Bathonian (Matsuoka, 1983, 1995). As we demonstrate by the Fludergraben fauna, *Tricolocapsa tetragona* occurs in the lower Oxfordian strata. This stratigraphic range prolongation is supported by the occurrence of *Tricolocapsa tetragona* in the Torinosu-type limestone of east Shikoku, Japan (Ishida, 1994). This fauna yields also *Kilinora spiralis*, suggesting an Oxfordian age. Although Ishida (1994) mentioned that the stratigraphic range of *Tricolocapsa tetragona* was not consistent with those of other early Late Jurassic radiolarian species, its occurrence is now regarded not as an exception but as the reflection of its real stratigraphic range.

6. 8 Redefinition of the *Williriedellum dierschei* Zone

In the Jurassic radiolarian zonation of the Northern Calcareous Alps the *Williriedellum dierschei* Subzone of the *Zhamoidellum ovum* Zone was first established by Suzuki and Gawlick (2003a) as the partial-range zone of the species *Williriedellum dierschei* Suzuki and Gawlick, and it is defined by the last occurrence horizon of *Protunuma lanosus* for the base and the last occurrence horizon of *Eucyrtidiellum unumaense* for the top, indicating an early to middle Oxfordian age (Auer *et al.*, 2007). However, as we demonstrate here, *Protunuma lanosus* occurs also in the lower Oxfordian Fludergraben section, so that the base of the *Williriedellum dierschei* Subzone lies within the lower Oxfordian or higher, if we follow the above-mentioned definition. Our purpose of the radiolarian zonation is to distinguish the lower Oxfordian radiolarian zone from the Callovian one. And to make an age determination, it is better to take a positive criterion, i.e. the first appearance

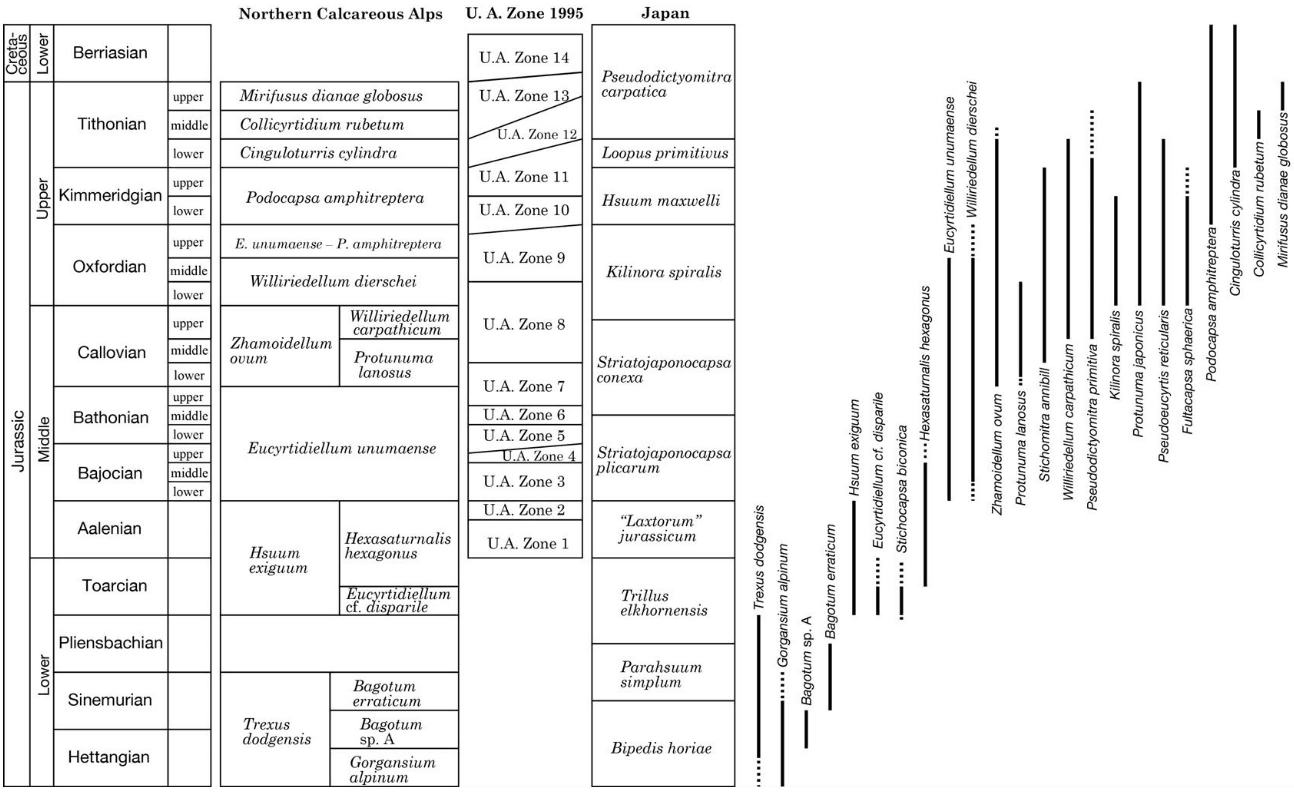

Fig. 8 Modified Jurassic radiolarian zonation for the Northern Calcareous Alps according to Suzuki and Gawlick (2003a), Steiger (1992), Gawlick *et al.* (2009) and this study. The U. A. Zone 1995 for the Western Tethyan realm of Baumgartner *et al.* (1995b) and the Japanese zonation of Matsuoka and Ito (2019) are shown on the side for comparison.

horizon, rather than a negative one, i.e. the last occurrence horizon. In this context, here we take the first appearance horizon of *Protunuma japonicus* as the definition of the base of the *Williriedellum dierschei* Subzone. *Fultacapsa sphaerica*, *Pseudoeucyrtis reticularis* and *Kilinora spiralis* are the subordinate marker species of this zone. Suzuki and Gawlick (2003a) and Gawlick *et al.* (2009) put it to the Subzone in the *Zhamoidellum ovum* Zone, because the faunal content of the Callovian-Oxfordian is very similar and no clear distinction was shown at that time. Because we can discriminate some early Oxfordian marker species among Callovian-Oxfordian-lasting species, we make this subzone ranked up as a zone apart from the *Zhamoidellum ovum* Zone of the Callovian, namely the *Williriedellum dierschei* Zone (Fig. 8). According as this, the overlying *Eucyrtidiellum unnumaense – Podocapsa amphitreptera* Interval Zone for the upper Oxfordian (Suzuki and Gawlick, 2003a) is also separated from the *Zhamoidellum ovum* Zone and it is here redefined as an independent zone (Fig. 8). And the upper limit of the *Williriedellum carpathicum* Subzone in the *Zhamoidellum ovum* Zone is also here emended as the first appearance horizon of *Protunuma japonicus.*

7. Conclusion

(1) 37 genera, 67 species and 2 subspecies of radiolarians are systematically described from the lower Oxfordian Fludergraben section that is calibrated by ammonites.

(2) Four radiolarian species have a potential to be marker for the base of Oxfordian. These are *Kilinora spiralis* Matsuoka, *Fultacapsa sphaerica* (Ozvoldova), *Protunuma japonicus* Matsuoka and Yao and *Pseudoeucyrtis reticularis* Matsuoka and Yao.

(3) The *Williriedellum dierschei* Zone is here redefined as the lower-middle Oxfordian radiolarian zone of the Northern Calcareous Alps.

(4) In the systematic part of radiolarians we have emended two genera and one species diagnoses, and redesignated of the type species of the genus *Loopus*.

Acknowledgments: We would like to express our sincere thanks to Dr. Satoshi Nakae (AIST) for his invitation and guidance to the special issue for INTERRAD XV of the Bulletin of the Geological Survey of Japan. We also thank specially to Dr. Naoto Ishida (Tottori University) and Dr. Takayuki Uchino (AIST) for their critical and positive remarks, which improve the manuscript significantly. We are deeply grateful to Dr. Sigrid Missoni and Dr. Eva Wegerer (Montanuniversität Leoben) for their help to make residues/preparations in laboratory for radiolarian analyses. This study was supported by the FWF Project P 16812 of Austria.

References

Aita, Y. (1987) Middle Jurassic to Lower Cretaceous radiolarian biostratigraphy of Shikoku with reference to selected sections in Rombardy Basin and Sicily. *Science Reports of the Tohoku University, Second Series (Geology)*, **58**, 1–91, pls. 1–14.

Auer, M., Gawlick, H.-J. and Suzuki, H. (2006) Die Unter-Oxford-Radiolarit-Megabrekzie am Nordrand des Dachstein-Blockes (Nördliche Kalkalpen, Österreich): Radiolarienfaunen, Mikrofazies des Komponentenbestandes und tektonische Bedeutung. *Jahrbuch der Geologischen Bundesanstalt*, **146**, 33–51. (in German with English abstract)

Auer, M., Suzuki, H., Schlagintweit, F. and Gawlick, H.-J. (2007) The late Middle to Late Jurassic sedimentary rocks of the Knallalm-Neualm area north of Gosau (northwestern Dachstein Block, central Northern Calcareous Alps). *Journal of Alpine Geology*, **48**, 117–140.

Auer, M., Gawlick, H.-J., Suzuki, H. and Schlagintweit, F. (2009) Spatial and temporal development of siliceous basin and shallow-water carbonate sedimentation in Oxfordian Northern Calcareous Alps. *Facies*, **55**, 63–87.

Baumgartner, P. O. (1980) Late Jurassic Hagiastridae and Patulibracchiidae (Radiolaria) from the Argolis Peninsula (Peloponnesus, Greece). *Micropaleontology*, **26**, 274–322.

Baumgartner, P. O. (1984) A Middle Jurassic-Early Cretaceous low-latitude radiolarian zonation based on Unitary Associations and age of Tethyan radiolarites. *Eclogae geologicae Helvetiae*, **77**, 729–837.

Baumgartner, P. O. and Matsuoka, A. (1995) New radiolarian data from DSDP Site 534A, Blake Bahama Basin, central northern Atlantic. *Mémoires de Géologie (Lausanne)*, **23**, 709–715.

Baumgartner, P. O., De Wever, P. and Kocher, R. (1980) Correlation of Tethyan Late Jurassic – Early Cretaceous radiolarian events. *Cahiers de Micropaléontologie*, **2**, 23–72, pls. 1–6.

Baumgartner, P. O., O'Dogherty, L., Goričan, Š., Dumitrica-Jud, R., Dumitrica, P., Pillevuit, A., Urquhart, E., Matsuoka, A., Danelian, T., Bartolini, A., Carter, E. S., De Wever, P., Kito, N., Marcucci, M. and Steiger, T. (1995a) Radiolarian catalogue and systematics of Middle Jurassic to Early Cretaceous Tethyan genera and species. *Mémoires de Géologie (Lausanne)*, **23**, 37–685.

Baumgartner, P. O., Bartolini, A., Carter, E. S., Conti, M., Cortese, G., Danelian, T., De Wever, P., Dumitrica, P., Dumitrica-Jud, R., Goričan, Š., Guex, J., Hull, D. M., Kito, N., Marcucci, M., Matsuoka, A., Murchey, B., O'Dogherty, L., Savary, J., Vishnevskaya, V., Widz, D. and Yao, A. (1995b) Middle Jurassic to Early Cretaceous radiolarian biochronology of Tethys based on Unitary Associations. *Mémoires de Géologie (Lausanne)*, **23**, 1013–1048.

Beccaro, P. (2004) Upper Jurassic radiolarians from Inici Mt. area (north-western Sicily, Italy): biochronology and calibration by ammonites. *Revista Italiana di Paleontologia e Stratigrafia*, **110**, 289–301.

Beccaro, P. (2006) Radiolarian correlation of Jurassic siliceous successions of the Rosso Ammonitico Formation in the Southern Alps and Western Sicily (Italy). *Eclogae geologicae Helvetiae*, **99**, 21–33.

Campbell, A. S. (1954) Radiolaria. *In* Moore, R. C. ed., *Treatise on Invertebrate Paleontology, (D) Protista 3*, The University of Kansas Press, Lawrence, 11–163.

Cayeux, L. (1897) Etude de quelques dépots siliceux secondaires et tertiaires du Bassin de Paris et de la Belgique Appendice paléontologique – Description des radiolaires de la smectique de Herve (Belgique). *Mémoires de la Société géologique du Nord*, **4**, 185–206, pls. 7–8. (in French)

Chiari, M., Cortese, G., Marcucci, M. and Nozzoli, N. (1997) Radiolarian biostratigraphy in the sedimentary cover of the ophiolites of south-western Tuscany, central Italy. *Eclogae geologicae Helvetiae*, **90**, 55–77.

Chiari, M., Marcucci, M. and Prela, M. (2002) New species of Jurassic radiolarians in the sedimentary cover of ophiolites in the Mirdita area, Albania. *Micropaleontology*, **48** (Supplement 1), 61–87.

Cortese, G. (1993) Radiolarian biostratigraphy of the Tuscan Cherts (Tuscan Succession) from Val di Lima, Tuscany, Northern Apennines. *Paleopelagos*, **3**, 169–189.

Danelian, T. (1995) *Emiluvia bisella. Mémoires de Géologie (Lausanne)*, **23**, 196–197.

Deflandre, G. (1953) Radiolaires fossiles. *In* Grassé, P. P. ed., *Traite de Zoologie*, **1**, Masson, Paris, 389–436. (in French)

De Wever, P. (1981) Une nouvelle sous-famille, les Poulpinae, et quatre nouvelles espèces de *Saitoum* radiolaires mésozoiques téthysiens. *Géobios*, **14**, 5–15. (in French with English abstract)

Diersche, V. (1980) Die Radiolarite des Oberjura im Mittelabschnitt der Nördlichen Kalkalpen. *Geotekonische Forschungen*, **58**, 1–217. (in German with English summary)

Donofrio, D. A. and Mostler, H. (1978) Zur Verbreitung der Saturnalidae (Radiolaria) im Mesozoikum der Nördlichen Kalkalpen und Südalpen. *Geologisch-Paläontologische Mitteilungen Innsbruck*, **7**, 1–55. (in German with English and Italian summaries)

Dumitrica, P. (1970) Cryptocephalic and cryptothoracic Nassellaria in some Mesozoic deposits of Romania. *Revue Roumaine de Géologie, Géophysique et Géographie, Série de Géologie*, **14**, 45–124.

Dumitrica, P. and Mello, J. (1982) On the age of the Meliata Group and the Silica Nappe radiolarites (localities Drzkovce and Buhúnovo, Slovak Karst, CSSR). *Geologické Práce*, **77**, 17–28, pls. 1–4.

Dumitrica, P., Immenhauser, A. and Dumitrica-Jud, R. (1997) Mesozoic radiolarian biostratigraphy from Masirah ophiolite, Sultanate of Oman. Part I Middle Triassic, uppermost Jurassic and Lower Cretaceous Spumellarians and multisegmented Nassellarians. *Bulletin of the National Museum of National Science*, **9**, 1–106.

Ehrenberg, C. G. (1839) Über die Bildung der Kreidefelsen und des Kreidemergels durch unsichtbare Organismen. *Abhandlungen der königlichen Akademie der Wissenschaften in Berlin*, **1838**, 59–147, Taf. 1–4, Tabelle-Anhänge. (in German)

Ehrenberg, C. G. (1876) Fortsetzung der mikrogeologischen Studien als Gesammt-Uebersicht der mikroskopischen Paläontologie gleichartig analysirter Gebirgsarten der Erde, mit specieller Rücksicht auf den Polycystinen-Mergel von Barbados. *Physikalische Abhandlungen der königlichen Akademie der Wissenschaften zu Berlin*, **1875**, 1–225, Taf. 1–30, Tabellen-Anhänge. (in German)

Fischli, H. (1916) Beitrag zur Kenntnis der fossilen radiolarien in der Riginagelfluh. *Mitteilungen der Naturwissenschaftlichen Gesellschaft in Winterthur*, **11**, 44–47. (in German)

Foreman, H. P. (1968) Upper Maestrichtian Radiolaria of California. *Special Papers in Palaeontology*, **3**, 1–82.

Foreman, H. P. (1973) Radiolaria from DSDP Leg 20. *In* Heezen, B. C. and MacGregor, J. D. *et al.* eds., *Initial Reports of the Deep Sea Drilling Project*, **20**, U. S. Government Printing Office, Washington, D. C., 249–305.

Frisch, W. and Gawlick, H.-J. (2003) The nappe structure of the central Northern Calcareous Alps and its disintegration during Miocene tectonic extrusion – a contribution to understanding the orogenic evolution of the Eastern Alps. *International Journal of Earth Sciences*, **92**, 712–727.

Gawlick, H.-J. and Frisch, W. (2003) The Middle to Late Jurassic carbonate clastic radiolaritic flysch sediments in the Northern Calcareous Alps: sedimentology, basin evolution and tectonics – an overview. *Neues Jahrbuch für Geologie und Paläontologie, Abhandlungen*, **230**, 163–213.

Gawlick, H.-J. and Missoni, S. (2019) Middle-Late Jurassic sedimentary mélange formation related to ophiolite obduction in the Alpine-Carpathian-Dinaridic Mountain Range. *Gondwana Research*, **74**, 144–172. doi: 10.1016/j.gr.2019.03.003

Gawlick, H.-J. and Suzuki, H. (1999) Zur stratigraphischen Stellung der Strubbergschichten in den Nördlichen Kalkalpen (Callovium-Oxfordium). *Neues Jahrbuch für Geologie und Paläontologie, Abhandlungen*, **211**, 233–262. (in German with English abstract)

Gawlick, H.-J., Suzuki, H., Vortisch, W. and Wegerer, E. (1999) Zur stratigraphischen Stellung der Tauglbodenschichten an der Typlokalität in der Osterhorngruppe (Nördliche Kalkalpen, Ober-Oxfordium – Unter-Tithonium). *Mitteilungen der Gesellschaft der Geologie und Bergbaustudenten in Österreich*, **42**, 1–20. (in German with English abstract)

Gawlick, H.-J., Schlagintweit, F., Ebli, O. and Suzuki, H. (2004) Die Plassen-Formation (Kimmeridgium) des Krahstein (Steirisches Salzkammergut, Österreich) und ihre Unterlagerung: neue Daten zur Fazies, Biostratigraphie und Sedimentologie. *Zentralblatt für Geologie und Paläontologie, Teil I*, **2003**, 295–334. (in German with English abstract)

Gawlick, H.-J., Suzuki, H. and Schlagintweit, F. (2006) Die Ober-Trias- und Jura-Sedimentgesteine der Sarsteinalm und ihre Bedeutung für die tektonische Gliederung des Dachstein-Blockes (Salzkammergut, Nördliche Kalkalpen, Österreich). *Neues Jahrbuch für Geologie und Paläontologie, Abhandlungen*, **239**, 101–160. (in German with English abstract)

Gawlick, H.-J., Schlagintweit, F. and Suzuki, H. (2007) Die Ober-Jura bis Unter-Kreide Schichtfolge des Gebietes Höherstein-Sandling (Salzkammergut, Österreich) – Implikationen zur Rekonstruktion des Block-Puzzles der zentralen Nördlichen Kalkalpen, der Gliederung der Radiolaritflyschbecken und der Plassen-Karbonatplattform. *Neues Jahrbuch für Geologie und Paläontologie, Abhandlungen*, **243**, 1–70. (in German with English abstract)

Gawlick, H.-J., Missoni, S., Schlagintweit, F., Suzuki, H., Frisch, W., Krystyn, L., Blau, J. and Lein, R. (2009) Jurassic tectonostratigraphy of the Austroalpine Domain. *Journal of Alpine Geology*, **50**, 1–152.

Gawlick, H.-J., Missoni, S., Schlagintweit, F. and Suzuki, H. (2010) Tiefwasser Beckengenese und Initiierung einer Karbonatplattform im Jura des Salzkammergutes (Nördliche Kalkalpen, Österreich). *Journal of Alpine Geology*, **53**, 63–136. (in German with English abstract)

Gawlick, H.-J., Suzuki, H. and Missoni, S. (2011) Neue Radiolarienfaunen aus der Ruhpolding-Formation im Liegenden der Rofan-Brekzie des Rofan-Sonnwendgebirges: Implikationen zur Deckenneugliederung der westlichen Nördlichen Kalkalpen. *Arbeitstagung 2011 der Geologischen Bundesanstalt – Geologisches Kartenblatt 88 Achenkirch*, 39–50. (in German)

Gawlick, H.-J., Missoni, S., Schlagintweit, F. and Suzuki, H. (2012) Jurassic active continental margin deep-water basin and carbonate platform formation in the north-western Tethyan realm (Austria, Germany). *Journal of Alpine Geology*, **54**, 189–292.

Gawlick, H.-J., Missoni, S., Suzuki, H., Sudar, M., Lein, R. and Jovanović, D. (2016) Triassic radiolarite and carbonate components from a Jurassic ophiolitic mélange (Dinaridic Ophiolite Belt). *Swiss Journal of Geosciences*, **109**, 473–494.

Gawlick, H.-J., Missoni, S., Sudar, M., Suzuki, H., Méres, Š, Lein, R. and Jovanović, D. (2018) The Jurassic Hallstatt Mélange of the Inner Dinarides (SW Serbia):

implications for Triassic-Jurassic geodynamic and palaeogeographic reconstructions of the Western Tethyan realm. *Neues Jahrbuch für Geologie und Paläontologie, Abhandlungen*, **288**, 1–47.

Goričan, Š. (1994) Jurassic and Cretaceous radiolarian biostratigraphy and sedimentary evolution of the Budava Zone (Dinarides, Montenegro). *Mémoires de Géologie (Lausanne)*, **18**, 1–177.

Grill, I. and Kozur, H. (1986) The first evidence of the *Unuma echinatus* radiolarian zone in the Rudabanya Mts. (northern Hungary). *Geologisch-Paläontologische Mitteilungen Innsbruck*, **13**, 239–275.

Haeckel, E. (1862) *Die Radiolarien (Rhizopoda Radiaria).* Georg Reimer, Berlin, 572p, Taf. 1–35. (in German)

Haeckel, E. (1881) Entwurf eines Radiolarien-Systems auf Grund von Studien der Challenger-Radiolarien. *Jenaische Zeitschrift für Naturwissenschaft*, **15**, 418–472. (in German and Latin)

Haeckel, E. (1887) Report on the radiolaria collected by H. M. S. Challenger during the years 1873-1876. *Report of the scientific results of the voyage of H.M.S. Challenger during the years 1873–76*, *Zoology*, **18**, Her Majesty's Government, London, CLXXXVIII+1803p, 140 pls.

Hatakeda, K., Suzuki, N. and Matsuoka, A. (2007) Quantitative morphological analyses and evolutionary history of the Middle Jurassic polycystine radiolarian genus *Striatojaponocapsa* Kozur. *Marine Micropaleontology*, **63**, 39–56.

Heitzer, I. (1930) Die Radiolarienfauna der mitteljurassischen Kieselmergel im Sonnwendgebirge. *Jahrbuch der Geologischen Bundesanstalt*, **80**, 381–406, Taf. 1–3. (in German)

Hori, N. (1999) Latest Jurassic radiolarians from the northeastern part of the Torinoko Block, Yamizo Mountains, central Japan. *Science Reports of the Institute of Geoscience, University of Tsukuba, Section B*, **20**, 47–114.

Hori, N., Saito, M. and Toshimitsu, S. (2002) Late Jurassic radiolarian fauna from the Ikenohara Formation of the Kurosegawa Belt in the Toyo-Izumi area, Kumamoto Prefecture, Kyushu, Japan. *Bulletin of the Geological Survey of Japan*, **53**, 689–724.

Hull, D. M. (1997) Upper Jurassic Tethyan and southern Boreal radiolarians from western North America. *Micropaleontology*, **43** (Supplement 2), 1–202.

Ichikawa, K. and Yao, A. (1976) Two new genera of Mesozoic cyrtoid radiolarians from Japan. *In* Takayanagi, Y. and Saito, T. eds., *Progress in Micropaleontology, Special Publication*, Micropaleontology Press, New York, 110–117.

Ishida, K. (1994) Radiolarian age of the Torinosu-type limestone in the north of the Shimanto Terrane, East Shikoku. *Journal of the Geological Society of Japan*, **100**, 312–315. (in Japanese with English figure captions)

Ishida, K. and Kozai, T. (2004) Stratigraphy and radiolarian ages of the Sakashu Group, South Kurosegawa Terrane (Sakashu Belt) in East Shikoku. *News of Osaka Micropaleontologists, Special Volume*, no. 13, 135–148. (in Japanese with English abstract)

Ishida, K., Tsujino, Y., Kozai, T., Sato, T. and Hirsch, F. (2009) Direct correlation of radiolarian *Kilinora spiralis* Zone with the Late Jurassic ammonite faunal succession in the Kurisaka Formation, Kurosegawa Terrane, SW Japan. *Science in China Series D, Earth Sciences*, **52**, 1910–1923.

Ishida, N. (2004) Lithostratigraphy of Mesozoic strata and Late Jurassic radiolarian assemblages in the Southern Chichibu terrane in the Hinohara area, southeastern part of the Kanto Massif, central Japan. *News of Osaka Micropaleontologists, Special Volume*, no. 13, 89–109. (in Japanese with English abstract)

Ishida, N. (2015) Late Middle Jurassic (Callovian) radiolarian assemblages from siliciclastic rocks in the Southern Chichibu belt, southwest Kanto Mountains, Japan. *News of Osaka Micropaleontologists, Special Volume*, no. 15, 181–205.

Isozaki, Y. and Matsuda, T. (1985) Early Jurassic radiolarians from bedded chert in Kamiaso, Mino Belt, Central Japan. *Earth Science (Chikyu Kagaku)*, **39**, 429–442, pls. 1–3.

Kemkin, I. V. and Taketani, Y. (2004) New radiolarian species from Late Jurassic chert-terrigenous deposits of the Taukha Terrane, Southern Sikhote-Alin. *Paleontological Research*, **8**, 325–336.

Kiessling, W. (1995) New radiolarians from the earliest Cretaceous of the Sultanate of Oman (Wahrah Formation, Jebel Buwaydah). *Paläontologische Zeitschrift*, **69**, 321–342.

Kiessling, W. (1999) Late Jurassic radiolarians from the Antarctic Peninsula. *Micropaleontology*, **45**, 1–96.

Kito, N. and De Wever, P. (1992) Novelles espèces d'Hagiastridae (Radiolaires) du Jurassique moyen de Sicily (Italy). *Revue de Micropaléontologie*, **35**, 127–141. (in French with English abstract)

Kobayashi, T. and Fukada, A. (1947) A new species of *Ataxioceras* in Nippon. *Japanese Journal of Geology and Geography*, **20**, 45–48, pl. 11.

Kocher, R. N. (1981) Biochronostratigraphische Untersuchungen oberjurassischer Radiolarienführender Gesteine, insbesondere der Südalpen. *Mitteilungen aus dem geologischen Institut der Eidgenossissche Technischen Hochschule und der Universität Zürich, Neue Folge*, Nr. 234, 1–184. (in German with English abstract)

Kozai, T., Ishida, K. and Kondo, Y. (2004) Radiolarian ages and bivalve fauna of the Birafu Formation, Central Shikoku. *News of Osaka Micropaleontologists, Special Volume*, no. 13, 149–165. (in Japanese with English abstract)

Kozur, H. (1984) New radiolarian taxa from the Triassic and Jurassic. *Geologisch-Paläontologische Mitteilungen Innsbruck*, **13**, 49–88.

Kozur, H. (1985) The radiolarian genus *Eoxitus* n. gen. from the *Unuma echinatus* zone (Bajocian) of the northern Hungary. *Proceedings of the Koninklijke Nederlandse Akademie van Wetenschappen, Series B*, **88**, 211–220.

Kozur, H. and Mostler, H. (1981) Beiträge zur Erforschung der mesozoischen Radiolarien. Teil IV: Thalassosphaeracea HAECKEL, 1862, Hexastylacea HEACKEL, 1882 emend. PETRUSEVSKAJA, 1979, Sponguracea HAECKEL, 1862 emend. und weitere triassische Lithocycliacea, Trematodiscacea, Actinommacea und Nassellaria. *Geologisch-Paläontologische Mitteilungen Innsbruck, Sonderband*, 1–208. (in German with English summary)

Kozur, H. and Mostler, H. (1982) Entactinaria subordo nov., a new radiolarian suborder. *Geologisch-Paläontologische Mitteilungen Innsbruck*, **11**, 399–414.

Krische, O., Suzuki, H. and Gawlick, H.-J. (2013) Mikrofazies und Radiolarienfauna der *Saccocoma*-Kalke in der westlichen Weitenau (Hochreith Einheit). *Jahrbuch der Geologischen Bundesanstalt*, **153**, 75–96. (in German with English abstract)

Krystyn, L. (1971) Stratigraphie, Fauna und Fazies der Klaus-Schichten (Aalenium-Oxford) in den Östlichen Nordalpen. *Verhandlungen der Geologischen Bundesanstalt*, **1971**, 486–509. (in German with English abstract)

Mandl, G. W. (1982) Jurassische Gleittektonik im Bereich der Hallstätter Zone zwischen Bad Ischl und Bad Aussee (Salzkammergut, Österreich). *Mitteilungen der Gesellschaft der Geologie- und Bergbaustudenten in Österreich*, **28**, 55–76. (in German with English abstract)

Matsuoka, A. (1982) Jurassic two-segmented Nassellarians (Radiolaria) from Shikoku, Japan. *Journal of Geosciences*, *Osaka City University*, **25**, 71–87.

Matsuoka, A. (1983) Middle and Late Jurassic radiolarian biostratigraphy in the Sakawa and adjacent areas, Shikoku, Southwest Japan. *Journal of Geosciences, Osaka City University*, **26**, 1–48.

Matsuoka, A. (1984) Late Jurassic four-segmented nassellarians (radiolaria) from Shikoku, Japan. *Journal of Geosciences, Osaka City University*, **27**, 143–153.

Matsuoka, A. (1986) *Tricolocapsa yaoi* assemblage (Late Jurassic radiolarians) from the Togano Group in Shikoku, Southwest Japan. *Journal of Geosciences, Osaka City University*, **29**, 101–115.

Matsuoka, A. (1991) Early Jurassic radiolarians from the Nanjo massiv in the Mino terrane, central Japan. *Transactions and Proceedings of the Palaeontological Society of Japan, New Series*, no. 161, 720–738.

Matsuoka, A. (1995) Jurassic and Lower Cretaceous radiolarian zonation in Japan and in the western Pacific. *The Island Arc*, **4**, 140–153.

Matsuoka, A. and Ito, T. (2019) Updated radiolarian zonation for the Jurassic in Japan and the western Pacific. *Science Reports of Niigata University (Geology)*, no. 34, 49–57.

Matsuoka, A. and Yao, A. (1985) Latest Jurassic radiolarians from the Torinosu Group in Southwest Japan. *Journal of Geosciences, Osaka City University*, **28**, 125–145.

Medd, A. W. (1982) Nannofossil zonation of the English Middle and Upper Jurassic. *Marine Micropaleontology*, **7**, 73–95.

Missoni, S. and Gawlick, H.-J. (2011) Jurassic mountain building and Mesozoic-Cenozoic geodynamic evolution of the Northern Calcareous Alps as proven in the Berchtesgaden Alps (Germany). *Facies*, **57**, 137–186.

Missoni, S., Schlagintweit, F., Suzuki, H. and Gawlick, H.-J. (2001) Die oberjurassische Karbonatplattform-entwicklung im Bereich der Berchtesgadener Kalkalpen (Deutschland) – eine Rekonstruktion auf der Basis von Untersuchungen polymikter Brekzienkörper in pelagischen Kieselsedimenten (Sillenkopf-Formation). *Zentralblatt für Geologie und Paläontologie, Teil I,* **2000**, 117–143. (in German with English abstract)

Missoni, S., Gawlick, H.-J., Suzuki, H. and Diersche, V. (2005) Die paläogeographische Stellung des Watzmann Blockes in den Berchtesgadener Kalkalpen–Neuergebnisse auf der Basis der Analyse der Trias- und Jura-Entwicklung. *Mitteilungen der Gesellschaft der Geologie und Bergbaustudenten in Österreich*, **47**, 169–209. (in German with English abstract)

Miyamoto, T., Nakamura, S. and Kuwazuru, J. (2001) Radiolarian biostratigraphy of the Jurassic Kawamata Group (new name) in the Bisho area of the Hinagu Belt, West Kyushu, Southwest Japan. *News of Osaka Micropaleontologists, Special Volume*, no.12, 227–251. (in Japanese with English abstract)

Mizutani, S. (1981) A Jurassic formation in the Hida-Kanayama area, central Japan. *Bulletin of the Mizunami Fossil Museum*, no. 8, 147–190, pls. 55–64. (in Japanese with English abstract and appendix)

Mizutani, S. and Kido, S. (1983) Radiolarians in Middle Jurassic siliceous shale from Kamiaso, Gifu Prefecture, Central Japan. *Transactions and Proceedings of the Palaeontological Society of Japan, New Series*, no. 132, 253–262, pls. 51–53.

Müller, J. (1858) Über die Thalassicollen, Polycystinen und Acanthometren des Mittelmeeres. *Abhandlungen der königlichen Akademie der Wissenschaften in Berlin*, **1858**, 1–62, Taf. 1–11. (in German)

Nakae, S. (2002) Triassic and Jurassic radiolarians from the Tamba Terrane in the Nishizu district, Fukui, Southwest Japan. *Bulletin of the Geological Survey of Japan*, **53**, 51–59.

Nishizono, Y. (1996) Mesozoic convergent process of the Southern Chichibu Terrane in West Kyushu, Japan, on the basis of Triassic to Early Cretaceous radiolarian biostratigraphy. *Kumamoto Journal of Science (Earth*

Science), **14**, 45–226. (in Japanese with English outline)

Nishizono, Y. (2001) Jurassic radiolarians from the Sakamoto Formation in the Kurosegawa Terrane, Kyushu, Southwest Japan. *News of Osaka Micropaleontologists, Special Volume*, no. 12, 203–214. (in Japanese with English abstract)

Nagai, H. and Mizutani, S. (1990) Jurassic *Eucyrtidiellum* (Radiolaria) in the Mino Terrane. *Transactions and Proceedings of the Palaeontological Society of Japan, New Series*, no. 159, 587–602.

O'Dogherty, L. (1994) Biochronology and Paleontology of Mid-Cretaceous radiolarians from Northern Appennines (Italy) and Betic Cordillera. *Mémoires de Géologie (Lausanne)*, **21**, xv+413p, pls. 1–74.

O'Dogherty, L., Bill, M., Goričan, Š., Dumitrica, P. and Masson, H. (2006) Bathonian radiolarians from an ophiolitic mélange of the Alpine Tethys (Gets Nappe, Swiss-French Alps). *Micropaleontology*, **51**, 425–485.

O'Dogherty, L., De Wever, P., Goričan, Š., Carter, E. S. and Dumitrica, P. (2011) Stratigraphic ranges of Mesozoic radiolarian families. *Palaeoworld*, **20**, 102–115.

O'Dogherty, L., Goričan, Š. and Gawlick, H.-J. (2017) Middle and Late Jurassic radiolarians from the Neotethys suture in the Eastern Alps. *Journal of Paleontology*, **91**, 25–72.

Ozvoldova, L. (1975) Upper Jurassic radiolarians from the Kisuca Series in the Klippen Belt. *Zapadne Karpaty, Seria Paleontologia*, **1**, 73–86.

Ozvoldova, L. (1988) Radiolarian associations from radiolarites of the Kysuca succession of the Klippen belt in the vicinity of Myjava – Tura Luka (west Carpathians). *Geologica Carpathica*, **39**, 369–392.

Ozvoldova, L. (1992) The discovery of a Callovian radiolarian association in the Upper Posidonia beds of the Pieniny succession of the Klippen belt (Western Carpathians). *Geologica Carpathica*, **43**, 111–122.

Ozvoldova, L. and Faupl, P. (1993) Radiolarien aus kieseligen Schichtgliedern des Juras der Grestener und Ybbsitzer Klippenzone (Ostalpen, Niederösterreich). *Jahresbericht der Geologischen Bundesanstalt*, **136**, 479–494. (in German with English abstract)

Ozvoldova, L. and Frantová, L. (1997) Jurassic radiolarians from the eastern part of the Pieniny Klippen Belt (western Carpathians). *Geologica Carpathica*, **48**, 49–61.

Parona, C. F. (1890) Radiolarie nei noduli selciosi del calcare giurese di Cittiglio presso Laverno. *Bollettino della Societa Geologica Italiana*, **9**, 132–175. (in Italian)

Pessagno, E. A. Jr. (1973) Upper Cretaceous Spumellariina from the Great Valley sequence, California Coast Ranges. *Bulletins of American Paleontology*, **63**, 49–102, pls. 9–21.

Pessagno, E. A. Jr. (1976) Radiolarian zonation and stratigraphy of the Upper Cretaceous portion of the Great Valley Sequence, California Coast Ranges. *Micropaleontology, Special Publication*, **2**, 1–95.

Pessagno, E. A. Jr. (1977a) Upper Jurassic radiolaria and radiolarian biostratigraphy of the California Coast Ranges. *Micropaleontology*, **23**, 56–113.

Pessagno, E. A. Jr. (1977b) Lower Cretaceous radiolarian biostratigraphy of the Great Valley Sequence and Franciscan complex, California Coast Ranges. *Cushman Foundation for Foraminiferal Research, Special Publication*, no. 15, 1–87.

Pessagno, E. A. Jr. and Blome, C. D. (1980) Upper Triassic and Jurassic Pantanelliinae from California, Oregon and British Columbia. *Micropaleontology*, **26**, 225–273.

Pessagno, E. A. Jr. and Whalen, P. A. (1982) Lower and Middle Jurassic radiolaria (multicyrtid Nassellariina) from California, east-central Oregon and the Queen Charlotte Islands, B. C. *Micropaleontology*, **28**, 111–169.

Pessagno, E. A. Jr., Blome, C. D., Hull, D. M. and Six, W. M. (1993) Jurassic Radiolaria from the Josephine ophiolite and overlying strata, Smith River subterrane (Klamath Mountains), northwestern California and southwestern Oregon. *Micropaleontology*, **39**, 93–166.

Petrushevskaya, M. G. (1981) Radioliarii otriada Nassellaria mirovogo okeana. *Opredeliteli po faune SSSR, Izdavaemye Zoologitcheskii Institutom Akademii Nauk SSSR*, **128**, Nauka, Leningradskoe Otdelenie, Leningrad, 405p. (in Russian)

Principi, P. (1909) Contributo allo studio dei Radiolari Miocenici Italiani. *Bollettino della Società Geologica Italiana*, **28**, 1–22, Tav. 1. (in Italian)

Riedel, W. R. (1967a) Some new families of radiolaria. *Proceedings of the Geological Society of London*, **1640**, 148–149.

Riedel, W. R. (1967b) Protozoa Subclass Radiolaria. *In* Harland, W. B. *et al.* eds., *The Fossil Record*, Geological Society of London, London, 291–298.

Riedel, W. R. (1971) Systematic classification of polycystine Radiolaria. *In* Funnel, B. M. and Riedel W. R. eds., *The Micropaleontology of Oceans,* Cambridge University Press, Cambridge, 649–661.

Riedel, W. R. and Sanfilippo, A. (1974) Radiolaria from the Southern Indian Ocean, DSDP Leg 26. *In* Davis, T. A., Luyendyk, B. P. *et al.* eds., *Initial Reports of Deep Sea Drilling Project*, **26**, 771–814, U. S. Government Printing Office, Washington, D. C.

Rood, A. P. and Barnars, T. (1972) On Jurassic Coccoliths: *Stephanolithion*, *Diadozygus* and related genera. *Eclogae geologicae Helvetiae*, **65**, 327–342.

Roth, P. H. (1983) Jurassic and Lower Cretaceous calcareous nannofossils in the western North Atlantic (Site 534): Biostratigraphy, preservation, and some observation on biogeography and paleoceanography. *Initial Reports of Deep Sea Drilling Project*, **76**, 587–621.

Rüst, D. (1885) Beiträge zur Kenntniss der fossilien Radiolarien aus Gesteinen des Jura. *Palaeontographica*, **31**, 269–321, Taf. 26–45. (in German)

Rüst, D. (1888) Beiträge zur Kenntniss der fossilien Radiolarien aus Gesteinen der Kreide. *Palaeontographica*, **34**, 181–213, Taf. 22–29. (in German)

Sashida, K., Munasri, Adachi, S. and Kamata, Y. (1999) Middle Jurassic radiolarian fauna from Rotti Island, Indonesia. *Journal of Asian Earth Sciences*, **17**, 561–572.

Sato, T., Tsujino, Y., Ishida, K., Kozai, T. and Hachiya, K. (2008) Newly collected Late Jurassic ammonites from Kurisaka, Tokushima Prefecture, Japan. *Bulletin of the Tokushima Prefectural Museum*, no. 18, 1–20.

Sher, S. A. (1974) The classification of *Tetylenchus* Filipjev, 1936, *Leipotylenchus* n. gen. (Leipotylenchinae n. subf.) and *Triversus* n. gen. (Nematoda: Tylenchoidea). *Nematologica*, **19**, 318–325.

Squinabol, S. (1903) Le Radiolarie dei Noduli selciosi nella Scaglia degli Euganei. *Rivista Italiana di Paleontologia*, **9**, 105–144, Tav. 8–10. (in Italian)

Steiger, T. (1992) Systematik, Stratigraphie und Palökologie der Radiolarien des Oberjura-Unterkreide-Grenzbereiches im Osterhorn-Trolikum (Nördliche Kalkalpen, Salzburg und Bayern). *Zitteliana*, **19**, 3–132, Taf. 1–27. (in German with English abstract)

Suzuki, H. (1995a) Das Verbreitungsmuster der *Canoptum*-Vergesellschaftung (jurassische Radiolarien) in der grauen Tonstein-Abfolge vom Kanoashi-Komplex, Südwestjapan. *Journal of Geological Society of Japan*, **101**, 451–461. (in Japanese with German abstract)

Suzuki, H. (1995b) Frühjurassische Radiolarienfauna aus dem mesozoischen akkretierten Komplex von Ost-Shikoku, Südwestjapan. *Neues Jahrbuch für Geologie und Paläontologie, Abhandlungen*, **198**, 275–296. (in German with English abstract)

Suzuki, H. and Gawlick, H.-J. (2003a) Die jurassischen Radiolarienzonen der Nördlichen Kalkalpen. *In* Weidinger, J. T., Lobitzer, H. and Spitzbart, I., Hrsg., *Beiträge zur Geologie des Salzkammergutes, Gmundner Geo-Studien*, **2**, 115–122. (in German with English abstract)

Suzuki, H. and Gawlick, H.-J. (2003b) Biostratigraphie und Taxonomie der Radiolarien aus den Kieselsedimenten der Blaa Alm und nördlich des Loser (Nördliche Kalkalpen, Callovium bis Oxfordium). *Mitteilungen der Gesellschaft der Geologie und Bergbaustudenten in Österreich*, **46**, 137–228. (in German with English and Japanese abstracts)

Suzuki, H. and Gawlick, H.-J. (2006) Middle Callovian radiolarian fauna from the ammonite-bearing Brielgraben of the Northern Calcareous Alps (Austria). *Abstracts of the 113th Annual Meeting of the Geological Society of Japan*, 116.

Suzuki, H. and Gawlick, H.-J. (2009) Jurassic radiolarians from cherty limestones below the Hallstatt salt mine (Northern Calcareous Alps, Austria). *Neues Jahrbuch für Geologie und Paläontologie, Abhandlungen*, **251**, 155–197.

Suzuki, H. and Kuwahara, K. (2005) Systematische Beschreibung jurassischer Radiolarien und Schwammnadeln aus dem Gebiet Takagamine (Stadt Kyoto, Japan). *Nature and its Environment*, **7**, 37–81. (in Japanese with German and English abstracts)

Suzuki, H. and Nakae, S. (1997) Lithostratigraphy and geologic age of the Furuya Formation of the Tamba Belt: Latest Jurassic radiolarians from Kutsuki, Shiga Prefecture, Southwest Japan. *News of Osaka Micropaleontologists, Special Volume*, no. 10, 205–210. (in Japanese with English abstract)

Suzuki, H. and Nakai, N. (2016) Topographic development of Mt. Hidari-Daimonji, a site of the Bonfire in conjunction with its lithologic distribution of the Tamba Terrane. *Chikyu Monthly, Special*, no. 66, 113–120. (in Japanese)

Suzuki, H., Wegerer, E. and Gawlick, H.-J. (2001) Zur Radiolarienstratigraphie im unteren Callovium in den Nördlichen Kalkalpen das Klauskogelbachprofil westlich von Hallstatt. *Zentralblatt für Geologie und Paläontologie, Teil I*, **2000** (1/2), 167–184. (in German with English abstract)

Suzuki, H., Prinz-Grimm, P. and Schmidt-Effing, R. (2002) Radiolarien aus dem Grenzbereich Hettangium/Sinemurium von Nordperu. *Paläontologische Zeitschrift*, **76**, 163–187. (in German with English and Spanish abstracts)

Suzuki, H., Kuwahara, K., Komine, A., Otsuji, K., Fujita, H., Kato, H., Matsumoto, T., Asada, S., Yoshida, Y. and Misaki, S. (2004a) Geologisches Alter der Tanba-Gruppe im Gebiet Takagamine der Stadt Kyoto, Japan. *Nature and its Environment*, **6**, 14–27. (in Japanese with German and English abstracts)

Suzuki, H., Maung Maung, Aye Ko Aung and Takai, M. (2004b) Jurassic radiolaria from chert pebbles of the Eocene Pondaung Formation, central Myanmar. *Neues Jahrbuch für Geologie und Paläontologie, Abhandlungen*, **213**, 369–393.

Suzuki, H., Shibata, M., Sudo, M., Tsujino, Y., Kogiso, T., Diersche, V. and Mikami, T. (2014) Die oberjurassische Radiolarienvergesellschaftung zum Tuffithorizont im Gscheidgraben, Unken-Gebiet, Österreich. *Annual Memoirs of the Otani University Shin Buddhist Comprehensive Research Institute*, **31**, 1–38. (in Japanese with German abstract and systematic part)

Suzuki, H., La Ja, Maung Maung, Aung Kyaw Thin and Kuwahara, K. (2020) The first report on Early Cretaceous Radiolaria from Myanmar. *Paleontological Research*, **24**, 103–112.

Sykora, M. and Ozvoldova, L. (1996) Lithoclasts of middle Jurassic radiolarites in debris flow sediments from Silica Nappe (locality Bleskovy pramen, Slovak Karst, Western Carpathians). *Mineralia Slovaca*, **28**, 21–25.

Takemura, A. (1986) Classification of Jurassic Nassellarians (Radiolaria). *Palaeontographica, Abteilung A*, **195**, 29–74, pls. 1–12.

Tan, S. H. (1927) Over de samenstelling en het ontstaan van krijt- en mergel-gesteenten van de Molukken. *Jaarboek van het Mijnwezen in Nederlandsch Oost-Indië*, **55**, 5–165, pls. 1–16. (in Dutch)

Tollmann, A. (1977) *Geologie von Österreich, Band 1: Die Zentralalpen*, Deuticke, Wien, 766p. (in German)

Vinassa de Regny, P. E. (1899) I radiolari delle ftaniti titoniane di Cárpena (Spezia). *Palaeontographica Italica*, **4**, 217–238, Tav. 17–18. (in Italian)

Wakita, K. (1988) Early Cretaceous melange in the Hida-Kanayama area, central Japan. *Bulletin of the Geological Survey of Japan*, **39**, 367–421.

Wegerer, E., Suzuki, H. and Gawlick, H.-J. (1999) Stratigraphische Einstufung von Radiolarienfaunen aus Kieselsedimenten im Bereich der Hallstätter Zone westlich von Hallstatt (Callovium - Oxfordium, Nördliche Kalkalpen). *Mitteilungen der Gesellschaft der Geologie und Bergbaustudenten in Österreich*, **42**, 93–108. (in German with English abstract)

Wegerer, E., Suzuki, H. and Gawlick, H.-J. (2001) Zur stratigraphischen Einstufung von Kieselsedimenten im Bereich des Sandling (Nördliche Kalkalpen, Callovium-Oxfordium). *Mitteilungen der Gesellschaft der Geologie und Bergbaustudenten in Österreich*, **45**, 67–82. (in German with English abstract)

Wegerer, E., Suzuki, H. and Gawlick, H.-J. (2003) Zur stratigraphischen Einstufung von Kieselsedimenten südöstlich des Plassen (Nördliche Kalkalpen, Österreich). *Jahrbuch der geologischen Bundesanstalt*, **143**, 323–335. (in German with English abstract)

Widz, D. and De Wever, P. (1993) Nouveaux Nassellaires (Radiolaria) des radiolarites jurassiques de la coupe de Szeligowy Potok (Zones de klippes de Pieniny, Carpathes, Pologne). *Revue de Micropaléontologie*, **36**, 77–91. (in French with English abstract)

Wisniowski, T. (1889) Beitrag zur Kenntniss der Mikrofauna aus den oberjurassischen Feuersteinknollen der Umgegend von Krakau. *Jahrbuch der kaiserlich-königlichen Geologischen Reichsanstalt*, **38**, 657–702, Taf. 12–13. (in German)

Wu, H. (1993) Upper Jurassic and Lower Cretaceous radiolarians of Xialu chert, Yarlung Zangbo ophiolite belt, southern Tibet. *In* Blueford, J. R. and Murchey, B., eds., *Radiolaria of giant and subgiant fields in Asia*. *Micropaleontology, Special Publication*, **6**, 115–136.

Yang, Q. (1993) Taxonomic studies of Upper Jurassic (Tithonian) radiolaria from the Taman Formation, east-central Mexico. *Palaeoworld*, **3**, 1–164.

Yao, A. (1972) Radiolarian fauna from the Mino belt in the northern part of the Inuyama area, central Japan. Part I. Spongosaturnalids. *Journal of Geosciences, Osaka City University*, **15**, 21–64, pls. 1–11.

Yao, A. (1979) Radiolarian fauna from the Mino belt in the northern part of the Inuyama area, central Japan. Part II: Nasselaria 1. *Journal of Geosciences, Osaka City University*, **22**, 21–73.

Yao, A. (1982) Middle Triassic to Early Jurassic radiolarians from the Inuyama area, central Japan. *Journal of Geosciences, Osaka City University,* **25**, 53–70, pls. 1–4.

Yao, A. (1997) Faunal change of Early-Middle Jurassic radiolarians. *News of Osaka Micropaleontologists, Special Volume*, no. 10, 155–182. (in Japanese with English abstract)

Yao, A., Matsuoka, A. and Nakatani, T. (1982) Triassic and Jurassic radiolarian assemblages in Southwest Japan. *News of Osaka Micropaleontologists, Special Volume*, **5**, 27–43. (in Japanese with English abstract)

Yeh, K.-Y. and Cheng, Y.-N. (1996) Jurassic radiolarians from the northeast coast of Busuanga Island, North Palawan Block, Philippines. *Micropaleontology*, **42**, 93–124.

Recieved July 9, 2019
Accepted July 17, 2020
Published on-line September 16, 2020

Plate 1 Scanning electron micrographs of radiolarians from the samples D1051 (1–2), D1023 (3–34) and D1024 (35–36), basal horizons of the Fludergraben section, Austria. A 50 µm scale bar applies to all photos.

1. *Williriedellum dierschei* Suzuki and Gawlick, 2004
2. *Archaeodictyomitra apiarium* (Rüst, 1885)
3. *Archaeospongoprunum* cf. *elegans* Wu, 1993
4. *Hsuum maxwelli* Pessagno, 1977a
5. *Loopus doliolum* Dumitrica, 1997
6. *Pseudodictyomitra primitiva* Matsuoka and Yao, 1985
7. *Parahsuum* sp. S sensu Matsuoka, 1986
8. *Tritrabs* cf. *exotica* (Pessagno, 1977a)
9. *Neorelumbra skenderbegi* Chiari *et al.*, 2002
10. *Archaeodictyomitra rigida* Pessagno 1977a
11. *Archaeodictyomitra apiarium* (Rüst, 1885)
12. *Hsuum brevicostatum* (Ozvoldova, 1975)
13. *Stichomitra annibill* Kocher, 1981
14. *Acanthocircus* cf. *suboblongus* (Yao, 1972)
15. *Cinguloturris carpatica* Dumitrica, 1982
16. *Takemuraella hungarica* (Kozur, 1985)
17. *Archaeodictyomitra mirabilis* Aita, 1987
18. *Takemuraella hexagonata* (Heitzer, 1930)
19. *Helvetocapsa matsuokai* (Sashida, 1999)
20. *Zhamoidellum ovum* Dumitrica, 1970
21. *Fultacapsa sphaerica* (Ozvoldova, 1988)
22. *Tricolocapsa undulata* (Heitzer, 1930)
23. *Stichocapsa robusta* Matsuoka, 1984
24. *Striatojaponocapsa synconexa* O'Dogherty *et al.*, 2006
25. *Zhamoidellum ventricosum* Dumitrica, 1970
26. *Gongylothorax favosus favosus* Dumitrica, 1970
27. *Williriedellum dierschei* Suzuki and Gawlick, 2004
28. *Stichocapsa cicciona* Chiari *et al.*, 2002
29. *Unuma gordus* Hull, 1997
30. *Protunuma japonicus* Matsuoka and Yao, 1985
31. *Kilinora* cf. *spiralis* (Matsuoka, 1982)
32. *Tricolocapsa tetragona* Matsuoka, 1983
33. *Eucyrtidiellum circumperforatum* Chiari *et al.*, 2002
34. *Eucyrtidiellum ptyctum* (Riedel and Sanfilippo, 1974)

35–36. *Eucyrtidiellum unumaense* (Yao, 1979)

Plate 1

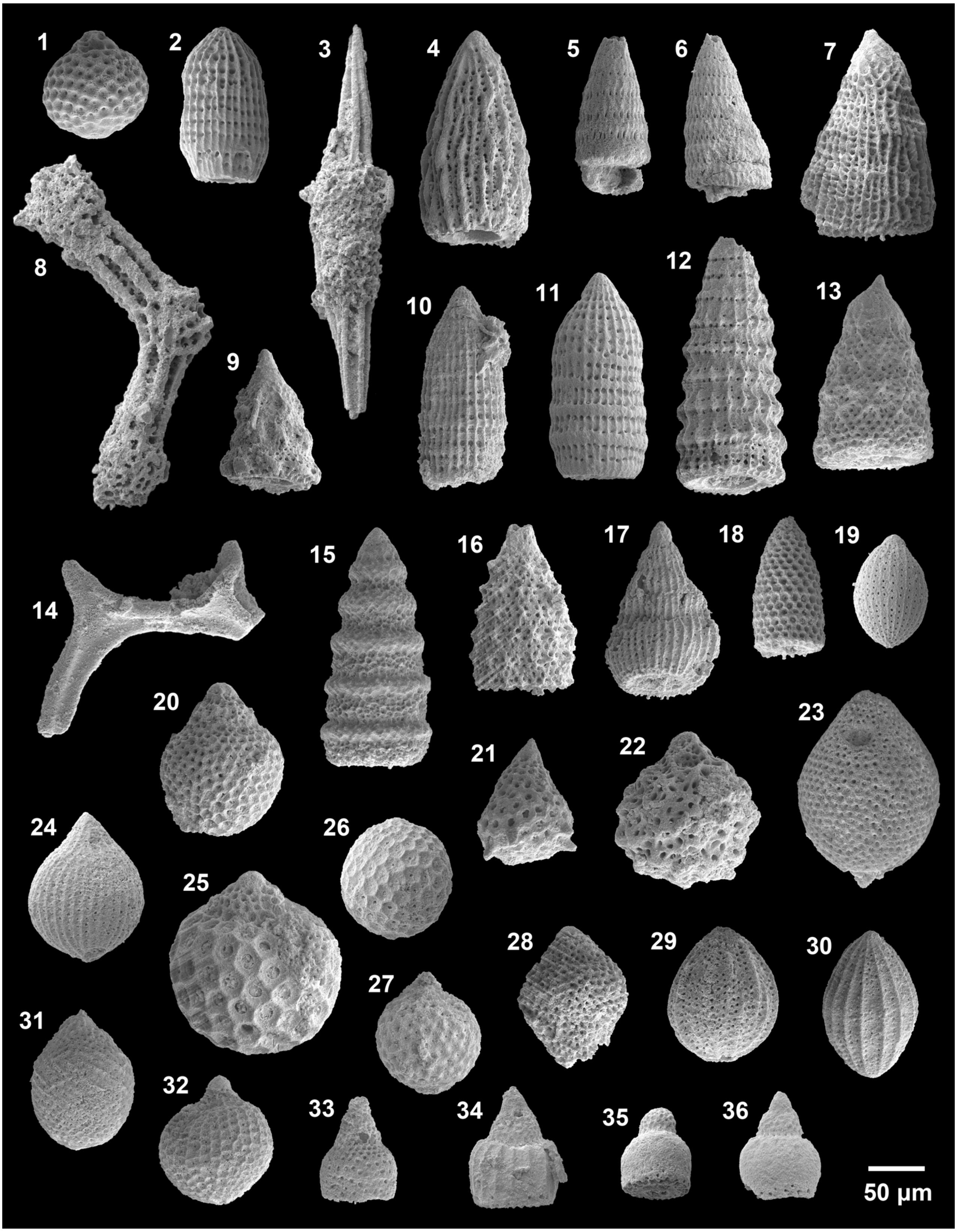
1
2
3
4
5
6
7
8
9
10
11
12
13
14
15
16
17
18
19
20
21
22
23
24
25
26
27
28
29
30
31
32
33
34
35
36
50 µm

Plate 2 Scanning electron micrographs of radiolarians from the samples D1024 (1–16) and D1052 (17–41), basal horizons of the Fludergraben section, Austria. A 50 μm scale bar applies to all photos.

1. *Archaeospongoprunum* cf. *elegans* Wu, 1993
2. *Parahsuum* sp. S sensu Matsuoka, 1986
3. *Cinguloturris carpatica* Dumitrica, 1982
4. *Dictyomitrella kamoensis* Mizutani and Kido, 1983
5. *Eucyrtidiellum nodosum* Wakita, 1988
6. *Unuma typicus* Ichikawa and Yao, 1976
7. *Gongylothorax favosus favosus* Dumitrica, 1970
8. *Protunuma lanosus* Ozvoldova, 1996
9. *Tricolocapsa tetragona* Matsuoka, 1983
10. *Williriedellum marcucciae* Cortese, 1993
11. *Striatojaponocapsa riri* O'Dogherty *et al.*, 2006
12. *Williriedellum dierschei* Suzuki and Gawlick, 2004
13. *Zhamoidellum ovum* Dumitrica, 1970
14. *Cyrtocapsa* sp. B
15. *Hsuum maxwelli* Pessagno, 1977a
16. *Williriedellum crystallinum* Dumitrica, 1970
17. *Ristola altissima* (Rüst, 1885)
18. *Pseudoeucyrtis reticularis* Matsuoka and Yao, 1985
19. *Stichomitra annibill* Kocher, 1981
20. *Williriedellum carpathicum* Dumitrica, 1970
21. *Striatojaponocapsa naradaniensis* (Matsuoka, 1984)
22. *Tritrabs exotica* (Pessagno, 1977a)
23. *Gongylothorax favosus oviformis* Suzuki and Gawlick, 2009
24. *Parahsuum* sp. S sensu Matsuoka, 1986
25. *Stichomitra annibill* Kocher, 1981
26. *Stichocapsa robusta* Matsuoka, 1984
27. *Tricolocapsa undulata* (Heitzer, 1930)
28. *Gongylothorax favosus favosus* Dumitrica, 1970
29. *Loopus doliolum* Dumitrica, 1997
30. *Williriedellum dierschei* Suzuki and Gawlick, 2004
31. *Podobursa nodosa* (Chiari *et al.*, 2002)
32. *Williriedellum sujkowskii* Widz and De Wever, 1993
33. *Striatojaponocapsa synconexa* O'Dogherty *et al.*, 2006
34. *Stichomitra* sp. A sensu Baumgartner *et al.*, 1995a
35. *Zhamoidellum ovum* Dumitrica, 1970
36. *Williriedellum crystallinum* Dumitrica, 1970
37. *Hsuum brevicostatum* (Ozvoldova, 1975)
38. *Pseudodictyomitra primitiva* Matsuoka and Yao, 1985
39. *Striatojaponocapsa conexa* (Matsuoka, 1983)
40. *Striatojaponocapsa riri* O'Dogherty *et al.*, 2006
41. *Unuma gordus* Hull, 1997

Plate 2

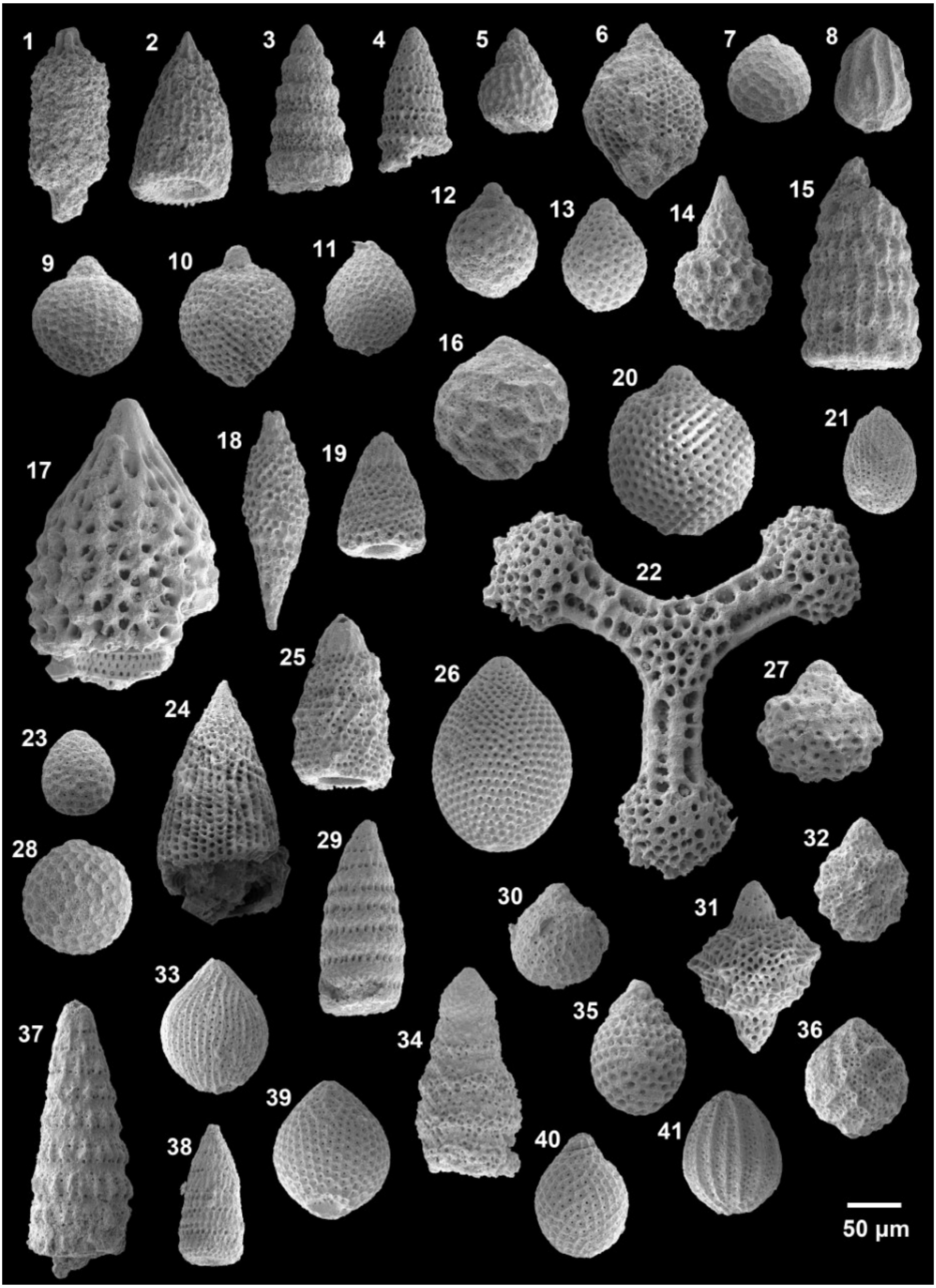
1
2
3
4
5
6
7
8
9
10
11
12
13
14
15
16
17
18
19
20
21
22
23
24
25
26
27
28
29
30
31
32
33
34
35
36
37
38
39
40
41
50 µm

Plate 3 Scanning electron micrographs of radiolarians from the samples D1052 (1–6), EW146 (7–17) and D1025 (18–45), basal horizons of the Fludergraben section, Austria. A 50 µm scale bar applies to all photos.

1. *Tetracapsa* sp. A sensu Suzuki and Gawlick, 2003b
2. *Eucyrtidiellum nodosum* Wakita, 1988
3. *Eucyrtidiellum circumperforatum* Chiari *et al.*, 2002
4. *Eucyrtidiellum ptyctum* (Riedel and Sanfilippo, 1974)
5. *Dictyomitrella kamoensis* Mizutani and Kido, 1983
6. *Cinguloturris carpatica* Dumitrica, 1982
7. *Hsuum baloghi* Grill and Kozur, 1986
8. *Archaeospongoprunum* cf. *imlayi* Pessagno, 1977a
9. *Cinguloturris carpatica* Dumitrica, 1982
10. *Cinguloturris primorika* Kemkin and Taketani, 2004
11. *Archaeodictyomitra minoensis* (Mizutani, 1981)
12. *Takemuraella hungarica* (Kozur, 1985)
13. *Parvicingula spinata* (Vinassa, 1899)
14. *Eucyrtidiellum unumaense* (Yao, 1979)
15. *Dictyomitrella* cf. *kamoensis* Mizutani and Kido, 1983
16. *Williriedellum carpathicum* Dumitrica, 1970
17. *Tricolocapsa undulata* (Heitzer, 1930)
18. *Saitoum pagei* Pessagno, 1977a
19. *Pseudodictyomitra primitiva* Matsuoka and Yao, 1985
20. *Archaeodictyomitra mirabilis* Aita, 1987
21. *Archaeospongoprunum* cf. *elegans* Wu, 1993
22. *Spongotripus* sp. D sensu Suzuki and Gawlick, 2003b
23. *Archaeodictyomitra patricki* Kocher, 1981
24. *Stichomitra annibill* Kocher, 1981
25. *Stichocapsa robusta* Matsuoka, 1984
26. *Zhamoidellum ovum* Dumitrica, 1970
27. *Protunuma fusiformis* Ichikawa and Yao, 1976
28–29. *Takemuraella hexagonata* (Heitzer, 1930)
30. *Striatojaponocapsa synconexa* O'Dogherty *et al.*, 2006
31. *Striatojaponocapsa conexa* (Matsuoka, 1983)
32. *Tetracapsa* sp. A sensu Suzuki and Gawlick, 2003b
33. *Tricolocapsa undulata* (Heitzer 1930)
34. *Stylocapsa oblongula* Kocher, 1981
35. *Gongylothorax favosus favosus* Dumitrica, 1970
36. *Gongylothorax favosus oviformis* Suzuki and Gawlick, 2009
37. *Eucyrtidiellum unumaense* (Yao, 1979)
38. *Eucyrtidiellum nodosum* Wakita, 1988
39. *Helvetocapsa matsuokai* (Sashida, 1999)
40. *Striatojaponocapsa naradaniensis* (Matsuoka, 1984)
41. *Japonocapsa tegiminis* (Yao, 1979)
42. *Gongylothorax* sp. C sensu Suzuki and Gawlick, 2003b
43. *Williriedellum* sp. C sensu Gawlick *et al.*, 2018
44. *Williriedellum marcucciae* Cortese, 1993
45. *Williriedellum dierschei* Suzuki and Gawlick, 2004
46. *Praewilliriedellum* aff. *spinosum* Kozur, 1984
47–48. *Japonocapsa fusiformis* (Yao, 1979)
49. *Droltus galerus* Suzuki, 1995b
50. *Archaeodictyomitra sixi* Yang, 1993

Plate 3

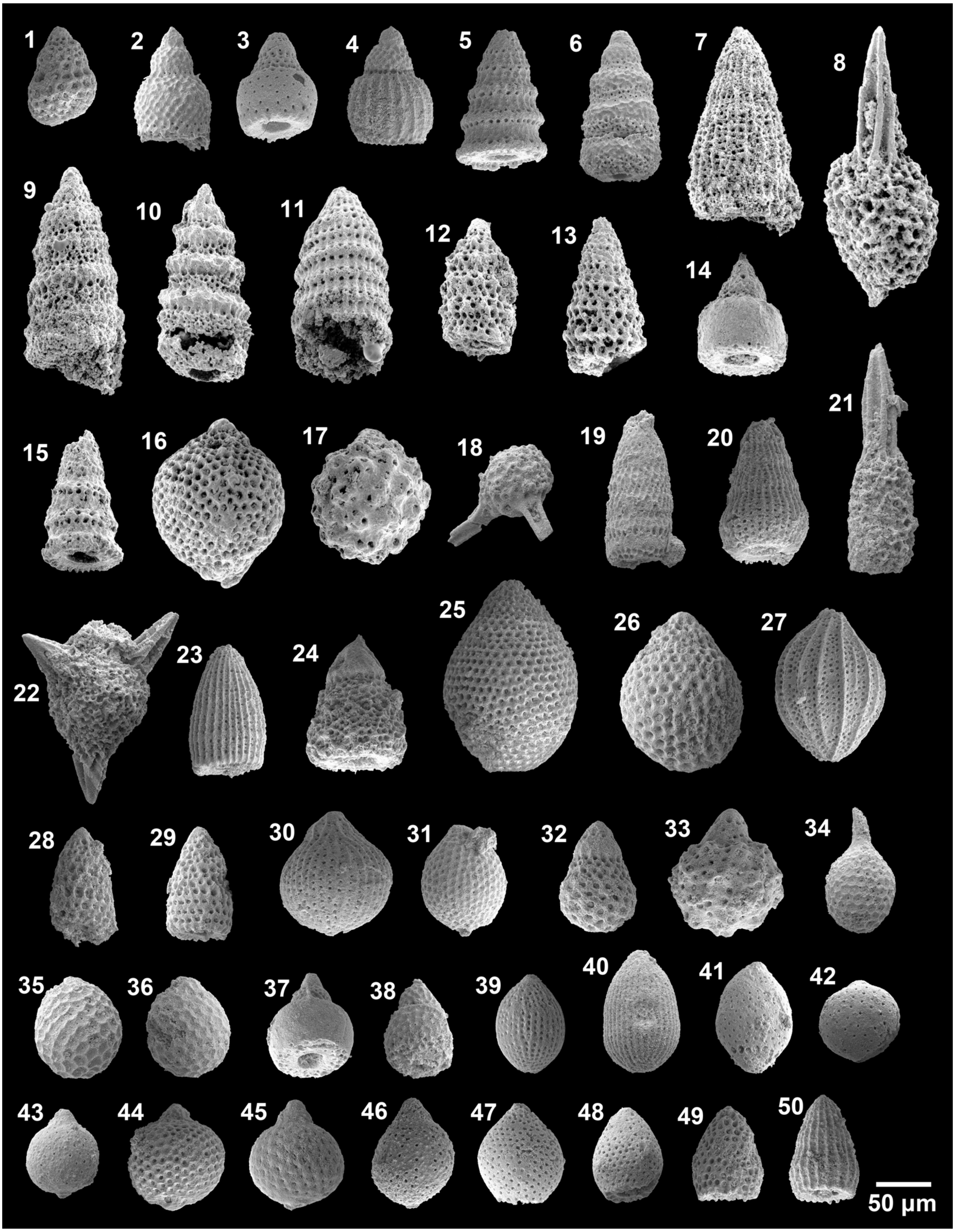
1
2
3
4
5
6
7
8
9
10
11
12
13
14
15
16
17
18
19
20
21
22
23
24
25
26
27
28
29
30
31
32
33
34
35
36
37
38
39
40
41
42
43
44
45
46
47
48
49
50
50 μm

Appendix 1

Updated inventory of radiolarian species from the sample BT1 of the middle Callovian Brielgraben section.

BT1: *Gorgansium xigazeense* Wu, 1993, *Stylosphaera* cf. *lanceola* Parona, 1890, *Archaeodictyomitra amabilis* Aita, 1987, *Archaeodictyomitra* cf. *minoensis* (Mizutani, 1981), *Archaeodictyomitra mitra* Dumitrica, 1997, *Archaeodictyomitra rigida* Pessagno, 1977a, *Cinguloturris carpatica* Dumitrica, 1982, *Dictyomitrella kamoensis* Mizutani and Kido, 1983, *Droltus galerus* Suzuki, 1995b, *Eucyrtidiellum ptyctum* (Riedel and Sanfilippo, 1974), *Eucyrtidiellum semifactum* Nagai and Mizutani, 1990, *Eucyrtidiellum takemurai* Hull, 1997, *Eucyrtidiellum unumaense dentatum* Baumgartner, 1995 in Baumgartner *et al.* (1995a), *Eucyrtidiellum unumaense unumaense* (Yao, 1979), *Gongylothorax favosus* Dumitrica, 1970, *Gongylothorax* sp. C sensu Suzuki and Gawlick (2003b), *Guexella nudata* (Kocher, 1980) in Baumgartner *et al.* (1980), *Helvetocapsa matsuokai* (Sashida, 1999), *Hiscocapsa magnipora* (Chiari *et al.*, 2002), *Hiscocapsa* cf. *acuta* Hull, 1997, *Hsuum brevicostatum* (Ozvoldova, 1975), *Hsuum maxwelli* Pessagno, 1977a, *Japonocapsa* aff. *fusiformis* (Yao, 1979), *Loopus doliolum* Dumitrica, 1997, *Parvifavus* sp. A, *Praezhamoidellum buekkense* Kozur, 1984, *Praezhamoidellum* cf. *parvipora* (Tan, 1927), *Protunuma lanosus* Ozvoldova, 1996, *Quarticella ovalis* Takemura, 1986, *Ristola procera* (Pessagno, 1977a), *Saitoum levium* De Wever, 1981, *Spongocapsula krahsteinensis* Suzuki and Gawlick, 2004, *Stichocapsa convexa* Yao, 1979, *Stichocapsa robusta* Matsuoka, 1984, *Striatojaponocapsa conexa* (Matsuoka, 1983), *Striatojaponocapsa naradaniensis* (Matsuoka, 1984), *Stylocapsa oblongula* Kocher, 1981, *Syringocapsa levis* (Hori, 1999), *Tetracapsa himedaruma* (Aita, 1987), *Tetracapsa* sp. A sensu Suzuki and Gawlick (2003b), *Theocapsomma* cf. *costata* Chiari *et al.*, 2002, *Theocapsomma cucurbiformis* Baumgartner, 1995 in Baumgartner *et al.* (1995a), *Tricolocapsa tetragona* Matsuoka, 1983, *Tricolocapsa undulata* (Heitzer, 1930), *Tricolocapsa* sp. C sensu Auer *et al.* (2007), *Tricolocapsa* sp. M sensu Baumgartner *et al.* (1995a), *Takemuraella hexagonata* (Heitzer, 1930), *Takemuraella hungarica* (Kozur, 1985), *Unuma gordus* Hull, 1997, *Williriedellum crystallinum* Dumitrica, 1970, *Williriedellum dierschei* Suzuki and Gawlick, 2004, *Williriedellum marcucciae* Cortese, 1993, *Zhamoidellum ovum* Dumitrica, 1970.

Appendix 2

The inventory of radiolarian species from the samples MR149 and MR175 of the lower part of the Knallalm-Neualm section, described by Auer *et al.* (2007). The lower part of the Knallalm-Neualm section is the stratum typicum of the *Williriedellum carpathicum* Subzone in the *Zhamoidellum ovum* Zone.

MR149: *Acanthocircus* cf. *suboblongus* (Yao, 1972), *Alievium* sp., *Archaeodictyomitra amabilis* Aita, 1987, *Archaeodictyomitra apiarium* (Rüst, 1885), *Archaeodictyomitra* cf. *minoensis* (Mizutani, 1981), *Archaeodictyomitra mitra* Dumitrica, 1997, *Archaeodictyomitra rigida* Pessagno, 1977a, *Archaeospongoprunum* sp. (this specimen is reidentified here as *Archaeospongoprunum* cf. *elegans* Wu, 1993), *Cinguloturris carpatica* Dumitrica, 1982, *Dictyomitrella kamoensis* Mizutani and Kido, 1983, *Emiluvia* cf. *bisellea* Danelian, 1995, *Eucyrtidiellum* cf. *circumperforatum* Chiari *et al.*, 2002, *Eucyrtidiellum nodosum* Wakita, 1988, *Eucyrtidiellum ptyctum* (Riedel and Sanfilippo, 1974), *Eucyrtidiellum unumaense pustulatum* Baumgartner, 1984, *Eucyrtidiellum unumaense* ssp. (Yao, 1979), *Gongylothorax favosus favosus* Dumitrica, 1970, *Gongylothorax favosus oviformis* Suzuki and Gawlick, 2009, *Gorgansium* sp., *Homoeoparonaella* sp., *Hsuum brevicostatum* (Ozvoldova, 1975), *Hsuum hisuikyoense* Isozaki and Matsuda, 1985, *Hsuum maxwelli* Pessagno, 1977a, *Lithocampium* sp. C sensu Auer *et al.* (2007), *Loopus doliolum* Dumitrica, 1997, *Neorelumbra skenderbegi* Chiari *et al.*, 2002, *Napora* sp., *Paronaella* sp., *Parvicingula cappa* Cortese, 1993, *Parvifavus* sp., *Podobursa triacantha* (Fischli, 1916), *Praewilliriedellum spinosum*

Kozur, 1984, *Praezhamoidellum* cf. *parvipora* (Tan, 1927), *Protunuma lanosus* Ozvoldova, 1996, *Pseudodictyomitra primitiva* Matsuoka and Yao, 1985, *Stylosphaera lanceola* Parona, 1890, *Spongocapsula krahsteinensis* Suzuki and Gawlick, 2004, *Stichocapsa convexa* Yao, 1979, *Stichocapsa robusta* Matsuoka, 1984, *Stichomitra* sp., *Striatojaponocapsa conexa* (Matsuoka, 1983), *Striatojaponocapsa synconexa* O'Dogherty *et al.*, 2006, *Stylocapsa oblongula* Kocher, 1981, *Syringocapsa lata* Yang, 1993, *Syringocapsa suavis* Yang, 1993, *Tetracapsa* sp. A sensu Suzuki and Gawlick (2003b), *Tetraditryma* sp., *Theocapsomma bicornis* Baumgartner, 1995 in Baumgartner *et al.* (1995a) *Theocapsomma cordis* Kocher, 1981, *Theocapsomma costata* Chiari *et al.*, 2002, *Tricolocapsa leiostraca* (Foreman, 1973), *Tricolocapsa undulata* (Heitzer, 1930), *Tricolocapsium* sp. A sensu Auer *et al.* (2007), *Tricolocapsium* sp. B sensu Auer *et al.* (2007), *Tritrabs* cf. *casmaliaensis* (Pessagno, 1977a), *Tritrabs rhododactylus* Baumgartner, 1980, *Takemuraella hexagonata* (Heitzer, 1930), *Takemuraella hungarica* (Kozur, 1985), *Unuma gordus* Hull, 1997, *Williriedellum carpathicum* Dumitrica, 1970, *Williriedellum dierschei* Suzuki and Gawlick, 2004, *Williriedellum marcucciae* Cortese, 1993, *Xitus magnus* Baumgartner, 1995 in Baumgartner *et al.* (1995a), *Zhamoidellum ovum* Dumitrica, 1970.

MR175: *Amphipyndax* cf. *tsunoensis* Aita, 1987, *Archaeodictyomitra* cf. *apiarium* (Rüst, 1885), *Archaeodictyomitra minoensis* (Mizutani, 1981), *Archaeodictyomitra mitra* Dumitrica, 1997, *Archaeodictyomitra rigida* Pessagno, 1977a, *Archaeodictyomitra sixi* Yang, 1993, *Cinguloturris carpatica* Dumitrica, 1982, *Crucella* sp., *Droltus galerus* Suzuki, 1995b, *Eucyrtidiellum nodosum* Wakita, 1988, *Eucyrtidiellum ptyctum* (Riedel and Sanfilippo, 1974), *Eucyrtidiellum semifactum* Nagai and Mizutani, 1990, *Eucyrtidiellum unumaense dentatum* Baumgartner, 1995 in Baumgartner *et al.* (1995a), *Eucyrtidiellum unumaense pustulatum* Baumgartner, 1984, *Eucyrtidiellum unumaense unumaense* (Yao, 1979), *Gongylothorax favosus oviformis* Suzuki and Gawlick, 2009, *Gongylothorax* aff. *siphonofer* Dumitrica, 1970, *Gorgansium* cf. *morganense* Pessagno and Blome, 1980, *Helvetocapsa matsuokai* (Sashida, 1999), *Hiscocapsa* cf. *hexagona* (Hori, 1999), *Homoeoparonaella* cf. *elegans* (Pessagno, 1977a), *Hsuum brevicostatum* (Ozvoldova, 1975), *Hsuum* cf. *exiguum* Yeh and Cheng, 1996, *Hsuum maxwelli* Pessagno, 1977a, *Lithocampium matsuokai* (Hull, 1997), *Loopus doliolum* Dumitrica, 1997, *Neorelumbra skenderbegi* Chiari *et al.*, 2002, *Parahsuum levicostatum* Takemura, 1986, *Parahsuum* aff. *simplum* Yao, 1982, *Parahsuum* sp. S sensu Matsuoka (1986), *Parvicingula cappa* Cortese, 1993, *Parvicingula spinata* (Vinassa, 1899), *Parvicingula dhimenaensis* Baumgartner, 1984, *Parvifavus wallacheri* (Grill and Kozur, 1986), *Parvifavus* sp. A sensu Auer *et al.* (2007), *Praewilliriedellum spinosum* Kozur, 1984, *Protunuma lanosus* Ozvoldova, 1996, *Protunuma ochiensis* Matsuoka, 1983, *Pseudodictyomitra venusta* (Chiari *et al.*, 1997) [= *Pseudodictyomitra* sp. D sensu Matsuoka and Yao (1985)], *Pseudoeucyrtis* sp. J sensu Baumgartner *et al.* (1995a), *Pseudodictyomitrella spinosa* Grill and Kozur, 1986, *Quarticella levis* Takemura, 1986, *Quarticella ovalis* Takemura, 1986, *Saitoum* cf. *pagei* Pessagno, 1977a, *Stylosphaera lanceola* Parona, 1890, *Spongotripus* sp. E, *Stichocapsa* aff. *biconica* Matsuoka, 1991, *Stichomitra* cf. *annibill* Kocher, 1981, *Stichomitra takanoensis* Aita, 1987, *Stylocapsa tecta* Matsuoka, 1983, *Striatojaponocapsa* cf. *conexa* (Matsuoka, 1983), *Striatojaponocapsa naradaniensis* (Matsuoka, 1984), *Striatojaponocapsa riri* O'Dogherty *et al.*, 2006 [= *Tricolocapsa* sp. A sensu Goričan (1994)], *Takemuraella hexagonata* (Heitzer, 1930), *Takemuraella hungarica* (Kozur, 1985), *Tetracapsa* sp. A sensu Suzuki and Gawlick (2003b), *Tetracapsa* sp. C sensu Auer *et al.* (2007), *Theocapsomma cordis* Kocher, 1981, *Theocapsomma* cf. *cucurbiformis* Baumgartner, 1995, *Tricolocapsa leiostraca* (Foreman, 1973), *Tricolocapsa undulata* (Heitzer, 1930), *Williriedellum* sp. C [= *Tricolocapsa* sp. A sensu Ozvoldova (1992)], *Tricolocapsa* sp. C sensu Auer *et al.* (2007), *Tritrabs* cf. *casmaliaensis* (Pessagno, 1977a), *Tritrabs simplex* Kito and De Wever, 1992, *Unuma gordus* Hull, 1997, *Williriedellum carpathicum* Dumitrica, 1970, *Williriedellum dierschei* Suzuki and Gawlick, 2004, *Williriedellum marcucciae* Cortese, 1993, *Xitus magnus* Baumgartner, 1995 in Baumgartner *et al.* (1995a), *Zhamoidellum kozuri* (Hull, 1997), *Zhamoidellum ovum* Dumitrica, 1970, *Zhamoidellum ventricosum* Dumitrica, 1970.

アンモナイト層準直上のジュラ系上部統基底フルダーグラーベン部層から産した放散虫化石（北部石灰アルプス，オーストリア）

鈴木　寿志・ハンス - ユルゲン　ガウリック

要　旨

北部石灰アルプスのフルダーグラーベン（オーストリア）において，アンモナイトで年代決定されたクラウス層石灰岩（ジュラ系中部統最上部）の直上に累重する放散虫岩から放散虫群集を記載した．この放散虫群集はジュラ系上部統最下部（Oxfordian）からのものであり，放散虫生層序を考える上で重要である．ジュラ系中部統から得られる長期間生存種が多い中で，上部統最下部から初めて出現する指標種 4 種（*Kilinora spiralis*，*Fultacapsa sphaerica*，*Protunuma japonicus*，*Pseudoeucyrtis reticularis*）を識別した．得られた放散虫種の生存期間について再検討し，ジュラ系中部統から産する種が引き続き上部統からも産する例を明らかにした．その結果，北部石灰アルプスのジュラ紀放散虫化石帯において，これまで *Zhamoidellum ovum* 帯中に含められていた *Williriedellum dierschei* 亜帯を，新たな指標種に基づき独立した帯として再定義した．古生物学的記載の章では 37 属 67 種 2 亜種を記載し，2 属（*Loopus* 属，*Pseudodictyomitra* 属）1 種（*Protunuma japonicus*）の標徴を改定するとともに，*Loopus* 属の模式種を再指定した．

Bulletin of the Geological Survey of Japan, vol. 71 (4), p. 281–296, 2020

Article

Middle Jurassic radiolarians from the ammonite bearing Toyora Group, Yamaguchi Prefecture, Southwest Japan

NISHIZONO Yukihisa[1,*] and YONEMITSU Isao[2]

NISHIZONO Yukihisa and YONEMITSU Isao (2020) Middle Jurassic radiolarians from the ammonite bearing Toyora Group, Yamaguchi Prefecture, Southwest Japan. *Bulletin of the Geological Survey of Japan*, vol. 71(4), p. 281–296, 6 figs.

Abstract: The Toyora Group is one of the typical Lower to Middle Jurassic strata in Japan that is distributed throughout Yamaguchi Prefecture, Southwest Japan. It yields abundant ammonoids. Although, microfossils, such as radiolarians, have not been previously reported from the group, radiolarian fossils are first discovered at seven localities from the uppermost Toyora Group. Those correspond to the *Transhsuum hisuikyoense* and *Striatojaponocapsa plicarum* zones and are determined to be from Aalenian to Bathonian in age. These radiolarian age determinations are a little older than those determined using ammonoids and inoceramids. According to previous studies, the assignment age of the first appearance of *Stj. plicarum* is only estimated to be near the Aalenian–Bajocian boundary. To discuss this issue, further study is required to correct the fossil data such as the Aalenian ammonoids that occur in the intervals of ammonoid and radiolarian localities.

Keywords: radiolaria, ammonoid, Jurassic, Toyora Group, Utano Formation, Yamaguchi Prefecture, Southwest Japan

1. Introduction

In Japan, most Jurassic strata are within accretionary complexes resulting from Mesozoic oceanic plate subduction. These strata are composed of various mixed rocks, such as oceanic plate-fragments, pelagic sediments and trench-filled clastic materials derived from the continent. The so-called shallow marine sediments are deposited on a continental shelf or in forearc basins composed of the accretionary strata. These shallow marine sediments overlie the accretionary strata on faulted or unconformable contacts. Before the rapid progress of research on the Jurassic accretionary complexes during the 1980s, these were a focus of stratigraphic research because of their abundant megafossils resulting from their comparatively limited mixing and weak deformation.

The geology of Southwest Japan is divided into the Inner (north) and Outer (south) zones by a major fault, the Median Tectonic Line, which formed in the Cretaceous. The Jurassic accretionary complexes are widely distributed in both zones.

The Lower to Middle Jurassic Toyora Group is one of the typical strata distributed in Yamaguchi Prefecture in the Inner Zone of Southwest Japan (Fig. 1). The Toyora Group comprises stratified clastic rocks, namely, sandstones and mudstones, with a small amount of conglomerates. They are deposited under shallow marine to brackish water conditions based on their sedimentary facies features and fossil associations, including characteristic black shale that indicates anoxic sedimentary conditions.

Various fossils, mainly ammonoids, bivalves, gastropods and plants, have been reported from the Toyora Group. As this area is a type locality of the Early to Middle Jurassic ammonoid biostratigraphy in Japan, these ammonoids have been studied in detail since the early twentieth century. However, research on fossil radiolarians from the Paleozoic and Mesozoic in Japan started during the late 1970s when samples of radiolarians were collected and analyzed from the accretionary complexes. Sedimentary rocks in Mesozoic accretionary complexes of Japan that yield megafossils are very rare. This study aims to find radiolarians in the shallow marine sediments, such as the Toyora Group, for correlation with geologic ages assigned from ammonoids. Radiolarians from the Torinosu Group and its equivalent beds in the Outer Zone of Southwest Japan were the focus of previous studies on Mesozoic

[1] Civil Engineering Headquarter, West Japan Engineering Consultants Inc., 1-1-1 Watanabe-dori, Chuo-ku, Fukuoka 810-0004, Japan.
[2] BOA Co. Ltd., 1-51 Fukuroshimameguri, Uguisuzawa, Kurihara, Miyagi 989-5401, Japan
[*] Corresponding author: NISHIZONO Y., Email: y-nishizono@wjec.co.jp

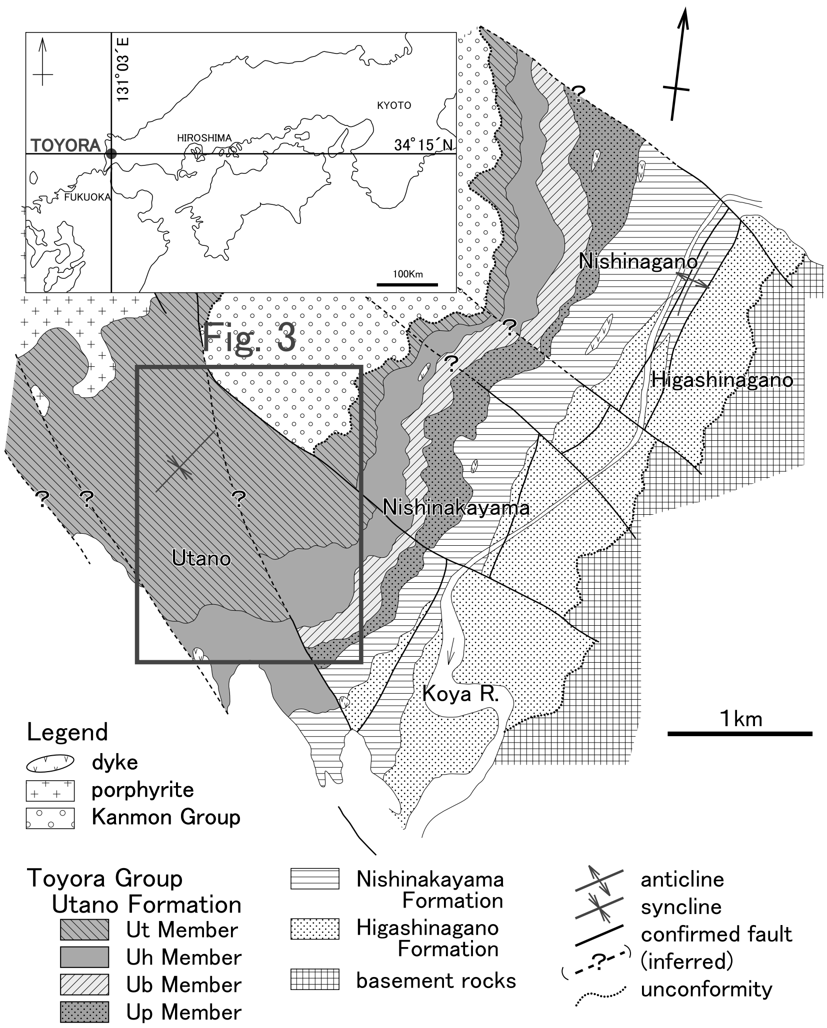

Fig. 1 Geological map of the Toyora Group around the Utano area, Yamaguchi Prefecture (modified from Hirano, 1971)

radiolarians (Matsumoto and Nishizono, 1985, Kozai *et al.*, 2006). Recently, Jurassic radiolarians were reported from shallow marine sediments of the Tetori Group on the Japan Sea side. On the basis of ammonoid biostratigraphy, radiolarians from this group are assigned to the Middle and Upper Jurassic (Callovian to Tithonian) (Hirasawa *et al.*, 2010). Sano and Kashiwagi (2015) explained that the high component ratio of Spumellaria (73–92 %) shows the Boreal element. This study, for the first time, describes radiolarians from the Toyora Group and the assignment of their geologic age and successfully correlates the geologic ages of the radiolarian biostratigraphy of the Middle Jurassic in Japan with the ammonoid one.

2. Geologic overview of the Toyora Group

Geological studies of the Toyora Group started with Yokoyama (1902) and Kobayashi (1926). Yokoyama (1902) described Jurassic ammonoids, while Kobayashi (1926) described inoceramids with lithostratigraphic notes. Toriyama (1938) showed the basic lithostratigraphic framework of the group. In the current study, the geologic overview is described on the basis of the studies by Hirano (1971, 1973a, b) who established the lithostratigraphy and ammonoid biostratigraphy of the northern distribution area of the Toyora Group. Based on his research, distribution area of the Toyora Group is divided into the northern and southern areas by the Kikugawa Fault. The effect of a granitic rock intrusion is comparatively very weak in the northern area of this group. Nakada and Matsuoka (2009, 2011) established a detailed ammonoid biostratigraphy of the Nishinakayama Formation of the group and discussed the exact stratigraphic location of the Pliensbachian–Toarcian boundary in this formation.

2. 1 Lithostratigraphy

The Toyora Group, comprising the Higashinagano, Nishinakayama, and Utano formations in ascending order, has a total thickness of 1800 m (Fig. 2). The Higashinagano Formation is 400 m in thickness and unconformably overlies the Sangun metamorphic rocks. It is composed of basal conglomerate, coarse sandstone, fine sandstone,

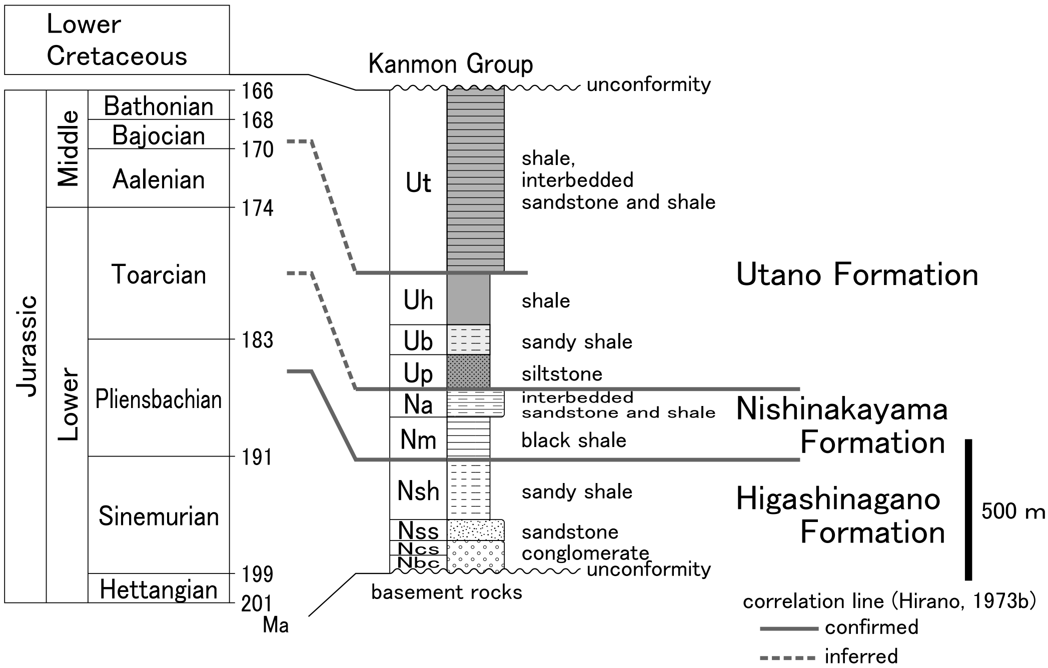

Fig. 2 Modified lithological succession and geologic age of the Toyora Group in the type locality after Hirano (1971, 1973a, b). Numerical ages are referred to the international chronostratigraphic chert ver. 2020/01 (Cohen *et al.*, 2013: updated in 2020). Abbreviations Nbc, Ncs, Nss and Nsh stand for the lower, middle, upper and uppermost members of the Higashinagano Formation; Nm and Na for the lower and upper members of the Nishinakayama Formation; Up, Ub, Uh and Ut for the lower, middle, upper and uppermost members of the Utano Formation.

and sandy shale in ascending order. This formation has been determined as a transgressive deposit because of its fining-upward sedimentary sequence. The Higashinagano Formation is subdivided into four members: the lower, middle, upper, and uppermost (abbreviated as the Nbc, Ncs, Nss and Nsh in Hirano, 1971, respectively) in ascending order. The Nishinakayama Formation is 250 m in thickness and is mainly composed of black shale, interbedding sandstone at its upper part. The black shale is recognized as the facies deposited under stagnant anoxic conditions because of the presence of sedimentary pyrite (Shikama and Hirano, 1970). This facies indicative of the shelf deposits records the early Toarcian oceanic anoxic event (Izumi *et al.*, 2012). The Nishinakayama Formation is divided into two members: the lower and upper (the Nm and Na, respectively) in ascending order. The Utano Formation is 1100 m in thickness and comprises silty shale, sandy shale, and interbedded sandstone and shale. In addition, the uppermost part of this formation has not been delimited because of a covering of the Lower Cretaceous Kanmon Group. The Utano Formation is recognized as a regressive sequence from its coarsening-upward sedimentation and is divided into four members: the lower, middle, upper, and uppermost (the Up, Ub, Uh, and Ut, respectivery) in ascending order. At the Utano Dam locality, the maximum thickness of the uppermost member (Ut) is 650 m.

2. 2 Biostratigraphy and geologic age based on megafossils

In studying the radiolarian assignment ages, it is effective to establish the biostratigraphy and geological age of each formation or member by the described megafossils, mainly ammonite (Fig. 2, Hirano, 1971, 1973a, b). Ammonoids are rarely found in the Higashinagano Formation but are abundant in the Nishinakayama Formation. The uppermost member of the Utano Formation (Ut) frequently yields ammonoids. Ammonoids have not been recognized in the lower member (Nbc) of the Higashinagano Formation. Abundant fossils, such as ammonoids, bivalves, gastropods, brachiopods, and corals, occur in the middle member (Ncs) of the Higashinagano Formation. The geologic age of Ncs is correlated with the early Sinemurian based on the occurrence of *Arietites* sp. That of the upper member (Nss), depending on its location, is correlated with the late Sinemurian to the Pliensbachian based on the age of Ncs in the northern area and the occurrences of the Pliensbachian ammonoid (*Amaltheus* cf. *stokes* (Sowerby) and *Arieticeras* aff. *apertum* Monestier) in the southern area. Based on the ages of Nss and the base of the Nishinakayama Formation above this member, the geological age of the uppermost member (Nsh) also depends on its location and is correlated with the latest Sinemurian to upper Pliensbachian.

Ammonoid fauna from the Nishinakayama Formation have been grouped into three zones: the *Fontanelliceras* *fontanellense*, *Protogrammoceras nipponicum*, and *Dactylioceras helianthoides*, in ascending order, and the lower (Nm) and upper (Na) members of the Nishinakayama Formation are assigned to the upper Pliensbachian to lower Toarcian and lower Toarcian, respectively (Hirano, 1973a, b). Furthermore, Nakada and Matsuoka (2011) established four ammonoid zones in Nm and correlated these with European zonations: the *Canavaria japonica*, *Paltarpites paltus*, *Dactylioceras helianthoides*, and *Harpoceras inouyei* zones in ascending order.

In the Utano Formation, the lower (Up) and middle (Ub) members are correlated with the upper Toarcian given the occurrences of *Grammoceras* and *Phymatoceras* in abundance in the Up and *Phymatoceras* sp. in the Ub. In this formation, the upper member (Uh) yields ammonoids such as *Planammatoceras* cf. *kitakamiensis* Buckman, *Dumortieria*? sp. and *Calliphylloceras* sp. These are assigned to the uppermost Toarcian to partially lower Bajocian. The uppermost member (Ut) is correlated with the Bathonian because of the occurrence of *Harpophylloceras* sp. and *Inoceramus utanoensis* (Hirano, 1973b). Based on the assigned age of the megafossils, the border between the Uh and Ut is in the lower Bajocian to Bathonian with a concordant stratigraphic contact.

2. 3 Pliensbachian–Toarcian boundary

Tanabe (1991) demonstrated that bituminous mudstones result from the deposition of marine sediments during anoxic events, which have occurred worldwide, based on the geochemical and sedimentological data and the extremely rare occurrence of benthic fossils. Nakada and Matsuoka (2011) determined that the Pliensbachian—Toarcian boundary is at the base of the *Paltarpites paltus* Zone based on the four established ammonoid zones and the lower member of the Nishinakayama Formation (Nm), which are correlated in detail with European zones.

3. Lithostratigraphy of the sampling section study route

Radiolarians were found from seven samples collected from the Utano B, C2, and D1 routes belonging to the Uh and Ut that crop out in the Utano Valley (along the current Utano Dam), where the thickest sequence of the Utano Formation is throughout distributed (Hirano, 1971). Hirano (1973a, b) has described ammonoids from the Utano A and D2 routes of this study (Fig. 3).

Utano A route

Along the Utano A route, the 400-m-thick Ut of the Utano Formation is exposed and mainly comprises interbedded sandstone and shale (Fig. 4). Sandy shale varying from 20 to 30 m in thickness occurs at three stratigraphic horizons. *Holcophylloceras* sp. described by Hirano (1973b: locality 59) occurs in the shale above the thick sandstone bed in the upper part of this route.

Utano B route

The lower part of the Utano B route (Fig. 4) is composed of the 150-m-thick massive sandy shale of the Uh of the Utano Formation. The upper part of this route consists of the interbedded sandstone and shale of the Ut of the Utano Formation with sandy shale; these are repeated every tens of meters. Their total thickness is 400 m. Tuffaceous shales are infrequently intercalated within the upper part of the strata. Radiolarian samples UT-4, UT-5, and UT-6 were collected from three horizons in the upper half of the Ut.

Utano C1 and C2 routes

The thickness and sedimentary facies of the Uh and Ut of the Utano Formation along the Utano C1 and C2 (C2n and C2s) routes are similar to those of the Utano B route (Fig. 4). The Ut is overlain unconformably by the Cretaceous Kanmon Group at the stratigraphic top of the Utano C2s route. A radiolarian sample UT-7 was collected at the horizon 70 m beneath this unconformity.

Utano D1 and D2 routes

The lower part of the Utano D1 and D2 routes comprises the 250-m-thick sandy shale of the Uh of the Utano Formation. The upper 200 m part consists of the interbedded sandstone, shale, and sandy shale of the Ut (Fig. 4). These lithologies are repeated every tens of meters. In the Utano D1 route, a radiolarian sample UT-1 was collected from the Uh, and samples UT-2 and UT-3 were collected from the middle part of the Ut. Hirano (1973a) reported ammonoids (*Dumortieria*? sp.) from shale in the lower part of the Uh in the Utano D2 route.

4. Radiolarian assemblages and age assignment

Seven radiolarian samples were collected from the studied route. Radiolarians from four samples (UT-1, UT-2, UT-5 and UT-7) were identified, whereas those from the other three samples could not be identified because of poor preservation. Age assignments of these identified radiolarians are mainly discussed on the basis of the radiolarian zonations of Nishizono *et al.* (1997) and Matsuoka (1995).

4. 1 Radiolarian assemblages

The locality and radiolarian assemblage of each sample are shown as follows.

Sample UT-1

Locality: Utano D1 route (sandy shale of the Uh).

Assemblage: Despite abundant Nassellaria and the poor preservation of the test surfaces in this sample, only *Praeparvicingula*? sp. A can be identified (Fig. 5m).

Sample UT-2

Locality: Utano D1 route (sandy shale of the Ut).

Assemblage: Abundant Spumellaria and Nassellaria are included in the sample; however, these are poorly preserved on the test surface. The following radiolarians were identified (Fig. 5b, e, j): *Canutus* sp., *Parahsuum* sp., and *Transhsuum* aff. *hisuikyoense*.

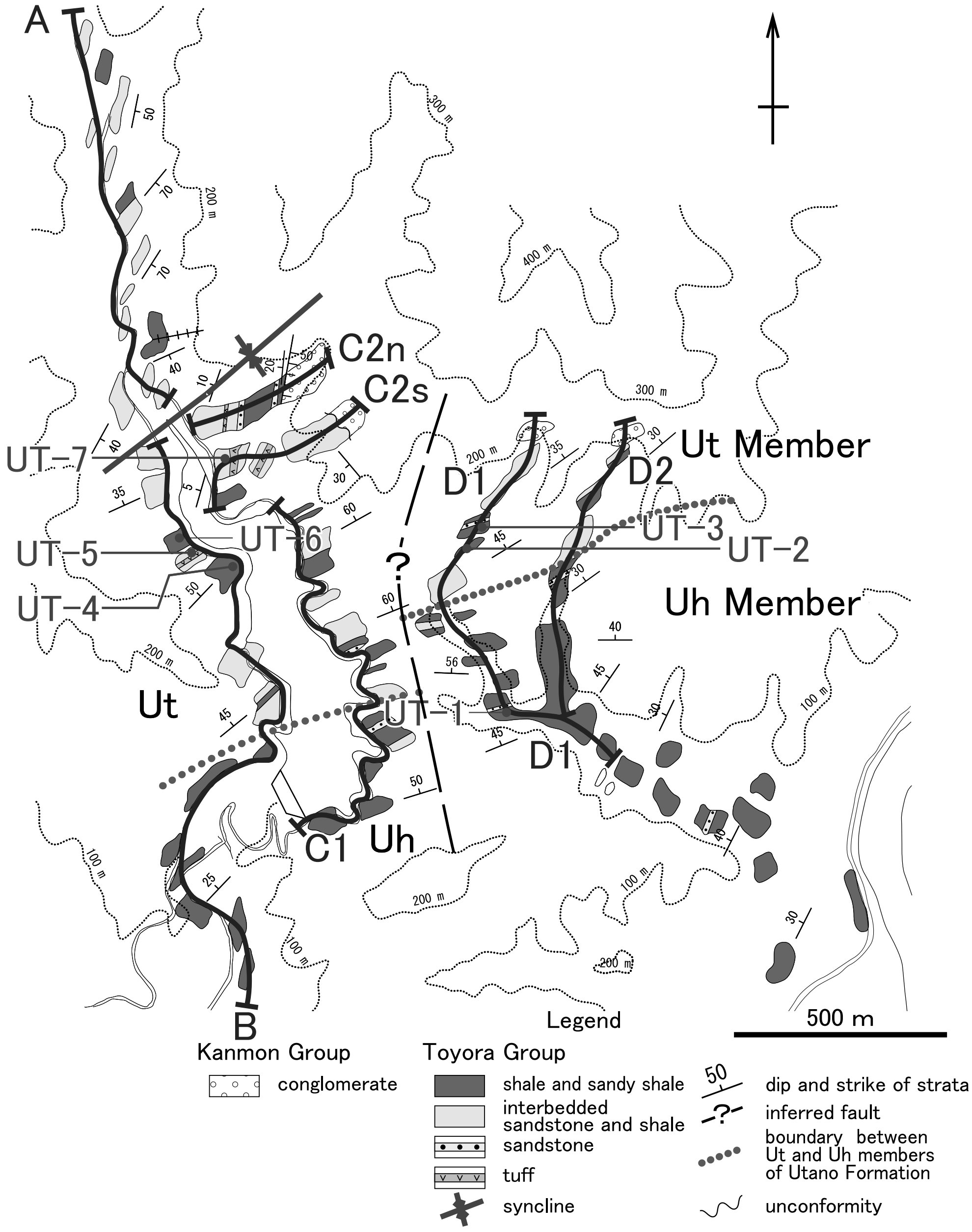

Fig. 3 Locality map for radiolarians and surveyed routes of Utano A, B, C1, C2, D1 and D2. UT-1 to Ut-7 are the locations of radiolarian occurrence.

Sample UT-3
Locality: Utano D1 route (sandy shale of the Ut located immediately above UT-2).
Assemblage: Despite the presence of abundant Nassellaria, no radiolarian species is identified because of their poor preservation on the test surfaces.

Sample UT-4
Locality: Utano B route (sandy shale of the Ut).
Assemblage: Despite abundant Nassellaria in the sample, no radiolarian species is identified due to their poor preservation on the test surfaces.

Sample UT-5
Locality: Utano B route (shale of the Ut).
Assemblage: Despite poor preservation, the following radiolarian species are identified (Fig. 5a, d, f, i, l, n–o, s, x–y): *Archicapsa pachyderma*, *Spongocapsula* sp. A, *Parahsuum* ? *hiconocosta*, *Transhsuum* aff. *brevicostatum*, *Praeparvicingula aculeata*, *Wrangellium* aff. *burnsensis*, *Droltus hecatensis*, *Unuma typicus*, *Stichocapsa convexa* and *Stichocapsa magnipora*.

Sample UT-6
Locality: Utano B route (sandy shale of the Ut)

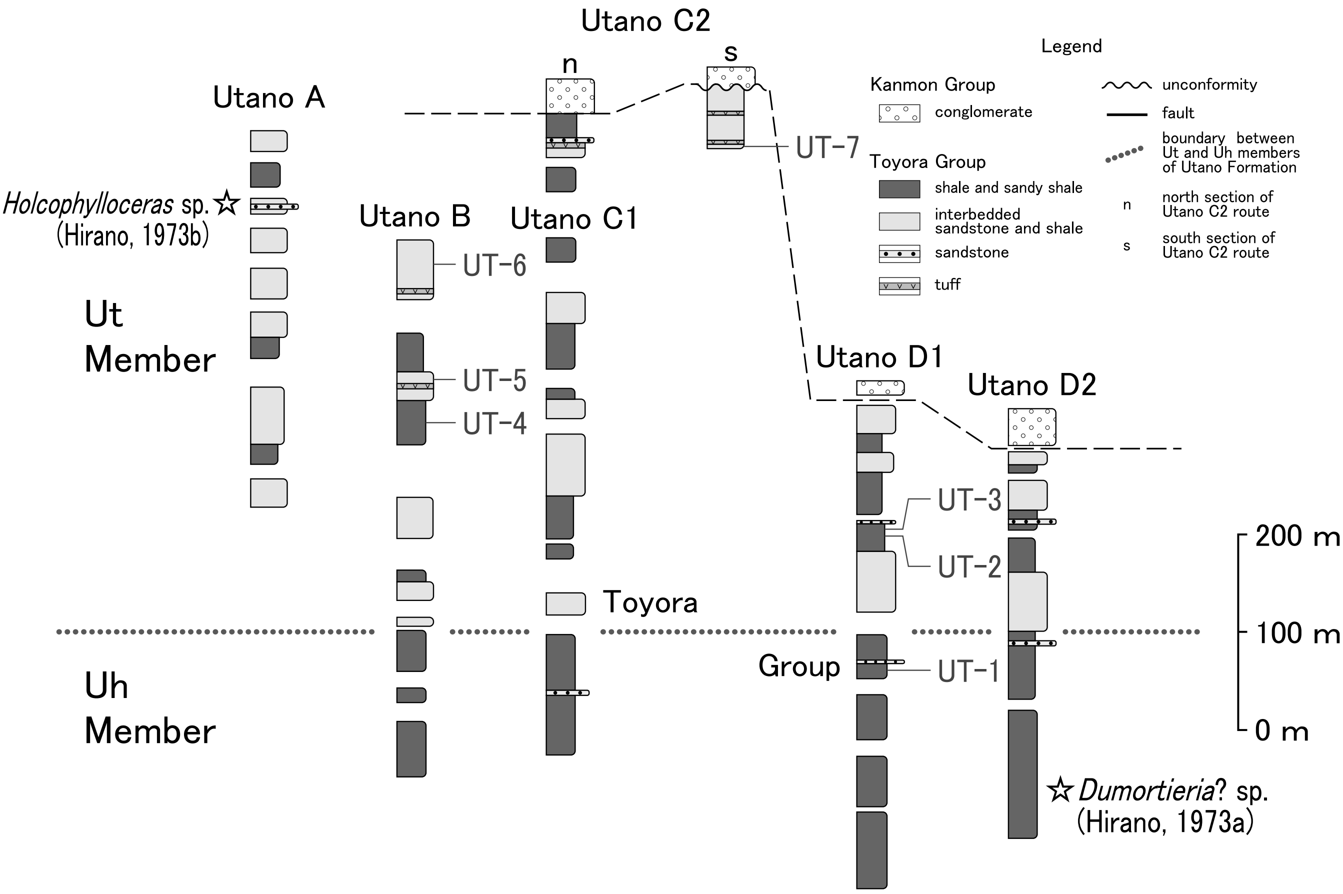

Fig. 4 Columnar sections of Utano A, B, C1, C2, D1 and D2 routes.

Assemblage: Despite the inclusion of radiolarians, no specimens is identified due to their poor preservation on the test surfaces.

Sample UT-7
Locality: Utano C2 route (nodule in the sandy shale of the Ut)
Assemblage: Well-preserved Nassellaria are included (Figs. 5c, g–h, k, p–r, t–w, z). The following radiolarians are identified: *Archicapsa pachyderma*, *Spongocapsula* aff. *krahsteinensis*, *Transhsuum maxwelli*, *Archaeodictyomitra* sp. H in Nishizono 1996, *Triversus hungaricus*, *Unuma latusicostatus*, *Unuma typicus*, *Podobursa nodosa*, *Striatojaponocapsa plicarum*, *Tricolocapsa undulata*, and *Eucyrtidiellum unumaense*.

4. 2 Correlation with radiolarian zonation and age assignment

According to Nishizono *et al.* (1997), the co-occurrence of *Archicapsa pachyderma*, *Stichocapsa convexa*, and *Striatojaponocapsa plicarum* in UT-7 collected from the Ut indicates the *Stj*. *plicarum* Zone (Nishizono *et al.*, 1997). UT-5 was collected from the stratigraphic level 240 m beneath sample UT-7 in the Ut. An assemblage with a co-occurrence of *A. pachyderma*, *Parahsuum*? *hiconocosta*, *Unuma typicus*, and *Stichocapsa convexa* but no *Str. plicarum* occurred in UT-5, which was correlated with the *Transhsuum hisuikyoense* Zone (Nishizono *et al.*, 1997). This correlation does not contradict the assemblage of the *Th. hisuikyoense* Zone of sample UT-2, which is in the lower part of the Ut. The *Th. hisuikyoense* and *Stj. plicarum* zones are assigned to the Aalenian and Bajocian to Bathonian, respectively (Nishizono *et al.*, 1997). Therefore, it is estimated that the boundary between the two zones is in the middle part of the Ut, which is 360 m above the Uh–Ut boundary at the stratigraphic level between the samples UT-5 and UT-7 (Fig. 6).

According to Matsuoka (1995), the co-occurrence of *Stj. plicarum* and *Eucyrtidiellum unumaense*, as seen in UT-7, correlates with the *Stj. plicarum* and *Stj. conexa* zones (Matsuoka, 1995; Matsuoka and Ito, 2019). However, the co-occurrence of *Stj. plicarum*, *Unuma typicus*, *Unuma latusicostatus*, *Stichocapsa convexa*, and *Eucyrtidiellum unumaense* but no *Stj conexa* shows that the radiolarians from UT-7 could be correlated with the *Stj. plicarum* Zone. Furthermore, the radiolaria in UT-5 could be correlated with the *Laxtorum*? *jurassicum* Zone (Matsuoka, 1995) because the co-occurrence of *A. pachyderma*, *Unuma typicus*, and *Stichocapsa convexa* but no *Stj. plicarum* is found in UT-5. Matsuoka (1995) correlated the *L.*?

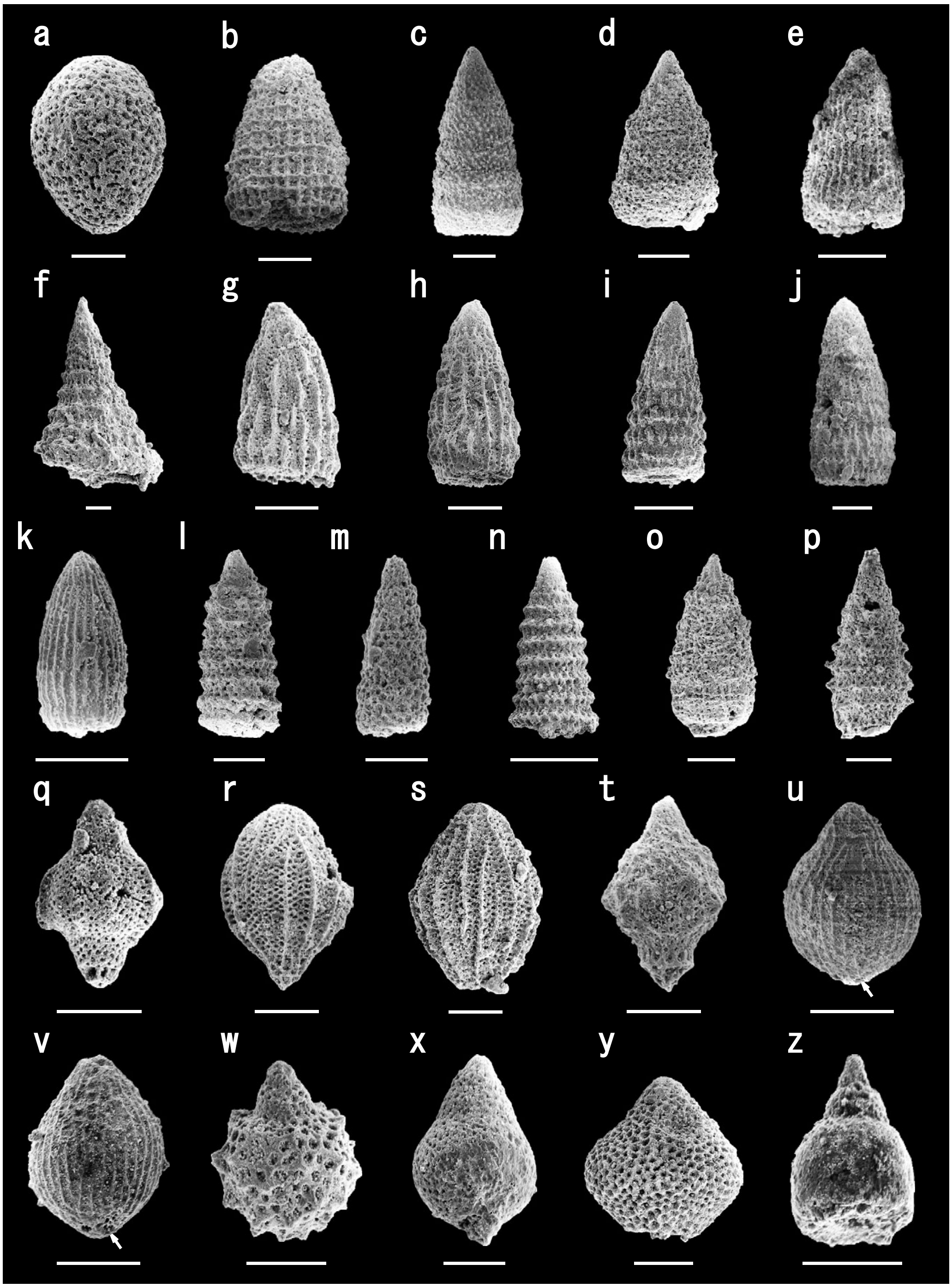

Fig. 5 SEM (Scanning Electron Microscope) photos of radiolarian.
a: *Archicapsa pachyderma* (Tan) (locality; UT-5). b: *Canutus* sp. (locality; UT-2). c: *Spongocapsula* aff. *S. krahsteinensis* Suzuki and Gawlick (UT-7). d: *Spongocapsula* sp. A (locality; UT-5). e: *Parahsuum* sp. (locality; UT-2). f: *Parahsuum*? *hiconocosta* Baumgartner and De Wever (locality; UT-5). g, h: *Transhsuum maxwelli* (Pessagno) (locality; UT-7). i: *Transhsuum* aff. *brevicostatum* (Ozvoldova) (locality; UT-5). j: *Transhsuum* aff. *hisuikyoense* (Isozaki and Matsuda) (locality; UT-2). k: *Archaeodictyomitra* sp. H in Nishizono (1996) (locality; UT-7). l: *Praeparvicingula aculeata* (Carter) (locality; UT-5). m: *Praeparvicingula*? sp. A (locality; UT-1). n: *Wrangellium* aff. *burnsensis* (Pessagno and Whalen) (locality; UT-5). o: *Droltus hecatensis* Pessagno and Whalen (locality; UT-5). p: *Triversus hungaricus* (Kozur) (locality; UT-7). q: *Unuma latusicostatus* (Aita) (locality; UT-7). r: *Unuma typicus* Ichikawa and Yao (locality; UT-7). s: *Unuma typicus* Ichikawa and Yao (locality; UT-5). t: *Podobursa nodosa* (Chiari, Marucucci and Prela) (locality; UT-7). u, v: *Striatojaponocapsa plicarum* (Yao) (locality; UT-7). Arrows of u and v show the circular area. w: *Tricolocapsa undulata* (Heitzer) (locality; UT-7). x: *Stichocapsa convexa* Yao (locality; UT-5). y: *Stichocapsa magnipora* Chiari, Marucci and Prela (locality; UT-5). z: *Eucyrtidiellum unumaense* (Yao) (locality; UT-7). All scale bars indicate 50 μm.

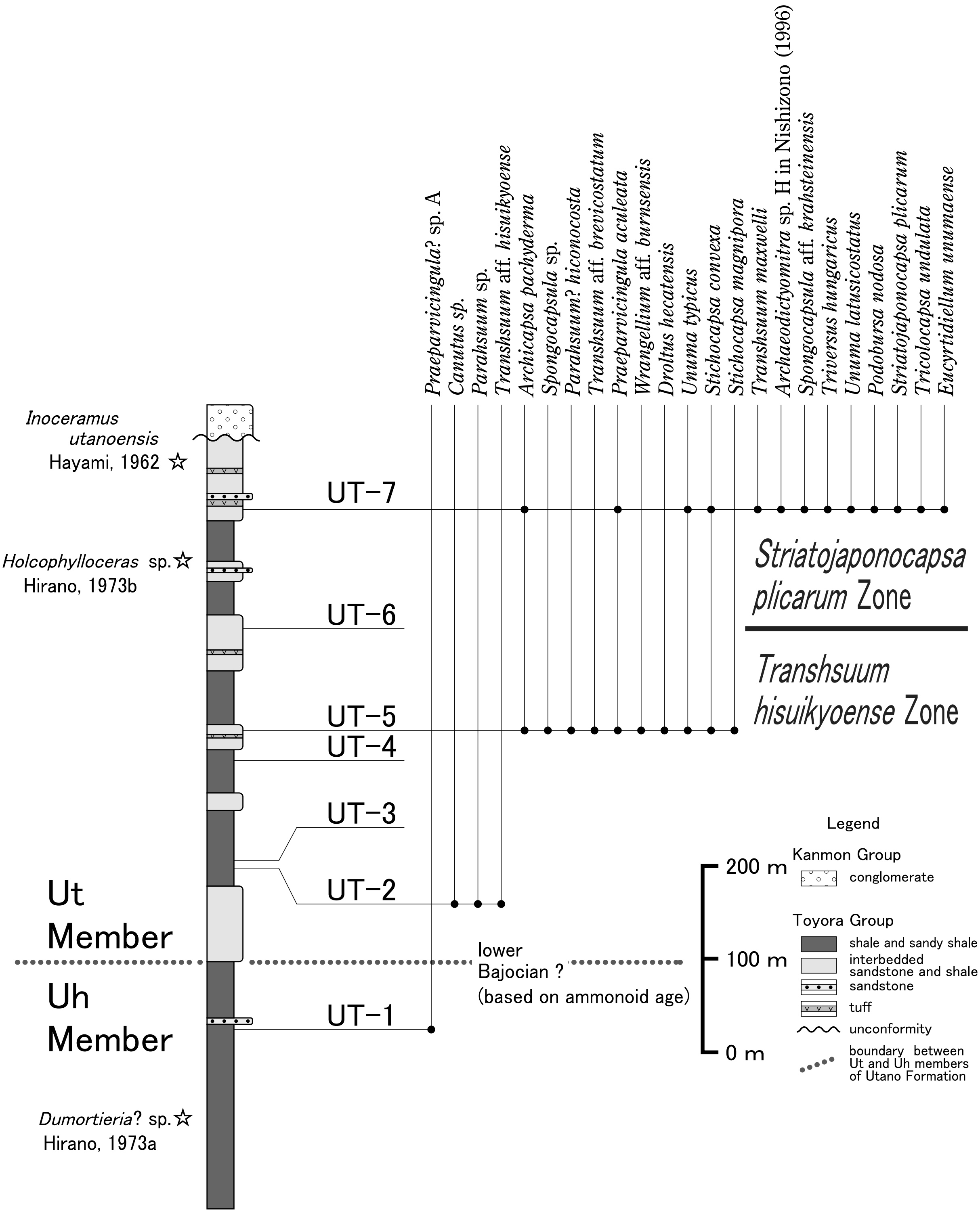

Fig. 6 Biostratigraphic distribution of radiolarian species in the Utano sections, the Toyora Group.

jurassicum and *Stj. plicarum* zones with the Aalenian and Bajocian to early Bathonian, respectively. Therefore, the geological ages assigned by radiolarians indicate that the boundary between the *Th. hisuikyoense* and *Stj. plicarum* zones (Nishizono *et al.*, 1997) is in the middle part of the Ut, which is the border of the Aalenian and Bajocian.

4. 3 Correlation between radiolarian and macrofossil age assignments

Find-spots of ammonoid are close to the two radiolarian sampling sites. *Dumortieria*? sp. occurs in the lower part of the upper member (Uh) in the Utano D2 route (Figs. 4 and 6), which is correlated with 280 m below UT-2; it is assigned to the Toarcian Stage of the Lower Jurassic (Hirano, 1973a). Hirano (1973b) showed that the Uh is assigned to the horizon ranging from the uppermost Toarcian to the Bajocian (mainly Aalenian) on the basis of an ammonoid *Planammatoceras* cf. *kitakamiensis* in the Uh, occurred outside of the study area. The stratigraphic level of *Holcophylloceras* sp. (Hirano, 1973b: locality 59) is 180 m above UT-5 and 60 m below UT-7 (Figs. 4 and 6), which is the upper part of the Ut in the Utano A route. The genus *Holcophylloceras* ranges in age from the Bajocian to the Aptian in the Early Cretaceous (Sandoval *et al.*, 2001, Majidifard, 2003). Furthermore, Hayami (1962) showed that *Inoceramus utanoensis* (Kobayashi), which occurred in the Ut, is very similar to *I. kystatymensis* as reported from the Bathonian in the Lena River, Russia (Koschelkina, 1963; Hirano, 1973b). This indicates that the uppermost member (Ut) includes at least the Bajocian to Bathonian in the Middle Jurassic.

Previous studies have shown the Aalenian–Bajocian boundary is in the Ut based on radiolarians (e.g. Matsuoka, 1995; Nishizono *et al.*, 1997) and in the upper part of the Uh based on ammonoids (Hirano, 1973b). The difference in the stratigraphic interval of the two ammonoid localities is 580 m, while that of the radiolarian localities (UT-5: Aalenian and UT-7: Bajocian) is 240 m (Fig. 6).

The assigned ages of ammonoids from the Utano Formation, indicate that the first appearance age of *Striatojaponocapsa plicarum* could be redefined from the Aalenian to the early Bajocian. According to Nishizono *et al.* (1997), *Stj. plicarum* first appeared in the lower Bajocian based on calibration by ammonoids occurring in the Kitakami Mountains, Tohoku district, central Kyushu district and Canada. Matsuoka (1995) showed that *Stj. Plicarum* appeared in the Bajocian based on the correlation data by ammonoids occurring in Spain, Italy and Japan. Furthermore, Baumgartner *et al.* (1995) set the range of *Stj. plicarum plicarum* from the upper Bajocian to the lower Bathonian (UA Zones 4 and 5). However, in previous studies (Matsuoka, 1995; Nishizono *et al.*, 1997), the first appearance age of *Stj. plicarum* could not be established for the assigned ages of ammonoid and was only estimated to be around the Aalenian/Bajocian boundary.

Considering this difference, further study is required to collect fossil data such as the Aalenian ammonoids from these intervals.

5. Conclusions

Radiolarian fossils were first discovered from the Lower to Middle Jurassic Toyora Group containing abundant ammonoids. The radiolarian fossils, found in seven localities from the uppermost Toyora Group, are assigned to the Aalenian–Bathonian based on the presence of ammonoids and inoceramids. According to Nishizono *et al.* (1997), these radiolarian assemblages are correlated to the *Transhsuum hisuikyoense* and *Striatojaponocapsa plicarum* zones which have been assigned to the Aalenian and Bajocian to lower Bathonian, respectively. Although the upper–uppermost member (Uh–Ut) boundary of the Utano Formation was correlated with the lower Bajocian based on megafossils (Hirano, 1973b), it should be assigned to the Aalenian based on the radiolarian zonation. The stratigraphic intervals of the two ammonoid localities and that of the radiolarian localities (UT-5: Aalenian and UT-7: Bajocian) are 580 m and 240 m, respectively. According to previous studies, the first appearance of *Stj. plicarum* could not be calibrated to the ammonoid assignment ages and is only estimated to be near the Aalenian/Bajocian boundary. To discuss this issue, further study is required to correct the fossil data such as the Aalenian ammonoid occurring in these intervals.

6. Systematic Paleontology

The familial classification system basically follows Takemura (1986), Suzuki *et al.* (2002), Suzuki and Gawlick (2003, 2009). The classification for genera *Archicapsa* and *Canutus* are based on Haeckel (1881), Pessagno and Whalen (1982), respectively.

Subclass **RADIOLARIA** Müller, 1858

Order **NASSELLARIA** Ehrenberg, 1875

Family **SETHOCAPSIDAE** Haeckel, 1881

Genus ***Archicapsa*** Rüst, 1885

Archicapsa pachyderma (Tan, 1927)
(UT-5, Fig. 5a)

1986 *Archicapsa pachyderma* (Tan) – Matsuoka and Yao, pl. 1, fig. 5.
1990 *Archicapsa pachyderma* (Tan) – Yao, pl. 2, fig. 15.
1990 *Archicapsa pachyderma* (Tan) – Hori, fig. 9.44.
1996 *Archicapsa pachyderma* (Tan) – Nishizono, pl. 12, fig. 4.

Remarks: Test is ellipsoidal with a spherical apical part and slightly pointed aperture side.
Range: This species occurs from the *Droltus*? sp. A–*Hsuum*? sp. G to *Striatojaponocapsa plicarum* zones in Outer zone of Southwest Japan (Nishizono, 1996).

Family **CANUTIDAE** Pessagno and Whalen, 1982

Genus ***Canutus*** Pessagno and Whalen, 1982

***Canutus* sp.**
(UT-2, Fig. 5b)
Remarks: Test is short, inflated and conical. Test surface consists of square symmetrical pore frames with nodes. In present specimen, the two or three layered structure and apical part are unclear due to poor preservation.

Family **THEOPERIDAE** Haeckel 1881;

emend. Takemura, 1986

Genus ***Spongocapsula*** Pessagno, 1977

Spongocapsula* sp. aff. *S. krahsteinensis Suzuki and Gawlick in Gawlick *et al.* (2004)
(UT-7, Fig. 5c)
1996 *Spongocapsula*? sp. – Nishizono, pl. 27, fig. 11.
aff. 2004 *Spongocapsula krahsteinensis* n. sp.– Gawlick *et al.*, p. 313–315, abb. 4.7–4.10.
Remarks: Test is short, inflated and spindle-shaped. Gawlick *et al.* (2004) regarded that underneath the microgranular outer layer of this species is spongy test. This specimen has a resemble test of *S. krahsteinensis*.
Range: late Bajocian to Callovian (Gawlick *et al.*, 2004)

***Spongocapsula* sp. A**
(UT-5, Fig. 5d)
Remarks: Test is conical shaped increasing slowly in height and moderately rapidly in width proximally, gradually decreasing in width distally. Cephalis and thorax are imperforate.

Genus ***Parahsuum*** Yao, 1982

***Parahsuum* sp.**
(UT-2, Fig. 5e)
Remarks: Test is conical and lacking ornamentation at cephalis, thorax and abdomen due to poor preservation of this sample. In a side view, sixteen edged costae are visible on post-abdominal chambers. Single row of square pore frames is arranged with circular, primary pores between costae.

Parahsuum*? *hiconocosta Baumgartner and De Wever in Baumgartner *et al.* (1995)
(UT-5, Fig. 5f)
1985 *Andromeda*? sp. – De Wever *et al.*, pl. 1, figs. 12, 13, 16.
1995 *Parahsuum*? *hiconocosta* n. sp. – Baumgartner *et al.*, p. 378, pl. 3011, figs. 1 (H) –6.
1996 *Andromeda* sp. B – Nishizono, pl. 26, fig. 18.
Remarks: Test is elongated conical form with concave and wedge-shaped outline in lateral view. Segments are well marked by a nodose circumferential ridge. The present species has rectangular and elevated vertical pore-frames with a protruding nodose as characteristic structures of this species.
Range: This species occurs from the *Transhsuum hisuikyoense* Zone in Outer zone of Southwest Japan (Nishizono, 1996). UA Zones 2–4, late Aalenian–late Bajocian (Baumgartner *et al.*, 1995)

Genus ***Transhsuum*** Takemura, 1986

Transhsuum maxwelli (Pessagno, 1977)
(UT-7, Fig. 5g, h)
1977 *Hsuum maxwelli* n. sp. – Pessagno, p.81, pl. 7, figs. 14–16.
1995 *Transhsuum maxwelli* group (Pessagno) – Baumgartner *et al.*, p. 582, pl. 3180, figs. 4, 5.
1997 *Hsuum maxwelli* Pessagno – Nishizono *et al.*, pl. III, fig. 10.
2009 *Hsuum maxwelli* Pessagno – Suzuki and Gawlick, p. 168, fig. 5.7.
Remarks: Test is conical. Cephalis is perforate without long and massive apical horn. The specimen shown in Fig. 5h has the test of increasing rapidly in width. Short, massive and discontinuous costae are distributed on a test.
Range: UA Zones 3–10, early–middle Bajocian to late Oxfordian–early Kimmeridgian. (Baumgartner *et al.*, 1995). The first appearance of *Transhsuum maxwelli* group is located in the upper part of *Striatojaponocapsa plicarum* Zone in Outer zone of Southwest Japan (Matsuoka, 1995: Bajocian to middle Bathonian).

Transhsuum* sp. aff. *T. brevicostatum (Ozvoldova, 1975)
(UT-5, Fig. 5i)
aff. 1975 *Lithostrobus brevicostatus* n. sp. – Ozvoldova, p. 84, pl. 102, fig. 1.
aff. 1979 *Lithostrobus brevicostatus* Ozvoldova – Ozvoldova, p. 259, pl. 5, fig. 2.
aff. 1995 *Transhsuum brevicostatum* group (Ozvoldova) –Baumgartner *et al.*, p. 578, pl. 3181, figs. 2, 4.
aff. 1996 *Hsuum brevicostatum* Ozvoldova – Nishizono, pl. 21, figs. 8, 9.
Remarks: Test is conical. Post-abdominal segments have short longitudinal ribs. The specimen shown in Fig. 5i could not be identified as *Transhsuum brevicostatum* because two longitudinal lines of pores are unclear due to poor preservation. *Th. brevicostatum* (Ozvoldova) is rare in the *Striatojaponocapsa plicarum* Zone after Nishizono (1996).
Range: UA Zones 3–11, early–middle Bajocian to late Kimmeridgian–early Tithonian. (Baumgartner *et al.*, 1995).

Transhsuum* sp. aff. *T. hisuikyoense (Isozaki and Matsuda 1985)
(UT-2, Fig. 5j)
Measurements (in μm): height 200, maximum width 100.
Remarks: General form and surface ornamentations of post-abdominal segments are very similar to *Hsuum hisuikyoense* Isozaki and Matsuda, 1985. However, details of apical part are unclear due to poor preservation.
Range: UA Zones 2–4, late Aalenian–late Bajocian (Baumgartner *et al.*, 1995).

Genus ***Archaeodictyomitra*** Pessagno, 1976

***Archaeodictyomitra* sp. H** in Nishizono, 1996
(UT-7, Fig. 5k)
1982 *Archaeodictyomitra* sp. A – Pessagno and Whalen,

p. 117, pl. 8, fig. 10.

1996 *Archaeodictyomitra* sp. H – Nishizono, pl. 24, fig. 4.

Remarks: This species has rounded test apically and constricted distally. Twelve costae are visible on post-abdominal chambers in a side view. This species occurs from the *Striatojaponocapsa plicarum* Zone in Outer zone of Southwest Japan (Nishizono, 1996).

Genus ***Praeparvicingula*** Pessagno, Blome and Hull in Pessagno *et al.*, 1993

Praeparvicingula aculeata (Carter in Carter *et al.*, 1988)
(UT-5, Fig. 5l)

1988 *Parvicingula aculeata* n. sp. – Carter *et al.*, p. 54–55, pl. 18, figs. 1, 2, 7.

1997 *Parvicingula dhimenaensis dhimenaensis* Baumgartner – Yao, pl. 13, fig. 625.

Remarks: Test is subcylindrical and maintaining same width of post-abdominal chamber. Cephalis and thorax are sparsely perforate without horn. Post-abdominal chambers has three lateral rows of pore frames between ridges. Those are depressed in central row. Sharp pointed nodes are clear, that separate the abdomen and first few post-abdominal chambers. The narrow tube is lacking on the final post-abdominal chamber. Goričan *et al.* (2006) clasified *Parvicingula aculeata* Carter to genus *Praepalvicingula* on the basis of the above test structures.
Range: middle Toarcian–Early Bajocian (Carter *et al.*, 1988) (no-data earlier than middle Toarcian in Carter *et al.*, 1988)

***Praeparvicingula*? sp. A.**
(UT-1, Fig. 5m)
Remarks: Test is subcylindrical with dome-shaped cephalis. Horn and terminal tube are unknown due to poor preservation. The present specimen is different from *Praeparvicingula tlellensis* Carter in having the non-parallel pore alignment to circumferential ridges.

Family **Amphipyndacidae** Riedel, 1967

Genus ***Wrangellium*** Pessagno and Whalen, 1982

Wrangellium* sp. aff. *W. burnsensis (Pessagno and Whalen, 1982)
(UT-5, Fig. 5n)

1988 *Parvicingula* sp. aff. *P. burnsensis* (Pessagno and Whalen) – Carter *et al.*, p. 55, pl. 18, figs. 10, 15.

Remarks: Test is characterized by having nodose circumferential ridges with H-linked structures. The specimen identified as *P.* aff. *burnsensis* Pessagno and Whalen (pl 18, figs 10 and 15 of Carter *et al.*, 1988) is considered to be classified as genus *Wrangellium* in having circumferential ridges with H-linked structures.
Range: middle Toarcian to early Bajocian (Carter *et al.*, 1988)

Genus ***Droltus*** Pessagno and Whalen, 1982

Droltus hecatensis Pessagno and Whalen, 1982
(UT-5, Fig. 5o)

1982 *Droltus hecatensis* n. sp. – Pessagno and Whalen, p. 121, pl. 1, figs. 12, 13, pl. 4, figs. 1, 2, 6, 10.

1998 *Droltus hecatensis* Pessagno and Whalen – Carter *et al.*, p. 63, pl. 15, fig.14.

2002 *Droltus hecatensis* Pessagno and Whalen – Suzuki *et al.*, 2002. p. 181–182, figs. 8G, 8H, 8L–8M.

2003 *Droltus hecatensis* Pessagno and Whalen – Suzuki and Gawlick, p. 191–192, fig. 6.72.

2009 *Droltus hecatensis* Pessagno and Whalen – Suzuki and Gawlick, p. 177, figs. 6.50A, 6.50B.

Remarks: Apical horn is ornamented with thick blades. Abdomen and several post-abdominal chambers have irregularly sized and shaped polygonal pore frames with solid small spines in somewhere. In lower one third, test consists of three longitudinal rows of pores between every adjacent pairs of costae.
Range: *Droltus hecatensis* occurs commonly in Lower Jurassic of west coast of Canada (Carter *et al.*, 1998) and Peru (Suzuki *et al.*, 2002). Suzuki and Gawlick (2003, 2009) described this species from the Callovian to Oxfordian in the Northern Calcareous Alps.

Genus ***Triversus*** Takemura, 1986

Triversus hungaricus (Kozur, 1985)
(UT-7, Fig. 5p)

1984 *Parvicingula dhimenaensis* n. sp. – Baumgartner, p. 778, pl. 7, fig. 4.

1985 *Eoxitus hungaricus* n. sp. – Kozur, p. 216, figs. 1a, 1b, 1d, 1e.

1995 *Parvicingula dhimenaensis* Baumgartner ssp. A – Baumgartner *et al.*, p. 406, pl. 4071, figs. 1–4.

1996 *Parvicingula dhimenaensis* Baumgartner – Nishizono, pl. 25, figs. 11–13.

2003 *Triversus hungaricus* (Kozur) – Suzuki and Gawlick, p. 195–196, fig. 6.58–6.60.

2009 *Triversus hungaricus* (Kozur) – Suzuki and Gawlick, p. 170, fig. 5.14; figs. 6.6A, 6.6B, 6.7, 6.8.

Remarks: Test has an elongated cephalis and is spindle-shaped with pronounced spines on circumferential ridges.
Range: UA Zones 3–8, early–middle Bajocian to middle Callovian (Baumgartner *et al.*, 1995).

Genus ***Unuma*** Ichikawa and Yao, 1976

Unuma latusicostatus (Aita, 1987)
(UT-7, Fig. 5q)

1987 *Tricolocapsa latusicostata* n. sp. – Aita, p. 76, pl. 4, figs. 7a–8b; pl. 10, figs. 8, 9.

1995 *Unuma latusicostatus* (Aita) – Baumgartner *et al.*, p. 622, pl. 4058, figs. 1, 4.

1996 *Tricolocapsa latusicostata* (Aita) – Nishizono, pl. 13, fig. 11.

Remarks: The present specimen has seven longitudinal plicae in a half side view, and four longitudinal rows of pores between neighboring plicae. No nodes or spines on the plicae.
Range: UA Zones 2–5, late Aalenian to latest Bajocian–early Bathonian (Baumgartner *et al,* 1995).

Unuma typicus Ichikawa and Yao, 1976
(UT-7, Fig. 5r; UT-5, Fig. 5s)
1976 *Unuma typicus* n. sp. – Ichikawa and Yao, p. 112, pl. 1, figs. 1–3.
1996 *Unuma typicus* Ichikawa and Yao – Nishizono, pl. 18, figs. 15, 16.
Remarks: The specimen shown in Fig. 5r (UT-7) has nine longitudinal plicae in a half side view, and four longitudinal rows of pores between neighboring plicae without spines. The specimen shown in Fig. 5s (UT-5) is very similar to *Unuma typicus* Ichikawa and Yao. Probably, this will be an immature (variation) specimen or basal appendage has been broken.
Range: This species occurs from the *Hsuum hisuikyoense* to *Striatojaponocapsa plicarum* zones in Outer zone of Southwest Japan (Nishizono, 1996). UA Zones 3–4, early–middle Bajocian to late Bathonian (Baumgartner *et al.*, 1995).

Genus ***Podobursa*** Wisniowski 1889; emend. Foreman, 1973

Podobursa nodosa (Chiari, Marucucci and Prela, 2002)
(UT-7, Fig. 5t)
2002 *Williriedellum nodosum* n. sp. – Chiari *et al.*, p. 84, pl. 5, figs. 15–19.
2009 *Podobursa nodosa* (Chiari, Marucucci and Prela) – Suzuki and Gawlick, p. 178, figs. 5.20, 5.21.
Remarks: Cephalis and thorax are conical. Abdomen is large globose with nodes surrounded by irregular pores. Final segment terminates in a prolonged tube with elongate pores and solid pore flames.
Range: UA Zone 5, latest Bajocian to early Bathonian (Chiari *et al,* 2002).

Family ***Arcanicapsidae*** Takemura, 1986

Genus ***Striatojaponocapsa*** Kozur, 1984

Striatojaponocapsa plicarum (Yao, 1979)
(UT-7, Fig. 5u, v)
1979 *Tricolocapsa plicarum* n. sp. –Yao, p. 32, pl. 4, figs. 1–11.
1984 *Striatojaponocapsa plicarum* (Yao) – Kozur, p. 56, pl. 7, fig. 3
1996 *Tricolocapsa plicarum* Yao – Nishizono, pl. 13, figs. 14–16.
2007 *Striatojaponocapsa plicarum* (Yao) – Hatakeda *et al.*, p. 16, pl. 1, figs. 1–10
2009 *Striatojaponocapsa plicarum* (Yao) – Suzuki and Gawlick, p. 182, figs. 5.39A, 5.39B.
Measurements (in μm): Fig. 5u; height 92, width 80, width of basal appendage 30, Fig. 5v; height 95 (broken cephalis), width 75, width of basal appendage 28.
Remarks: Abdomen is spherical with eighteen longitudinal plicae along an equator in a side view. One row of small pores are arranged in neighboring two longitudinal plicae. The basal appendage of the specimen shown in Fig. 5u is small with unclear circular area. In the specimen of the shown in Fig. 5v, circular area without surrounding ridges (Hatakeda *et al.*, 2007) is wider than that of the specimen shown in Fig. 5u.
Range: *Stj. plicarum* with small appendage (30 to 35 μm) occurs in near the last horizon of this species (Hatakeda *et al.*, 2007). UA Zones 4–5, late Bajocian to latest Bajocian–early Bathonian (Baumgartner *et al.*, 1995). This species occurs from the *Striatojaponocapsa plicarum* to *Cinguloturris carpatica* zones in Outer zone of Southwest Japan (Nishizono, 1996).

Genus ***Tricolocapsa*** Haeckel, 1881

Tricolocapsa undulata (Heitzer, 1930)
(UT-7, Fig. 5w)
1930 *Lithobotrys undulata* n. sp. – Heitzer, p.390, pl. 28, fig. 22.
1987 *Sethocapsa funatoensis* n. sp. – Aita, p. 73, pl. 2, figs. 6a–11; pl. 7, figs. 14, 15.
1993 *Tricolocapsa undulata* (Heitzer) – Ozvoldova and Faupl, pl. 3, fig. 12.
1996 *Sethocapsa funatoensis* Aita – Nishizono, pl. 16, figs. 5, 6.
2003 *Tricolocapsa undulata* (Heitzer) – Suzuki and Gawlick, p. 210, fig. 5.41; fig. 6.39.
2009 *Tricolocapsa undulata* (Heitzer) – Suzuki and Gawlick, p. 183, figs. 5.44A, 5.44B, 5.45A, 5.45B; figs. 6.18A, 6.18B, 6.19A, 6.19B.
Remarks: This species was described by Aita (1987) as *Sethocapsa funatoensis*. This species differs from *Sethoc. yahazuensis* by having rather spinose or pointed nodes on the last segment (Aita, 1987). Suzuki and Gawlick (2003) regarded these two species as younger synonyms of *Lithobotrys undulata* Heitzer.
Range: This species occurs from the *Striatojaponocapsa plicarum* to *Stylocapsa*? *spiralis* zones in the Outer zone of Southwest Japan (Nishizono, 1996).

Genus ***Stichocapsa*** Haeckel, 1881

Stichocapsa convexa Yao, 1979
(UT-5, Fig. 5x)
1979 *Stichocapsa convexa* n. sp. – Yao, p. 35, pl. 5, figs. 14–16; pl. 6, figs. 1–7.
1986 *Stichocapsa convexa* Yao – Takemura, p. 55, pl. 7, figs. 9, 10.
1996 *Stichocapsa convexa* Yao – Nishizono, pl. 14, fig. 13.
Remarks: Test consists of four segments, conical at upper

half. Forth segment is a truncated sphere with small aperture.
Range: This species occurs mainly from middle of the *Transhsuum hisuikyoense* to the uppermost of the *Striatojaponocapsa plicarum* zones in the Outer zone of Southwest Japan (Nishizono 1996).

Stichocapsa magnipora Chiari, Marucci and Prela, 2002
(UT-5, Fig. 5y)
2002 *Stichocapsa magnipora* – Chiari *et al.*, p. 76–77, pl. 3, figs. 13–17.
Remarks: Last segment is inflated with flattened base and aperture. Test has a large depression between the third chamber and the final one. Size of pores is smaller than holotype.
Range: UA Zones 4–7, late Bajocian to late Bathonian–early Callovian. (Chiari *et al.*, 2002).

Family **EUCYRTIDIELLIDAE** Takemura, 1986

Genus ***Eucyrtidiellum*** Baumgartner, 1984

Eucyrtidiellum unumaense (Yao, 1979)
(UT-7, Fig. 5z)
1979 *Eucyrtidium*? *unumaensis* n. sp. – Yao, p. 39, pl. 9, figs. 1–11.
1984 *Eucyrtidiellum putsulatum* Yao – Baumgartner, p. 765, pl. 4, figs. 4, 5.
1986 *Monosera unumaensis* (Yao) – Takemura and Nakaseko, p. 1022, figs. 4.1–4.9.
1990 *Eucyrtidiellum unumaense* (Yao) – Nagai and Mizutani, p. 597, figs. 4.6, 4.7.
1995 *Eucyrtidiellum unumaense putsulatum* Baumgartner – Baumgartner *et al.*, p. 220, pl. 3013, figs. 1, 2.
Remarks: Shell of four segments. Cephalis with a horn where the root remains. Thorax nodose with the sutural pores at distal part. Most of the abdomen is not preserved. However, the part of it with nodes in proximal portion. The fourth segment is lost due to poor preservation. These features show that this specimen similar to *Eucyrtidiellum unumaense putsulatum* Baumgartner *et al.*, 1995.
Range: UA Zones 3–8, early–middle Bajocian to middle Callovian – early Oxfordian (Baumgartner *et al.*, 1995).

Acknowledgments: This study is mainly based on the master's thesis of YONEMITSU Isao, a second author of this paper. We wish to express our gratitude to their supervisor, Dr. MURATA Masafumi (honorary professor of the Kumamoto University). We would also like to thank members of the InterRad XV in Niigata, 2017, organizing committee, Dr. MATSUOKA Atsushi (chairperson), and especially, Dr. NAKAE Satoshi (Geological Survey of Japan, AIST) for providing the opportunity to publish our study. Finally, we gratefully acknowledge Dr. SUZUKI Hisashi (professor of the Otani University) and Dr. UCHINO Takayuki (Geological Survey of Japan, AIST) for their appropriate reviews.

References

Aita, Y. (1987) Middle Jurassic to Lower Cretaceous radiolarian biostratigraphy of Shikoku with reference to selected sections Lombardy basin and Sicily. *Science Reports of the Tohoku university, Second Series (Geology)*, **58**, 1–91.

Baumgartner, P. O. (1984) A Middle Jurassic–Early Cretaceous low latitude radiolarian zonation based on unitary association and age of Tethyan radiolarites. *Eclogae Geologicae Helvetiae*, **77**, 729–837.

Baumgartner, P. O., O' Dogherty, L., Goričan S., Dumitrica-Jud, R., Dumitrica, P., Pillevuit, A., Urquhart, E., Matsuoka, A., Danellian, T., Bartolini, A., Carter, E. S., De Wever P., Kito, N., Marcucci, M. and Steiger, T. (1995) Radiolarian catalogue and systematics of Middle Jurassic to Early Cretaceous Tethyan genera and species. *Memoires de Geologie (Lausanne)*, no. 23, 37–685.

Carter, E. S., Cameron, B. E. B. and Smith, P. L. (1988) Lower and Middle Jurassic radiolarian biostratigraphy and systematic paleontology, Queen Charlotte Islands, British Columbia. *Geological Survey of Canada Bulletin*, **386**, 1–109.

Carter E. S., Whalen, P. A. and Guex, J. (1998) Biochronology and paleontology of Lower Jurassic (Hettangian and Sinemurian) radiolarians, Queen Charlotte Island, British Columbia. *Geological Survey of Canada Bulletin*, **496**, 1–161.

Chiari, M., Marcucci, M. and Prela, M. (2002) New species of Jurassic radiolarians in the sedimentary cover of ophiolites in Mirdita area, Albania. *Micropaleontology*, **48**, 61–87.

Cohen, K. M., Harper, D. A., Gibbard, P. L. and Fan, J. -X. (2013) International Chronostratigraphic Chart. *Episodes*, **36**, 199–204 (updated in 2020, https://stratigraphy.org/icschart/ChronostratChart2020-01.pdf, Accessed: 2020-01-23).

De Wever, P., Duée, G. and El Kadiri, K. (1985) Les sériesstratigraphiques des klippes de Chrafate (Rif septentrional, Maroc). *Bulletin de la Sociéte Géologique de France, série 8*, **1**, 363–379 (in French with English abstract).

Ehrenberg, C. G. (1875) Fortsetzung der mikrogeologischen Studien als Gesammt-Uebersicht der mikroskopischen Paläontologie gleichartig analysirter Gebirgsarten der Erde, mit specieller Rücksicht auf den Polycystinen-Mergel von Barbados. *Abhandlungen der Königlichen Preussichen Akademie der Wissenschaften zu Berlin*, **1875**, 1–225 (in German).

Forman, H. P. (1973) Radiolaria from DSDP Leg 20, *In* Heezen, C., MacGregor, D., Forman, P., Hekel, H., Hesse, R., Hoskins, A., Okada, H. and Ruef, H. eds., *Initial Reports of the Deep See Drilling Project.*, **20**, 249–305.

Gawlick, H., Schlagintweit, F., Ebli, O. and Suzuki, H. (2004) Die Plassen-Formation (Kimmeridgium) des

Krahstein (Steirisches Salzkammergut, Österreich) und ihre Unterlagerung: neue Daten zur Fazies, Biostratigraphie und Sedimentologie. *Zentralblatt für Geologie und Paläontologie*, **2003**, 295–334 (in German with English abstract).

Goričan, Š., Carter, E. S., Dumitrica, P., Whalen, P., Hori, R., De Wever, P., O'Dogherty, L., Matsuoka, A. and Guex, J. (2006) *Catalogue and systematics of Pliensbachian, Toarcian and Aalenian radiolarian genera and species*. Založba ZRC Publishing, SAZU, Ljubljana, 1–446.

Hatakeda, K., Suzuki, N. and Matsuoka, A. (2007) Quantitative morphological analyses and evolutionary history of the Middle Jurassic polycystine radiolarian genus *Striatojaponocapsa* Kozur. *Marine Micropaleontology*, **63**, 39–56.

Haeckel, H. (1881) Entwurf eines Radiolarien-Systems auf Grund von Studien der Challenger-Radiolarien. *Jenaische Zeitschrift für Naturwissenschaft*, **15**, 418–472 (in German).

Hayami, I. (1962) Jurassic pelecypod fauna in Japan with special reference to their stratigraphical provinces. *Journal of Geological Society of Japan*, **68**, 96–108 (in Japanese with English abstract).

Heitzer, I. (1930) Die Radiolarienfauna der mitteljurassischen kieselmergel im Sonnwendgebirge. *Jahrebuch der Geologischen Bundesanstalt*, **80**, 381–406 (in German).

Hirano, H. (1971) Biostratigraphic study of the Jurassic Toyora Group part 1. *Memoirs of the Faculty of Science, Kyushu University. Series D, Geology*, **21**, 93–128.

Hirano, H. (1973a) Biostratigraphic study of the Jurassic Toyora Group part 2. *Transactions and Proceedings of the Palaeontological Society of Japan, New Series*, **89**, 1–14.

Hirano, H. (1973b) Biostratigraphic study of the Jurassic Toyora Group part 3. *Transactions and Proceedings of the Palaeontological Society of Japan, New Series*, **90**, 45–71.

Hirasawa, S., Kashiwagi, K. and Fujita, M. (2010) Marine strata and dinosaur footprints of the Upper Jurassic to Lower Cretaceous Tetori Group, Toyama Prefecture. *Journal of Geological Society of Japan*, **116**, Supplement, 103–121 (in Japanese).

Hori, R. (1990) Lower Jurassic radiolarian zones of Japan. *Transactions and Proceedings of the Palaeontological Society of Japan, New Series*, **159**, 562–586.

Ichikawa, K. and Yao, A. (1976) Two new genera of Mesozoic cyrtoid radiolarians from Japan. *In* Takayanagi, Y. and Saito, T. eds., *Progress in micropaleontology, special publication*, Micropaleontology Press, 110–117.

Isozaki, Y. and Matsuda, T. (1985) Early Jurassic radiolarians from bedded chert in Kamiaso, Mino Belt, central japan. *Earth Science (Journal of the Association for the Geological Collaboration in Japan)*, **39**, 429–442.

Izumi, K., Miyaji, T. and Tanabe, K. (2012) Early Toarcian (Early Jurassic) oceanic anoxic event recorded in the shelf deposits in the northwestern Panthalassa: evidence from the Nishinakayama Formation in the Toyora area, west Japan. *Palaeogeography, Palaeoclimatology, Palaeoecology*, **315–316**, 100–108.

Kobayashi, T. (1926) Note on the Mesozoic formations in prov. Nagato. *Journal of Geological Society of Japan*, **33**, 1–19.

Koschelkina, Z. V. (1963) Stratigraphy and bivalve mollusks of the Jurassic deposits of Viluysk syncline and near Verhojansk foredeep. *Transactions of the Northeast, Integrated Research Institute, Siberian Branch of the USSR Academy of Sciences*, **5**, 1–219 (in Russian).

Kozai, T., Ishida, K. and Kondo, Y. (2006) Jurassic–Cretaceous boundary and Cretaceous formations in the Tosayamada–Birafu area, Kochi Prefecture. *Journal of Geological Society of Japan*, **112**, Supplement, 89–99 (in Japanese).

Kozur, H. (1984) New radiolarian taxa from the Triassic and Jurassic. *Geologisch-Paläontlogische Mitteilungen Innsbruck*, **13**, 49–88.

Kozur, H. (1985) The radiolarian genus Eoxitus n. gen. from the *Unuma echinathus* Zone (Bajocian) of the northern Hungary. *Proceedings of the Koninklijke Nederlandse Akademie van Wetenschappen, series B*, **88**, 211–220.

Majidifard, M. (2003) Biostratigraphy, lithostratigraphy, ammonite taxonomy and microfacies analysis of the Middle and Upper Jurassic of northeastern Iran. *Dissertation zur Erlangung des Naturwissenschaftlichen Doktorgrades Der Bayerischen Julius-Maximilians-Universität Würzburg*, **2003**, 1–201.

Matsuoka, A. (1995) Jurassic and Lower Cretaceous radiolarian zonation in Japan and in the western Pacific. *The Island Arc*, **4**, 140–153.

Matsuoka, A. and Yao, A. (1986) A newly proposed radiolarian zonation for the Jurassic of Japan. *Marine Micropaleontology*, **11**, 91–105.

Matsuoka, A. and Ito, T. (2019) Updated radiolarian zonation for the Jurassic in Japan and the western Pacific. *Science Reports of Niigata University (Geology)*, **34**, 49–57.

Matsumoto, T. and Nishizono, Y. (1985) *Decipia* from the Ebirase Formation of Kyushu. *Journal of Geolological Society of Japan*, **91**, 421–423 (in Japanese).

Müller, J. (1858) Einige neue bei St. Tropezam Mittelmeer beobachetete Polycystinen und Acanthometren. *Königlich-Preußische Akademie der Wissenschaften zu Berlin, Monatsberichte*, Jahrgang **1858**, 154–155 (in German).

Nakada, K and Matsuoka, A. (2009) On the Pliensbachian/ Toarcian boundary in the Lower Jurassic Toyora Group in southwest Japan. *Volumina Jurassica*, **7**, 47–54.

Nakada, K. and Matsuoka, A. (2011) International correlation on the Pliensbachian/Toarcian (Lower Jurassic) ammonoid biostratigraphy of the Nishinakayama Formation in the Toyora Group, Southwest Japan. *Newsletter on Stratigraphy*, **44**, 89–111.

Nagai, H. and Mizutani, S. (1990) Jurassic *Eucyrtidiellum* (radiolaria) in the Mino terrane. *Transactions and Proceedings of the Palaeontological Society of Japan, New Series*, **159**, 587–602.

Nishizono, Y. (1996) Mesozoic convergent process of the Southern Chichibu Terrane in West Kyushu, Japan, on the basis of Triassic to Early Cretaceous radiolarian biostratigraphy. *Kumamoto Journal of Science, Earth Sciences*, **14**, 45–226 (in Japanese with English abstract).

Nishizono, Y., Sato, T. and Murata, M. (1997) A revised Jurassic radiolarian zonation for the South Belt of the Chichibu terrane, western Kyushu, Southwest Japan. *Marine Micropaleontology*, **30**, 117–138.

Ozvoldova, L. (1975) Upper Jurassic radiolarians from the Kisuca Series in the Klippen Belt. *Západné karpaty, Séria Paleontologia*, **1**, 73–86.

Ozvoldova, L. (1979) Radiolarian assemblage of radiolarian cherts of Podbiel locality (Slovakia). *Casopis pro Mineralogii a Geologii*, **24**, 249–261.

Ozvoldova, L. and Faupl, P., (1993) Radiolarien aus kieseligen Schichtgliedern des Juras der Grestener und Ybbsitzer Klippenzone (Ostalpen, Niedrösterreich). *Jahrbuch der Geologischen Bundesanstalt*, **136**, 479–494 (in German with English abstract).

Pessagno, E. A. (1976) Radiolarian zonation and stratigraphy of the Upper Cretaceous portion of the Great Valley Sequence, California Coast Ranges. *Micropaleontology Special Publication*, **2**, 1–95.

Pessagno, E. A. (1977) Upper Jurassic radiolarian biostratigraphy of the California Coast Ranges. *Micropaleontology*, **23**, 56–113.

Pessagno, E. A. and Whalen, A. P. (1982) Lower and Middle Jurassic radiolaria (multicyrtid Nassellariina) from California, east-central Oregon and the Queen Charlotte Islands, B.C. *Micropaleontology*, **28**, 111–169.

Pessagno, E. A., Blome, C. D., Hull, D. M. and Six, W. M. (1993) Jurassic radiolaria from the Josephine ophiolite and overlying strata, Smith River subterrane (Klamath Mountains), northwestern California and southwestern Oregon. *Micropaleontology*, **39**, 93–166.

Riedel, R. (1967) Some new families of radiolaria. *Proceedings of the Geological Society of London*, **1640**, 148–149.

Rüst, D. (1885) Beiträge zur Kenntniss der fossilen Radiolarien aus Gesteinen des Jura. *Palaeontographica*, **31**, 269–321 (in German).

Sandoval, J., O' Dogherty, L. and Guex, J. (2001) Evolutionary rates of Jurassic ammonites in relation to sea-level fluctuations. *Palaios*, **16**, 311–335.

Sano, K. and Kashiwagi, K. (2015) The comparison of Middle to Late Jurassic, shallow-marine radiolarian assemblages between the Inner and Outer zones of Southwest Japan. *Proceedings of 164th Regular Meeting of Palaeontological Society of Japan*, 48 (in Japanese).

Shikama, T. and Hirano, H. (1970) On the mode of occurrence of ammonites in the Nishinakayama Formation, Toyora Group. *Science Reports of Yokohama National University, Section 2*, **16**, 61–71.

Suzuki, H. and Gawlick, H. (2003) Biostratigraphie und Taxonomie der Radiolarien aus den Kieselsedimenten der Blaa Alm und nördlich des Loser (Nördliche Kalkalpen, Callovium-Oxfordium). *Mitteilungen der Gesellschaft der Geologie und Bergbaustudenten Österreichs*, **46**, 137–228 (in German with English abstract).

Suzuki, H. and Gawlick, H. (2009) Jurassic radiolarians from cherty limestones below the Hallstatt salt mine (Northern Calcareous Alps, Austria). *Neues Jahrbuch für Geologie und Paläontologie, Abhandlungen*, **251**, 155–197.

Suzuki, H., Prinz, P. and Schmidt-Effing, R. (2002) Radiolarien aus dem Grenzbereich Hettangum/ Sinemurium von Nordperu. *Paläontologische Zeitschrift*, **76**, 163–187 (in German with English abstract).

Tan, S. H. (1927) Over de samenstelling en het ontstaan van krijten mergel-gesteenten van de Molukken. *Jaarboek van het Mijinwezen in Nederlandsch Oost-Indië*, **55**, 5–165 (in Dutch).

Takemura, A. (1986) Classification of Jurassic Nassellarians (radiolaria). *Palaeontographica, Abteilung A: Palaozoologie- Stratigrahie*, **195**, 29–74.

Takemura, A. and Nakaseko, K. (1986) The cephalic skeletal structure of Jurassic "*Eucyrtidium*" (radiolaria). *Journal of Paleontology*, **60**, 1016–1024.

Tanabe, K. (1991) Early Jurassic macrofauna of the oxygen-depleted epicontinental marine basin in the Toyora area West Japan. *Saito Ho-on Kai Special Publication*, no. 3, 147–161.

Toriyama, R. (1938) Geology of the Toyora Group in the Toyora Country, Yamaguchi Prefecture. *Journal of Geological Society of Japan*, **45**, 247–258 (in Japanese).

Wisniowski, T. (1889) Beitrag zur Kenntniss der Mikrofauna aus den oberjurassischen Feuersteinknollen der Umgegend von Krakau. *Jahrbuch der Kaiseriche-Königlichen Geologischen Reichsanstalt*, **38**, 657–702 (in German).

Yao, A. (1979) Radiolarian fauna from the Mino Belt in the northern part of the Inuyama area, central Japan. Part 2: Nassellaria 1. *Journal of Geosciences, Osaka City University*, **22**, 21–72.

Yao, A. (1982) Middle Triassic to Early Jurassic radiolarians from the Inuyama area, central Japan. *Journal of Geosciences, Osaka City University*, **25**,

53–70.
Yao, A. (1990) Triassic and Jurassic radiolarians. *Pre-Cretaceous terranes of Japan*, Publication of IGCP Project no. 224, Osaka, 329–345.
Yao, A. (1997) Faunal change of Early–Middle Jurassic radiolarians. *News of Osaka Micropaleontologist, Special Volume*, no. 10, 155–182 (in Japanese with English abstract).
Yokoyama, M. (1902) Jurassic ammonites from Echizen and Nagato. *Journal of the College of Science, Imperial University of Tokyo,* **14**, 1–17.

Recieved January 10, 2019
Accepted May 26, 2020
Published on-line August 21, 2020

西南日本，山口県に分布するアンモナイトを含む豊浦層群から産出した放散虫

西園　幸久・米光　功雄

要　旨

豊浦層群は西南日本山口県に分布する日本における下部－中部ジュラ系模式地の一つであり，アンモナイト化石を多産する．しかし，放散虫のような微化石の報告は今まで知られていない．豊浦層群最上部 7 か所から *Transhsuum hisuikyoense* 帯および *Striatojaponocapsa plicarum* 帯の放散虫を見出した．これらの放散虫は，中期ジュラ紀 Aalenian から Bathonian を指示すると考えられる．この放散虫指示年代は，アンモナイトやイノセラムスで決定された地質年代よりもやや古い．先行研究によれば *Stj. plicarum* の初出現年代は，Aalenian と Bajocian の境界付近と推定されているにすぎない．この課題を検討するためには，アンモナイトと放散虫の産出間隙から Aalenian を指示するアンモナイトのような化石資料のさらなる蓄積が必要である．

Bulletin of the Geological Survey of Japan, vol. 71 (4), p. 297–312, 2020

Report

Radiolarian age of Triassic striped chert within the Jurassic accretionary complex of the Ashio terrane in the Ashikaga area, Tochigi Prefecture, central Japan

ITO Tsuyoshi[1,*]

ITO Tsuyoshi (2020) Radiolarian age of Triassic striped chert within the Jurassic accretionary complex of the Ashio terrane in the Ashikaga area, Tochigi Prefecture, central Japan. *Bulletin of the Geological Survey of Japan*, vol. 71(4), p. 297–312, 9 figs, 1 table.

Abstract: A striped structure within a single chert bed has been observed in the Tamba–Mino and Ashio terranes, Jurassic accretionary complexes of the Inner Zone of Southwest Japan. This study reports striped chert beds in four sections of the Ashio terrane in Ashikaga and Sano cities of Tochigi Prefecture, namely, Hikoma, Oiwa, Tsukiya and Orihime sections, and their radiolarian ages, except for the Hikoma section. The striped chert comprises streaks and spacing. The streak indicates a thin part of a pin-striped structure within a chert bed and consists mainly of clay minerals. The spacings indicate a thick part between the streaks and is composed mainly of cryptocrystalline quartz. The Oiwa section, which contains numerous striped chert beds, partially corresponds to the middle Carnian–middle Norian (Upper Triassic). The Tsukiya and Orihime sections, which include a few striped chert beds, partially correspond to the middle–upper Anisian (Middle Triassic) and upper Norian–lower Rhaetian (Upper Triassic), respectively.

Keywords: radiolaria, accretionary complex, Ashio terrane, striped chert, Triassic

1. Introduction

Chert is a hard and dense microcrystalline or cryptocrystalline sedimentary rock (Bates and Jackson, 1984) and is one of the major components of Jurassic accretionary complexes (ACs) of East Asia. The age of chert had not been determined because index fossils were unobtainable. Extraction methods for microfossils such as conodont and radiolaria had been proposed in the 1960s to 1970s (e.g. Hayashi, 1968, 1969; Pessagno and Newport, 1972). This development made microfossils valuable age indexes and allowed the age of the Jurassic ACs to be clarified in the strata which had been treated as the Paleozoic (e.g. Yao and Mizutani, 1993; Isozaki *et al.*, 2010; Agematsu-Watanabe and Kamata, 2018). The age of chert within the Jurassic ACs ranges from Pennsylvanian (Carboniferous) to Late Jurassic (e.g. Matsuoka *et al.*, 1998; Nakae, 2000).

As stated above, microfossils within chert such as radiolaria are valuable index fossils. However, they cannot be always obtained from chert because of several reasons such as the diagenetic effect. The determination of an alternative age index for chert would be valuable for the investigation of geologic units without fossils.

The author discovered a striped structure within a single chert bed in the Ashikaga area of Tochigi Prefecture, Japan. The structure was reported from the Tamba–Mino and Ashio terranes in the previous studies (e.g. Iijima *et al.*, 1978; Kido, 1982; Yoshimura *et al.*, 1982; Kakuwa, 1991; Nikaido and Matsuoka, 2008, 2009, 2011). Based on these previous studies, the occurrences of the striped chert might be dominant in a specific age.

This study describes the striped chert beds in the Ashikaga area and determines their microfossil ages. Furthermore, the ages of striped chert reported in the previous studies are compiled for future references. This information would contribute to the discussion about the potential of the striped chert as an alternative age index for the Jurassic ACs in the Tamba–Mino and Ashio terranes.

2. Previous studies on the striped structure and terminology

Structures within chert beds were described in several international studies, particularly in the 1970s (e.g. Davis, 1918; Bastin, 1933; McBride and Thomson, 1970; Folk, 1973; Lowe, 1976; McBride and Folk, 1979). A research group from the University of Tokyo studied structures within the chert beds within the Jurassic ACs of Southwest Japan in the 1970s to early 1990s (e.g. Iijima *et al.*, 1978, 1979, 1985; Iijima and Utada, 1983; Kakuwa, 1991). Imoto (1983, 1984a, 1984b) focused on several characteristics

[1] AIST, Geological Survey of Japan, Research Institute of Geology and Geoinformation

[*] Corresponding author: ITO, T., Central 7, 1-1-1 Higashi, Tsukuba, Ibaraki 305-8567, Japan. Email: ito-t@aist.go.jp

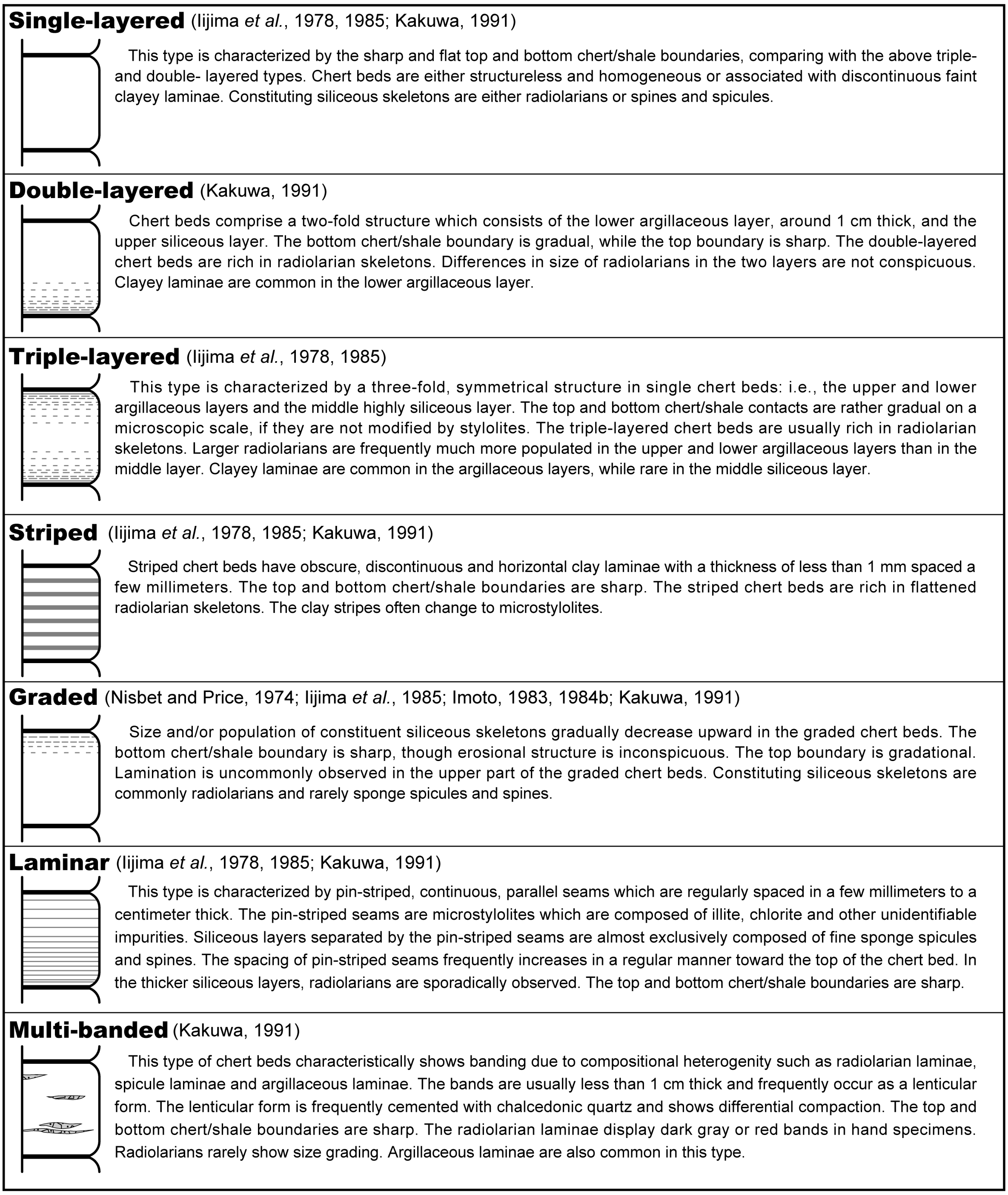

Fig. 1 Classification of the structure within a single chert bed based on previous studies with their characteristics and simplified images. The simplified images are based on Iijima and Utada (1983) and Kakuwa (1991). The characteristics of each structure are from Kakuwa (1991).

of chert, such as color and bed thickness, and classified their differences by age. Sugiyama (1997) classified chert into two types: B-type chert rather argillaceous and rich in siliceous organic remains; F-type chert highly silicified with very rare organic remains. The B- and F-types sensu Sugiyama (1997) can be corresponded to the B- and F-types sensu Imoto (1984b), respectively. Furthermore, Sugiyama (1997) proposed A-type alternating occurrences of B- and F-type chert beds within short interval (ca. less than 1 m).

Figure 1 shows classification of structures within chert bed and their images in the previous studies. Iijima *et al.* (1978) recognized four types of single chert beds showing the Triassic age: single-layered, triple-layered, laminar

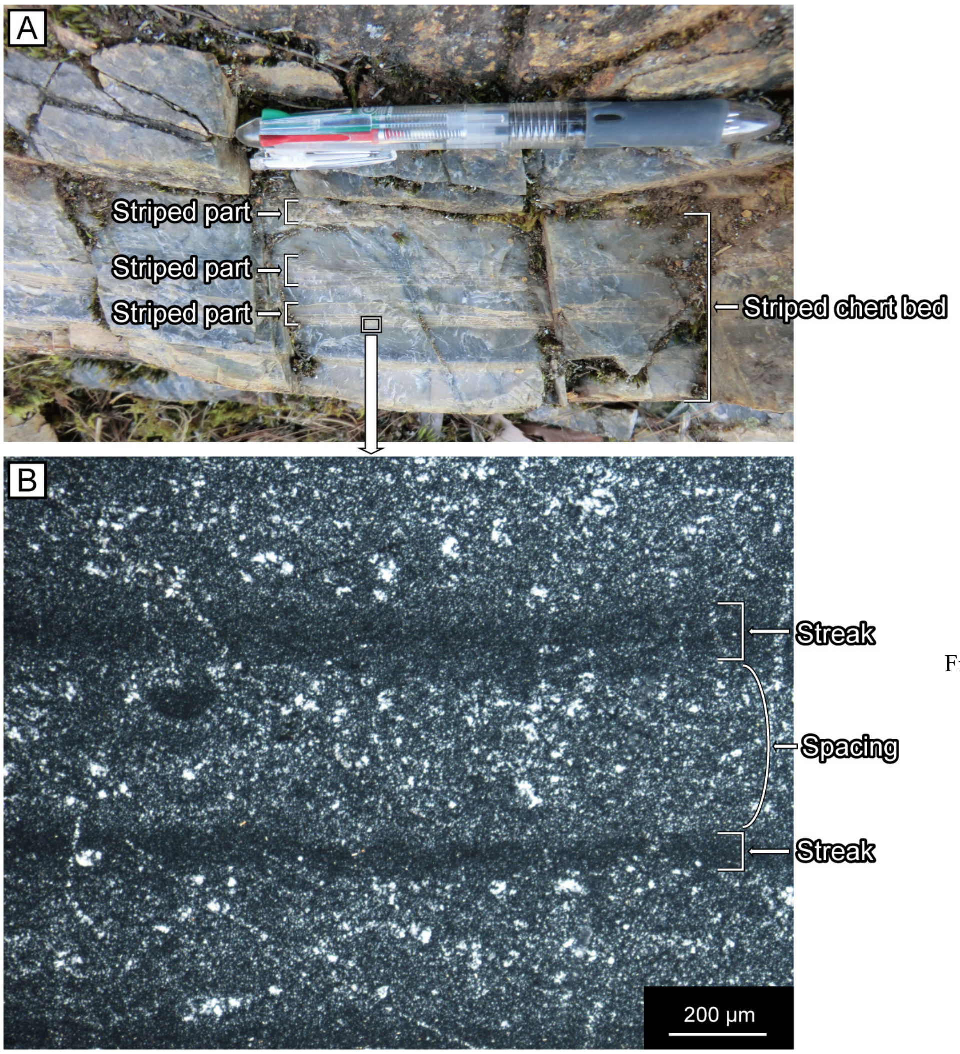

Fig. 2 Terminology of the description in this study. Field occurrence (A) and thin section (B) are from the lower part of the Tsukiya section. Striped chert bed: chert bed including striped part(s). Striped part: dominant part of the pin-striped structures. Streak: thin part of the pin-striped structure within the striped part. Spacing: a thick part between two streaks.

and striped. Iijima and Utada (1983) and Iijima *et al.* (1985) compiled siliceous rocks from Japan and reported a new graded type of single chert beds. Furthermore, Kakuwa (1991) recognized two additional types of chert beds: double-layered and multi-banded. Kakuwa (1991) synonymized the stylolite chert sensu Yoshimura *et al.* (1982) with the laminar chert. Sugiyama (1997) noted that the B-type is predominated by single-layered chert, whereas F-type by various degrees of triple-layered, striped and laminar types of Kakuwa (1991). Nikaido and Matsuoka (2009) described striped chert and classified them into three types according to the thickness changes of spacings between streaks in single chert beds: constant in thickness, thinning upward and thickening upward.

Both striped and laminar chert is characterized by having horizontal clay lamina-like structure (Kakuwa, 1991). Based on the description by Kakuwa (1991), the major difference between the striped and laminar chert is richness of the radiolarian skeletons. However, it can be greatly affected by secondary factors such as a surrounding igneous activity. The lamina-like structure of the striped chert often changes to microstylolite, and those of the laminar chert do likewise. This article regards the laminar chert as a type of the striped chert, i.e. the striped chert that has stylolite and less radiolarian skeletons with thickening-upward spacing is the laminar chert. The previous studies also used the name of "varved chert" (Yamada *et al.*, 1985; Mizutani and Koido, 1992; Nakano *et al.*, 1995); however, the term of "varve" is an annual layer and has a petrogenetic meaning. For these reasons, the stylolite and varved chert are used synonymously with the striped chert in this study.

The terminology of the description in this article is shown in Fig. 2. Striped chert bed is a chert bed including the striped part(s) (Fig. 2A). The striped part is dominant part of the pin-striped structures composed of streaks and spacing (Fig. 2B). The streak indicates a thin part of the pin-striped structure. The spacing indicates a thick part between the streaks.

3. Geologic setting

The Tamba–Mino and Ashio terranes are distributed over the Inner Zone of Southwest Japan (Nakae, 2000;

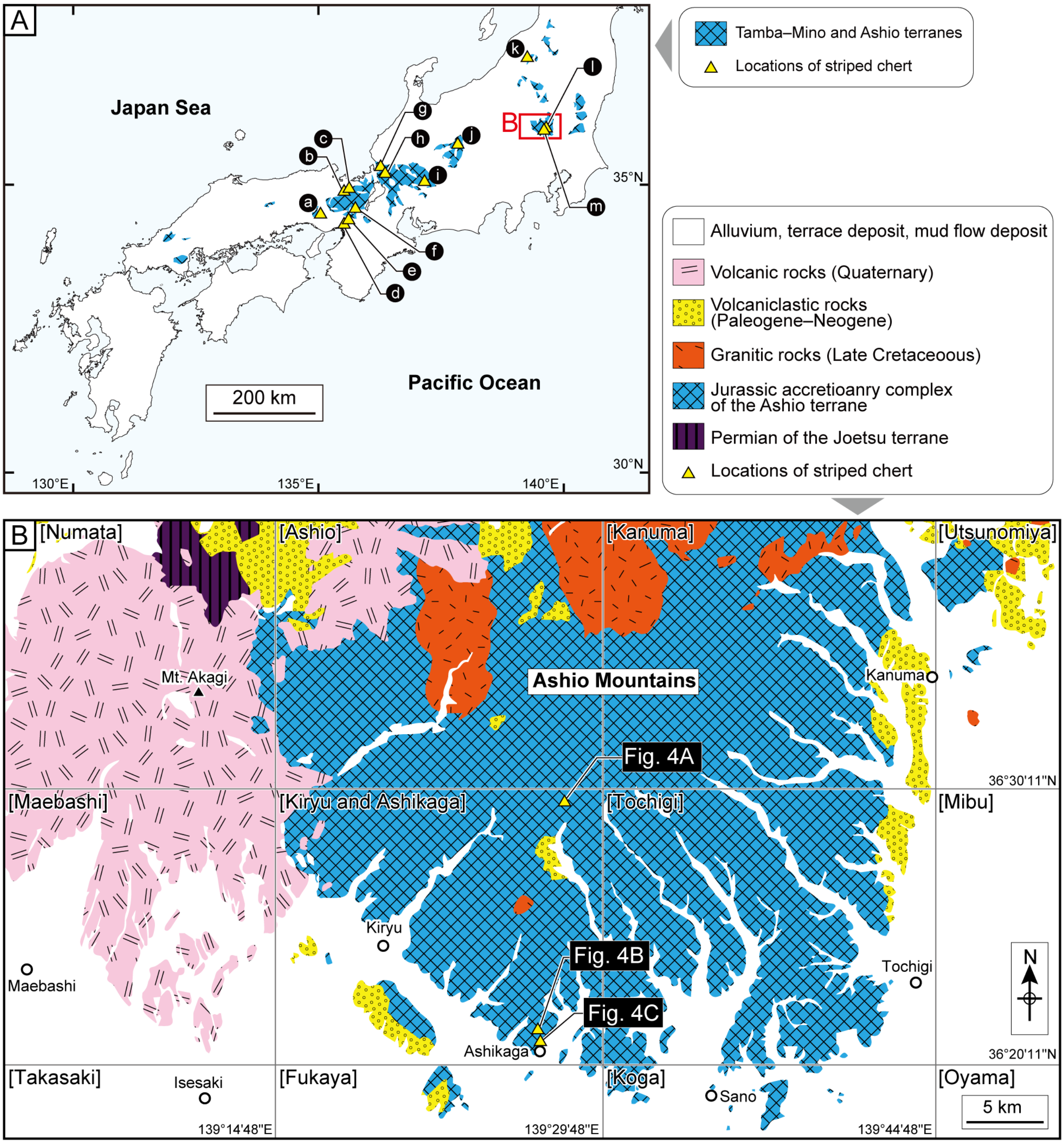

Fig. 3 Index maps of the study area. (A) Distribution of the Tamba–Mino and Ashio terranes (modified from Geological Survey of Japan, AIST, 2018) with locations of striped and related chert in the present and previous studies. The alphabets of lower-case within the black circle correspond to the locations (Loc.) shown in Table 1. (B) Simplified geologic map of the Ashio terrane in the Ashio Mountains (modified after Sudo *et al.*, 1991; Geological Survey of Japan, AIST, 2018). The geographical names in brackets indicate 1:50,000 topographic maps published by the Geospatial Information Authority of Japan.

Kojima *et al.*, 2016) (Fig. 3A). The Tamba–Mino terrane corresponds to the Ashio terrane. The terranes are mainly composed of late Carboniferous–Permian ocean ridge basalt and pelagic carbonate, late Carboniferous–Jurassic pelagic chert, Jurassic hemipelagic siliceous mudstone and trench-fill clastics, such as mudstone and sandstone (e.g. Nakae, 2000).

The components of the Ashio terrane are exposed in the Ashio Mountains in central Japan (Fig. 3B). The occurrences of microfossils such as radiolaria and conodont have been reported in this area since the 1960s (e.g. Hayashi, 1963, 1968; Koike *et al.*, 1971; Hayashi and Hasegawa, 1981; Aono, 1985; Kamata, 1996, 1997; Takayanagi *et al.*, 2001; Ito, 2019, 2020).

Kamata (1996) divided the Ashio terrane of the Ashio Mountains into three tectonostratigraphic units, namely, the Kuzu, Kurohone–Kiryu and Omama complexes. The Kuzu Complex is characterized by coherent facies and is mainly composed of repeated chert–clastic sequences with basalt–limestone blocks. The Kuzu Complex can be subdivided into three units: 1, 2 and 3 (Kamata, 1997). The Omama and Kurohone–Kiryu complexes are characterized by mixed facies that is represented by muddy mixed rocks including several types and sizes of blocks. Both complexes include chert, limestone and sandstone blocks. The Omama Complex contains large amounts of basalt and limestone, whereas the Kurohone–Kiryu Complex includes small amounts of these rocks.

4. Striped chert in the Ashikaga area

4. 1 Study sections

This study investigated four sections in Sano and Ashikaga cities, Tochigi Prefecture (Fig. 4). The Hikoma, Tsukiya, Orihime and Oiwa sections include one to several striped chert beds (Fig. 5). According to the tectonostratigraphic division by Kamata (1996) and the geological maps of Sudo *et al.* (1991), the Hikoma section is located in the distributional area of the Kurohone–Kiryu Complex, whereas the Oiwa, Tsukiya and Orihime sections in unit 3 of the Kuzu Complex. The chert of all sections predominantly corresponds to the F-type chert sensu Imoto (1984b) and Sugiyama (1997).

The Hikoma section crops out along the prefectural road 208 in Hikoma, Sano City (Fig. 4A). The total stratigraphic thickness of this section is about 4 m. The chert in this section is generally dark-gray and weakly bedded. The single bed thickness of the individual chert is 5–15 cm and accompanies claystone with sizes less than 1 mm. One striped chert bed is interbedded.

The Oiwa section is exposed on a hiking trail in Oiwa-cho, Ashikaga City and is located above the Oiwa Tunnel (Fig. 4B). The total stratigraphic thickness of this section is about 15 m. The chert from this section is generally bright-gray and clearly bedded. The single bed thickness of the individual chert is 3–15 cm and accompanies claystone with sizes less than 1 mm. Numerous striped chert beds can be observed in this section. The lower part of this sequence is folded.

The Tsukiya section crops out along a road in Tsukiya-cho, Ashikaga City (Fig. 4B). The total stratigraphic thickness of this section is about 2 m. The chert of this section is generally gray and clearly bedded. The single bed thickness of the chert is 3–15 cm and accompanies claystone with sizes less than 1 mm. The gray chert includes a 1–2 cm wide black-colored part. Five striped chert beds are observed.

The Orihime section crops out along the road to the Orihime-jinja Shrine in Nishinomiya-cho, Ashikaga City (Fig. 4C). The total stratigraphic thickness of this section is about 3 m. The chert from this section is generally gray to dark-gray and bedded. The single bed thickness of the gray chert is 5–10 cm and accompanies claystone with sizes less than 1 mm. Four striped chert beds are observed. Folded chert is recognized in the middle part.

4. 2 Characteristics of striped chert

The striped chert is continuously and laterally distributed, at least at the outcrop (Fig. 6A, B). The maximum thickness of the streaks is about 1 mm (Fig. 6C). The streaks are almost parallel to the bed surface (Fig. 6B, C). A large amount of the striped chert is observed in the Oiwa section (Fig. 6D). The streaks are also folded by a small fault within the bed (Fig. 6E).

The color of the streaks are generally paler than the spacings at the outcrop. For example, the streaks in the Tsukiya and Oiwa sections are caramel color whereas the spacings are dark-gray (Fig. 6). However, marginal parts of the spacings along the streaks represent paler color like the streaks. Consequently, the color of the streaks may be due to fading during the diagenesis.

The thin section observations indicate that the striped chert is composed of cryptocrystalline quartz and a few clay minerals (Fig. 7). The streaks are almost parallel (Fig. 7A, B), and the thickness of the spacing between the streaks is several hundred micrometres. The streaks are composed mainly of clay minerals; the spacings consist mainly of cryptocrystalline quartz. The streaks are composed of finer material than that found in the spacing (Fig. 7B, C). The streaks are stylolitic in some samples (Fig. 7D, E). The stylolitic seam is about 5 μm in thickness and is slightly undulated.

5. Microfossil occurrence and age assignment

A total of 17 chert samples were collected from the study sections. The following methods were used to extract microfossils from the samples. The samples were crushed into about 1 cm fragments and then soaked in hydrofluoric acid (ca. 5 %) at room temperature (ca. 20 °C–25 °C) for 24 h. The residues were collected using a sieve with a mesh diameter of 0.054 mm and then enclosed within a slide prepared with a photocrosslinkable mounting medium (GJ-4006, Gluelabo Ltd.). The slides were analyzed using a transmitted light microscope and then photographed. Several specimens from the residues were mounted on stubs, analyzed and then photographed using scanning electron microscopy.

Six chert samples, including one striped chert sample, were collected from the Hikoma section. However, microfossils for age determination could not be obtained from these samples.

Four samples of striped chert were collected from the Oiwa section. Two samples (IT18101413 and IT18101415) yielded radiolarian remains. The twisted spine (Fig. 8A) from sample IT18101413 resembles a spine of *Capnuchosphaera deweveri* Kozur and Mostler. On the basis of the occurrence range of Sugiyama

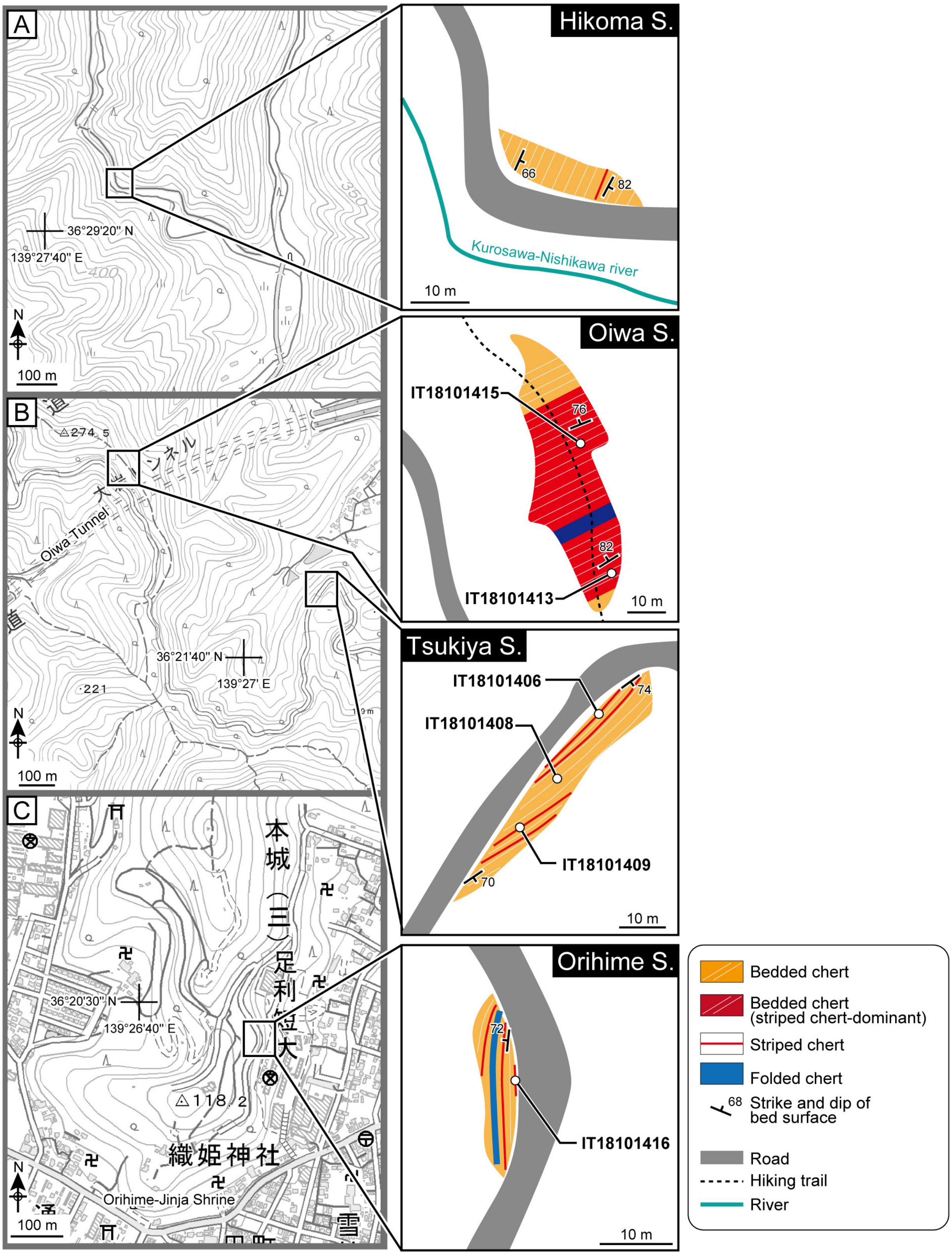

Fig. 4 Traverse maps of sections studied in this article. The maps are modified from the 1:25000 map of 'Bamba' and 'Ashikaga-Hokubu' by the Geospatial Authority of Japan. S.: section.

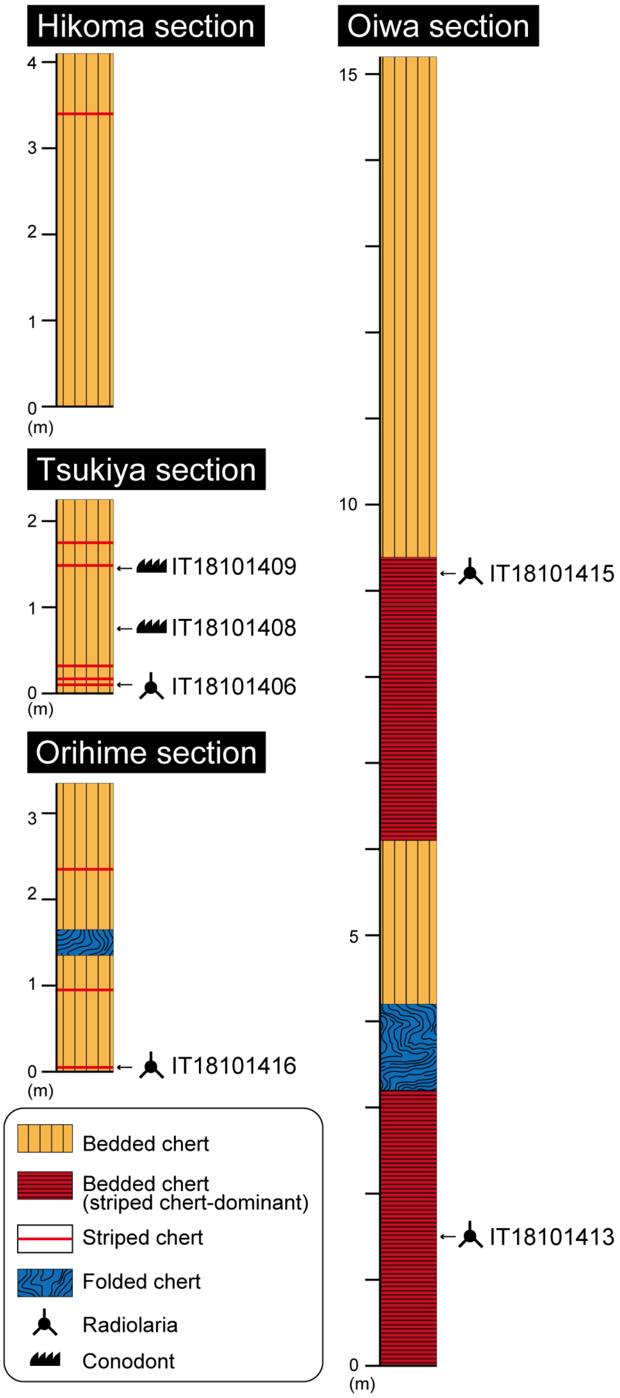

Fig. 5 Columnar illustration of the studied sections with microfossil horizons.

(1997), *C. deweveri* occurred in the *Capnuchosphaera* Lowest-Occurrence Zone (TR5A) to the *Trialatus robustus*–*Lysemelas olbia* Partial-Range Zone (TR6B). The results of this study indicate that sample IT 18101413 corresponds to the middle Carnian–middle Norian.

Six chert samples, including two striped chert samples, were collected from the Tsukiya section. Two chert samples (IT18101408 and IT18101409) yielded conodont fragments (Fig. 8B, C). One striped chert sample (IT18101406) yielded radiolarian fossils: *Paroertlispongus*? sp. (Fig. 8D), *Pararchaeospongoprunum*? sp. (Fig. 8E), twisted spine (Fig. 8F) and *Spinotriassocampe*? sp. (Fig. 8G). According to O'Dogherty *et al.* (2009), *Paroertlispongus*, *Pararchaeospongoprunum* and *Spinotriassocampe* occurred in the middle Anisian–lower Carnian, upper Permian–upper Anisian and middle Anisian–lower Carnian, respectively. Consequently, sample IT 18101406 might correspond to the middle–upper Anisian.

Two chert samples, including one striped chert sample, were collected from the Orihime section. Only one sample from the striped chert bed (IT18101416) yielded *Lysemelas* sp. cf. *L. olbia* Sugiyama (Fig. 8H). On the basis of the occurrence range reported by Sugiyama (1997), *L. olbia* occurred in the *L. olbia* Lowest-Occurrence Zone (TR7) to Skirt F Lowest-Occurrence Zone (TR8C). Sample IT 18101416 might correspond to the upper Norian–lower Rhaetian.

6. Ages of striped chert in other areas

6. 1 Tamba–Mino and Ashio terranes

Several researchers have noted the presence of the striped chert in the Tamba–Mino and Ashio terranes (Fig. 3A). In this chapter, the previous studies on the striped chert and their ages are reviewed (Table 1).

Kido (1982) described four sections including striped chert beds, namely, the Kashibara, Kamiaso Bridge, Hisuikyo and Hosobi-dani sections, and determined the ages of the former three sections. The striped chert bed in the Kashibara section is about 8 m below the sampling point of sample KC1 yielding *Praemesosaturnalis gracilis* Kozur and Mostler, which occurred in TR8A to TR8C (Sugiyama, 1997). One striped chert bed in the Kamiaso Bridge section is located between samples BC2 and BC3, which include several species of the genus *Pseudostylosphaera* Kozur and Mostler. *Pseudostylosphaera compacta* (Nakaseko and Nishimura) is observed in both samples, and *Pseudostylosphaera goestlingensis* (Kozur and Mostler) is observed in BC3. The occurrence range of the latter species is TR4A to TR5A (Sugiyama, 1997). Another chert bed in the Kamiaso Bridge section is located between samples BC4 and BC5. Sample BC5 yielded *Capnodoce sarisa* De Wever, which occurred in TR6A to TR7 (Sugiyama, 1997). One striped chert bed in the Hisuikyo section is about 5 m below sample HC1, which yielded *Yeharaia elegans* Nakaseko and Nishimura. The occurrence range of *Y. elegans* is TR3B to TR4A, Ladinian (Sugiyama, 1997). Another chert bed in the Hisuikyo section is located between samples HC2 and HC3. Sample HC2 yielded *Pentactinocarpus* sp. cf. *P. fusiformis* Dumitrica and sample HC3 yielded *Hexasaturnalis hexagonus* (Yao). *Pentactinocarpus fusiformis* occurred in TR3B (Sugiyama, 1997). Meanwhile, an occurrence range of *H. hexagonus* is from the late *Trillus elkhornensis* zone (JR2)

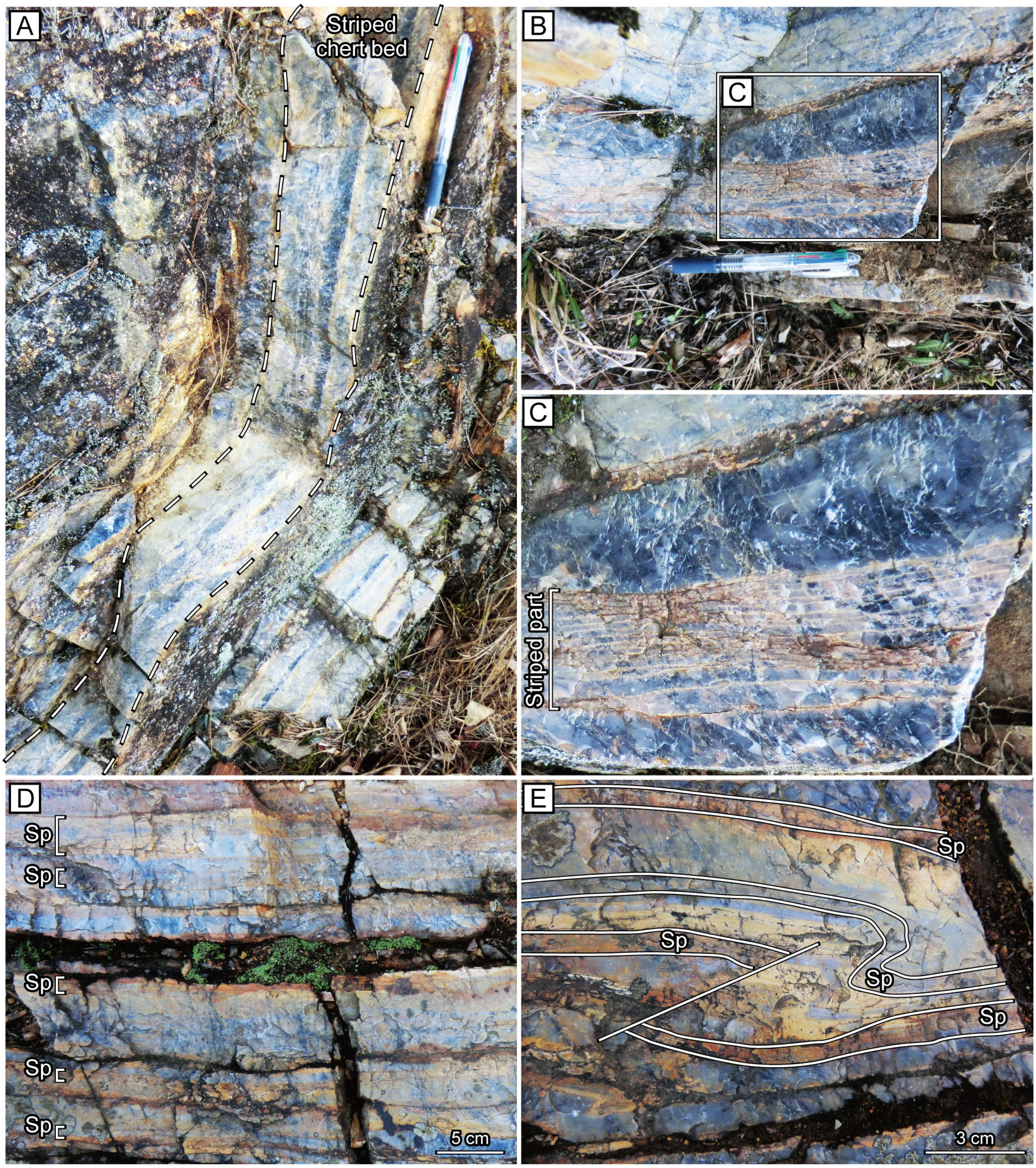

Fig. 6 Field occurrences of striped chert beds. (A) Laterally continuous striped chert beds from the lower part of the Tsukiya section. (B, C) Striped chert bed from the lower part of the Tsukiya section. The striped part is observed in the middle part within the striped chert bed. The bed surface and the streaks are almost parallel. (D) Bedded chert containing several striped parts (Sp) from the lower part of the Oiwa section. (E) Fold and fault within the chert bed and deformed striped parts (Sp) from the lower part of the Oiwa section. The streaks were deformed along the deformation of the chert beds by the fold and fault.

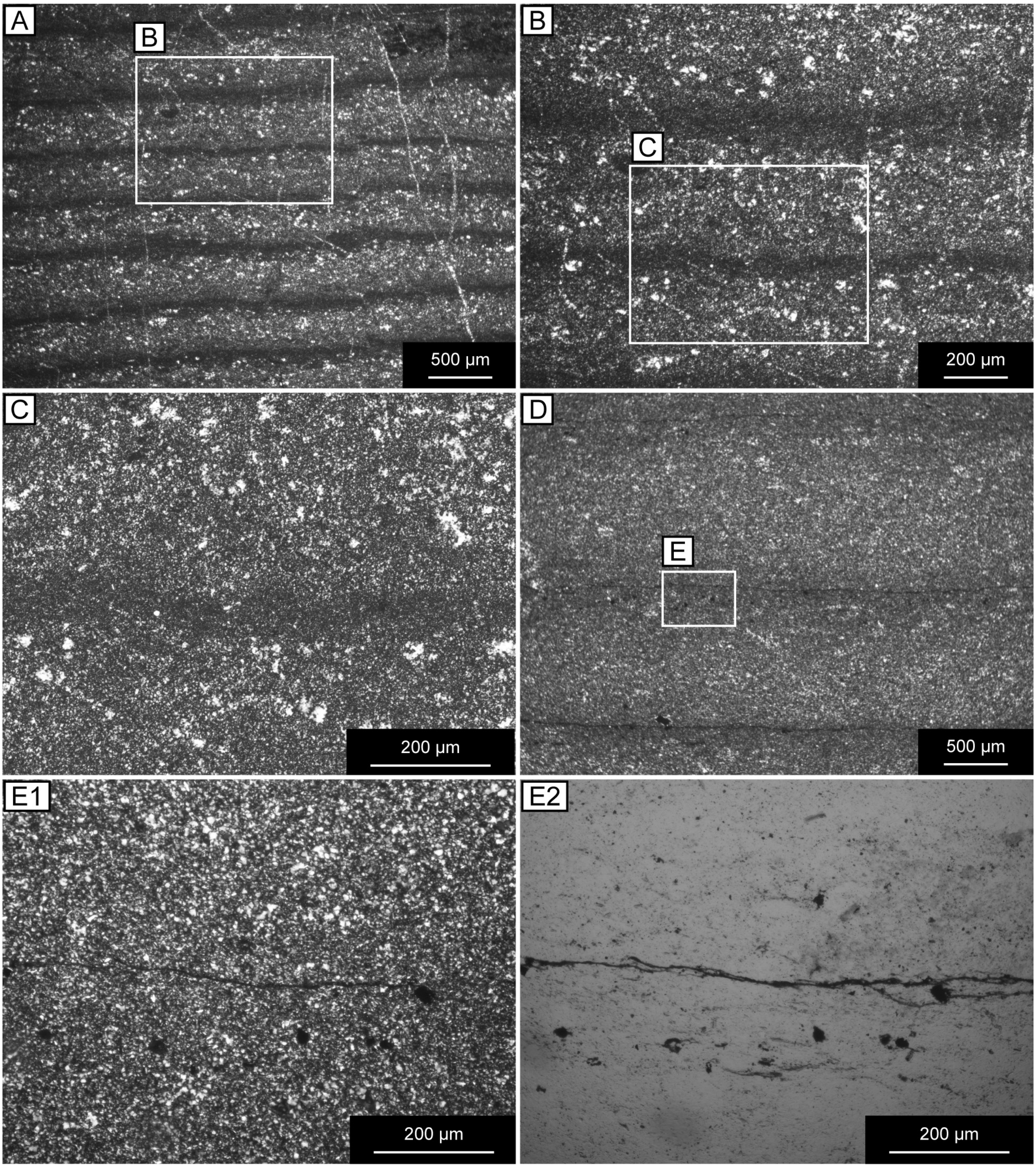

Fig. 7 Thin sections of the striped chert consisting of cryptocrystalline quartz and a few clay minerals. (A–C) Striped chert from the lower part of the Tsukiya section (sample IT18101406). The streaks are almost parallel. The thickness of the spacing is several hundred micrometres. The streaks are composed of finer material (mainly of clay minerals) than that found in the spacings. (D, E) Striped chert from the upper part of the Hikoma section (sample IT18101404). The streaks are stylolitic and slightly undulated in some samples. (A–D, E1) Crossed nicols. (E2) Open nicols.

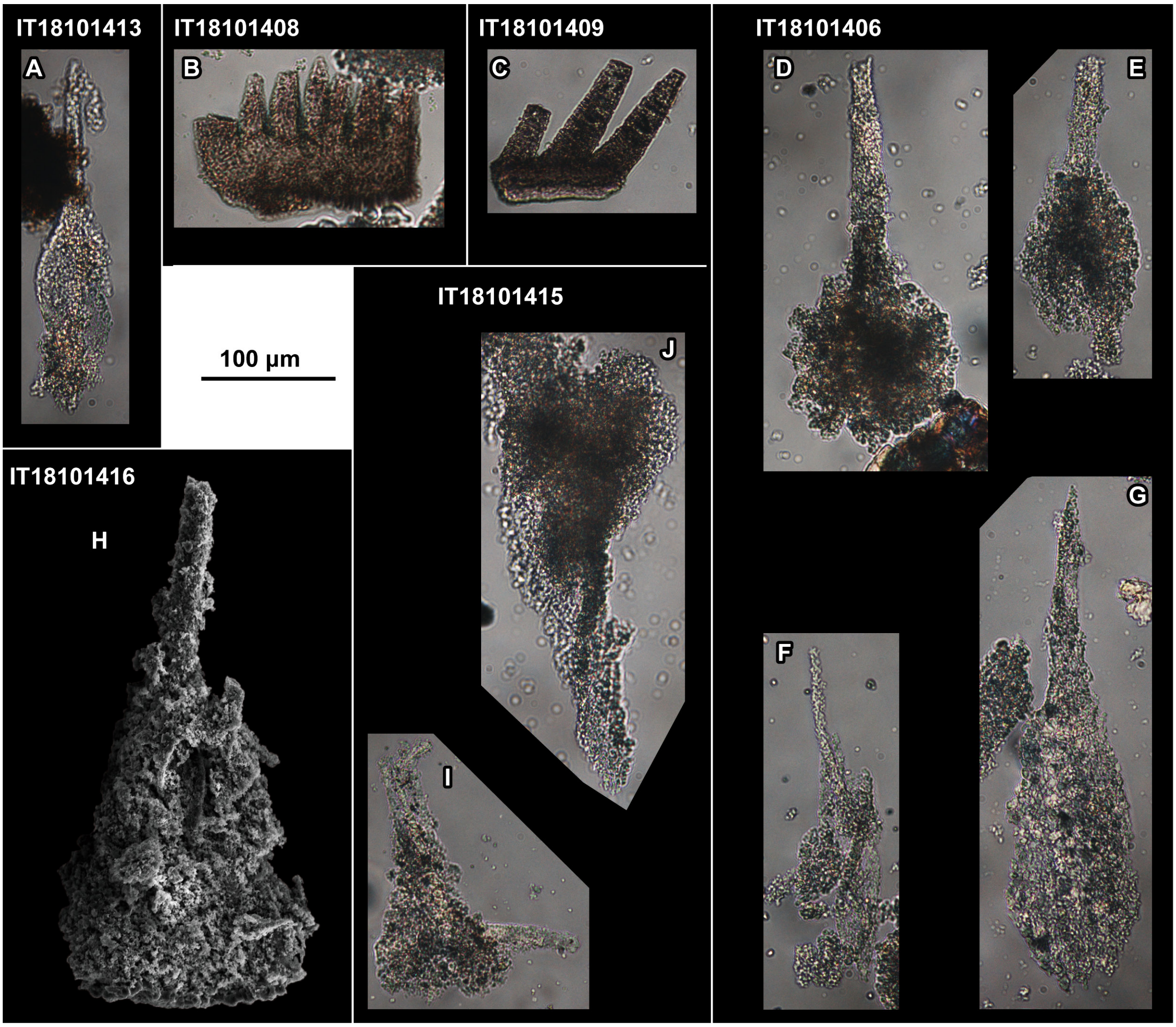

Fig. 8 Radiolarian and conodont fossils obtained from the studied sections. (A, F) Twisted spine. (B, C) Conodont fragment. (D) *Paroertlispongus*? sp. (E): *Pararchaeospongoprunum*? sp. (G) *Spinotriassocampe*? sp. (H) *Lysemelas* sp. cf. *L. olbia* Sugiyama. (I, J) Spumellaria gen. et sp. indet. with twisted spine.

to *Striatojaponocapsa plicarum* zone (JR4) (Matsuoka, 1995) corresponding to the Toarcian–middle Bathonian, late Early–Middle Jurassic (Matsuoka and Ito, 2019). Consequently, the age of the striped chert bed between samples HC2 and HC3 is some age between the Late Triassic and Early Jurassic.

Yoshimura *et al.* (1982) described "stylolitic chert" in the Imajo area of the Nanjo Massif, Fukui Prefecture. The age of the "stylolitic chert" was undetermined.

Imoto (1984a, b) studied Paleozoic and Mesozoic chert in the Tamba area. Imoto (1984b) noted that both Permian and Triassic–Jurassic chert contains sedimentary structures such as parallel lamination, and showed their photographs.

Yamada *et al.* (1985), Mizutani and Koido (1992) and Nakano *et al.* (1995) noted the presence of "varved chert". Yamada *et al.* (1985) stated that the age of the "varved chert" is the Triassic.

Kakuwa (1991) focused on structures within single chert beds and described them in several areas. Most of the striped chert beds of these sections correspond to the Triassic (Table 1). Among the sections including the striped chert beds studied by Kakuwa (1991), better ages were obtained from four sections by using conodont and radiolaria. The Koze section corresponds to the Spathian, Anisian and Norian; the Unuma section corresponds to the Norian; the Hisuikyo section corresponds to the Carnin–Rhaetian; and the Karasawa section corresponds to the Carnian.

The Sakahogi section, which is exposed along the Kiso River, mainly consists of successive Triassic bedded chert. Therefore, most researchers have studied this section and

Table 1 The description of the striped chert and related chert based on previous studies. The alphabets of lower-case in the locations (Loc.) correspond to Fig. 3A.

Reference	Loc.	Area or section	Chert description	Stage, Series and System
Kido (1982)	i	Kashibara section	Striped chert	Norian–Rhatian (Upper Triassic)
	i	Kamiaso Bridge section	Striped chert	Ladinian–Carnian (Middle–Upper Triassic)
	i	Hisuikyo section	Striped chert	Triassic–Jurassic?
	i	Hosobi-dani section	Striped chert	-
Yoshimura *et al*. (1982)	g	Imajo	Stylolitic chert	-
Imoto(1984b)	c	Yagi	Parallel lamination	middle Prmian and Triassic
Yamada *et al*. (1985)	j	Takayama	Varved chert	Upper Triassic
Kakuwa (1991)	d	Kinzoji section	Laminar chert	Triassic–Jurassic
	e	Kurio section	Laminar chert	Upper Triassic
	a	Kuwahara section	Striped chert	Triassic–Jurassic
	f	Okuhatcho section	Laminar chert; Striped chert	Triassic–Jurassic
	b	Ohtaki-kita section	Laminar chert	Triassic–Jurassic
	d	Koze sction	Striped chert	Spathian, Anisian, Norian (Lower, Middle and Upper Triassic)
	i	Unuma secion	Laminar chert	Norian (Upper Triassic)
	i	Hisuikyo section	Laminar chert	Carnin–Rhaetian (Upper Triassic)
	h	Kammuriyama section	Laminar chert	Triassic–Jurassic
	m	Yamamae section	Laminar chert	Triassic–Jurassic
	l	Karasawa section	Laminar chert; Striped chert	Carnin (Upper Triassic) and lower Jurassic
	k	Kuromatagawa section	Laminar chert	Triassic–Jurassic
Mizutani and Koido (1992)	i	Kanayama	Varved chert	-
Nakano *et al.* (1995)	j	Norikuradake	Varved chert	-
Nikaido and Matsuoka (2009)	i	Sakahogi section	Striped chert	upper Ladinian–upper Norian (Middle–Upper Triassic)
This study	m	Hikoma section	Striped chert	-
	m	Oiwa section	Striped chert	middle Carnian–middle Norian (Upper Triassic)
	m	Tsukiya section	Striped chert	upper Anisian (Middle Triassic)
	m	Orihime section	Striped chert	upper Norian–lower Rhaetian (Upper Triassic)

the surrounding area in detail (e.g. Sugiyama, 1997; Onoue *et al.*, 2012, 2016, 2017; Nozaki *et al.*, 2019). Nikaido and Matsuoka (2009) studied the stratigraphic distribution of the striped chert beds of the Sakahogi section and correlated it with the radiolarian zonation proposed by Sugiyama (1997). On the basis of the correlation, the first occurrence of the striped chert is TR4A, their dominant intervals are in TR5A to TR6B, and their last occurrence is observed in TR8A (Fig. 9).

6. 2 Permian and Jurassic ACs in other areas

Permian and Jurassic ACs other than the Tamba–Mino and Ashio terranes exist in the Japanese Islands such as the Akiyoshi terrane (Permian AC) of the Inner Zone of Southwest Japan, Chichibu composite terrane of the Outer Zone of Southwest Japan and the North Kitakami terrane of Northeast Japan (e.g. Kojima *et al.*, 2016). Furthermore, the Jurassic ACs extend to adjacent regions of Japan, such as Northeast China, Far Eastern Russia and the Philippines (e.g. Kojima and Kametaka, 2000). The occurrence of the striped chert in geologic units other than the Tamba–Mino and Ashio terranes is noted in this section for future reference.

According to the results of fieldworks (e.g. Ito and Matsuoka, 2018 and reference therein), the presence of striped chert beds has rarely been noted in the Chichibu composite terrane. The author discovered striped chert beds near Mt. Gusuku on Ie Island, Okinawa Prefecture. Although the age of the striped chert beds has not been determined, the chert in Ie Island ranges from upper Permian to Lower Jurassic (Shen *et al.*, 1996; Ito and Matsuoka, 2017). The author could not find the description of stripe chert beds from the North Kitakami terrane and corresponding geologic units in Northeast China and Far East Russia. The author studied the Akiyoshi terrane (Ito and Matsuoka, 2015, 2016); however, according to field works and the literature, striped chert beds have never been found.

Matsuoka (2002) and Matsuoka *et al.* (2009) noted a large number of striped chert beds in the North Palawan Block of the Philippines which is the southwestern extension of the Jurassic ACs on the Japanese Islands. Matsuoka *et al.* (2009) found Early Jurassic radiolarians from intervals of dominant striped chert beds in the North Palawan Block.

Previous studies proposed that global cyclic phenomena, such as the 20 kyr- to Myr-scale Milankovitch cycle, led to the rhythmical bedding of chert (e.g. Hori *et al.*, 1993; Ikeda *et al.*, 2010, 2017). Matsuoka *et al.* (2009), however, noted that the mm-scale striped structure within a single chert bed is probably related to shorter periodic events on ~kyr timescale. Therefore, other factors might have affected the formation of striped chert beds.

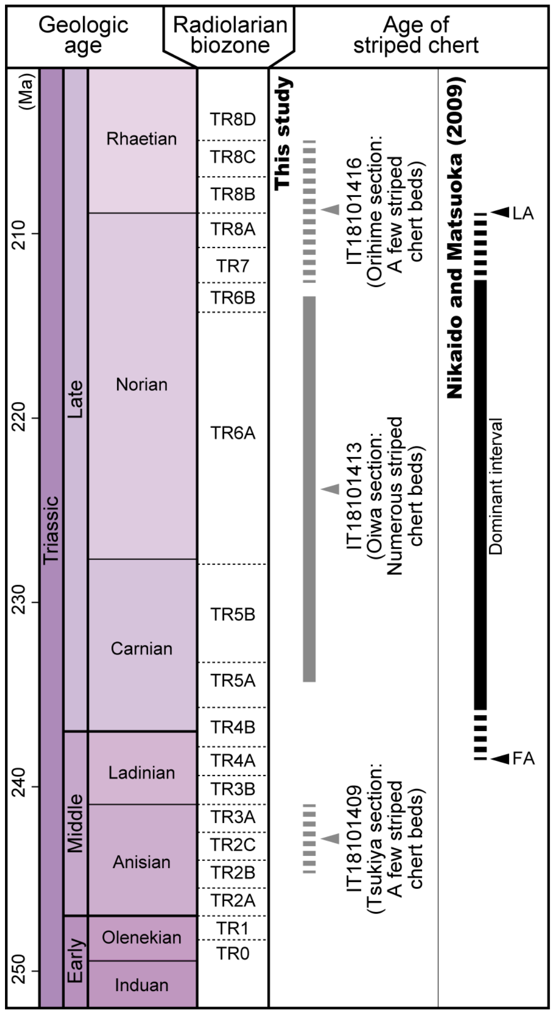

Fig. 9 Geologic time scale of the Triassic including the distribution of striped chert beds. Geologic time scale is after Ogg *et al.* (2016). Radiolarian biozones are after Sugiyama, 1997 and are partially modified based on the calibration by Yamashita *et al.* (2018).

7. Concluding remarks

The ages of the sections including the striped chert beds in the Ashikaga area were determined in this study. The Tsukiya and Orihime sections, including a few striped chert beds, correspond to the middle–upper Anisian and upper Norian, respectively. The Oiwa section, which contains numerous striped chert beds, corresponds to the middle Carnian–lower Norian. The results of the present study are consistent with the description of Nikaido and Matsuoka (2009) (Fig. 9). Likewise, the age determinations for other areas (e.g. Kido, 1982; Kakuwa, 1991) indicated that the striped chert beds are generally the Carnian–lower Norian.

Consequently, the striped chert might be used as an alternative age index, at least for studies in the Tamba–Mino and Ashio terranes. That is, several striped chert beds likely indicate the Triassic age, and the dominant interval of the striped chert beds is probably the Carnian–lower Norian. Meanwhile, a few striped chert beds correspond to the Permian (Imoto, 1984a) and Lower Jurassic (Kakuwa, 1991). Further descriptions and age assignments of striped chert beds, including petrogenetic work, will provide additional information on past ocean conditions.

Acknowledgments: This study was conceived from discussion with Prof. MATSUOKA Atsushi (Niigata University). The author thanks Dr. KAMATA Yoshihito (University of Tsukuba) for the comment on the earlier version of the manuscript; an anonymous reviewer and an editor, Dr. UCHINO Takayuki (Geological Survey of Japan, AIST) for the careful review and constructive suggestion that greatly improved the manuscript. The thin sections observed in this study (Fig. 7) were made by the thin section preparation laboratory at the Geological Survey of Japan.

References

Agematsu-Watanabe, S. and Kamata, Y. (2018) Recent progress in Paleozoic–Mesozoic microfossil research in deep-sea sediments of Japanese accretionary complexes: current status and future direction on study of radiolarians and conodonts. *The Journal of the Geological Society of Japan*, **124**, 951–965. (in Japanese with English abstract)

Aono, H. (1985) Geologic structure of the Ashio and Yamizo Mountains with special reference to its tectonic evolution. *Science Reports of the Institute of Geoscience, University of Tsukuba, Section B, Geological Sciences*, **6**, 21–57.

Bastin, E. S. (1933) Relations of cherts to stylolites at Carthage, Missouri. *Journal of Geology*, **41**, 371–383.

Bates, R. L. and Jackson, J. A. (1984) *Dictionary of Geological Terms: Third Edition (Rocks, Minerals and Gemstones)*. Anchor Books, New York.

Davis, E. F. (1918) The radiolarian cherts of the Franciscan Group. *University of California Publications, Bulletin of the Department of Geological Sciences*, **11**, 235–432.

Folk, R. L. (1973) Evidence for Peritidal Deposition of Devonian Caballos Novaculite, Marathon Basin, Texas. *AAPG Bulletin*, **57**, 702–725.

Geological Survey of Japan, AIST (2018) Seamless digital geological map of Japan 1: 200,000. January 26, 2018 version. Geological Survey of Japan, AIST. https://gbank.gsj.jp/seamless/v2full/ (Accessed:2018-1-26)

Hayashi, S. (1963) On the Conodonts newly discovered from the Ashio Mountains, central Japan. *Earth Science (Chikyu Kagaku),* **68**, 9–12. (in Japanese with English abstract)

Hayashi, S. (1968) The Permian conodonts in chert of the Adoyama Formation, Ashio Mountains, central Japan. Earth Science (Chikyu Kagaku), **22**, 63–77. (in Japanese with English abstract)

Hayashi, S. (1969) Extraction of conodont by HF methods*. *Fossil Club Bulletin*, **2**, 1–9. (in Japanese)

Hayashi, S. and Hasegawa, Y. (1981) Chichibu System in the Ashio Belt: Macrofossil- and conodont-based age (Part 2)*. *Studies on Late Mesozoic Tectonism in Japan*, **3**, 233–249. (in Japanese with English abstract)

Hori, R. S., Cho, C. F. and Umeda, M. (1993) Origin of cyclicity in Triassic–Jurassic radiolarian bedded cherts of the Mino accretionary complex from Japan. *The Island Arc*, **65**, 351–361.

lijima, A., Inagaki, H. and Kakuwa, Y. (1979) Nature and origin of the Paleogene cherts in the Setogawa Terrain, Shizuoka, central Japan. *Journal of the Faculty of Science, University of Tokyo, Section 2*, **20**, 1–30.

lijima, A., Kakuwa, Y., Yamazaki, K. and Yanagimoto, Y. (1978) Shallow-sea, organic origin of the Triassic bedded chert in central Japan. *Journal of the Faculty of Science, University of Tokyo, Section 2*, **19**, 369–400.

lijima, A., Matsumoto, R. and Tada, R. (1985) Mechanism of sedimentation of rhythmically bedded chert. *Sedimentary Geology*, **41**, 221–233.

Iijima, A. and Utada, M. (1983) Recent developments in sedimentology of siliceous deposits in Japan. *In* Iijima, A., Hein, J. R., Siever, R., eds., *Siliceous Deposits in the Pacific Region*. Elsevier, Amsterdam, 45–64.

Ikeda, M., Tada, R. and Sakuma, H. (2010) Astronomical cycle origin of bedded chert; a middle Triassic bedded chert sequence, Inuyama, Japan. *Earth and Planetary Science Letters*, **297**, 369–378.

Ikeda, M., Tada, R. and Ozaki, K. (2017) Astronomical pacing of the global silica cycle recorded in Mesozoic bedded cherts. *Nature Communications*, **8**, 15532.

Imoto, N. (1983) Sedimentary structures of Permian-Triassic cherts in the Tamba District. Southwest Japan. *In* Iijima, A., Hein, J. R., Siever, R., eds., *Siliceous Deposits in the Pacific Region*. Elsevier, Amsterdam, 377–394.

Imoto, N. (1984a) Late Paleozoic and Mesozoic cherts in the Tamba Belt, Southwest Japan (part 1). *Bulletin of Kyoto University of Education, Series B*, **65**, 15–40.

Imoto, N. (1984b) Late Paleozoic and Mesozoic cherts in the Tamba Belt, Southwest Japan (part 2). *Bulletin of Kyoto University of Education, Series B*, **65**, 41–71.

Isozaki, Y., Aoki, K., Nakama, T. and Yanai, S. (2010) New insight into a subduction-related orogen: A reappraisal of the geotectonic framework and evolution of the Japanese Islands. *Gondwana Research*, **18**, 82–105.

Ito, T. (2019) A report of Permian, Triassic, and Jurassic radiolarian occurrences from the Ashio terrane in the Hachioji Hills, eastern Gunma Prefecture, central Japan. *Bulletin of the Geological Survey of Japan*, **70**, 225–247.

Ito, T. (2020) A Cisuralian (early Permian) radiolarian assemblage and a new species of *Latentibifistula* Nazarov and Ormiston from central Japan. *Revue de Micropaléontologie*, **66**, 100407.

Ito, T. and Matsuoka, A. (2015) Imbricate structure of the Permian Yoshii Group in the Otakeyama area, Okayama Prefecture, southwest Japan. *Frontiers of Earth Science*, **9**, 152–163.

Ito, T. and Matsuoka, A. (2016) Ductilely deformed cherts within intrusive sandstones of the Yoshii Group of the Akiyoshi terrane in Southwest Japan: Consolidation time of Permian cherts. *News of Osaka Micropaleontologists (NOM), Special Volume*, no. 16, 95–104.

Ito, T. and Matsuoka, A. (2017) Permian–Cretaceous radiolarians from Ie Island, Okinawa Prefecture, Japan. *Science Reports of Niigata University (Geology)*, no. 32 (supplement), 125–136.

Ito, T. and Matsuoka, A. (2018) Lithology and radiolarian age of the Ryokami-yama Chert Formation in eastern Mt. Ryokami: Possible décollement zone in Permian pelagic sequence in mid-Mesozoic accretionary complexes of Southwest Japan. *Island Arc*, **27**, e12273.

Kakuwa, Y. (1991) Lithology and petrography of Triassic–Jurassic bedded cherts of the Ashio, Mino and Tamba belts in Southwest Japan. *Scientific Papers of the College of General Education, University of Tokyo*, **41**, 7–57.

Kamata, Y. (1996) Tectonostratigraphy of sedimentary complex in the southern part of the Ashio Terrane, central Japan. *Science Reports of the Institute of Geoscience, University of Tsukuba, Section B, Geological Sciences*, **17**, 71–107.

Kamata, Y. (1997) Reconstruction of chert–clastic sequence of the Ashio Terrane in the Kuzu area, central Japan. *The Journal of the Geological Society of Japan*, **103**, 343–356. (in Japanese with English abstract)

Kido, S. (1982) Occurrence of Triassic chert and Jurassic siliceous shale at Kamiaso, Gifu Prefecture, central Japan. *News of Osaka Micropaleontologists (NOM), Special Volume*, no. 5, 135–151. (in Japanese with English abstract)

Koike, T., Kinoshita, T., Igo, H. and Takizawa, S. (1971) Conodonts from the Tochigi Group and the discovery of the thrust fault in the vicinity of Kuzuu, Tochigi Prefecture. *The Journal of the Geological Society of Japan*, **77**, 221–222. (in Japanese with English abstract)

Kojima, S., Hayasaka, Y., Hiroi, Y., Matsuoka, A., Sano, H., Sugamori, Y., Suzuki, N., Takemura, S., Tsujimori, T. and Uchino, T. (2016) Pre-Cretaceous accretionary complexes. *In* Moreno, T., Wallis, S. and Gibbons, W., eds., *The Geology of Japan*, Geological Society of London, London, 61–100.

Kojima, S. and Kametaka, M. (2000) Jurassic accretionary complexes in East Asia. *The Memoirs of the Geological Society of Japan*, no. 55, 61–72. (in Japanese with English abstract)

Lowe, D. R. (1976) Nonglacial varves in Lower Member of Arkansas Novaculite (Devonian), Arkansas and Oklahoma. *AAPG Bulletin*, **60**, 2103–2116.

Matsuoka, A. (1995) Jurassic and Lower Cretaceous radiolarian zonation in Japan and in the western Pacific. *Island Arc*, **4**, 140–153.

Matsuoka, A. (2002) Paleoceanography of radiolarian ocean in the Paleozoic–Mesozoic*. *Chikyu Monthly (Gekkan Chikyu)*, **24**, 444–448. (in Japanese)

Matsuoka, A. and Ito, T. (2019) Updated radiolarian zonation for the Jurassic in Japan and the western Pacific. *Science Reports of Niigata University (Geology)*, no. 34, 49–57.

Matsuoka, A., Nikaido, T., Onoue, T. and Zamoras, L.R. (2009) Striped cherts in Jurassic accretionary complexes in the Mino Terrane, central Japan and in the North Palawan Block, Philippines. *Abstracts of Japan Geosciences Union Meeting 2009*, J236-007.

Matsuoka, A., Yamakita, S., Sakakibara, M. and Hisada, K. (1998) Unit division for the Chichibu Composite Belt from a view point of accretionary tectonics and geology of western Shikoku, Japan. *The Journal of the Geological Society of Japan*, **104**, 634–653. (in Japanese with English abstract)

McBride, E. F. and Folk, R. L. (1979) Features and origin of Italian Jurassic radiolarites deposited on continental crust. *Journal of Sedimentary Petrology*, **49**, 837–868.

McBride, E. F. and Thomson, A. (1970) *The Caballos Novaculite, Marathon Region, Texas.* Geological Society of America, Special Paper, **122**, 129p.

Mizutani, S. and Koido, Y. (1992) *Geology of the Kanayama district*. With Geological Sheet Map at 1:50,000, Geological Survey of Japan, 111p. (in Japanese with English abstract)

Nakae, S. (2000) Regional correlation of the Jurassic accretionary complex in the Inner Zone of Southwest Japan. *The Memoirs of the Geological Society of Japan*, no. 55, 73–98. (in Japanese with English abstract)

Nakano, S., Otsuka, T., Adachi, M., Harayama, S. and Yoshioka, T. (1995) *Geology of the Norikuradake district*. With Geological Sheet Map at 1:50,000, Geological Survey of Japan, 139p. (in Japanese with English abstract)

Nikaido, T. and Matsuoka, A. (2008) Lithostratigraphy and radiolarian biostratigraphy of Triassic bedded chert of the Sakahogi section in the Mino Terrane, Japan. *Abstracts of Japan Geosciences Union Meeting 2008*, J240-004.

Nikaido, T. and Matsuoka, A. (2009) Radiolarian biostratigraphy and striped chert of the Sakahogi section in the Mino Terrane, Japan. *Abstracts of Japan Geosciences Union Meeting 2009*, J236-P003.

Nikaido, T. and Matsuoka, A. (2011) Detailed examination on upper Triassic radiolarian biostratigraphy in the Sakahogi section of the Mino Terrane, Japan. *Abstracts of Japan Geosciences Union Meeting 2011*, MIS025-03.

Nisbet, E. G. and Grice, I. (1984) Siliceous Turbidites: Bedded Cherts as Redeposited Ocean Ridge-Derived Sediments. *In* Hsü, K. J. and Jenkyns, H. C., eds., *Pelagic Sediments: On Land and under the Sea*, Burgess & Son Ltd., Abingdon, 351–366.

Nozaki, T., Nikaido, T., Onoue, T., Takaya, Y., Sato, K., Kimura, J-I., Chang, Q., Yamashita, D., Sato, J., Suzuki, K., Kato, Y. and Matsuoka, A. (2019) Triassic marine Os isotope record from a pelagic chert succession, Sakahogi section, Mino Belt, southwest Japan. *Journal of Asian Earth Sciences: X*, **1**, 100004.

O'Dogherty, L., Carter, E. S., Dumitrica, P., Goričan, Š., De Wever, P., Hungerbühler, A., Bandini, A. N. and Takemura, A. (2009) Catalogue of Mesozoic radiolarian genera. Part 1: Triassic. *Geodiversitas*, **31**, 213–270.

Ogg, J. G., Ogg, G. M. and Gradstein, F. M. (2016)

A Concise Geologic Time Scale 2016. Elsevier, Amsterdam.

Onoue, T., Hori, R. S. and Kojima, S. (2017) Triassic and Jurassic radiolarian response to global catastrophic events in the Panthalassa Ocean, as recorded in the Mino Belt, central Japan. *Science Reports of Niigata University (Geology)*, no. 32 (supplement), 29–69.

Onoue, T., Sato, H., Nakamura, T., Noguchi, T., Hidaka, Y., Shirai, N., Ebihara, M., Osawa, T., Hatsukawa, Y., Toh, Y., Koizumi, M., Harada, H., Orchard, M. J. and Nedachi, M. (2012) Deep-sea record of impact apparently unrelated to mass extinction in the Late Triassic. *Proceedings of the National Academy of Sciences of the United States of America*, **109**, 19134–19139.

Onoue, T., Sato, H., Yamashita, D., Ikehara, M., Yasukawa, K., Fujinaga, K., Kato, Y. and Matsuoka, A. (2016) Bolide impact triggered the Late Triassic extinction event in equatorial Panthalassa. *Scientific Reports*, **6**, doi:ARTN 2960910.1038/srep29609.

Pessagno, E. A. and Newport, J. N. (1972) A technique for extracting Radiolaria from radiolarian cherts. *Micropaleontology*, **18**, 231–234.

Shen, G. P., Ujiié, H. and Sashida, K. (1996) Off-scraped Permian–Jurassic bedded chert thrust on Jurassic–early Cretaceous accretionary prism: Radiolarian evidence from Ie Island, central Ryukyu Island Arc. *The Island Arc*, **5**, 156–165.

Sudo, S., Makimoto, H., Hata, M., Unozawa, A., Takizawa, F. and Sakamoto, T. (1991) *Geological map of the Utsunomiya district*. Quadrangle Series, 1:200,000, Geological Survey of Japan.

Sugiyama, K. (1997) Triassic and Lower Jurassic radiolarian biostratigraphy in the siliceous claystone and bedded chert units of the southeastern Mino terrane, central Japan. *Bulletin of the Mizunami Fossil Museum*, no. 24, 79–193.

Takayanagi, A., Hori, N. and Sashida, K. (2001) Tectonostratigraphy of sedimentary complex of the Ashio Terrane in the northern part of the Ashikaga area, Tochigi Prefecture, and the occurrence of radiolarians. *News of Osaka Micropaleontologists (NOM), Special Volume*, no. 12, 113–127. (in Japanese with English abstract)

Yamashita, D., Kato, H., Onoue, T. and Suzuki, N. (2018) Integrated Upper Triassic conodont and radiolarian biostratigraphies of the Panthalassa Ocean. *Paleontological Research*, **22**, 167–198.

Yamada, N., Adachi, M., Kajita, S., Hirayama, S., Yamazaki, H. and Bunno, H. (1985) *Geology of the Takayama district*. Quadrangle Series, scale 1:50,000, Geological Survey of Japan, 111p. (in Japanese with English abstract)

Yao, A. and Mizutani, S. (1993) Research on radiolarian fossils and re-examination of Paleozoic–Mesozoic stratigraphy in Japan. *In* Geological Society of Japan, ed., *Hundred Years of Geology in Japan: Centennial Volume of the Geological Society of Japan*, Soubun Printing Co. Ltd., 131–137. (in Japanese)

Yoshimura, M., Kido, S. and Hattori, I. (1982) Stylolitic cherts and radiolarian fossils in the Imajo area of the Nanjo Massif, Fukui Prefecture, central Japan. *Memoirs of the Faculty of Education, Fukui University, Series II*, **31**, 65–89. (in Japanese with English abstract)

* Translated by the authors

Recieved July 12, 2019
Accepted May 29, 2020
Published on-line August 7, 2020

栃木県足利地域の足尾テレーンジュラ紀付加体に含まれる三畳系ストライプチャートの放散虫年代

伊藤　剛

要　旨

チャートの単層中に発達するストライプ構造は，西南日本内帯のジュラ紀付加体丹波 - 美濃テレーン及び足尾テレーンでみられる．本研究では，栃木県足利市及び佐野市の 4 セクション（飛駒・大岩・月谷・織姫セクション）中にみられるストライプチャートについて記載するとともに，飛駒セクションを除く 3 セクションの放散虫化石年代について検討する．ストライプチャートは，ストリークとスペーシングからなる．ストリークは，ピンストライプ状構造における薄い部分を指し，主に粘土鉱物からなる．スペーシングは，ストリークの間の厚い部分であり，隠微晶質石英を主体とする．ストライプチャートに富む大岩セクションは，上部三畳系カーニアン階中部～ノーリアン階中部に部分的に対比される．ストライプチャートを部分的に含む月谷セクションと織姫セクションは，中部三畳系アニシアン階中部～上部と上部三畳系ノーリアン階上部～レーティアン階下部にそれぞれ対比される．

Bulletin of the Geological Survey of Japan, vol. 71 (4), p. 313–330, 2020

Article

Late Jurassic radiolarians from mudstone near the U–Pb-dated sandstone of the North Kitakami Belt in the northeastern Shimokita Peninsula, Tohoku, Japan

UCHINO Takayuki[1,*] and SUZUKI Noritoshi[2]

UCHINO Takayuki and SUZUKI Noritoshi (2020) Late Jurassic radiolarians from mudstone near the U–Pb-dated sandstone of the North Kitakami Belt in the northeastern Shimokita Peninsula, Tohoku, Japan. *Bulletin of the Geological Survey of Japan*, vol. 71(4), p. 313–330, 7 figs, 1 table, 2 plates.

Abstract: In the northeastern Shimokita Peninsula, Aomori Prefecture, a Jurassic accretionary complex (AC) belonging to the North Kitakami Belt is distributed in three hilly areas of the Kuwabatayama, Katasakiyama and Omori. Although the AC in the Kuwabatayama area has been extensively studied and subdivided into the Late Jurassic Iwaya Unit and the Early Cretaceous Shitsukari Unit, those in the other areas are not fully understood except for a recent report of the detrital zircon U–Pb age from sandstone in the Omori area.

We extracted radiolarian fossils such as *Eucyrtidiellum* cf. *pyramis* indicating the Late Jurassic (probably Kimmeridgian) from mudstone near the U–Pb-dated sandstone in the Omori area. Because this radiolarian age is close to the zircon U–Pb age, and the horizons of the mudstone and sandstone are close without any recognizable distinctive tectonic discontinuity between them, the clastic rocks in the Omori area may be stratigraphically continuous or contemporaneous sequences deposited around the Kimmeridgian.

The ACs in the Katasakiyama and Omori areas are correlative to the Iwaya Unit in the Kuwabatayama area based on the lithology, geologic structure and clastic rock age. Therefore, the ACs in the northeastern Shimokita Peninsula can be divided into the Late Jurassic and the Early Cretaceous units; the former is the Iwaya Unit in the Kuwabatayama area and the unnamed ACs in the Omori and Katasakiyama areas, while the latter is the Shitsukari Unit in the Kuwabatayama area.

Keywords: radiolarian fossil, Late Jurassic, Kimmeridgian, accretionary complex, Shimokita Peninsula, North Kitakami Belt, Northeast Japan

1. Introduction

The North Kitakami Belt, located in the northern region of the Kitakami Massif of Tohoku (Northeast Japan), is mainly occupied by a Jurassic accretionary complex (AC). This AC is also sparsely exposed in the northward and westward areas of the massif because of the broad-scale coverage of Cenozoic volcanic and sedimentary rocks; only small amounts of the AC crop out in the Shimokita Peninsula, the south of Hirosaki City, the west of Lake Towada, the north of Mt. Hachimantai and the north of Mt. Moriyoshi (Fig. 1). A northeastern part in the Shimokita Peninsula, Aomori Prefecture, is marked by the Shimokita Hill, which is bounded by an escarpment along its east coast on the Pacific Ocean. The ACs in the northeastern Shimokita Peninsula are distributed in the Kuwabatayama, Katasakiyama and Omori areas from the north to south of Higashidori Village (Fig. 2a). The ACs in these areas are exposed as a coastal terrace with a 200- to 300-m elevated steep escarpment although they are mainly overlaid by the Neogene sediments of the Sunakomata or Tomari formations (Imai,1961) at the foot of the terrace. This paper mainly focuses on the ACs in the Katasakiyama and Omori areas.

The AC in the Kuwabatayama area crops out well along the seashore of Cape Shiriya and contains huge limestone blocks with fossils. Although it has been the subject of study by many researchers, the Katasakiyama and Omori areas have been little studied because of poor and fragmental exposures inland. Because the ACs in these two areas have not been mapped in detail despite the existence of 1:50,000 quadrangle series geologic maps, named “Chikagawa” (Imai, 1961) and “Shiriyazaki” (Tsushima and Takizawa, 1977), their geologic ages and

[1] AIST, Geological Survey of Japan, Research Institute of Geology and Geoinformation

[2] Department of Earth Science, Graduate School of Science, Tohoku University, Sendai 980-8578, Japan

[*] Corresponding author: UCHINO, T., Central 7, 1-1-1 Higashi, Tsukuba, Ibaraki 305-8567, Japan. Email: t-uchino@aist.go.jp

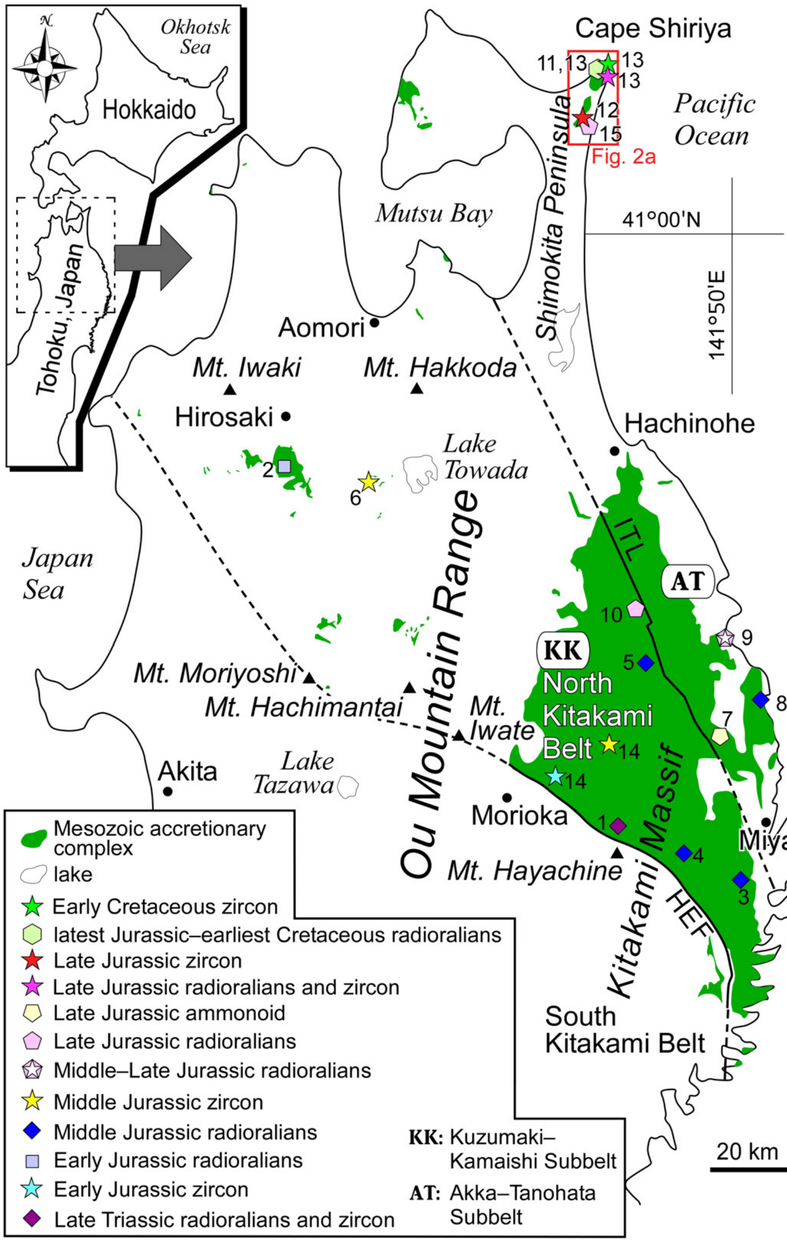

Fig. 1 Distribution map of Mesozoic accretionary complexes (green regions) in the North Kitakami Belt derived from the Seamless Digital Geological Map of Japan (1:200,000) V2 of the Geological Survey of Japan, AIST (2019). Symbols with numbers indicate the locations for which fossil and zircon ages from terrigenous clastic rocks were reported. 1: Kawamura *et al.* (2013); Uchino (2017), 2: Ueda *et al.* (2009), 3: Yoshihara *et al.* (2002); Suzuki and Ogane (2004), 4: Suzuki *et al.* (2007a), 5: Suzuki *et al.* (2007b); Ehiro *et al.* (2008), 6: Uchino (2018a), 7: Suzuki *et al.* (2007a), 8: Matsuoka and Oji (1990), 9: Minoura and Tsushima (1984), 10: Nakae and Kamada (2003), 11: Matsuoka (1987), 12: Uchino (2018b), 13: Ueda *et al.* (2018), 14: Uchino (2019), 15: this study.
HEF: Hayachine Eastern Marginal Fault, ITL: Iwaizumi Tectonic Line. The broken line shows an inferred fault.

tectonostratigraphy are not well understood. Recently, Uchino (2018b) obtained a zircon U–Pb age of ca. 155 Ma for the sandstone of the undated AC in the Omori area, indicating that it is slightly older than the latest Jurassic–earliest Cretaceous age for the clastic rocks (Matsuoka, 1987) in Cape Shiriya, which are regarded as the youngest in the North Kitakami Belt. To understand the tectonostratigraphy of the Shimokita Peninsula, more data, such as radiolarian fossil ages, are required for this region. This paper reports radiolarians from mudstone near the location of sandstone dated using detrital zircon U–Pb geochronology, and discusses the local geologic correlation based on lithology and ages.

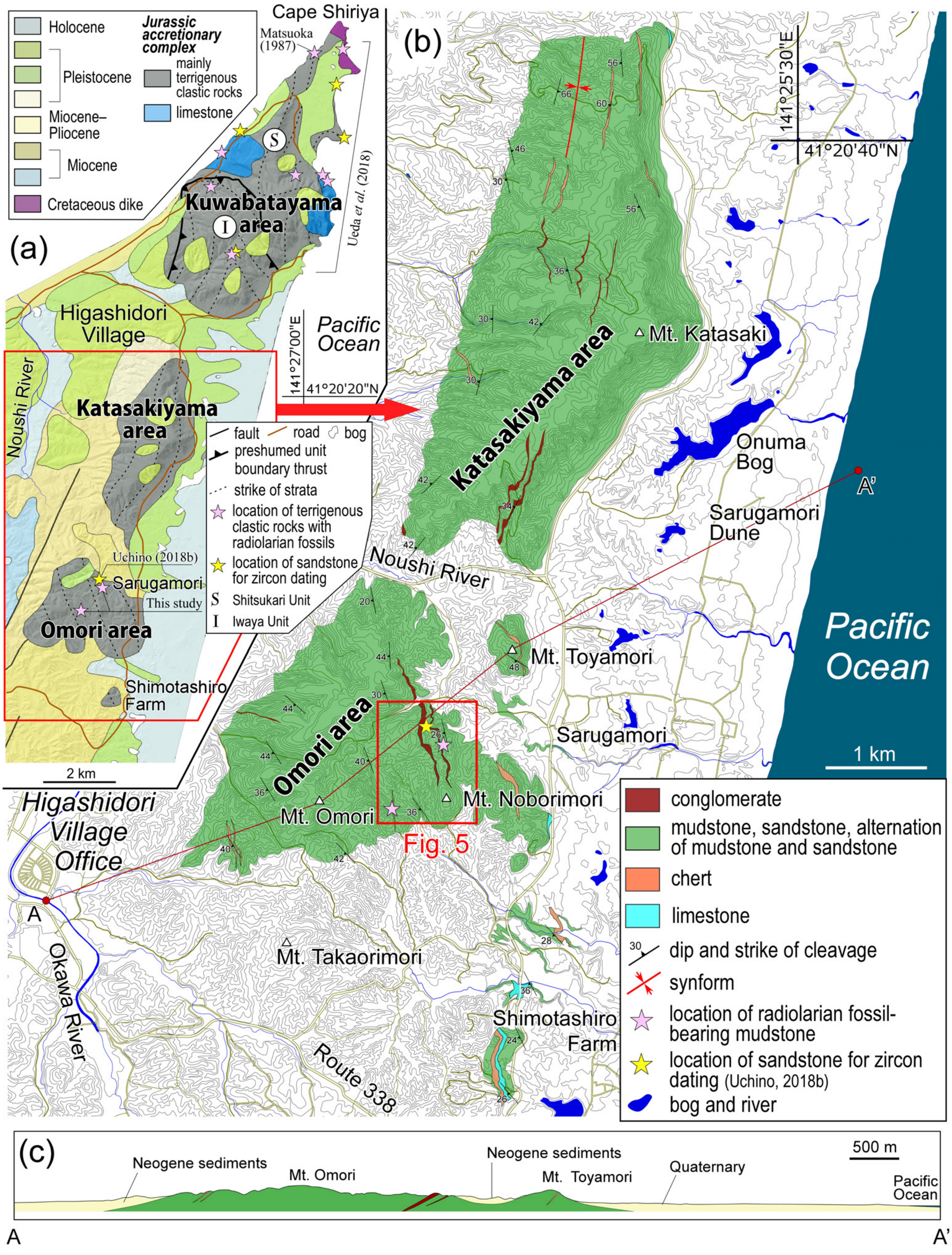

Fig. 2 (a) Index map of the northeastern Shimokita Peninsula, Aomori Prefecture. The geologic map was derived from the Seamless Digital Geological Map of Japan (1:200,000) V2 of the Geological Survey of Japan, AIST (2019). (b) Detailed geologic map of the accretionary complex in the Katasakiyama and Omori areas. The Quaternary deposits on the accretionary complexes in the two areas are not shown. (c) Geologic profile from the southwest (A) through Mt. Omori and Mt. Toyamori to the northeast (A').

<table>
<tr><th>Reference / Area</th><th>Imai (1961)</th><th colspan="2">Murata (1962)</th><th colspan="2">Tsushima and Takizawa (1977)</th><th>Kawamura et al. (1994)</th><th>Kamada (2000)</th><th colspan="2">Ueda et al. (2018)</th></tr>
<tr><td rowspan="3">Kuwabata-yama</td><td rowspan="5">Shiriya Formation</td><td rowspan="4">Shimokita Group</td><td>Tatemachijima Formation</td><td rowspan="4">Shiriya Group</td><td>A formation</td><td rowspan="5">Shiriya Complex</td><td rowspan="3">Shiriya Complex</td><td rowspan="3">Shiriya Complex</td><td rowspan="2">Shitsukari Unit</td></tr>
<tr><td>Kuwabatakeyama Formation</td><td>B formation</td></tr>
<tr><td>Iwaya Formation</td><td>C formation</td><td>Iwaya Unit</td></tr>
<tr><td>Katasaki-yama</td><td>Katasakiyama Formation</td><td>C formation?</td><td></td><td colspan="2"></td></tr>
<tr><td>Omori</td><td colspan="2"></td><td colspan="2"></td><td></td><td colspan="2"></td></tr>
</table>

Fig. 3 Nomenclatural history of the stratigraphic units of the accretionary complexes in the northeastern Shimokita Peninsula, Aomori Prefecture. Tsushima and Takizawa (1977) indicates that the C formation in the Kuwabatayama area is probably correlative to the northern unit in the Katasakiyama area.

2. Geological outline

The North Kitakami Belt is divided into two sub-belts, namely the southwestward Kuzumaki–Kamaishi Subbelt and the northeastward Akka–Tanohata Subbelt, based on sandstone composition (dominated by plagioclase or K-feldspars), presence or absence of Paleozoic marine fossils and presence or absence of Late Jurassic coral-bearing limestone (Ehiro *et al.*, 2005; Kojima *et al.*, 2016) (Fig. 1). The AC in the Shimokita Peninsula belongs to the Akka–Tanohata Subbelt (e.g. Kamada, 2000; Ehiro *et al.*, 2008). The accretion age generally becomes younger from the southwest to the northeast (e.g. Suzuki *et al.*, 2007a; Ehiro *et al.*, 2008) although this trend does not always hold in the entire area (Nakae and Kamada, 2003). Of note, the youngest marine sediment in the North Kitakami Belt, from terrigenous clastic rocks in Cape Shiriya, was dated to the Early Cretaceous (Matsuoka, 1987; Ueda *et al.*, 2018) (Fig. 1).

2. 1 Nomenclature of stratigraphic units

The stratigraphic divisional scheme in the northeastern Shimokita Peninsula has changed over time (Imai, 1961; Murata, 1962; Tsushima and Takizawa, 1977; Kawamura *et al.*, 1994; Kamada, 2000; Kojima *et al.*, 2016; Ueda *et al.*, 2018) (Fig. 3). The pre-Neogene sedimentary rocks in this peninsula were previously thought to be "Paleozoic strata" and were named the Shiriya Formation in the 1:50,000 quadrangle series geologic map "Chikagawa" (Imai, 1961). In consideration of Mesozoic hexacorals reported from the "Paleozoic strata" in the Kuwabatayama area (Onuki, 1959), the stratigraphic divisional scheme in the northeastern Shimokita Peninsula was revised to comprise the Katasakiyama Formation in the Katasakiyama area, and the Tatemachijima, Kuwabatakeyama and Iwaya formations in the Kuwabatayama area. These four formations were grouped as the Shimokita Group (Murata, 1962). However, the name Shimokita Group was already used as a formal Miocene stratigraphic unit. Therefore, Tsushima and Takizawa (1977) renamed the four formations to the Shiriya Group. Because the strata of the North Kitakami Belt were thought to be an AC (e.g. Minoura, 1985), the Shiriya Group was renamed to the Shiriya Complex. A tectonostratigraphic continuity of this complex to the ACs of the Oshima Belt in southern Hokkaido has been found (Kawamura *et al.*, 1994). Allocation of the Shiriya Complex was expanded by Kawamura *et al.* (1994) to any ACs in the Shimokita Peninsula. Kamada (2000) confined this allocation to only the AC in the Kuwabatayama area. Recent geologic mapping, petrology, radiolarian ages and zircon U–Pb dating of the Shiriya Complex by Ueda *et al.* (2018) have led to the proposal of using the Shitsukai and Iwaya units as sub-stratigraphic units of the Shiriya Complex in the Kuwabatayama area.

We withhold specific geologic division names for the Katasakiyama and Omori areas because the first author is still engaged in a study of these areas, although the ACs in the Katasakiyama and Omori areas are likely to be correlative to the Iwaya Unit in the Kuwabatayama area, as discussed later.

2. 2 Brief overview of geology and paleontology in study areas

2. 2. 1 AC in Kuwabatayama area

The Kuwabatayama area in the present paper covers nearly the entire study areas of Murata (1962), Oho and Iwamatsu (1986), Kamada (2000), Sano *et al.* (2009) and Ueda *et al.* (2018). The Shiriya Complex (Kawamura *et al.*, 1994; Kamada, 2000) is characterized by imbricated stacks of coherent chert and clastic rock layers, and characteristic kilometer-long limestone blocks (Ueda *et al.*, 2018). The AC in Cape Shiriya is intruded by diorite 122.1+1.4 (2σ) Ma in age (Ueda *et al.*, 2018). Oho and Iwamatsu (1986) considered this AC as an olistostrome of submarine landslide deposits based on a slump with huge limestone olistoliths and the presence of a microbrecciated matrix. Recently, Ueda *et al.* (2018) divided the AC in this area into two tectonostratigraphic units (Iwaya and Shitsukari units) based on lithology and radiolarian and zircon U–Pb ages. They found that the Iwaya Unit is composed of mudstone, sandstone, chert, siliceous mudstone, and minor amounts of limestone and conglomerate. The Shitsukari Unit is composed of conglomerate, sandstone, mudstone, siliceous mudstone, chert, limestone and a minor amount of metabasalt. The Iwaya Unit, which has an approximately N–S to NW–SE trending synform, is supposed to lie structurally above the Shitsukari Unit, which has a NE–SW trending synform and antiform pair (Fig. 2a). Ueda *et al.* (2018) also found that the Shitsukari Unit formed as an imbricated accretionary wedge which was composed of debrite from an inner trench slope.

The limestone was dated to the Late Jurassic using Hexacorallia and Stromatoporoidea fossils (Onuki, 1959; Murata, 1962) and another limestone was dated to the Late Triassic using megalodontoid bivalves (Sano *et al.*, 2009). The microfossil ages of chert range from the Middle Triassic (Anisian) to the Late Jurassic (Kimmeridgian) (Toyohara *et al.*, 1980; Oho and Iwamatsu, 1986; Matsuoka, 1987; Ueda *et al.*, 2018). Siliceous mudstone yields Middle Jurassic to latest Jurassic radiolarians (Ueda *et al.*, 2018), and tuffaceous mudstone yields latest Jurassic to earliest Cretaceous radiolarians (Matsuoka, 1987). The zircon U–Pb ages of clastic rocks, including intercalated tuff layers, are correlated to the Early Cretaceous (Berriasian to Barremian) (Ueda *et al.*, 2018).

2. 2. 2 AC in Katasakiyama area

The AC in the Katasakiyama area shows a 7 km × 2.5 km lenticular distribution pattern around Mt. Katasaki. The northern part of the Katasakiyama area was partly covered by Murata (1962), who mapped a synform in the southern margin of his map. A detailed geologic map of the AC is shown in Fig. 2b, along with that in the Omori area (see next section). The AC exceeds over 1,200 m in thickness. It consists mainly of mudstone with minor amounts of chert, alternating beds of sandstone and mudstone, sandstone, conglomerate and limestone. The sheets or lens of oceanic rocks such as limestone and chert are less than several meters in thickness. The AC trends in the NNW–SSE to NNE–SSW directions and dips at a low–middle angle to the west (Fig. 2c). A thin limestone sheet several meters in thickness occurs at the northeastern edge of this area.

2. 2. 3 AC in Omori area

The AC in the Omori area shows a 2.7 km × 2.9 km elliptical distribution pattern around Mt. Omori. The thickness of the AC exceeds over 2,000 m. It consists mainly of mudstone with minor amounts of limestone, chert, alternating beds of sandstone and mudstone, sandstone and conglomerate. Similar to the limestone sheet at the northeastern edge of the Katasakiyama area, a limestone sheet <25 m in thickness is aligned, from place to place, along the eastern margin of the Omori area with a NNW–SSE trend, suggesting a possible southern extension of the limestone sheet from the Katasakiyama area. The AC trends in the NW–SE to NNW–SSE directions and dips at a low–middle angle to the west (Fig. 2b, c).

3. Lithology

The lithologies of the ACs in the Katasakiyama and Omori areas are very similar and are thus described collectively in this section. That in the Kuwabatayama area is not explained here because it has been described in previous reports.

Limestone, which accounts for ca. 0.4 % of the mapped distribution area of the AC, is gray to pale gray and mostly recrystallized. Macroscopic and microscopic calcite veins less than 1 cm in width frequently crosscut the limestone, and some of them are dark pink. Matrix-supported and poorly sorted calcirudite infrequently occurs with preserving as an original sedimentary structure. The limestone clasts in the calcirudite do not exceed 4 cm in length. Chert, which accounts for ca. 1 % of the mapped distribution area, is gray. It has a bedded structure, where several-centimeter-thick chert layers alternate with ca. 1-mm-thick claystone layers. The chert is mostly recrystallized. Dark gray mudstone is the most dominant rock type in the AC. The mudstone is more or less slaty, and frequently contains radiolarian fossil pseudomorphs. Quartz veins less than 1 cm in width occasionally intrude into the mudstone.

Sandstone, which accounts for a ca. 1 % of the mapped distribution area, occurs as feldspathic arenite (Fig. 4a) and lithic arenite to wacke. Quartz grains are more common than feldspar ones, which have nearly equal amounts of plagioclase and K-feldspar. This sandstone varies from fine to very coarse grains and is in general poorly sorted. It also contains many lithic fragments such as chert and siliceous mudstone, and frequently contains contemporaneous mud chips. It is occasionally intruded by quartz veins less than 5 cm in width. The sandstone sometimes alternates with mudstone in the form of layers with a thickness on the order of several millimeters. Rarely, pale purple tuffaceous sandstone appears.

Poorly sorted, granule to pebbly conglomerates (Fig. 4b, c) account for 1 % of the mapped distribution area of the AC in these two areas. They are mostly characterized by a clast-supported fabric with coarse quartz grains, angular to sub-rounded variable clasts of chert (gray, dark gray, white and rarely red), siliceous mudstone, mudstone and sandstone.

These sedimentary rocks have undergone extensive post-depositional alteration and deformation, with layer-parallel slaty cleavage in the fissile mudstone and considerably flattened clasts in the conglomerate (Fig. 4c). The mudstone sometimes exhibits whitish parts caused by

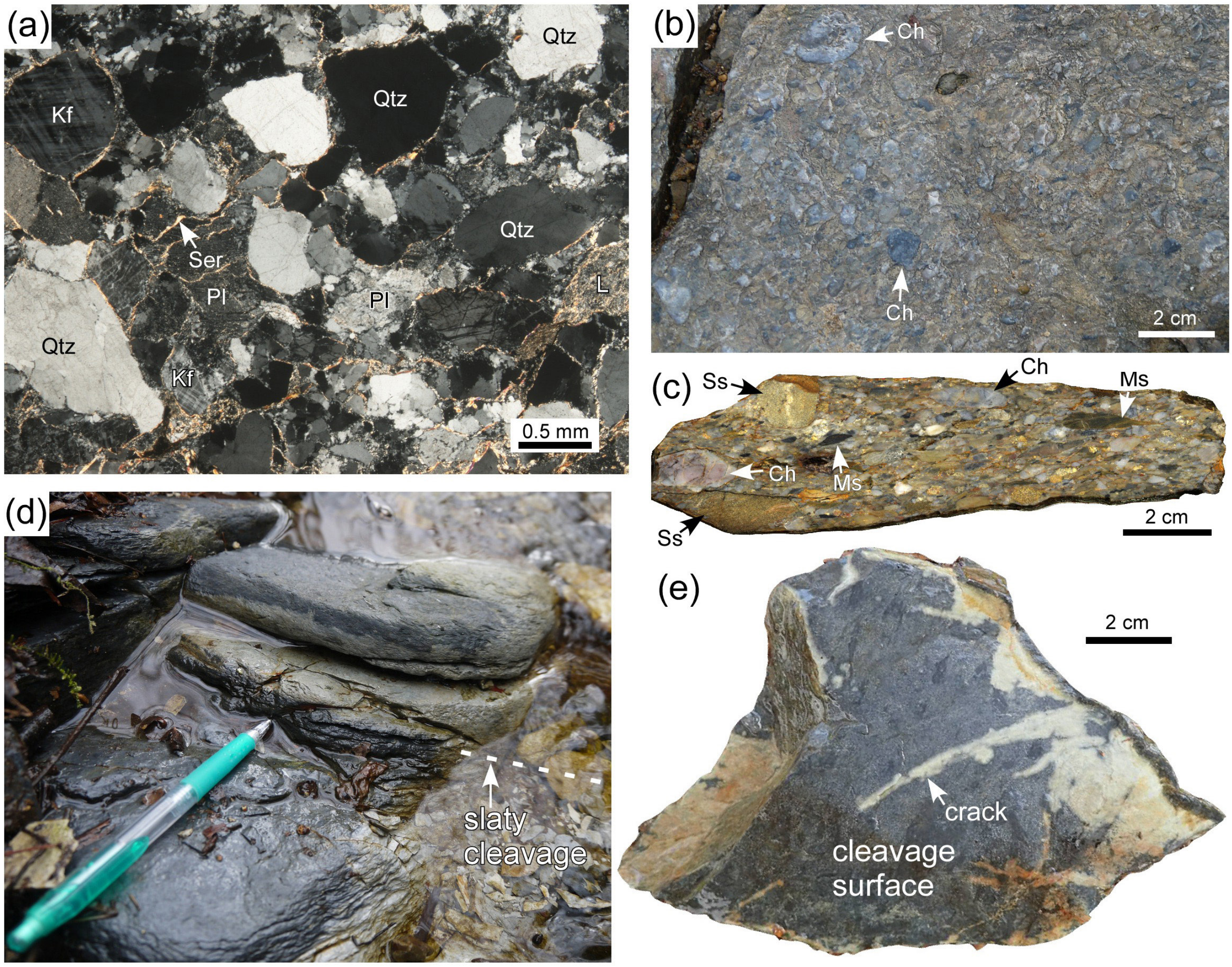

Fig. 4 (a) Photomicrograph of feldspathic arenite. Cross-polarized light. Mizunashi Stream, east ramp of Mt. Katasaki. Kf: K-feldspar, Pl: plagioclase, Qtz: quartz, Ser: sericite, L: lithic fragment (mudstone). (b) Conglomerate outcrop. Stream to the west of Sarugamori hamlet. Ch: chert. (c) Conglomerate specimen. Ch: chert, Ms: mudstone, Ss: sandstone. (d) Altered mudstone outcrop. The pen is 15 cm long. (e) Altered mudstone specimen. Stream to the west of Mt. Toyamori.

fluid flow along the slaty cleavages and cracks, and looks as if it was tuffaceous or calcareous mudstone (Fig. 4d, e). Fine clay minerals such as sericite, which are mostly in a unidirectional polarization extinction position, are found between the clastic grains (Fig. 4a). Very fine ferric oxyhydroxide minerals frequently develop along the cleavages and cracks or between the clastic grains. Calcite spots (<0.2 mm in diameter) that are not aligned with the cleavages are occasionally present in the clastic rocks, and quartz spots (<0.2 mm) containing very fine dusty inclusions appear in the matrix of limestone and calcite veins.

4. Radiolarian fossil

4. 1 Sample location and extraction method

Samples containing radiolarian fossils were recovered from mudstone at two outcrops in the stream: Loc. 1 (41°17′05″N, 141°22′35″E) ca. 550 m west and Loc. 2 (41°17′25″N, 141°22′56″E) ca. 550 m north of Mt. Noborimori (Fig. 2b). The mudstone is dark gray and does not exhibit the apparent deformation or alteration. A route map and a columnar section around these outcrops are shown in Figs. 5 and 6, respectively. Of note, Loc. 2 is close to an outcrop of the Late Jurassic sandstone dated using detrital zircon U–Pb geochronology (Uchino, 2018b).

Rock chips were soaked in 5 % HF for ca. 18 hours and then residual fractions were collected with sieves of #65 and #250 meshes. After these steps were repeated three times, radiolarian samples were picked with a brush under a stereomicroscope and subsequently examined with a scanning electron microscope.

Regarding taxonomy, the species was determined by strictly referring to the holotype or other type series images in original publications, and the genus was determined by

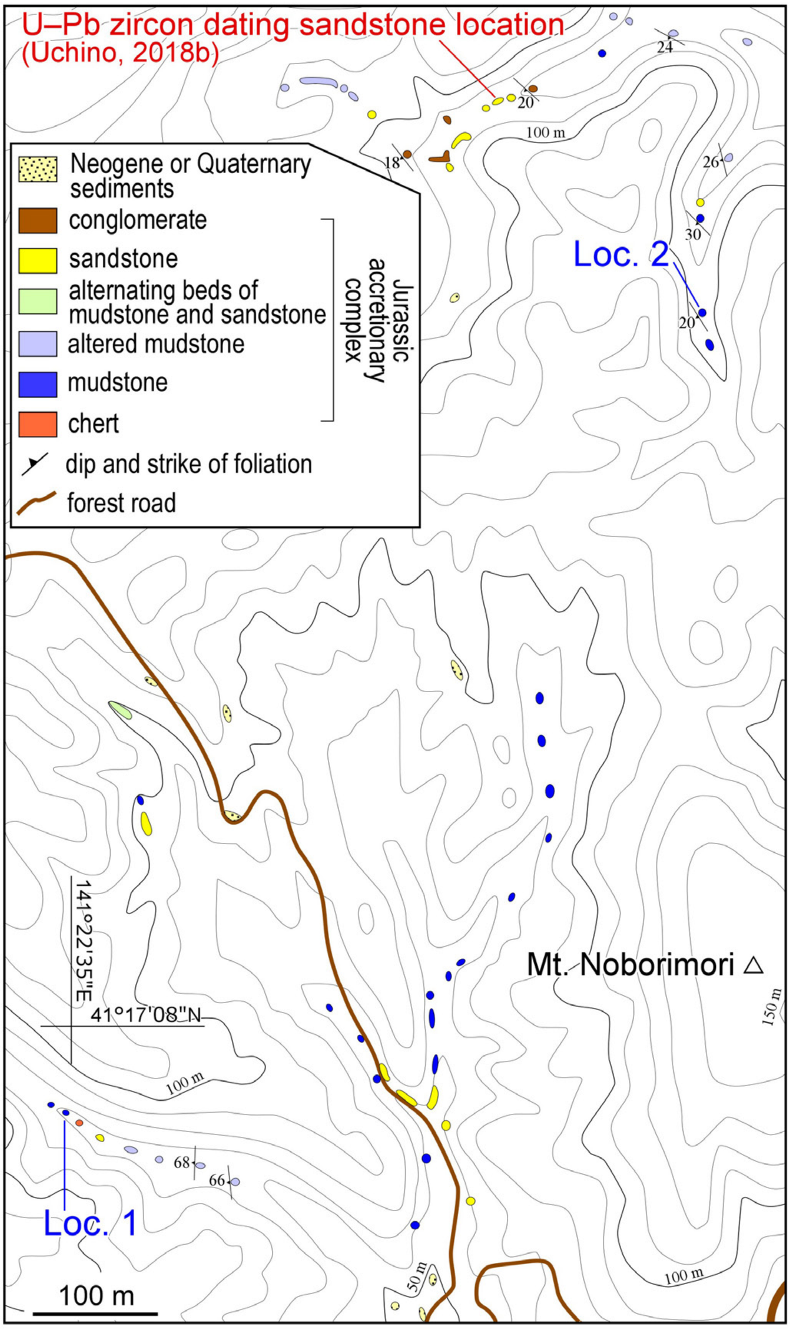

Fig. 5 Route map around the location of radiolarian fossil-bearing mudstone. Contour lines were derived from digital elevation model data (10-m mesh) from the Geospatial Information Authority of Japan.

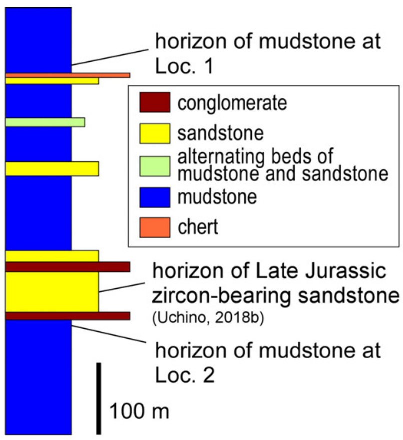

Fig. 6 Columnar section around the location of radiolarian fossil-bearing mudstone.

referring to updated concepts if possible (e.g. O'Dogherty *et al.*, 2017). The biostratigraphic correlation to the geologic time scale at the stage level was largely based on the Jurassic standard radiolarian zones proposed by Matsuoka (1995) and some revisions in subsequent papers (Hatakeda *et al.*, 2007; Ishida *et al.*, 2009). Because of a contradiction in the denoted geologic stages of the same fauna among Japan, Europe and North America, the assigned geologic time scale was converted from biozones in other regions to those of Japan by referencing Baumgartner *et al.* (1995), Yang and Matsuoka (1997) and Goričan *et al.* (2018).

4. 2 Identification and age

4. 2. 1 Radiolarians at Loc. 1

Many of the radiolarian fossils were deformed and recrystallized. Although their surface structure is hard to be recognized, 33 species or species levels are identified.

Table 1 List of radiolarian fossils. Red and blue numbers indicate individuals from the mudstone at Loc. 1 and Loc. 2, respectively.

Fossil	Loc. 1	Loc. 2	Individual number in plate
Archaeodictyomitra cf. *inornata* Hull	*	*	21–23, 4
Archaeodictyomitra cf. *unica* Wu	*		15
Archaeodictyomitra aff. *prisca* Kozur and Mostler in Grill and Kozur (1986)	*		7
Archaeodictyomitra aff. *rigida* Pessagno	*	*	16, 17, 1, 2
Archaeodictyomitra spelae Chiari, Cortese and Marcucci	*		1–3
Archaeodictyomitra cf. *spelae* Chiari, Cortese and Marcucci	*		4–6
Archaeodictyomitra aff. *suzukii* Aita	*		18–20
Archaeodictyomitra cf. *tyaughtonensis* Cordey		*	3
Archaeodictyomitra aff. *vulgaris* Pessagno	*		11–14
Archaeodictyomitra sp. A	*		8
Archaeodictyomitra sp. B	*		9, 10
Archaeodictyomitra sp. C	*		24
Archaeodictyomitra sp. D	*		25
Archaeospongoprunum cf. *mizutanii* Ožvoldová in Ožvoldová *et al.* (2000)	*		109
Archaeospongoprunum sp.	*		108
Bistarkum aff. *mangartense* Goričan, Šmuc and Baumgartner	*		112, 113
Cinguloturris cf. *carpatica* Dumitrică in Dumitrică and Mello (1982)	*	*	38–43, 17
Cinguloturris cf. *floridicingula* (Li)		*	15
Cinguloturris cf. *getsensis* O'Dogherty, Goričan and Dumitrică in O'Dogherty *et al.* (2006)		*	16
Cinguloturris cf. *latiannulatum* (Grill and Kozur)	*		44
Cinguloturris sp.	*		45
Crococapsa aff. *truncata* (Wu)	*		63
Eucyrtidiellum cf. *nodosum* Wakita	*		62
Eucyrtidiellum cf. *pyramis* (Aita) in Aita and Okada (1986)	*		59–61
Eucyrtidiellum sp.		*	29
Favosyringium cf. *affine* (Rüst) sensu Steiger (1992)	*		111
Kilinora sp.	*		69
Loopus cf. *venusta* (Chiari, Cortese and Marucci)	*		37
Minutosolla sp.	*		88, 89
Parahsuum mudongensis (Li) sensu lato	*		26–28
Podobursa sp.	*		110
Praewilliriedellum sp.	*		78
Hiscocapsa robusta (Matsuoka)	*		91, 92
Hemicryptocapsa cf. *yaoi* (Kozur)	*		93
Hemicryptocapsa carpathica (Dumitrică)	*		79
Praezhamoidellum sp.	*		94–98
Praezhamoidellum ? sp.	*		90
Quarkus sp.		*	30
Spongocapsula palmerae Pessagno	*		29–31
Spongocapsula sp.	*		32, 33
Spongocapsula ? sp.	*		34–36
Striatojaponocapsa cf. *conexa* (Matsuoka)	*		70
Striatojaponocapsa synconexa O'Dogherty, Goričan and Dumitrică in O'Dogherty *et al.* (2006)	*		71–76
Striatojaponocapsa sp.	*		77
Svinitzium sp.	*		46, 47
Tetracapsa sp.		*	31
Transhsuum sp.	*		49–55
Wrangellium sp.	*		48
Williriedellum sp.	*	*	80–87, 20–23
Complexapora aff. *kiesslingi* Hull	*		105, 106
Zhamoidellum cf. *mikamense* Aita		*	19
Zhamoidellum ovum Dumitrică	*		101–104
Zhamoidellum cf. *ventricosum* Dumitrică	*		100
Zhamoidellum sp.	*		99
Minocapsidae gen. et sp. indet.	*		107
Pyloniodea gen. et sp. indet.	*		58
Multisegmented nassellarians		*	5–14
Spherical radiolarians		*	18
Williriedelloidea gen. et sp. indet.		*	24–26
Syringocapsidae? gen. et sp. indet.		*	27, 28
Few segmented nassellarians		*	32–35
Four-armed flat Pylonioidea		*	36
Nassellaria gen. et sp. indet.	*		56, 57, 64–68, 114

A total of approximately 15 species coexisted in the early to middle Late Jurassic (roughly Oxfordian or Kimmeridgian): *Archaeodictyomitra* cf. *inornata* Hull, *Archaeodictyomitra* cf. *unica* Wu, *Archaeodictyomitra spelae* Chiari *et al.* (a single report from the Oxfordian), *Archaeospongoprunum* cf. *mizutanii* Ožvoldová [known from Oxfordian and Tithonian], *Cinguloturris* cf. *carpatica* Dumitrică, *Cinguloturris* cf. *latiannulatum* (Grill and Kozur), *Eucyrtidiellum* cf. *nodosum* Wakita, *Eucyrtidiellum* cf. *pyramis* (Aita) (Kimmeridgian and later), *Loopus* cf. *venusta* (Chiari *et al.*), *Parahsuum mudongensis* (Li) sensu lato, *Hiscocapsa robusta* (Matsuoka), *Hemicryptocapsa* cf. *yaoi* (Kozur), *Spongocapsula palmerae* Pessagno, *Striatojaponocapsa* cf. *conexa* (Matsuoka), *Hemicryptocapsa carpathica* (Dumitrică), *Zhamoidellum ovum* Dumitrică, and *Zhamoidellum* cf. *ventricosum* Dumitrică. By contrast, 12 species, such as *Striatojaponocapsa synconexa* O’Dogherty *et al.*, are referable to the late Middle Jurassic (roughly Callovian). Eight species are common in the late Late Jurassic (Tithonian). These eight species, however, range down to the middle Late Jurassic (Kimmeridgian), and are thus not necessarily from the Tithonian. Therefore, the fauna from Loc. 1 is roughly dated to the early to middle Late Jurassic. Based on species whose ranges are well documented (Aita, 1987; Matsuoka, 1995; Nishizono, 1996; Hori, 1999; Hatakeda *et al.*, 2007), the co-occurrence of *Striatojaponocapsa* cf. *conexa* (Matsuoka) and *Striatojaponocapsa synconexa* O’Dogherty *et al.* is correlative to JR5 (*S. conexa* Zone) to JR6 (*Kilinora spiralis* Zone) of Matsuoka (1995). These two zones are generally correlated to the Bathonian and Callovian. However, Ishida *et al.* (2009) reported the earliest Kimmeridgian ammonoid, *Ataxioceras* (*Ataxioceras*) *kurisakense*, from bioturbated sandy mudstone 1.5 m above the horizon of the JR6 fauna with *S. conexa* and *S. synconexa* (= *Stichocapsa naradaniensis* Matsuoka shown in Fig. 7.9 of Ishida *et al.*, 2009) from the Kurisaka Formation of the Kurosegawa Belt in Shikoku, Southwest Japan. This suggests that an extension of geologic time ranges up to the earliest Kimmeridgian from the Callovian, or an age revision from the Callovian to a significantly younger age is needed. The contradiction of ranges of the radiolarian zone shown by Matsuoka (1995) was pointed out for stratigraphically important *Kilinora spiralis*, *Loopus primitivus* (Matsuoka and Yao), *Striatojaponocapsa plicarum* (Yao) and *S. conexa* by Hori *et al.* (2002). Because the occurrence of *S. conexa* and *S. synconexa* can also be explained by reworking to the lowest Kimmeridgian strata, we focus on *Eucyrtidiellum* cf. *pyramis*, whose ranges are the youngest among the fauna from Loc. 1. The genus *Eucyrtidiellum* is composed of 19 species. The form of *E. pyramis* is quite distinctive, with widely spaced longitudinal plicae on both the thorax and abdomen and a smooth cone shape, from any other *Eucyrtidiellum* species. The first occurrence of *E. pyramis* was correlative to the radiolarian *Ditrabs sansalvadorensis* Zone of Aita (1987) and UAZ 12 of Baumgartner *et al.* (1995), indicating the Tithonian according to Aita (1987) and Goričan *et al.* (2018). The oldest occurrence of *E. pyramis* is from the Nusplingen Lithographic Limestone in Germany, which yielded late Kimmeridgian ammonoids indicative of the *Lithacoceras ulmense* Subzone of Zügel *et al.* (1998). Although it is unclear why *E.* cf. *pyramis*, *S.* cf. *conexa* and *S. synconexa* co-exist in the same sample, the sample can be roughly dated to the Kimmeridgian (157.3±1.0 Ma to 152.1±0.9 Ma).

4. 2. 2 Radiolarians at Loc. 2

Radiolarian fossils at Loc. 2 were more deformed and recrystallized than those at Loc. 1. Their surface structure was difficult to identify. A total of 11 taxa at the genus or species level were identified in this sample. Identified taxa at the species level are *Archaeodictyomitra* cf. *inornata*, *Archaeodictyomitra* aff. *rigida*, *Archaeodictyomitra* cf. *tyaughtonensis* Cordey, *Cinguloturris* cf. *carpatica*, *Cinguloturris* cf. *floridicingula* (Li), *Cinguloturris* cf. *getsensis* O’Dogherty *et al.* and *Zhamoidellum* cf. *mikamense* Aita. Although three of these seven species (*A*. cf. *inornata*, *A*. aff. *rigida* and *C*. cf. *carpatica*) were also found at Loc. 1, they are generally dated to the late Middle Jurassic (probably Callovian) to middle Late Jurassic (probably Kimmeridgian). There were no taxa that could be certainly assigned to a geologic age later than this suggested age. It was impossible to determine ages at higher resolution. Most of these species (e.g. *A*. cf. *tyaughtonensis*) are rarely reported after their first description or they cannot be used for age determination. For example, *Cinguloturris carpatica* belongs to the latter case. It is subdivided into several *Cinguloturris* species, such as *C. floridicingula* and *C. getsensis*. *Zhamoidellum mikamense* was combined with *Zhamoidellum ovum* Dumitrică as a junior synonym (Baumgartner *et al.*, 1995). Thus, taxonomic confirmation of these two species is needed to determine the precise age. In consideration of the insufficient number of reports for the rare taxa and incomplete updating of the taxonomic concept of age-index species, we retain the radiolarian age for the Loc. 2 sample as the late Middle Jurassic (probably Callovian) to middle Late Jurassic (probably Kimmeridgian).

5. Discussion

5. 1 Depositional age of clastic rocks

The youngest cluster U–Pb ages of detrital zircon from sandstone in the Omori area are 154.7±1.5 Ma (1σ) and 155.6±3.2 Ma (2σ), obtained using different calculation methods (Uchino, 2018b). These ages correspond to the latest Oxfordian–Kimmeridgian under the geologic time scale of Cohen *et al.* (2013). A detrital zircon age suggests only a possible lower limit of a depositional age of sandstone, although the zircon age can approximate the depositional age if volcanism in its hinterland was very active. However, volcanism in eastern Asia, including the paleo-Japanese islands, was not very active during the Late Jurassic–earliest Cretaceous (e.g. Sagong *et al.*, 2005; Kiminami and Imaoka, 2013; Lee *et al.*, 2018). The low age spectrum peak of the youngest cluster of the detrital zircon from the sandstone in the Omori area shown by Uchino (2018b) probably reflects this weak volcanism in the hinterland. Therefore, the sandstone was deposited in the latest Oxfordian–Kimmeridgian or later.

The radiolarian fossil age from mudstone can directly indicate the depositional age of the mudstone if the fossils were not reworked. In consideration of the reliability of the assigned radiolarian ages for the mudstone at Locs. 1 and 2, the mudstone ages of the Kimmeridgian at Loc. 1 and the late Middle Jurassic (probably Callovian) to middle Late Jurassic (probably Kimmeridgian) at Loc. 2 are close to the U–Pb age of the sandstone in the Omori area. In addition, the horizons of the mudstone and sandstone are close to each other without any recognizable distinctive tectonic discontinuity between them (Figs. 5, 6), indicating that these clastic rocks may be stratigraphically continuous or contemporaneous sequences. Therefore, the clastic rocks in the Omori area were deposited in a trench around the Kimmeridgian (middle Late Jurassic).

5. 2 Tectonostratigraphic correlation

The ACs identified in the Shimokita Peninsula are, from north to south, the Shiriya Complex (the Iwaya and Shitsukari units) in the Kuwabatayama area, an unnamed AC in the Katasakiyama area and an unnamed AC in the Omori area. Tsushima and Takizawa (1977) pointed out that the Iwaya Unit (“C formation” in the original paper) of the Shiriya Complex in the Kuwabatayama area is similar to the northernmost part of the AC in the Katasakiyama area (Fig. 3). In consideration of the trends in geologic structures, such as the NE–SW strikes of the Shitsukai Unit in the northern Kuwabatayama area, the N–S to NW–SE strikes of the Iwaya Unit in the southern Kuwabatayama area, the NNE–SSW to NNW–SSE strikes of the AC in the Katasakiyama area and the NW–SE to NNW–SSE strikes in the Omori area, the Iwaya Unit in the Kuwabatayama area and the ACs in the Katasakiyama and Omori areas are presumably tectonically continuous (Fig. 2a).

According to Ueda *et al.* (2018) and other previous papers, the Iwaya Unit differs from the Shitsukari Unit in that the latter exclusively contains basalt, huge limestone blocks and lithic sandstone, and is characterized by slump facies indicating debrite (Figs. 2a, 3). In addition, the age of the clastic rocks in the Iwaya Unit is the Late Jurassic, younger than the Early Cretaceous age of the clastic rocks in the Shitsukai Unit.

The lithologies of the ACs in the Katasakiyama and Omori areas are more similar to that in the Iwaya Unit than that in the Shitsukai Unit, in particular in terms of the presence of characteristic quartzo-feldspathic sandstone (Fig. 4a) and small amounts of limestone and conglomerate. The assigned age of the Kimmeridgian (the Late Jurassic) to the clastic rocks of the AC in the Omori area overlaps the age of the Iwaya Unit in the southern Kuwabatayama area, which supports the probable tectonostratigraphic continuity of the ACs in the Katasakiyama and Omori areas to the Iwaya Unit in the Kuwabatayama area.

Although more detailed studies are needed to confirm this assumption, the ACs in the northeastern Shimokita Peninsula are likely to comprised a Late Jurassic tectonostratigraphic unit and an overlain Early Cretaceous unit. The former is the Iwaya Unit in the southern Kuwabatayama area and the unnamed ACs in the Katasakiyama and Omori areas, and the latter is the Shitsukari Unit, which has only been found in the northern Kuwabatayama area so far.

5. 3 Younging polarity

It has been reported that a younging polarity of accretion ages for trench-fill terrigenous clastic rocks in the North Kitakami Belt is detectable from the southwest to the northeast, in a direction perpendicular to the general NW–SE to NNW–SSE distribution trends of the ACs in the belt (e.g. Suzuki *et al.*, 2007a; Ehiro *et al.*, 2008; Kojima *et al.*, 2016) (Figs. 1, 7). The geologic columns of the ocean plate stratigraphy reconstructed in each area are compiled in Fig. 7, although the terms “complex” and “unit” are mixed in the figure. The depositional ages of terrigenous rocks within the ACs in the “B” zone of Otoh and Sasaki (2003) range from the Late Triassic in the Kadoma Complex (Uchino, 2017), through the Early Jurassic in the Nishimatayama Unit and the Nakatsugawa Complex (Ueda *et al.*, 2009; Uchino, 2019), to the Middle Jurassic in the Shibamori Complex, possibly the Nakatsugawa Complex, and the Tsugaruishi Unit (Yoshihara *et al.*, 2002; Suzuki and Ogane, 2004; Suzuki *et al.*, 2007a; Uchino, 2018a; Uchino, 2019). No age data for the trench-fill terrigenous rocks has been reported in the “C” zone excluding the Late Jurassic coral fossils from possible shallow marine deposits. The “D” and “E” zones range from the Middle Jurassic to the Late Jurassic in the Kado–Akka areas (Nakae and Kamada, 2003; Suzuki *et al.*, 2007b; Ehiro *et al.*, 2008).

The “B”–“E” zones belong to the Kuzumaki–Kamaishi Subbelt, and the “A” zone belongs to the Nedamo Belt. The Akka–Tanohata Subbelt fully corresponds to the “F” and “G” zones, whose depositional ages range from the Middle–Late Jurassic in the Takayashiki and Magisawa units (Minoura and Tsushima, 1984; Matsuoka and Oji, 1990; Suzuki *et al.*, 2007a), through the Late Jurassic in the Iwaya Unit and its equivalent (Matsuoka, 1987; Ueda *et al.*, 2018; this study), to the late Late Jurassic to the early Early Cretaceous in the Shitsukari Unit (Matsuoka, 1987; Ueda *et al.*, 2018). The present study confirmed that the Late Jurassic ACs in the northeastern Shimokita Peninsula are distributed in the Kuwabatayama area as the Iwaya Unit and in the Omori area as an unnamed AC, and probably in the Katasakiyama area as an unnamed AC.

A well-ordered younging polarity was found in the

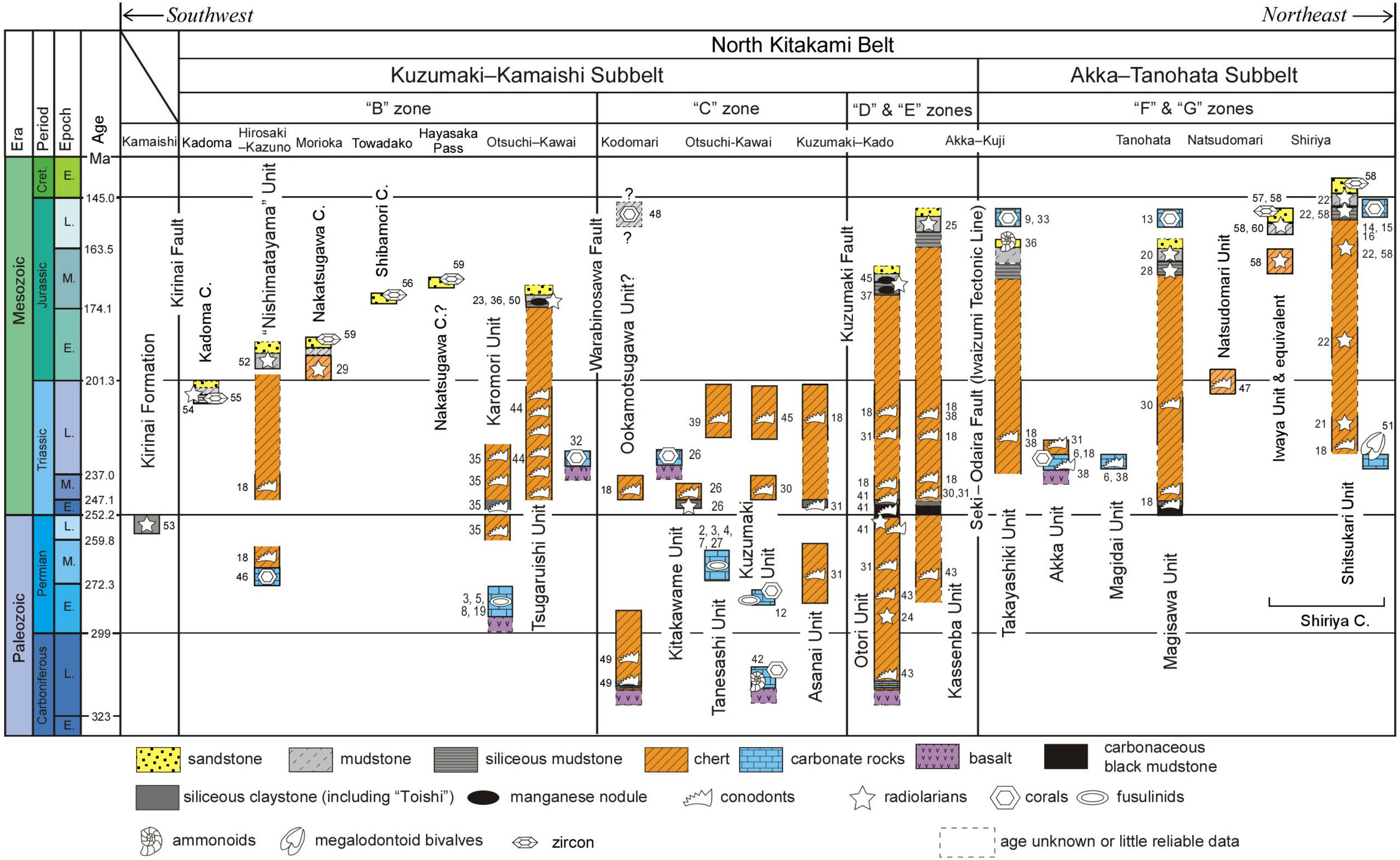

Fig. 7 Schematic compilation diagram of age and lithostratigraphic column of the North Kitakami Belt. This diagram was revised based on Fig. 42 of Suzuki *et al.* (2007a), Fig. 3 of Ehiro *et al.* (2008) and Fig. 2b. 41 of Kojima *et al.* (2016). Numbers beside fossil and zircon symbols correspond to literature references. See Suzuki *et al.* (2007a) for nos. 1–35 and Ehiro *et al.* (2008) for nos. 36–45. 46: Fujimoto and Kobayashi (1961), 47: Murata and Nagai (1972), 48: Kato (1972), 49: Murata *et al.* (1974), 50: Yoshihara *et al.* (2002); 51: Sano *et al.* (2009), 52: Ueda *et al.* (2009), 53: Nakae and Kurihara (2011), 54: Kawamura *et al.* (2013), 55: Uchino (2017), 56: Uchino (2018a), 57: Uchino (2018b), 58: Ueda *et al.* (2018), 59: Uchino (2019), 60: this study. See Otoh and Sasaki (2003) for “A”–“G” zones. L.: Late, M.: Middle, E.: Early, C.: Complex. Tectonostratigraphic names are taken from the original papers or Fig. 2b. 41 of Kojima *et al.* (2016), and the appropriateness of the terms “complex” and “unit” are not discussed in the present paper.

Kuzumaki–Kamaishi Subbelt. By contrast, the age polarity in the Akka–Tanohata Subbelt appears somewhat disordered, as shown in Fig. 7. Possible reasons for this disorder include wrong reconstruction of complexes/units, no age data for the terrigenous clastic rocks of the Magidai Unit in the Tanohata area, and repeated distribution of the same tectonostratigraphic units by folding or out-of-sequence thrust. Despite this, when viewing the younging polarity from a broad perspective, the trend from the Late Triassic of the southwesternmost AC (Kadoma Complex) of the Kuzumaki–Kamaishi Subbelt to the early Early Cretaceous of the northeasternmost AC (Shitsukari Unit of the Shiriya Complex) of the Akka–Tanohata Subbelt is well constrained in the North Kitakami Belt based on the data in this study.

6. Conclusion

Radiolarian fossils from around the Kimmeridgian (middle Late Jurassic) were extracted from mudstone in the AC in the Omori area, northeastern Shimokita Peninsula. The ACs in the Kasakiyama and Omori areas are correlative to the Iwaya Unit, the southern unit in the Kuwabatayama area, based on the lithology, geologic structure and clastic rock ages.

Acknowledgments:We are grateful to Dr. Kamata, Y. (University of Tsukuba) for reviewing the manuscript.

References

Aita, Y. (1987) Middle Jurassic to Lower Cretaceous radiolarian biostratigraphy of Shikoku with reference to selected sections in Lombardy basin and Sicily. *The Science Reports of the Tohoku University, Second Series (Geology)*, **58**, 1–91.

Aita, Y. and Okada, H. (1986) Radiolarians and calcareous nannofossils from the uppermost Jurassic and Lower Cretaceous strata of Japan and Tethyan regions. *Micropaleontology*, **32**, 97–128.

Baumgartner, P. O., Bartolini, A., Carter, E. S., Conti, M., Cortese, G., Danelian, T., DeWever, P., Dumitrica, P., Dumitrica-Jud, R., Gorican, S., Guex, J., Hull, D. M., Kito, N., Marcucci, M., Matsuoka, A., Murchey, B., O'Dogherty, J., Savaray, J.,Vishnevskaya, V.,Widz, D. and Yao, A. (1995) Middle Jurassic to Early Cretaceous radiolarian biochronology of Tethys based on UnitaryAssociations. *Memories de Geologie (Lausanne)*, no. 23, 1013–1048.

Cohen, K. M., Finney, S. C., Gibbard, P. L. and Fan, J. -X. (2013) The ICS International Chronostratigraphic Chart. *Episodes*, **36**, 199–204.

Dumitrică, P. and Mello, J. (1982) On the age of the Meliata Group and the Silica Nappe radiolarites (localities Držkovce and Bohúňovo, Slovak Karst, ČSSR). *Geologické Práce,* **77**, 17–28.

Ehiro, M., Kawamura, M. and Kawamura, T. (2005) *Appendix for the Geology of Japan: General Geology and Divisions, Meso–Paleozoic of the Tohoku district*. 49–50, Kyoritsu Publishing, Tokyo (in Japanese).

Ehiro, M., Yamakita, S., Takahashi, S. and Suzuki, N. (2008) Jurassic accretionary complexes of the North Kitakami Belt in the Akka–Kuji area, Northeast Japan. *The Journal of the Geological Society of Japan*, **114** Supplement, 121–139 (in Japanese).

Fujimoto, H. and Kobayashi, F. (1961) On the Paleozoic deposites of the Inner Zone of the Ou region. *The Journal of the Geological Society of Japan*, **67**, 221–227 (in Japanese with English abstract).

Geological Survey of Japan, AIST (2019) *Seamless Digital Geological Map of Japan (1:200,000) V2*, https://gbank.gsj.jp/seamless/ (Accessed: 2019-02-14).

Goričan, S., O'Dogherty, L., Baumgartner, P. O., Carter, E. S. and Matsuoka, A. (2018) Mesozoic radiolarian biochronology – current status and future directions. *Revue de Micropaléontologie*, **61**, 165–189.

Grill, J. and Kozur, H. (1986) The first evidence of the *Unuma echinatus* radiolarian zone in the Rudabanya Mts. (Northern Hungary). *Geologisch-Paläontologische Mitteilungen Innsbruck*, **13**, 239–275.

Hatakeda, K., Suzuki, N. and Matsuoka, A. (2007) Quantitative morphological analyses and evolutionary history of the Middle Jurassic polycystine radiolarian genus *Striatojaponocapsa* Kozur. *Marine Micropaleontology*, **63**, 39–56.

Hori, N. (1999) Latest Jurassic radiolarians from the northeastern part of the Torinoko Block, Yamizo Mountains, central Japan. *Science Reports of the Institute of Geoscience, University of Tsukuba, Section B: Geological Sciences*, **20**, 27–114.

Hori, N., Saito, M. and Toshimitsu, S. (2002) Late Jurassic radiolarian fauna from the Ikenohara Formation of the Kurosegawa Belt in the Toyo-Izumi area, Kumamoto Prefecture, Kyushu, Japan. *Bulletin of the Geological Survey of Japan*, **69**, 37–46.

Imai, I. (1961) *Geological Sheet Map 1:50,000 "Chikagawa"*, Geological Survey of Japan. 45p (in Japanese with English abstract).

Ishida, K, Tsujino, Y, Kozai, T, Sato, T. and Hirsch, F. (2009) Direct correlation of radiolarian *Kilinora spiralis* Zone with the Late Jurassic ammonite faunal succession in the Kurisaka Formation, Kurosegawa Terrane, SW Japan. *Science in China Series D Earth Sciences*, **52**, 1910–1923.

Kamada, K. (2000) Shiriya Complex: Pre-Tertiary accretional complex at Cape Shiriya, northern Japan. *Bulletin of the Faculty of Education, Hirosaki University*, **83**, 39–47 (in Japanese with English abstract).

Kato, M. (1972) "Paleozoic strata" in the Tsugaru Peninsula, Aomori Prefecture. *The Journal of the Geological Society of Japan*, **78**, 515 (in Japanese).

Kawamura, M., Otsu, S., Terada, T. and Yasuda, N. (1994) Geology and internal structure of the Oshima accretionary complex. *Field Trip Guidebook, 101st Annual Meeting of Geological Society of Japan*, 175–195, Nakanishi Printing Office, Sapporo (in Japanese).

Kawamura, T., Uchino, T. and Kawamura, M. (2013) Chapter 8, Jurassic of the North Kitakami Terrane, *Geology of the Hayachine San District*. Quadrangle Series, 1:50,000, Geological Survey of Japan, AIST, 62–67 (in Japanese with English abstract).

Kiminami, K. and Imaoka, T. (2013). Spatiotemporal variations of Jurassic–Cretaceous magmatism in eastern Asia (Tan-Lu Fault to SW Japan): Evidence for flat-slab subduction and slab rollback. *Terra Nova*, **25**, 414–422.

Kojima, S., Hayasaka, Y., Hiroi, Y. Matsuoka, A., Sano, H., Sugamori, Y., Suzuki, N., Takemura, S., Tsujimori T. and Uchino, T. (2016) 2b Pre-Cretaceous accretionary complexes. *In* Moreno, T., Wallis, S., Kojima, T. and Gibbons, W., eds., *The Geology of Japan*, Geological Society of London, 61–100.

Lee, T.-H., Park, K.-H. and Yi, K. (2018) SHRIMP U–Pb ages of detrital zircons from the Early Cretaceous Nakdong Formation, south east Korea: Timing of initiation of the Gyeongsang Basin and its provenance. *Island Arc*, **27**, e12258. doi:10.1111/iar.12258.

Matsuoka, A. (1987) Radiolarian age of the Shiriya Group in Aomori Prefecture, northeast Japan. *Fossils*, **42**, 7–13 (in Japanese with English abstract).

Matsuoka, A. (1995) Jurassic and Lower Cretaceous radiolarian zonation in Japan and in the western Pacific. *The Island Arc*, **4**, 140–153.

Matsuoka, A. and Oji, T. (1990) Middle Jurassic radiolarian fossils from the Magisawa Formation in the Taro Belt, North Kitakami Mountains. *The Journal of the Geological Society of Japan*, **96**, 239–241 (in Japanese).

Minoura, K. (1985) Where did the Kitakami and Abukuma Massif come from?: How to develop the geological structure of the Tohoku of Japan. *Kagaku*, **55**, 14–23 (in Japanese).

Minoura, K. and Tsushima, H. (1984) Geology of the Omoto district in the eastern margin of the North Kitakami Massif. *The Science Report of the Hirosaki University*, no. 31, 93–107 (in Japanese).

Murata, M. (1962) The Upper Jurassic of Cape Shiriya, Aomori Prefecture, Japan. *The Science Reports of the Tohoku University, Series 2, Special Volume*, no. 5, 119–126.

Murata, M. and Nagai, T. (1972) Discovery of conodonts from Sekkenai, Hiranai-cho, Higashi-Tsugaru-gun, Aomori Prefecture, Japan. *Professor Jun-ichi Iwai Memorial Volume*, 709–717.

Murata, M., Nagai, T. and Kawamura, S. (1974) Signification and occurrence of late Carboniferous conodont fossil from Cape Kodomari, Tsugaru Peninsula, Aomori Prefecture, Japan. *Aomori-Chigaku*, no. 26, 3–5 (in Japanese). http://aomorichigaku.web.fc2.com/fc2-imageviewer/?aid=1&iid=24 (Accessed:2019-02-14)

Nakae, S. and Kamada, K. (2003) Late Jurassic radiolarians from the Rikuchu-Seki district in the North Kitakami Belt, Northeast Japan. *The Journal of the Geological Society of Japan*, **109**, 722–725 (in Japanese with English abstract).

Nakae, S. and Kurihara, T. (2011) Direct age determination for an Upper Permian accretionary complex (Kirinai Formation), Kitakami Mountains, Northeast Japan. *Palaeoworld*, **20**, 146–157.

Nishizono, Y. (1996) Mesozoic convergent process of the Southern Chichibu Terrane in west Kyushu, Japan, on the basis of Triassic to Early Cretaceous radiolarian biostratigraphy. *Kumamoto Journal of Science, Earth Sciences*, **14**, 45–226.

O'Dogherty, L., Bill, M., Goričan, S., Dumitrica, P. and Masson, H. (2006) Bathonian radiolarians from an ophiolitic mélange of the Alpine Tethys (Gets Nappe, Swiss–French Alps). *Micropaleontology*, **51**, 425–485.

O'Dogherty, L., Goričan, Š. and Gawlick, H.-J. (2017) Middle and Late Jurassic radiolarians from the Neotethys suture in the Eastern Alps. *Journal of Paleontology*, **91**, 25–72.

Oho, Y. and Iwamatsu, A. (1986) Olistostrome in the Shiriyazaki area of the Shimokita Peninsula, Northeast Japan. *The Journal of the Geological Society of Japan*, **92**, 109–118 (in Japanese with English abstract).

Onuki, Y. (1959) Discovery of Hexacorals from the Shiriya district, Aomori Prefecture, Northeast Japan. *The Journal of the Geological Society of Japan*, **65**, 248 (in Japanese).

Otoh, S. and Sasaki, M. (2003) Tectonostratigraphic division and regional correlation of the sedimentary complex of the North Kitakami Belt. *Journal of Geography (Chigaku Zasshi)*, **112**, 406–410.

Ožvoldová, L., Jablonsky, J. and Frantova, L. (2000) Upper Jurassic radiolarites of the Czertezic succession and comparison with the Kysuca succession in the east-Slovak part of the Pienny Klippen Belt (western Carpathians, Slovakia). *Geologica Carpathica*, **51**, 109–119.

Sano, S., Sugisawa, N. and Shimaguchi, T. (2009) Discovery of megalodontoid bivalves in the Shiriya area, northern Honshu, Northeast Japan, and its geological implications. *Memoir of the Fukui Prefectural Dinosaur Museum*, **8**, 51–57 (in Japanese with English abstract).

Sagong, H., Kwon, S.-T. Ree, J.-H. (2005) Mesozoic episodic magmatism in South Korea and its tectonic implication. *Tectonics*, **24**, TC5002, doi:10.1029/2004TC001720.

Steiger, T. (1992) Systematik, stratigraphie und Palökologie der Radiolarien des Oberjura-Unterkrieden-Grenzbereiches im Osterhorn-Tirolikum (Nördliche Kalkalpen, Salzburg und Bayern). *Zitteliana*, **19**, 3–188.

Suzuki, N. and Ogane, K. (2004) Paleoceanographic affinities of radiolarian faunas in late Aalenian time (Middle Jurassic) recorded in the Jurassic accretionary complex of Japan. *Journal of Asian Earth Sciences*, **23**, 343–357.

Suzuki, N., Ehiro, M., Yoshihara, K., Kimura, Y., Kawashima, G., Yoshimoto, H. and Nogi, T. (2007a) Geology of the Kuzumaki–Kamaishi Subbelt of the North Kitakami Belt (a Jurassic accretionary complex), Northeast Japan: Case study of the Kawai–Yamada area, eastern Iwate Prefecture. *Bulletin of the Tohoku University Museum*, no. 6, 103–174.

Suzuki, N., Yamakita, S., Takahashi, S. and Ehiro, M. (2007b) Middle Jurassic radiolarians from carbonate manganese nodules in the Otori Formation in the eastern part of the Kuzumaki–Kamaishi Subbelt, the North Kitakami Belt, Northeast Japan. *The Journal of the Geological Society of Japan*, **113**, 274–277 (in Japanese with English abstract).

Toyohara, F., Uesugi, K., Kimura, T., Ito, T., Murata, A. and Iwamatsu, A. (1980) Northern Kitakami Massif: Geosynclines in the Oshima Peninsula. *In* Kimura, T., ed., *Reexamination of geosynclines and tectonic division on the northern part of the Japanese Islands*, Science Report (Fund type A) for Grants-in-Aid for Scientific Research (The Ministry of Education, Science, Sports and Culture), Tokyo University, 27–36 (in Japanese).

Tsushima, K. and Takizawa, F. (1977) *Geology of the Shiriyazaki District. With Geological Sheet Map at 1:50,000*, Geological Survey of Japan. 36p (in Japanese with English abstract).

Uchino, T. (2017) Late Triassic U–Pb-zircon age from tuffaceous mudstone in the Kadoma Complex, North Kitakami Belt, Northeast Japan. *The Journal of the Geological Society of Japan*, **123**, 977–982 (in Japanese with English abstract).

Uchino, T. (2018a) Detrital zircon U–Pb age of the Jurassic accretionary complex in the western area of Lake Towada located between Akita and Aomori prefectures, Northeast Japan. *Bulletin of Geological Survey of Japan*, **69**, 37–46 (in Japanese with English abstract).

Uchino, T. (2018b) Detrital zircon U–Pb age of sandstone within the Jurassic accretionary complex in the Omori area, northeastern Shimokita Peninsula, Northeast Japan. *Bulletin of Geological Survey of Japan*, **69**, 125–133 (in Japanese with English abstract).

Uchino, T. (2019) Detrital zircon U–Pb ages of sandstone within the Jurassic accretionary complex in the North Kitakami Belt of the Sotoyama District, Iwate Prefecture, Northeast Japan. *Bulletin of Geological Survey of Japan*, **70**, 357–372 (in Japanese with English abstract).

Ueda, H., Mori, M. and Sato, I. (2009) Early Jurassic radiolarian fossils from mudstone within an accretionary complex south of Hirosaki City, Aomori Prefecture, Japan. *The Journal of the Geological Society of Japan*, **115**, 610–613 (in Japanese with English abstract).

Ueda, H., Kimura, S., Saito, T., Takano, Y., Iizuka, N. and Orihashi, Y. (2018) Material recycling in a sediment-starved trench recorded in the Early Cretaceous Shiriya accretionary complex, Northeast Japan. *Island Arc*, **27**, e12272. doi:10.1111/iar.12272.

Yang, Q. and Matsuoka, A. (1997) A comparative study on Upper Jurassic radiolarian biostratigraphy of the Taman Formation, east-central Mexico and the ODP Site 801B Section, west Pacific. *Science Reports of Niigata University, Series E (Geology)*, no. 12, 29–49.

Yoshihara, K., Suzuki, N. and Ehiro, M. (2002) Middle Jurassic radiolarian-bearing nodules from the Kuzumaki-Kamaishi Subbelt in the northern Kitakami Massif and its significance. *The Journal of the Geological Society of Japan*, **108**, 536–539 (in Japanese with English abstract).

Zügel, P., Riegraf, W., Schweigert, G. and Dietl, G. (1998) Radiolaria from the Nusplingen Lithographic Limestone (Late Kimmeridgian, SW Germany). *Stuttgarter Beiträge zur Naturkunde, Serie B*, no. 268, 1–44.

Recieved July 9, 2019
Accepted March 12, 2020
Published on-line May 7, 2020

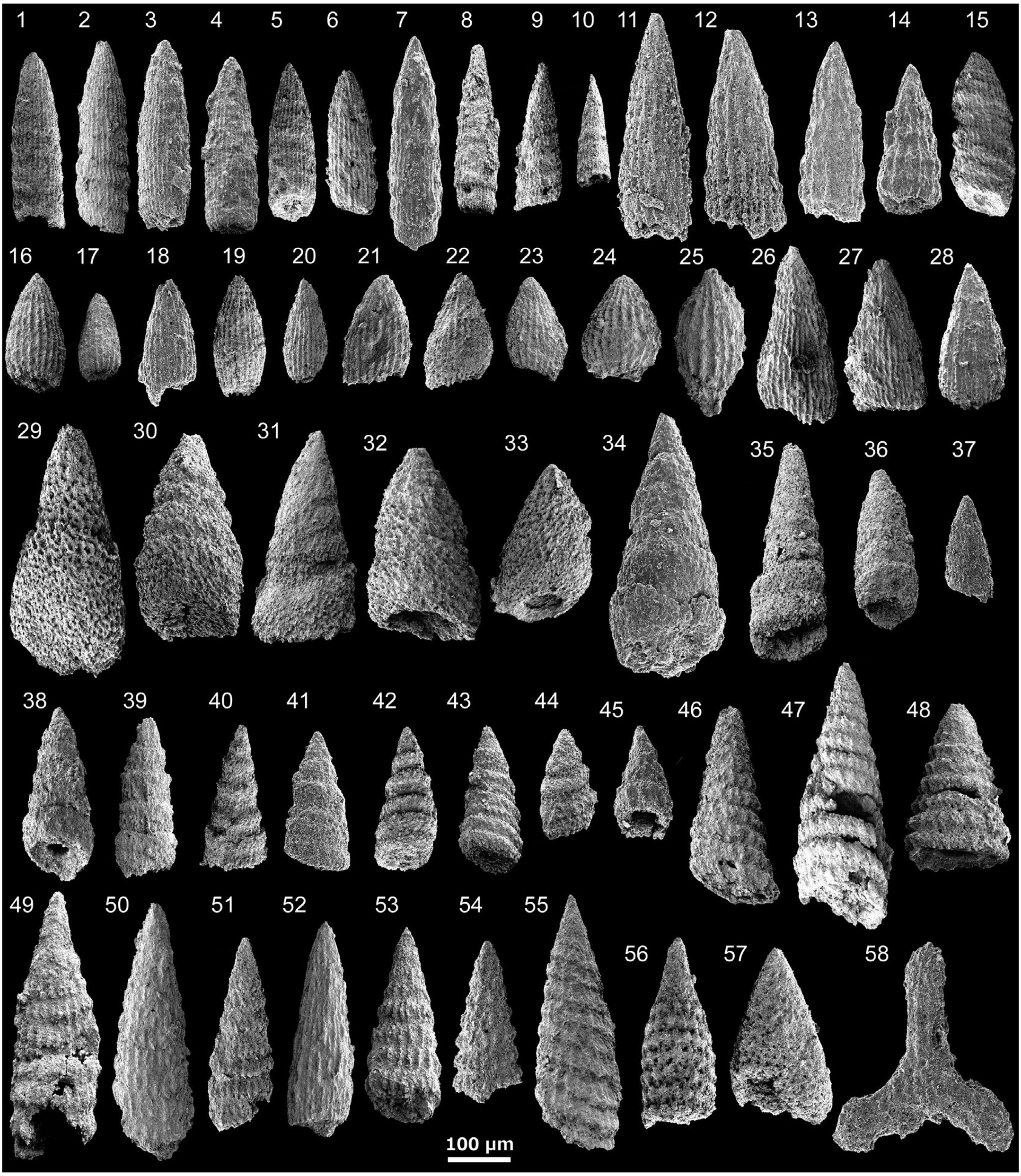

Plate 1 Scanning electron microscopy images of the Kimmeridgian (middle Late Jurassic) radiolarians extracted from mudstone at Loc. 1. **1**–**3**: *Archaeodictyomitra spelae* Chiari, Cortese and Marcucci, **4**–**6**: *Archaeodictyomitra* cf. *spelae* Chiari, Cortese and Marcucci, **7**: *Archaeodictyomitra* aff. *prisca* Kozur and Mostler, **8**: *Archaeodictyomitra* sp. A, **9**–**10**: *Archaeodictyomitra* sp. B, **11**–**14**: *Archaeodictyomitra* aff. *vulgaris* Pessagno, **15**: *Archaeodictyomitra* cf. *unica* Wu, **16**–**17**: *Archaeodictyomitra* aff. *rigida* Pessagno, **18**–**20**: *Archaeodictyomitra* aff. *suzukii* Aita, **21**–**23**: *Archaeodictyomitra* cf. *inornata* Hull, **24**: *Archaeodictyomitra* sp. C, **25**: *Archaeodictyomitra* sp. D, **26**–**28**: *Parahsuum mudongensis* (Li) sensu lato, **29**–**31**: *Spongocapsula palmerae* Pessagno, **32**–**33**: *Spongocapsula* sp., **34–36**: *Spongocapsula*? sp., **37:** *Loopus* cf. *venusta* (Chiari, Cortese and Marucci), **38**–**43**: *Cinguloturris* cf. *carpatica* Dumitrică, **44**: *Cinguloturris* cf. *latiannulatum* (Grill and Kozur), **45**: *Cinguloturris* sp., **46**–**47**: *Svinitzium* sp., **48**: *Wrangellium* sp., **49**–**55**: *Transhsuum* sp., **56**–**57**: Nassellaria gen. et sp. indet., **58**: Pyloniodea et sp. indet.

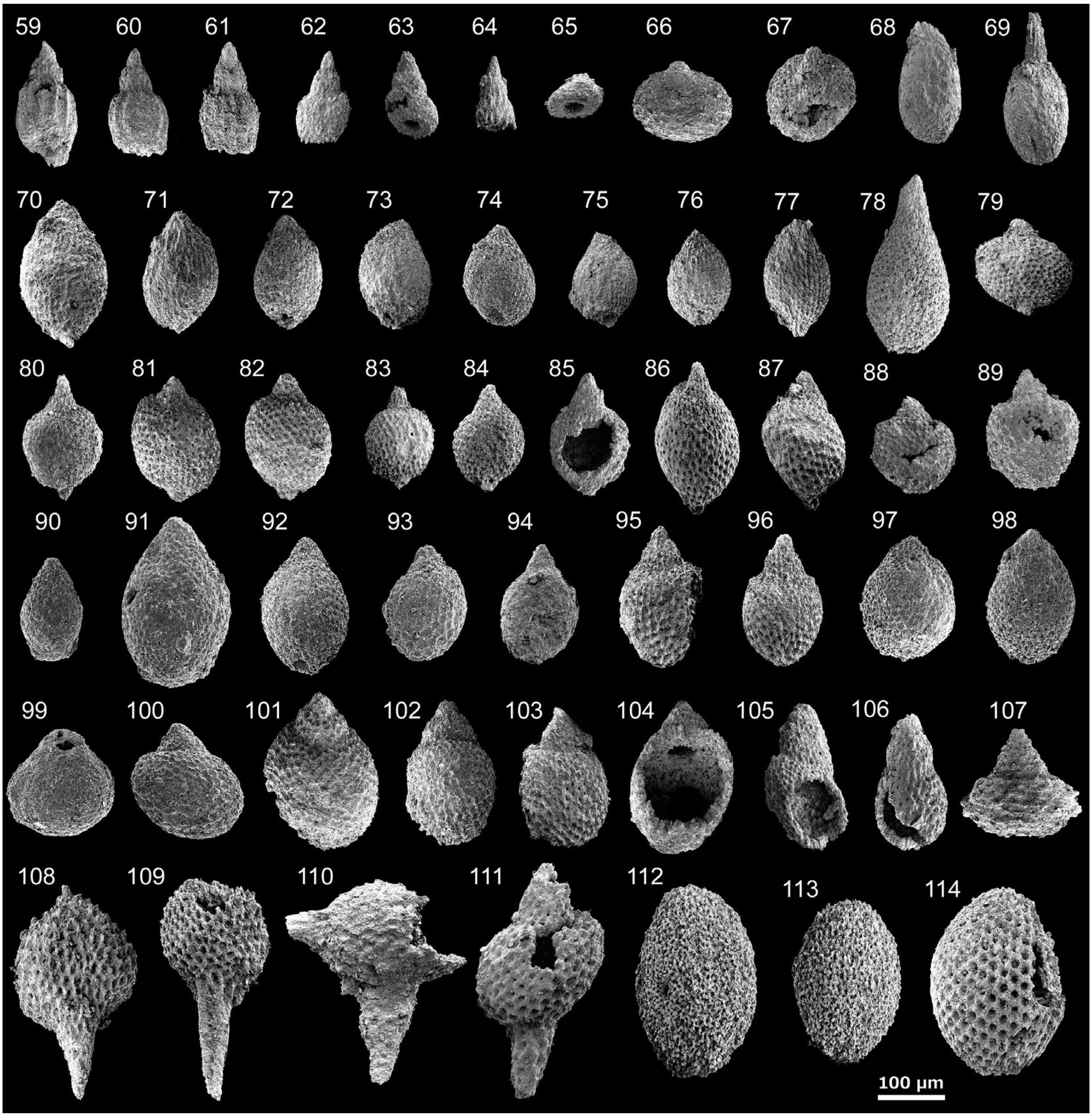

Plate 1 (Continued)
59–**61**: *Eucyrtidiellum* cf. *pyramis* (Aita), **62**: *Eucyrtidiellum* cf. *nodosum* Wakita, **63**: *Crococapsa* aff. *truncata* (Wu), **64**–**68**: Nassellaria gen. et sp. indet., **69**: *Kilinora* sp., **70**: *Striatojaponocapsa* cf. *conexa* (Matsuoka), **71**–**76**: *Striatojaponocapsa synconexa* O'Dogherty, Goričan and Dumitrică, **77**: *Striatojaponocapsa* sp., **78**: *Praewilliriedellum* sp., **79**: *Hemicryptocapsa carpathica* (Dumitrică), **80**–**87**: *Williriedellum* sp., **88**–**89**: *Minutosolla* sp., **90**: *Praezhamoidellum*? sp., **91**–**92**: *Hiscocapsa robusta* (Matsuoka), **93**: *Hemicryptocapsa* cf. *yaoi* (Kozur), **94**–**98**: *Praezhamoidellum* sp., **99**: *Zhamoidellum* sp., **100**: *Zhamoidellum* cf. *ventricosum* Dumitrică, **101**–**104**: *Zhamoidellum ovum* Dumitrică, **105**–**106**: *Complexapora* aff. *kiesslingi* Hull, **107**: Minocapsidae gen. et sp. indet., **108**: *Archaeospongoprunum* sp., **109**: *Archaeospongoprunum* cf. *mizutanii* Ožvoldová, **110**: *Podobursa* sp., **111**: *Favosyringium* cf. *affine* (Rüst) sensu Steiger (1992), **112**–**113**: *Bistarkum* aff. *mangartense* Goričan, Šmuc and Baumgartner, **114**: Nassellaria gen. et sp. indet.

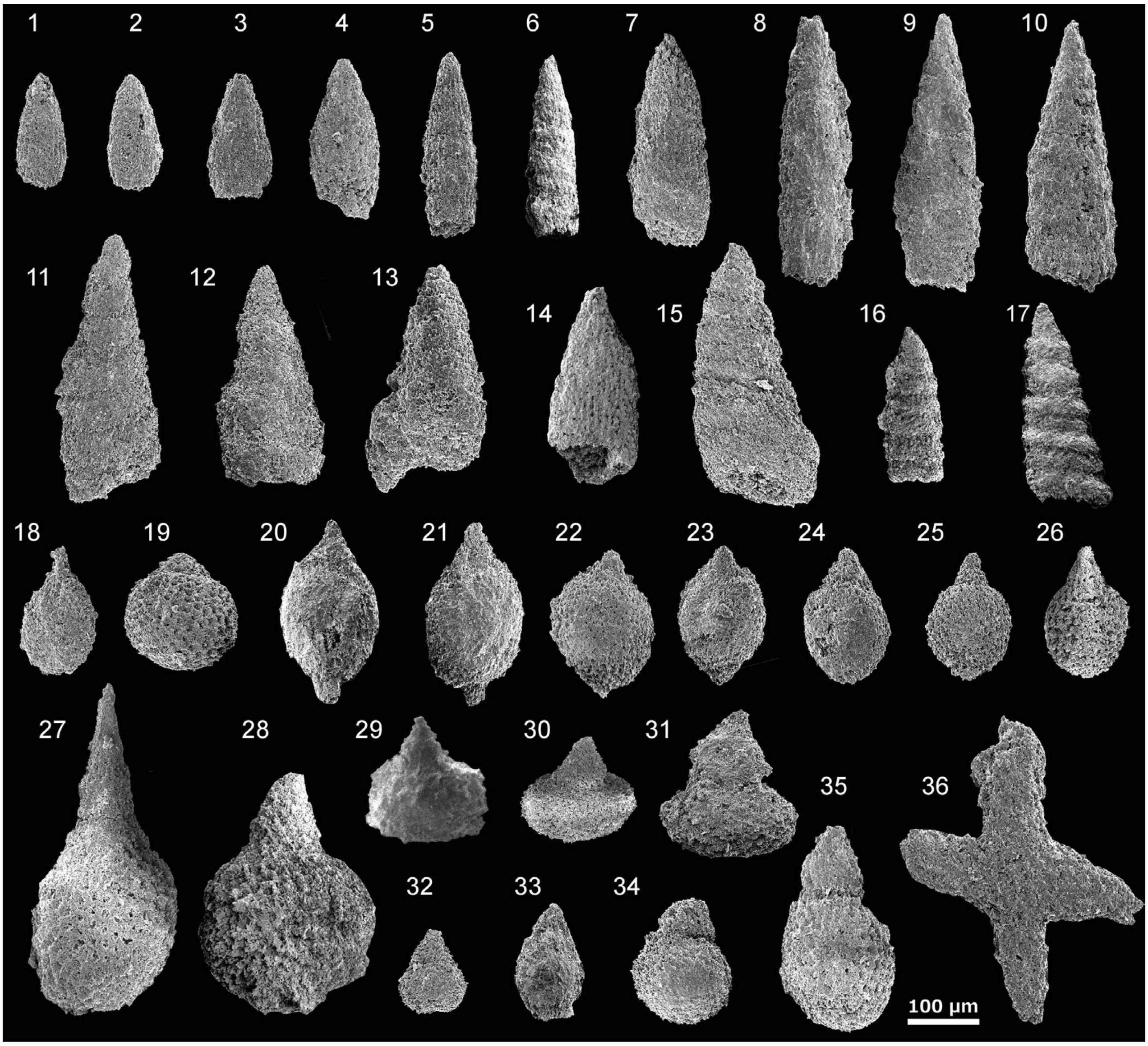

Plate 2 Scanning electron microscopy images of probably Callovian–Kimmeridgian radiolarians extracted from mudstone at Loc. 2. **1–2**: *Archaeodictyomitra* aff. *rigida* Pessagno, **3**: *Archaeodictyomitra* cf. *tyaughtonensis* Cordey, **4**: *Archaeodictyomitra* cf. *inornata* Hull, **5–14**: Multisegmented nassellarians, **15**: *Cinguloturris* cf. *floridicingula* (Li), **16**: *Cinguloturris* cf. *getsensis* O'Dogherty, Goričan and Dumitrică, **17**: *Cinguloturris* cf. *carpatica* Dumitrică, **18**: Spherical radiolarians, **19**: *Zhamoidellum* cf. *mikamense* Aita, **20–23**: *Williriedellum* sp., **24–26**: Williriedelloidea gen. et sp. indet., **27–28**: Syringocapsidae? gen. et sp. indet., **29**: *Eucyrtidiellum* sp., **30**: *Quarkus* sp., **31**: *Tetracapsa* sp., **32–35**: Few segmented nassellarians, **36**: Four-armed flat Pylonioidea.

下北半島北東部，北部北上帯の U–Pb 年代測定砂岩近傍の泥岩から得られた後期ジュラ紀放散虫化石

内野　隆之・鈴木　紀毅

要　旨

青森県下北半島の北東部では，北部北上帯に属する付加体が，桑畑山（くわばたやま）地域，片崎山地域，大森地域に分布している．桑畑山地域の付加体については，後期ジュラ紀の岩屋ユニットと前期白亜紀前半の尻労（しつかり）ユニットに区分されるなど，これまで多くの研究がなされているものの，片崎山・大森地域の付加体については，大森地域の砂岩から砕屑性ジルコン U–Pb 年代が得られているほかは，詳しいデータはほとんどない．

本研究ではジルコン年代が測定された砂岩近傍の泥岩から *Eucyrtidiellum* cf. *pyramis* をはじめとする後期ジュラ紀（おそらくキンメリッジアン期）の放散虫化石が見出された．この泥岩の化石年代と砂岩のジルコン年代とは大差なく，また泥岩と砂岩との層準の間に不連続構造面も確認されないことから，両者の堆積年代に大きな乖離はないと考えられる．

岩相・地質構造・放散虫化石年代から，片崎山・大森地域の付加体と，桑畑山地域の岩屋ユニットは対比可能である．つまり，下北半島北東部の付加体は，後期ジュラ紀に形成された桑畑山地域の岩屋ユニット及び片崎山・大森地域の未命名ユニットと，前期白亜紀に形成された桑畑山地域の尻労ユニットとに区分される．

難読･重要地名

Chikagawa：近川，Higashidori：東通，Iwaya：岩屋，Kadoma：門馬，Katasakiyama；Mt. Katasaki：片崎山，Kuwabatayama；Kuwabatakeyama；Mt. Kuwabata：桑畑山，Mt. Noborimori：登森，Mt. Omori；Omori：大森，Mt. Toyamori：トヤ森，Magisawa：槇木沢，Magidai：間木平，Sarugamori：猿ヶ森，Shimokita：下北，Shiriya：尻屋，Shiriyazaki：尻屋崎，Shitsukari：尻労，Takayashiki：高屋敷，Tatemachijima：立待島

Bulletin of the Geological Survey of Japan, vol. 71 (4), p. 331–353, 2020

Article

SIMS analysis of Si isotope for radiolarian test in Mesozoic bedded chert, Inuyama, central Japan

Maximilien BÔLE[1, 2, 3*], IKEDA Masayuki[2, 3], Peter O. BAUMGARTNER[1], HORI S. Rie[4] and Anne-Sophie BOUVIER[1]

Maximilien BÔLE, IKEDA Masayuki, Peter O. BAUMGARTNER, HORI S. Rie and Anne-Sophie BOUVIER (2020) SIMS analysis of Si isotope for radiolarian test in Mesozoic bedded chert, Inuyama, central Japan. *Bulletin of the Geological Survey of Japan*, vol. 71(4), p. 331–353, 5 figs, 2 tables, 2 appendicies.

Abstract: The global silica cycle is an important component of the long-term climate system, yet its controlling factors are largely uncertain due to poorly constrained proxy records. Because radiolarians and other organisms preferentially extract lighter ^{28}Si from the ocean, the $\delta^{30}Si$ of biosiliceous tests can thus be used for a potential proxy of productivity. Additionally, $\delta^{30}Si$ of oceanic silica could have reflected changes in the isotopic ratio of sources and sinks.

Here we show $\delta^{30}Si$ records measured by secondary ion mass spectrometer (SIMS) in radiolarian silica, precipitated inside radiolarian molds in early Mesozoic bedded chert of the Inuyama section, central Japan. Range of measured $\delta^{30}Si$ between -0.3 and 2 ‰ is consistent with that of modern and Cenozoic radiolarian tests. Relatively large intra-chert bed variability up to ~ 0.8 ‰ (1SD) support that $\delta^{30}Si$ of the Mesozoic radiolarian molds are not perfectly homogenized in a chert bed during diagenesis. We found an overall inverse correlation between 10-Myr scale $\delta^{30}Si$ and biogenic silica (BSi) burial flux, which contradicts with a conventional interpretation of $\delta^{30}Si$ as paleoproductivity proxy, despite the low-resolution and scattered our $\delta^{30}Si$ records. Although most of the factors controlling oceanic $\delta^{30}Si$ are difficult to be constrained, this inverse relation might be explained by changes in $\delta^{30}Si$ of mafic/felsic rock weathering ratio, which inferred from paleogeography. Further high-resolution $\delta^{30}Si$ records will allow a better understanding of the past silica cycle.

Keywords: Silicon isotopes, $\delta^{30}Si$, Radiolarites, Mesozoic oceanic silica cycle, SIMS

1. Introduction

The global silica cycle is linked to long-term changes in Earth's climate through feedback mechanisms between atmospheric CO_2, climate and the rate of silicate weathering, followed by carbonate and biogenic silica (BSi) deposition. Changes in Si and C cycle dynamics are linked to global climate changes throughout Earth's history, a relationship, which in turn, allows numerical models to reconstruct past atmospheric pCO_2 (Berner, 1991). Understanding the global silica cycle is therefore crucial to elucidate the response of Earth's surface system to changes in external (astronomical) and internal (tectonic and volcanic) forcings.

Silicate weathering and BSi burial are important to constrain the silica cycle as major source and sink, respectively, but are difficult to quantify, and poorly understood their dynamic relation due to large uncertainties in the proxy records. Radiolarians dominated as producers of BSi during much of the Phanerozoic (Hein *et al.*, 1987), whereas siliceous sponges are largely restricted to marginal settings, and diatoms became quantitatively important only in the Cenozoic (Racki and Cordey, 2000; Kidder and Erwin, 2001). Radiolarites were deposited in a broad low-latitude belt, while radiolarian-bearing siliceous mudstones dominated in mid-latitudes (Baumgartner, 2013).

The volume of Paleozoic and Mesozoic Radiolarian-rich deposits is largely underestimated, because much of the ocean floor has been subducted. Plate tectonic reconstructions of Panthalassa and Tethys, based on accreted remnants preserved in Circum-Caribbean,

[1] Institute of Earth Sciences (ISTE), Faculty of Geoscience, Geopolis, University of Lausanne, 1015 Lausanne, Switzerland
[2] Department of Geosciences, Faculty of Sciences, Shizuoka University, 836 Ohya Suruga, Shizuoka 422-8529, Japan.
[3] Department of Earth and Planetary Science, Graduate School of Science, The University of Tokyo, 7-3-1 Hongo, Bunkyo-ku, Tokyo 113-0033 Japan
[4] Department of Earth Sciences, Faculty of Science, Ehime University, Bunkyo-cho 2-5, Matsuyama, Ehime 790-8577, Japan
[*] Corresponding author: M, BÔLE., Rue des Envers 13, 2400 Le Locle, Switzerland

Circum-Pacific and Himalayan terranes, suggest that radiolarian-rich sediments covered more than 80 % of the area of the Mesozoic ocean (Baumgartner *et al.*, 2018).

The modern oceanic silica cycle is relatively well-known, and is considered to be close to steady state (Tréguer and De La Rocha, 2013). Rivers are the main suppliers of silicic acid to oceans followed by seafloor weathering, groundwater, hydrothermal and aeolian inputs. The surface BSi production of diatoms overpasses by two orders of magnitude of the total silicon input to the ocean resulting in high dissolved silica (DSi) undersaturation and strong recycling. With depth, the undersaturation becomes weaker due to silicon recycling, but never reaches the saturation of any silica phases. Only about 3 % of BSi produced in the photic zone is trapped in sediments (Tréguer and De La Rocha, 2013). If steady state is assumed, the total BSi burial has to be proportional to the total input from all sources on timescales longer than the residence time of oceanic DSi (Treguer and De La Rocha, 2013).

BSi of radiolarian silica in bedded cherts is potentially a unique proxy for past Si cycle, because the estimated radiolarian BSi burial flux in the low-latitude pelagic Panthalassa was comparable with the modern global BSi flux, and was the possible major sink of DSi (Ikeda *et al.*, 2017). This hypothesis is consistent with overall in-phase relation between radiolarian BSi flux and global silicate weathering flux calculated by GEOCARBSULFvolc model (Ikeda *et al.*, 2017), implying that the estimated BSi burial flux can be proportional to silicate weathering flux over timescales longer than residence time of oceanic Si (<100 kyr; Ritterbush *et al.*, 2015).

However, controlling factors for the BSi burial are still controversial. Although changes in oceanic upwelling intensity and consequent BSi productivity are proposed as potential controlling factors (Hori *et al.*, 1993; De Wever *et al.*, 2014), their temporal variations are also difficult to be understood due to large uncertainty in their proxy records, such as Al/Ti ratio (Murray *et al.*, 1993; Murray and Leinen, 1996; Dymond *et al.*, 1997). On the other hand, controlling factors for siliceous weathering are also still debated. Today, more than 70 % of silicate weathering occurs only in <10 % land area with highly-weatherable volcanic rock region under humid monsoonal climate (Hartmann *et al.*, 2014). Considering the Mesozoic paleogeography, wide distribution of the volcanic islands and large igneous provinces under intensified mega-monsoonal climate could have further modulate the global silicate weathering (Ikeda *et al.*, 2017), despite of lack of quantitative constraints.

Si isotope of BSi is a potential proxy to understand past Si cycle. Glacial-Interglacial scale δ^{30}Si variations have been documented (e.g. Brzezinski *et al.*, 2002), potentially due to an increase of the diatom productivity and extraction of light silicon by diatoms during interglacial periods (De La Rocha *et al.*, 1998).

Only few scattered data of δ^{30}Si from radiolaria are published. (Wu *et al.*, 1997; Egan *et al.* 2012; Ding *et al.*, 1996; Hendry *et al.* 2014; Abelmann *et al.*, 2015; Fontorbe *et al.*, 2016). Silicon fractionation by modern radiolarians varies between -0.8 ‰ and -2.1 ‰ (Egan *et al.*, 2012; Abelmann *et al.*, 2015), which is similar to that by diatom (Frings *et al.*, 2016). Although factors controlling of δ^{30}Si records of radiolarian test are still debated, even for Cenozoic (e.g. Fontorbe *et al.*, 2016), early Mesozoic Si cycle seems to be a simpler system due to lack of diatom in continent and ocean. In this paper, we investigated the past oceanic silica cycle through in situ δ^{30}Si in radiolarian molds of Mesozoic bedded cherts. Then we compared our δ^{30}Si records with BSi burial flux (Ikeda *et al.*, 2017), to constrain the early Mesozoic Si cycle.

2. Material

We sampled material from bedded cherts from the Inuyama area, central Japan (Fig. 1). These cherts are part of an accretionary prism and are incorporated into several tectonic imbricates (Matsuda and Isozaki, 1991; Kimura and Hori, 1993). High-resolution radiolarian and conodont biostratigraphy, chemo-cyclostratigraphy in this succession have allowed to reconstruct the best studied Early Triassic to Early Jurassic bedded chert sequence (Yao *et al.*, 1980, Hori, 1990; Sugiyama, 1997; Ikeda *et al.*, 2010; Ikeda and Tada, 2013, 2014). Based on biostratigraphic age constraints, average duration of a chert-shale couplet are ~20 kyr throughout the early Mesozoic (Ikeda *et al.*, 2010; Ikeda and Tada, 2014), which is consistent with the precession-scale changes in the accumulation rate of BSi under the extremely slow accumulation of shale mostly composed of aeolian dust (e.g. Hori *et al.*, 1993). Estimated BSi fluctuations should be proportional to DSi input from chemical weathering paced with the monsoon dynamics, over timescales longer than the residence time of oceanic DSi (20 kyr; Tréguer and De La Rocha, 2013; <~100 kyr; Ritterbush *et al.*, 2015), because low-mid-latitude BSi burial flux (Ikeda *et al.*, 2017) is ~90 % of the modern global ocean (Tréguer and De La Rocha, 2013) and was a major sink for oceanic DSi.

Bedded cherts are rocks composed of chert layers (Si-rich), interbedded with clay-rich shale partings (Si-poor), produced by differential compaction and diagenetic reactions of dissolution-precipitation usually forming opal-CT and later quartz (Isaacs, 1981; Tada, 1991). Radiolarian molds filled with nearly pure microquartz and/or chalcedony are found in the silica-rich matrix of cherts. The radiolarian molds that we measured are commonly spherical. Therefore, they could result from Spumellaria, which have regularly a spherical morphology, dwelling in a photic zone due to their symbiotic relation with photosynthetic algae (e.g. Swanberg and Anderson, 1985; Takahashi *et al.*, 2003).

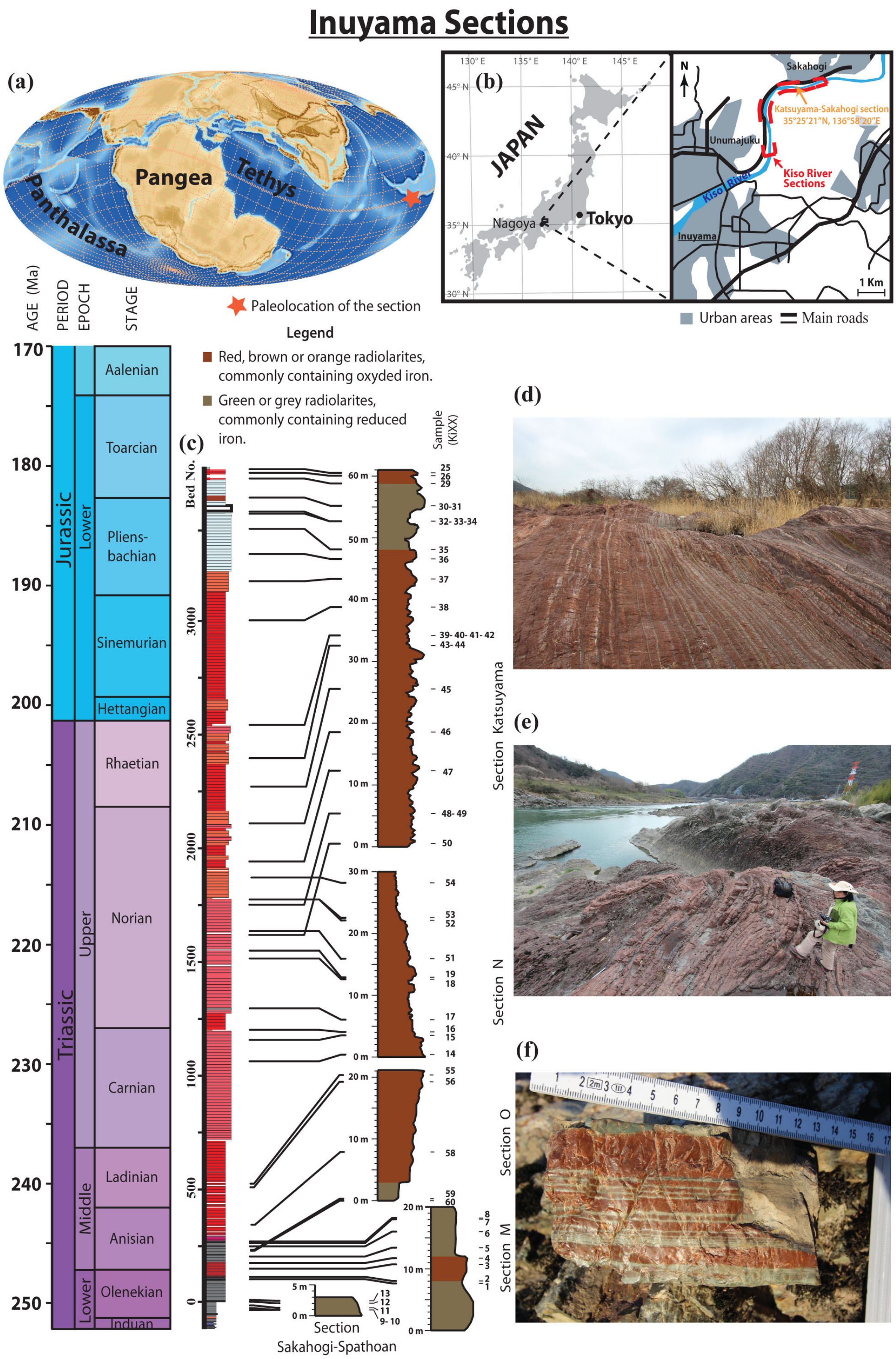

Fig. 1 Log of the Inuyama sections with their Triassic-Early Jurassic paleogeography on a map of Middle Jurassic (a) and their current location (b). The Paleomap (a) is from the Stampfli model developed at the University of Lausanne (Stampfli and Borel, 2002). The bed number log (c) is from Ikeda and Tada (2014). Additional information on the Kiso River sections can be found in Sugiyama (1997). These radiolarites are illustrated through (d) the nice parallel bedding for Late Triassic bedded chert (35°23'57" N, 136°57'34" E), (e) outcropping of Rhatian bedded chert along the Kiso River (35°25'21" N, 136°58'16" E) and (f) millimetric laminations inside single Norian bed (Ki18).

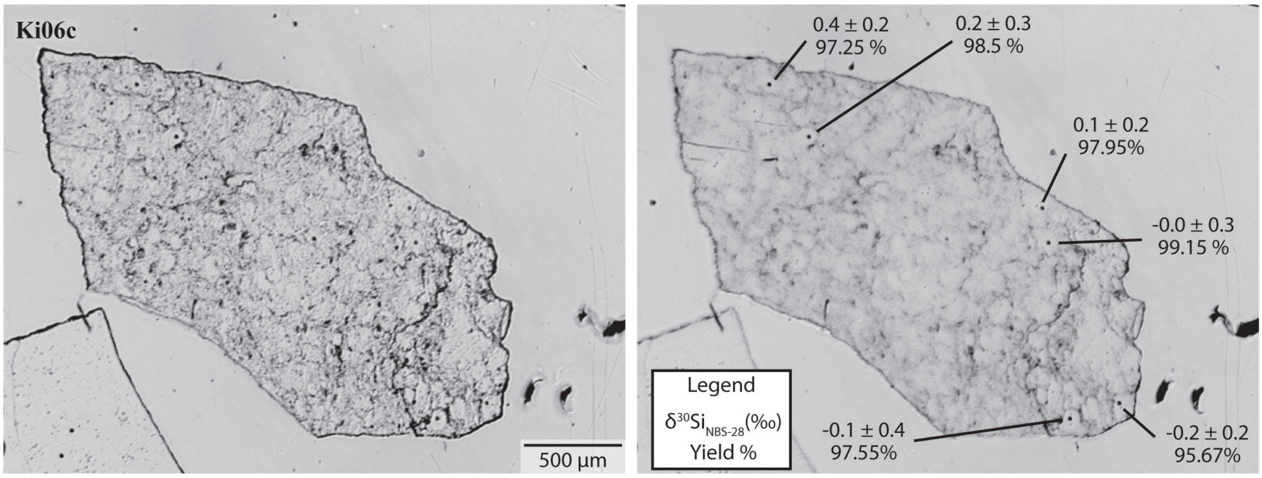

Fig. 2 $\delta^{30}Si_{NBS-28}$ measurements on sample Ki06c with analytical yield percent relative to the yield of the Paine Quartz Standard (UNIL_Q1). Image on the right are out of focus to better distinguish the analytical spots.

3. Methods

In total, 34 cherts were analysed for the Inuyama section. Sample holders consists of ten fragments of different samples mounted into epoxide around an internal standard. These fragments were previously polished into trapezoidal shapes and the presence of radiolarian molds was checked by optical methods.

The $\delta^{30}Si$ of micro-crystalline quartz precipitated inside radiolarian molds was measured by SIMS at University of Lausanne with a primary Cs^+ ion beam intensity of 2 nA, resulting in a ~10 µm spot (cf. Seitz *et al.*, 2017), to avoid contamination from other sources of silicon in radiolarites (detrital/aeolian minerals). Secondary ions ^{30}Si and ^{28}Si were analyzed at 3000 MRP and collected on Faraday cups (FC) multi-collection mode. The resistances of the L'2 and H'2 FC were 10^{11} Ω for the detection of ^{28}Si and ^{30}Si, respectively. FCs were calibrated in the beginning of each session, using the calibration routine. Mass calibration was performed at the beginning of each session and every 12 h. Samples were gold coated to dissipated charges. Each analysis consists of 20 cycles of 5 sec, and starts with a presputtering time of 30 sec to remove gold and stabilize the secondary ion emission. The standard deviation of each analysis is expressed as analytical standard deviation. The data have been obtained in 7 different sessions for $\delta^{30}Si$ measurements, over 7 months.

For each chert sample, we made 4-10 measurements within about 0.5 cm stratigraphic interval (Fig. 2). A quartz internal standard (UNIL_Q1; Paine Quartz; Seitz *et al.*, 2017 for $\delta^{18}O$ and method; $\delta^{30}Si_{NBS-28}$ = -0.13 ± 0.02 ‰ (2SD)) was analysed every 6-10 measurements for instrumental drift correction and calibration.

We subsequently controlled by optical methods that the ion beam actually hit the radiolarian molds for each measurement. In addition, data were postprocessed using the analytical yield and the analytical deviation of each measurement. The analytical yield depends on the nature of the analysed material (mineral species and matrix effect) and on the topography of the analysed surface which modifies the incident angle of the primary ion beam. In addition to instrumental instabilities, the high analytical deviation can also indicate heterogeneity and the analyse of a mixture of silica, clays minerals and/ or oxides. Regarding these considerations, the analytical yield and deviation are objective parameters to decide if a measurement must be rejected.

The drift correction was realized using a least square regression line weighted for incertitude (σ_i^2). For the calibration, we calculated the least square $\delta^{30}Si$-mean ($\underset{\cdot}{x}$) and standard deviation (σ_i) for the internal standard also weighted for incertitude (Equation 1 and 2) to keep consistent data processing with the least square drift correction. The calibrated $\delta^{30}Si$ for samples ($\delta^{30}\ Si_{NBS\text{-}28}\ Spl$) depend on each sample measurement ($\delta^{30}\ Si\ Spl_{measured}$) and are proportional to the measured least square $\delta^{30}Si$-mean and the true $\delta^{30}Si_{NBS-28}$ from the internal standard ($\delta^{30}\ Si\ Std_{measured}$ and $\delta^{30}\ Si_{NBS\text{-}28}\ Std$, respectively) (Equation 3). The errors on the calibrated $\delta^{30}Si$ ($\sigma(\delta^{30}\ Si_{NBS\text{-}28}\ Spl)$) were obtained by error propagation (Equation 4). The weighted means and standard deviations (Table 2 and Appendix Tables A1 and A2) were then calculated for each sample following equation 1 and 2. Raw, drift corrected and calibrated data are indicated in appendix tables. The $\delta^{30}Si$-data were then filtered with a 10 Ma moving windows average with a step of 5 Ma and compared with estimation of the BSi burial rates in the Inuyama area (Ikeda *et al.*, 2017).

Equation 1

$$\underset{\cdot}{x} = \sum \left(\frac{1}{\sigma_i^2} \times x_i\right) / \left(\frac{1}{\sigma_i^2}\right)$$

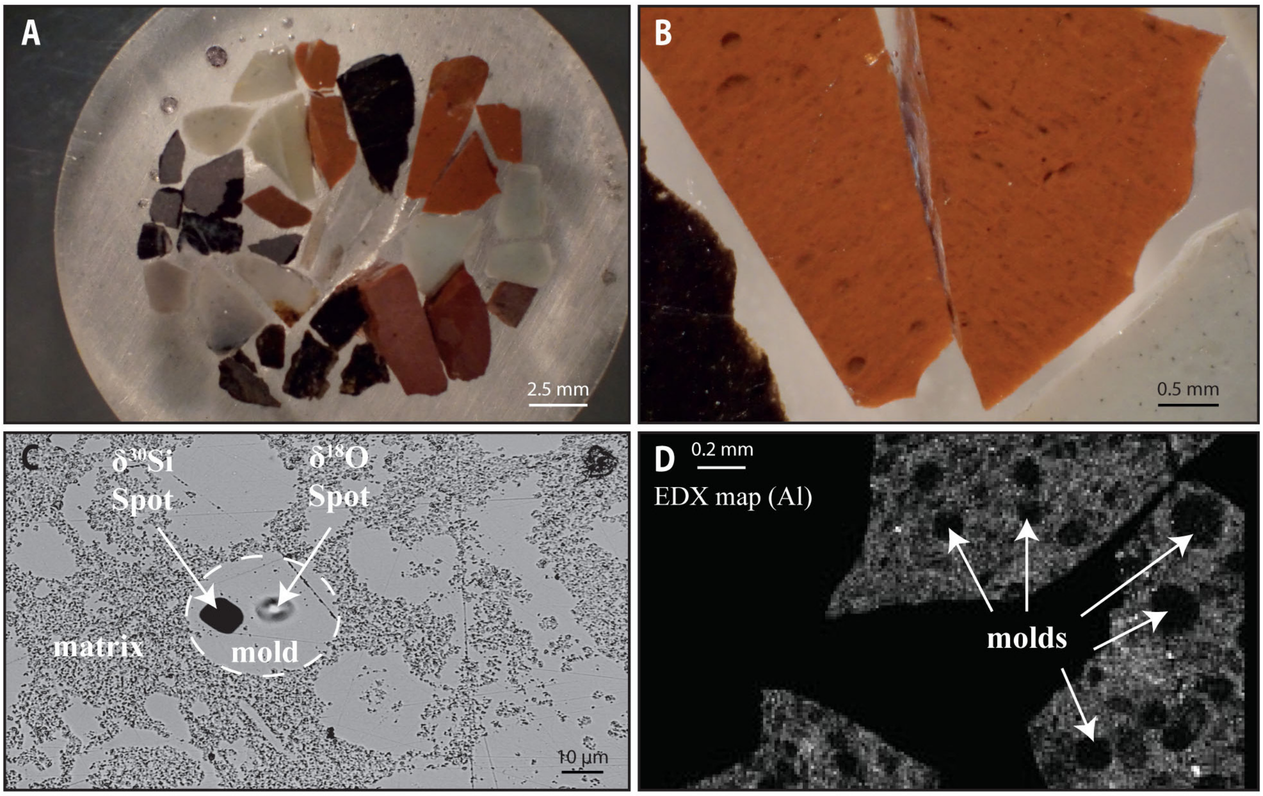

Fig. 3 Illustration of the analyzed materials. A) epoxy sample mount (Br7) including several fragments of about 10 samples. B) Zoom on a sample in this mount with binocular. C) Image of two spots left by a SIMS analysis ($\delta^{18}O$ and $\delta^{30}Si$) in radiolarian silica (radiolarian molds) on a gold coated sample mount. The $\delta^{18}O$-spot on the right is covered by a new gold coating. The difference of polishing between the radiolarian molds of nearly pure microcrystalline quartz and the matrix is well illustrated on this image. D) SEM imaging of the aluminium distribution in the sample Ki08c (EDX map). Radiolarian molds are aluminium-free on this image.

Equation 2

$$\dot{\sigma}_\iota = \sqrt{\sum \left(\frac{1}{\sigma_i^2} \times (x_i - \dot{\underline{x}})^2\right) / \sum \left(\frac{1}{\sigma_i^2}\right) \times \frac{N}{N-1}}$$

Equation 3

$$\delta^{30}Si_{NBS-28}\,Spl = \left(\left(\left(1 + \frac{\delta^{30}Si\,Spl_{measured}}{1000}\right) / \frac{(1 + \delta^{30}Si\,Std_{measured} / 1000)}{(1 + \delta^{30}Si_{NBS-28}\,Std / 1000)}\right) - 1\right) \times 1000$$

Equation 4

$$\sigma(\delta^{30}Si_{NBS-28}\,Spl) = \sqrt{\left(\frac{\partial F}{\partial V_1} \times dV_1\right)^2 + \left(\frac{\partial F}{\partial V_2} \times dV_2\right)^2 + \left(\frac{\partial F}{\partial V_3} \times dV_3\right)^2}$$

With $F = \delta^{30}Si_{NBS-28}\,Spl$, $V_1 = \delta^{30}Si\,Spl_{measured}$, $V_2 = \delta^{30}Si\,Std_{measured}$ and $V_3 = \delta^{30}Si_{NBS-28}\,Std$

For the SIMS analyses, it is common to use 2SD, which make sense considering the high accuracy of the method or when measuring very homogenous samples. 2SD was thus also used to discuss the UNIL-Q1 $\delta^{30}Si$. We used 1SD for the LS-mean of samples and for their moving average, following usage in palaeoceanography, such as $\delta^{13}C$ and $\delta^{18}O$ in low magnesium calcium shells through time (e.g. Veizer *et al.*, 1999).

We also use scanning electron microscopy-energy dispersive X-ray spectrometry (SEM-EDS) in Lausanne University to map the elemental distribution in chert (Fig. 3).

4. Results

All the analytical dataset of our samples and a standard is presented in Appendix Tables, and is summarised in Tables 1 and 2. The means and standard deviations (2SD) of the raw $\delta^{30}Si$ from UNIL-Q1 range from -41.77 ‰ to -45.6 ‰ and from 0.33 ‰ to 0.69 ‰, respectively (Table 1). The drift correction only slightly reduced the standard deviations (0.29 ‰ to 0.68 ‰; 2SD). Calibrating data using the LS-means of standard, the arithmetic means and standard deviation (2SD) of the $\delta^{30}Si_{NBS-28}$ values

Table 1 Raw, drift corrected and calibrated δ^{30}Si means and standard deviations (2 SD) for the UNIL-Q1 standard (in ‰) between our different sessions. Instrumental fractionation is calculated based on the least square mean and standard deviation of the drift corrected δ^{30}Si. The δ^{30}Si$_{NBS-28}$ mean and standard deviation (2 SD) of calibrated data are given for all standard measured through a session and for the average δ^{30}Si$_{NBS-28}$ of the different standard clusters. Reproducibility of the δ^{30}Si$_{NBS-28}$ based on the average δ^{30}Si$_{NBS-28}$ of the different standard clusters is much better than on all standard measured (< 0.37 ‰, 2SD vs < 0.71 ‰).

Session	Number of bracketing standard	Raw δ^{30}Si (‰) All standard		drift corrected δ^{30}Si (‰) All standard				Fractionation based on LS-mean	Calibrated δ^{30}Si$_{NBS-28}$ (‰) All standard		Standard clusters		Reproducibility of δ^{30}Si$_{NBS-28}$ (‰) All standard	Standard clusters
		mean	2 SD	mean	2 SD	LS-mean	LS-STD (1SD)		mean	2SD	mean	2SD	2SD	2SD
Br2	36	-42.67	0.38	-42.67	0.38	-42.65	0.19	1.0444	-0.15	0.40	-0.15	0.21	0.40	0.21
Br3	28	-42.84	0.33	-42.84	0.31	-42.84	0.16	1.0446	-0.13	0.33	-0.13	0.15	0.33	0.15
Br4	16	-45.60	0.49	-45.60	0.39	-45.61	0.19	1.0477	-0.12	0.40	-0.12	0.36	0.40	0.36
Br4v2	18	-43.08	0.69	-43.08	0.68	-43.12	0.37	1.0449	-0.09	0.71	-0.09	0.02	0.71	0.03
Br6	40	-45.36	0.67	-45.38	0.66	-45.36	0.31	1.0474	-0.15	0.69	-0.15	0.20	0.69	0.21
Br7	40	-42.44	0.35	-42.44	0.33	-42.44	0.17	1.0442	-0.13	0.35	-0.13	0.25	0.35	0.25
Br1	24	-41.77	0.37	-41.77	0.29	-41.76	0.12	1.0434	-0.14	0.30	-0.14	0.13	0.30	0.13
Br5	44	-41.79	0.39	-41.79	0.39	-41.80	0.19	1.0435	-0.12	0.41	-0.12	0.17	0.41	0.17
mean		-43.19		-43.20		-43.20			-0.13		-0.13			
2SD		2.97		2.98		2.98			0.04		0.04			

from our standards vary from -0.09 ‰ to -0.15 ‰ and from 0.30 ‰ to 0.71 ‰, respectively. The average of the arithmetic δ^{30}Si$_{NBS-28}$ means obtained during different sessions is thus -0.13 ± 0.04 ‰ (2SD) which is relatively similar to the bulk UNIL-Q1 δ^{30}Si$_{NBS-28}$ (-0.13 ± 0.02 ‰; 2SD) and bellow the reproducibility of all δ^{30}Si$_{NBS-28}$ from standard during a single session. We removed 6 on 189 measurements of samples which had yield deviating more than 10 % from the yield of the quartz standard or their analytical deviation (2SD) exceeding 0.37 ‰.

LS-mean δ^{30}Si of measured radiolarian molds ranges from -0.3 ‰ to 2 ‰ (Table 2). δ^{30}Si-means have an inter-sample range of up to 2.3 ‰, which is higher than their standard deviation (Table 2). The intra-sample standard deviations (1SD) of the δ^{30}Si-means varies between 0.1 ‰ and 0.75 ‰. The δ^{30}Si-means from our samples range from -0.3 ‰ to 0.8 ‰ during the Early Triassic, from -0.3 ‰ to 1 ‰ during the Middle Triassic, from -0.3 ‰ to 1.5 ‰ during the Late Triassic, and from 0.5 ‰ to 2 ‰ during the Early Jurassic (Fig. 4). The low δ^{30}Si-values from 10-Myr moving windows average are overall associated with high BSi burial rates (Ikeda *et al.*, 2017). A mapping of the aluminium content by SEM-EDS shows that clay minerals are concentrated in the matrix (Fig. 3).

5. Discussion

5. 1 δ^{30}Si of radiolarian molds and diagenesis

SIMS-measured δ^{30}Si for Mesozoic radiolarian molds ranges from -0.3 ‰ to 2 ‰ (Fig. 4), which overlap with the range of Cenozoic radiolarian tests (e.g. Fontorbe *et al.*, 2016; Fig. 5), potentially supporting that the Mesozoic radiolarian molds preserve the original values to some extent.

Radiolarian skeletons are originally composed of biogenic opal (opal-A), which is the most soluble silica phase (Walther and Helgeson 1977; Fournier and Rowe, 1977; Gunnarsson and Arnórsson, 2000). During the phase transitions from opal-A to opal-CT and quartz, silicon isotope of radiolarian molds might have changed by contamination of pore water DSi. However, migration of Si from the layers with low Si content (shale bed) to layers with high Si content (chert bed) allows us to ignore interbed migration of Si (Tada, 1991). The lower solubility of quartz (<1000 ppm) than opal-A (<2000 ppm) and opal-CT (<1500 ppm) (e.g. Gunnarsson and Arnórsson, 2000) further implicates the negligible effect of aeolian/detrital quartz dissolution on DSi of pore water. Additionally, clay mineral diagenesis occurs at higher temperature (80 °C; Chamley, 1989; Fagel 2007) than opal-CT transition (65 °C; Matheney and Knauth, 1993), which segregated biosiliceous sediments (Tada, 1991). Considering mass balance in the chert-dominant bedded chert succession with minor-clay component in the Inuyama area (Sugiyama, 1997), we can thus assume that the bulk δ^{30}Si of radiolarian molds in cherts would be equal to that of former opal-A.

Table 2 List of samples with their age, their $\delta^{30}Si_{NBS-28}$ Least square mean (LS-mean) and their $\delta^{30}Si$ least square standard deviation (LS-std; 1SD). The $\delta^{30}Si_{NBS-28}$ was averaged with a 10 Ma windows moving average (5 Ma step) and compared with BSi.

Sample	Age (Ma)	Number of measurements	Results		Curves	
			$\delta^{30}Si_{NBS-28}$ (‰)		$\delta^{30}Si_{NBS-28}$ (‰)	Biosilica burial rate (g cm^{-2} Kyr^{-1})
			This study		This study	Ikeda *et al.*, 2017
			LS-mean	LS-std (1SD)	10 Ma moving average	10 Ma smooth
Ki20	174.00	5	2.0	0.7	1.42	
Ki22c1	178.00	8	1.1	0.1	1.24	
Ki22c2	178.00	3	0.8	0.2	1.24	
Ki21	178.00	9	1.2	0.3	1.24	
Ki27	180.99	6	0.5	0.6	1.26	0.26
Ki24	182.00	6	1.9	0.2	1.31	0.26
Ki32	184.20	10	2.0	0.4	1.43	0.26
Ki34	184.37	10	1.0	0.3	1.43	0.26
Ki35	185.62	9	2.0	0.2	1.45	0.25
Ki38	193.31	10	0.8	0.4	0.96	0.19
Ki40	201.50	5	0.8	0.5	1.22	0.23
Ki39	201.50	5	1.4	0.3	1.22	0.23
Ki41	201.50	1	1.1		1.22	0.23
Ki42	201.50	10	1.4	0.3	1.22	0.23
Ki44	204.82	9	1.4	0.1	1.22	0.25
ki43	204.82	6	1.2	0.3	1.22	0.25
Ki46	210.27	10	-0.3	0.6	-0.09	0.27
Ki54	214.40	6	0.0	0.5	0.40	0.26
ki48	217.09	4	1.0	0.4	0.71	0.25
Ki51	219.00	6	1.1	0.3	0.94	0.25
Ki15	228.00	10	1.1	0.3	1.10	0.21
Ki57	241.00	9	1.0	0.4	0.52	0.36
Ki58	243.48	6	0.6	0.5	0.39	0.36
Ki08	244.90	10	-0.2	0.3	0.32	0.35
Ki07	245.00	6	0.9	0.2	0.32	0.35
Ki06	245.25	6	0.0	0.3	0.31	0.35
Ki06s	245.25	14	-0.1	0.4	0.31	0.35
Ki05	246.20	6	-0.3	0.2	0.30	0.33
Ki04	246.60	9	0.7	0.3	0.30	0.33
Ki03	247.20	10	0.2	0.6	0.29	0.32
Ki02	247.80	7	0.4	0.4	0.28	0.31
Ki01	248.00	10	0.3	0.5	0.28	0.31
Ki10	250.20	6	-0.2	0.3	0.25	
Ki09	250.30	9	0.7	0.3	0.25	

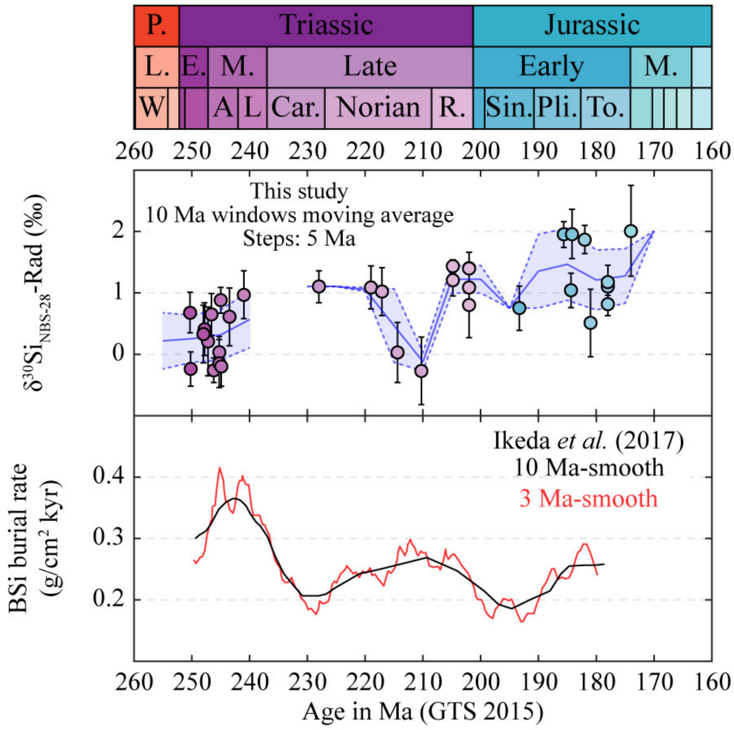

Fig. 4 Evolution of $\delta^{30}Si_{NBS-28}$ through time from radiolarian silica in the Inuyama Area (this study). Our results are compared with estimations of the BSi burial rate (Ikeda *et al.*, 2017). The trend and variation of $\delta^{30}Si$ can be correlated (R= -0.73) with the trend and/or variations observed in the BSi burial rate. The geological timescale (GTS 2015) used for this figure is the timescale of the international commission of stratigraphy (Cohen *et al.* 2013). The color filling inside markers corresponds to the color of the geological stage. The boundaries of curves, when plotted, are equivalent to 1SD. The moving average for radiolarian silica is realized using a 10 Ma windows and 5 Ma steps. The $\delta^{30}Si_{NBS-28}$ error bars correspond to the least square standard deviation of samples presented in Table 2.

The relatively large internal $\delta^{30}Si$-scattering up to 0.8 ‰ (1SD) for each sample suggests that kyr-scale $\delta^{30}Si$ heterogeneity within each chert sample still exist after the diagenesis. Micrometric isotopic variations have been previously observed even in Precambrian cherts, supporting that the $\delta^{30}Si$ is not homogenised through time in cherts (Marin-Carbonne *et al.*, 2011, 2012). Even fragments of cherts included as enclave in tonalitic intrusions (>700 °C) or metamorphosed in amphibolite facies seem to preserve their $\delta^{30}Si$ (André *et al.*, 2006). Therefore, it is reasonable to assess $\delta^{30}Si$ records of radiolarian molds in Mesozoic bedded chert as those in Mesozoic radiolarian tests, despite of diagenetic homogenization to some extent.

5. 2 Evolution of radiolarian $\delta^{30}Si$

The increasing trend of radiolarian $\delta^{30}Si$ through the Triassic might be interpreted as an increase of the radiolarian productivity resulting in a higher biogenic fractionation (e.g. De La Rocha *et al.* 1998), despite of large scattering and complex fractionation of $\delta^{30}Si$ (Fig. 4). However, this conventional interpretation contradicts with low $\delta^{30}Si$ mainly associated with higher BSi burial rates (Ikeda *et al.*, 2017) (Fig. 5). Upwelling of isotopically-light DSi might have affected the observed negative correlation between $\delta^{30}Si$ and BSi flux in equatorial Panthalassa. Regarding the radiolarian BSi as major sink of DSi in the Mesozoic ocean before the post-Cretaceous rise of diatoms (Ikeda *et al.*, 2017), however, radiolarian $\delta^{30}Si$ could have reflected $\delta^{30}Si$ of oceanic DSi on timescale longer than residence time of oceanic DSi (~100 kyr: Ritterbush *et al.*, 2015).

$\delta^{30}Si$ of oceanic DSi is controlled by changes in $\delta^{30}Si$ values of sources and sinks (e.g. Frings *et al.*, 2016). Major source of oceanic DSi is river input, which $\delta^{30}Si$ currently varies from 0 ‰ to 4 ‰, mainly depending on diatom uptake and rock types of provenance (e.g. Frings *et al.*, 2016). However, before the rise of diatom, biogenic uptake in continent can be negligible. Small difference exists between continental felsic rocks ($\delta^{30}Si$ = -0.5 to 0.5 ‰) and mantle-origin mafic rocks ($\delta^{30}Si$ = -1 to 0 ‰) (Opfergelt and Delmelle, 2012). Up to 1 ‰ amplitudes of 10-Myr scale $\delta^{30}Si$ data can be explained by changes in felsic/mafic ratios, although our $\delta^{30}Si$ data is too low-resolution to discuss its <10-Myr scale dynamics.

On another hand, $\delta^{30}Si$ of siliceous sponges varies from -6 ‰ to -1 ‰ (Frings *et al.*, 2016), whereas that of radiolarias and diatoms varies from -1.1 ‰ to 1.7‰ (Abelmann *et al.*, 2015; Fontorbe *et al.*, 2016) and from -1 ‰ to 3 ‰ (e.g. Frings *et al.*, 2016), respectively. Changes in the relative contribution of sponge BSi deposition might be a candidate to explain $\delta^{30}Si$ variations, despite of lack of evidence of massive sponge deposition, except for some biotic events after Carnian Pluvial Event, Norian Manicouagan impact, and the end-Triassic extinction (Thibodeau *et al.*, 2016; Onoue *et al.*, 2016; Shi *et al.*, 2017). However, there are no significant $\delta^{30}Si$ variations across the end-Triassic extinction, implying negligible effect of sponge deposition on Si cycle at this event (Fig. 4).

On the other hand, 10-Myr scale BSi burial flux also correlates with calculated global silicate weathering rate, which potentially linked with changes in weathering of highly-weatherable volcanic rocks with lighter silicon isotope (Ikeda *et al.*, 2017). This idea is consistent with

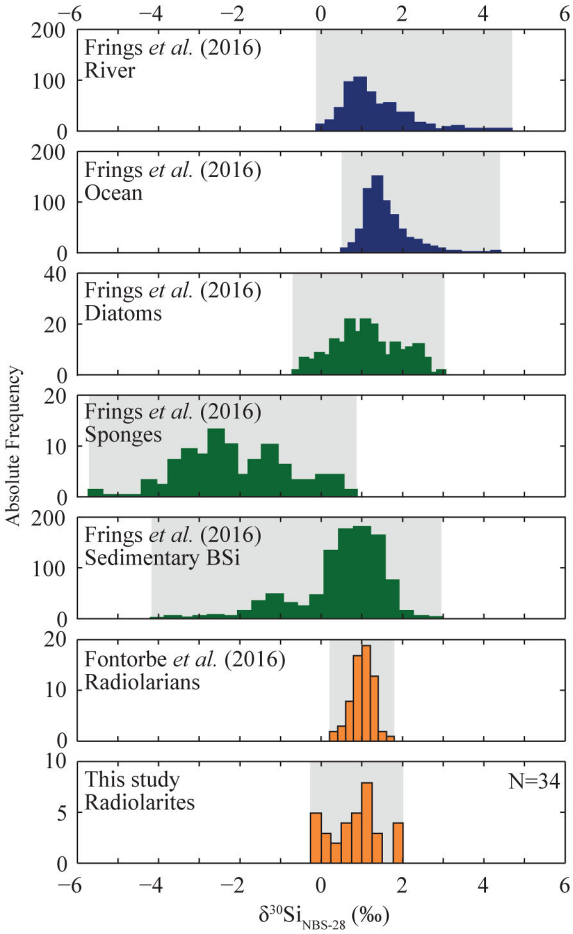

Fig. 5 $\delta^{30}Si_{NBS\text{-}28}$-distribution in rivers, oceans, diatoms, sponges and sedimentary biogenic silica from Frings *et al.* (2016) compared with $\delta^{30}Si_{NBS\text{-}28}$-distribution for Cenozoic radiolarians (Fontorbe *et al.*, 2016) and for the Triassic to Jurassic radiolarites from the Inuyama Area (this study). The relative similar range between Cenozoic radiolarians and Mesozoic radiolarites supports that the Mesozoic radiolarian molds preserve the original values.

the overall negative correlation between radiolarian $\delta^{30}Si$ and the BSi burial flux in the Inuyama area, despite of large scattering and low-resolution $\delta^{30}Si$ records (Fig. 4). Further high-resolution works are necessary to improve our understanding of $\delta^{30}Si$ cycle of radiolarian molds and unravelling some radiolarian crisis through geologic events, in response to bolide impact, massive volcanism, oceanic acidification, and oceanic anoxic events.

6. Conclusion and perspective

We measured $\delta^{30}Si$ of the Mesozoic radiolarian molds in Inuyama chert by SIMS. Range of $\delta^{30}Si$ between -0.3 and 2 ‰ is consistent with that of modern and Cenozoic radiolarian tests. Relatively large $\delta^{30}Si$ up to 0.8 ‰ (1SD) in intra-chert bed supports that $\delta^{30}Si$ of the Mesozoic radiolarian molds is not perfectly homogenized in a chert bed during the diagenesis, and potentially record of kyr-scale changes in radiolarian $\delta^{30}Si$. 10-Myr scale trend of $\delta^{30}Si$ of the Mesozoic radiolarian molds from 250 Ma to 180 Ma is overall out-of-phase relation with BSi burial flux. This relation contradicts with interpretation of $\delta^{30}Si$ as a productivity proxy, despite of low-resolution and scattered $\delta^{30}Si$ records. Further high-resolution analysis will allow a better understanding of the past silica cycle, opening the possibility of accurate estimations of the past oceanic silica cycle and the contribution of past radiolarian productivity.

Acknowledgements:We thank the Swiss National Science Foundation (Project Numbers 200021_185067 and 200020_162670) and the University of Lausanne for their financial support. We acknowledge Nakae, S. and Okazaki, Y. and an anonymous reviewer for fruitful comments on our manuscript.

References

Abelmann, A., Gersonde, R., Knorr, G., Zhang, X., Chapligin, B., Maier, E., Esper, O., Friedrichsen, H., Lohmann, G., Meyer, H. and Tiedemann, R. (2015) The seasonal sea-ice zone in the glacial Southern Ocean as a carbon sink. *Nature Communications*, **6**, 1–13p.

André, L., Cardinal, D., Alleman, L. Y. and Moorbath, S. (2006) Silicon isotopes in ~3.8 Ga West Greenland rocks as clues to the Eoarchaean supracrustal Si cycle. *Earth and Planetary Science Letters*, **245**, 162–173.

Baumgartner, P. O. (2013) Mesozoic radiolarites–accumulation as a function of sea surface fertility on Tethyan margins and in ocean basins. *Sedimentology*, **60**, 292–318.

Baumgartner, P. O., Andjic, G., Sandoval-Gutierrez, M., Bandini-Maeder, A., Diserens, M-C., Baumgartner-Mora, C. and Kukoc, C. (2018) Radiolarian biochronology and paleoceanography of Pacific Terranes in Central America and the Caribbean. *Abstracts of AAPG Hedberg Conference*, 10–16, https://www.researchgate.net/publication/329196576 (Accessed:2018-12-23).

Berner, R. A. (1991) A model for atmospheric CO_2 over phanerozoic time. *American Journal of Science*, **291**, 339–376.

Brzezinski, M. A., Pride, C. J., Franck, V. M., Sigman, D. M., Sarmiento, J. L., Matsumoto, K., Gruber, N., Rau, G. H. and Coale, K. H. (2002). A switch from $Si(OH)_4$ to NO_3^- depletion in the glacial Southern Ocean. *Geophysical Research Letters*, **29**, 1–4.

Chamley, H. (1989) *Clay Sedimentology*, Springer - Verlag, Berlin Heidelberg, 623p.

Cohen, K. M., Finney, S. C., Gibbard, P. L. and Fan, J.-X. (2013; updated) The ICS International Chronostratigraphic Chart. *Episodes*, **36**, 199–204.

De La Rocha, C. L, Brzezinski, M. A., DeNiro M. J. and Shemesh A. (1998) Silicon-isotope composition of diatoms as an indicator of past oceanic change. *Nature*, **395**, 680–683.

De Wever P., O'Dogherty L. and Gorican S. (2014) Monsoon as a cause of radiolarite in the Tethyan realm. *Comptes Rendus Geoscience*, **346**, 287–297.

Ding, T., Jiang, S., Wan, D., Li, Y., Song, H., Liu, Z., Yao, X. (1996) *Silicon isotope Geochemistry*, Geological Publishing House, Beijing, China, 125p.

Dymond, J., Collier, R., McManus, J., Honjo, S. and Manganini, S. (1997) Can the aluminum and titanium contents of ocean sediments be used to determine the paleoproductivity of the oceans? *Paleoceanography*, **12**, 586–593.

Egan, K. E., Rickaby, R. E. M, Leng, M. J., Hendry, K. R., Hermoso, M., Sloane, H. J., Bostock, H. and Halliday, A. N. (2012) Diatom silicon isotopes as proxy for silicic acid utilisation. A Southern Ocean core top calibration. *Geochimica et Cosmochimica Acta*, **96**, 174–192.

Fagel, N. (2007) Clay minerals, deep circulation and climate. *Development in Marin Geology*, **1**, 139–184.

Fontorbe, G., Frings, P. J., De La Rocha, C. L., Hendry, J. R. and Conley, D. J. (2016) A silicon depleted North Atlantic since the Palaeogene: Evidence from sponge and radiolarian silicon isotopes. *Earth and Planetary Science Letters*, **453**, 67–77.

Fournier, R. O. and Rowe J. J. (1997) The solubility of amorphous silica in water at high temperatures and high pressures. *American Mineralogist*, **62**, 1052–1056.

Frings, P. J., Clymans, W., Fontorbe, G., De La Rocha, C. L. and Conley, D. J. (2016) The continental Si cycle and its impact on the ocean Si isotope budget. *Chemical Geology*, **425**, 12–36.

Gunnarsson, I. and Arnórsson, S. (2000) Amorphous silica solubility and the thermodynamic properties of H_4SiO_4 in the range of 0 °C to 350 °C at Psat. *Geochimica et Cosmochimica Acta*, **64**, 2295–2307.

Hartmann, J., Moosdorf, N., Lauerwald, R., Hinderer, M. and West, A. J. (2014) Global chemical weathering and associated P-release – The role of lithology, temperature and soil properties. *Chemical Geology*, **363**, 145–163.

Hein, J. R., Park, M. and Parrish, J. T. (1987) Distribution of siliceous deposits in space and time. *In* Hein, J. R., ed., *Siliceous sedimentary rock-hosted ores and petroleum*, Van Nostrand Reinhold Company, Inc., New York, 10–57.

Hendry, K.R., Robinson, L.F., McManus, J.F. and Hays, J.D. (2014) Silicon isotopes indicate enhanced carbon export efficiency in the North Atlantic during deglaciation. *Nature Communications*, **5** (3107), 1–9.

Hori, R. (1990) Lower Jurassic radiolarian zones of SW Japan. *Transactions and proceedings of the Paleontological Society of Japan. New Series*., no. 159, 562–586.

Hori, R. S., Cho, C. and Umeda, H. (1993) Origin of cyclicity in Triassic-Jurassic radiolarian bedded cherts of the Mino accretionary complex from Japan. *Island Arc*, **2**, 170–180.

Ikeda, M. and Tada, R. (2014) A 70 million year astronomical time scale for the deep-sea bedded chert sequence (Inuyama, Japan): Implications for Triassic–Jurassic geochronology. *Earth and Planetary Science Letters*, **399**, 30–43.

Ikeda, M. and Tada, R. (2013) Long period astronomical cycles from the Triassic to Jurassic bedded chert sequence (Inuyama, Japan); Geologic evidences for the chaotic behavior of solar planets. *Earth, Planets and Space*, **65**, 351–360.

Ikeda, M., Tada, R. and Ozaki, K. (2017) Astronomical pacing of the global silica cycle recorded in Mesozoic bedded cherts. *Nature Communications*, **8**, 1–9.

Ikeda, M., Tada, R. and Sakuma, H. (2010) Astronomical cycle origin of bedded chert: A middle Triassic bedded chert sequence, Inuyama, Japan. *Earth and Planetary Science Letters*, **297**, 369–378.

Isaacs, C. M. (1981) Porosity reduction during diagenesis of the Monterey Formation, Santa Barbara coastal area, California. *In* Garrison, R. E. and Douglas, R. G., eds., *The Monterey Formation and related siliceous rocks of California*, Los Angeles, Pacific Section, SEPM, 257–271.

Kimura, K. and Hori, R. (1993) Offscraping accretionary process of Jurassic chert-clastic complexes in the Mino-Tamba belt, central Japan. *Journal of Structural Geology*, **15**, 145–161.

Kidder, D. L. and Erwin, D. H. (2001) Secular Distribution of Biogenic Silica through the Phanerozoic: Comparison of Silica-Replaced Fossils and Bedded Cherts at the Series Level. *Journal of Geology*, **109**, 509–522.

Marin-Carbonne, J., Chaussidon, M., Boiron, M. C. and Robert, F. (2011) A combined in situ oxygen, silicon isotopic and fluid inclusion study of a chert sample from Onverwacht Group (3.35 Ga, South Africa): New constraints on fluid circulation. *Chemical Geology*, **286**, 59–71.

Marin-Carbonne, J., Chaussidon, M. and Robert, F. (2012) Micrometer-scale chemical and isotopic criteria (O and Si) on the origin and history of Precambrian cherts: Implications for paleo-temperature reconstructions. *Geochimica et Cosmochimica Acta*, **92**, 129–147.

Matheney, R.K. and Knauth, L.P. (1993) New isotopic temperature estimates for early silica diagenesis in bedded cherts. *Geology*, **21**, 519–522.

Matsuda, T. and Isozaki, Y. (1991) Well-documented travel history of Mesozoic pelagic chert in Japan: from remote ocean to subduction zone. *Tectonics*, **10**, 475–499.

Murray, R. W., Leinen, M. and Isern, A. (1993) Biogenic flux of Al to sediment in the central equatorial Pacific Ocean: Evidence for increased productivity during glacial periods. *Paleoceanography*, **8**, 651–670.

Murray, R. W. and Leinen, M. (1996) Scavenged excess aluminum and its relationship to bulk titanium in biogenic sediment from the central equatorial Pacific Ocean. *Geochimica et Cosmochimica Acta*, **60**, 3869–3878.

Onoue, T., Sato, H., Yamashita, D., Ikehara, M., Yasukawa, K., Fujinaga, K., Kato, Y. and Matsuoka, A. (2016) Bolide impact triggered the Late Triassic extinction event in equatorial Panthalassa. *Scientific Reports*, **6**, 29609.

Opfergelt, S. and Delmelle, P. (2012) Silicon isotopes and continental weathering processes: Assessing controls on Si transfer to the ocean. *Comptes Rendus Geoscience*, **344**, 723–738.

Racki, G. and Cordey, F. (2000) Radiolarian palaeoecology and radiolarites: Is the present the key to the past? *Earth-Science Reviews*., **52**, 83–120.

Ritterbush, K. A., Rosas, S., Corsetti, F. A., Bottjer, D. J. and West, A. J. (2015) Andean sponges reveal long-term benthic ecosystem shifts following the end-Triassic mass extinction. *Palaeogeography, Palaeoclimatology, Palaeoecology*, **420**, 193–209.

Seitz, S., Baumgartner, L. P., Bouvier, A. S., Putlitz, B. and Vennemann, T. (2017) Quartz reference materials for oxygen isotope analysis by SIMS. *Geostandards and Geoanalytical Research*, **41**, 69–75.

Shi, Z., Preto, N., Jiang, H., Krystyn, L., Zhang, Y., Ogg, J. G. and Du, Y. (2017) Demise of Late Triassic sponge mounds along the northwestern margin of the Yangtze Block, South China: Related to the Carnian Pluvial Phase? *Palaeogeography, Palaeoclimatology, Palaeoecology*, **474**, 247–263.

Stampfli, G. M. and Borel G. D. (2002). A plate tectonic model for Paleozoic and Mesozoic constrained by daynamic plate boundaries and restored synthetic oceanic isochrons. *Earth and Planetary Science Letters*, **196**, 17–33.

Sugiyama, K. (1997) Triassic and Lower Jurassic radiolarian biostratigraphy in the siliceous claystone and bedded chert units of the southeastern Mino Terrane, Central Japan. *Bulletin of the Mizunami Fossil Museum*, **24**, 79–193.

Swanberg, N. R. and Anderson, O. R. (1985) The nutrition of radiolarians: Tropic activity of some Spumellaria. *Limnology and Oceanography*, **30**, 646–652.

Tada, R. (1991) Origin of rhythmical bedding in middle Miocene siliceous rocks of the Onnagawa Formation, northern Japan. *Journal of Sedimentary Research*, **61**, 1123–1145.

Takahashi O., Mayama S. and Matsuoka A. (2003) Host-symbiont association of polycystine Radiolaria: Epifluorescence microscopic observation of living Radiolaria. *Marine Micropaleontology*, **49**, 187–194.

Thibodeau A.M., Ritterbush K., Yager J.A., West A.J., Ibarra Y., Bottjer D.J. and Corsetti F.A. (2016). Mercury anomalies and the timing of biotic recovery following the end-Triassic mass extinction. *Nature Communications*, **7**, 1–8.

Tréguer P. J. and De La Rocha C. L. (2013) The world ocean silica cycle. *Annual Review of Marine Science*, **5**, 477–501.

Veizer J., Ala D., Azmy K., Bruckschen P., Buhl D., Bruhn F., Carden G. A. F., Diener A., Ebneth S. and Godderis Y. (1999) $^{87}Sr/^{86}Sr$, $\delta^{13}C$ and $\delta^{18}O$ evolution of Phanerozoic seawater. *Chemical Geology*, **161**, 59–88.

Walther, J. V, and Helgeson, H. C. (1977) Calculation of the thermodynamic properties of aqueous silica and the solubility of quartz and its polymorphs at high pressure and temperatures. *American Journal of Science*, **277**, 1315–1351.

Wu, S., Ding, T., Meng, X. and Bai, L. (1997) Determination and geological implication of O-Si isotope of the sediment core in the CC area, the Pacific Ocean. *Chinese Science Bulletin*, **42**, 1462–1465.

Yao, A., Matsuda, T. and Isozaki, Y. (1980) Triassic and Jurassic radiolarians from the Inuyama area, central Japan. *Journal of Geoscience, Osaka City University*, **23**, 135–154.

Recieved January 7, 2019
Accepted March 27, 2020
Published on-line June 5, 2020

Appendix

Table A1 Least square drift corrected and calibrated $\delta^{30}Si$ measurements (‰) for each sample. The LS-mean and standard deviation for each sample is indicated in bold font. All $\delta^{30}Si$ are relative to NBS-28 and all standard deviations are given as 2σ. Analytical standard deviation is sometime higher than 0.37 (2SD) due the use of error propagation during calibration.

Sample	Ki20	Ki22c2	Ki22c1	Ki21	Ki27	Ki24	Ki32	Ki34	Ki35	Ki38	Ki41	Ki39
age	174.00	178.00	178.00	178.00	180.99	182.00	184.20	184.37	185.62	193.31	201.50	201.50
LS-mean ($\delta^{30}Si_{NBS-28}$) and LS-SD (2 SD) (‰)	**2.01 ± 1.47**	**0.82 ± 0.37**	**1.10 ± 0.29**	**1.18 ± 0.54**	**0.51 ± 1.10**	**1.87 ± 0.47**	**1.96 ± 0.79**	**1.04 ± 0.56**	**1.95 ± 0.42**	**0.75 ± 0.72**	**1.09 ± 0.20**	**1.40 ± 0.53**
Number of measurements	5	6	9	9	6	6	10	10	9	10	2	5
Accepted measurements	5	5	8	9	6	6	10	10	9	10	1	4
Rejected measurements	0	1	1	0	0	0	0	0	0	0	1	1
$\delta^{30}Si_{NBS-28}$ and analytical standard deviation (2SD) of all accepted measurements (‰) 1	3.00 ± 0.31	0.79 ± 0.28	0.92 ± 0.28	1.17 ± 0.29	0.37 ± 0.25	2.02 ± 0.26	1.37 ± 0.20	0.58 ± 0.29	1.96 ± 0.26	1.39 ± 0.19	1.09 ± 0.20	1.68 ± 0.27
2	2.13 ± 0.26	0.66 ± 0.27	0.93 ± 0.39	1.08 ± 0.21	1.16 ± 0.24	1.75 ± 0.20	1.92 ± 0.28	1.25 ± 0.21	2.22 ± 0.23	0.73 ± 0.33		1.31 ± 0.22
3	2.52 ± 0.27	1.03 ± 0.33	1.08 ± 0.21	0.67 ± 0.28	0.96 ± 0.21	1.87 ± 0.27	1.74 ± 0.16	1.30 ± 0.25	2.06 ± 0.30	0.84 ± 0.34		1.62 ± 0.15
4	1.16 ± 0.17		1.11 ± 0.28	1.52 ± 0.29	0.19 ± 0.19	2.16 ± 0.21	2.02 ± 0.24	0.85 ± 0.28	1.53 ± 0.19	1.14 ± 0.30		1.03 ± 0.17
5	1.56 ± 0.19		1.18 ± 0.34	1.15 ± 0.24	-0.39 ± 0.33	1.92 ± 0.18	1.82 ± 0.19	1.18 ± 0.22	2.06 ± 0.24	0.64 ± 0.31		1.41 ± 0.24
6			0.97 ± 0.34	1.06 ± 0.27	0.56 ± 0.48	1.49 ± 0.22	2.19 ± 0.33	0.99 ± 0.28	2.08 ± 0.26	0.64 ± 0.17		
7			1.31 ± 0.25	1.44 ± 0.29			2.25 ± 0.24	1.19 ± 0.23	1.93 ± 0.30	0.74 ± 0.25		
8			1.24 ± 0.24	1.03 ± 0.20			2.84 ± 0.24	1.36 ± 0.22	1.81 ± 0.29	0.49 ± 0.22		
9				1.53 ± 0.26			1.73 ± 0.22	0.60 ± 0.25	2.03 ± 0.30	0.05 ± 0.37		
10							1.86 ± 0.22	0.99 ± 0.29		0.63 ± 0.36		
11												
12												
13												
14												
Session	Br6	Br2	Br2	Br2	Br1	Br3	Br7	Br7	Br2	Br5	Br4v2	Br4
Sample order during the session	5	3	2	4	3	5	7	9	9	2	3	5

Sample	Ki40	Ki42	Ki43	Ki44	Ki46	Ki54	Ki48	Ki51	Ki15	Ki57	Ki58	Ki08
age	201.50	201.50	204.82	204.82	210.27	214.4	217.09	219.00	228.00	241.00	243.48	244.90
LS-mean ($\delta^{30}Si_{NBS-28}$) and LS-SD (2 SD) (‰)	**0.80 ± 1.06**	**1.40 ± 0.52**	**1.21 ± 0.52**	**1.43 ± 0.22**	**-0.27 ± 1.10**	**0.03 ± 0.97**	**1.02 ± 0.78**	**1.09 ± 0.69**	**1.10 ± 0.52**	**0.97 ± 0.78**	**0.61 ± 0.93**	**-0.20 ± 0.64**
Number of measurements	5	10	6	9	10	6	5	6	10	10	6	10
Accepted measurements	5	10	6	9	10	6	4	6	10	9	6	10
Rejected measurements	0	0	0	0	0	0	1	0	0	1	0	0
$\delta^{30}Si_{NBS-28}$ and analytical standard deviation (2SD) of all accepted measurements (‰) 1	-0.11 ± 0.18	1.47 ± 0.28	0.82 ± 0.24	1.44 ± 0.24	-0.57 ± 0.21	-0.12 ± 0.23	1.54 ± 0.22	0.51 ± 0.20	1.31 ± 0.35	0.65 ± 0.19	0.85 ± 0.23	0.27 ± 0.23
2	0.88 ± 0.21	1.59 ± 0.29	1.03 ± 0.17	1.41 ± 0.31	0.83 ± 0.25	0.15 ± 0.33	0.63 ± 0.15	1.20 ± 0.19	1.31 ± 0.31	1.46 ± 0.26	0.91 ± 0.28	0.15 ± 0.20
3	1.21 ± 0.20	1.38 ± 0.24	1.17 ± 0.26	1.30 ± 0.29	-1.06 ± 0.22	-0.67 ± 0.24	1.08 ± 0.32	1.36 ± 0.29	0.98 ± 0.29	1.23 ± 0.24	0.92 ± 0.24	-0.03 ± 0.23
4	1.09 ± 0.17	1.37 ± 0.19	1.51 ± 0.23	1.26 ± 0.25	-0.62 ± 0.27	0.75 ± 0.21	0.91 ± 0.16	0.93 ± 0.25	1.14 ± 0.28	0.66 ± 0.25	0.90 ± 0.23	0.00 ± 0.20
5	0.97 ± 0.18	0.76 ± 0.20	1.32 ± 0.27	1.43 ± 0.19	-0.01 ± 0.27	0.25 ± 0.27		1.45 ± 0.18	0.88 ± 0.24	1.54 ± 0.21	0.15 ± 0.26	-0.69 ± 0.18
6		1.38 ± 0.25	1.40 ± 0.20	1.45 ± 0.22	-0.24 ± 0.19	-0.16 ± 0.17		1.09 ± 0.24	1.04 ± 0.24	1.04 ± 0.23	-0.15 ± 0.27	-0.17 ± 0.27
7		1.56 ± 0.25		1.63 ± 0.18	-0.02 ± 0.20				1.55 ± 0.20	0.45 ± 0.27		-0.34 ± 0.28
8		1.56 ± 0.35		1.41 ± 0.26	0.05 ± 0.25				0.99 ± 0.18	0.67 ± 0.23		-0.21 ± 0.32
9		1.67 ± 0.21		1.52 ± 0.21	-0.01 ± 0.26				1.25 ± 0.22	0.98 ± 0.29		-0.29 ± 0.26
10		1.36 ± 0.23			-0.90 ± 0.20				0.67 ± 0.22			-0.64 ± 0.20
11												
12												
13												
14												
Session	Br4	Br7	Br6	Br2	Br7	Br1	Br6	Br3	Br2	Br7	Br3	Br7
Sample order during the session	1	3	4	8	5	5	2	4	5	1	7	4

Sample	Ki07	Ki06	Ki06s	Ki05	Ki04	Ki3s	Ki03	Ki02	Ki01	Ki10	Ki09	
age	245.00	245.25	245.25	246.20	246.60	247.20	247.20	247.80	248.00	250.2	250.30	
LS-mean ($\delta^{30}Si_{NBS-28}$) and LS-SD (2 SD) (‰)	**0.88 ± 0.42**	**0.03 ± 0.53**	**-0.15 ± 0.78**	**-0.26 ± 0.40**	**0.65 ± 0.67**		**0.21 ± 1.11**	**0.41 ± 0.85**	**0.33 ± 0.94**	**-0.24 ± 0.57**	**0.68 ± 0.65**	**Total**
Number of measurements	6	6	14	6	9	8	10	7	10	6	9	266
Accepted measurements	6	6	14	6	9	0	10	7	10	6	9	252
Rejected measurements	0	0	0	0	0	8	0	0	0	0	0	14
$\delta^{30}Si_{NBS-28}$ and analytical standard deviation (2SD) of all accepted measurements (‰) 1	1.11 ± 0.24	0.43 ± 0.19	-0.03 ± 0.39	-0.09 ± 0.49	0.75 ± 0.29		0.31 ± 0.26	0.86 ± 0.23	0.63 ± 0.27	-0.38 ± 0.26	0.33 ± 0.26	
2	0.96 ± 0.31	0.16 ± 0.28	0.02 ± 0.32	-0.37 ± 0.30	0.83 ± 0.19		0.17 ± 0.28	-0.16 ± 0.30	0.79 ± 0.13	-0.42 ± 0.25	0.80 ± 0.29	
3	0.79 ± 0.16	0.07 ± 0.20	0.16 ± 0.22	-0.46 ± 0.25	1.14 ± 0.23		0.73 ± 0.27	0.77 ± 0.22	0.71 ± 0.19	-0.02 ± 0.25	0.97 ± 0.37	
4	1.14 ± 0.29	-0.10 ± 0.32	-0.19 ± 0.20	0.01 ± 0.25	0.59 ± 0.23		0.84 ± 0.33	0.52 ± 0.29	0.44 ± 0.21	-0.52 ± 0.28	0.26 ± 0.31	
5	0.70 ± 0.25	-0.23 ± 0.18	0.11 ± 0.25	-0.39 ± 0.23	0.26 ± 0.24		0.08 ± 0.17	0.72 ± 0.25	-0.27 ± 0.30	0.34 ± 0.42	1.03 ± 0.26	
6	0.64 ± 0.26	-0.23 ± 0.36	0.24 ± 0.24	-0.14 ± 0.33	0.19 ± 0.16		-0.23 ± 0.18	0.23 ± 0.19	0.77 ± 0.21	-0.20 ± 0.30	0.35 ± 0.26	
7			-0.24 ± 0.40		0.39 ± 0.28		0.73 ± 0.27	-0.16 ± 0.23	0.51 ± 0.19		0.72 ± 0.18	
8			0.22 ± 0.47		0.83 ± 0.25		0.46 ± 0.34		-0.48 ± 0.16		0.52 ± 0.28	
9			-0.23 ± 0.43		1.02 ± 0.34		0.43 ± 0.18		0.12 ± 0.18		1.15 ± 0.27	
10			0.14 ± 0.37				-1.00 ± 0.21		-0.14 ± 0.31			
11			-0.65 ± 0.20									
12			-1.06 ± 0.20									
13			-0.09 ± 0.23									
14			-0.03 ± 0.29									
Session	Br3	Br3	Br5	Br1	Br2	Br2	Br7	Br3	Br7	Br1	Br2	
Sample order during the session	3	6	8	2	7	1	2	8	6	1	6	

Table A2 All the analytical dataset of the samples and a standard.

	SIMS ANALYSES								Mount: BR2	Standard: UNIL-Q1 (Paine)		Analyse: δ^{30}Si			Value= -0.13±0.02 (NBS-28, 2σ)					Date: 03.09.2015	
	Beam	H'2/L'2 (30Si/28Si)		L'2 (30Si/Coeff)		H'2 (28Si/Coeff)		Time	Yield	mean	Measurements		mean	Drift correction			Calibration			Comment	
	nA	CPS	2SD	CPS	2SD	CPS	2SD		CPS/nA	2SD	$\delta^{30}Si$	2SD int	2SD	$\delta^{30}Si$	2SD		$\delta^{30}Si_{NBS-28}$	2SD			
d30Si_030915_BR2_Paine_test@1	2.26	3.2687E-02	1.5872E-02	7.0687E+07	1.1240E-01	2.3118E+06	1.0604E-01	16:57	3.1284E+07	3.1148E+07	-42.75	0.32	-42.66							Setting: Standard	
d30Si_030915_BR2_Paine_test@2	2.26	3.2689E-02	1.0757E-02	7.0462E+07	1.1922E-01	2.3047E+06	1.1042E-01	17:01	3.1152E+07	1.5384E+05	-42.68	0.22	0.16							Setting: Standard	
d30Si_030915_BR2_Paine_test@3	2.26	3.2694E-02	1.3079E-02	7.0423E+07	1.1688E-01	2.3039E+06	1.0647E-01	17:04	3.1126E+07		-42.55	0.26								Setting: Standard	
d30Si_030915_BR2_Paine_test@4	2.26	3.2688E-02	1.5435E-02	7.0486E+07	1.1414E-01	2.3042E+06	1.1717E-01	17:07	3.1147E+07		-42.71	0.31								Setting: Standard	
d30Si_030915_BR2_Paine_test@5	2.26	3.2693E-02	1.6394E-02	7.0499E+07	1.3955E-01	2.3048E+06	1.4128E-01	17:10	3.1136E+07		-42.58	0.33								Setting: Standard	
d30Si_030915_BR2_Paine_test@6	2.26	3.2688E-02	1.3543E-02	7.0292E+07	1.1098E-01	2.2976E+06	1.0713E-01	17:14	3.1046E+07		-42.71	0.27								Setting: Standard	
d30Si_030915_BR2_Paine@1	2.26	3.2694E-02	1.5181E-02	6.9683E+07	1.1456E-01	2.2783E+06	1.0862E-01	17:17	3.0782E+07	3.0755E+07	-42.55	0.30	-42.77	-42.57	0.30	-42.79	-0.04	0.25	-0.27	Standard	
d30Si_030915_BR2_Paine@02	2.27	3.2682E-02	1.1378E-02	6.9711E+07	1.2302E-01	2.2785E+06	1.1625E-01	17:21	3.0759E+07	7.4196E+04	-42.89	0.23	0.36	-42.90	0.23	0.31	-0.39	0.23	0.33	Standard	
d30Si_030915_BR2_Paine@03	2.27	3.2680E-02	1.6388E-02	6.9728E+07	1.2192E-01	2.2785E+06	1.2124E-01	17:24	3.0779E+07		-42.95	0.33		-42.96	0.33		-0.46	0.26		Standard	
d30Si_030915_BR2_Paine@04	2.27	3.2688E-02	1.4874E-02	6.9620E+07	1.0511E-01	2.2769E+06	9.4673E-02	17:27	3.0702E+07		-42.71	0.30		-42.72	0.30		-0.21	0.25		Standard	
d30Si_030915_Ki3S_rad@1	2.27	3.2749E-02	1.6859E-02	5.1262E+07	2.4876E-01	1.6786E+06	2.4497E-01	17:30	2.2626E+07	2.2818E+07	-40.93	0.34	-40.88							Ki3S	Yield
d30Si_030915_Ki3S_rad@2	2.26	3.2766E-02	1.3178E-02	4.8409E+07	2.2682E-01	1.5859E+06	2.2852E-01	17:34	2.1376E+07	2.2135E+06	-40.43	0.26	0.89							Ki3S	Yield
d30Si_030915_Ki3S_rad@3	2.27	3.2749E-02	2.0690E-02	4.8957E+07	5.6754E-02	1.6038E+06	5.7820E-02	17:37	2.1605E+07		-40.93	0.41								Ki3S	Yield
d30Si_030915_Ki3S_rad@4	2.27	3.2720E-02	1.6079E-02	5.6224E+07	2.0840E-01	1.8396E+06	2.0247E-01	17:40	2.4820E+07		-41.79	0.32								Ki3S	Yield
d30Si_030915_Ki3S_rad@5	2.27	3.2763E-02	1.7839E-02	5.2504E+07	1.0394E-01	1.7200E+06	1.0313E-01	17:44	2.3169E+07		-40.52	0.36								Ki3S	Yield
d30Si_030915_Ki3S_rad@6	2.27	3.2762E-02	1.6637E-02	5.2583E+07	1.6773E-01	1.7229E+06	1.6217E-01	17:47	2.3173E+07		-40.56	0.33								Ki3S	Yield
d30Si_030915_Ki3S_rad@7	2.27	3.2756E-02	1.5645E-02	5.0516E+07	3.1287E-01	1.6548E+06	3.1276E-01	17:50	2.2285E+07		-40.73	0.31								Ki3S	Yield
d30Si_030915_Ki3S_rad@8	2.27	3.2740E-02	2.0530E-02	5.3220E+07	7.4002E-02	1.7424E+06	7.8460E-02	17:53	2.3487E+07		-41.18	0.41								Ki3S	Yield
d30Si_030915_Ki22c1_rad@1	2.27	3.2748E-02	1.4319E-02	6.2360E+07	2.5919E-02	2.0419E+06	2.6538E-02	17:57	2.7525E+07	2.8729E+07	-40.96	0.29	-41.43							Ki22C1	Yield
d30Si_030915_Ki22c1_rad@2	2.27	3.2724E-02	1.3817E-02	6.5276E+07	1.0292E-01	2.1358E+06	1.0897E-01	18:00	2.8815E+07	1.7030E+06	-41.66	0.28	0.44	-41.67	0.28		0.90	0.24		Ki22C1	
d30Si_030915_BR2_Paine@05	2.27	3.2698E-02	9.9477E-03	6.9788E+07	1.1346E-01	2.2831E+06	1.0870E-01	18:03	3.0781E+07	3.0675E+07	-42.41	0.20	-42.69	-42.42	0.20	-42.70	0.11	0.22	-0.18	Standard	
d30Si_030915_BR2_Paine@06	2.27	3.2683E-02	1.4823E-02	6.9573E+07	1.2514E-01	2.2741E+06	1.2135E-01	18:07	3.0657E+07	2.1453E+05	-42.87	0.30	0.40	-42.88	0.30	0.34	-0.37	0.25	0.36	Standard	
d30Si_030915_BR2_Paine@07	2.29	3.2685E-02	1.2259E-02	6.9774E+07	1.0113E-01	2.2806E+06	9.8226E-02	18:10	3.0533E+07		-42.79	0.25		-42.80	0.25		-0.29	0.23		Standard	
d30Si_030915_BR2_Paine@08	2.27	3.2689E-02	1.0243E-02	6.9756E+07	9.9679E-02	2.2804E+06	1.0233E-01	18:13	3.0729E+07		-42.68	0.20		-42.69	0.20		-0.18	0.22		Standard	
d30Si_030915_Ki22c1_rad@3	2.27	3.2724E-02	1.9482E-02	6.3715E+07	2.2270E-01	2.0850E+06	2.2781E-01	18:17	2.8094E+07		-41.65	0.39		-41.66	0.39		0.90	0.28		Ki22C1	
d30Si_030915_Ki22c1_rad@4	2.27	3.2729E-02	1.0581E-02	6.5590E+07	5.8589E-02	2.1469E+06	5.6218E-02	18:20	2.8907E+07		-41.50	0.21		-41.51	0.21		1.06	0.23		Ki22C1	
d30Si_030915_Ki22c1_rad@5	2.27	3.2730E-02	1.4120E-02	6.3659E+07	1.3707E-01	2.0852E+06	1.2918E-01	18:23	2.8049E+07		-41.48	0.28		-41.49	0.28		1.08	0.25		Ki22C1	
d30Si_030915_Ki22c1_rad@6	2.27	3.2732E-02	1.6827E-02	6.7115E+07	9.6219E-02	2.1968E+06	8.8619E-02	18:26	2.9583E+07		-41.41	0.34		-41.42	0.34		1.15	0.26		Ki22C1	
d30Si_030915_Ki22c1_rad@7	2.27	3.2726E-02	1.6874E-02	6.3738E+07	2.6734E-02	2.0859E+06	3.2168E-02	18:30	2.8062E+07		-41.61	0.34		-41.62	0.34		0.95	0.26		Ki22C1	
d30Si_030915_Ki22c1_rad@8	2.27	3.2737E-02	1.2569E-02	6.8121E+07	1.1726E-01	2.2314E+06	1.0650E-01	18:33	3.0018E+07		-41.28	0.25		-41.29	0.25		1.29	0.24		Ki22C1	
d30Si_030915_Ki22c1_rad@9	2.27	3.2734E-02	1.1850E-02	6.6993E+07	8.3217E-02	2.1928E+06	8.0588E-02	18:36	2.9511E+07		-41.36	0.24		-41.36	0.24		1.21	0.23		Ki22C1	
d30Si_030915_Ki22C2_rad@1	2.27	3.2720E-02	1.4179E-02	6.6657E+07	1.2513E-01	2.1822E+06	1.1069E-01	18:40	2.9368E+07	2.7029E+07	-41.78	0.28	-41.00	-41.79	0.28		0.76	0.25		Ki22C2	
d30Si_030915_Ki22C2_rad@2	2.27	3.2715E-02	1.3497E-02	6.5550E+07	6.6668E-01	2.1445E+06	6.6701E-01	18:43	2.8892E+07	5.3019E+06	-41.91	0.27	1.72	-41.92	0.27		0.63	0.24		Ki22C2	
d30Si_030915_Ki22C2_rad@3	2.27	3.2757E-02	1.5328E-02	6.0644E+07	9.8168E-02	1.9861E+06	9.5456E-02	18:46	2.6714E+07		-40.69	0.31								Ki22C2	Yield
d30Si_030915_Ki22C2_rad@4	2.27	3.2728E-02	1.6302E-02	6.6806E+07	8.3038E-02	2.1864E+06	7.9917E-02	18:49	2.9436E+07		-41.56	0.33		-41.56	0.33		1.01	0.26		Ki22C2	
d30Si_030915_BR2_Paine@09	2.27	3.2692E-02	1.1050E-02	7.0310E+07	1.0519E-01	2.2986E+06	1.0531E-01	18:53	3.0988E+07	3.0837E+07	-42.61	0.22	-42.57	-42.61	0.22	-42.58	-0.09	0.23	-0.05	Standard	
d30Si_030915_BR2_Paine@10	2.27	3.2692E-02	1.2444E-02	6.9922E+07	8.9388E-02	2.2848E+06	9.4032E-02	18:56	3.0792E+07	2.1480E+05	-42.60	0.25	0.08	-42.61	0.25	0.07	-0.09	0.24	0.08	Standard	
d30Si_030915_BR2_Paine@11	2.27	3.2694E-02	1.1138E-02	6.9982E+07	9.7723E-02	2.2882E+06	9.7959E-02	18:59	3.0831E+07		-42.53	0.22		-42.54	0.22		-0.01	0.23		Standard	
d30Si_030915_BR2_Paine@12	2.27	3.2694E-02	1.5243E-02	6.9871E+07	1.0025E-01	2.2842E+06	1.0330E-01	19:03	3.0738E+07		-42.54	0.30		-42.54	0.30		-0.02	0.25		Standard	
d30Si_030915_Ki22C2_rad@5	2.27	3.2775E-02	1.7302E-02	5.5381E+07	7.9738E-02	1.8149E+06	8.6541E-02	19:06	2.4376E+07		-40.17	0.35								Ki22C2	Yield
d30Si_030915_Ki22C2_rad@6	2.27	3.2784E-02	2.2939E-02	5.3142E+07	1.5654E-01	1.7424E+06	1.5735E-01	19:09	2.3387E+07		-39.92	0.46								Ki22C2	Yield
d30Si_030915_Ki21_rad@1	2.27	3.2732E-02	1.4682E-02	6.7028E+07	8.2338E-02	2.1939E+06	8.5387E-02	19:13	2.9512E+07	2.9310E+07	-41.42	0.29	-41.41	-41.43	0.29		1.15	0.25		Ki21	
d30Si_030915_Ki21_rad@2	2.27	3.2729E-02	1.0343E-02	6.8106E+07	8.4599E-02	2.2290E+06	8.2063E-02	19:16	2.9987E+07	2.6665E+06	-41.51	0.21	0.53	-41.51	0.21		1.06	0.23		Ki21	
d30Si_030915_Ki21_rad@3	2.27	3.2716E-02	1.3917E-02	6.9057E+07	1.0325E-01	2.2591E+06	1.0358E-01	19:19	3.0389E+07		-41.90	0.28		-41.91	0.28		0.64	0.24		Ki21	
d30Si_030915_Ki21_rad@4	2.27	3.2744E-02	1.4509E-02	6.1416E+07	2.1616E-01	2.0108E+06	2.1450E-01	19:22	2.7024E+07		-41.09	0.29		-41.09	0.29		1.50	0.25		Ki21	
d30Si_030915_Ki21_rad@5	2.27	3.2732E-02	1.2205E-02	6.8046E+07	8.9280E-02	2.2273E+06	8.4314E-02	19:26	2.9953E+07		-41.44	0.24		-41.44	0.24		1.13	0.23		Ki21	
d30Si_030915_Ki21_rad@6	2.27	3.2728E-02	1.3732E-02	6.6905E+07	6.4271E-02	2.1899E+06	6.0335E-02	19:29	2.9446E+07		-41.53	0.27		-41.54	0.27		1.03	0.24		Ki21	
d30Si_030915_Ki21_rad@7	2.27	3.2741E-02	1.4288E-02	6.1453E+07	5.9736E-02	2.0120E+06	5.6079E-02	19:32	2.7062E+07		-41.16	0.29		-41.17	0.29		1.42	0.25		Ki21	
d30Si_030915_Ki21_rad@8	2.27	3.2727E-02	1.0176E-02	6.7868E+07	1.7685E-01	2.2210E+06	1.7127E-01	19:36	2.9860E+07		-41.56	0.20		-41.56	0.20		1.01	0.22		Ki21	
d30Si_030915_BR2_Paine@13	2.27	3.2699E-02	1.3770E-02	7.0232E+07	1.0871E-01	2.2967E+06	1.0425E-01	19:39	3.0913E+07	3.0838E+07	-42.39	0.28	-42.49	-42.40	0.28	-42.49	0.13	0.24	0.04	Standard	
d30Si_030915_BR2_Paine@14	2.27	3.2709E-02	1.1614E-02	7.0162E+07	1.0142E-01	2.2958E+06	9.1776E-02	19:42	3.0867E+07	1.2775E+05	-42.11	0.23	0.64	-42.11	0.23	0.55	0.43	0.23	0.58	Standard	
d30Si_030915_BR2_Paine@15	2.27	3.2692E-02	8.7517E-03	7.0003E+07	9.8259E-02	2.2884E+06	9.9923E-02	19:45	3.0796E+07		-42.59	0.18		-42.59	0.18		-0.07	0.22		Standard	
d30Si_030915_BR2_Paine@16	2.27	3.2683E-02	1.4489E-02	7.0002E+07	1.0497E-01	2.2881E+06	1.0610E-01	19:49	3.0775E+07		-42.86	0.29		-42.87	0.29		-0.35	0.25		Standard	
d30Si_030915_Ki21_rad@9	2.27	3.2744E-02	1.3202E-02	6.9458E+07	9.2310E-02	2.2743E+06	8.6229E-02	19:52	3.0552E+07		-41.08	0.26		-41.08	0.26		1.51	0.24		Ki21	
d30Si_030915_Ki15_rad@1	2.27	3.2737E-02	1.7317E-02	6.7385E+07	1.2935E-01	2.2062E+06	1.2653E-01	19:55	2.9622E+07	3.0009E+07	-41.29	0.35	-41.48	-41.29	0.35		1.29	0.26		Ki15	
d30Si_030915_Ki15_rad@2	2.27	3.2737E-02	1.5466E-02	6.7060E+07	1.6278E-01	2.1953E+06	1.6678E-01	19:59	2.9496E+07	1.4397E+06	-41.29	0.31	0.49	-41.29	0.31		1.29	0.25		Ki15	
d30Si_030915_Ki15_rad@3	2.27	3.2726E-02	1.4656E-02	6.9494E+07	1.0328E-01	2.2743E+06	1.0459E-01	20:02	3.0549E+07		-41.61	0.29		-41.61	0.29		0.96	0.25		Ki15	
d30Si_030915_Ki15_rad@4	2.27	3.2731E-02	1.3983E-02	6.8310E+07	1.1537E-01	2.2361E+06	1.1834E-01	20:05	3.0046E+07		-41.45	0.28		-41.45	0.28		1.12	0.24		Ki15	
d30Si_030915_Ki15_rad@5	2.28	3.2723E-02	1.1931E-02	7.1562E+07	8.4753E-02	2.3420E+06	8.6113E-02	20:09	3.1452E+07		-41.70	0.24		-41.70	0.24		0.86	0.23		Ki15	
d30Si_030915_Ki15_rad@6	2.28	3.2728E-02	1.1754E-02	6.8359E+07	8.5718E-02	2.2381E+06	7.7042E-02	20:12	3.0030E+07		-41.55	0.24		-41.55	0.24		1.02	0.23		Ki15	
d30Si_030915_Ki15_rad@7	2.28	3.2745E-02	9.7906E-03	6.5598E+07	1.3139E-01	2.1495E+06	1.2014E-01	20:15	2.8828E+07		-41.06	0.20		-41.06	0.20		1.53	0.22		Ki15	
d30Si_030915_Ki15_rad@8	2.28	3.2726E-02	9.2152E-03	6.8204E+07	7.7514E-02	2.2321E+06	8.0069E-02	20:18	2.9964E+07		-41.59	0.18		-41.59	0.18		0.97	0.22		Ki15	
d30Si_030915_Ki15_rad@9	2.28	3.2735E-02	1.1172E-02	6.7281E+07	1.1389E-01	2.2017E+06	1.1129E-01	20:22	2.9563E+07		-41.35	0.22		-41.35	0.22		1.23	0.23		Ki15	

Table A2 Continued.

SIMS ANALYSES						Mount: BR2			Standard: UNIL-Q1 (Paine)		Analyse: δ^{30}Si			Value= -0.13±0.02 (NBS-28, 2σ)						Date: 03.09.2015
	Beam	H'2/L'2 (30Si/28Si)		L'2 (30Si/Coeff)		H'2 (28Si/Coeff)		Time	Yield	mean	Measurements		mean	Drift correction			Calibration			Comment
	nA	*CPS*	*2SD*	*CPS*	*2SD*	*CPS*	*2SD*		CPS/nA	*2SD*	$\delta^{30}Si$	*2SD int*	*2SD*	$\delta^{30}Si$	*2SD*		$\delta^{30}Si_{NBS-28}$	*2SD*		
d30Si_030915_BR2_Paine@17	2.27	3.2690E-02	1.4568E-02	7.0136E+07	1.1794E-01	2.2941E+06	1.0669E-01	20:25	3.0836E+07	3.0799E+07	-42.67	0.29	-42.59	-42.67	0.29	-42.59	-0.15	0.25	-0.07	Standard
d30Si_030915_BR2_Paine@18	2.28	3.2688E-02	1.8037E-02	7.0093E+07	1.1699E-01	2.2925E+06	1.0701E-01	20:28	3.0800E+07	1.3591E+05	-42.71	0.36	0.27	-42.71	0.36	0.23	-0.20	0.27	0.24	Standard
d30Si_030915_BR2_Paine@19	2.28	3.2698E-02	1.1392E-02	7.0237E+07	1.0615E-01	2.2967E+06	1.0721E-01	20:32	3.0857E+07		-42.41	0.23		-42.41	0.23		0.12	0.23		Standard
d30Si_030915_BR2_Paine@20	2.28	3.2693E-02	1.5741E-02	6.9948E+07	1.0087E-01	2.2868E+06	9.9959E-02	20:35	3.0703E+07		-42.57	0.31		-42.57	0.31		-0.04	0.25		Standard
d30Si_030915_Ki15_rad@10	2.28	3.2716E-02	1.0776E-02	6.9531E+07	1.0497E-01	2.2759E+06	9.4792E-02	20:38	3.0537E+07		-41.90	0.22		-41.90	0.22		0.65	0.23		Ki15
d30Si_030915_Ki9_rad@1	2.28	3.2705E-02	1.3044E-02	7.0936E+07	1.2251E-01	2.3214E+06	1.0837E-01	20:42	3.1151E+07	3.0274E+07	-42.23	0.26	-41.89	-42.23	0.26		0.31	0.24		Ki09
d30Si_030915_Ki9_rad@2	2.28	3.2720E-02	1.4574E-02	6.7386E+07	7.8828E-02	2.2049E+06	7.7565E-02	20:45	2.9604E+07	1.6946E+06	-41.78	0.29	0.63	-41.78	0.29		0.78	0.25		Ki09
d30Si_030915_Ki9_rad@3	2.28	3.2725E-02	1.8691E-02	6.5120E+07	1.1842E-01	2.1314E+06	1.1876E-01	20:48	2.8592E+07		-41.62	0.37		-41.62	0.37		0.95	0.27		Ki09
d30Si_030915_Ki9_rad@4	2.28	3.2702E-02	1.5312E-02	7.0892E+07	1.2606E-01	2.3185E+06	1.2108E-01	20:51	3.1112E+07		-42.29	0.31		-42.29	0.31		0.25	0.25		Ki09
d30Si_030915_Ki9_rad@5	2.28	3.2727E-02	1.3002E-02	6.7699E+07	1.1528E-01	2.2158E+06	1.1386E-01	20:55	2.9729E+07		-41.56	0.26		-41.56	0.26		1.01	0.24		Ki09
d30Si_030915_Ki9_rad@6	2.28	3.2705E-02	1.2780E-02	7.0346E+07	1.1938E-01	2.3019E+06	1.1071E-01	20:58	3.0867E+07		-42.21	0.26		-42.20	0.26		0.34	0.24		Ki09
d30Si_030915_Ki9_rad@7	2.28	3.2717E-02	9.1153E-03	6.9233E+07	9.0624E-02	2.2649E+06	8.9704E-02	21:01	3.0376E+07		-41.86	0.18		-41.85	0.18		0.70	0.22		Ki09
d30Si_030915_Ki9_rad@8	2.28	3.2711E-02	1.4062E-02	7.0284E+07	8.1807E-02	2.2993E+06	8.1119E-02	21:05	3.0846E+07		-42.04	0.28		-42.04	0.28		0.51	0.24		Ki09
d30Si_030915_Ki9_rad@9	2.28	3.2732E-02	1.3680E-02	6.8839E+07	1.1557E-01	2.2530E+06	1.1352E-01	21:08	3.0184E+07		-41.44	0.27		-41.44	0.27		1.14	0.24		Ki09
d30Si_030915_BR2_Paine@21	2.28	3.2681E-02	1.0822E-02	7.1908E+07	9.6591E-02	2.3502E+06	9.7210E-02	21:11	3.1578E+07	3.1513E+07	-42.92	0.22	-42.79	-42.92	0.22	-42.79	-0.41	0.23	-0.27	Standard
d30Si_030915_BR2_Paine@22	2.28	3.2691E-02	1.4090E-02	7.1814E+07	9.0667E-02	2.3477E+06	9.1274E-02	21:14	3.1505E+07	1.0345E+05	-42.63	0.28	0.24	-42.62	0.28	0.21	-0.10	0.24	0.22	Standard
d30Si_030915_BR2_Paine@23	2.28	3.2686E-02	1.1573E-02	7.1704E+07	1.0805E-01	2.3449E+06	9.7910E-02	21:18	3.1452E+07		-42.78	0.23		-42.78	0.23		-0.26	0.23		Standard
d30Si_030915_BR2_Paine@24	2.28	3.2684E-02	1.3058E-02	7.1842E+07	9.6674E-02	2.3484E+06	9.4787E-02	21:21	3.1517E+07		-42.83	0.26		-42.83	0.26		-0.31	0.24		Standard
d30Si_030915_Ki4C_rad@1	2.28	3.2718E-02	1.4400E-02	6.7128E+07	9.9781E-02	2.1963E+06	9.6489E-02	21:24	2.9444E+07	3.0239E+07	-41.83	0.29	-41.91	-41.82	0.29		0.74	0.25		Ki04C
d30Si_030915_Ki4C_rad@2	2.28	3.2721E-02	9.5208E-03	6.9043E+07	1.3916E-01	2.2605E+06	1.2690E-01	21:28	3.0302E+07	1.1552E+06	-41.75	0.19	0.64	-41.75	0.19		0.81	0.22		Ki04C
d30Si_030915_Ki4C_rad@3	2.28	3.2731E-02	1.1254E-02	6.7751E+07	9.2481E-02	2.2172E+06	8.8627E-02	21:31	2.9706E+07		-41.45	0.23		-41.45	0.23		1.13	0.23		Ki04C
d30Si_030915_Ki4C_rad@4	2.28	3.2713E-02	1.1513E-02	6.8764E+07	1.1598E-01	2.2495E+06	1.1234E-01	21:34	3.0172E+07		-41.98	0.23		-41.97	0.23		0.58	0.23		Ki04C
d30Si_030915_Ki4C_rad@5	2.28	3.2702E-02	1.1848E-02	6.9922E+07	1.6186E-01	2.2870E+06	1.6041E-01	21:38	3.0691E+07		-42.30	0.24		-42.29	0.24		0.24	0.23		Ki04C
d30Si_030915_Ki4C_rad@6	2.28	3.2700E-02	8.0270E-03	7.0885E+07	9.0174E-02	2.3180E+06	8.9241E-02	21:41	3.1081E+07		-42.36	0.16		-42.35	0.16		0.18	0.22		Ki04C
d30Si_030915_Ki4C_rad@7	2.28	3.2706E-02	1.3764E-02	6.9897E+07	9.2811E-02	2.2859E+06	9.5888E-02	21:44	3.0652E+07		-42.17	0.28		-42.17	0.28		0.38	0.24		Ki04C
d30Si_030915_Ki4C_rad@8	2.28	3.2721E-02	1.2281E-02	6.9777E+07	8.4784E-02	2.2829E+06	8.6294E-02	21:47	3.0591E+07		-41.75	0.25		-41.74	0.25		0.82	0.23		Ki04C
d30Si_030915_Ki4C_rad@9	2.28	3.2727E-02	1.6765E-02	6.7343E+07	9.6880E-02	2.2040E+06	9.4344E-02	21:51	2.9507E+07		-41.57	0.34		-41.56	0.34		1.01	0.26		Ki04C
d30Si_030915_Ki44_rad@1	2.28	3.2741E-02	1.1908E-02	6.8848E+07	8.6897E-02	2.2544E+06	8.7865E-02	21:54	3.0182E+07		-41.16	0.24		-41.15	0.24		1.43	0.23		Ki44
d30Si_030915_BR2_Paine@25	2.28	3.2683E-02	1.4298E-02	7.1742E+07	9.6409E-02	2.3450E+06	8.8822E-02	21:57	3.1455E+07	3.1416E+07	-42.87	0.29	-42.69	-42.86	0.29	-42.68	-0.35	0.25	-0.16	Standard
d30Si_030915_BR2_Paine@26	2.28	3.2687E-02	9.2350E-03	7.1687E+07	1.0528E-01	2.3435E+06	1.0246E-01	22:01	3.1438E+07	7.5919E+04	-42.74	0.18	0.37	-42.73	0.18	0.32	-0.21	0.22	0.33	Standard
d30Si_030915_BR2_Paine@27	2.28	3.2698E-02	1.4460E-02	7.1556E+07	1.0853E-01	2.3397E+06	1.0437E-01	22:04	3.1370E+07		-42.43	0.29		-42.42	0.29		0.11	0.25		Standard
d30Si_030915_BR2_Paine@28	2.28	3.2688E-02	7.0230E-03	7.1697E+07	9.2215E-02	2.3435E+06	8.8595E-02	22:07	3.1401E+07		-42.72	0.14		-42.71	0.14		-0.19	0.21		Standard
d30Si_030915_Ki44_rad@2	2.28	3.2740E-02	1.5265E-02	6.9974E+07	1.1253E-01	2.2910E+06	1.1307E-01	22:10	3.0655E+07	3.0551E+07	-41.19	0.31	-41.18	-41.19	0.31		1.40	0.25		Ki44
d30Si_030915_Ki44_rad@3	2.28	3.2736E-02	1.4482E-02	7.1225E+07	8.6454E-02	2.3326E+06	7.7928E-02	22:14	3.1193E+07	8.0769E+05	-41.30	0.29	0.21	-41.29	0.29		1.29	0.25		Ki44
d30Si_030915_Ki44_rad@4	2.28	3.2735E-02	1.2597E-02	7.0045E+07	1.2242E-01	2.2931E+06	1.2202E-01	22:17	3.0685E+07		-41.34	0.25		-41.33	0.25		1.25	0.24		Ki44
d30Si_030915_Ki44_rad@5	2.28	3.2740E-02	9.2657E-03	6.9955E+07	1.2491E-01	2.2906E+06	1.2356E-01	22:20	3.0641E+07		-41.18	0.19		-41.17	0.19		1.42	0.22		Ki44
d30Si_030915_Ki44_rad@6	2.28	3.2741E-02	1.1069E-02	6.8689E+07	1.2902E-01	2.2505E+06	1.1969E-01	22:24	3.0079E+07		-41.15	0.22		-41.14	0.22		1.44	0.23		Ki44
d30Si_030915_Ki44_rad@7	2.28	3.2747E-02	8.9239E-03	7.0431E+07	1.0452E-01	2.3063E+06	1.0159E-01	22:27	3.0847E+07		-40.98	0.18		-40.97	0.18		1.62	0.22		Ki44
d30Si_030915_Ki44_rad@8	2.28	3.2740E-02	1.2774E-02	7.0208E+07	8.7631E-02	2.2976E+06	8.0694E-02	22:30	3.0739E+07		-41.20	0.26		-41.19	0.26		1.40	0.24		Ki44
d30Si_030915_Ki44_rad@9	2.29	3.2743E-02	1.0382E-02	6.8420E+07	1.3881E-01	2.2401E+06	1.3814E-01	22:33	2.9940E+07		-41.09	0.21		-41.08	0.21		1.51	0.23		Ki44
d30Si_030915_Ki35_rad@1	2.28	3.2758E-02	1.2989E-02	6.9064E+07	1.2380E-01	2.2638E+06	1.1696E-01	22:37	3.0249E+07		-40.67	0.26		-40.66	0.26		1.95	0.24		Ki35
d30Si_030915_BR2_Paine@29	2.28	3.2680E-02	1.2319E-02	7.1696E+07	9.8828E-02	2.3444E+06	9.1310E-02	22:40	3.1391E+07	3.1377E+07	-42.94	0.25	-42.76	-42.93	0.25	-42.75	-0.42	0.23	-0.23	Standard
d30Si_030915_BR2_Paine@30	2.28	3.2687E-02	1.3720E-02	7.1770E+07	1.0328E-01	2.3458E+06	1.0042E-01	22:44	3.1429E+07	1.3094E+05	-42.73	0.27	0.26	-42.72	0.27	0.22	-0.20	0.24	0.23	Standard
d30Si_030915_BR2_Paine@31	2.28	3.2687E-02	1.5268E-02	7.1711E+07	9.6995E-02	2.3443E+06	9.6941E-02	22:47	3.1408E+07		-42.75	0.31		-42.74	0.31		-0.22	0.25		Standard
d30Si_030915_BR2_Paine@32	2.28	3.2691E-02	1.0132E-02	7.1428E+07	9.8129E-02	2.3351E+06	9.5767E-02	22:50	3.1282E+07		-42.63	0.20		-42.62	0.20		-0.10	0.22		Standard
d30Si_030915_Ki35_rad@2	2.28	3.2766E-02	1.1402E-02	6.8756E+07	1.0508E-01	2.2527E+06	1.0399E-01	22:53	3.0152E+07	2.9876E+07	-40.42	0.23	-40.67	-40.41	0.23		2.21	0.23		Ki35
d30Si_030915_Ki35_rad@3	2.28	3.2761E-02	1.4989E-02	6.8978E+07	1.6074E-01	2.2596E+06	1.6210E-01	22:57	3.0233E+07	1.0492E+06	-40.58	0.30	0.38	-40.56	0.30		2.05	0.25		Ki35
d30Si_030915_Ki35_rad@4	2.28	3.2744E-02	9.3645E-03	6.8504E+07	1.2516E-01	2.2429E+06	1.2349E-01	23:00	3.0049E+07		-41.08	0.19		-41.07	0.19		1.52	0.22		Ki35
d30Si_030915_Ki35_rad@5	2.28	3.2761E-02	1.2068E-02	6.6329E+07	1.5829E-01	2.1746E+06	1.4430E-01	23:03	2.9096E+07		-40.58	0.24		-40.56	0.24		2.05	0.23		Ki35
d30Si_030915_Ki35_rad@6	2.28	3.2762E-02	1.3199E-02	6.9467E+07	1.1818E-01	2.2759E+06	1.1377E-01	23:07	3.0459E+07		-40.56	0.26		-40.54	0.26		2.07	0.24		Ki35
d30Si_030915_Ki35_rad@7	2.28	3.2757E-02	1.4762E-02	6.6260E+07	1.0846E-01	2.1716E+06	1.0019E-01	23:10	2.9057E+07		-40.70	0.30		-40.69	0.30		1.92	0.25		Ki35
d30Si_030915_Ki35_rad@8	2.28	3.2753E-02	1.4295E-02	6.7238E+07	1.5922E-01	2.2023E+06	1.5517E-01	23:13	2.9482E+07		-40.81	0.29		-40.80	0.29		1.80	0.25		Ki35
d30Si_030915_Ki35_rad@9	2.28	3.2760E-02	1.5032E-02	6.8657E+07	1.3825E-01	2.2507E+06	1.2435E-01	23:16	3.0110E+07		-40.60	0.30		-40.59	0.30		2.02	0.25		Ki35
d30Si_030915_BR2_Paine@33	2.28	3.2690E-02	1.5042E-02	7.1276E+07	8.5477E-02	2.3301E+06	8.8889E-02	23:20	3.1269E+07	3.1133E+07	-42.66	0.30	-42.65	-42.65	0.30	-42.64	-0.13	0.25	-0.12	Standard
d30Si_030915_BR2_Paine@34	2.28	3.2681E-02	1.2069E-02	7.1028E+07	1.0906E-01	2.3212E+06	1.0489E-01	23:23	3.1115E+07	2.0383E+05	-42.93	0.24	0.45	-42.91	0.24	0.39	-0.40	0.23		Standard
d30Si_030915_BR2_Paine@35	2.28	3.2690E-02	1.2324E-02	7.1001E+07	1.3126E-01	2.3212E+06	1.2931E-01	23:27	3.1124E+07		-42.65	0.25		-42.63	0.25		-0.11	0.23		Standard
d30Si_030915_BR2_Paine@36	2.28	3.2700E-02	8.2229E-03	7.0813E+07	1.1254E-01	2.3154E+06	1.0918E-01	23:30	3.1022E+07		-42.37	0.16		-42.36	0.16		0.18	0.22		Standard

Table A2 Continued.

SIMS ANALYSES									Mount: BR3	Standard: UNIL-Q1 (Paine)	Analyse: $\delta^{30}Si$			Value= -0.13±0.02 (NBS-28, 2σ)						Date: 03.09.2015
	Beam	H'2/L'2 (30Si/28Si)		L'2 (30Si/Coeff)		H'2 (28Si/Coeff)		Time	Yield	mean	Measurements		mean	Drift correction			Calibration			Comment
	nA	CPS	2SD	CPS	2SD	CPS	2SD		CPS/nA	2SD	$\delta^{30}Si$	2SD int	2SD	$\delta^{30}Si$	2SD		$\delta^{30}Si_{NBS-28}$	2SD		
d30Si_030915_BR3_Paine_test@1	2.95	3.2675E-02	6.2872E-03	1.1213E+08	1.0747E-01	3.6642E+06	1.0556E-01	10:05	3.7981E+07	3.7351E+07	-43.09	0.13	-42.91							Setting: Standard
d30Si_030915_BR3_Paine_test@2	2.96	3.2682E-02	1.2070E-02	1.1171E+08	6.2295E-02	3.6510E+06	6.7105E-02	10:09	3.7698E+07	7.5902E+05	-42.88	0.24	0.30							Setting: Standard
d30Si_030915_BR3_Paine_test@3	2.97	3.2682E-02	1.0184E-02	1.1100E+08	9.7157E-02	3.6278E+06	9.1043E-02	10:12	3.7420E+07		-42.88	0.20								Setting: Standard
d30Si_030915_BR3_Paine_test@4	2.96	3.2686E-02	9.6006E-03	1.1084E+08	1.1302E-01	3.6246E+06	1.0309E-01	10:15	3.7397E+07		-42.76	0.19								Setting: Standard
d30Si_030915_BR3_Paine_test@5	2.97	3.2675E-02	1.1150E-02	1.1050E+08	1.5044E-01	3.6109E+06	1.4508E-01	10:18	3.7217E+07		-43.08	0.22								Setting: Standard
d30Si_030915_BR3_Paine_test@6	2.97	3.2676E-02	7.6194E-03	1.1095E+08	1.0389E-01	3.6256E+06	9.9872E-02	10:22	3.7352E+07		-43.07	0.15								Setting: Standard
d30Si_030915_BR3_Paine_test@7	2.97	3.2685E-02	1.0739E-02	1.0979E+08	1.0918E-01	3.5888E+06	1.0592E-01	10:25	3.6941E+07		-42.79	0.21								Setting: Standard
d30Si_030915_BR3_Paine_test@8	2.97	3.2687E-02	8.3907E-03	1.0939E+08	1.0076E-01	3.5774E+06	9.3054E-02	10:28	3.6806E+07		-42.73	0.17								Setting: Standard
d30Si_030915_BR3_Paine@1	2.24	3.2688E-02	1.5603E-02	7.9842E+07	1.2759E-01	2.6100E+06	1.2215E-01	10:32	3.5719E+07	3.5859E+07	-42.70	0.31	-42.76	-42.79	0.31	-42.83	-0.07	0.23	-0.11	Standard
d30Si_030915_BR3_Paine@02	2.24	3.2685E-02	1.5305E-02	8.0251E+07	1.0616E-01	2.6242E+06	1.0085E-01	10:35	3.5820E+07	2.2364E+05	-42.79	0.31	0.31	-42.87	0.31	0.08	-0.16	0.23	0.09	Standard
d30Si_030915_BR3_Paine@03	2.24	3.2692E-02	1.2761E-02	8.0502E+07	9.5218E-02	2.6318E+06	9.7118E-02	10:39	3.5960E+07		-42.59	0.26		-42.67	0.26		0.05	0.21		Standard
d30Si_030915_BR3_Paine@04	2.24	3.2680E-02	1.0213E-02	8.0475E+07	1.1060E-01	2.6301E+06	1.1363E-01	10:42	3.5937E+07		-42.96	0.20		-43.03	0.20		-0.33	0.20		Standard
d30Si_030915_BR3_Paine@05	2.24	3.2687E-02	1.1033E-02	8.0389E+07	1.1222E-01	2.6277E+06	1.1142E-01	11:21	3.5880E+07	3.5835E+07	-42.74	0.22	-42.77	-42.80	0.22	-42.82	-0.08	0.20	-0.11	Standard
d30Si_030915_BR3_Paine@06	2.24	3.2691E-02	1.6327E-02	8.0645E+07	1.1874E-01	2.6364E+06	1.2532E-01	11:25	3.5958E+07	2.6308E+05	-42.62	0.33	0.36	-42.67	0.33	0.31	0.05	0.24	0.33	Standard
d30Si_030915_BR3_Paine@07	2.24	3.2677E-02	9.0856E-03	7.9925E+07	1.5800E-01	2.6120E+06	1.5538E-01	11:28	3.5649E+07		-43.03	0.18		-43.08	0.18		-0.38	0.19		Standard
d30Si_030915_BR3_Paine@08	2.24	3.2689E-02	7.7881E-03	8.0391E+07	1.0209E-01	2.6293E+06	9.3148E-02	11:31	3.5852E+07		-42.68	0.16		-42.73	0.16		-0.01	0.19		Standard
d30Si_030915_Ki7C_rad@1	2.24	3.2726E-02	1.2216E-02	7.7732E+07	5.8207E-02	2.5441E+06	5.4915E-02	11:38	3.4695E+07	3.4951E+07	-41.61	0.24	-41.83	-41.66	0.24		1.11	0.21		Ki07C
d30Si_030915_Ki7C_rad@2	2.24	3.2721E-02	1.5353E-02	7.7458E+07	1.4446E-01	2.5345E+06	1.4418E-01	11:41	3.4547E+07	7.5457E+05	-41.76	0.31	0.41	-41.80	0.31		0.96	0.23		Ki07C
d30Si_030915_Ki7C_rad@3	2.24	3.2715E-02	8.0328E-03	7.8936E+07	9.3491E-02	2.5827E+06	9.2580E-02	11:45	3.5226E+07		-41.92	0.16		-41.96	0.16		0.79	0.19		Ki07C
d30Si_030915_Ki7C_rad@4	2.24	3.2726E-02	1.4500E-02	7.8267E+07	9.9890E-02	2.5626E+06	9.2018E-02	11:48	3.4901E+07		-41.59	0.29		-41.63	0.29		1.14	0.22		Ki07C
d30Si_030915_Ki7C_rad@5	2.24	3.2712E-02	1.2513E-02	7.8019E+07	2.2485E-01	2.5518E+06	2.2597E-01	11:51	3.4775E+07		-42.02	0.25		-42.05	0.25		0.70	0.21		Ki07C
d30Si_030915_Ki7C_rad@6	2.24	3.2710E-02	1.3116E-02	7.9702E+07	1.1500E-01	2.6070E+06	1.1933E-01	11:54	3.5563E+07		-42.07	0.26		-42.10	0.26		0.64	0.21		Ki07C
d30Si_030915_Ki51_rad@1	2.24	3.2706E-02	1.0172E-02	7.9344E+07	9.1960E-02	2.5949E+06	8.9846E-02	11:58	3.5395E+07	3.4445E+07	-42.20	0.20	-41.65	-42.23	0.20		0.51	0.20		Ki51
d30Si_030915_Ki51_rad@2	2.24	3.2728E-02	9.6286E-03	7.6583E+07	1.4323E-01	2.5063E+06	1.4759E-01	12:01	3.4135E+07	1.0735E+06	-41.54	0.19	0.64	-41.57	0.19		1.20	0.19		Ki51
d30Si_030915_Ki51_rad@3	2.24	3.2733E-02	1.4440E-02	7.7664E+07	1.1995E-01	2.5422E+06	1.1313E-01	12:04	3.4630E+07		-41.39	0.29		-41.42	0.29		1.36	0.22		Ki51
d30Si_030915_BR3_Paine@09	2.24	3.2693E-02	1.0410E-02	8.0844E+07	1.0599E-01	2.6429E+06	1.0371E-01	12:07	3.6022E+07	3.6101E+07	-42.57	0.21	-42.73	-42.60	0.21	-42.75	0.13	0.20	-0.03	Standard
d30Si_030915_BR3_Paine@10	2.24	3.2686E-02	1.1547E-02	8.1105E+07	9.3516E-02	2.6511E+06	9.4209E-02	12:11	3.6137E+07	1.0794E+05	-42.76	0.23	0.23	-42.79	0.23	0.20	-0.07	0.20	0.21	Standard
d30Si_030915_BR3_Paine@11	2.24	3.2687E-02	1.1975E-02	8.1047E+07	1.0351E-01	2.6506E+06	9.9416E-02	12:14	3.6134E+07		-42.73	0.24		-42.75	0.24		-0.04	0.21		Standard
d30Si_030915_BR3_Paine@12	2.24	3.2683E-02	1.2928E-02	8.1028E+07	1.0004E-01	2.6498E+06	9.4833E-02	12:17	3.6112E+07		-42.85	0.26		-42.87	0.26		-0.16	0.21		Standard
d30Si_030915_Ki51_rad@4	2.24	3.2719E-02	1.2741E-02	7.7336E+07	1.3237E-01	2.5303E+06	1.2756E-01	12:21	3.4478E+07		-41.81	0.25		-41.83	0.25		0.93	0.21		Ki51
d30Si_030915_Ki51_rad@5	2.25	3.2736E-02	8.9637E-03	7.6079E+07	1.1530E-01	2.4919E+06	1.1045E-01	12:24	3.3880E+07		-41.31	0.18		-41.33	0.18		1.45	0.19		Ki51
d30Si_030915_Ki51_rad@6	2.24	3.2724E-02	1.2074E-02	7.6651E+07	1.6499E-01	2.5084E+06	1.6341E-01	12:27	3.4151E+07		-41.66	0.24		-41.68	0.24		1.09	0.21		Ki51
d30Si_030915_Ki24_rad@1	2.24	3.2754E-02	1.2907E-02	7.6934E+07	1.1669E-01	2.5197E+06	1.1309E-01	12:30	3.4283E+07	3.3452E+07	-40.77	0.26	-40.92	-40.78	0.26		2.02	0.21		Ki24
d30Si_030915_Ki24_rad@2	2.25	3.2745E-02	9.9085E-03	7.4673E+07	8.7587E-02	2.4440E+06	8.1973E-02	12:34	3.3259E+07	1.3202E+06	-41.04	0.20	0.45	-41.05	0.20		1.75	0.20		Ki24
d30Si_030915_Ki24_rad@3	2.24	3.2749E-02	1.3585E-02	7.4489E+07	1.3498E-01	2.4395E+06	1.3067E-01	12:37	3.3209E+07		-40.92	0.27		-40.93	0.27		1.87	0.22		Ki24
d30Si_030915_Ki24_rad@4	2.24	3.2759E-02	1.0536E-02	7.5011E+07	8.4256E-02	2.4570E+06	7.9608E-02	12:40	3.3439E+07		-40.64	0.21		-40.65	0.21		2.16	0.20		Ki24
d30Si_030915_Ki24_rad@5	2.26	3.2751E-02	8.9260E-03	7.3293E+07	9.4002E-02	2.4002E+06	9.5443E-02	12:43	3.2450E+07		-40.88	0.18		-40.88	0.18		1.92	0.19		Ki24
d30Si_030915_Ki24_rad@6	2.24	3.2737E-02	1.0813E-02	7.6411E+07	8.5403E-02	2.5015E+06	8.3864E-02	12:47	3.4075E+07		-41.29	0.22		-41.29	0.22		1.49	0.20		Ki24
d30Si_030915_Ki6C_rad@1	2.24	3.2702E-02	9.3909E-03	7.7473E+07	7.5322E-02	2.5335E+06	7.3156E-02	12:50	3.4541E+07		-42.31	0.19		-42.31	0.19		0.43	0.19		Ki06C
d30Si_030915_BR3_Paine@13	2.24	3.2676E-02	9.1282E-03	7.9346E+07	1.0639E-01	2.5929E+06	1.0458E-01	12:53	3.5373E+07	3.5520E+07	-43.07	0.18	-42.88	-43.07	0.18	-42.88	-0.37	0.19	-0.17	Standard
d30Si_030915_BR3_Paine@14	2.24	3.2689E-02	8.7227E-03	7.9790E+07	9.5323E-02	2.6068E+06	1.0172E-01	12:57	3.5556E+07	1.9670E+05	-42.70	0.17	0.30	-42.70	0.17	0.27	0.02	0.19	0.28	Standard
d30Si_030915_BR3_Paine@15	2.24	3.2682E-02	1.3738E-02	7.9844E+07	9.7867E-02	2.6107E+06	9.1314E-02	13:00	3.5576E+07		-42.89	0.27		-42.89	0.27		-0.18	0.22		Standard
d30Si_030915_BR3_Paine@16	2.24	3.2683E-02	9.0427E-03	7.9789E+07	1.0031E-01	2.6075E+06	9.8651E-02	13:03	3.5574E+07		-42.87	0.18		-42.86	0.18		-0.15	0.19		Standard
d30Si_030915_Ki6C_rad@2	2.24	3.2693E-02	1.4200E-02	7.8499E+07	1.0089E-01	2.5676E+06	8.9339E-02	13:06	3.4985E+07	3.4695E+07	-42.57	0.28	-42.71	-42.56	0.28		0.16	0.22		Ki06C
d30Si_030915_Ki6C_rad@3	2.24	3.2690E-02	1.0032E-02	7.8042E+07	1.1918E-01	2.5512E+06	1.1967E-01	13:10	3.4788E+07	8.4980E+05	-42.66	0.20	0.50	-42.66	0.20		0.07	0.20		Ki06C
d30Si_030915_Ki6C_rad@4	2.25	3.2684E-02	1.5786E-02	7.9072E+07	1.0154E-01	2.5856E+06	8.9306E-02	13:13	3.5219E+07		-42.82	0.32		-42.81	0.32		-0.10	0.23		Ki06C
d30Si_030915_Ki6C_rad@5	2.25	3.2680E-02	8.8349E-03	7.6306E+07	1.2811E-01	2.4938E+06	1.2812E-01	13:16	3.3980E+07		-42.95	0.18		-42.94	0.18		-0.23	0.19		Ki06C
d30Si_030915_Ki6C_rad@6	2.25	3.2680E-02	1.7941E-02	7.7819E+07	1.1470E-01	2.5429E+06	1.2079E-01	13:20	3.4654E+07		-42.95	0.36		-42.94	0.36		-0.23	0.25		Ki06C
d30Si_030915_Ki56_rad@1	2.24	3.2715E-02	1.1438E-02	7.6875E+07	7.1230E-02	2.5149E+06	6.6858E-02	13:23	3.4250E+07	3.3596E+07	-41.92	0.23	-42.17	-41.90	0.23		0.85	0.20		Ki58
d30Si_030915_Ki56_rad@2	2.24	3.2717E-02	1.3821E-02	7.4950E+07	1.3737E-01	2.4525E+06	1.3439E-01	13:26	3.3398E+07	1.4770E+06	-41.86	0.28	0.92	-41.84	0.28		0.91	0.22		Ki58
d30Si_030915_Ki56_rad@3	2.24	3.2717E-02	1.1866E-02	7.3754E+07	1.1540E-01	2.4132E+06	1.1335E-01	13:29	3.2866E+07		-41.86	0.24		-41.84	0.24		0.92	0.21		Ki58
d30Si_030915_Ki56_rad@4	2.25	3.2716E-02	1.1655E-02	7.3258E+07	8.1070E-02	2.3967E+06	7.6710E-02	13:33	3.2630E+07		-41.88	0.23		-41.86	0.23		0.90	0.21		Ki58
d30Si_030915_Ki56_rad@5	2.24	3.2692E-02	1.3222E-02	7.6566E+07	1.2848E-01	2.5031E+06	1.2903E-01	13:36	3.4110E+07		-42.60	0.26		-42.57	0.26		0.15	0.21		Ki58
d30Si_030915_BR3_Paine@17	2.24	3.2687E-02	1.1110E-02	8.0028E+07	9.0278E-02	2.6159E+06	8.8983E-02	13:39	3.5658E+07	3.5626E+07	-42.75	0.22	-43.00	-42.73	0.22	-42.97	-0.01	0.20	-0.27	Standard
d30Si_030915_BR3_Paine@18	2.25	3.2672E-02	1.1292E-02	7.9880E+07	1.0023E-01	2.6100E+06	9.8988E-02	13:42	3.5556E+07	1.0604E+05	-43.19	0.23	0.37	-43.16	0.23	0.32	-0.46	0.20	0.33	Standard
d30Si_030915_BR3_Paine@19	2.25	3.2679E-02	1.5750E-02	7.9964E+07	9.2994E-02	2.6131E+06	1.0240E-01	13:46	3.5616E+07		-42.99	0.31		-42.96	0.31		-0.25	0.23		Standard
d30Si_030915_BR3_Paine@20	2.25	3.2676E-02	1.2143E-02	8.0111E+07	9.3055E-02	2.6177E+06	9.0982E-02	13:49	3.5675E+07		-43.08	0.24		-43.05	0.24		-0.34	0.21		Standard
d30Si_030915_Ki56_rad@6	2.24	3.2682E-02	1.3729E-02	7.7046E+07	1.2286E-01	2.5182E+06	1.1980E-01	13:52	3.4324E+07		-42.90	0.27		-42.87	0.27		-0.15	0.22		Ki58
d30Si_030915_Ki2C_rad@1	2.24	3.2715E-02	1.1563E-02	7.7323E+07	1.5357E-01	2.5296E+06	1.5306E-01	13:56	3.4454E+07	3.4314E+07	-41.93	0.23	-42.38	-41.90	0.23		0.86	0.21		Ki02C
d30Si_030915_Ki2C_rad@2	2.25	3.2682E-02	1.4893E-02	8.0727E+07	9.4518E-02	2.6383E+06	9.3060E-02	13:59	3.5942E+07	2.1155E+06	-42.90	0.30	0.83	-42.87	0.30		-0.16	0.23		Ki02C
d30Si_030915_Ki2C_rad@3	2.25	3.2712E-02	1.0820E-02	7.3531E+07	6.8995E-02	2.4060E+06	7.2550E-02	14:02	3.2727E+07		-42.02	0.22		-41.98	0.22		0.77	0.20		Ki02C
d30Si_030915_Ki2C_rad@4	2.25	3.2703E-02	1.4432E-02	7.5308E+07	1.9525E-01	2.4630E+06	1.9113E-01	14:05	3.3532E+07		-42.26	0.29		-42.22	0.29		0.52	0.22		Ki02C
d30Si_030915_Ki2C_rad@5	2.25	3.2710E-02	1.2445E-02	7.6289E+07	1.0249E-01	2.4955E+06	1.0129E-01	14:09	3.3968E+07		-42.07	0.25		-42.03	0.25		0.72	0.21		Ki02C
d30Si_030915_Ki2C_rad@6	2.25	3.2694E-02	9.5069E-03	7.7190E+07	1.2376E-01	2.5238E+06	1.2561E-01	14:12	3.4374E+07		-42.54	0.19		-42.50	0.19		0.23	0.19		Ki02C
d30Si_030915_Ki2C_rad@7	2.25	3.2681E-02	1.1661E-02	7.9063E+07	1.0516E-01	2.5837E+06	1.0263E-01	14:15	3.5202E+07		-42.91	0.23		-42.87	0.23		-0.16	0.21		Ki02C
d30Si_030915_BR3_Paine@21	2.25	3.2689E-02	1.2409E-02	7.9822E+07	1.0844E-01	2.6092E+06	1.0585E-01	14:25	3.5529E+07	3.5461E+07	-42.69	0.25	-42.86	-42.64	0.25	-42.81	0.08	0.21	-0.09	Standard
d30Si_030915_BR3_Paine@22	2.25	3.2680E-02	1.1089E-02	7.9602E+07	1.0520E-01	2.6029E+06	9.9791E-02	14:29	3.5394E+07	1.1169E+05	-42.94	0.22	0.25	-42.88	0.22	0.21	-0.17	0.20	0.22	Standard
d30Si_030915_BR3_Paine@23	2.25	3.2679E-02	1.2876E-02	7.9646E+07	1.1004E-01	2.6030E+06	1.1131E-01	14:32	3.5448E+07		-42.97	0.26		-42.91	0.26		-0.20	0.21		Standard
d30Si_030915_BR3_Paine@24	2.25	3.2683E-02	1.3000E-02	7.9762E+07	1.0126E-01	2.6068E+06	9.8114E-02	14:35	3.5472E+07		-42.86	0.26		-42.80	0.26		-0.08	0.21		Standard
d30Si_030915_BR3_Paine@25	2.25	3.2691E-02	9.2987E-03	7.9703E+07	1.3082E-01	2.6055E+06	1.2737E-01	15:11	3.5441E+07	3.5550E+07	-42.64	0.19	-42.91	-42.56	0.19	-42.83	0.17	0.19	-0.09	Standard
d30Si_030915_BR3_Paine@26	2.25	3.2678E-02	9.6762E-03	7.9991E+07	1.1212E-01	2.6141E+06	1.1492E-01	15:15	3.5546E+07	1.6123E+05	-43.02	0.19	0.36	-42.94	0.19	0.31	-0.23	0.19	0.36	Standard
d30Si_030915_BR3_Paine@27	2.25	3.2679E-02	1.0628E-02	8.0073E+07	9.0828E-02	2.6179E+06	8.1637E-02	15:18	3.5582E+07		-42.98	0.21		-42.90	0.21			0.20		Standard
d30Si_030915_BR3_Paine@28	2.25	3.2678E-02	1.2869E-02	8.0209E+07	8.7631E-02	2.6212E+06	8.9838E-02	15:21	3.5632E+07		-43.00	0.26		-42.92	0.26		-0.21	0.21		Standard

Table A2 Continued.

	SIMS ANALYSES						Mount: BR4		Standard: UNIL-Q1 (Paine)		Analyse: δ^{30}Si			Value= -0.13±0.02 (NBS-28, 2σ)						Date: 03.09.2015	
	Beam	H'2/L'2 (30Si/28Si)		L'2 (30Si/Coeff)		H'2 (28Si/Coeff)		Time	Yield	mean	Measurements		mean	Drift correction		Calibration				Comment	
	nA	CPS	2SD	CPS	2SD	CPS	2SD		CPS/nA	2SD	$\delta^{30}Si$	2SD int	2SD	$\delta^{30}Si$	2SD		$\delta^{30}Si_{NBS-28}$	2SD			
d30Si_020915_Paine@1	2.82	3.2523E-02	9.9294E-03	7.4151E+07	2.1783E-01	2.4112E+06	2.1018E-01	10:02	2.6325E+07	3.0863E+07	-47.54	0.20	-46.82							Setting: Standard	
d30Si_020915_Paine@2	2.82	3.2528E-02	1.0860E-02	7.3971E+07	2.3800E-01	2.4060E+06	2.3489E-01	10:05	2.6188E+07	8.7974E+06	-47.40	0.22	0.84							Setting: Standard	
d30Si_020915_Paine@3	2.82	3.2544E-02	1.7757E-02	7.4083E+07	1.8241E-01	2.4107E+06	1.7446E-01	10:09	2.6229E+07		-46.94	0.36								Setting: Standard	
d30Si_020915_Paine@4	2.83	3.2535E-02	1.3506E-02	7.4297E+07	2.2129E-01	2.4177E+06	2.1739E-01	10:12	2.6295E+07		-47.20	0.27								Setting: Standard	
d30Si_020915_Paine@5	2.83	3.2546E-02	1.2153E-02	7.4337E+07	2.2347E-01	2.4195E+06	2.1606E-01	10:15	2.6308E+07		-46.88	0.24								Setting: Standard	
d30Si_020915_Paine@6	2.82	3.2552E-02	1.0820E-02	9.8091E+07	1.2170E-01	3.1949E+06	1.1625E-01	10:23	3.4741E+07		-46.71	0.22								Setting: Standard	
d30Si_020915_Paine@7	2.83	3.2551E-02	9.7748E-03	9.7926E+07	9.5872E-02	3.1892E+06	8.5702E-02	10:26	3.4611E+07		-46.73	0.20								Setting: Standard	
d30Si_020915_Paine@8	2.83	3.2561E-02	1.2064E-02	9.8059E+07	9.5963E-02	3.1943E+06	8.4903E-02	10:29	3.4689E+07		-46.45	0.24								Setting: Standard	
d30Si_020915_Paine@9	2.83	3.2558E-02	8.7009E-03	9.8186E+07	9.7307E-02	3.1983E+06	8.7008E-02	10:32	3.4729E+07		-46.51	0.17								Setting: Standard	
d30Si_020915_Paine@10	2.83	3.2568E-02	9.8810E-03	9.8148E+07	8.3126E-02	3.1948E+06	8.6428E-02	10:36	3.4674E+07		-46.22	0.20								Setting: Standard	
d30Si_020915_Paine@11	2.83	3.2560E-02	8.2523E-03	9.8191E+07	9.1561E-02	3.1971E+06	8.8840E-02	10:39	3.4705E+07		-46.47	0.17								Setting: Standard	
d30Si_020915_Paine@12	2.82	3.2582E-02	9.3217E-03	9.7986E+07	8.6879E-02	3.1940E+06	7.8282E-02	11:13	3.4772E+07	3.4669E+07	-45.81	0.19	-45.85	-45.63	0.19	-45.68	-0.15	0.22	-0.20	Standard	
d30Si_020915_Paine@13	2.83	3.2581E-02	1.0729E-02	9.4161E+07	1.1472E-01	3.0658E+06	1.0770E-01	11:16	3.3318E+07	1.9675E+06	-45.85	0.21	0.14	-45.67	0.21	0.13	-0.19	0.23	0.14	Standard	
d30Si_020915_Paine@14	2.83	3.2583E-02	1.1800E-02	9.8710E+07	1.1136E-01	3.2164E+06	1.1121E-01	11:19	3.4912E+07		-45.80	0.24		-45.63	0.24		-0.15	0.23		Standard	
d30Si_020915_Paine@15	2.83	3.2577E-02	1.2392E-02	1.0100E+08	3.3931E-02	3.2902E+06	3.0999E-02	11:22	3.5673E+07		-45.95	0.25		-45.79	0.25		-0.32	0.23		Standard	
d30Si_020915_Ki40C_rad@1	2.83	3.2584E-02	8.7786E-03	9.4593E+07	1.2279E-01	3.0822E+06	1.2206E-01	11:26	3.3434E+07	3.2967E+07	-45.74	0.18	-44.86	-45.59	0.18		-0.11	0.22		Ki40	
d30Si_020915_Ki40C_rad@2	2.83	3.2617E-02	1.0446E-02	9.4750E+07	7.9341E-02	3.0916E+06	6.9655E-02	11:29	3.3468E+07	9.9949E+05	-44.79	0.21	1.02	-44.65	0.21		0.88	0.23		Ki40	
d30Si_020915_Ki40C_rad@3	2.83	3.2628E-02	9.7511E-03	9.3534E+07	1.4252E-01	3.0516E+06	1.3927E-01	11:32	3.3012E+07		-44.47	0.20		-44.33	0.20		1.21	0.22		Ki40	
d30Si_020915_Ki40C_rad@4	2.83	3.2624E-02	8.3011E-03	9.1656E+07	6.7558E-02	2.9904E+06	6.2500E-02	11:35	3.2376E+07		-44.58	0.17		-44.45	0.17		1.09	0.22		Ki40	
d30Si_020915_Ki40C_rad@5	2.83	3.2621E-02	9.2252E-03	9.2147E+07	1.2059E-01	3.0057E+06	1.2020E-01	11:39	3.2544E+07		-44.69	0.18		-44.56	0.18		0.97	0.22		Ki40	
d30Si_020915_Ki40C_mat@1	2.83	3.2614E-02	1.2897E-02	9.0044E+07	1.3905E-01	2.9367E+06	1.3680E-01	11:42	3.1794E+07	2.9199E+07	-44.87	0.26	-44.35	-44.75	0.26		0.77	0.24		Ki40 matrix	
d30Si_020915_Ki40C_mat@2	2.83	3.2636E-02	1.0807E-02	7.8346E+07	7.9853E-02	2.5568E+06	8.0175E-02	11:45	2.7665E+07	3.9851E+06	-44.22	0.22	0.89	-44.11	0.22		1.44	0.23		Ki40 matrix	Yield
d30Si_020915_Ki40C_mat@3	2.83	3.2627E-02	1.5059E-02	8.4163E+07	2.1239E-01	2.7463E+06	2.1605E-01	11:48	2.9732E+07		-44.49	0.30		-44.38	0.30		1.16	0.25		Ki40 matrix	
d30Si_020915_Ki40C_mat@4	2.83	3.2651E-02	1.2098E-02	7.8254E+07	8.0917E-02	2.5548E+06	8.3633E-02	11:52	2.7605E+07		-43.81	0.24		-43.72	0.24		1.85	0.23		Ki40 matrix	Yield
d30Si_020915_Paine@16	2.83	3.2588E-02	1.0207E-02	1.0062E+08	9.4110E-02	3.2789E+06	9.6070E-02	12:08	3.5502E+07	3.5259E+07	-45.63	0.20	-45.69	-45.57	0.20	-45.72	-0.09	0.22	-0.24	Standard	
d30Si_020915_Paine@17	2.84	3.2580E-02	9.9793E-03	1.0088E+08	1.5463E-01	3.2869E+06	1.5225E-01	12:11	3.5575E+07	8.2022E+05	-45.87	0.20	0.37	-45.82	0.20	0.21	-0.34	0.22	0.22	Standard	
d30Si_020915_Paine@18	2.84	3.2582E-02	8.9222E-03	1.0008E+08	6.8048E-02	3.2607E+06	6.5209E-02	12:14	3.5287E+07		-45.82	0.18		-45.77	0.18		-0.30	0.22		Standard	
d30Si_020915_Paine@20	2.84	3.2597E-02	1.2129E-02	9.9828E+07	1.4368E-01	3.2562E+06	1.3573E-01	12:57	3.5204E+07	3.4480E+07	-45.37	0.24	-45.29	-45.43	0.24	-45.35	0.06	0.23	0.14	Standard	
d30Si_020915_Paine@21	2.84	3.2600E-02	1.3150E-02	9.5795E+07	1.7153E-01	3.1230E+06	1.6685E-01	13:00	3.3759E+07	1.2667E+06	-45.28	0.26	0.18	-45.34	0.26	0.15	0.16	0.24	0.16	Standard	
d30Si_020915_Paine@22	2.84	3.2604E-02	1.0883E-02	9.7063E+07	1.0209E-01	3.1647E+06	1.0152E-01	13:03	3.4197E+07		-45.17	0.22		-45.23	0.22		0.27	0.23		Standard	
d30Si_020915_Paine@23	2.84	3.2598E-02	1.1110E-02	9.8760E+07	1.0897E-01	3.2210E+06	1.0148E-01	13:07	3.4760E+07		-45.33	0.22		-45.41	0.22		0.08	0.23		Standard	
d30Si_020915_Ki39C_rad@1	2.84	3.2652E-02	1.3611E-02	9.3237E+07	1.7241E-01	3.0444E+06	1.7475E-01	13:29	3.2797E+07	3.2782E+07	-43.76	0.27	-44.00	-43.89	0.27		1.68	0.24		Ki39	
d30Si_020915_Ki39C_rad@2	2.84	3.2641E-02	1.0819E-02	9.2177E+07	1.2077E-01	3.0086E+06	1.1730E-01	13:33	3.2415E+07	1.2128E+06	-44.10	0.22	0.49	-44.23	0.22		1.31	0.23		Ki39	
d30Si_020915_Ki39C_rad@3	2.84	3.2651E-02	7.4558E-03	9.1870E+07	9.1450E-02	2.9996E+06	9.2586E-02	13:36	3.2327E+07		-43.80	0.15		-43.94	0.15		1.62	0.21		Ki39	
d30Si_020915_Ki39C_rad@4	2.84	3.2632E-02	8.6803E-03	9.6095E+07	1.1948E-01	3.1375E+06	1.0888E-01	13:39	3.3820E+07		-44.36	0.17		-44.51	0.17		1.03	0.22		Ki39	
d30Si_020915_Ki39C_rad@5	2.84	3.2644E-02	1.1935E-02	9.2526E+07	1.5894E-01	3.0205E+06	1.5687E-01	13:42	3.2553E+07		-43.99	0.24		-44.14	0.24		1.41	0.23		Ki39	
d30Si_020915_Paine@24	2.84	3.2598E-02	1.0019E-02	9.9604E+07	1.0829E-01	3.2469E+06	1.0848E-01	13:46	3.5060E+07	3.4594E+07	-45.36	0.20	-45.56	-45.52	0.20	-45.73	-0.04	0.22	-0.26	Standard	
d30Si_020915_Paine@25	2.84	3.2588E-02	1.0454E-02	9.9646E+07	1.7489E-01	3.2474E+06	1.7248E-01	13:49	3.5030E+07	1.1051E+06	-45.65	0.21	0.29	-45.82	0.21	0.26	-0.35	0.22	0.27	Standard	
d30Si_020915_Paine@26	2.85	3.2587E-02	8.8288E-03	9.6531E+07	1.6169E-01	3.1456E+06	1.5969E-01	13:52	3.3917E+07		-45.68	0.18		-45.85	0.18		-0.38	0.22		Standard	
d30Si_020915_Paine@27	2.85	3.2591E-02	1.1541E-02	9.7847E+07	9.1926E-02	3.1903E+06	8.7533E-02	13:55	3.4368E+07		-45.55	0.23		-45.73	0.23		-0.26	0.23		Standard	

Table A2 Continued.

SIMS ANALYSES								Mount: BR4v2	Standard: UNIL-Q1 (Paine)		Analyse: δ^{30}Si			Value= -0.13±0.02 (NBS-28, 2σ)						Date: 03.09.2015
	Beam	H'2/L'2 (30Si/28Si)		L'2 (30Si/Coeff)		H'2 (28Si/Coeff)		Time	Yield	mean	Measurements		mean	Drift correction			Calibration			Comment
	nA	CPS	2SD	CPS	2SD	CPS	2SD		CPS/nA	2SD	$\delta^{30}Si$	2SD int	2SD	$\delta^{30}Si$	2SD		$\delta^{30}Si_{NBS-28}$	2SD		
d30Si_040915_BR4_Paine@1	2.33	3.2677E-02	1.1111E-02	8.4303E+07	1.4469E-01	2.7567E+06	1.3319E-01	0	3.6219E+07	3.5641E+07	-43.04	0.22	-43.01							Setting: Standard
d30Si_040915_BR4_Paine@2	2.34	3.2691E-02	7.3868E-03	8.1704E+07	1.1866E-01	2.6711E+06	1.1937E-01	1	3.4961E+07	2.6970E+06	-42.63	0.15	0.78							Setting: Standard
d30Si_040915_BR4_Paine@3	2.34	3.2677E-02	9.2090E-03	8.2091E+07	1.5683E-01	2.6826E+06	1.5533E-01	2	3.5121E+07		-43.04	0.18								Setting: Standard
d30Si_040915_BR4_Paine@4	2.34	3.2693E-02	1.1562E-02	8.1632E+07	1.1860E-01	2.6690E+06	1.1802E-01	3	3.4904E+07		-42.56	0.23								Setting: Standard
d30Si_040915_BR4_Paine@5	2.34	3.2676E-02	1.4900E-02	7.4776E+07	1.6760E-01	2.4436E+06	1.6393E-01	4	3.1937E+07		-43.07	0.30								Setting: Standard
d30Si_040915_BR4_Paine@6	2.34	3.2659E-02	1.2601E-02	8.7057E+07	1.1632E-01	2.8433E+06	1.1725E-01	5	3.7203E+07		-43.56	0.25								Setting: Standard
d30Si_040915_BR4_Paine@7	2.34	3.2679E-02	7.0994E-03	8.3225E+07	1.5934E-01	2.7219E+06	1.4642E-01	6	3.5509E+07		-42.99	0.14								Setting: Standard
d30Si_040915_BR4_Paine@8	2.34	3.2680E-02	7.7632E-03	8.0416E+07	2.1591E-01	2.6282E+06	2.1209E-01	7	3.4298E+07		-42.95	0.16								Setting: Standard
d30Si_040915_BR4_Paine@9	2.34	3.2679E-02	1.2674E-02	8.3395E+07	1.2314E-01	2.7236E+06	1.3337E-01	8	3.5578E+07		-42.97	0.25								Setting: Standard
d30Si_040915_BR4_Paine@10	2.34	3.2644E-02	1.3700E-02	8.6099E+07	1.9825E-01	2.8106E+06	1.9444E-01	9	3.6740E+07		-43.99	0.27								Setting: Standard
d30Si_040915_BR4_Paine@11	2.35	3.2679E-02	7.9642E-03	8.5974E+07	1.6549E-01	2.8095E+06	1.6395E-01	10	3.6659E+07		-42.96	0.16								Setting: Standard
d30Si_040915_BR4_Paine@12	2.34	3.2657E-02	1.4912E-02	8.8997E+07	1.9070E-01	2.9089E+06	1.7753E-01	11	3.8079E+07		-43.62	0.30								Setting: Standard
d30Si_040915_BR4_Paine@13	2.35	3.2684E-02	9.0542E-03	8.2865E+07	1.2373E-01	2.7085E+06	1.2587E-01	12	3.5333E+07		-42.83	0.18								Setting: Standard
d30Si_040915_BR4_Paine@14	2.35	3.2686E-02	8.3286E-03	8.4266E+07	9.1881E-02	2.7544E+06	9.0038E-02	13	3.5931E+07		-42.78	0.17								Setting: Standard
d30Si_040915_BR4_Paine@15	2.35	3.2694E-02	9.2168E-03	8.3456E+07	1.3326E-01	2.7285E+06	1.3149E-01	14	3.5589E+07		-42.53	0.18								Setting: Standard
d30Si_040915_BR4_Paine@16	2.35	3.2677E-02	1.5127E-02	8.5898E+07	1.3879E-01	2.8047E+06	1.5102E-01	15	3.6618E+07		-43.03	0.30								Setting: Standard
d30Si_040915_BR4_Paine@17	2.35	3.2689E-02	9.5313E-03	8.2581E+07	1.1661E-01	2.6993E+06	1.1507E-01	16	3.5216E+07		-42.69	0.19								Setting: Standard
d30Si_040915_BR4_Paine@18	2.34	3.2679E-02	9.5366E-03	8.5453E+07	1.4558E-01	2.7923E+06	1.4702E-01	17	3.6583E+07	3.6642E+07	-42.98	0.19	-43.12	-42.93	0.19	-43.07	0.07	0.40	-0.08	Standard
d30Si_040915_BR4_Paine@19	2.35	3.2661E-02	1.0937E-02	8.6477E+07	1.5850E-01	2.8244E+06	1.5749E-01	18	3.6868E+07	1.3429E+06	-43.52	0.22	0.82	-43.47	0.22	0.71	-0.49	0.40	0.74	Standard
d30Si_040915_BR4_Paine@20	2.35	3.2665E-02	8.3444E-03	8.7634E+07	1.7846E-01	2.8648E+06	1.6951E-01	19	3.7359E+07		-43.38	0.17		-43.33	0.17		-0.35	0.40		Standard
d30Si_040915_BR4_Paine@21	2.35	3.2692E-02	1.0079E-02	8.3962E+07	8.1061E-02	2.7449E+06	7.9766E-02	20	3.5757E+07		-42.61	0.20		-42.56	0.20		0.45	0.40		Standard
d30Si_040915_BR4_Paine@22	2.35	3.2678E-02	9.5927E-03	8.4321E+07	1.5606E-01	2.7554E+06	1.5549E-01	31	3.5888E+07	3.6211E+07	-43.02	0.19	-43.08	-43.00	0.19	-43.08	-0.01	0.40	-0.09	Standard
d30Si_040915_BR4_Paine@23	2.35	3.2684E-02	8.4275E-03	8.4676E+07	1.1396E-01	2.7693E+06	1.0541E-01	32	3.6004E+07	1.8631E+06	-42.84	0.17	0.80	-42.83	0.17	0.76	0.17	0.40	0.79	Standard
d30Si_040915_BR4_Paine@24	2.35	3.2687E-02	1.0581E-02	8.5300E+07	1.6291E-01	2.7880E+06	1.6437E-01	33	3.6262E+07		-42.74	0.21	0.80	-42.73	0.21		0.28	0.40		Standard
d30Si_040915_BR4_Paine@25	2.35	3.2659E-02	1.1782E-02	8.9236E+07	1.2595E-01	2.9145E+06	1.2747E-01	34	3.7931E+07		-43.56	0.24		-43.55	0.24		-0.58	0.41		Standard
d30Si_040915_BR4_Paine@26	2.35	3.2651E-02	7.1539E-03	8.8410E+07	1.8994E-01	2.8868E+06	1.9097E-01	35	3.7664E+07		-43.81	0.14		-43.81	0.14		-0.85	0.39		Standard
d30Si_040915_BR4_Paine@27	2.35	3.2683E-02	1.7097E-02	8.3575E+07	1.3612E-01	2.7317E+06	1.3510E-01	36	3.5514E+07		-42.86	0.34		-42.86	0.34		0.15	0.42		Standard
d30Si_040915_BR4_Paine@28	2.35	3.2659E-02	1.1533E-02	8.6054E+07	1.5429E-01	2.8105E+06	1.5585E-01	37	3.6589E+07		-43.55	0.23		-43.56	0.23		-0.59	0.40		Standard
d30Si_040915_BR4_Paine@29	2.35	3.2686E-02	1.3047E-02	8.3492E+07	1.0558E-01	2.7291E+06	1.0150E-01	38	3.5498E+07		-42.76	0.26		-42.77	0.26		0.24	0.41		Standard
d30Si_040915_BR4_Paine@30	2.35	3.2682E-02	1.1241E-02	8.2751E+07	1.2243E-01	2.7060E+06	1.1355E-01	39	3.5183E+07		-42.89	0.22		-42.90	0.22		0.10	0.40		Standard
d30Si_040915_BR4_Paine@31	2.35	3.2686E-02	1.0208E-02	8.3726E+07	1.3262E-01	2.7367E+06	1.3139E-01	40	3.5581E+07		-42.78	0.20		-42.79	0.20		0.22	0.40		Standard
d30Si_040915_Ki41_rad@1	2.36	3.2720E-02	1.0150E-02	7.7345E+07	1.3637E-01	2.5306E+06	1.3666E-01	49	3.2841E+07	3.3730E+07	-41.76	0.20	-42.01	-41.80	0.20		1.25	0.40		Ki41
d30Si_040915_Ki41_rad@2	2.35	3.2729E-02	1.8727E-02	7.7343E+07	6.1451E-02	2.5317E+06	6.4292E-02	50	3.2853E+07	3.0611E+06	-41.51	0.37	1.32		1.64			1.72		Ki41 intenal error
d30Si_040915_BR4_Paine@32	2.35	3.2681E-02	9.9304E-03	8.2620E+07	1.4261E-01	2.7002E+06	1.4438E-01	51	3.5093E+07	3.5617E+07	-42.90	0.20	-43.04	-42.95	0.20	-43.09	0.05	0.40	-0.10	Standard
d30Si_040915_BR4_Paine@33	2.36	3.2673E-02	1.0927E-02	8.4653E+07	1.0648E-01	2.7661E+06	1.0690E-01	52	3.5935E+07	7.4899E+05	-43.16	0.22	0.22	-43.20	0.22	0.19	-0.21	0.40	0.20	Standard
d30Si_040915_BR4_Paine@34	2.36	3.2678E-02	1.1001E-02	8.3915E+07	1.2060E-01	2.7420E+06	1.2043E-01	53	3.5610E+07		-43.01	0.22		-43.06	0.22		-0.07	0.40		Standard
d30Si_040915_BR4_Paine@35	2.36	3.2675E-02	1.1106E-02	8.4421E+07	9.5202E-02	2.7584E+06	9.2224E-02	54	3.5830E+07		-43.10	0.22		-43.15	0.22		-0.16	0.40		Standard

Table A2 Continued.

SIMS ANALYSES						Mount: BR6			Standard: UNIL-Q1 (Paine)		Analyse: δ^{30}Si			Value= -0.13±0.02 (NBS-28, 2σ)						Date: 03.09.2015	
	Beam	H'2/L'2 (30Si/28Si)		L'2 (30Si/Coeff)		H'2 (28Si/Coeff)		Time	Yield	mean	Measurements		mean	Drift correction			Calibration			Comment	
	nA	CPS	2SD	CPS	2SD	CPS	2SD		CPS/nA	2SD	$\delta^{30}Si$	2SD int	2SD	$\delta^{30}Si$	2SD		$\delta^{30}Si_{NBS28}$	2SD			
d30Si_020915_BR6_Paine@1	2.85	3.2600E-02	1.0308E-02	9.8177E+07	8.3010E-02	3.2019E+06	7.4661E-02	15:10	3.4493E+07	3.4162E+07	-45.29	0.21	-45.10							Setting: Standard	
d30Si_020915_BR6_Paine@2	2.85	3.2608E-02	8.4777E-03	9.8585E+07	1.3462E-01	3.2148E+06	1.3181E-01	15:13	3.4531E+07	1.5657E+06	-45.05	0.17	0.24							Setting: Standard	
d30Si_020915_BR6_Paine@3	2.86	3.2611E-02	1.1375E-02	9.6759E+07	9.7800E-02	3.1569E+06	9.1071E-02	15:17	3.3884E+07		-44.97	0.23								Setting: Standard	
d30Si_020915_BR6_Paine@4	2.86	3.2603E-02	9.7271E-03	9.8461E+07	7.8345E-02	3.2103E+06	7.9922E-02	15:20	3.4484E+07		-45.21	0.19								Setting: Standard	
d30Si_020915_BR6_Paine@5	2.86	3.2609E-02	1.1222E-02	9.9675E+07	1.9120E-01	3.2501E+06	1.9022E-01	15:23	3.4875E+07		-45.04	0.22								Setting: Standard	
d30Si_020915_BR6_Paine@6	2.86	3.2608E-02	7.9083E-03	9.3462E+07	3.1953E-01	3.0474E+06	3.1779E-01	15:26	3.2703E+07		-45.06	0.16								Setting: Standard	
d30Si_020915_BR6_Paine@9	2.85	3.2598E-02	9.7991E-03	9.3629E+07	1.8584E-01	3.0549E+06	1.6920E-01	15:48	3.2819E+07	3.3782E+07	-45.36	0.20	-45.25	-45.34	0.20	-45.23	-0.10	0.34	0.01	Standard	
d30Si_020915_BR6_Paine@9	duplicate							15:48		1.9693E+06			0.25			0.21			0.22	Standard	duplicate
d30Si_020915_BR6_Paine@10	2.86	3.2606E-02	1.0866E-02	9.6410E+07	1.3948E-01	3.1457E+06	1.2793E-01	15:51	3.3690E+07		-45.11	0.22		-45.09	0.22		0.15	0.34		Standard	
d30Si_020915_BR6_Paine@11	2.86	3.2600E-02	1.1102E-02	1.0067E+08	1.5093E-01	3.2838E+06	1.3535E-01	15:54	3.5151E+07		-45.29	0.22		-45.27	0.22		-0.03	0.34		Standard	
d30Si_020915_BR6_Paine@12	2.86	3.2600E-02	1.3121E-02	9.5810E+07	1.2286E-01	3.1253E+06	1.1224E-01	15:58	3.3468E+07		-45.29	0.26		-45.27	0.26		-0.04	0.35		Standard	
d30Si_020915_BR6_Paine@13	2.87	3.2592E-02	9.9742E-03	9.9673E+07	2.0366E-01	3.2516E+06	1.9003E-01	16:21	3.4778E+07	3.4004E+07	-45.52	0.20	-45.34	-45.50	0.20	-45.33	-0.28	0.34	-0.10	Standard	
d30Si_020915_BR6_Paine@14	2.87	3.2602E-02	9.6423E-03	9.7008E+07	1.2312E-01	3.1624E+06	1.2123E-01	16:24	3.3824E+07	1.0669E+06	-45.24	0.19	0.33	-45.22	0.19	0.29	0.02	0.34	0.30	Standard	
d30Si_020915_BR6_Paine@15	2.87	3.2595E-02	1.0272E-02	9.7065E+07	1.3454E-01	3.1640E+06	1.3189E-01	16:27	3.3856E+07		-45.45	0.21		-45.43	0.21		-0.20	0.34		Standard	
d30Si_020915_BR6_Paine@16	2.87	3.2604E-02	6.4968E-03	9.6249E+07	1.1832E-01	3.1381E+06	1.1709E-01	16:30	3.3557E+07		-45.17	0.13		-45.16	0.13		0.09	0.33		Standard	
d30Si_020915_Ki48_rad@1	2.87	3.2654E-02	1.0835E-02	9.1341E+07	7.4821E-02	2.9829E+06	7.3635E-02	16:34	3.1866E+07	2.4983E+07	-43.71	0.22	-44.19	-43.69	0.22		1.62	0.34		Ki48	
d30Si_020915_Ki48_rad@2	2.87	3.2624E-02	7.7468E-03	9.1638E+07	1.8806E-01	2.9898E+06	1.8353E-01	16:37	3.1974E+07	2.8041E+07	-44.58	0.15	0.73	-44.57	0.15		0.70	0.33		Ki48	
d30Si_020915_Ki48_rad@3	2.87	3.2639E-02	1.6026E-02	9.1689E+07	1.4856E-01	2.9926E+06	1.4161E-01	16:40	3.1989E+07		-44.15	0.32		-44.13	0.32		1.15	0.36		Ki48	
d30Si_020915_Ki48_rad@4	2.87	3.2634E-02	7.9662E-03	8.3345E+07	5.4489E-02	2.7198E+06	5.3755E-02	16:43	2.9085E+07		-44.31	0.16		-44.29	0.16		0.99	0.33		Ki48	
d30Si_020915_Ki48_rad@5	2.87	-2.9223E-01		4.9264E+02		-7.6538E+03	4.1698E-02	16:47	1.7166E+02		-9558.22									Ki48	Yield
d30Si_020915_BR6_Paine@17	2.87	3.2597E-02	9.3871E-03	9.8864E+07	1.9022E-01	3.2258E+06	1.7664E-01	16:50	3.4495E+07	3.4504E+07	-45.38	0.19	-45.38	-45.37	0.19	-45.37	-0.14	0.34	-0.13	Standard	
d30Si_020915_BR6_Paine@18	2.87	3.2579E-02	1.1024E-02	1.0322E+08	2.2235E-01	3.3632E+06	2.1936E-01	16:53	3.5976E+07	2.1273E+06	-45.91	0.22	0.77	-45.90	0.22	0.66	-0.69	0.34	0.70	Standard	
d30Si_020915_BR6_Paine@19	2.87	3.2609E-02	1.1687E-02	9.6092E+07	9.7992E-02	3.1335E+06	9.3768E-02	16:57	3.3491E+07		-45.02	0.23		-45.01	0.23		0.24	0.34		Standard	
d30Si_020915_BR6_Paine@20	2.87	3.2603E-02	9.7614E-03	9.7703E+07	9.6057E-02	3.1853E+06	9.2870E-02	17:00	3.4055E+07		-45.20	0.20		-45.19	0.20		0.05	0.34		Standard	
d30Si_020915_BR6_Paine@21	2.87	3.2609E-02	1.4716E-02	9.6472E+07	1.1339E-01	3.1459E+06	1.0780E-01	17:26	3.3601E+07	3.3866E+07	-45.04	0.29	-45.41	-45.03	0.29	-45.40	0.21	0.36	-0.17	Standard	
d30Si_020915_BR6_Paine@22	2.87	3.2587E-02	1.1020E-02	1.0016E+08	1.6617E-01	3.2639E+06	1.6556E-01	17:29	3.4868E+07	1.3777E+06	-45.66	0.22	0.56	-45.65	0.22	0.49	-0.43	0.34	0.51	Standard	
d30Si_020915_BR6_Paine@23	2.87	3.2589E-02	9.7018E-03	9.5567E+07	1.1007E-01	3.1163E+06	9.9105E-02	17:33	3.3299E+07		-45.60	0.19		-45.59	0.19		-0.37	0.34		Standard	
d30Si_020915_BR6_Paine@24	2.87	3.2598E-02	1.4101E-02	9.6797E+07	1.1054E-01	3.1554E+06	1.0929E-01	17:36	3.3697E+07		-45.34	0.28		-45.34	0.28		-0.11	0.35		Standard	
d30Si_020915_Ki43_rad@1	2.87	3.2631E-02	1.1986E-02	9.1151E+07	1.9092E-01	2.9743E+06	1.8759E-01	17:39	3.1737E+07	3.1679E+07	-44.40	0.24	-44.02	-44.39	0.24		0.89	0.35		Ki43	
d30Si_020915_Ki43_rad@2	2.87	3.2637E-02	8.4439E-03	9.5318E+07	1.2148E-01	3.1111E+06	1.1630E-01	17:42	3.3169E+07	2.0334E+06	-44.19	0.17	0.49	-44.19	0.17		1.10	0.34		Ki43	
d30Si_020915_Ki43_rad@3	2.87	3.2642E-02	1.2908E-02	9.0341E+07	1.5164E-01	2.9489E+06	1.4815E-01	17:46	3.1432E+07		-44.06	0.26		-44.06	0.26		1.24	0.35		Ki43	
d30Si_020915_Ki43_rad@4	2.87	3.2653E-02	1.1564E-02	8.6235E+07	1.8871E-01	2.8158E+06	1.8712E-01	17:49	3.0004E+07		-43.73	0.23		-43.73	0.23		1.58	0.34		Ki43	
d30Si_020915_Ki43_rad@5	2.88	3.2647E-02	1.3404E-02	9.1568E+07	4.9230E-02	2.9897E+06	4.5444E-02	17:54	3.1802E+07		-43.91	0.27		-43.91	0.27		1.39	0.35		Ki43	
d30Si_020915_Ki43_rad@6	2.88	3.2650E-02	1.0058E-02	9.1817E+07	1.2289E-01	2.9997E+06	1.2973E-01	17:57	3.1930E+07		-43.84	0.20		-43.83	0.20		1.47	0.34		Ki43	
d30Si_020915_BR6_Paine@25	2.87	3.2616E-02	1.1356E-02	9.0220E+07	1.6610E-01	2.9426E+06	1.6369E-01	18:00	3.1410E+07	3.2103E+07	-44.83	0.23	-45.41	-44.83	0.23	-45.41	0.43	0.34	-0.18	Standard	
d30Si_020915_BR6_Paine@26	2.88	3.2564E-02	1.1604E-02	8.8765E+07	3.3713E-01	2.8908E+06	3.3163E-01	18:04	3.0869E+07	2.3901E+06	-46.33	0.23	1.35	-46.33	0.23	1.17	-1.15	0.34	1.22	Standard	
d30Si_020915_BR6_Paine@27	2.87	3.2610E-02	1.1234E-02	9.6270E+07	1.1286E-01	3.1395E+06	1.0608E-01	18:07	3.3527E+07		-45.00	0.22		-44.99	0.22		0.25	0.34		Standard	
d30Si_020915_BR6_Paine@28	2.87	3.2594E-02	1.6649E-02	9.3602E+07	3.2507E-01	3.0508E+06	3.1861E-01	18:10	3.2607E+07		-45.48	0.33		-45.48	0.33		-0.25	0.36		Standard	
d30Si_020915_Ki20C_rad@1	2.87	3.2702E-02	1.5311E-02	7.2862E+07	1.1359E-01	2.3846E+06	1.3011E-01	18:14	2.5376E+07		-42.31	0.31		-42.31	0.31		3.07	0.36		Ki20	
d30Si_020915_Ki20C_rad@2	2.87	3.2674E-02	1.3194E-02	7.5096E+07	9.7037E-02	2.4536E+06	9.7677E-02	18:17	2.6136E+07		-43.14	0.26		-43.14	0.26		2.20	0.35		Ki20	
d30Si_020915_Ki20C_rad@3	2.87	3.2686E-02	1.3627E-02	6.8071E+07	1.0142E-01	2.2250E+06	1.0136E-01	18:20	2.3702E+07		-42.77	0.27		-42.77	0.27		2.59	0.35		Ki20	
d30Si_020915_Ki20C_rad@4	2.88	3.2642E-02	8.6278E-03	8.4333E+07	1.7955E-01	2.7526E+06	1.8100E-01	18:23	2.9319E+07		-44.07	0.17		-44.07	0.17		1.22	0.34		Ki20	
d30Si_020915_Ki20C_rad@5	2.87	3.2655E-02	9.5962E-03	7.9734E+07	1.5535E-01	2.6037E+06	1.5697E-01	18:27	2.7745E+07		-43.69	0.19		-43.69	0.19		1.62	0.34		Ki20	
d30Si_020915_BR6_Paine@29	2.87	3.2601E-02	1.0628E-02	1.0025E+08	1.3549E-01	3.2686E+06	1.3637E-01	18:30	3.4895E+07	3.5215E+07	-45.26	0.21	-45.54	-45.27	0.21	-45.54	-0.03	0.34	-0.32	Standard	
d30Si_020915_BR6_Paine@30	2.88	3.2590E-02	8.2813E-03	9.9192E+07	1.8276E-01	3.2328E+06	1.8266E-01	18:33	3.4498E+07	2.3817E+06	-45.59	0.17	0.80	-45.59	0.17	0.69	-0.37	0.33	0.72	Standard	
d30Si_020915_BR6_Paine@31	2.87	3.2573E-02	9.0740E-03	1.0625E+08	1.6989E-01	3.4634E+06	1.6183E-01	18:36	3.6978E+07		-46.08	0.18		-46.08	0.18		-0.89	0.34		Standard	
d30Si_020915_BR6_Paine@32	2.87	3.2603E-02	1.0416E-02	9.9135E+07	1.2055E-01	3.2339E+06	1.1218E-01	18:40	3.4488E+07		-45.21	0.21		-45.22	0.21		0.02	0.34		Standard	
d30Si_020915_BR6_Paine@33	2.87	3.2604E-02	1.0537E-02	9.9222E+07	1.3592E-01	3.2372E+06	1.2450E-01	19:03	3.4537E+07	3.4917E+07	-45.17	0.21	-45.38	-45.18	0.21	-45.39	0.06	0.34	-0.16	Standard	
d30Si_020915_BR6_Paine@34	2.88	3.2605E-02	1.0568E-02	9.8211E+07	9.2263E-02	3.2024E+06	8.9789E-02	19:06	3.4146E+07	2.1810E+06	-45.15	0.21	0.55	-45.16	0.21	0.47	0.08	0.34	0.50	Standard	
d30Si_020915_BR6_Paine@35	2.87	3.2585E-02	8.6040E-03	1.0499E+08	1.3089E-01	3.4232E+06	1.2243E-01	19:09	3.6533E+07		-45.73	0.17		-45.74	0.17		-0.53	0.34		Standard	
d30Si_020915_BR6_Paine@36	2.87	3.2594E-02	1.0620E-02	9.9013E+07	3.7047E-01	3.2274E+06	3.7127E-01	19:12	3.4451E+07		-45.46	0.21		-45.47	0.21		-0.25	0.34		Standard	
d30Si_020915_BR6_Paine@37	2.88	3.2595E-02	7.1932E-03	9.7245E+07	3.1926E-01	3.1697E+06	3.1870E-01	19:35	3.3816E+07	3.4381E+07	-45.44	0.14	-45.44	-45.45	0.14	-45.46	-0.23	0.33	-0.23	Standard	
d30Si_020915_BR6_Paine@38	2.88	3.2567E-02	1.2160E-02	1.0084E+08	3.1313E-01	3.2843E+06	3.1290E-01	19:38	3.5037E+07	1.0468E+06	-46.26	0.24	1.16	-46.28	0.24	1.00	-1.09	0.35	1.05	Standard	
d30Si_020915_BR6_Paine@39	2.88	3.2610E-02	1.1544E-02	9.8269E+07	5.8766E-02	3.2045E+06	5.2910E-02	19:42	3.4151E+07		-45.01	0.23		-45.02	0.23		0.22	0.34		Standard	
d30Si_020915_BR6_Paine@40	2.87	3.2608E-02	7.0475E-03	9.9229E+07	6.1553E-02	3.2357E+06	6.0752E-02	19:45	3.4522E+07		-45.06	0.14		-45.07	0.14		0.17	0.33		Standard	
d30Si_020915_BR6_Paine@41	2.88	3.2603E-02	8.5709E-03	9.9529E+07	8.6408E-02	3.2449E+06	8.6704E-02	20:08	3.4612E+07	3.4870E+07	-45.22	0.17	-45.27	-45.23	0.17	-45.28	0.01	0.34	-0.05	Standard	
d30Si_020915_BR6_Paine@42	2.88	3.2598E-02	1.4648E-02	9.7471E+07	1.5305E-01	3.1774E+06	1.5411E-01	20:11	3.3868E+07	1.5840E+06	-45.34	0.29	0.24	-45.35	0.29	0.21	-0.12	0.36	0.22	Standard	
d30Si_020915_BR6_Paine@43	2.88	3.2596E-02	9.4263E-03	1.0251E+08	1.0588E-01	3.3430E+06	9.7777E-02	20:14	3.5583E+07		-45.40	0.19		-45.41	0.19		-0.19	0.34		Standard	
d30Si_020915_BR6_Paine@44	2.88	3.2606E-02	1.1674E-02	1.0199E+08	7.4907E-02	3.3270E+06	6.6900E-02	20:17	3.5420E+07		-45.12	0.23		-45.14	0.23		0.10	0.34		Standard	
d30Si_020915_BR6_Paine@45	2.88	3.2602E-02	8.0255E-03	1.0007E+08	1.0896E-01	3.2640E+06	1.0119E-01	20:40	3.4734E+07	3.4243E+07	-45.24	0.16	-45.21	-45.26	0.16	-45.23	-0.03	0.33	0.01	Standard	
d30Si_020915_BR6_Paine@46	2.88	3.2598E-02	7.9395E-03	1.0098E+08	8.9550E-02	3.2919E+06	8.5410E-02	20:44	3.5064E+07	1.6072E+06	-45.34	0.16	0.32	-45.36	0.16	0.28	-0.13	0.33	0.29	Standard	
d30Si_020915_BR6_Paine@47	2.88	3.2611E-02	1.1262E-02	9.7611E+07	2.7802E-01	3.1829E+06	2.8087E-01	20:47	3.3876E+07		-44.97	0.23		-45.00	0.23		0.25	0.34		Standard	
d30Si_020915_BR6_Paine@48	2.88	3.2600E-02	8.7302E-03	9.6003E+07	5.6955E-02	3.1295E+06	5.2194E-02	20:50	3.3300E+07		-45.28	0.17		-45.30	0.17		-0.07	0.34		Standard	

Table A2 Continued.

	SIMS ANALYSES									Mount: BR7	Standard: UNIL-Q1 (Paine)	Analyse: $\delta^{30}Si$					Value= -0.13±0.02 (NBS-28, 2σ)				Date: 03.09.2015
	Beam	H'2/L'2 (30Si/28Si)		L'2 (30Si/Coeff)		H'2 (28Si/Coeff)		Time	Yield	mean	Measurements		mean	Drift correction			Calibration			Comment	
	nA	CPS	2SD	CPS	2SD	CPS	2SD		CPS/nA	2SD	$\delta^{30}Si$	2SD int	2SD	$\delta^{30}Si$	2SD		$\delta^{30}Si_{NBS-28}$	2SD			
d30Si_040915_BR7_Paine_test@1	2.35	3.2698E-02	8.2542E-03	7.8392E+07	1.8327E-01	2.5630E+06	1.8224E-01	13:49	3.3338E+07	3.3096E+07	-42.42	0.17	-42.55							Setting: Standard	
d30Si_040915_BR7_Paine_test@2	2.36	3.2695E-02	8.3876E-03	8.0136E+07	1.2329E-01	2.6203E+06	1.2045E-01	13:53	3.3979E+07	2.3352E+06	-42.50	0.17	0.47							Setting: Standard	
d30Si_040915_BR7_Paine_test@3	2.36	3.2697E-02	1.5089E-02	7.8788E+07	1.3377E-01	2.5780E+06	1.2222E-01	13:56	3.3396E+07		-42.45	0.30								Setting: Standard	
d30Si_040915_BR7_Paine_test@4	2.36	3.2695E-02	1.1602E-02	8.0159E+07	1.2819E-01	2.6208E+06	1.2989E-01	13:59	3.3978E+07		-42.51	0.23								Setting: Standard	
d30Si_040915_BR7_Paine_test@5	2.36	3.2699E-02	1.0142E-02	7.8873E+07	1.2755E-01	2.5804E+06	1.1404E-01	14:03	3.3394E+07		-42.38	0.20								Setting: Standard	
d30Si_040915_BR7_Paine_test@6	2.36	3.2686E-02	9.6415E-03	8.0167E+07	1.2827E-01	2.6205E+06	1.2985E-01	14:06	3.3940E+07		-42.78	0.19								Setting: Standard	
d30Si_040915_BR7_Paine_test@7	2.36	3.2702E-02	1.0227E-02	7.2379E+07	3.9660E-01	2.3665E+06	3.9300E-01	14:09	3.0636E+07		-42.30	0.20								Setting: Standard	
d30Si_040915_BR7_Paine_test@8	2.36	3.2678E-02	1.1543E-02	7.5878E+07	2.7898E-01	2.4797E+06	2.7848E-01	14:13	3.2104E+07		-43.01	0.23								Setting: Standard	
d30Si_040915_BR7_Paine@1	2.36	3.2700E-02	1.6150E-02	7.7564E+07	1.7097E-01	2.5364E+06	1.6831E-01	14:17	3.2867E+07	3.3035E+07	-42.35	0.32	-42.37	-42.43	0.32	-42.45	-0.13	0.24	-0.15	Standard	
d30Si_040915_BR7_Paine@02	2.37	3.2700E-02	7.3254E-03	7.9038E+07	1.5356E-01	2.5865E+06	1.4316E-01	14:20	3.3411E+07	5.1591E+05	-42.38	0.15	0.04	-42.46	0.15	0.03	-0.15	0.19	0.03	Standard	
d30Si_040915_BR7_Paine@03	2.36	3.2700E-02	1.3863E-02	7.7696E+07	1.4544E-01	2.5388E+06	1.5577E-01	14:23	3.2865E+07		-42.37	0.28		-42.45	0.28		-0.14	0.22		Standard	
d30Si_040915_BR7_Paine@04	2.36	3.2699E-02	1.1811E-02	7.8019E+07	1.4630E-01	2.5511E+06	1.4873E-01	14:27	3.2997E+07		-42.40	0.24		-42.47	0.24		-0.17	0.21		Standard	
d30Si_040915_Ki57_rad@1	2.36	3.2726E-02	9.7275E-03	7.7400E+07	1.3478E-01	2.5330E+06	1.3156E-01	14:30	3.2735E+07	3.1285E+07	-41.61	0.19	-41.14	-41.68	0.19		0.65	0.20		Ki57	
d30Si_040915_Ki57_rad@2	2.36	3.2752E-02	1.3111E-02	6.9962E+07	1.7990E-01	2.2916E+06	1.7616E-01	14:33	2.9602E+07	2.1509E+06	-40.83	0.26	1.28	-40.91	0.26		1.46	0.22		Ki57	
d30Si_040915_Ki57_rad@3	2.36	3.2744E-02	1.2240E-02	7.4255E+07	1.3508E-01	2.4315E+06	1.3284E-01	14:37	3.1399E+07		-41.06	0.24		-41.13	0.24		1.23	0.21		Ki57	
d30Si_040915_Ki57_rad@4	2.37	3.2726E-02	1.2459E-02	7.5864E+07	1.5457E-01	2.4845E+06	1.4234E-01	14:40	3.2057E+07		-41.60	0.25		-41.68	0.25		0.66	0.21		Ki57	
d30Si_040915_Ki57_rad@5	2.37	3.2755E-02	1.0355E-02	7.3148E+07	1.8908E-01	2.3959E+06	1.8647E-01	14:43	3.0922E+07		-40.76	0.21		-40.83	0.21		1.54	0.20		Ki57	
d30Si_040915_Ki57_rad@6	2.37	3.2738E-02	1.1352E-02	7.3339E+07	1.6555E-01	2.4013E+06	1.6167E-01	14:47	3.0989E+07		-41.24	0.23		-41.31	0.23		1.04	0.21		Ki57	
d30Si_040915_Ki57_rad@7	2.36	3.2719E-02	1.3351E-02	7.6744E+07	1.2646E-01	2.5109E+06	1.2384E-01	14:50	3.2468E+07		-41.81	0.27		-41.88	0.27		0.45	0.22		Ki57	
d30Si_040915_Ki57_rad@8	2.37	3.2726E-02	1.1628E-02	7.5207E+07	9.0513E-02	2.4612E+06	9.3291E-02	14:53	3.1789E+07		-41.60	0.23		-41.66	0.23		0.67	0.21		Ki57	
d30Si_040915_Ki57_rad@9	2.37	3.2793E-02	1.3895E-02	6.9961E+07	1.0132E-01	2.2956E+06	7.9234E-02	14:56	2.9555E+07		-39.63	0.28								Ki57	yield
d30Si_040915_Ki57_rad@10	2.37	3.2736E-02	1.4276E-02	7.4133E+07	2.5698E-01	2.4299E+06	2.3483E-01	15:00	3.1336E+07		-41.31	0.29		-41.38	0.29		0.98	0.23		Ki57	
d30Si_040915_Ki3c_rad@1	2.37	3.2714E-02	1.2811E-02	7.7656E+07	1.5262E-01	2.5403E+06	1.4815E-01	15:03	3.2821E+07		-41.95	0.26		-42.01	0.26		0.31	0.22		Ki03C	
d30Si_040915_BR7_Paine@05	2.36	3.2701E-02	1.1867E-02	7.9516E+07	1.3463E-01	2.6004E+06	1.3081E-01	15:07	3.3631E+07	3.3415E+07	-42.33	0.24	-42.33	-42.39	0.24	-42.39	-0.09	0.21	-0.08	Standard	
d30Si_040915_BR7_Paine@06	2.37	3.2702E-02	1.0781E-02	7.7973E+07	1.3932E-01	2.5497E+06	1.3343E-01	15:10	3.2949E+07	6.2761E+05	-42.29	0.22	0.17	-42.35	0.22	0.14	-0.05	0.20	0.15	Standard	
d30Si_040915_BR7_Paine@07	2.37	3.2704E-02	1.2501E-02	7.9432E+07	1.5085E-01	2.5977E+06	1.4955E-01	15:13	3.3556E+07		-42.24	0.25		-42.31	0.25		0.01	0.21		Standard	
d30Si_040915_BR7_Paine@08	2.37	3.2697E-02	1.2610E-02	7.9350E+07	1.5563E-01	2.5947E+06	1.5621E-01	15:16	3.3526E+07		-42.44	0.25		-42.50	0.25		-0.20	0.22		Standard	
d30Si_040915_Ki3c_rad@2	2.37	3.2709E-02	1.4099E-02	7.8436E+07	1.6892E-01	2.5658E+06	1.6788E-01	15:20	3.3137E+07	3.2645E+07	-42.09	0.28	-42.01	-42.15	0.28		0.17	0.22		Ki03C	
d30Si_040915_Ki3c_rad@3	2.37	3.2727E-02	1.3517E-02	7.3853E+07	2.5015E-01	2.4170E+06	2.4799E-01	15:23	3.1199E+07	1.4913E+06	-41.56	0.27	1.06	-41.61	0.27		0.73	0.22		Ki03C	
d30Si_040915_Ki3c_rad@4	2.37	3.2731E-02	1.6375E-02	7.4904E+07	1.0126E-01	2.4519E+06	9.9863E-02	15:26	3.1633E+07		-41.45	0.33		-41.50	0.33		0.84	0.24		Ki03C	
d30Si_040915_Ki3c_rad@5	2.37	3.2706E-02	8.2757E-03	7.8671E+07	1.3618E-01	2.5732E+06	1.3386E-01	15:30	3.3225E+07		-42.18	0.17		-42.23	0.17		0.08	0.19		Ki03C	
d30Si_040915_Ki3c_rad@6	2.37	3.2696E-02	9.1298E-03	7.9000E+07	1.5135E-01	2.5833E+06	1.4940E-01	15:33	3.3381E+07		-42.47	0.18		-42.53	0.18		-0.23	0.20		Ki03C	
d30Si_040915_Ki3c_rad@7	2.37	3.2727E-02	1.3385E-02	7.6718E+07	1.4830E-01	2.5108E+06	1.4374E-01	15:36	3.2405E+07		-41.56	0.27		-41.61	0.27		0.73	0.22		Ki03C	
d30Si_040915_Ki3c_rad@8	2.37	3.2718E-02	1.7101E-02	7.7635E+07	1.3033E-01	2.5416E+06	1.1748E-01	15:40	3.2795E+07		-41.82	0.34		-41.87	0.34		0.46	0.24		Ki03C	
d30Si_040915_Ki3c_rad@9	2.37	3.2717E-02	8.9040E-03	7.6749E+07	1.5763E-01	2.5127E+06	1.4171E-01	15:43	3.2430E+07		-41.85	0.18		-41.90	0.18		0.43	0.20		Ki03C	
d30Si_040915_Ki3c_rad@10	2.37	3.2671E-02	1.0620E-02	7.9130E+07	1.4139E-01	2.5854E+06	1.3634E-01	15:46	3.3427E+07		-43.22	0.21		-43.27	0.21		-1.00	0.20		Ki03C	
d30Si_040915_Ki42_rad@1	2.37	3.2752E-02	1.4032E-02	7.2386E+07	2.0918E-01	2.3730E+06	1.9782E-01	15:50	3.0594E+07		-40.85	0.28		-40.90	0.28		1.47	0.22		Ki42	
d30Si_040915_BR7_Paine@09	2.37	3.2696E-02	1.1891E-02	8.0320E+07	1.3071E-01	2.6276E+06	1.1872E-01	15:53	3.3926E+07	3.3536E+07	-42.48	0.24	-42.60	-42.53	0.24	-42.64	-0.22	0.21	-0.34	Standard	
d30Si_040915_BR7_Paine@10	2.37	3.2693E-02	1.3240E-02	7.9106E+07	1.3460E-01	2.5862E+06	1.3099E-01	15:56	3.3397E+07	7.0590E+05	-42.56	0.26	0.21	-42.61	0.26	0.18	-0.31	0.22	0.19	Standard	
d30Si_040915_BR7_Paine@11	2.37	3.2687E-02	1.0073E-02	7.9791E+07	1.3410E-01	2.6083E+06	1.3452E-01	16:00	3.3703E+07		-42.73	0.20		-42.78	0.20		-0.49	0.20		Standard	
d30Si_040915_BR7_Paine@12	2.37	3.2691E-02	1.1246E-02	7.8429E+07	1.3907E-01	2.5642E+06	1.3735E-01	16:03	3.3118E+07		-42.61	0.22		-42.65	0.22		-0.36	0.21		Standard	
d30Si_040915_Ki42_rad@2	2.37	3.2755E-02	1.4653E-02	7.2759E+07	1.1304E-01	2.3845E+06	1.0210E-01	16:06	3.0726E+07	3.1870E+07	-40.75	0.29	-40.92	-40.79	0.29		1.59	0.23		Ki42	
d30Si_040915_Ki42_rad@3	2.37	3.2748E-02	1.2128E-02	7.3407E+07	1.4083E-01	2.4040E+06	1.3832E-01	16:10	3.0995E+07	1.7750E+06	-40.95	0.24	0.48	-40.99	0.24		1.38	0.21		Ki42	
d30Si_040915_Ki42_rad@4	2.37	3.2748E-02	9.4508E-03	7.6768E+07	1.5635E-01	2.5157E+06	1.4288E-01	16:13	3.2390E+07		-40.96	0.19		-41.00	0.19		1.37	0.20		Ki42	
d30Si_040915_Ki42_rad@5	2.37	3.2728E-02	1.0159E-02	7.8410E+07	1.4340E-01	2.5684E+06	1.2855E-01	16:16	3.3094E+07		-41.54	0.20		-41.58	0.20		0.76	0.20		Ki42	
d30Si_040915_Ki42_rad@6	2.37	3.2748E-02	1.2327E-02	7.7803E+07	1.4448E-01	2.5496E+06	1.3323E-01	16:20	3.2843E+07		-40.95	0.25		-40.99	0.25		1.38	0.21		Ki42	
d30Si_040915_Ki42_rad@7	2.37	3.2754E-02	1.2484E-02	7.4738E+07	1.5139E-01	2.4478E+06	1.4943E-01	16:23	3.1534E+07		-40.78	0.25		-40.81	0.25		1.56	0.21		Ki42	
d30Si_040915_Ki42_rad@8	2.37	3.2754E-02	1.7647E-02	7.5432E+07	8.3375E-02	2.4708E+06	7.7791E-02	16:26	3.1834E+07		-40.79	0.35		-40.82	0.35		1.56	0.25		Ki42	
d30Si_040915_Ki42_rad@9	2.37	3.2757E-02	1.0388E-02	7.6180E+07	1.0354E-01	2.4955E+06	9.7220E-02	16:30	3.2121E+07		-40.68	0.21		-40.71	0.21		1.67	0.20		Ki42	
d30Si_040915_Ki42_rad@10	2.37	3.2747E-02	1.1595E-02	7.7232E+07	1.0593E-01	2.5293E+06	9.9794E-02	16:33	3.2573E+07		-40.97	0.23		-41.00	0.23		1.36	0.21		Ki42	
d30Si_040915_Ki8C_rad@1	2.37	3.2712E-02	1.1604E-02	7.7547E+07	1.5599E-01	2.5386E+06	1.4424E-01	16:36	3.2724E+07		-42.02	0.23		-42.05	0.23		0.27	0.21		Ki08C	
d30Si_040915_BR7_Paine@13	2.37	3.2700E-02	1.3691E-02	8.0261E+07	1.2938E-01	2.6245E+06	1.3295E-01	16:40	3.3839E+07	3.3527E+07	-42.37	0.27	-42.36	-42.40	0.27	-42.39	-0.09	0.22	-0.08	Standard	
d30Si_040915_BR7_Paine@14	2.37	3.2702E-02	8.3553E-03	7.8908E+07	1.3886E-01	2.5803E+06	1.3841E-01	16:43	3.3280E+07	7.2116E+05	-42.32	0.17	0.18	-42.34	0.17	0.16	-0.03	0.19	0.16	Standard	
d30Si_040915_BR7_Paine@15	2.37	3.2703E-02	7.6391E-03	8.0293E+07	1.3009E-01	2.6259E+06	1.2846E-01	16:46	3.3832E+07		-42.28	0.15		-42.30	0.15		0.01	0.19		Standard	
d30Si_040915_BR7_Paine@16	2.37	3.2696E-02	1.2995E-02	7.8639E+07	1.4622E-01	2.5714E+06	1.4354E-01	16:50	3.3155E+07		-42.49	0.26		-42.51	0.26		-0.21	0.22		Standard	
d30Si_040915_Ki8C_rad@2	2.39	3.2707E-02	1.0117E-02	7.9204E+07	1.3837E-01	2.5904E+06	1.4382E-01	16:53	3.3126E+07	3.3048E+07	-42.15	0.20	-42.48	-42.17	0.20		0.15	0.20		Ki08C	
d30Si_040915_Ki8C_rad@3	2.38	3.2702E-02	1.1450E-02	7.8792E+07	9.7952E-02	2.5765E+06	9.7218E-02	16:56	3.3103E+07	5.9433E+05	-42.31	0.23	0.60	-42.34	0.23		-0.03	0.21		Ki08C	
d30Si_040915_Ki8C_rad@4	2.38	3.2702E-02	9.7923E-03	7.8952E+07	1.5730E-01	2.5821E+06	1.5384E-01	17:00	3.3200E+07		-42.29	0.20		-42.31	0.20		0.00	0.20		Ki08C	
d30Si_040915_Ki8C_rad@5	2.38	3.2680E-02	9.0114E-03	7.8552E+07	1.4236E-01	2.5691E+06	1.3202E-01	17:03	3.3033E+07		-42.95	0.18		-42.97	0.18		-0.69	0.20		Ki08C	
d30Si_040915_Ki8C_rad@6	2.38	3.2697E-02	1.3315E-02	7.9130E+07	1.4645E-01	2.5894E+06	1.3265E-01	17:06	3.3272E+07		-42.45	0.27		-42.47	0.27		-0.17	0.22		Ki08C	
d30Si_040915_Ki8C_rad@7	2.38	3.2691E-02	1.3943E-02	7.9173E+07	1.3667E-01	2.5883E+06	1.3841E-01	17:09	3.3306E+07		-42.62	0.28		-42.64	0.28		-0.34	0.22		Ki08C	
d30Si_040915_Ki8C_rad@8	2.38	3.2695E-02	1.5903E-02	7.7481E+07	1.4995E-01	2.5332E+06	1.4558E-01	17:13	3.2583E+07		-42.50	0.32		-42.52	0.32		-0.21	0.24		Ki08C	
d30Si_040915_Ki8C_rad@9	2.38	3.2693E-02	1.2909E-02	7.7631E+07	1.5343E-01	2.5382E+06	1.5118E-01	17:16	3.2665E+07		-42.57	0.26		-42.59	0.26		-0.29	0.22		Ki08C	
d30Si_040915_Ki8C_rad@10	2.38	3.2681E-02	9.9828E-03	7.9547E+07	1.3007E-01	2.5997E+06	1.2859E-01	17:19	3.3470E+07		-42.91	0.20		-42.92	0.20		-0.64	0.20		Ki08C	
d30Si_040915_Ki4c_rad@1	2.38	3.2683E-02	1.0581E-02	7.8571E+07	1.4618E-01	2.5697E+06	1.2978E-01	17:23	3.3075E+07		-42.85	0.21		-42.86	0.21		-0.57	0.20		Ki04C	
d30Si_040915_BR7_Paine@17	2.37	3.2698E-02	1.1616E-02	7.9776E+07	1.5064E-01	2.6085E+06	1.5216E-01	17:26	3.3599E+07	3.3439E+07	-42.41	0.23	-42.49	-42.42	0.23	-42.50	-0.11	0.21	-0.20	Standard	
d30Si_040915_BR7_Paine@18	2.38	3.2700E-02	9.2503E-03	7.8698E+07	1.3669E-01	2.5735E+06	1.3640E-01	17:29	3.3105E+07	5.6407E+05	-42.37	0.19	0.29	-42.37	0.19	0.25	-0.07	0.20	0.26	Standard	
d30Si_040915_BR7_Paine@19	2.38	3.2689E-02	1.2761E-02	8.0168E+07	1.2207E-01	2.6208E+06	1.2007E-01	17:33	3.3733E+07		-42.70	0.26		-42.70	0.26		-0.41	0.22		Standard	
d30Si_040915_BR7_Paine@20	2.38	3.2696E-02	8.3351E-03	7.9140E+07	1.1313E-01	2.5875E+06	1.1307E-01	17:36	3.3318E+07		-42.49	0.17		-42.50	0.17		-0.20	0.19		Standard	

Table A2 Continued.

SIMS ANALYSES									Mount: BR7		Standard: UNIL-Q1 (Paine)		Analyse: δ^{30}Si		Value= -0.13±0.02 (NBS-28, 2σ)					Date: 03.09.2015
	Beam	H'2/L'2 (30Si/28Si)		L'2 (30Si/Coeff)		H'2 (28Si/Coeff)		Time	Yield	mean	Measurements		mean	Drift correction			Calibration			Comment
	nA	*CPS*	*2SD*	*CPS*	*2SD*	*CPS*	*2SD*		CPS/nA	*2SD*	$\delta^{30}Si$	*2SD int*	*2SD*	$\delta^{30}Si$	*2SD*		$\delta^{30}Si_{NBS-28}$	*2SD*		
d30Si_040915_Ki4c_rad@2	2.37	3.2729E-02	1.2325E-02	7.6127E+07	1.9181E-01	2.4913E+06	1.8649E-01	17:39	3.2063E+07	3.2878E+07	-41.52	0.25	-42.56	-41.52	0.25		0.83	0.21		Ki04C
d30Si_040915_Ki4c_rad@3	2.37	3.2667E-02	1.0837E-02	7.8304E+07	1.3228E-01	2.5580E+06	1.2756E-01	17:43	3.2974E+07	6.9141E+05	-43.33	0.22	1.06	-43.33	0.22		-1.06	0.21		Ki04C
d30Si_040915_Ki4c_rad@4	2.37	3.2681E-02	1.3559E-02	7.8335E+07	1.4863E-01	2.5601E+06	1.4785E-01	17:46	3.3005E+07		-42.91	0.27		-42.91	0.27		-0.62	0.22		Ki04C
d30Si_040915_Ki4c_rad@5	2.37	3.2701E-02	1.3728E-02	7.8715E+07	1.3996E-01	2.5743E+06	1.3648E-01	17:49	3.3148E+07		-42.32	0.27		-42.32	0.27		-0.01	0.22		Ki04C
d30Si_040915_Ki4c_rad@6	2.37	3.2694E-02	9.7254E-03	7.9001E+07	1.4777E-01	2.5827E+06	1.4588E-01	17:53	3.3264E+07		-42.54	0.19		-42.54	0.19		-0.24	0.20		Ki04C
d30Si_040915_Ki4c_rad@7	2.38	3.2701E-02	1.0231E-02	7.7888E+07	1.5143E-01	2.5472E+06	1.5421E-01	17:56	3.2794E+07		-42.34	0.20		-42.33	0.20		-0.02	0.20		Ki04C
d30Si_040915_Ki4c_rad@8	2.38	3.2703E-02	1.2546E-02	7.7486E+07	1.7084E-01	2.5342E+06	1.6635E-01	17:59	3.2620E+07		-42.26	0.25		-42.26	0.25		0.05	0.21		Ki04C
d30Si_040915_Ki4c_rad@9	2.37	3.2701E-02	1.2891E-02	7.7773E+07	1.4372E-01	2.5436E+06	1.3778E-01	18:03	3.2766E+07		-42.32	0.26		-42.32	0.26		-0.01	0.22		Ki04C
d30Si_040915_Ki4c_rad@10	2.38	3.2672E-02	9.7734E-03	7.8574E+07	1.4518E-01	2.5670E+06	1.4134E-01	18:06	3.3075E+07		-43.18	0.20		-43.17	0.20		-0.90	0.20		Ki04C
d30Si_040915_Ki1R_rad@1	2.38	3.2722E-02	1.3647E-02	7.4896E+07	9.0437E-02	2.4499E+06	8.1294E-02	18:09	3.1531E+07		-41.71	0.27		-41.71	0.27		0.63	0.22		Ki01
d30Si_040915_BR7_Paine@21	2.37	3.2709E-02	1.0353E-02	7.8733E+07	1.4037E-01	2.5751E+06	1.3639E-01	18:13	3.3166E+07	3.3423E+07	-42.10	0.21	-42.33	-42.09	0.21	-42.32	0.23	0.20	-0.01	Standard
d30Si_040915_BR7_Paine@22	2.38	3.2703E-02	1.5345E-02	7.9892E+07	1.3314E-01	2.6127E+06	1.3371E-01	18:16	3.3631E+07	6.0414E+05	-42.28	0.31	0.39	-42.27	0.31	0.33	0.05	0.23	0.35	Standard
d30Si_040915_BR7_Paine@23	2.38	3.2699E-02	1.0750E-02	7.8776E+07	1.3540E-01	2.5759E+06	1.3198E-01	18:19	3.3162E+07		-42.39	0.22		-42.37	0.22		-0.07	0.20		Standard
d30Si_040915_BR7_Paine@24	2.38	3.2693E-02	9.0273E-03	8.0209E+07	1.2220E-01	2.6225E+06	1.2037E-01	18:23	3.3733E+07		-42.56	0.18		-42.55	0.18		-0.25	0.20		Standard
d30Si_040915_Ki1R_rad@2	2.38	3.2727E-02	6.6060E-03	7.1271E+07	8.3266E-02	2.3325E+06	7.9401E-02	18:26	3.0004E+07	3.2318E+07	-41.57	0.13	-42.03	-41.56	0.13		0.79	0.19		Ki01
d30Si_040915_Ki1R_rad@3	2.38	3.2725E-02	9.5079E-03	7.6277E+07	1.4698E-01	2.4963E+06	1.4784E-01	18:29	3.2094E+07	2.1061E+06	-41.64	0.19	0.90	-41.63	0.19		0.71	0.20		Ki01
d30Si_040915_Ki1R_rad@4	2.38	3.2716E-02	1.0750E-02	7.6057E+07	1.3781E-01	2.4881E+06	1.3567E-01	18:33	3.1998E+07		-41.90	0.22		-41.89	0.22		0.44	0.20		Ki01
d30Si_040915_Ki1R_rad@5	2.38	3.2692E-02	1.5202E-02	7.8438E+07	1.5438E-01	2.5664E+06	1.3945E-01	18:36	3.3025E+07		-42.59	0.30		-42.57	0.30		-0.27	0.23		Ki01
d30Si_040915_Ki1R_rad@6	2.38	3.2726E-02	1.0371E-02	7.5802E+07	1.6710E-01	2.4807E+06	1.6308E-01	18:39	3.1874E+07		-41.59	0.21		-41.57	0.21		0.77	0.20		Ki01
d30Si_040915_Ki1R_rad@7	2.38	3.2718E-02	9.4345E-03	7.8006E+07	8.1243E-02	2.5522E+06	8.3504E-02	18:43	3.2817E+07		-41.84	0.19		-41.82	0.19		0.51	0.20		Ki01
d30Si_040915_Ki1R_rad@8	2.38	3.2685E-02	8.1087E-03	7.9685E+07	1.2523E-01	2.6047E+06	1.2536E-01	18:46	3.3523E+07		-42.79	0.16		-42.77	0.16		-0.48	0.19		Ki01
d30Si_040915_Ki1R_rad@9	2.38	3.2705E-02	9.2173E-03	7.8350E+07	1.4268E-01	2.5623E+06	1.4096E-01	18:49	3.2982E+07		-42.21	0.18		-42.19	0.18		0.12	0.20		Ki01
d30Si_040915_Ki1R_rad@10	2.38	3.2696E-02	1.5368E-02	7.9151E+07	1.4851E-01	2.5900E+06	1.4061E-01	18:53	3.3326E+07		-42.47	0.31		-42.44	0.31		-0.14	0.23		Ki01
d30Si_040915_Ki32_rad@1	2.38	3.2746E-02	9.9746E-03	7.6427E+07	1.5956E-01	2.5029E+06	1.5584E-01	18:56	3.2177E+07		-41.03	0.20		-41.00	0.20		1.37	0.20		Ki32
d30Si_040915_BR7_Paine@25	2.37	3.2705E-02	1.0661E-02	8.0291E+07	1.4897E-01	2.6256E+06	1.4693E-01	18:59	3.3811E+07	3.3515E+07	-42.22	0.21	-42.34	-42.19	0.21	-42.32	0.12	0.20	0.00	Standard
d30Si_040915_BR7_Paine@26	2.38	3.2698E-02	1.1091E-02	7.8955E+07	1.4315E-01	2.5815E+06	1.4135E-01	19:03	3.3211E+07	5.7907E+05	-42.42	0.22	0.21	-42.39	0.22	0.18	-0.08	0.21	0.19	Standard
d30Si_040915_BR7_Paine@27	2.38	3.2697E-02	1.2416E-02	8.0114E+07	1.3865E-01	2.6211E+06	1.2694E-01	19:06	3.3707E+07		-42.44	0.25		-42.41	0.25		-0.11	0.21		Standard
d30Si_040915_BR7_Paine@28	2.38	3.2702E-02	1.3578E-02	7.9193E+07	1.4346E-01	2.5915E+06	1.3255E-01	19:09	3.3331E+07		-42.30	0.27		-42.27	0.27		0.04	0.22		Standard
d30Si_040915_Ki32_rad@2	2.38	3.2763E-02	1.4155E-02	7.2852E+07	8.8968E-02	2.3856E+06	8.0526E-02	19:13	3.0657E+07	3.0895E+07	-40.50	0.28	-40.46	-40.47	0.28		1.92	0.23		Ki32
d30Si_040915_Ki32_rad@3	2.38	3.2758E-02	8.1320E-03	7.4174E+07	1.8626E-01	2.4297E+06	1.8332E-01	19:16	3.1221E+07	1.9450E+06	-40.67	0.16	0.75	-40.64	0.16		1.74	0.19		Ki32
d30Si_040915_Ki32_rad@4	2.38	3.2767E-02	1.2007E-02	7.4106E+07	1.9446E-01	2.4280E+06	1.9182E-01	19:19	3.1175E+07		-40.41	0.24		-40.38	0.24		2.02	0.21		Ki32
d30Si_040915_Ki32_rad@5	2.38	3.2760E-02	9.4522E-03	7.1487E+07	1.8862E-01	2.3420E+06	1.8708E-01	19:23	3.0072E+07		-40.60	0.19		-40.57	0.19		1.82	0.20		Ki32
d30Si_040915_Ki32_rad@6	2.38	3.2772E-02	1.6343E-02	7.1276E+07	2.0414E-01	2.3359E+06	1.9883E-01	19:26	2.9999E+07		-40.25	0.33		-40.21	0.33		2.19	0.24		Ki32
d30Si_040915_Ki32_rad@7	2.38	3.2774E-02	1.1828E-02	6.9365E+07	2.1179E-01	2.2734E+06	2.0952E-01	19:29	2.9184E+07		-40.19	0.24		-40.15	0.24		2.25	0.21		Ki32
d30Si_040915_Ki32_rad@8	2.38	3.2793E-02	1.1851E-02	7.2993E+07	2.2250E-01	2.3937E+06	2.2439E-01	19:33	3.0718E+07		-39.63	0.24		-39.59	0.24		2.84	0.21		Ki32
d30Si_040915_Ki32_rad@9	2.38	3.2757E-02	1.1189E-02	7.4943E+07	1.0623E-01	2.4551E+06	1.0541E-01	19:36	3.1515E+07		-40.69	0.22		-40.65	0.22		1.73	0.21		Ki32
d30Si_040915_Ki32_rad@10	2.38	3.2761E-02	1.0789E-02	7.6603E+07	1.6177E-01	2.5097E+06	1.5683E-01	19:39	3.2237E+07		-40.58	0.22		-40.53	0.22		1.86	0.21		Ki32
d30Si_040915_BR7_Paine@29	2.38	3.2699E-02	1.0052E-02	7.8953E+07	1.2690E-01	2.5832E+06	1.1595E-01	19:46	3.3243E+07	3.3342E+07	-42.39	0.20	-42.44	-42.34	0.20	-42.39	-0.03	0.20	-0.09	Standard
d30Si_040915_BR7_Paine@30	2.38	3.2705E-02	1.0667E-02	8.0284E+07	1.3436E-01	2.6270E+06	1.2416E-01	19:49	3.3775E+07	7.9618E+05	-42.21	0.21	0.36	-42.16	0.21	0.31	0.16	0.20	0.32	Standard
d30Si_040915_BR7_Paine@31	2.38	3.2692E-02	1.1636E-02	7.9674E+07	1.5080E-01	2.6064E+06	1.3727E-01	19:53	3.3509E+07		-42.58	0.23		-42.54	0.23		-0.24	0.21		Standard
d30Si_040915_BR7_Paine@32	2.38	3.2693E-02	1.4567E-02	7.8079E+07	1.4935E-01	2.5544E+06	1.3539E-01	19:56	3.2842E+07		-42.58	0.29		-42.53	0.29		-0.23	0.23		Standard
d30Si_040915_Ki34S_rad@1	2.38	3.2718E-02	1.4395E-02	7.2962E+07	3.7414E-01	2.3870E+06	3.7193E-01	20:29	3.0681E+07		-41.82	0.29		-41.76	0.29		0.58	0.23		Ki34
d30Si_040915_BR7_Paine@33	2.38	3.2699E-02	1.1880E-02	7.9544E+07	1.5090E-01	2.6009E+06	1.4877E-01	20:33	3.3431E+07	3.3038E+07	-42.38	0.24	-42.43	-42.32	0.24	-42.36	-0.01	0.21	-0.06	Standard
d30Si_040915_BR7_Paine@34	2.38	3.2697E-02	1.1580E-02	7.7549E+07	1.5769E-01	2.5358E+06	1.5553E-01	20:36	3.2582E+07	1.7158E+06	-42.45	0.23	0.07	-42.39	0.23	0.06	-0.08	0.21	0.06	Standard
d30Si_040915_BR7_Paine@35	2.38	3.2697E-02	1.0881E-02	8.0952E+07	1.1373E-01	2.6487E+06	1.0839E-01	20:39	3.4029E+07		-42.45	0.22		-42.39	0.22		-0.08	0.21		Standard
d30Si_040915_BR7_Paine@36	2.38	3.2698E-02	1.4187E-02	7.6419E+07	1.8788E-01	2.4985E+06	1.8414E-01	20:43	3.2109E+07		-42.43	0.28		-42.36	0.28		-0.05	0.22		Standard
d30Si_040915_Ki34S_rad@2	2.38	3.2740E-02	1.0332E-02	7.8865E+07	1.3088E-01	2.5821E+06	1.3295E-01	20:46	3.3192E+07	3.3004E+07	-41.18	0.21	-41.40	-41.12	0.21		1.25	0.20		Ki34
d30Si_040915_Ki34S_rad@3	2.38	3.2742E-02	1.2278E-02	7.9581E+07	1.4501E-01	2.6054E+06	1.4147E-01	20:49	3.3440E+07	1.8242E+06	-41.13	0.25	0.53	-41.06	0.25		1.30	0.21		Ki34
d30Si_040915_Ki34S_rad@4	2.38	3.2727E-02	1.3991E-02	7.7557E+07	1.5705E-01	2.5402E+06	1.4536E-01	20:53	3.2598E+07		-41.56	0.28		-41.49	0.28		0.85	0.22		Ki34
d30Si_040915_Ki34S_rad@5	2.38	3.2738E-02	1.1103E-02	7.9996E+07	1.3153E-01	2.6190E+06	1.2928E-01	20:56	3.3603E+07		-41.25	0.22		-41.18	0.22		1.18	0.21		Ki34
d30Si_040915_Ki34S_rad@6	2.38	3.2732E-02	1.3780E-02	7.8167E+07	1.6674E-01	2.5587E+06	1.6541E-01	20:59	3.2824E+07		-41.44	0.28		-41.37	0.28		0.99	0.22		Ki34
d30Si_040915_Ki34S_rad@7	2.38	3.2738E-02	1.1524E-02	7.9965E+07	1.7029E-01	2.6177E+06	1.6526E-01	21:03	3.3614E+07		-41.24	0.23		-41.17	0.23		1.19	0.21		Ki34
d30Si_040915_Ki34S_rad@8	2.38	3.2744E-02	1.0931E-02	7.8033E+07	1.4801E-01	2.5567E+06	1.3571E-01	21:06	3.2790E+07		-41.08	0.22		-41.01	0.22		1.36	0.21		Ki34
d30Si_040915_Ki34S_rad@9	2.38	3.2719E-02	1.2330E-02	8.0386E+07	1.5851E-01	2.6299E+06	1.5703E-01	21:09	3.3815E+07		-41.81	0.25		-41.73	0.25		0.60	0.21		Ki34
d30Si_040915_Ki34S_rad@10	2.38	3.2731E-02	1.4680E-02	7.9626E+07	1.6714E-01	2.6061E+06	1.6125E-01	21:13	3.3488E+07		-41.44	0.29		-41.36	0.29		0.99	0.23		Ki34
d30Si_040915_BR7_Paine@37	2.37	3.2695E-02	1.4404E-02	7.5378E+07	2.1280E-01	2.4668E+06	1.9983E-01	21:16	3.1741E+07	3.4492E+07	-42.51	0.29	-42.71	-42.43	0.29	-42.63	-0.12	0.23	-0.34	Standard
d30Si_040915_BR7_Paine@38	2.38	3.2695E-02	9.7545E-03	8.2600E+07	1.0324E-01	2.7006E+06	9.9784E-02	21:19	3.4748E+07	4.3771E+06	-42.50	0.20	0.50	-42.42	0.20	0.43	-0.12	0.20	0.45	Standard
d30Si_040915_BR7_Paine@39	2.38	3.2683E-02	1.2191E-02	8.1758E+07	2.0009E-01	2.6719E+06	1.9608E-01	21:23	3.4393E+07		-42.85	0.24		-42.77	0.24		-0.48	0.21		Standard
d30Si_040915_BR7_Paine@40	2.38	3.2678E-02	1.0592E-02	8.8088E+07	1.4745E-01	2.8764E+06	1.6072E-01	21:26	3.7085E+07		-43.00	0.21		-42.92	0.21		-0.63	0.20		Standard

Table A2 Continued.

	SIMS ANALYSES						Mount: BR1			Standard: UNIL-Q1 (Paine)		Analyse: $\delta^{30}Si$			Value= -0.13±0.02 (NBS-28, 2σ)					Date: 03.09.2015
	Beam	H'2/L'2 (30Si/28Si)		L'2 (30Si/Coeff)		H'2 (28Si/Coeff)		Time	Yield	mean	Measurements		mean	Drift correction			Calibration			Comment
	nA	CPS	2SD	CPS	2SD	CPS	2SD		CPS/nA	2SD	$\delta^{30}Si$	2SD int	2SD	$\delta^{30}Si$	2SD		$\delta^{30}Si_{NBS-28}$	2SD		
d30Si_030316_Paine@1	2.41	3.2711E-02	1.0759E-02	8.9319E+07	1.0787E-01	2.9214E+06	1.0921E-01	9:33	3.7112E+07	3.7091E+07	-42.03	0.22	-41.96							Setting: Standard
d30Si_030316_Paine@2	2.41	3.2713E-02	1.0975E-02	8.9839E+07	9.2660E-02	2.9392E+06	9.2405E-02	9:37	3.7203E+07	1.3945E+05	-41.97	0.22	0.16							Setting: Standard
d30Si_030316_Paine@3	2.42	3.2713E-02	1.3642E-02	8.9735E+07	8.8443E-02	2.9358E+06	9.1665E-02	9:40	3.7140E+07		-41.97	0.27								Setting: Standard
d30Si_030316_Paine@4	2.42	3.2715E-02	1.6678E-02	8.9320E+07	8.2644E-02	2.9218E+06	9.3164E-02	9:43	3.6965E+07		-41.91	0.33								Setting: Standard
d30Si_030316_Paine@5	2.41	3.2715E-02	2.0306E-02	8.9446E+07	9.7514E-02	2.9263E+06	1.0197E-01	9:46	3.7068E+07		-41.94	0.41								Setting: Standard
d30Si_030316_Paine@6	2.42	3.2718E-02	1.5530E-02	8.9677E+07	9.6322E-02	2.9346E+06	1.0047E-01	9:50	3.7077E+07		-41.82	0.31								Setting: Standard
d30Si_030316_Paine@7	2.42	3.2709E-02	2.0341E-02	8.9911E+07	9.0500E-02	2.9411E+06	9.6693E-02	9:53	3.7110E+07		-42.09	0.41								Setting: Standard
d30Si_030316_Paine@8	2.42	3.2714E-02	1.0389E-02	8.9782E+07	9.1614E-02	2.9380E+06	9.6711E-02	9:56	3.7050E+07		-41.94	0.21								Setting: Standard
d30Si_030316_Paine1@1	2.39	3.2737E-02	2.4704E-02	8.7680E+07	1.4409E-01	2.8709E+06	1.4169E-01	10:47	3.6690E+07	3.6679E+07	-41.29	0.49	-41.50			-41.71			-0.08	Standard internal variation
d30Si_030316_Paine1@02	2.40	3.2725E-02	1.2921E-02	8.7934E+07	1.3623E-01	2.8785E+06	1.3639E-01	10:51	3.6678E+07	9.3305E+04	-41.63	0.26	0.39	-41.76	0.26	0.27	-0.13	0.18	0.28	Standard
d30Si_030316_Paine1@03	2.41	3.2733E-02	1.5435E-02	8.8164E+07	1.1103E-01	2.8859E+06	1.1988E-01	10:54	3.6617E+07		-41.39	0.31		-41.52	0.31		0.11	0.20		Standard
d30Si_030316_Paine1@04	2.41	3.2722E-02	1.2299E-02	8.8485E+07	1.1525E-01	2.8957E+06	1.1686E-01	10:57	3.6730E+07		-41.71	0.25		-41.84	0.25		-0.21	0.18		Standard
d30Si_030316_KI10@1	2.40	3.2717E-02	1.3073E-02	8.7666E+07	1.2726E-01	2.8685E+06	1.2708E-01	11:00	3.6459E+07	3.6069E+07	-41.87	0.26	-41.71	-41.99	0.26		-0.38	0.18		Ki10
d30Si_030316_KI10@2	2.41	3.2715E-02	1.2622E-02	8.7628E+07	1.1817E-01	2.8670E+06	1.2151E-01	11:04	3.6379E+07	1.5050E+06	-41.91	0.25	0.60	-42.03	0.25		-0.42	0.18		Ki10
d30Si_030316_KI10@3	2.41	3.2728E-02	1.2585E-02	8.7514E+07	1.2743E-01	2.8643E+06	1.2805E-01	11:07	3.6247E+07		-41.53	0.25		-41.65	0.25		-0.02	0.18		Ki10
d30Si_030316_KI10@4	2.42	3.2712E-02	1.4220E-02	8.8558E+07	9.9412E-02	2.8971E+06	1.0848E-01	11:10	3.6538E+07		-42.02	0.28		-42.13	0.28		-0.52	0.19		Ki10
d30Si_030316_KI10@5	2.42	3.2740E-02	2.0834E-02	8.3629E+07	1.2022E-01	2.7363E+06	1.3343E-01	11:13	3.4552E+07		-41.20	0.42		-41.31	0.42		0.34	0.24		Ki10
d30Si_030316_KI10@6	2.42	3.2722E-02	1.4942E-02	8.7734E+07	9.5698E-02	2.8703E+06	9.7849E-02	11:17	3.6238E+07		-41.72	0.30		-41.82	0.30		-0.20	0.20		Ki10
d30Si_030316_KI5C@1	2.42	3.2725E-02	2.4343E-02	8.8286E+07	9.8969E-02	2.8898E+06	1.0265E-01	11:20	3.6409E+07	3.6454E+07	-41.62	0.49	-41.77	-41.72	0.49		-0.09	0.27		Ki05C
d30Si_030316_KI5C@2	2.43	3.2716E-02	1.5099E-02	8.8658E+07	8.9288E-02	2.9010E+06	9.8341E-02	11:23	3.6538E+07	2.3928E+05	-41.89	0.30	0.37	-41.99	0.30		-0.37	0.20		Ki05C
d30Si_030316_KI5C@3	2.42	3.2713E-02	1.2623E-02	8.8169E+07	1.0078E-01	2.8844E+06	1.0301E-01	11:26	3.6405E+07		-41.98	0.25		-42.07	0.25		-0.46	0.18		Ki05C
d30Si_030316_KI5C@4	2.42	3.2729E-02	1.2654E-02	8.7773E+07	1.0371E-01	2.8725E+06	1.0607E-01	11:30	3.6265E+07		-41.53	0.25		-41.62	0.25		0.01	0.18		Ki05C
d30Si_030316_KI5C@5	2.42	3.2715E-02	1.1420E-02	8.8240E+07	9.8707E-02	2.8869E+06	9.9694E-02	11:33	3.6511E+07		-41.92	0.23		-42.01	0.23		-0.39	0.17		Ki05C
d30Si_030316_KI5C@6	2.42	3.2723E-02	1.6568E-02	8.8408E+07	1.0311E-01	2.8930E+06	1.0044E-01	11:36	3.6599E+07		-41.68	0.33		-41.76	0.33		-0.14	0.21		Ki05C
d30Si_030316_Paine1@05	2.51	3.2727E-02	2.2749E-02	8.9040E+07	1.1418E-01	2.9136E+06	1.2071E-01	11:39	3.5493E+07	3.6463E+07	-41.56	0.45	-41.73	-41.64	0.45	-41.81	-0.01	0.26	-0.18	Standard
d30Si_030316_Paine1@06	2.42	3.2713E-02	2.2219E-02	8.9003E+07	1.2129E-01	2.9116E+06	1.2608E-01	11:43	3.6782E+07	1.2978E+06	-41.97	0.44	0.35	-42.05	0.44	0.30	-0.43	0.26	0.31	Standard
d30Si_030316_Paine1@07	2.42	3.2723E-02	2.2491E-02	8.9000E+07	1.0947E-01	2.9125E+06	1.1177E-01	11:46	3.6721E+07		-41.68	0.45		-41.75	0.45		-0.13	0.26		Standard
d30Si_030316_Paine1@08	2.42	3.2722E-02	1.8381E-02	8.9223E+07	1.0292E-01	2.9197E+06	1.0827E-01	11:49	3.6856E+07		-41.72	0.37		-41.79	0.37		-0.16	0.22		Standard
d30Si_030316_KI27@1	2.42	3.2739E-02	1.2491E-02	8.6257E+07	9.2205E-02	2.8248E+06	9.9921E-02	11:52	3.5704E+07	3.5900E+07	-41.21	0.25	-41.12	-41.28	0.25		0.37	0.18		Ki27
d30Si_030316_KI27@2	2.41	3.2765E-02	1.1935E-02	8.4843E+07	9.0573E-02	2.7799E+06	9.6118E-02	11:56	3.5177E+07	1.4009E+06	-40.45	0.24	1.08	-40.52	0.24		1.16	0.17		Ki27
d30Si_030316_KI27@3	2.41	3.2758E-02	1.0698E-02	8.4489E+07	1.0628E-01	2.7681E+06	1.0827E-01	11:59	3.5044E+07		-40.65	0.21		-40.71	0.21		0.96	0.17		Ki27
d30Si_030316_KI27@4	2.42	3.2733E-02	9.3970E-03	8.8642E+07	9.4396E-02	2.9021E+06	9.9339E-02	12:02	3.6656E+07		-41.39	0.19		-41.45	0.19		0.19	0.16		Ki27
d30Si_030316_KI27@5	2.42	3.2714E-02	1.6537E-02	8.8413E+07	1.0798E-01	2.8933E+06	9.4731E-02	12:05	3.6594E+07		-41.96	0.33		-42.01	0.33		-0.39	0.21		Ki27
d30Si_030316_KI27@6	2.41	3.2745E-02	2.3863E-02	8.7409E+07	1.1510E-01	2.8623E+06	1.1974E-01	12:09	3.6226E+07		-41.05	0.48		-41.10	0.48		0.56	0.27		Ki27
d30Si_030316_Paine1@09	2.41	3.2723E-02	1.4878E-02	8.9375E+07	9.3278E-02	2.9244E+06	9.5865E-02	12:31	3.7053E+07	3.7010E+07	-41.68	0.30	-41.85	-41.70	0.30	-41.87	-0.07	0.20	-0.25	Standard
d30Si_030316_Paine1@10	2.41	3.2723E-02	9.7175E-03	8.9112E+07	8.3263E-02	2.9160E+06	8.3455E-02	12:35	3.6925E+07	1.7022E+05	-41.68	0.19	0.39	-41.70	0.19	0.33	-0.07	0.16	0.35	Standard
d30Si_030316_Paine1@11	2.41	3.2712E-02	2.0510E-02	8.8989E+07	9.0197E-02	2.9113E+06	9.1713E-02	12:38	3.6953E+07		-42.01	0.41		-42.03	0.41		-0.42	0.24		Standard
d30Si_030316_Paine1@12	2.41	3.2712E-02	2.4919E-02	8.9316E+07	1.0257E-01	2.9223E+06	1.0884E-01	12:41	3.7107E+07		-42.02	0.50		-42.03	0.50		-0.42	0.28		Standard
d30Si_030316_KI54@1	2.41	3.2721E-02	1.1635E-02	8.9080E+07	1.3214E-01	2.9155E+06	1.3217E-01	12:45	3.6955E+07	3.6623E+07	-41.74	0.23	-41.60	-41.75	0.23		-0.12	0.17		Ki54
d30Si_030316_KI54@2	2.41	3.2730E-02	1.6300E-02	8.8868E+07	1.1907E-01	2.9080E+06	1.2089E-01	12:48	3.6843E+07	1.0533E+06	-41.48	0.33	0.91	-41.49	0.33		0.15	0.21		Ki54
d30Si_030316_KI54@3	2.41	3.2703E-02	1.2153E-02	8.8962E+07	1.2166E-01	2.9094E+06	1.2365E-01	12:51	3.6853E+07		-42.27	0.24		-42.27	0.24		-0.67	0.18		Ki54
d30Si_030316_KI54@4	2.41	3.2750E-02	1.0544E-02	8.5753E+07	1.1821E-01	2.8084E+06	1.1738E-01	12:54	3.5584E+07		-40.91	0.21		-40.91	0.21		0.75	0.16		Ki54
d30Si_030316_KI54@5	2.40	3.2733E-02	1.3503E-02	8.7922E+07	1.3833E-01	2.8781E+06	1.4030E-01	12:57	3.6573E+07		-41.39	0.27		-41.39	0.27		0.25	0.19		Ki54
d30Si_030316_KI54@6	2.40	3.2720E-02	8.5859E-03	8.8770E+07	1.4404E-01	2.9045E+06	1.4309E-01	13:01	3.6928E+07		-41.79	0.17		-41.78	0.17		-0.16	0.15		Ki54
d30Si_030316_Paine1@13	2.41	3.2727E-02	1.2941E-02	8.9585E+07	6.1890E-02	2.9314E+06	6.4085E-02	13:24	3.7236E+07	3.7082E+07	-41.58	0.26	-41.77	-41.55	0.26	-41.73	0.08	0.18	-0.11	Standard
d30Si_030316_Paine1@14	2.41	3.2716E-02	1.3135E-02	8.9363E+07	1.0831E-01	2.9241E+06	1.1719E-01	13:27	3.7109E+07	2.5074E+05	-41.88	0.26	0.29	-41.85	0.26	0.25	-0.23	0.18	0.26	Standard
d30Si_030316_Paine1@15	2.41	3.2716E-02	1.7074E-02	8.9123E+07	9.0650E-02	2.9162E+06	9.4825E-02	13:30	3.6935E+07		-41.89	0.34		-41.85	0.34		-0.23	0.21		Standard
d30Si_030316_Paine1@16	2.41	3.2722E-02	1.9889E-02	8.9360E+07	8.8332E-02	2.9246E+06	9.1550E-02	13:33	3.7050E+07		-41.73	0.40		-41.69	0.40		-0.06	0.24		Standard
d30Si_030316_Paine1@17	2.41	3.2717E-02	2.0220E-02	8.9435E+07	9.7479E-02	2.9261E+06	9.9900E-02	14:06	3.7148E+07	3.7218E+07	-41.86	0.40	-41.85	-41.78	0.40	-41.77	-0.16	0.24	-0.15	Standard
d30Si_030316_Paine1@18	2.41	3.2714E-02	1.0900E-02	8.9699E+07	8.5840E-02	2.9343E+06	8.7235E-02	14:09	3.7229E+07	9.8011E+04	-41.95	0.22	0.21	-41.87	0.22	0.18	-0.25	0.17	0.19	Standard
d30Si_030316_Paine1@19	2.41	3.2722E-02	1.6915E-02	8.9744E+07	1.0809E-01	2.9369E+06	1.1677E-01	14:13	3.7263E+07		-41.71	0.34		-41.62	0.34		0.01	0.21		Standard
d30Si_030316_Paine1@20	2.41	3.2716E-02	1.1862E-02	8.9669E+07	8.8921E-02	2.9336E+06	9.5004E-02	14:16	3.7231E+07		-41.90	0.24		-41.81	0.24		-0.19	0.17		Standard
d30Si_030316_Paine1@21	2.39	3.2721E-02	1.0923E-02	8.9023E+07	8.3748E-02	2.9129E+06	8.6352E-02	14:48	3.7243E+07	3.7281E+07	-41.76	0.22	-41.84	-41.63	0.22	-41.71	0.00	0.17	-0.08	Standard
d30Si_030316_Paine1@22	2.39	3.2716E-02	1.1678E-02	8.9116E+07	9.3004E-02	2.9160E+06	9.4926E-02	14:52	3.7296E+07	1.0114E+05	-41.89	0.23	0.21	-41.76	0.23	0.18	-0.14	0.17	0.19	Standard
d30Si_030316_Paine1@23	2.39	3.2714E-02	8.4705E-03	8.9145E+07	1.0339E-01	2.9162E+06	1.0703E-01	14:55	3.7346E+07		-41.96	0.17		-41.83	0.17		-0.20	0.15		Standard
d30Si_030316_Paine1@24	2.39	3.2721E-02	1.4403E-02	8.9111E+07	8.4870E-02	2.9159E+06	9.3423E-02	14:58	3.7238E+07		-41.74	0.29		-41.61	0.29		0.03	0.19		Standard

Table A2 Continued.

	SIMS ANALYSES							Mount: BR5				Standard: UNIL-Q1 (Paine)		Analyse: δ^{30}Si		Value= -0.13±0.02 (NBS-28, 2σ)				Date: 03.09.2015
	Beam	H'2/L'2 (30Si/28Si)		L'2 (30Si/Coeff)		H'2 (28Si/Coeff)		Time	Yield	mean	Measurements		mean	Drift correction			Calibration			Comment
	nA	*CPS*	*2SD*	*CPS*	*2SD*	*CPS*	*2SD*		CPS/nA	*2SD*	$\delta^{30}Si$	*2SD int*	*2SD*	$\delta^{30}Si$	*2SD*		$\delta^{30}Si_{NBS-28}$	*2SD*		
d30Si_030316_PaineBR5@1	2.39	3.2730E-02	1.2599E-02	8.9573E+07	1.0093E-01	2.9319E+06	1.0717E-01	16:17	3.7465E+07	3.7413E+07	-41.50	0.25	-41.84	-41.50	0.25	-41.85	0.18	0.23	-0.18	Setting: Standard
d30Si_030316_PaineBR5@02	2.39	3.2721E-02	1.0458E-02	8.9823E+07	1.0913E-01	2.9390E+06	1.0732E-01	16:21	3.7539E+07	2.3644E+05	-41.76	0.21	0.40	-41.76	0.21	0.37	-0.09	0.22	0.39	Setting: Standard
d30Si_030316_PaineBR5@03	2.39	3.2725E-02	1.2325E-02	8.9977E+07	1.0489E-01	2.9438E+06	1.0862E-01	16:24	3.7605E+07		-41.62	0.25		-41.63	0.25		0.05	0.23		Setting: Standard
d30Si_030316_PaineBR5@04	2.39	3.2711E-02	2.1218E-02	8.9126E+07	9.7604E-02	2.9159E+06	9.8091E-02	16:27	3.7230E+07		-42.03	0.42		-42.04	0.42		-0.38	0.29		Setting: Standard
d30Si_030316_PaineBR5@05	2.39	3.2716E-02	2.1827E-02	8.9233E+07	1.1680E-01	2.9191E+06	1.1611E-01	16:30	3.7355E+07		-41.90	0.44		-41.91	0.44		-0.24	0.29		Setting: Standard
d30Si_030316_PaineBR5@06	2.40	3.2712E-02	1.3882E-02	8.9614E+07	9.7443E-02	2.9324E+06	1.0325E-01	16:34	3.7386E+07		-42.02	0.28		-42.03	0.28		-0.37	0.24		Setting: Standard
d30Si_030316_PaineBR5@07	2.40	3.2715E-02	1.4699E-02	8.9665E+07	9.7678E-02	2.9335E+06	9.8519E-02	16:37	3.7371E+07		-41.92	0.29		-41.93	0.29		-0.26	0.24		Setting: Standard
d30Si_030316_PaineBR5@08	2.40	3.2712E-02	9.9247E-03	8.9736E+07	1.1275E-01	2.9354E+06	1.1201E-01	16:40	3.7355E+07		-42.00	0.20		-42.01	0.20		-0.34	0.22		Setting: Standard
d30Si_030316_PaineBR5@09	2.40	3.2722E-02	1.1383E-02	8.9731E+07	9.3143E-02	2.9363E+06	9.5543E-02	17:32	3.7343E+07	3.7437E+07	-41.72	0.23	-41.79	-41.73	0.23	-41.79	-0.06	0.22	-0.12	Standard
d30Si_030316_PaineBR5@10	2.40	3.2707E-02	1.6588E-02	9.0586E+07	1.0616E-01	2.9632E+06	1.0919E-01	17:35	3.7812E+07	5.0357E+05	-42.15	0.33	0.49	-42.15	0.33	0.42	-0.50	0.25	0.44	Standard
d30Si_030316_PaineBR5@11	2.39	3.2726E-02	1.1308E-02	8.9312E+07	8.5992E-02	2.9228E+06	8.8626E-02	17:39	3.7316E+07		-41.60	0.23		-41.60	0.23		0.08	0.22		Standard
d30Si_030316_PaineBR5@12	2.39	3.2723E-02	1.1822E-02	8.8908E+07	9.9542E-02	2.9094E+06	1.0273E-01	17:42	3.7276E+07		-41.68	0.24		-41.69	0.24		-0.01	0.23		Standard
d30Si_030316_KI38@1	2.38	3.2767E-02	9.6572E-03	8.7401E+07	1.1483E-01	2.8638E+06	1.1743E-01	17:45	3.6678E+07	3.6738E+07	-40.40	0.19	-41.03	-40.40	0.19		1.33	0.22		Ki38
d30Si_030316_KI38@2	2.39	3.2745E-02	1.6468E-02	8.8321E+07	1.0313E-01	2.8895E+06	1.1617E-01	17:48	3.7001E+07	4.6645E+05	-41.04	0.33	0.69	-41.04	0.33		0.66	0.25		Ki38
d30Si_030316_KI38@3	2.39	3.2749E-02	1.6855E-02	8.7888E+07	1.2609E-01	2.8783E+06	1.2716E-01	17:52	3.6789E+07		-40.92	0.34		-40.93	0.34		0.78	0.26		Ki38
d30Si_030316_KI38@4	2.39	3.2759E-02	1.4869E-02	8.6769E+07	9.4572E-02	2.8429E+06	9.8309E-02	17:55	3.6235E+07		-40.63	0.30		-40.64	0.30		1.08	0.24		Ki38
d30Si_030316_KI38@5	2.40	3.2742E-02	1.5259E-02	8.7890E+07	9.5538E-02	2.8782E+06	1.0338E-01	17:58	3.6660E+07		-41.12	0.31		-41.13	0.31		0.57	0.25		Ki38
d30Si_030316_KI38@6	2.39	3.2743E-02	8.3122E-03	8.8221E+07	1.2460E-01	2.8887E+06	1.2989E-01	18:01	3.6855E+07		-41.12	0.17		-41.12	0.17		0.58	0.21		Ki38
d30Si_030316_KI38@7	2.39	3.2746E-02	1.2357E-02	8.7202E+07	1.1260E-01	2.8553E+06	1.1156E-01	18:05	3.6523E+07		-41.02	0.25		-41.02	0.25		0.69	0.23		Ki38
d30Si_030316_KI38@8	2.39	3.2738E-02	1.0977E-02	8.8044E+07	1.1828E-01	2.8824E+06	1.2185E-01	18:08	3.6892E+07		-41.26	0.22		-41.26	0.22		0.43	0.22		Ki38
d30Si_030316_KI38@9	2.39	3.2723E-02	1.8451E-02	8.8567E+07	1.0884E-01	2.8986E+06	1.1093E-01	18:11	3.7007E+07		-41.68	0.37		-41.69	0.37		-0.01	0.27		Ki38
d30Si_030316_KI38@10	2.40	3.2742E-02	1.8200E-02	8.8034E+07	1.0554E-01	2.8807E+06	1.1634E-01	18:14	3.6744E+07		-41.13	0.36		-41.13	0.36		0.57	0.27		Ki38
d30Si_030316_PaineBR5@13	2.39	3.2723E-02	2.5206E-02	8.9681E+07	8.3345E-02	2.9349E+06	8.0731E-02	18:18	3.7470E+07	3.7493E+07	-41.69	0.50	-41.92	-41.70	0.50	-41.92	-0.02	0.32	-0.26	Standard
d30Si_030316_PaineBR5@14	2.39	3.2709E-02	9.5730E-03	8.9554E+07	9.9818E-02	2.9297E+06	1.0143E-01	18:21	3.7506E+07	1.4107E+05	-42.09	0.19	0.35	-42.10	0.19	0.30	-0.44	0.22	0.32	Standard
d30Si_030316_PaineBR5@15	2.39	3.2712E-02	1.6328E-02	8.9727E+07	1.0251E-01	2.9355E+06	1.0840E-01	18:24	3.7582E+07		-42.01	0.33		-42.01	0.33		-0.35	0.25		Standard
d30Si_030316_PaineBR5@16	2.40	3.2717E-02	1.4308E-02	8.9624E+07	8.3673E-02	2.9329E+06	8.7202E-02	18:27	3.7414E+07		-41.87	0.29		-41.88	0.29		-0.21	0.24		Standard
d30Si_030316_PaineBR5@17	2.39	3.2714E-02	2.0163E-02	8.9743E+07	8.7382E-02	2.9369E+06	8.7169E-02	19:10	3.7581E+07	3.7565E+07	-41.96	0.40	-41.68	-41.96	0.40	-41.68	-0.29	0.28	-0.01	Standard
d30Si_030316_PaineBR5@18	2.39	3.2733E-02	1.3335E-02	8.9291E+07	9.2416E-02	2.9227E+06	9.7886E-02	19:13	3.7429E+07	2.1225E+05	-41.39	0.27	0.47	-41.39	0.27	0.41	0.30	0.24	0.42	Standard
d30Si_030316_PaineBR5@19	2.38	3.2721E-02	9.5349E-03	8.9482E+07	1.0740E-01	2.9281E+06	1.1118E-01	19:16	3.7562E+07		-41.74	0.19		-41.75	0.19		-0.07	0.22		Standard
d30Si_030316_PaineBR5@20	2.39	3.2725E-02	1.0092E-02	8.9967E+07	9.9850E-02	2.9442E+06	1.0295E-01	19:19	3.7688E+07		-41.64	0.20		-41.64	0.20		0.04	0.22		Standard
d30Si_030316_PaineBR5@21	2.38	3.2713E-02	8.0536E-03	8.9526E+07	1.0469E-01	2.9286E+06	1.0780E-01	20:12	3.7688E+07	3.7556E+07	-41.99	0.16	-41.74	-41.99	0.16	-41.74	-0.33	0.21	-0.06	Standard
d30Si_030316_PaineBR5@22	2.38	3.2719E-02	1.0759E-02	8.9650E+07	1.0102E-01	2.9334E+06	1.0200E-01	20:15	3.7641E+07	2.6451E+05	-41.80	0.22	0.56	-41.80	0.22	0.49	-0.13	0.22	0.51	Standard
d30Si_030316_PaineBR5@23	2.39	3.2735E-02	1.8993E-02	8.9235E+07	8.2768E-02	2.9202E+06	8.7244E-02	20:18	3.7402E+07		-41.34	0.38		-41.34	0.38		0.35	0.27		Standard
d30Si_030316_PaineBR5@24	2.38	3.2719E-02	1.8026E-02	8.9227E+07	8.9843E-02	2.9197E+06	9.5974E-02	20:21	3.7493E+07		-41.82	0.36		-41.82	0.36		-0.15	0.26		Standard
d30Si_030316_PaineBR5@25	2.37	3.2725E-02	9.4497E-03	8.9020E+07	9.3873E-02	2.9132E+06	9.4630E-02	20:57	3.7497E+07	3.7523E+07	-41.62	0.19	-41.68	-41.62	0.19	-41.68	0.05	0.22	0.00	Standard
d30Si_030316_PaineBR5@26	2.37	3.2714E-02	9.4758E-03	8.9036E+07	1.2596E-01	2.9128E+06	1.2561E-01	21:00	3.7552E+07	6.1096E+04	-41.94	0.19	0.40	-41.94	0.19	0.34	-0.28	0.22	0.36	Standard
d30Si_030316_PaineBR5@27	2.38	3.2724E-02	1.1021E-02	8.9323E+07	9.4406E-02	2.9231E+06	9.7635E-02	21:04	3.7547E+07		-41.67	0.22		-41.67	0.22		0.01	0.22		Standard
d30Si_030316_PaineBR5@28	2.38	3.2731E-02	2.3450E-02	8.9223E+07	8.0472E-02	2.9228E+06	8.5623E-02	21:07	3.7496E+07		-41.47	0.47		-41.47	0.47		0.22	0.30		Standard
d30Si_030316_PaineBR5@29	2.38	3.2722E-02	1.7666E-02	8.9386E+07	1.0125E-01	2.9250E+06	1.0752E-01	21:59	3.7602E+07	3.7442E+07	-41.71	0.35	-41.73	-41.71	0.35	-41.73	-0.03	0.26	-0.06	Standard
d30Si_030316_PaineBR5@30	2.39	3.2717E-02	1.7077E-02	8.9014E+07	7.6190E-02	2.9124E+06	7.6389E-02	22:02	3.7318E+07	2.3680E+05	-41.86	0.34	0.22	-41.86	0.34	0.19	-0.19	0.26	0.20	Standard
d30Si_030316_PaineBR5@31	2.38	3.2720E-02	2.1973E-02	8.9071E+07	8.3952E-02	2.9145E+06	8.9301E-02	22:05	3.7436E+07		-41.77	0.44		-41.76	0.44		-0.09	0.29		Standard
d30Si_030316_PaineBR5@32	2.37	3.2726E-02	1.5505E-02	8.8837E+07	8.3440E-02	2.9078E+06	8.6051E-02	22:09	3.7411E+07		-41.59	0.31		-41.59	0.31		0.09	0.25		Standard
d30Si_030316_PaineBR5@33	2.38	3.2721E-02	1.3838E-02	8.9275E+07	2.0890E-01	2.9211E+06	2.1479E-01	23:01	3.7505E+07	3.7453E+07	-41.76	0.28	-41.84	-41.75	0.28	-41.84	-0.08	0.24	-0.17	Standard
d30Si_030316_PaineBR5@34	2.39	3.2725E-02	9.0185E-03	8.9135E+07	8.3633E-02	2.9171E+06	8.6517E-02	23:04	3.7365E+07	2.1759E+05	-41.63	0.18	0.40	-41.63	0.18	0.34	0.05	0.21	0.36	Standard
d30Si_030316_PaineBR5@35	2.38	3.2709E-02	1.0680E-02	8.9046E+07	7.4305E-02	2.9131E+06	7.8298E-02	23:07	3.7359E+07		-42.10	0.21		-42.09	0.21		-0.44	0.22		Standard
d30Si_030316_PaineBR5@36	2.38	3.2717E-02	1.4468E-02	8.9289E+07	1.1296E-01	2.9197E+06	1.2456E-01	23:11	3.7581E+07		-41.87	0.29		-41.87	0.29		-0.20	0.24		Standard
d30Si_030316_KI6CS@1	2.38	3.2722E-02	1.9406E-02	8.7653E+07	1.1806E-01	2.8679E+06	1.1871E-01	23:14	3.6853E+07	3.6480E+07	-41.71	0.39	-41.79	-41.71	0.39		-0.03	0.27		Ki06cs
d30Si_030316_KI6CS@02	2.38	3.2724E-02	1.5753E-02	8.7284E+07	1.2918E-01	2.8560E+06	1.3197E-01	23:17	3.6609E+07	3.7636E+05	-41.66	0.32	0.68	-41.66	0.32		0.02	0.25		Ki06cs
d30Si_030316_KI6CS@03	2.39	3.2729E-02	1.1059E-02	8.7634E+07	1.0250E-01	2.8686E+06	1.0664E-01	23:20	3.6684E+07		-41.53	0.22		-41.52	0.22		0.16	0.22		Ki06cs
d30Si_030316_KI6CS@04	2.38	3.2717E-02	1.0195E-02	8.6466E+07	1.1364E-01	2.8289E+06	1.1619E-01	23:24	3.6270E+07		-41.86	0.20		-41.85	0.20		-0.19	0.22		Ki06cs
d30Si_030316_KI6CS@05	2.38	3.2727E-02	1.2670E-02	8.6605E+07	1.2435E-01	2.8346E+06	1.2345E-01	23:27	3.6401E+07		-41.57	0.25		-41.57	0.25		0.11	0.23		Ki06cs
d30Si_030316_KI6CS@06	2.38	3.2731E-02	1.2047E-02	8.6069E+07	1.3062E-01	2.8174E+06	1.3209E-01	23:30	3.6140E+07		-41.45	0.24		-41.44	0.24		0.24	0.23		Ki06cs
d30Si_030316_KI6CS@07	2.39	3.2715E-02	2.0194E-02	8.6460E+07	7.6094E-02	2.8291E+06	8.9311E-02	23:33	3.6238E+07		-41.91	0.40		-41.91	0.40		-0.24	0.28		Ki06cs
d30Si_030316_KI6CS@08	2.38	3.2730E-02	2.3637E-02	8.7172E+07	1.0617E-01	2.8539E+06	1.1325E-01	23:37	3.6559E+07		-41.47	0.47		-41.47	0.47		0.22	0.31		Ki06cs
d30Si_030316_KI6CS@09	2.38	3.2716E-02	2.1692E-02	8.6667E+07	1.2336E-01	2.8359E+06	1.2215E-01	23:40	3.6440E+07		-41.90	0.43		-41.90	0.43		-0.23	0.29		Ki06cs
d30Si_030316_KI6CS@10	2.38	3.2728E-02	1.8277E-02	8.6594E+07	1.0120E-01	2.8339E+06	1.0515E-01	23:43	3.6394E+07		-41.54	0.37		-41.54	0.37		0.15	0.27		Ki06cs
d30Si_030316_KI6CS@11	2.38	3.2702E-02	9.8627E-03	8.7268E+07	1.0338E-01	2.8539E+06	1.0495E-01	23:46	3.6597E+07		-42.30	0.20		-42.29	0.20		-0.64	0.22		Ki06cs
d30Si_030316_KI6CS@12	2.39	3.2689E-02	9.9951E-03	8.7275E+07	7.8217E-02	2.8530E+06	7.9221E-02	23:50	3.6579E+07		-42.69	0.20		-42.68	0.20		-1.05	0.22		Ki06cs
d30Si_030316_KI6CS@13	2.38	3.2721E-02	1.1297E-02	8.6792E+07	1.3359E-01	2.8398E+06	1.3558E-01	23:53	3.6487E+07		-41.76	0.23		-41.75	0.23		-0.08	0.22		Ki06cs
d30Si_030316_KI6CS@14	2.38	3.2722E-02	1.4451E-02	8.6860E+07	1.1513E-01	2.8422E+06	1.2289E-01	23:56	3.6475E+07		-41.71	0.29		-41.70	0.29		-0.03	0.24		Ki06cs
d30Si_030316_PaineBR5@37	2.39	3.2729E-02	1.7262E-02	8.9669E+07	9.5199E-02	2.9330E+06	1.0826E-01	23:59	3.7575E+07	3.7601E+07	-41.50	0.35	-41.76	-41.49	0.35	-41.75	0.19	0.26	-0.08	Standard
d30Si_030316_PaineBR5@38	2.40	3.2716E-02	9.9543E-03	9.0157E+07	1.1405E-01	2.9500E+06	1.1168E-01	0:03	3.7643E+07	2.6371E+05	-41.90	0.20	0.36	-41.89	0.20	0.31	-0.22	0.22	0.32	Standard
d30Si_030316_PaineBR5@39	2.40	3.2720E-02	1.3629E-02	9.0501E+07	9.3523E-02	2.9616E+06	9.3058E-02	0:06	3.7750E+07		-41.79	0.27		-41.78	0.27		-0.11	0.24		Standard
d30Si_030316_PaineBR5@40	2.40	3.2718E-02	1.0085E-02	8.9845E+07	9.4685E-02	2.9395E+06	9.5942E-02	0:09	3.7435E+07		-41.85	0.20		-41.84	0.20		-0.17	0.22		Standard
d30Si_030316_PaineBR5@41	2.40	3.2719E-02	1.2431E-02	8.9440E+07	1.0284E-01	2.9266E+06	1.0764E-01	1:01	3.7325E+07	3.7387E+07	-41.80	0.25	-41.88	-41.79	0.25	-41.87	-0.12	0.23	-0.20	Standard
d30Si_030316_PaineBR5@42	2.39	3.2715E-02	1.7413E-02	8.9710E+07	8.6706E-02	2.9354E+06	9.4042E-02	1:04	3.7473E+07	2.6215E+05	-41.93	0.35	0.30	-41.92	0.35	0.26	-0.25	0.26	0.27	Standard
d30Si_030316_PaineBR5@43	2.39	3.2710E-02	1.7304E-02	8.9676E+07	8.7877E-02	2.9342E+06	9.4081E-02	1:08	3.7517E+07		-42.07	0.35		-42.06	0.35		-0.40	0.26		Standard
d30Si_030316_PaineBR5@44	2.39	3.2722E-02	2.1597E-02	8.9067E+07	9.5382E-02	2.9147E+06	1.0388E-01	1:11	3.7234E+07		-41.73	0.43		-41.72	0.43		-0.04	0.29		Standard

二次イオン質量分析法（SIMS）を用いた 中部日本犬山地域中生代層状チャート中の放散虫殻 Si 同位体分析

Maximilien BÔLE・池田　昌之・Peter O. BAUMGARTNER・
堀　利栄・Anne-Sophie BOUVIER

要　旨

全球シリカ循環は長期的気候システムの重要な要素だが，その制御要因は古環境指標の制約に乏しいため，不確実性が大きい．本論では，二次イオン質量分析計（SIMS）によって測定された犬山地域の中生代チャートに含まれる放散虫化石のシリカ変動（δ^{30}Si）を報告する．測定の結果，放散虫殻 δ^{30}Si は -0.3 ～ 2 ‰で，現在及び新生代の放散虫殻の値と調和的であった．さらに，予察的な δ^{30}Si 変動は低解像度にもかかわらず，1,000 万年スケールでは生物起源シリカ（BSi）埋没速度と逆相関し，従来の古生産性プロキシとしての δ^{30}Si の解釈に矛盾する結果となった．この時間スケールでは BSi 埋没速度は風化速度に依存するため，風化しやすく低 δ^{30}Si の苦鉄質岩の風化速度変化によって，この逆相関は説明されるかもしれない．さらに高解像度で δ^{30}Si 記録を測定することで，過去のシリカ循環をより深く理解できると期待される．

Bulletin of the Geological Survey of Japan, vol. 71 (4), p. 355–393, 2020

Article

Oxygen isotope analysis of Mesozoic radiolarites using SIMS

Maximilien BÔLE[1, 2, 3*], IKEDA Masayuki[2, 3], Peter O. BAUMGARTNER[1], HORI S. Rie[4],
Anne-Sophie BOUVIER[1] and Duje KUKOČ[1, 5]

Maximilien BÔLE, IKEDA Masayuki, Peter O. BAUMGARTNER, HORI S. Rie, Anne-Sophie BOUVIER and Duje KUKOČ (2020) Oxygen isotope analysis of Mesozoic radiolarites using SIMS. *Bulletin of the Geological Survey of Japan*, vol. 71(4), p. 355–393, 8 figs, 3 tables, 2 appendicies.

Abstract: The oxygen isotope ($\delta^{18}O$) analysis of carbonate fossils is widely applied for palaeoceanographic analysis, whereas that of siliceous fossils is only limited partly due to technical constraints and uncertain fractionation factors. Here we used a secondary ion mass spectrometer (SIMS) for $\delta^{18}O$ of radiolarian silica, precipitated inside radiolarian molds in Mesozoic radiolarites from Japan, Italy, Switzerland and Romania in order to examine its potential for palaeoceanographic proxy. 507 measurements of the isotopic oxygen signature relative to the Vienna Standard Mean Ocean Water ($\delta^{18}O_{VSMOW}$) of 53 chert samples range between 19.8 to 35.3 ‰ overlapping with that of modern and Cenozoic radiolarian tests in the equatorial Pacific. Relatively large intra-chert variability supports that $\delta^{18}O$ of the Mesozoic radiolarian tests are not perfectly homogenized within a chert bed during the diagenetic segregation. The temporal changes in the $\delta^{18}O$ values of radiolarians ($\delta^{18}O_{radiolarians}$) show an Early-Middle Triassic slight positive excursion, a Late Triassic high plateau, an Early Jurassic negative excursion with up to 8 ‰ , a Middle Jurassic slight positive excursion, and a few light values for the Cretaceous despite of their low resolution. A comparison of $\delta^{18}O$ between radiolarian molds, conodont apatite, and the low magnesium calcium shells show overall similar secular variations during the Triassic, but different trends was observed during the Early Jurassic. Because our data is low-resolution, further cross check of $\delta^{18}O_{radiolarians}$ is necessary to use as a proxy for paleoceanography.

Keywords: $\delta^{18}O$, Mesozoic, radiolarites, radiolarians, SIMS

1. Introduction

One of the most widely used palaeoceanographic techniques is the oxygen isotope ($\delta^{18}O$) analysis of carbonate shells which reflects past environmental changes, such as temperature, ice sheet volume, and precipitation/evaporation ratio (e.g., Emiliani, 1955; Shackleton and Kennett, 1975). However, a significant caveat in the paleoceanographic analyses using carbonate shells is their scarcity or complete absence in some sediments for large sections of the globe and deep past, due to dissolution below carbonate compensation depth (CCD) and/or carbonate organism evolution in pelagic ocean after the Late Triassic. The most easily available archive of seawater $\delta^{18}O$ for such sediments is biogenic silica (BSi), such as diatoms, sponges, and radiolarians (e.g. Jaffrés *et al.*, 2007). At least, $\delta^{18}O$ values of opal have been recognized as a potential proxy of past seawater temperature and isotopic composition as referred for diatoms (Labeyrie, 1974; Mikkelsen *et al.*, 1978; Juillet-Leclerc and Labeyrie, 1987; Shemesh *et al.*, 1992, 2001; Schmidt *et al.*, 1997; Swann *et al.*, 2008; Swann and Leng, 2009; Maier *et al.*, 2013), even if this is still debated. In Southern Ocean cores, $\delta^{18}O$ values of diatoms and radiolarians show similar patterns with similar values from 43 ‰ to 45 ‰ for at least last 30 ky (cf. Abelmann *et al.*, 2015). Therefore, $\delta^{18}O_{radiolarians}$ might also be a potential proxy for paleoceanography.

Radiolarians dominated as BSi producers in Paleozoic and Mesozoic open ocean (Hein and Parrish, 1987), whereas siliceous sponges were and are today largely restricted to marginal settings, and diatoms became quantitatively important in the Cenozoic (Racki and Cordey, 2000; Kidder and Erwin, 2001). Radiolarites were deposited in

[1] Institute of Earth Sciences (ISTE), Faculty of Geoscience, Geopolis, University of Lausanne, 1015 Lausanne, Switzerland
[2] Department of Geosciences, Faculty of Sciences, Shizuoka University, 836 Ohya Suruga, Shizuoka 422-8529, Japan.
[3] Department of Earth and Planetary Science, Graduate School of Science, The University of Tokyo, 7-3-1 Hongo, Bunkyo-ku, Tokyo 113-0033 Japan
[4] Department of Earth Sciences, Faculty of Science, Ehime University, Bunkyo-cho 2-5, Matsuyama, Ehime 790-8577, Japan
[5] Croatian Geological Survey, Sachsova 2, Hr-10000 Zagreb, Croatia
[*] Corresponding author: M, BÔLE., Rue des Envers 13, 2400 Le Locle, Switzerland. Email: maximilien.bole@gmail.com

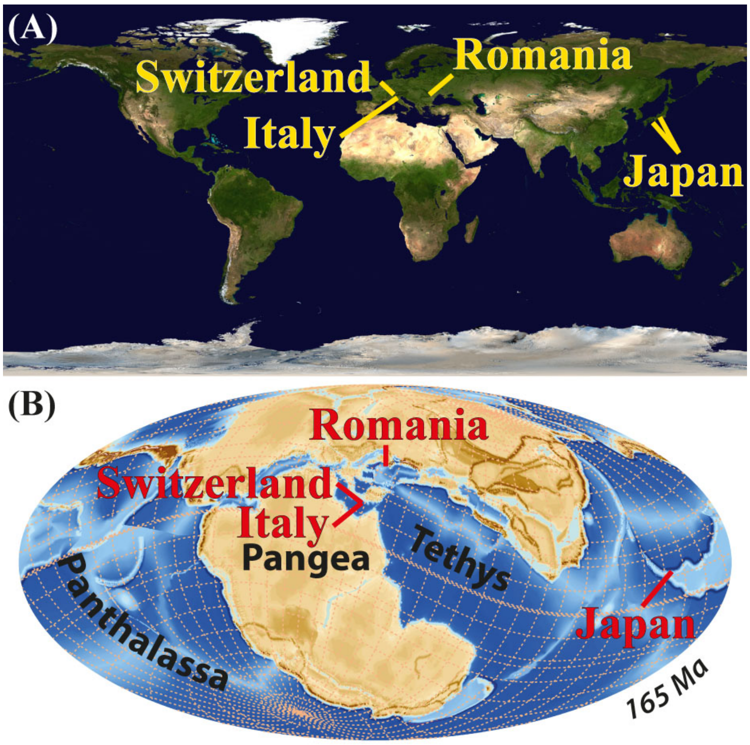

Fig. 1 Location of the studied sections (A) and their paleogeography during the Middle Jurassic (B). The Paleomap is from the Stampfli model developed at the University of Lausanne (Stampfli and Borel, 2002).

a broad low-latitude belt, and radiolarian-bearing siliceous mudstones also dominated in mid-latitudes (Baumgartner, 2013). Therefore, radiolarian $\delta^{18}O$ provides potentially important information for paleoceanography of the Paleozoic and Mesozoic.

Some evidence supports that radiolarian $\delta^{18}O$ may reflect environmental change (Knauth and Epstein, 1976; Wu *et al.*, 1997; Abelmann *et al.*, 2015). Although diagenetic isotopic fractionation of radiolarian test is still debated, even for Cenozoic (e.g. Fontorbe *et al.*, 2016), that for early Mesozoic bedded chert might be more simple system due to diagenetic segregation; This segregation results from the migration of silica from layers with low-Si content to layers with high-Si content during the transformation from opal-A to opal-CT (Isaacs, 1981; Tada, 1991). Thus, the cm-scale alternations of chert and shale might have limited migration of BSi within a chert-shale couplet. Contrary to this advantage, such diagenetic processes make extraction and picking of radiolarian molds without strong chemical procedures quite hard. To solve this disadvantage, secondary ion mass spectrometer (SIMS) is a powerful technique to measure the Mesozoic radiolarian molds on ~10 µm scale. Here we used SIMS for the Mesozoic radiolarian $\delta^{18}O$ to examine their paleoceanographic and diagenetic imprints.

2. Materials

We collected 55 chert samples from Mesozoic radiolarites in Japan, Italy, Switzerland and Romania (Fig. 1). Only fresh cherts were sampled to avoid alteration. The Triassic to Early Jurassic Panthalassan bedded cherts are distributed in the Inuyama Area from Japan (Kiso River sections; Nakaseko and Nishimura, 1979; Yao *et al.*, 1980; Mizutani and Koike, 1982; Hori, 1988; Sugiyama, 1997; Yao and Kuwahara, 1997; Carter and Hori, 2005; Ikeda and Tada, 2014). These bedded cherts consist of several tectonic imbricates outcropping along the Kiso River which were formed during the Jurassic accretion (Kimura and Hori, 1993). The Cretaceous Panthalassan radiolarites come from the Goshikikahama section (Okamura and Uto, 1982; Kodama *et al.*, 1983). We sampled Middle Jurassic Tethyan radiolarites from the Sogno section (Gaetani and Poliani, 1978; Baumgartner *et al.*, 1980; Kocher, 1981; Baumgartner, 1984; Baumgartner *et al.*, 1995; Ikeda *et al.*, 2016). Additional material (Pi01, Pe01, Ro01 and Ca01) are a Middle Jurassic radiolarite sample from the southern part of Switzerland (45°54′12″N, 8°59′55″E), a Late Permian radiolarian chert from Neo section, Japan (35°41′39″N, 136°39′25″E), a Middle Jurassic radiolarian chert from the Rarau synclinal of the Carpathian Mountain along a road going to Lagu Rosu, Romania (46°47′29″N, 25°47′32″E; Dumitrica, 1995) and a Berriasian diagenetic chert nodule from the Capriolo section in the Lombardian basin, Italy (45°38′40″N, 9°57′32″E; Weissert *et al.*, 1979; Channell *et al.*, 1987; Lini *et al.*, 1992; Föllmi *et al.*, 2012), respectively.

Bedded chert is composed of silica-rich chert layers interbedded with silica-poorer shale partings (Davis, 1918; Tada, 1991; Hori *et al.*, 1993). In radiolarian cherts, radiolarian silica can be easily distinguished from a stained matrix enclosing radiolarian molds often filled with nearly

Table 1 Raw, drift corrected, calibrated for our $\delta^{18}O_{VSMOW}$ least square mean and standard deviations on the UNIL-Q1 standard (in ‰; 2SD). The identic raw and drift corrected $\delta^{18}O_{VSMOW}$ suggests that there was no major instrumental drift during our sessions. Overall, the reproductivity of the UNIL-Q1 on the 269 measurements after calibration is 0.3 ‰ (2SD). The raw $\delta^{18}O_{VSMOW}$ of the PRIM123 session for Ki08C, Pi01 and Ca01 is in average 2.5 ‰ higher than the other session due to instrumental fractionation differences.

Session	Number of measurements	Raw $\delta^{18}O_{VSMOW}$ (‰)		Drift corrected $\delta^{18}O_{VSMOW}$ (‰)		Calibrated $\delta^{18}O_{VSMOW}$ (‰)	
		LSmean	LSstd	LSmean	LSstd	LSmean	LSstd
Prim123	48	6.5	0.3	6.5	0.3	9.8	0.3
Br2	47	4.4	0.5	4.4	0.5	9.8	0.5
Br3	31	4.5	0.4	4.4	0.4	9.8	0.3
Br4	52	3.8	0.3	3.8	0.3	9.8	0.3
Br6	28	3.7	0.3	3.7	0.3	9.8	0.3
Br7	63	3.9	0.3	3.9	0.3	9.8	0.3
All UNIL-Q1 measurements	269					9.8	0.3

pure microquartz and/or chalcedony (Bôle *et al.*, 2020). Most of these microquartz are early diagenetic products from opal-A precipitating in the pore space produced by radiolarian skeletons which are the target of this study.

3. Methods

Secondary ion mass spectrometer (SIMS) can achieve accurate in situ analyses of very small sample amount. The aim of in situ analyses in the infills radiolarian molds by SIMS is to measure the oxygen derived from their microquartz without contamination from clays or aeolian/detrital minerals present in the matrix. Microquartz infills in radiolarian molds, which are likely an early silica precipitation derived from biosilica, were analysed with a CAMECA IMS 1280HR at the University of Lausanne (e.g. Seitz *et al.*, 2016).

About 10 subsamples were mounted in each 1-inch micron-polished epoxy sample holder (Epofit resin) around an internal standard. An amorphous glass standard from the National Institute of Standard and Technology (NIST-610) was used for the initial three mounts with samples Ki08C, Pi01, and Ca01, to control instrumental drift in absence of a proper quartz standard. The quartz internal standard UNIL-Q1 (Seitz *et al.*, 2016) have been used for all mounts, including initial three samples reanalysed, to correct instrumental drift and mass fractionation. As instrumental mass fractionation on SIMS depend on minerals species (Marin *et al.*, 2010), data from chert samples are calibrated with UNIL-Q1. Before SIMS measurements, radiolarian molds and their microcrystalline quartz infill was carefully examined on each subsample on mount by optical and/or scanning electrons microscopy (SEM).

The $\delta^{18}O$ from 532 points of radiolarian molds was measured with a primary Cs+ ion beam intensity of ~2 nA, resulting in a beam diameter of ~10 µm. Electrical charges were compensated using an electron flood gun, with normal incidence and the conductivity of the sample surface was assured by a gold coating connected to electrical ground. ^{16}O and ^{18}O secondary ions, accelerated at 10 kV, were analyzed at a mass resolving power of 3000 and collected on Faraday cups (FC) multi-collection mode. The resistances of the L'2 and H'2 FC were set to 10^{10} Ω and 10^{11} Ω for the detection of ^{16}O and ^{18}O, respectively. FC were calibrated in the beginning of each session, using the calibration routine. Mass calibration was performed at the beginning of each session and every 12 h.

Each analysis took less than 4 minutes and consists of 20 cycles of 5 seconds starting with a presputtering time of 30 seconds to remove gold, stabilized the secondary ion emission allowing automatic centring of the secondary ion beam. This setting allowed an average reproducibility better than 0.3 ‰ (2 standard deviation, 2SD) on UNIL-Q1 (Seitz *et al.*, 2016; Table 1) at the beginning each session, and analytical standard deviation for each analysis lower than 0.3 ‰ (2SD). The analytical standard deviation expressed here is the standard deviation of each data from different analytical cycles. A minimum set of 4 analyses of UNIL-Q1 quartz standard (9.18 ± 0.14 ‰ (VSMOW); Seitz *et al.*, 2016), inserted in each mount, has been measured every 6-10 analyses for monitoring the instrument stability, and for accurately correcting the instrumental mass fractionation, as it can slightly differ from mount to mount. The data have been obtained in 10 different sessions for $\delta^{18}O$ measurements, over 11 months. The variation of the UNIL-Q1 quartz standard over the entire sessions is < 0.3‰ (2SD after the drift correction (Table 1).

The target locations were controlled by optical methods and SEM for each measurement to check that radiolarian molds were effectively hit. Analytical yield and standard deviation of each measurement were also used to check the validation. The analytical yield is the quantity of elements measured relative to the intensity of primary ion beam (cps/nA), and here we used relative analytical yield normalized

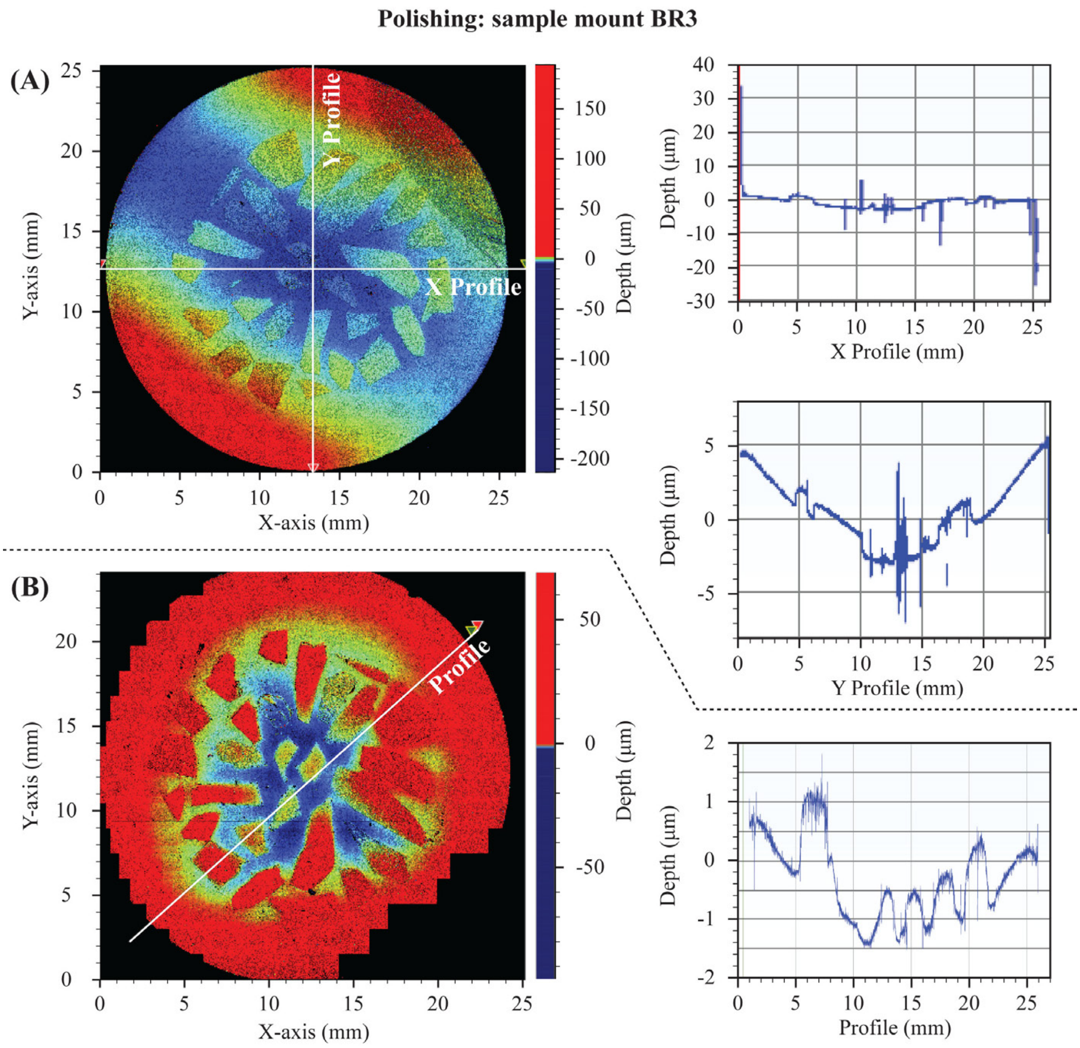

Fig.2 Topography of the sample mount BR3 after polishing. (A) Between the lower part of the rim and the centre of the sample mount, there is a difference of about 7.5 μm in depth. This difference was due to an internal tension triggered by a screw which initially hold the sample holder during the polishing. (B) After a second polishing without the screw, the topography of the rim is better and the difference between the rim and the center is reduced to 0.25 μm. The profiles on the right part are represented by white lines on the surface of the sample mount.

by that of internal standard UNIL-Q1. Different analytical yields result from the nature of the analysed material (mineral species and matrix effect) and from the topography of the analysed surface, which modifies the incident angle of the primary ion beams and thus the energy per surface of the primary ion beam. Therefore, the planarity of our sample mounts after polishing up to 0.25 μm was checked using white light profilometer (Brucker: Countour GT; Fig. 2) to have elevation differences of less than 1.5 μm between the standard and the samples. High analytical standard deviation depends on isotopic heterogeneities in the analysed minerals, but also on modifications of the instrumental mass fractionation which could be triggered by changes of the analytical conditions (topography, beam and analyser stability) or by the analyses of a mixture of silica, clay minerals and oxides. Overall, analytical yield similar to the one of our UNIL-Q1 standard (~ 7.9 cps/nA, but depends on sessions) and analytical standard deviation lower than 0.35 ‰ (2SD) are objective criterions to decide if a measurement should be accepted.

The drift correction was realized using a least square regression line weighted for incertitude (σ_i^2). For the calibration, the weighted δ^{18}O-mean ($\underset{\cdot}{x}$) and standard deviation ($\dot{\sigma}_i$) for the internal standard was calculated also using the incertitude (Equation 1 and 2) to keep consistent data processing with the least square drift correction. The calibrated δ^{18}O for samples ($\delta^{18}O_{VSMOW}\ Spl$), depend on each sample measurement ($\delta^{18}O\ Spl_{measured}$) and are proportional to the measured least square δ^{18}O-mean and the true $\delta^{18}O_{VSMOW}$ from the internal standard ($\delta^{18}O\ Std_{measured}$ and $\delta^{18}O_{VSMOW}\ Std$, respectively) (Equation 3). The errors on the calibrated δ^{18}O (σ ($\delta^{18}O_{VSMOW}\ Spl$)) were obtained by error propagation (Equation 4). The weighted means and standard deviations (Table 2 and Appendix Table A1) were then calculated for each sample following equation 1 and 2. Conversion from VSMOW to VPDB was realized using the Equation 5 (Kim *et al.*, 2015). For comparison, $\delta^{18}O$ values relative to the Vienna Pee Dee Belemnite standard for low magnesium calcium shells ($\delta^{18}O_{VPDB}$ LMC) from Grossman (2012) were digitalized using PlotDigitizer (2.6.8).

Equation 1

$$\dot{\underline{x}} = \sum \left(\frac{1}{\sigma_i^2} \times x_i\right) / \left(\frac{1}{\sigma_i^2}\right)$$

Equation 2

$$\dot{\sigma_i} = \sqrt{\sum \left(\frac{1}{\sigma_i^2} \times (x_i - \dot{\underline{x}})^2\right) / \sum \left(\frac{1}{\sigma_i^2}\right) \times \frac{N}{N-1}}$$

Equation 3

$$\delta^{18}O_{VSMOW}\ Spl = x_i = \left(\left(\left(1 + \frac{\delta^{18}O\ Spl_{measured}}{1000}\right) \Big/ \frac{(1 + \delta^{18}O\ Std_{measured} / 1000)}{(1 + \delta^{18}O_{VSMOW}\ Std / 1000)}\right) - 1\right) \times 1000$$

Equation 4

$$\sigma(\delta^{18}O_{VSMOW}\ Spl) = \sqrt{\left(\frac{\partial F}{\partial V_1} \times dV_1\right)^2 + \left(\frac{\partial F}{\partial V_2} \times dV_2\right)^2 + \left(\frac{\partial F}{\partial V_3} \times dV_3\right)^2}$$

With $F = \delta^{18}O_{VSMOW}\ Spl$, $V_1 = \delta^{18}O\ Spl_{measured}$, $V_2 = \delta^{18}O\ Std_{measured}$ and $V_3 = \delta^{18}O_{VSMOW}\ Std$

Equation 5

$$\delta^{18}O_{VSMOW} = 1.0392 \times \delta^{18}O_{VPDB} + 30.92\ ‰$$

4. Results

Here we present some raw data from the SIMS to illustrate the measurements of single radiolarian molds and their validation. Raw results from repetitive measurements on some samples are also described to highlight reproducibility of our analyses. Finally, we present the $\delta^{18}O_{VSMOW}$ trends from our measurements through the Mesozoic.

4. 1 Quality 234 check of SIMS analyses

We validate the quality of the SIMS measurement by post-checking of analysed spots by optical and/or SEM, and relative analytical yield. Illustrating the necessity of the pre- and post-checking, some spherical zones on the Late Triassic Inuyama chert sample Ki48 (Fig. 3A and B) are difficult to be identified as radiolarian molds or epoxy, and have been measured with very low analytical yield (~3 % of the UNIL-Q1 yield) and very light $\delta^{18}O_{RAW}$ (uncalibrated $\delta^{18}O$) (<-30 ‰) (Appendix Table A2). The normal analytical yield and $\delta^{18}O_{RAW}$ of this sample (e.g. Fig. 3C) are ~97.8 % and ~25 ‰, respectively, with calibrated $\delta^{18}O_{VSMOW}$ of ~31.3 ‰.

The measurements of mixings of epoxy and radiolarian molds for some analytical spots have low analytical yields and light $\delta^{18}O_{RAW}$-values. Such value can be found in an Early Triassic siliceous mudstone sample Ki12s from Inuyama (e.g. Fig. 3E). The detection of potential analytical sites in this sample is particularly difficult due to scarcity of radiolarian molds. Alternatively, we also commonly observed quartz patches, which could be the result from radiolarian silica precipitation, aleatory distributed that we tried to analyse (Fig. 3D). The post checking of these patches was nearly impossible due to their small size (smaller or equal to the 10 μm beam size) and we exclude them because they have usually low analytical yield (<90 %). The measurement of one of these patches has however a relatively good yield (94.9 %) but an uncommon light $\delta^{18}O_{RAW}$ (2.8 ‰), corresponding to a calibrated $\delta^{18}O_{VSMOW}$ of 8.7 ‰ (Fig. 3D).

High analytical $\delta^{18}O$-yields were measured in the Middle Jurassic Sogno sample So29 (~130.2 %). SEM-EDX analyses demonstrate that the molds in this sample were filled with carbonates, and that the matrix is more siliceous (Fig. 4). This observation contrasts with the radiolarian molds being commonly more siliceous than the matrix, which contains clays (Fig. 5 and Fig. 6).

4. 2 Reproducibility of SIMS measurements for radiolarian δ18O

Three chert samples (Pi01, Ki08C, Ca01) have been initially measured in detail relative to the NIST-610 standard, and then together relative to UNIL-Q1 standard (Table 3). NIST-610 was used to correct instrumental drift, but not to calibrate $\delta^{18}O$ measurements because the instrument fractionation depends on matrix and structure of the material analysed, mainly chert in this study. Overall, reproducibility on the UNIL-Q1 standard was 0.3 ‰ for $\delta^{18}O$ over all SIMS sessions (Table 1).

In detail, $\delta^{18}O$-measurements on Pi01 (a Middle Jurassic radiolarite sample in the southern Switzerland) with NIST-610 were done during two sessions. Uncalibrated $\delta^{18}O$-results for Pi01 after drift correction for the first and second sequences are 28.2 ± 1.5 ‰ (10 points, 2SD) and 28.4 ± 5.1 ‰ (27 points, 2SD) with NIST-610 values at 10.4 ± 0.2 ‰ (5 points, 2SD) and 10.8 ± 0.4 ‰ (16 points, 2SD), respectively. $\delta^{18}O$-measurements on Ki08C (a Middle Triassic chert in Inuyama) and Ca01 (a diagenetic chert lacking radiolarian molds in the Cretaceous Maiolica Formation of the Lombardian basin) were measured relative to NIST-610 during single session. Uncalibrated $\delta^{18}O$-results for Ki08C after drift correction

Table 2 List of samples with their age, the number of measurements, their $\delta^{18}O$ least square mean (LS-mean) and their $\delta^{18}O$ least square standard deviation (LS std; 1SD). The $\delta^{18}O$ was average with a 10 Ma windows moving average (5 Ma step) and compared with $\delta^{18}O$ from low magnesium carbonate shells for tropical and temperate regions (Grossman, 2012).

Sample	Age (Ma)	Number of measurements	Results		Curves			
			$\delta^{18}O_{Vsmow}$ (‰)		$\delta^{18}O_{VSMOW}$ Radiolarian molds (‰)		$\delta^{18}O_{VPDB}$ LMC shells (‰)	
			This study		This study		Grossman, 2012	
			LS-mean	LS-std	Panthalassa	Tethys	Tropical	Temperate
					10 Ma moving average		4 Ma moving average	
Pe01	253.15	10	24.0	0.2	27.21		-3.0	
Ki09	250.30	9	29.3	0.4	28.15			
Ki01	248.00	10	30.9	1.4	28.57			
Ki02	247.80	6	30.8	1.0	28.60			
Ki03s	247.20	4	20.9	2.3	28.69			
Ki03s	247.20	5	23.9	1.1	28.69			
Ki03	247.20	10	30.4	0.7	28.69			
Ki04	246.60	9	31.3	0.9	28.79			
Ki06	245.25	6	31.9	1.2	29.00		-4.0	
Ki07	245.00	6	29.3	1.8	29.04		-4.1	
Ki08	244.90	10	30.6	1.0	29.06		-4.1	
Ki08	244.90	86	30.8	0.6	29.06		-4.1	
Ki58C	243.48	6	31.2	0.7	29.24		-4.3	
Ki57	241.00	9	26.8	1.8	29.56		-3.8	
Ki15	228.00	10	31.5	0.7	31.49		-2.5	
Ki51	219.00	6	31.9	0.3	31.35		-2.1	
Ki48	217.09	3	30.6	0.9	31.52		-2.1	
Ki46	210.27	10	32.6	1.6	32.55		-1.8	
Ki44	204.82	9	31.6	0.4	31.48		-1.7	
Ki43s	204.82	6	31.3	0.4	31.48		-1.7	
Ki39	201.50	9	31.4	0.5	31.48			
Ki40	201.50	10	31.7	0.6	31.48			
Ki41	201.50	10	31.4	0.8	31.48			
Ki42	201.50	10	31.4	0.5	31.48			
Ki35	185.62	9	30.0	0.4	28.92		-0.8	
Ki34s	184.37	1	30.8	0.0	28.66		-1.0	
Ki34s	184.37	8	25.8	1.4	28.66		-1.0	
Ki32	184.20	10	30.2	0.9	28.62		-1.1	
Ki24	182.00	6	30.8	0.7	28.22		-1.9	
Ki25	180.66	8	25.2	2.5	27.97		-2.4	
Ki22c1	178.00	9	27.0	1.2	26.90		-2.7	
Ki22c2	178.00	6	26.1	1.5	26.90		-2.7	
Ki21	178.00	10	27.2	1.1	26.90		-2.7	
Ki20	174.00	5	21.9	1.9	24.76		-2.3	
So07	169.50	6	32.5	0.8		33.53		0.3
So08	169.50	7	34.0	0.4		33.53		0.3
So09	169.30	6	34.3	0.4		33.54		0.3
So12	168.27	6	35.0	0.5		33.63		0.3
So13	168.13	9	34.3	0.4		33.64		0.3
So15	167.54	6	34.7	0.5		33.69		0.4
So17	166.89	9	32.7	2.6		33.75		0.5
So21	166.09	6	32.3	1.0		33.81		0.5
Ro01	166.00	6	30.9	0.8		33.82		0.5
So23	165.10	6	34.0	0.6		33.90		0.4
So25	164.31	9	35.3	0.3		34.06		0.3
Pi01	163.00	32	34.6	0.4		34.35		-0.1
So26	162.65	6	35.1	0.3		34.43		-0.2
So28	161.14	8	34.7	0.7		34.76		-0.4
So31	159.97	9	35.2	0.3		35.02		-0.5
Ca01	139.00	10	34.3	0.2		34.36		-0.3
Go68	131.70	6	26.5	0.6	26.49		-0.3	
Go73	97.95	9	28.5	1.0	24.09		-2.6	
Go74	97.59	10	19.8	0.7	24.09		-2.8	

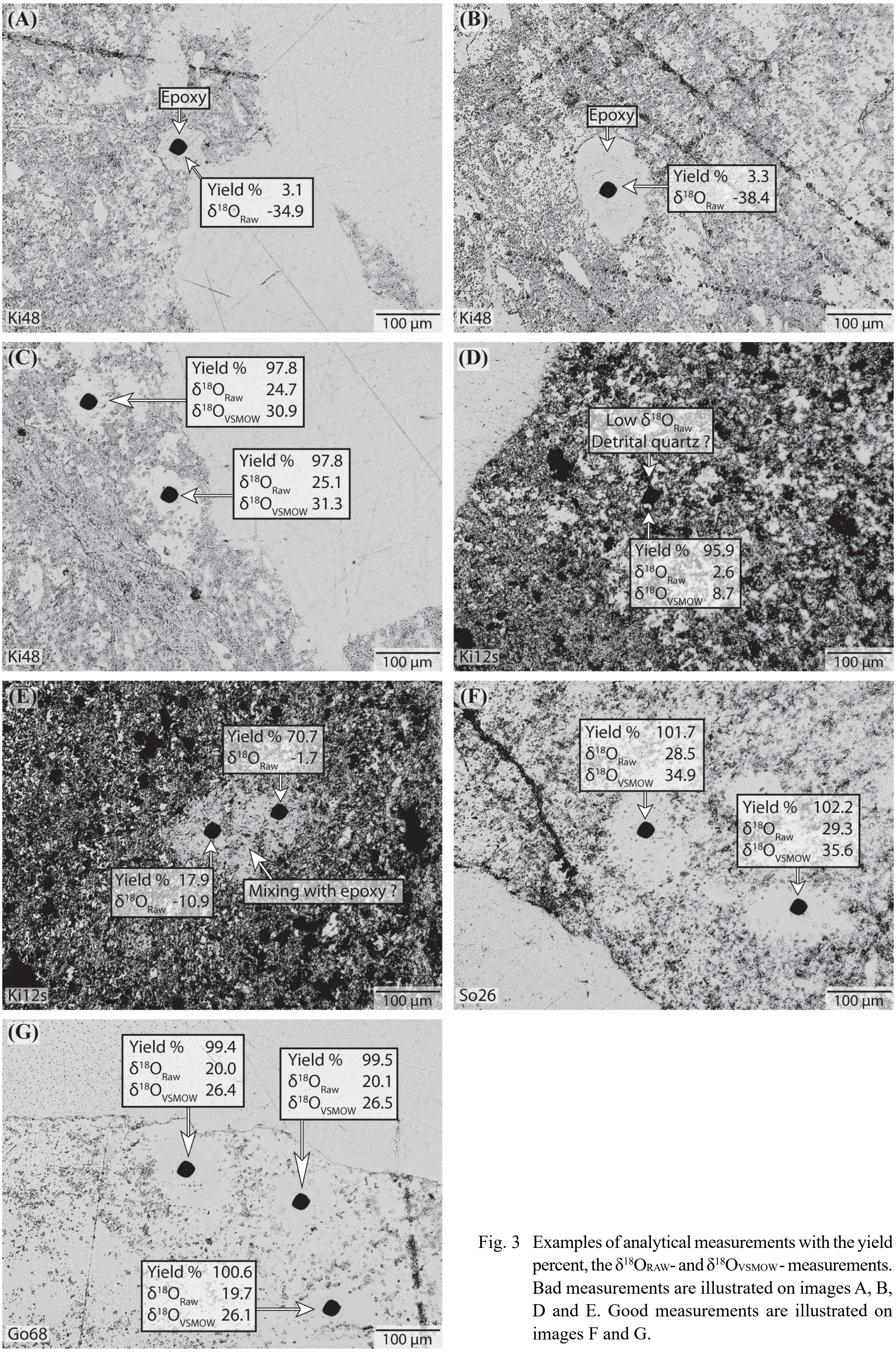

Fig. 3 Examples of analytical measurements with the yield percent, the $\delta^{18}O_{RAW}$- and $\delta^{18}O_{VSMOW}$- measurements. Bad measurements are illustrated on images A, B, D and E. Good measurements are illustrated on images F and G.

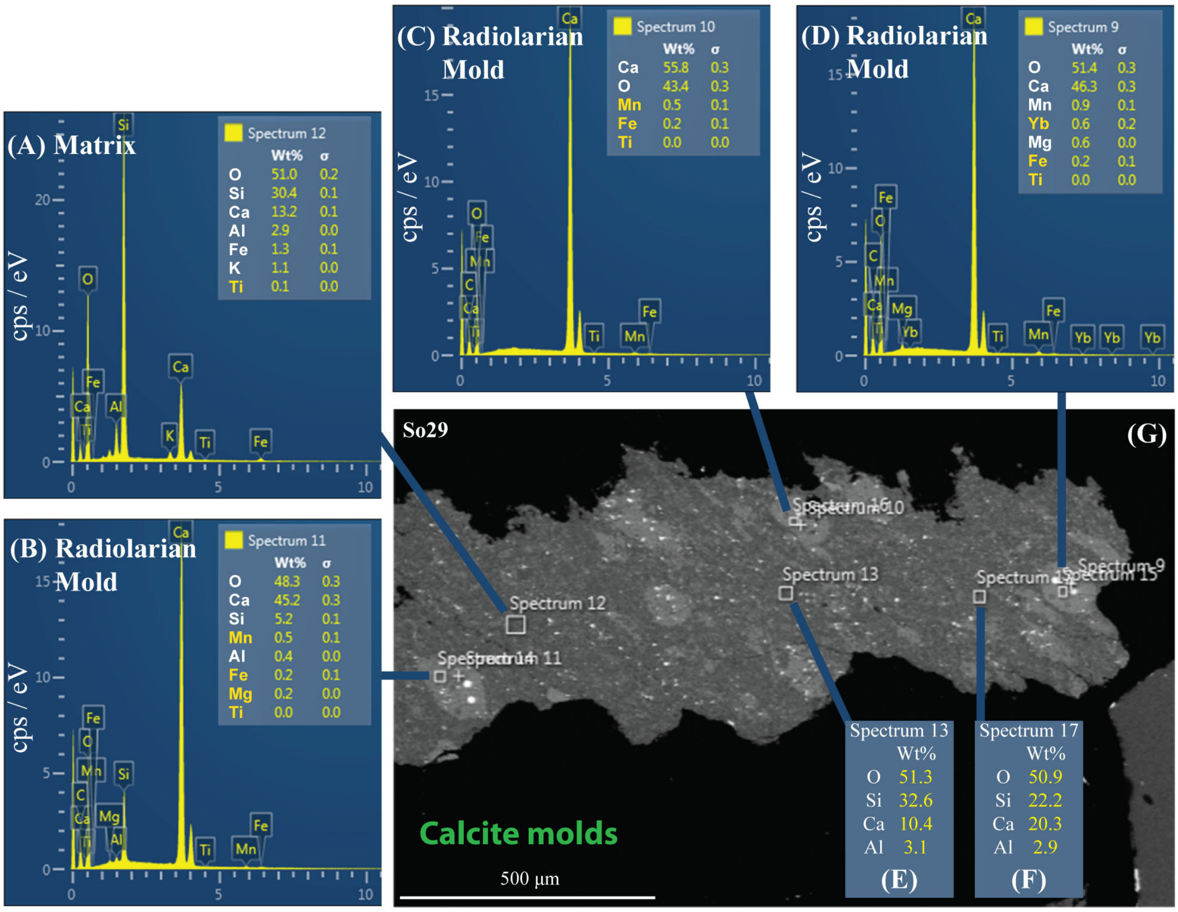

Fig. 4 EDX analyses of sample So29 with SEM. The EDX spectrums prove that the molds were filled with calcites in this sample (B, C and D) during diagenesis. The δ^{18}O- and δ^{30}Si-yields were respectively about 130.2 % and 11 % of the UNIL-Q1 quartz standard yield. The matrix is more siliceous but also included some carbonates (A, E, F). BSE image is show in (G).

are 25.4 ± 1.8 ‰ (27 points, 2SD) for radiolarians, 23.6 ± 1.2 ‰ (3 points, 2SD) for the matrix and 10.5± 0.4 ‰ (16 points, 2SD) for NIST-610. Uncalibrated δ^{18}O-results for Ca01 after drift correction are 29.0 ± 1.6 ‰ (11 points, 2SD) for sample and 10.6 ± 0.2 ‰ (8 points, 2SD) for NIST-610.

The samples Pi01, Ca01 and Ki08C were then measured together during a single session relative to UNIL-Q1 (PRIM123) to calibrate oxygen isotopes correcting instrumental mass fractionation due to the mineralogy of samples (chemical composition and crystal structure). Uncalibrated δ^{18}O-results after drift correction for this UNIL-Q1 session are 6.5 ± 0.3 ‰ (48 points, 2SD) for UNIL-Q1, 31.2 ± 0.7 ‰ (32 points, 2SD) for Pi01, 27.4 ± 1.2 ‰ (86 points, 2SD) for Ki08C, and 30.9 ± 0.4 ‰ (10 points, 2SD) for Ca01, respectively. Measurements of the base, middle and top of samples Ki08C are 27.3 ± 0.6 ‰ (4 points, 2SD), 27.9 ± 1 ‰ (28 points, 2SD) and 27.0 ± 1 ‰ (15 points, 2SD), respectively, with the average value of 27.4 ± 1.2 ‰ (86 points, 1SD).

Between the NIST-610 and the UNIL-Q1 sessions, we observed an δ^{18}O-offset of ~2.4 ± 1.2 ‰ for the uncalibrated δ^{18}O of the samples Pi01, Ki08C and Ca01. However, the δ^{18}O-results for Ki08C are systematically lighter of about 3.3 ± 0.9 ‰ (2SD) than the two other samples (Pi01 and Ca01). Moreover, it is interesting to note that UNIL-Q1 has an uncalibrated δ^{18}O of 6.5 ± 0.3 ‰ during the PRIM123 session whereas UNIL-Q1 has an average value of 4.0 ± 0.7 ‰ during the other session, and that correspond relatively well with the ~2.4 ± 1.2 ‰ offset detected (Table 2).

4. 3 Mesozoic $\delta^{18}O_{radiolarians}$ trends and fluctuations

Here, we present the $\delta^{18}O_{VSMOW}$ trends after having checked and calibrated our results (Fig. 7 and Fig. 8). The Early Triassic to Early Jurassic Panthalassan samples from the Inuyama area have least square means (LS-means) $\delta^{18}O_{VSMOW}$ range from 20.9 ‰ to 32.6 ‰. The Early to Middle Triassic LS-means $\delta^{18}O_{VSMOW}$ range from 20.9 ‰ to 31.9 ‰ with a slightly increasing trend. The Late Triassic LS-means $\delta^{18}O_{VSMOW}$ range has relatively low variation between 30.6 ‰ to 32.6 ‰. The Early Jurassic LS-means $\delta^{18}O_{VSMOW}$ range from 21.9 ‰ to 30.8 ‰ with a decreasing trend.

In the Middle Jurassic Lombardian basin of the Tethys, the LS-means $\delta^{18}O_{VSMOW}$ values are relatively high from

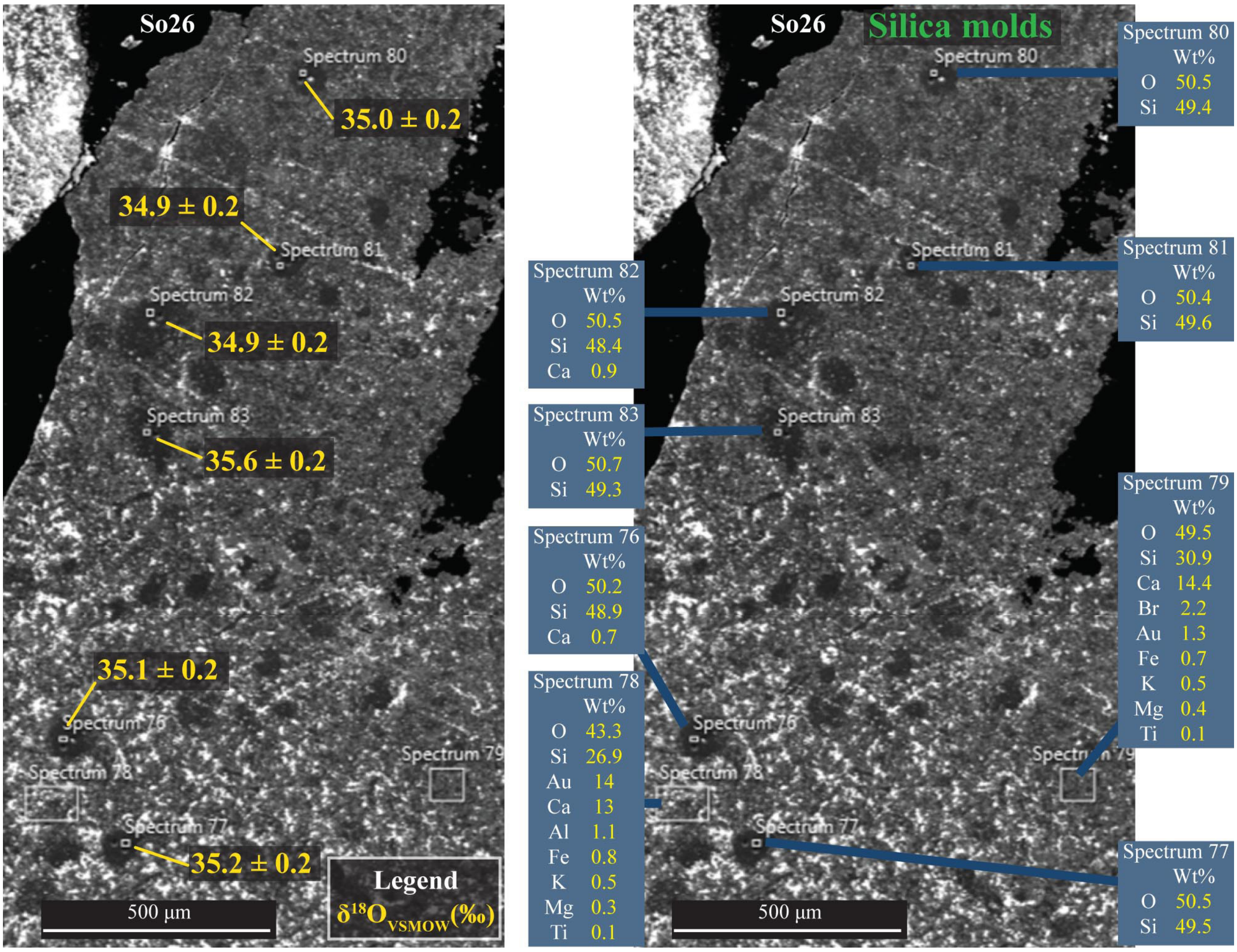

Fig. 5 Comparison between $\delta^{18}O_{VSMOW}$ and the chemical composition estimated by SEM-EDX spectrum in sample So26.

32.3 ‰ to 35.3 ‰. Our Middle Jurassic radiolarite sample from southern Switzerland (Pi01) has a LS-mean of 34.6 ‰, which is coherent with the other $\delta^{18}O$ range from the Sogno section in north Italy. A Berriasian diagenetic chert (Ca01) from the Lombardian basin has similar LS-means of 34.3 ‰. However, our Middle Jurassic Romanian sample (Ro01) has lighter $\delta^{18}O_{VSMOW}$ (30.9 ‰).

For the Cretaceous, the $\delta^{18}O_{VSMOW}$ values of the Goshikigahama samples are relatively light. A Hauterivian sample has a LS-mean 26.5 ‰, and two other Cenomanian samples have LS-means of 28.5 ‰ and 19.8 ‰.

5. Discussion

5. 1 Quality of the SIMS analysis

To evaluate quality of SIMS results, we examined analytical yields relative to UNIL-Q1 yield, in addition to optical check. We rejected analytical spots with low yield values, generally <90 %, potentially the measurement of a mixing with epoxy or other minerals. Even if the spot analysed of the Early Triassic Inuyama shale sample Ki12s on Fig. 3D was discarded after optical control, it is interesting to note that it has one of the best analytical yield (94.9 %) of the spots measured in Ki12s. In this sample, radiolarian molds are scarce, but quartz patches are common. The quartz patches are potentially precipitated radiolarian silica, but could be a diagenetic product. Its $\delta^{18}O_{RAW}$ is very light (2.8 ‰), corresponding to a calibrated $\delta^{18}O_{VSMOW}$ of 8.7 ‰. Such light value is common for igneous quartz (e.g. Seitz *et al.*, 2016), metamorphic quartz or eventually diagenetic quartz (cf. Bindeman, 2008), but not for radiolarian molds (e.g. Viswanathan and Mahabaleswar, 2014). We thus discarded this measurement.

The chemical composition of some excluded molds was also checked by SEM-EDX. SEM-EDX shows calcium as the first major element of the radiolarian molds in chert sample So29 from Sogno section (Fig. 4), and too high analytical $\delta^{18}O$-yields (~130.2 %) were measured in this sample. Therefore, the chemical composition of these radiolarian molds is necessary to be checked before interpretation of isotopic data. In total, 53 samples and 507 measurements passed our checking from the initial 55 samples and 532 measurements.

Calibration of our measurements requires to know the nature of our samples (mineralogy and chemical

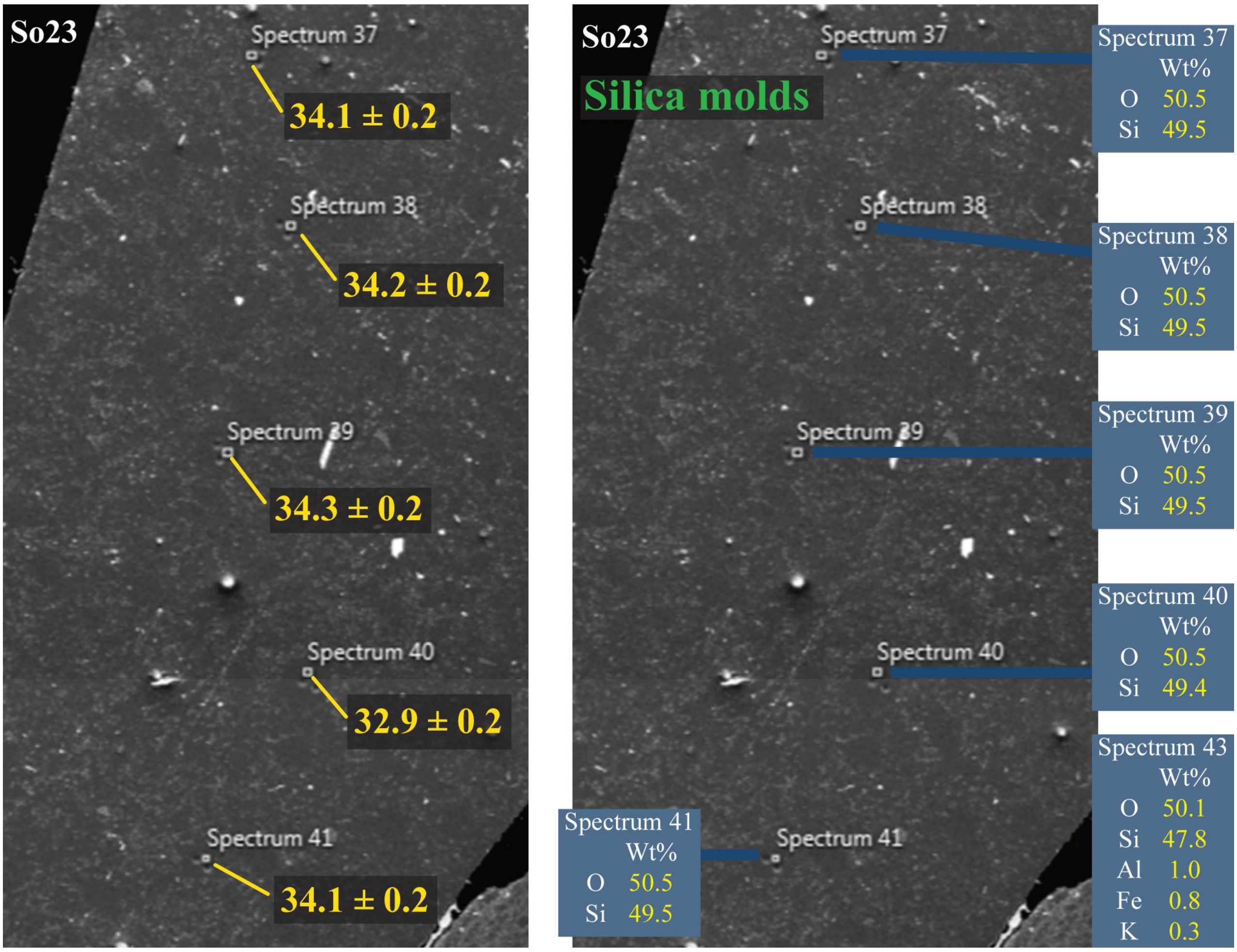

Fig. 6 Comparison between $\delta^{18}O_{VSMOW}$ and the chemical composition estimated by SEM-EDX spectrum in sample So23.

composition), because it affects the instrumental fractionation. If we correct the offset of 2.4 ± 1.2 ‰ between the NIST-610 glass standard and the UNIL-Q1 quartz standard using the initial chert samples (Pi01, Ki08C, and Ca01) as references, values of the UNIL-Q1 standards should be about 6.4 ‰ lighter than the NIST standard. This difference is in contradiction with absolute value of UNIL-Q1 standard (9.81 ± 0.14 ‰, VSMOW, 2SD) and of NIST-610 standard (10.79 ‰, VSMOW following GEOREM database from Jochum *et al.*, 2005), and might be explained by different instrumental fractionations between quartz and silica glass (amorphous material). Similar instrumental fractionations having already been inferred between microquartz, filling radiolarian molds, and quartz (Marin *et al.*, 2010), it is likely that the instrumental fractionation is different with silica glass. Higher uncalibrated $\delta^{18}O$ values for radiolarian molds (25.4 ± 1.8 ‰, 2SD) than for the matrix (23.6 ± 1.2 ‰, 2SD) in sample Ki08C might also be the result of a different instrumental fractionation between pure quartz in radiolarian molds and the mineral mixture in the matrix (matrix effect).

The $\delta^{18}O$-values relative to VSMOW calibrated by UNIL-Q1 are 34.55 ± 0.4 ‰ (32 points, 1SD) for Pi01, 30.75 ± 0.61 ‰ (86 points, 1SD) for Ki08C and 34.33 ± 0.23 ‰ (10 points, 1SD) for Ca01. These intra-sample and inter-sample $\delta^{18}O$-variability in radiolarite molds are larger than instrumental resolution (<0.3 ‰, 2SD), indicating that our measurements represent some signatures in addition to instrumental uncertainties.

Our $\delta^{18}O_{VSMOW}$ ranges from LS-means (19.8 ‰ to 35.3 ‰; Fig. 8) is also consistent with the 18 ‰ to 38 ‰ of bulk $\delta^{18}O_{VSMOW}$ of Phanerozoic cherts by Knauth (1973). This further supports the validity of our SIMS $\delta^{18}O$ measurements and our calibration routine.

5. 2 SIMS $\delta^{18}O$ from radiolarian molds and diagenetic effects

We here discuss some of the factors influencing the $\delta^{18}O_{radiolarians}$ based on our data and comparison with other dataset. Numbers of factors could have influenced on $\delta^{18}O_{radiolarians}$ in Mesozoic cherts, including such as: 1) temperature and $\delta^{18}O$ of seawater for oxygen in original radiolarian opal-A as referred for diatoms (e.g. Juillet-Leclerc and Labeyrie, 1987; Brandriss *et al.*, 1998), 2) Vital effects (Swann *et al.* 2007), 3) Dissolution and

Table 3 Comparison of our SIMS δ^{18}O least square means and standard deviations (in ‰; 2SD) for the samples Pi01, Ki08C and Ca01 between their NIST-610 and UNIL-Q1 sessions. Raw δ$^{18}O_{VSMOW}$ of our samples are slightly shifted between the NIST-610 and UNIL-Q1 sessions due to changes of the analytical parameters but they conserve a similar pattern (~2.5 ‰). Least square standard deviations do not change between raw and drift corrected δ$^{18}O_{VSMOW}$ indicating that there were no major instrumental drifts during our sessions.

Session	Sample	Points	Yield (CPS/nA) Mean	Yield (CPS/nA) Std	Yield % relative to NIST-610	Raw δ$^{18}O_{VSMOW}$ (‰) LS-Mean	Raw δ$^{18}O_{VSMOW}$ (‰) LS-Std	Drift corrected δ$^{18}O_{VSMOW}$ (‰) LS-Mean	Drift corrected δ$^{18}O_{VSMOW}$ (‰) LS-Std	Calibrated δ$^{18}O_{VSMOW}$ (‰) LS-Mean	Calibrated δ$^{18}O_{VSMOW}$ (‰) LS-Std
NIST Sessions	NIST-610	5	9.37E+08	4.55E+06		10.5	0.2	10.4	0.2		
	Pi01	10	9.65E+08	6.18E+06	102.9%	28.2	1.5	28.2	1.5		
	NIST	16	9.28E+08	3.43E+07		10.8	0.4	10.8	0.4		
	Pi01	27	9.49E+08	3.29E+07	102.2%	28.4	5.1	28.4	5.1		
	NIST-610	16	9.04E+08	7.96E+06		10.5	0.4	10.5	0.4		
	Ki08C	27	9.17E+08	1.65E+07	101.5%	25.4	1.8	25.4	1.8		
	Matrix	3	8.96E+08	1.49E+07	99.1%	23.6	1.2	23.6	1.2		
	NIST-610	8	9.41E+08	1.65E+07		10.6	0.2	10.6	0.1		
	Ca01	11	9.52E+08	6.01E+06	101.1%	29.0	1.6	29.0	1.6		
UNIL-Q1 Session	UNIL-Q1	48				6.5	0.3	6.5	0.3	9.8	0.3
	Ki08C base	4				27.3	0.6	27.3	0.6	30.7	0.6
	Ki08C med	28				27.9	1.0	27.9	1.0	31.2	1.0
	Ki08C top	15				27.0	1.0	27.0	1.0	30.4	1.0
	Total Ki08C	86				27.4	1.2	27.4	1.2	30.8	1.2
	Pi01	32				31.2	0.7	31.2	0.7	34.6	0.8
	Ca01	10				30.9	0.4	30.9	0.4	34.3	0.5

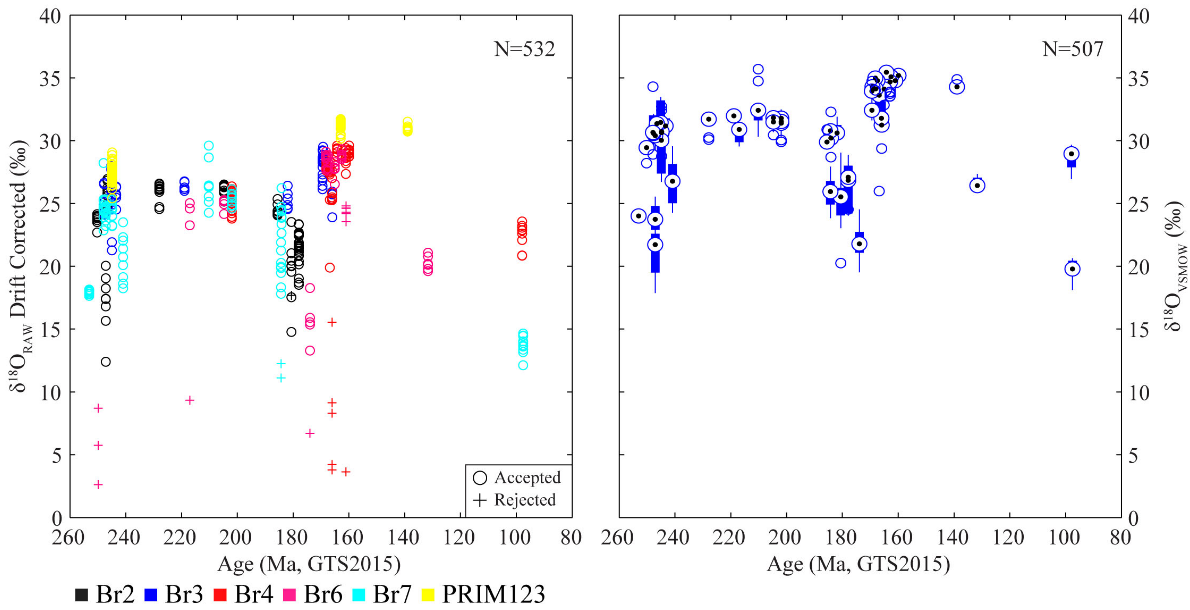

Fig. 7 δ^{18}O-measurements in function of sample mounts on left and boxplot for each sample on the right. For the measurements, each color corresponds to a sample mount showing that samples of similar age tend to converge toward similar δ^{18}O. Cross makers correspond to analyses with lower analytical yields, uncommon internal analytical errors or which did not pass the microscopic checking. Based on these parameters, these values are not considered as valid and excluded for the boxplot diagrams and the average values of samples. Br2 to 7 and PRIM123 are the session names.

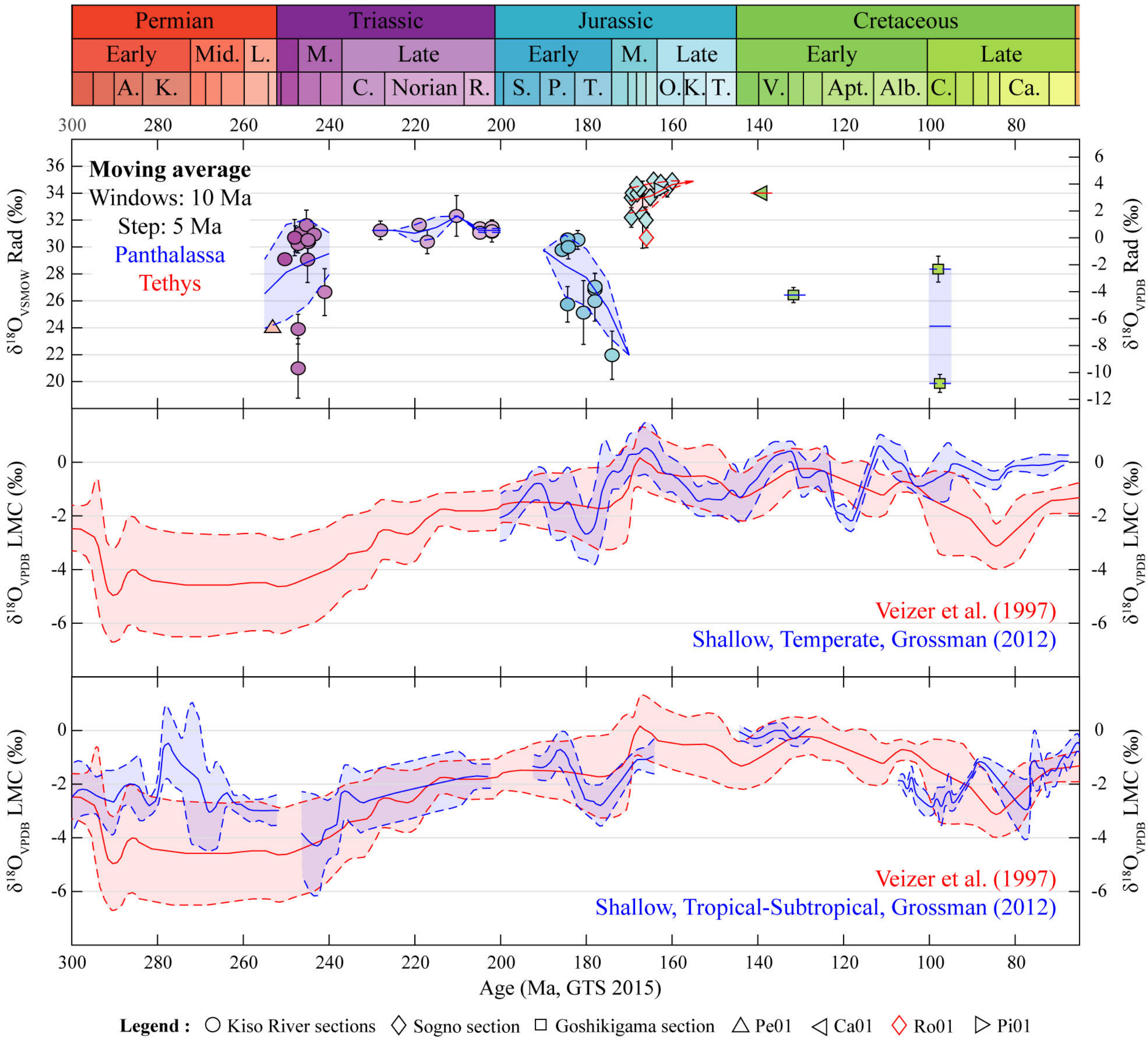

Fig. 8 Comparison between $\delta^{18}O$ from radiolarian silica ($\delta^{18}O$ Rad; this study) and digitalized curves for $\delta^{18}O$ from low magnesium calcite shells ($\delta^{18}O$ LMC; Veizer *et al.*, 1999 and Grossman, 2012), expressed either relative to the Vienna Standard Mean Ocean Water ($\delta^{18}O_{VSMOW}$) or to the Vienna Pee Dee Belemnite standard ($\delta^{18}O_{VPDB}$). The minimum values of $\delta^{18}O$ measured in radiolarian silica correspond to light values in the LMC curves during the Early Triassic, the Toarcian and eventually during the Early Cretaceous. In addition, the Middle Jurassic acme is also recorded with heavier $\delta^{18}O$ in the radiolarites. The geological timescale (GTS 2015) used for this figure is the timescale of the international commission of stratigraphy in 2015 based on Cohen *et al.* (2013). The color filling inside markers corresponds to the color of the geological stage. The boundaries of curves, when plotted, are equivalent to 1SD. The moving averages for radiolarian silica are realized separately for Panthalassa and Tethys using both a 10 Ma windows and 5 Ma steps. The $\delta^{18}O$ error bars correspond to the least square standard deviation of samples presented in Table 2.

dehydroxylation during settling and early diagenesis preferentially releasing light ^{16}O as for diatom frustules (see Schmidt *et al.* 2001; Moschen *et al.*, 2006; Swann and Leng, 2009), 4) Diagenetic temperature and isotopic composition of sediment pore water (e.g. Matheney and Knauth, 1993). In addition to these factors, we can not exclude that $\delta^{18}O$ is also influenced by 5) degree of diagenetic migration of opal-A during the phase transitions from opal-A to quartz via opal-CT, which is mainly controlled by the solubilities of the different phases (e.g. Gunnarsson *et al.*, 2000) and 6) partially by kinetic isotopic fractionation associated with silica tetrahedrons, which at least occur for $\delta^{30}Si$ during silica precipitation under 200 °C (see He and Liu, 2015; Pollington *et al.*, 2016). Factors influencing the kinetic of the phase transitions from opal-A to quartz via opal-CT, such as temperature

(Ernst and Calvert, 1969; Dralus *et al.*, 2011) and pH of pore water associated with the presence of accessory minerals (c.f. Kastner *et al.*, 1977; Isaacs, 1981; Hinman, 1998) might thus also have some influences.

In the Cenozoic unconsolidated sediments, $\delta^{18}O_{radiolarians}$ ranges from 21 ‰ to 35 ‰ in equatorial Pacific (Wu *et al.*, 1997) and from 42 ‰ to 45 ‰ in Southern Ocean (e.g. Abelmann *et al.*, 2015), possibly related with different oceanographic setting. The former $\delta^{18}O_{radiolarians}$ from equatorial Pacific are within the range of our measurements on low latitude Mesozoic deep-sea bedded cherts (19.8 ‰ to 35.3 ‰). Contrary to ~6 ‰ changes in Cenozoic $\delta^{18}O_{benthic\ foraminifera}$ (Zachos *et al.*, 2008), different dwelling depth of radiolarians might be attributed to ~7 ‰ (Katz *et al.*, 2010; Xu *et al.*, 2012; Völpel *et al.*, 2017). Other factor is partial silica dissolution and isotopic enrichment of up to 6.8 ‰ for diatom (Moschen *et al.*, 2006). Because dissolution rate mainly depends on Si undersaturation and pH, fluctuation of $\delta^{18}O$ values amplified the temperature effect. Although contamination of siliciclastics with light $\delta^{18}O$ values, ranging from 10 to 20 ‰ (Eiler, 2001), cannot be rejected, similar ~10 ‰ large fluctuations in pelagic equatorial (paleo-) Pacific $\delta^{18}O_{radiolarians}$ during the Cenozoic and Mesozoic might imply that diagenetic $\delta^{18}O$ shift is insignificant relative to unconsolidated biosiliceous sediments, and that $\delta^{18}O$ from radiolarian molds still preserve an environmental signature after diagenesis.

The cause of spatial variations of $\delta^{18}O_{radiolarians}$ needs to be examined. Our equatorial paleo-Pacific $\delta^{18}O_{radiolarians}$ from Triassic-Early Jurassic Inuyama and Cretaceous Goshikigahama sections (~20 to 32 ‰) is slightly lighter than the low-middle latitude $\delta^{18}O_{radiolarians}$ from the Middle Jurassic Tethys regions (~30 to 35 ‰), although our data cannot reject the possibility of age difference (Fig. 8). In the Tethys region, oppositely, a higher latitude $\delta^{18}O_{radiolarians}$ from Romania is slightly lighter than other data from Italy (Fig. 8). Further spatio-temporal comparison will be needed to understand the nature of $\delta^{18}O_{radiolarians}$ in the past.

The intra-chert variability of $\delta^{18}O$ (0.16 to 2.49 ‰) larger than analytical errors could be related with different degree of diagenesis and/or original variations. Such $\delta^{18}O$ microvariations in cherts have also described from Precambrian chert (Marin *et al.*, 2010). During the transformation from opal-A to opal-CT, the diagenetic migration of opal-A from layers with low-Si content to layers with high-Si content could have homogenized $\delta^{18}O$ within a chert (Isaacs, 1981; Tada, 1991). Subsequent transformation from opal-CT to quartz could have also homogenized through similar mechanism. Nevertheless, significant $\delta^{18}O$-variability in each chert suggests that such diagenetic segregation could not have perfectly homogenized $\delta^{18}O$ within each chert bed, and original variability might be larger.

If original, the intra-sample variations within cherts (0.16 to 2.49 ‰) corresponds to temperature differences of 2.3 to 40.9 °C, using equation from Brandriss *et al.* (1998) with an initial seawater $\delta^{18}O$ of about 0 ‰. A temperature difference of 40.9 °C is certainly too high to reflect original $\delta^{18}O$ from radiolarian skeletons, suggesting possible changes in degree of diagenesis and/or paleoceanographic condition, such as global ice volume, precipitation/evaporation, and/or upwelling of deep-water. Because most of the Mesozoic is ice-free in polar region (e.g. Frakes *et al.*, 1992) and because Triassic-Jurassic Inuyama samples were deposited under equatorial pelagic Panthalassa, changes in upwelling of deep-water, dwelling depth of radiolarians, partial silica dissolution, and diagenesis might be likely cause of the intra-sample variations. The sedimentary rhythms of bedded chert are hypothesized to be linked with periodic changes in upwelling intensity and associated radiolarian productivity based on the systematic changes in cosmic spherule content between chert and mudstone (e.g. Hori *et al.*, 1993). The average duration of a chert-shale couplet is ~20 kyr based on radiolarian and conodont biostratigraphic age model in the early Mesozoic bedded chert sequence in the Inuyama area, Japan, which is consistent with a dominant periodicity of a precession cycle (Hori *et al.*, 1993; Ikeda *et al.*, 2010; Ikeda and Tada, 2014). Therefore, <20 kyr-scale oscillation in radiolarian $\delta^{18}O$ might be preserved in bedded chert to some extent after diagenesis. Further detailed works are necessary to understand this issue.

5. 3 Mesozoic $\delta^{18}O$ trends of radiolarian silica and other proxies

$\delta^{18}O$ of low magnesium carbonate shells (LMC shells) are widely used for paleo-$\delta^{18}O$ of seawater during the Paleozoic and Mesozoic because of their less diagenetic overprint (e.g. Veizer *et al.* 1999; Grossman, 2012). The Mesozoic $\delta^{18}O$ of LMC shells from Tethys ocean shows a ~2 ‰ positive excursion during the Early-Middle Triassic, a relatively stable plateau during the Late Triassic, a large variation with <10-Myr variations during the Early Jurassic, a slight positive excursion during the Middle Jurassic (Fig. 8; Veizer *et al.* 1999; Grossman, 2012).

Although our SIMS measurement of $\delta^{18}O_{radiolarians}$ is low-resolution, our LS-mean data also shows a positive excursion during the Early-Middle Triassic, and relatively stable plateau during the Late Triassic, but up to ~8 ‰ negative excursion is not present in $\delta^{18}O$ curves of LMC shells (Fig. 8). Subsequent ~2 ‰ positive excursion during the Middle Jurassic seems to be also similar (Fig. 8). Although <10 Myr scale variability in our data is also large, similar repetitive measurements on sample Pi01 (uncalibrated LS-means of 28.2 ± 1.5 ‰ and 28.4 ± 5.1 ‰ from 10 and 27 measurements, respectively (2SD)) and Ki08C (27.3 ± 0.6 ‰, 27.9 ± 1.0 ‰, and 27.0 ± 1.0 ‰ from 4, 28, and 15 measurements (2SD)) imply that heterogeneities are well distributed in each chert and that chert could be relatively homogenous at bigger scale. Similar $\delta^{18}O$ trends of LMC shells and radiolarians might imply similar factors controlling these $\delta^{18}O$ records during the Triassic and the Middle Jurassic (Fig. 8).

The cause of the ~8 ‰ negative excursion of radiolarian $\delta^{18}O$ during the Early Jurassic is unclear. Because our data is radiolarian silica of equatorial Panthalassa, various factors can be related, such as differences in paleoceanographic setting, temperature and pH of water column and sediment pore water for early dissolution, diagenetic processes. Considering large scattering of LMC shells records (e.g. Veizer *et al.* 1999; Grossman, 2012), further high-resolution and multi-proxy works are needed to examine this issue.

The $\delta^{18}O$ of conodont apatite ($\delta^{18}O_{conodont}$) is recently used for paleoceanographic analysis, and also shows similar positive excursion during the Early-Middle Triassic, and relatively stable plateau during the Late Triassic (e.g. Trotter *et al.*, 2015). Unfortunately, $\delta^{18}O_{conodont}$ cannot be applied for post-Triassic successions due to the complete extinction of conodont at the end-Triassic extinction (e.g. Clark, 1983). The $\delta^{18}O_{conodont}$ could be useful to compare with $\delta^{18}O_{radiolarians}$ with high-resolution because conodonts co-occur with radiolarians in chert and other siliceous sediments. Further crosscheck with other $\delta^{18}O$-signatures, such as conodont, have to be done to validate radiolarian silica as a paleoceanographic proxy.

6. Concluding remarks

Here we report the in situ $\delta^{18}O_{VPDB}$ -values from Mesozoic radiolarian molds show range between 19.8 to 35.8 ‰, which is consistent with that of modern and Cenozoic radiolarian tests from deep-sea core of equatorial Pacific (Wu *et al.*, 1997). Relatively large variability of $\delta^{18}O$ in intra-chert bed could support $\delta^{18}O$ of the Mesozoic radiolarian tests are not perfectly homogenized in a chert bed during the diagenetic segregation and through time.

The temporal changes in the $\delta^{18}O_{VSMOW}$ values from Mesozoic radiolarian molds show an Early-Middle Triassic slight positive excursion, a Late Triassic high plateau, an Early Jurassic negative excursion with up to 8 ‰, a Middle Jurassic slight positive excursion, and few light values for the Cretaceous. Although the Early Jurassic negative excursion is not consistent with the $\delta^{18}O$ trend of less-diagenetic low-Mg calcite shells in shallow marine Tethys, similar $\delta^{18}O$ trends among radiolarians, LMC shells, and conodonts during the Triassic and the Middle Jurassic imply potential preservation of an environmental component even after diagenesis of biogenic silica. Further crosscheck with other $\delta^{18}O$-signatures have to be done to validate radiolarian silica as a paleoceanographic proxy.

Acknowledgements:We thank the Swiss National Science Foundation (Project Numbers 200021_185067 and 200020_162670) and the University of Lausanne for their financial support. This research was partly supported by grants from the JSPS 2680026 awarded to MI and JSPS Postdoctoral Fellowship for Foreign Researchers awarded to BM.

References

Abelmann, A., Gersonde, R., Knorr, G., Zhang, X., Chapligin, B., Maier, E., Esper, O., Friedrichsen, H., Lohmann, G., Meyer, H. and Tiedemann, R. (2015) The seasonal sea-ice zone in the glacial Southern Ocean as a carbon sink. *Nature Communications*, **6**, 1–13.

Baumgartner, P. O. (1984) A Middle Jurassic−Early Cretaceous low latitude radiolarian zonation based on Unitary Associations and age of Tethyan radiolarites. *Eclogae Geologicae Helvetiae*, **77**, 729–841.

Baumgartner, P. O. (2013) Mesozoic radiolarites–accumulation as a function of sea surface fertility on Tethyan margins and in ocean basins. *Sedimentology*, **60**, 292–318.

Baumgartner, P. O., De Wever, P. and Kocher, R. (1980) Correlation of Tethyan Late Jurassic−Early Cretaceous radiolarian events. *Cahiers de Micropaléontologie*, **2**, 23–86.

Baumgartner, P. O., Matire, L., Goričan, Š., O'Dogherty, L., Erba, E. and Pillevuit, A. (1995) New Middle and Upper Jurassic radiolarian assemblage co-occurring with ammonites and nannofossils from the Southern Alps (Nothern Italy). *In* Baumgartner, P. O., O'Dogherty, L. *et al.*, eds., *Middle Jurassic to Lower Cretaceous radiolaria of Tethys: Occurences, systematics, biochronology. Mémoires Géologie (Lausanne)*, **23**, 737–750.

Bindeman, I. (2008) Oxygen Isotopes in Mantle and Crustal Magmas as Revealed by Single Crystal Analysis. *Reviews in Mineralogy and Geochemistry*, **69**, 445–478.

Bôle, M., Ikeda, M., Baumgartner, P. O., Hori, R. S. and Bouvier A.-S. (2020) SIMS analysis of Si isotope for radiolarian test in Mesozoic bedded chert, Inuyama, central Japan, *Bulletin of Geological Survey of Japan*, **71**, 331–353.

Brandriss, M. E., O'Neil, J. R., Edlund, M. B. and Stoermer, E. F. (1998) Oxygen isotope fractionation between diatomaceous silica and water. *Geochimica et Cosmochima Acta*, **62**, 1119–1125.

Carter, E. S. and Hori, R. S. (2005) Global correlation of the radiolarian faunal change across the Triassic Jurassic boundary. *Canadian Journal of Earth Sciences*, **42**, 777–790.

Channell, J. E. T., Bralower, T. J. and Grandesso, P. (1987) Biostratigraphic correlation of Mesozoic polarity chrons CM1 to CM23 at Capriolo and Xausa (Southern Alps, Italy). *Earth and Planetary Science Letters*, **85**, 203–221.

Clark, D. L. (1983) Extinction of conodonts. *Journal of Paleontology*, **57**, 652–661.

Cohen, K. M., Finney, S. C., Gibbard, P. L. and Fan, J.-X. (2013; updated) The ICS International Chronostratigraphic Chart. *Episodes*, **36**, 199–204.

Davis, E. F. (1918) The radiolarian cherts of the Franciscan

Group. *University of California Publications Bulletin of the Department of Geology*, **11**, 252–432.

Dralus, D., Peters, K. E., Lewan, M. D., Schenk, O., Herron, M. and Tsuchida, K. (2011) Kinetics of the Opal-CT to Quartz Phase Transition Control Diagenetic Traps in Siliceous Shale Source Rock from the San Joaquin Basin and Hokkaido. *AAPG Search and Discovery*, Article # 40771.

Dumitrica, P. (1995) Biostratigraphy of the radiolarites at Pojorîta (Rarău syncline, East Carpathians). *In* Baumgartner, P. O., O'Dogherty, L. *et al.*, eds., *Middle Jurassic to Lower Cretaceous Radiolaria of Tethys: Occurences, systematics, biochronology. Mémoires de Géologie (Lausanne)*, **23**, 907–914.

Eiler, J. M. (2001) Oxygen isotope variations of basaltic lavas and upper mantle rocks. *Reviews in mineralogy and geochemistry*, **43**, 319–364.

Emiliani, C. (1955) Pleistocene temperatures. *The Journal of Geology*, **63**, 538–578.

Ernst, W. G. and Calvert, S. E. (1969) An experimental study of the recrystallization of porcelanite and its bearing on the origin of some bedded cherts. *American Journal of Science*, **267**, 114–133.

Föllmi, K. B., Bôle, M., Jammet, N., Froidevaux, P., Godet, A., Bodin, S., Adatte, T., Matera, V., Fleitmann, D. and Spangenberg, J. E. (2012) Bridging the Faraoni and Selli oceanic anoxic events: late Hauterivian to early Aptian dysaerobic to anaerobic phases in the Tethys. *Climate of the Past*, **8**, 171–189.

Fontorbe, G., Frings, P. J., De La Rocha, C. L., Hendry, J. R. and Conley, D. J. (2016) A silicon depleted North Atlantic since the Palaeogene: Evidence from sponge and radiolarian silicon isotopes. *Earth and Planetary Science Letters*, **453**, 67–77.

Frakes, L. A., Francis, J. E. and Syktus, J. L. (1992) *Climate Modes of the Phanerozoic: the history of the earth's climate over the past 600 million years,* Cambridge Univ Press, 274pp.

Gaetani, M. and Poliani, G. (1978) Il Toarciano ed il Giurassico medio in Albenza (Bergamo). *Rivista Italalina di Paleontologia e Stratigrafia*, **84**, 349–382.

Grossman, E. L. (2012) Oxygen isotope stratigraphy. *In* Gradstein, F.M., Ogg, J.G., Schmitz, M. and Ogg, G., eds., *The Geologic Time Scale 2012*, Elsevier B.V., 181–206.

Gunnarsson, I., Arnorsson, S. and Arnórsson, S. (2000) Amorphous silica solubility and the thermodynamic properties of H_4SiO_4 in the range of 0° to 350 °C at Psat. *Geochimica et Cosmochima Acta*, **64**, 2295–2307.

He, H. and Liu, Y. (2015) Silicon isotope fractionation during the precipitation of quartz and the adsorption of H_4SiO_4(aq) on Fe(III)-oxyhydroxide surfaces. *Chinese Journal of Geochemistry*, **34**, 459–468.

Hein, J. R. and Parrish, J. T. (1987) Distribution of Siliceous Deposits in Space and Time. *In* Hein, J. R., ed., *Siliceous Sediment Rock-Hosted Ores and Petroleum*, Van Nostrand Reinhold Compagny, Inc., New York, 10–57.

Hinman, N. W. (1998) Sequences of silica phase transitions: effects of Na, Mg, K, Al, and Fe ions. *Marine Geology*, **147**, 13–24.

Hori, R. (1988) Some characteristic radiolarians from Lower Jurassic bedded cherts of the Inuyama area, Southwest Japan. *Transactions and proceedings of the Paleontological Society of Japan, New series*, **151**, 543–563.

Hori, R. S., Cho, C. and Umeda, H. (1993) Origin of cyclicity in Triassic-Jurassic radiolarian bedded cherts of the Mino accretionary complex from Japan. *Island Arc*, **2**, 170–180.

Ikeda, M. and Tada, R. (2014) A 70 million year astronomical time scale for the deep-sea bedded chert sequence (Inuyama, Japan): Implications for Triassic–Jurassic geochronology. *Earth and Planetary Science Letters*, **399**, 30–43.

Ikeda, M., Tada, R. and Sakuma, H. (2010) Astronomical cycle origin of bedded chert: A middle Triassic bedded chert sequence. *Earth and Planetary Science Letters*, **297**, 369–378.

Ikeda, M., Bôle, M. and Baumgartner, P. O. (2016) Orbital-scale changes in redox condition and biogenic silica/ detrital fluxes of the Middle Jurassic Radiolarite in Tethys (Sogno, Lombardy, N-Italy): Possible link with glaciation? *Palaeogeography, Palaeoclimatology, Palaeoecology*, **457**, 247–257.

Isaacs, C. M. (1981) Porosity reduction during diagenesis of the Monterey Formation, Santa Barbara coastal area, California. *In* Garrison, R. E. and Douglas, R. G., eds., *The Monterey Formation and related siliceous rocks of California: Los Angeles*. Pacific Section, SEPM, 257–271.

Jaffrés, J. B. D., Shields, G. A. and Wallmann, K. (2007) The oxygen isotope evolution of seawater: A critical review of a long-standing controversy and an improved geological water cycle model for the past 3.4 billion years. *Earth-Science Reviews*, **83**, 83–122.

Jochum, K. P., Nohl, U., Herwig, K., Lammel, E., Stoll, B. and Hoffman, A. W. (2005) GeoReM: A New Geochemical Database for Reference Materials and Isotopic Standards. *Geostandards and Geoanalytical Research*, **29**, 333–338.

Juillet-Leclerc, A. and Labeyrie, L. (1987) Temperature dependence of the oxygen isotopic fractionation between diatom silica and water. *Earth and Planetary Science Letters*, **84**, 69–74.

Kastner, M., Keene, J. B. and Gieskes, J. M. (1977) Diagenesis of siliceous oozes—I. Chemical controls on the rate of opal-A to opal-CT transformation—an experimental study. *Geochimica et Cosmochimica Acta*, **41**, 1041–1059.

Katz, M. E., Cramer, B. S., Franzese, A., Hönisch, B., Miller, K. G., Rosenthal, Y. and Wright, J. D. (2010) Traditional and emerging geochemical proxies in foraminifera. *The Journal of Foraminiferal Research*, **40**, 165–192.

Kidder, D. L. and Erwin, D. H. (2001) Secular Distribution of Biogenic Silica through the Phanerozoic: Comparison of Silica-Replaced Fossils and Bedded Cherts at the Series Level. *The Journal of Geology*, **109**, 509–522.

Kim, S. T., Coplen, T. B. and Horita, J. (2015) Normalization of stable isotope data for carbonate minerals: Implementation of IUPAC guidelines. *Geochimica et Cosmochima Acta*, **158**, 276–289.

Kimura, K. and Hori, R. (1993) Offscraping accretionary process of Jurassic chert-clastic complexes in the Mino-Tamba belt, central Japan. *Journal of Structural Geology*, **15**, 145–161.

Knauth, L. P. (1973) Oxygen and hydrogen isotope ratios in cherts and related rocks. *Doctoral dissertation, California Institute of Technology*, 378p.

Knauth, L. P. and Epstein, S. (1976) Hydrogen and oxygen isotope ratios in nodular and bedded cherts. *Geochimica et Cosmochimic Acta*, **40**, 1095–1108.

Kocher, R. N. (1981) Biochronostratigraphische Untersuchungen oberjurassischer radiolarian führender Gesteine, insbesondere der Südalpen. *Mitteilungen aus dem Geologischen Institut der Eidgenössischen Technische Hochschule und der Univerität Zürich*, **234**, 184p.

Kodama, K., Taira, A., Okamura, M. and Saito, Y. (1983) Paleomagnetism of the Shimanto Belt in Shikoku, Southwest Japan. *In* Hashimoto, M. and Uyeda, H., eds., *Accretion Tectonics in the Circum-Pacific Region*, Terra Scientific Publishing Company, Tokyo, 231–241.

Labeyrie, L. D. (1974) New approach to surface seawater palaeotemperatures using $^{18}O/^{16}O$ ratios in silica of diatom frustules. *Nature*, **248**, 40–42.

Lini, A., Weissert, H. and Erba, E. (1992) The Valanginian carbon isotope event: a first episode of greenhouse climate conditions during the Cretaceous. *Terra Nova*, **4**, 374–384.

Maier, E., Chapligin, B., Abelmann, A., Gersonde, R., Esper, O., Ren, J., Friedrichsen, H., Meyer, H. and Tiedemann, R. (2013) Combined oxygen and silicon isotope analysis of diatom silica from a deglacial subarctic Pacific record. *Journal of Quaternary Science*, **28**, 571–581.

Marin, J., Chaussidon, M. and Robert, F. (2010) Microscale oxygen isotope variations in 1.9 Ga Gunflint cherts: Assessments of diagenesis effects and implications for oceanic paleotemperature reconstructions. *Geochimica et Cosmochimica Acta*, **74**, 116–130.

Matheney, R. K. and Knauth, L. P. (1993) New isotopic temperature estimates for early silica diagenesis cherts. *Geology*, **21**, 519–522.

Mikkelsen, N., Labeyrie, Jr L. and Berger, W. H. (1978) Silica oxygen isotopes in diatoms: A 20,000 yr record in deep-sea sediments. *Nature*, **271**, 536–538.

Mizutani, S. and Koike, T. (1982) Radiolarians in the Jurassic siliceous shale and in the Triassic bedded chert of Unuma, Kagamigahara City, Gifu Prefecture, central Japan. *News of Osaka Micropaleontologists Special Volume*, no. 5, 117–134. (in Japanese with English abstract)

Moschen, R., Lücke, A., Parplies, J., Radtke, U. and Schleser, G. H. (2006) Transfer and early diagenesis of biogenic silica oxygen isotope signals during settling and sedimentation of diatoms in a temperate freshwater lake (Lake Holzmaar, Germany). *Geochimica et Cosmochimica Acta*, **70**, 4367–4379.

Nakaseko, K. and Nishimura, A. (1979) Upper Triassic radiolaria from Southwest Japan. *Science Reports, College of General Education, Osaka University*, **28**, 61–109.

Okamura, M. and Uto, H. (1982) Notes on stratigraphic distributions of radiolarians from the Lower Cretaceous sequence of chert in the Yokonami Melange of Shimanto Belt, Kochi Prefecture, Shikoku. *Research Reports of Kochi University Natural Science*, **31**, 87–94. (in Japanese with English abstract)

Pollington, A. D., Kozdon, R., Anovitz, L. M., Georg, R. B., Spicuzza, M. J. and Valley, J. W. (2016) Experimental calibration of silicon and oxygen isotope fractionations between quartz and water at 250 °C by in situ microanalysis of experimental products and application to zoned low $\delta^{30}Si$ quartz overgrowths. *Chemical Geology*, **421**, 127–142.

Racki, G. and Cordey, F. (2000) Radiolarian palaeoecology and radiolarites: Is the present the key to the past? *Earth-Science Reviews*, **52**, 83–120.

Schmidt, M., Botz, R., Stoffers, P., Anders, T. and Bohrmann, G. (1997) Oxygen isotopes in marine diatoms: a comparative study of analytical techniques and new results on the isotope composition of recent marine diatoms. *Geochimica et Cosmochimica Acta*, **61**, 2275–2280.

Schmidt, M., Botz, R., Rickert, D., Bohrmann, G., Hall, S. R. and Mann, S. (2001) Oxygen isotopes of marine diatoms and relations to opal-A maturation. *Geochimica et Cosmochimica Acta*, **65**, 201–211.

Seitz, S., Baumgartner, L. P., Bouvier, A. S., Putlitz, B. and Vennemann, T. (2016) Quartz Reference Materials for Oxygen Isotope Analysis by SIMS. *Geostandards and Geoanalytical Research*, **41**, 69–75.

Shackleton, N. J. and Kennett, J. P. (1975) Paleotemperature history of the Cenozoic and the initiation of Antarctic glaciation: oxygen and carbon isotope analyses in DSDP Sites 277, 279, and 281. *In* Kennett, J. O., Houtz, R. E. *et al.*, eds., *Initial Reports of the Deep Sea Drilling Project*, **29**, 743–755.

Shemesh, A., Charles, C. D. and Fairbanks, R. G. (1992) Oxygen isotopes in biogenic silica: global changes in ocean temperature and isotopic composition. *Science*, **256**, 1434–1436.

Shemesh, A., Rietti-Shati, M., Rioual, P., Battarbee, R., de

Beaulieu, J.-L., Reille, M., Andrieu, V. and Svobodova, H. (2001) An oxygen isotope record of lacustrine opal from a European Maar indicates climatic stability during the last interglacial. *Geophysical Research Letters*, **28**, 2305–2308.

Stampfli, G. M. and Borel G. D. (2002) A plate tectonic model for Paleozoic and Mesozoic constrained by dynamic plate boundaries and restored synthetic oceanic isochrons. *Earth and Planetary Science Letters*, **196**, 17–33.

Sugiyama, K. (1997) Triassic and Lower Jurassic radiolarian biostratigraphy in the siliceous claystone and bedded chert units of the southeastern Mino Terrane, Central Japan. *Bulletin of the Mizunami Fossil Museum*, **24**, 79–193.

Swann, G. E. A. and Leng, M. J. (2009) A review of diatom $\delta^{18}O$ in palaeoceanography. *Quaternary Science Reviews*, **28**, 384–398.

Swann, G. E. A., Leng, M. J., Sloane, H. J., Maslin, M. A. and Onodera, J. (2007) Diatom oxygen isotopes: evidence of a species effect in the sediment record. *Geochemistry, Geophysics, Geosystems*, **8**, 1–10.

Swann, G. E. A., Leng, M. J., Sloane, H. J. and Maslin, M. A. (2008) Isotope offsets in marine diatom $\delta^{18}O$ over the last 200 ka. *Journal of Quaternary Science*, **23**, 389–400.

Tada, R. (1991) Origin of rhythmical bedding in middle Miocene siliceous rocks of the Onnagawa Formation, northern Japan. *Journal of Sedimentary Research*, **61**, 1123–1145.

Trotter, J. A., Williams, I. S., Nicora, A., Mazza, M. and Rigo, M. (2015) Long-term cycles of Triassic climate change: a new $\delta^{18}O$ record from conodont apatite. *Earth and Planetary Science Letters*, **415**, 165–174.

Veizer, J., Ala, D., Azmy, K., Bruckschen, P., Buhl, D., Bruhn, F., Carden, G. A. F., Diener, A., Ebneth, S. and Godderis, Y. (1999) $^{87}Sr/^{86}Sr$, $\delta^{13}C$ and $\delta^{18}O$ evolution of Phanerozoic seawater. *Chemical Geology*, **161**, 59–88.

Viswanathan, S. and Mahabaleswar, B. (2014) Silicate oxygen isotope geochemistry: History, principles, techniques, and application to petrological problems. *Journal of the Geological Society of India*, **83**, 47–53.

Völpel, R., Paul, A., Krandick, A., Mulitza, S. and Schulz, M. (2017) Stable water isotopes in the MITgcm. Geoscientific Model Development, 10, 3125-3144.

Weissert, H., McKenzie, J. and Hochuli, P. (1979) Cyclic anoxic events in the Early Cretaceous Tethys Ocean. *Geology*, **7**, 147–151.

Wu, S., Ding, T., Meng, X. and Bai, L. (1997) Determination and geological implication of 0-Si isotope of the sediment core in the CC area, the Pacific Ocean. *Chinese Science Bulletin*, **42**, 1462–1465.

Xu, X., Werner, M., Butzin, M. and Lohmann, G. (2012) Water isotope variations in the global ocean model MPI-OM. *Geoscience Model Development*, **5**, 809–818.

Yao, A., Matsuda, T. and Isozaki, Y. (1980) Triassic and Jurassic radiolarians from the Inuyama area, central Japan. *Journal of Geosciences Osaka City University*, **23**, 135–154.

Yao, A. and Kuwahara, K. (1997) Radiolarian faunal change from Late Permian to Middle Triassic times. *News of Osaka Micropaleontolists, Special Volume*, no. 10, 87–96.

Zachos, J. C., Dickens, G. R. and Zeebe, R. E. (2008) An early Cenozoic perspective on greenhouse warming and carbon-cycle dynamics. *Nature*, **451**, 279–283.

Recieved January 7, 2019
Accepted October 20, 2020

Appendix

Table A1 Least square drift corrected and calibrated $\delta^{18}O$ measurements for each sample and for each accepted analyses. All $\delta^{18}O$ are relative to VPDB and all standard deviations are given as 2SD.

Sample		Pe01	Ki09	Ki12s	Ki01	Ki02	Ki03s	Ki03s	Ki03	Ki04	Ki06	Ki07
age		253.15	250.30	249.9	248	247.80	247.20	247.20	247.20	246.60	245.25	245.00
LS-mean ($\delta^{18}O_{VSMOW}$) and LS-Standard deviation (2SD) (‰)		23.99 ± 0.33	29.27 ± 0.88		30.93 ± 2.81	30.83 ± 2.01	20.92 ± 4.61	23.92 ± 2.29	30.44 ± 1.38	31.27 ± 1.8	31.88 ± 2.32	29.25 ± 3.55
Number of measurements		10	9	6	10	6	4	5	10	9	6	6
Accepted measurements		10	9	0	10	6	4	5	10	9	6	6
Rejected measurements				6								
$\delta^{18}O_{VSMOW}$ and analytical standard deviation (2SD) of all accepted measurements (‰)	1	24.04 ± 0.18	29.2 ± 0.31		28.91 ± 0.2	29.59 ± 0.21	22.31 ± 0.32	24.55 ± 0.25	30.24 ± 0.2	30.04 ± 0.12	31.42 ± 0.13	30.39 ± 0.25
	2	23.86 ± 0.22	29.45 ± 0.19		30.53 ± 0.18	32.13 ± 0.19	22.9 ± 0.22	22.92 ± 0.19	30.87 ± 0.19	30.19 ± 0.19	30.81 ± 0.19	31.03 ± 0.24
	3	23.97 ± 0.2	29.48 ± 0.16		30.59 ± 0.13	30.58 ± 0.16	21.15 ± 0.2	22.9 ± 0.22	30.5 ± 0.13	30.5 ± 0.27	31.49 ± 0.23	27.39 ± 0.25
	4	23.99 ± 0.22	29.35 ± 0.18		31.29 ± 0.13	30.18 ± 0.15	17.87 ± 0.14	23.75 ± 0.24	31.37 ± 0.2	31.36 ± 0.17	33.2 ± 0.19	29.99 ± 0.24
	5	23.67 ± 0.25	29.54 ± 0.19		31.38 ± 0.26	30.57 ± 0.2		25.55 ± 0.21	30.09 ± 0.33	32.5 ± 0.21	30.93 ± 0.17	26.73 ± 0.21
	6	24.15 ± 0.19	29.68 ± 0.18		30.97 ± 0.25	32.02 ± 0.22			30.31 ± 0.18	31.15 ± 0.18	33.48 ± 0.17	30.08 ± 0.23
	7	23.79 ± 0.21	29.47 ± 0.19		34.3 ± 0.17				31.4 ± 0.26	31.6 ± 0.25		
	8	24.15 ± 0.24	28.21 ± 0.2		30.45 ± 0.23				29.7 ± 0.23	31.8 ± 0.18		
	9	24.07 ± 0.21	29.05 ± 0.17		29.96 ± 0.2				30.78 ± 0.17	32.36 ± 0.16		
	10	24.18 ± 0.23			30.72 ± 0.2				29.26 ± 0.13			
	11											
	12											
	13											
	14											
	15											
	16											
	17											
	18											
	19											
	20											
Session		Br7	Br2	Br6	Br7	Br3	Br2	Br2	Br7	Br2	Br3	Br3
Sample order during the session		8	6	7	11	8	1	2	5	8	6	3

Sample		Ki08	Ki08					Ki58C	Ki57	Ki15	Ki51	Ki48
age		244.9	244.9					243.48	241.00	228.00	219.00	217.09
LS-mean ($\delta^{18}O_{VSMOW}$) and LS-Standard deviation (2SD) (‰)		30.58 ± 2.05	30.75 ± 1.21					31.16 ± 1.32	26.76 ± 3.62	31.49 ± 1.43	31.91 ± 0.68	30.61 ± 1.83
Number of measurements		10	86					6	10	10	6	6
Accepted measurements		10	86					6	9	10	6	3
Rejected measurements									1			3
$\delta^{18}O_{VSMOW}$ and analytical standard deviation (2SD) of all accepted measurements (‰)	1	30.05 ± 0.23	30.9 ± 0.2	32.43 ± 0.17	30.12 ± 0.1	30.81 ± 0.18	30.34 ± 0.12	31.78 ± 0.2	24.27 ± 0.25	31.74 ± 0.18	31.76 ± 0.22	29.55 ± 0.21
	2	30.58 ± 0.18	30.64 ± 0.18	31.25 ± 0.23	29.77 ± 0.17	30.4 ± 0.16	30.01 ± 0.12	31.22 ± 0.24	26.78 ± 0.24	31.47 ± 0.2	32.23 ± 0.25	31.33 ± 0.19
	3	32.72 ± 0.22	30.89 ± 0.15	30.79 ± 0.22	30.11 ± 0.2	30.78 ± 0.1	30 ± 0.17	30 ± 0.24	27.45 ± 0.18	30.25 ± 0.2	31.49 ± 0.16	30.9 ± 0.18
	4	29.25 ± 0.23	30.25 ± 0.17	30.68 ± 0.17	30.3 ± 0.15	30.91 ± 0.11	30.9 ± 0.21	31.84 ± 0.22	26.13 ± 0.22	32.13 ± 0.26	32.2 ± 0.24	
	5	30.92 ± 0.31	31.73 ± 0.14	30.68 ± 0.16	30.09 ± 0.27	30.36 ± 0.12	30.54 ± 0.14	31.13 ± 0.17	29.56 ± 0.18	31.92 ± 0.16	31.63 ± 0.2	
	6	29.3 ± 0.2	31.02 ± 0.14	31.04 ± 0.16	30.35 ± 0.17	30.94 ± 0.15	30.26 ± 0.16	30.95 ± 0.21	28.09 ± 0.19	31.69 ± 0.25	32.25 ± 0.17	
	7	30.7 ± 0.19	30.31 ± 0.16	30.91 ± 0.2	29.84 ± 0.17	30.63 ± 0.14			24.64 ± 0.23	32.07 ± 0.25		
	8	31.35 ± 0.21	31.01 ± 0.2	30.95 ± 0.18	30.25 ± 0.1	30.08 ± 0.17			28.36 ± 0.26	31.88 ± 0.2		
	9	30.9 ± 0.21	30.96 ± 0.19	31.24 ± 0.12	30.49 ± 0.1	30.15 ± 0.12			25.16 ± 0.19	30.09 ± 0.26		
	10	30.08 ± 0.26	31.3 ± 0.22	30.52 ± 0.18	31.19 ± 0.18	30.23 ± 0.16				31.61 ± 0.24		
	11		31.22 ± 0.21	30.66 ± 0.17	30.64 ± 0.2	31 ± 0.18						
	12		31.16 ± 0.16	32.22 ± 0.14	30.32 ± 0.15	30.64 ± 0.14						
	13		30.83 ± 0.14	30.51 ± 0.17	30.54 ± 0.21	30.8 ± 0.14						
	14		31.48 ± 0.11	31.11 ± 0.23	30.34 ± 0.15	28.77 ± 0.16						
	15		31.25 ± 0.14	31.44 ± 0.19	29.51 ± 0.13	30.61 ± 0.16						
	16		31.31 ± 0.16	31.17 ± 0.14	31.93 ± 0.15	30.64 ± 0.14						
	17		31.74 ± 0.19	30.4 ± 0.18	30.88 ± 0.2	31 ± 0.12						
	18		31.7 ± 0.18	29.8 ± 0.17	31.79 ± 0.19	30.63 ± 0.17						
	19		31.81 ± 0.21	30.9 ± 0.18	30.42 ± 0.18	31.22 ± 0.16						
	20		31.77 ± 0.15	30.24 ± 0.16	30.58 ± 0.19	30.76 ± 0.15						
Session		Br7	PRIM123					Br3	Br7	Br2	Br3	Br6
Sample order during the session		3	1					7	6	7	4	2

Table A1 Continued.

Sample	Ki46	Ki43s	Ki44	Ki39	Ki40	Ki41	Ki42	Ki35	Ki34s	Ki34s	Ki32
age	210.27	204.82	204.82	201.50	201.50	201.50	201.5	185.62	184.37	184.37	184.20
LS-mean ($\delta^{18}O_{VSMOW}$) and LS-Standard deviation (2SD) (‰)	**32.59 ± 3.13**	**31.3 ± 0.89**	**31.65 ± 0.86**	**31.41 ± 1.05**	**31.72 ± 1.17**	**31.38 ± 1.57**	**31.42 ± 0.94**	**29.98 ± 0.81**	**25.82 ± 2.74**	**30.79 ± 0.3**	**30.21 ± 1.83**
Number of measurements	10	6	9	9	10	10	10	9	9	1	10
Accepted measurements	10	6	9	9	10	10	10	9	8	1	10
Rejected measurements									1		
$\delta^{18}O_{VSMOW}$ and analytical standard deviation (2SD) of all accepted measurements (‰) 1	31.63 ± 0.22	31.47 ± 0.25	31.44 ± 0.19	30.79 ± 0.15	31.88 ± 0.17	31.46 ± 0.25	32.2 ± 0.19	29.95 ± 0.25	23.83 ± 0.12	30.79 ± 0.3	29.98 ± 0.17
2	30.32 ± 0.19	31.57 ± 0.14	31.95 ± 0.2	31.51 ± 0.12	31.46 ± 0.24	32.49 ± 0.16	31.2 ± 0.18	30.47 ± 0.28	27.29 ± 0.21		30.43 ± 0.22
3	32.43 ± 0.21	31.25 ± 0.22	32 ± 0.22	32.08 ± 0.24	32.28 ± 0.16	31.33 ± 0.18	30.66 ± 0.25	29.88 ± 0.17	25.5 ± 0.28		29.41 ± 0.16
4	32.51 ± 0.15	31.52 ± 0.22	32.06 ± 0.24	32.16 ± 0.19	31.79 ± 0.23	31.84 ± 0.15	30.94 ± 0.18	29.72 ± 0.2	26 ± 0.21		30.55 ± 0.2
5	34.75 ± 0.22	30.46 ± 0.18	30.69 ± 0.22	30.52 ± 0.17	32.12 ± 0.21	29.91 ± 0.19	30.88 ± 0.2	29.59 ± 0.26	27.94 ± 0.29		28.69 ± 0.25
6	32.41 ± 0.14	31.56 ± 0.19	31.91 ± 0.19	31.39 ± 0.14	31.71 ± 0.26	30.34 ± 0.18	31.85 ± 0.19	29.65 ± 0.14	24.35 ± 0.26		29.96 ± 0.18
7	32.47 ± 0.18		31.83 ± 0.19	31.69 ± 0.28	31.79 ± 0.2	31.28 ± 0.2	31.51 ± 0.19	29.92 ± 0.22	26.31 ± 0.19		30.44 ± 0.24
8	31.2 ± 0.24		31.57 ± 0.19	31.35 ± 0.15	31.94 ± 0.14	31.9 ± 0.19	31.57 ± 0.15	29.9 ± 0.18	25.9 ± 0.2		32.3 ± 0.21
9	32.38 ± 0.2		31.4 ± 0.18	31.55 ± 0.14	30.06 ± 0.24	31.14 ± 0.2	31.73 ± 0.22	30.89 ± 0.29			29.92 ± 0.21
10	35.7 ± 0.18				31.76 ± 0.16	31.96 ± 0.19	31.56 ± 0.16				30.45 ± 0.24
11											
12											
13											
14											
15											
16											
17											
18											
19											
20											
Session	Br7	Br6	Br2	Br4	Br4	Br4	Br7	Br2	Br7	Br7	Br7
Sample order during the session	10	4	9	3	6	8	4	11	2	2	9

Sample	Ki24	Ki25	Ki22c2	Ki22c1	Ki21	Ki20	So07	So08	So09	So12	So13
age	182.00	180.66	178.00	178.00	178.00	174.00	169.50	169.50	169.30	168.27	168.13
LS-mean ($\delta^{18}O_{VSMOW}$) and LS-Standard deviation (2SD) (‰)	**30.76 ± 1.45**	**25.19 ± 4.92**	**26.07 ± 3.07**	**26.97 ± 2.44**	**27.16 ± 2.11**	**21.92 ± 3.73**	**32.47 ± 1.52**	**33.99 ± 0.82**	**34.35 ± 0.83**	**34.96 ± 0.9**	**34.31 ± 0.83**
Number of measurements	6	9	6	9	10	6	6	7	6	6	9
Accepted measurements	6	8	6	9	10	5	6	7	6	6	9
Rejected measurements		1				1					
$\delta^{18}O_{VSMOW}$ and analytical standard deviation (2SD) of all accepted measurements (‰) 1	31.9 ± 0.23	23.04 ± 0.28	24.03 ± 0.25	26.42 ± 0.22	26.33 ± 0.21	19.52 ± 0.21	32.8 ± 0.29	34.01 ± 0.14	34.21 ± 0.22	34.93 ± 0.16	33.99 ± 0.26
2	30.88 ± 0.22	25.56 ± 0.18	26.76 ± 0.31	27.1 ± 0.22	28.02 ± 0.19	21.61 ± 0.26	32.34 ± 0.14	34.74 ± 0.16	33.99 ± 0.15	35.19 ± 0.22	34.36 ± 0.19
3	30.36 ± 0.2	25.96 ± 0.24	24.21 ± 0.22	28.86 ± 0.25	27.14 ± 0.14	21.79 ± 0.28	33.81 ± 0.22	33.89 ± 0.21	34.68 ± 0.31	34.01 ± 0.28	33.74 ± 0.24
4	30.03 ± 0.26	26.56 ± 0.17	26.93 ± 0.2	26.33 ± 0.2	26.64 ± 0.2	22.14 ± 0.24	32.52 ± 0.18	33.95 ± 0.18	34.38 ± 0.14	35.05 ± 0.15	34.83 ± 0.18
5	30.11 ± 0.17	20.26 ± 0.3	27.4 ± 0.26	24.53 ± 0.19	27.95 ± 0.19	24.53 ± 0.21	31.62 ± 0.18	34.15 ± 0.18	33.96 ± 0.14	35.44 ± 0.15	34.04 ± 0.13
6	31.25 ± 0.19	29.06 ± 0.28	27.12 ± 0.21	27.36 ± 0.19	27.04 ± 0.22		31.89 ± 0.21	33.4 ± 0.17	35.02 ± 0.2	34.9 ± 0.19	34.13 ± 0.27
7		25.07 ± 0.17		28.21 ± 0.24	28.88 ± 0.2			33.76 ± 0.22			33.96 ± 0.2
8		25.51 ± 0.13		26.91 ± 0.26	25.91 ± 0.17						34.9 ± 0.12
9				27.22 ± 0.13	28.12 ± 0.21						34.53 ± 0.21
10					25.67 ± 0.2						
11											
12											
13											
14											
15											
16											
17											
18											
19											
20											
Session	Br3	Br2	Br2	Br2	Br2	Br6	Br3	Br3	Br3	Br6	Br4
Sample order during the session	5	10	4	3	5	5	2	1	10	9	4

Table A1 Continued.

Sample		So15	So17	So21	Ro01	So23	So25	P01		So26	So28	So29
age		167.54	166.89	166.09	166.00	165.10	164.31	163.00		162.65	161.14	161.06
LS-mean ($\delta^{18}O_{VSMOW}$) and LS-Standard deviation (2SD) (‰)		**34.68 ± 1.05**	**32.69 ± 5.18**	**32.27 ± 2.04**	**30.92 ± 1.54**	**34.02 ± 1.18**	**35.3 ± 0.65**	**34.55 ± 0.8**		**35.12 ± 0.55**	**34.71 ± 1.37**	
Number of measurements		6	9	11	6	6	9	32		6	9	6
Accepted measurements		6	9	6	6	6	9	32		6	8	0
Rejected measurements				5							1	6
$\delta^{18}O_{VSMOW}$ and analytical standard deviation (2SD) of all accepted measurements (‰)	1	34.58 ± 0.18	33.73 ± 0.15	31.96 ± 0.25	31.2 ± 0.16	34.61 ± 0.2	35.74 ± 0.21	34.74 ± 0.15	34.69 ± 0.17	35.03 ± 0.2	35.38 ± 0.22	
	2	34.99 ± 0.19	33.93 ± 0.28	31.49 ± 0.17	30.85 ± 0.13	34.06 ± 0.16	35.5 ± 0.25	33.54 ± 0.15	34.92 ± 0.1	34.85 ± 0.18	34.52 ± 0.2	
	3	35.18 ± 0.2	33.44 ± 0.23	33.75 ± 0.16	29.38 ± 0.21	32.85 ± 0.2	35.23 ± 0.2	33.53 ± 0.2	34.56 ± 0.18	34.89 ± 0.2	34.81 ± 0.24	
	4	33.92 ± 0.26	25.99 ± 0.21	31.39 ± 0.26	31.29 ± 0.22	34.32 ± 0.17	34.88 ± 0.19	34.73 ± 0.1	33.75 ± 0.14	35.62 ± 0.22	35.15 ± 0.17	
	5	34.12 ± 0.21	31.42 ± 0.2	31.62 ± 0.2	31.42 ± 0.24	34.15 ± 0.16	34.91 ± 0.27	34.75 ± 0.16	34.55 ± 0.17	35.15 ± 0.22	34.75 ± 0.17	
	6	35.15 ± 0.22	33.59 ± 0.13	33.15 ± 0.24	31.39 ± 0.21	34.07 ± 0.17	35.45 ± 0.17	34.59 ± 0.14	34.74 ± 0.1	35.22 ± 0.18	34.33 ± 0.19	
	7		34.01 ± 0.17				34.89 ± 0.18	34.66 ± 0.12	34.48 ± 0.1		33.49 ± 0.13	
	8		34.26 ± 0.24				35.5 ± 0.18	34.88 ± 0.13	35 ± 0.17		35.56 ± 0.2	
	9		33.62 ± 0.17				35.55 ± 0.2	34.71 ± 0.2	34.33 ± 0.14			
	10							34.77 ± 0.15	34.62 ± 0.17			
	11							35.09 ± 0.22	34.84 ± 0.2			
	12							34.92 ± 0.15	34.73 ± 0.11			
	13							34.47 ± 0.16				
	14							34.62 ± 0.1				
	15							33.87 ± 0.13				
	16							33.89 ± 0.2				
	17							34.68 ± 0.13				
	18							34.72 ± 0.17				
	19							34.8 ± 0.16				
	20							34.43 ± 0.16				
Session		Br6	Br4	Br4	Br3	Br6	Br4	PRIM123		Br6	Br4	Br6
Sample order during the session		1	2	10	9	3	7	2		8	1	6

Sample		So31	Ca01	Go68	Go73	Go74
age		159.97	139.00	131.70	97.95	97.59
LS-mean ($\delta^{18}O_{VSMOW}$) and LS-Standard deviation (2SD) (‰)		**35.25 ± 0.57**	**34.33 ± 0.45**	**26.53 ± 1.16**	**28.52 ± 1.99**	**19.76 ± 1.4**
Number of measurements		9		6	9	10
Accepted measurements		9		6	9	10
Rejected measurements						
$\delta^{18}O_{VSMOW}$ and analytical standard deviation (2SD) of all accepted measurements (‰)	1	35.42 ± 0.22	34.27 ± 0.14	27.06 ± 0.26	29.68 ± 0.2	18.12 ± 0.29
	2	35.09 ± 0.19	34.3 ± 0.12	25.89 ± 0.19	26.95 ± 0.18	19.61 ± 0.22
	3	35.76 ± 0.15	34.89 ± 0.17	26.39 ± 0.17	28.71 ± 0.14	20.49 ± 0.23
	4	34.87 ± 0.22	34.18 ± 0.17	26.47 ± 0.26	28.2 ± 0.15	19.36 ± 0.13
	5	34.9 ± 0.24	34.1 ± 0.13	26.06 ± 0.18	28.96 ± 0.18	19.16 ± 0.15
	6	35.1 ± 0.19	34.13 ± 0.13	27.36 ± 0.17	26.96 ± 0.17	20.03 ± 0.14
	7	35.19 ± 0.18	34.36 ± 0.19		29.33 ± 0.19	20.45 ± 0.19
	8	35.42 ± 0.16	34.28 ± 0.17		29 ± 0.22	19.89 ± 0.11
	9	35.32 ± 0.24	34.51 ± 0.2		29.19 ± 0.23	20.65 ± 0.22
	10		34.4 ± 0.19			19.7 ± 0.17
	11					
	12					
	13					
	14					
	15					
	16					
	17					
	18					
	19					
	20					
Session		Br4	PRIM123	Br6	Br4	Br7
Sample order during the session		9	3	10	5	1

Table A2 All the analytical dataset of the samples and standards. This data set include raw information such as the beam intensity (nA) during the analyses, counts per second on the L'2 and H'2 FC for ^{16}O and ^{18}O, respectively, time at which was realized (HH:MM). The raw isotopic ratios (H'2/L'2 ($^{18}O/^{16}O$)) is computed from the counts per second on the L'2 and H'2 FC and transformed into raw $\delta^{18}O$ using the regular formula ($\delta^{18}O=[(^{18}O / ^{16}O)spl / (^{18}O / ^{16}O)ref]- 1$) with VSMOW as reference. For each standard and sample cluster, we calculated mean and standard deviation for raw $\delta^{18}O$. Raw $\delta^{18}O$ were drifted corrected and calibrated using the procedure described in methods. The analytical yield (cps/nA) is calculated from the counts per second on the L'2 FC and the beam intensity.

SIMS ANALYSES							Mount: Pi01		Standard: UNIL-Q1 (Paine)	Analyse: $\delta^{18}O$			Value= 9.81±0.14 (VSMOW, 2σ)				Date: 06.12.2013	
	Beam	H'2/L'2 ($^{18}O/^{16}O$)		L'2 (^{18}O/Coeff)		H'2 (^{16}O/Coeff)		Time	Yield	Measurements (‰)		mean	Drift correction (‰)		Calibration (‰)		Comment	
	nA	*CPS*	*2SD*	*CPS*	*2SD*	*CPS*	*2SD*		CPS/nA	*$\delta^{18}O$*	*2SD int*	*2SD*	*$\delta^{18}O$*	*2SD*	*$\delta^{18}O_{VSMOW}$*	*2SD*		
d18O_NIST_051213	1.76	2.03E-03	6.74E-03	1.65E+09	1.69E-01	3.34E+06	1.71E-01	18:40	937036723.6	10.53	0.07		10.50	0.07			Standard	
d18O_NIST_051213@00	1.75	2.03E-03	9.37E-03	1.62E+09	2.22E-01	3.29E+06	2.24E-01	18:46	929754014.2	10.44	0.09		10.42	0.09			Standard	
d18O_NIST_051213@01	1.76	2.03E-03	8.94E-03	1.66E+09	2.19E-01	3.36E+06	2.21E-01	18:52	940293982.6	10.55	0.09		10.52	0.09			Standard	
d18O_NIST_051213@02	1.75	2.03E-03	8.15E-03	1.65E+09	1.78E-01	3.34E+06	1.77E-01	18:57	940747052.5	10.26	0.08		10.25	0.08			Standard	
d18O_CSDT_051213_Rad@1	1.73	2.06E-03	8.40E-03	1.69E+09	1.88E-01	3.48E+06	1.87E-01	19:03	975833586.0	28.25	0.08		28.24	0.08			Pi01	
d18O_CSDT_051213_Rad@2	1.74	2.06E-03	8.93E-03	1.69E+09	1.88E-01	3.49E+06	1.86E-01	19:09	970639709.1	28.52	0.09		28.51	0.09			Pi01	matrix
d18O_CSDT_051213_Rad@3	1.74	2.06E-03	7.66E-03	1.68E+09	1.39E-01	3.46E+06	1.39E-01	19:14	965642159.9	28.34	0.07		28.33	0.07			Pi01	
d18O_CSDT_051213_Rad@4	1.73	2.06E-03	9.30E-03	1.66E+09	1.75E-01	3.43E+06	1.72E-01	19:20	962178241.0	28.39	0.09		28.39	0.09			Pi01	
d18O_CSDT_051213_Rad@5	1.74	2.06E-03	6.68E-03	1.66E+09	1.47E-01	3.43E+06	1.46E-01	19:25	958772118.2	28.61	0.06		28.62	0.06			Pi01	
d18O_CSDT_051213_Rad@6	1.72	2.06E-03	8.69E-03	1.66E+09	1.76E-01	3.42E+06	1.74E-01	19:31	964038027.7	26.02	0.08		26.03	0.08			Pi01	
d18O_CSDT_051213_Rad@7	1.73	2.06E-03	7.49E-03	1.66E+09	1.85E-01	3.41E+06	1.84E-01	19:37	956921826.6	28.62	0.07		28.64	0.07			Pi01	matrix
d18O_CSDT_051213_Rad@8	1.73	2.06E-03	7.25E-03	1.68E+09	1.75E-01	3.46E+06	1.75E-01	19:43	971843241.2	27.63	0.07		27.65	0.07			Pi01	matrix
d18O_CSDT_051213_Rad@9	1.73	2.06E-03	7.20E-03	1.66E+09	1.67E-01	3.43E+06	1.65E-01	19:48	961408328.6	28.58	0.07		28.60	0.07			Pi01	
d18O_CSDT_051213_Rad@10	1.73	2.06E-03	7.88E-03	1.66E+09	1.76E-01	3.42E+06	1.78E-01	19:54	960327526.0	28.13	0.08		28.16	0.08			Pi01	
d18O_NIST_051213@03	1.74	2.03E-03	9.51E-03	1.64E+09	1.88E-01	3.32E+06	1.89E-01	19:59	939541026.8	10.44	0.09		10.48	0.09			Standard	
d18O_NIST_051213@04	1.74	-5.54E-02	6.84E-03	8.08E+08	2.00E+01	1.61E+06	2.07E+01	20:04	465282628.7	-28621.71	0.00						Standard	Rejected
d18O_NIST_CSDT1_061213_test	1.97	2.03E-03	9.82E-03	1.91E+09	2.92E-01	3.86E+06	2.95E-01	10:08	966977620.6	10.66	0.10						Standard	
d18O_NIST_CSDT1_061213_test@0	1.99	2.03E-03	4.46E-03	1.90E+09	2.65E-01	3.86E+06	2.65E-01	10:13	958449755.8	10.62	0.04						Standard	
d18O_NIST_CSDT1_061213_test@1	1.99	2.03E-03	6.66E-03	1.91E+09	2.76E-01	3.86E+06	2.77E-01	10:19	958940040.1	10.90	0.07						Standard	
d18O_NIST_CSDT1_061213_test@2	1.99	2.03E-03	4.97E-03	1.89E+09	2.14E-01	3.83E+06	2.17E-01	10:24	946796831.9	10.95	0.05						Standard	
d18O_NIST_CSDT1_061213	1.99	2.03E-03	8.31E-03	1.89E+09	2.01E-01	3.82E+06	2.01E-01	10:30	945772952.2	10.94	0.08		10.93	0.08			Standard	
d18O_NIST_CSDT1_061213@1	1.99	2.03E-03	1.01E-02	1.88E+09	1.95E-01	3.81E+06	1.98E-01	10:35	942748647.2	11.09	0.10		11.07	0.10			Standard	
d18O_NIST_CSDT1_061213@2	1.99	2.03E-03	6.50E-03	1.88E+09	2.05E-01	3.82E+06	2.06E-01	10:41	944925425.5	11.04	0.06		11.02	0.06			Standard	
d18O_NIST_CSDT1_061213@3	1.99	2.03E-03	8.73E-03	2.08E+09	3.33E-01	4.21E+06	3.28E-01	10:46	1044254888.4	10.13	0.09		10.12	0.09			Standard	
d18O_CSDT_051213_Rad@2b	1.99	2.06E-03	5.88E-03	1.92E+09	1.03E-01	3.96E+06	1.02E-01	10:52	962957678.9	28.96	0.06		28.95	0.06			Pi01	matrix
d18O_CSDT_051213_Rad@2c	1.99	2.06E-03	8.72E-03	1.90E+09	1.29E-01	3.93E+06	1.30E-01	10:57	957509062.5	28.87	0.08		28.85	0.08			Pi01	matrix
d18O_CSDT_051213_Rad@6b	1.98	2.06E-03	7.34E-03	1.91E+09	1.51E-01	3.94E+06	1.52E-01	11:03	964028824.2	28.66	0.07		28.65	0.07			Pi01	
d18O_CSDT_051213_Rad@7b	1.98	2.06E-03	6.87E-03	1.89E+09	1.17E-01	3.90E+06	1.19E-01	11:09	956315169.9	28.74	0.07		28.73	0.07			Pi01	matrix
d18O_CSDT_051213_Rad@7c	1.97	2.06E-03	7.44E-03	1.90E+09	1.51E-01	3.93E+06	1.54E-01	11:14	964120635.3	28.51	0.07		28.50	0.07			Pi01	matrix
d18O_CSDT_051213_Rad@7d	1.97	2.06E-03	8.10E-03	1.87E+09	1.10E-01	3.86E+06	1.09E-01	11:20	948241294.4	28.67	0.08		28.66	0.08			Pi01	matrix
d18O_CSDT_051213_Rad@8b	1.97	2.06E-03	4.89E-03	1.89E+09	1.25E-01	3.90E+06	1.25E-01	11:25	957616444.5	28.53	0.05		28.52	0.05			Pi01	matrix
d18O_NIST_CSDT1_061213@4	1.97	2.03E-03	8.08E-03	1.82E+09	1.67E-01	3.68E+06	1.67E-01	11:31	923048549.4	10.79	0.08		10.78	0.08			Standard	
d18O_NIST_CSDT1_061213@5	1.96	2.03E-03	6.45E-03	1.81E+09	1.18E-01	3.67E+06	1.18E-01	11:36	920637037.3	10.77	0.06		10.77	0.06			Standard	
d18O_NIST_CSDT1_061213@6	1.96	2.03E-03	1.03E-02	1.81E+09	1.59E-01	3.67E+06	1.58E-01	11:42	925487784.3	10.81	0.10		10.80	0.10			Standard	
d18O_NIST_CSDT1_061213@7	1.95	2.03E-03	6.81E-03	1.82E+09	1.42E-01	3.68E+06	1.43E-01	11:47	929622947.4	10.85	0.07		10.84	0.07			Standard	
d18O_CSDT_051213_Rad@11	1.95	2.06E-03	4.48E-03	1.84E+09	1.64E-01	3.80E+06	1.62E-01	11:53	943272631.9	28.80	0.04		28.80	0.04			Pi01	
d18O_CSDT_051213_Rad@12	1.95	2.06E-03	6.32E-03	1.81E+09	6.63E-02	3.72E+06	6.70E-02	11:58	925184905.1	28.54	0.06		28.54	0.06			Pi01	
d18O_CSDT_051213_Rad@13	1.95	2.06E-03	7.19E-03	1.78E+09	6.82E-02	3.66E+06	7.24E-02	12:04	911993098.8	27.48	0.07		27.47	0.07			Pi01	
d18O_CSDT_051213_Rad@14	1.94	2.06E-03	7.07E-03	1.80E+09	8.37E-02	3.71E+06	8.49E-02	12:09	930176591.5	28.85	0.07		28.85	0.07			Pi01	
d18O_CSDT_051213_Rad@15	1.94	2.06E-03	8.55E-03	1.79E+09	7.33E-02	3.69E+06	7.08E-02	12:15	922862978.0	27.99	0.08		27.99	0.08			Pi01	
d18O_CSDT_051213_Rad@16	1.93	2.06E-03	5.83E-03	1.87E+09	9.65E-02	3.85E+06	8.70E-02	12:21	969055053.1	25.64	0.06		25.64	0.06			Pi01	
d18O_CSDT_051213_Rad@17	1.93	2.06E-03	5.99E-03	1.88E+09	1.39E-01	3.86E+06	1.39E-01	12:26	973256076.8	25.40	0.06		25.40	0.06			Pi01	
d18O_CSDT_051213_Rad@18	1.93	2.05E-03	1.32E-02	2.03E+09	3.54E-01	4.16E+06	3.44E-01	12:32	1052497605.5	22.41	0.13		22.41	0.13			Pi01	
d18O_CSDT_051213_Rad@19	1.92	2.06E-03	8.04E-03	1.89E+09	3.20E-02	3.88E+06	3.50E-02	12:37	985122842.5	25.51	0.08		25.51	0.08			Pi01	
d18O_CSDT_051213_Rad@20	1.92	2.06E-03	7.13E-03	1.81E+09	7.41E-02	3.71E+06	7.50E-02	12:43	942994176.3	24.94	0.07		24.95	0.07			Pi01	
d18O_NIST_CSDT1_061213@8	1.92	2.03E-03	7.31E-03	1.73E+09	1.17E-01	3.50E+06	1.10E-01	12:48	901636040.5	11.01	0.07		11.01	0.07			Standard	
d18O_NIST_CSDT1_061213@9	1.92	2.03E-03	7.52E-03	1.75E+09	1.22E-01	3.56E+06	1.21E-01	12:54	916158385.4	10.78	0.07		10.78	0.07			Standard	
d18O_NIST_CSDT1_061213@10	1.90	2.03E-03	6.85E-03	1.75E+09	1.42E-01	3.54E+06	1.45E-01	12:59	916750362.4	10.90	0.07		10.91	0.07			Standard	
d18O_NIST_CSDT1_061213@11	1.90	2.03E-03	7.97E-03	1.71E+09	1.15E-01	3.47E+06	1.17E-01	13:05	900903011.1	10.74	0.08		10.75	0.08			Standard	
d18O_CSDT_051213_Rad@22	1.90	2.07E-03	6.08E-03	1.76E+09	7.42E-02	3.65E+06	7.48E-02	13:11	929756446.0	31.64	0.06		31.64	0.06			Pi01	
d18O_CSDT_051213_Rad@23	1.88	2.07E-03	6.79E-03	1.70E+09	8.30E-02	3.53E+06	8.85E-02	13:16	903009555.7	34.29	0.07		34.30	0.07			Pi01	
d18O_CSDT_051213_Rad@24	1.89	2.07E-03	6.94E-03	1.71E+09	6.15E-02	3.55E+06	5.80E-02	13:22	907660798.1	33.70	0.07		33.71	0.07			Pi01	
d18O_CSDT_051213_Rad@25	1.87	2.07E-03	7.01E-03	1.72E+09	8.74E-02	3.56E+06	9.03E-02	13:27	917764595.2	32.04	0.07		32.05	0.07			Pi01	
d18O_CSDT_051213_Rad@26	1.88	2.07E-03	8.10E-03	1.72E+09	9.19E-02	3.56E+06	9.30E-02	13:33	919271595.5	30.29	0.08		30.30	0.08			Pi01	
d18O_CSDT_051213_Rad@27	1.87	2.06E-03	8.31E-03	1.74E+09	9.35E-02	3.58E+06	9.55E-02	13:38	925963968.3	29.62	0.08		29.63	0.08			Pi01	
d18O_CSDT_051213_Rad@28	1.86	2.06E-03	8.30E-03	1.74E+09	8.43E-02	3.58E+06	8.64E-02	13:44	932452157.7	28.93	0.08		28.95	0.08			Pi01	matrix
d18O_CSDT_051213_Rad@29	1.87	2.06E-03	5.50E-03	1.72E+09	8.35E-02	3.54E+06	9.09E-02	13:49	923602679.3	25.03	0.05		25.04	0.05			Pi01	matrix
d18O_CSDT_051213_Rad@30	1.87	2.06E-03	7.72E-03	1.85E+09	4.00E-02	3.81E+06	4.19E-02	13:55	989775408.6	26.11	0.08		26.12	0.08			Pi01	
d18O_CSDT_051213_Rad@31	1.86	2.06E-03	7.54E-03	1.85E+09	1.91E-01	3.81E+06	1.88E-01	14:00	995048477.8	25.93	0.07		25.95	0.07			Pi01	
d18O_NIST_CSDT1_061213@12	1.84	2.03E-03	7.14E-03	1.68E+09	1.22E-01	3.40E+06	1.26E-01	14:06	909700126.4	10.85	0.07		10.87	0.07			Standard	
d18O_NIST_CSDT1_061213@13	1.85	2.03E-03	5.27E-03	1.69E+09	1.06E-01	3.42E+06	1.06E-01	14:12	913009652.7	10.66	0.05		10.68	0.05			Standard	
d18O_NIST_CSDT1_061213@14	1.84	2.03E-03	9.58E-03	1.68E+09	1.14E-01	3.40E+06	1.16E-01	14:17	910940934.0	11.17	0.09		11.18	0.09			Standard	
d18O_NIST_CSDT1_061213@15	1.84	2.03E-03	6.22E-03	1.66E+09	1.14E-01	3.36E+06	1.15E-01	14:23	902535113.2	10.77	0.06		10.79	0.06			Standard	

Table A2 Continued.

SIMS ANALYSES								Mount: Ca01	Standard: UNIL-Q1 (Paine)	Analyse: $\delta^{18}O$			Value= 9.81±0.14 (VSMOW, 2σ)				Date: 06.12.2013
	Beam	H'2/L'2 ($^{18}O/^{16}O$)		L'2 (^{18}O/Coeff)		H'2 (^{16}O/Coeff)		Time	Yield	Measurements (‰)		mean	Drift correction (‰)		Calibration (‰)		Comment
	nA	CPS	2SD	CPS	2SD	CPS	2SD		CPS/nA	$\delta^{18}O$	2SD int	2SD	$\delta^{18}O$	2SD	$\delta^{18}O_{VSMOW}$	2SD	
d18O_NIST_CSDT3_061213@1	1.82	2.0264E-03	6.2543E-03	1.7811E+09	1.6631E-01	3.6091E+06	1.6931E-01	14:43	977287741.6	10.55	0.06		10.60	0.06			Standard
d18O_NIST_CSDT3_061213@2	1.86	2.0262E-03	6.6390E-03	1.7215E+09	1.3108E-01	3.4878E+06	1.3042E-01	14:49	923326071.4	10.46	0.07		10.50	0.07			Standard
d18O_NIST_CSDT3_061213@3	1.83	2.0264E-03	8.2308E-03	1.7213E+09	1.3329E-01	3.4882E+06	1.3440E-01	14:54	940427324.4	10.59	0.08		10.63	0.08			Standard
d18O_NIST_CSDT3_061213@4	1.83	2.0265E-03	6.9264E-03	1.7292E+09	1.6352E-01	3.5041E+06	1.6538E-01	15:00	944087859	10.60	0.07		10.64	0.07			Standard
d18O_CSDT3_061213@1	1.83	2.0633E-03	8.1094E-03	1.7540E+09	1.7668E-01	3.6189E+06	1.7420E-01	15:06	959941221.2	28.95	0.08		28.98	0.08			Ca01
d18O_CSDT3_061213@02	1.82	2.0637E-03	6.5090E-03	1.7317E+09	1.5226E-01	3.5737E+06	1.5606E-01	15:11	953843306.6	29.17	0.06		29.19	0.06			Ca01
d18O_CSDT3_061213@03	1.82	2.0628E-03	9.2159E-03	1.7281E+09	1.9555E-01	3.5647E+06	1.9694E-01	15:17	949098048.9	28.71	0.09		28.73	0.09			Ca01
d18O_CSDT3_061213@04	1.82	2.0631E-03	7.4815E-03	1.7261E+09	1.6595E-01	3.5612E+06	1.6541E-01	15:22	947365734.6	28.87	0.07		28.89	0.07			Ca01
d18O_CSDT3_061213@05	1.81	2.0640E-03	7.1060E-03	1.7193E+09	1.1586E-01	3.5489E+06	1.1650E-01	15:28	949698680.4	29.35	0.07		29.35	0.07			Ca01
d18O_CSDT3_061213@06	1.80	2.0639E-03	7.6013E-03	1.7005E+09	1.8841E-01	3.5096E+06	1.8826E-01	15:33	943666450.4	29.28	0.07		29.28	0.07			Ca01
d18O_CSDT3_061213@07	1.80	2.0629E-03	9.5068E-03	1.7158E+09	1.7008E-01	3.5395E+06	1.7215E-01	15:39	952188802.9	28.78	0.09		28.77	0.09			Ca01
d18O_CSDT3_061213@08	1.81	2.0641E-03	6.0840E-03	1.7249E+09	1.2808E-01	3.5603E+06	1.2892E-01	15:44	955612863.9	29.40	0.06		29.38	0.06			Ca01
d18O_CSDT3_061213@09	1.81	2.0587E-03	7.5731E-03	1.7426E+09	1.7302E-01	3.5874E+06	1.7638E-01	15:50	961179866.4	26.67	0.07		26.65	0.07			Ca01
d18O_CSDT3_061213@10	1.81	2.0641E-03	6.2662E-03	1.7066E+09	1.4075E-01	3.5226E+06	1.4065E-01	15:56	942681882.7	29.38	0.06		29.35	0.06			Ca01
d18O_CSDT3_061213@11	1.81	2.0646E-03	5.8261E-03	1.7274E+09	1.1620E-01	3.5661E+06	1.1581E-01	16:01	954562560.4	29.60	0.06		29.57	0.06			Ca01
d18O_NIST_CSDT3_061213@5	1.80	2.0265E-03	7.0211E-03	1.7018E+09	1.7275E-01	3.4489E+06	1.7323E-01	16:07	942963434.6	10.62	0.07		10.58	0.07			Standard
d18O_NIST_CSDT3_061213@6	1.81	2.0264E-03	6.0760E-03	1.7091E+09	1.5355E-01	3.4632E+06	1.5199E-01	16:12	942730682.2	10.55	0.06		10.50	0.06			Standard
d18O_NIST_CSDT3_061213@7	1.81	2.0267E-03	8.1140E-03	1.6881E+09	1.3467E-01	3.4211E+06	1.3457E-01	16:18	930517467.1	10.73	0.08		10.68	0.08			Standard
d18O_NIST_CSDT3_061213@8	1.81	2.0266E-03	7.1672E-03	1.6836E+09	1.2255E-01	3.4117E+06	1.2340E-01	16:23	929121369.4	10.67	0.07		10.62	0.07			Standard

SIMS ANALYSES								Mount: Ki08	Standard: UNIL-Q1 (Paine)	Analyse: $\delta^{18}O$			Value= 9.81±0.14 (VSMOW, 2σ)				Date: 06.12.2013
	Beam	H'2/L'2 ($^{18}O/^{16}O$)		L'2 (^{18}O/Coeff)		H'2 (^{16}O/Coeff)		Time	Yield	Measurements (‰)		mean	Drift correction (‰)		Calibration (‰)		Comment
	nA	CPS	2SD	CPS	2SD	CPS	2SD		CPS/nA	$\delta^{18}O$	2SD int	2SD	$\delta^{18}O$	2SD	$\delta^{18}O_{VSMOW}$	2SD	
d18O_NIST_K108_061213@1	1.78	2.03E-03	5.80E-03	1.63E+09	1.56E-01	3.29E+06	1.58E-01	17:07	913329556.4	10.31	0.06		10.32	0.06			Standard
d18O_NIST_K108_061213@2	1.78	2.03E-03	8.59E-03	1.62E+09	1.17E-01	3.28E+06	1.10E-01	17:12	907935802.6	10.61	0.08		10.63	0.08			Standard
d18O_NIST_K108_061213@3	1.79	2.03E-03	1.03E-02	1.60E+09	1.01E-01	3.24E+06	1.01E-01	17:18	895583374.2	10.45	0.10		10.46	0.10			Standard
d18O_NIST_K108_061213@4	1.78	2.03E-03	8.80E-03	1.59E+09	1.22E-01	3.22E+06	1.24E-01	17:24	893204020.0	10.58	0.09		10.59	0.09			Standard
d18O_K108_061213_Rad@1	1.78	2.06E-03	8.25E-03	1.67E+09	9.66E-02	3.43E+06	9.83E-02	17:29	935865704.8	25.57	0.08		25.59	0.08			Ki08
d18O_K108_061213_Rad@2	1.78	2.05E-03	9.49E-03	1.67E+09	1.19E-01	3.43E+06	1.20E-01	17:35	935067212.9	24.15	0.09		24.16	0.09			Ki08
d18O_K108_061213_Rad@3	1.78	2.05E-03	7.41E-03	1.66E+09	1.18E-01	3.41E+06	1.14E-01	17:40	930860841.3	24.30	0.07		24.31	0.07			Ki08
d18O_K108_061213_Rad@4a	1.78	2.06E-03	8.00E-03	1.68E+09	3.41E-01	3.46E+06	3.42E-01	17:46	946623505.0	26.90	0.08		26.91	0.08			Ki08
d18O_K108_061213_Rad@4b1	1.80	2.06E-03	8.19E-03	1.69E+09	1.34E-01	3.48E+06	1.33E-01	17:51	941500427.1	25.60	0.08		25.61	0.08			Ki08
d18O_K108_061213_Rad@4c	1.78	2.05E-03	9.94E-03	1.67E+09	9.72E-02	3.43E+06	9.17E-02	17:57	936396816.4	24.28	0.10		24.29	0.10			Ki08
d18O_K108_061213_Rad@5a	1.77	2.06E-03	8.09E-03	1.65E+09	7.29E-02	3.40E+06	7.15E-02	18:02	936503855.7	26.70	0.08		26.70	0.08			Ki08
d18O_K108_061213_Rad@5b	1.77	2.06E-03	8.51E-03	1.65E+09	9.43E-02	3.40E+06	9.60E-02	18:08	936336153.4	26.46	0.08		26.47	0.08			Ki08
d18O_K108_061213_Rad@6	1.75	2.06E-03	7.56E-03	1.64E+09	7.53E-02	3.37E+06	7.84E-02	18:13	935726935.9	25.14	0.07		25.14	0.07			Ki08
d18O_K108_061213_Rad@7	1.75	2.05E-03	7.95E-03	1.61E+09	6.58E-02	3.30E+06	6.67E-02	18:19	920237746.2	24.16	0.08		24.17	0.08			Ki08
d18O_NIST_K108_061213@5	1.74	2.03E-03	1.04E-02	1.57E+09	1.14E-01	3.17E+06	1.12E-01	18:25	899689925.4	10.35	0.10		10.36	0.10			Standard
d18O_NIST_K108_061213@6	1.74	2.03E-03	9.43E-03	1.57E+09	5.84E-02	3.17E+06	5.71E-02	18:30	901186676.2	10.71	0.09		10.72	0.09			Standard
d18O_NIST_K108_061213@7	1.73	2.03E-03	8.34E-03	1.58E+09	1.25E-01	3.19E+06	1.27E-01	18:36	909775738.3	10.36	0.08		10.36	0.08			Standard
d18O_NIST_K108_061213@8	1.73	2.03E-03	8.06E-03	1.56E+09	1.24E-01	3.17E+06	1.23E-01	18:41	905524233.3	10.51	0.08		10.52	0.08			Standard
d18O_K108_061213_Rad@8	1.72	2.06E-03	8.50E-03	1.60E+09	5.16E-02	3.29E+06	4.85E-02	18:47	929426857.6	26.77	0.08		26.77	0.08			Ki08
d18O_K108_061213_Rad@9	1.73	2.06E-03	8.72E-03	1.55E+09	6.61E-02	3.19E+06	6.47E-02	18:52	898925923.2	25.53	0.08		25.53	0.08			Ki08
d18O_K108_061213_Rad@10	1.72	2.06E-03	5.80E-03	1.55E+09	6.32E-02	3.19E+06	6.22E-02	18:58	902282757.9	25.43	0.06		25.44	0.06			Ki08
d18O_K108_061213_Rad@11a	1.71	2.06E-03	7.01E-03	1.56E+09	4.67E-02	3.20E+06	4.86E-02	19:03	908354883.7	25.38	0.07		25.38	0.07			Ki08
d18O_K108_061213_Rad@11b	1.72	2.05E-03	8.52E-03	1.56E+09	6.65E-02	3.20E+06	6.94E-02	19:09	904497693.1	24.79	0.08		24.79	0.08			Ki08
d18O_K108_061213_Rad@11c	1.72	2.06E-03	8.61E-03	1.53E+09	2.83E-02	3.16E+06	2.51E-02	19:15	893300584.6	25.48	0.08		25.48	0.08			Ki08
d18O_K108_061213_Rad@12	1.71	2.06E-03	9.33E-03	1.54E+09	7.27E-02	3.18E+06	7.04E-02	19:20	903770057.3	26.61	0.09		26.61	0.09			Ki08
d18O_K108_061213_argile@1	1.71	2.05E-03	1.02E-02	1.55E+09	8.98E-02	3.18E+06	9.21E-02	19:26	907442845.9	23.48	0.10		23.48	0.10			Ki08 Clay
d18O_K108_061213_argile@2	1.71	2.05E-03	9.01E-03	1.54E+09	1.94E-02	3.16E+06	1.91E-02	19:31	900282302.0	23.12	0.09		23.12	0.09			Ki08 Clay
d18O_K108_061213_argile@3	1.71	2.05E-03	9.48E-03	1.50E+09	4.46E-02	3.09E+06	4.49E-02	19:37	878889186.9	24.26	0.09		24.26	0.09			Ki08 Clay
d18O_NIST_K108_061213@9	1.70	2.03E-03	8.56E-03	1.52E+09	1.07E-01	3.07E+06	1.06E-01	19:42	890615758.4	10.60	0.08		10.60	0.08			Standard
d18O_NIST_K108_061213@10	1.70	2.03E-03	7.13E-03	1.53E+09	1.02E-01	3.10E+06	1.03E-01	19:48	897582878.4	10.86	0.07		10.86	0.07			Standard
d18O_NIST_K108_061213@11	1.71	2.03E-03	7.53E-03	1.53E+09	1.04E-01	3.10E+06	1.06E-01	19:53	895962799.3	10.48	0.07		10.48	0.07			Standard
d18O_NIST_K108_061213@12	1.69	2.03E-03	1.04E-02	1.53E+09	4.86E-02	3.11E+06	5.73E-02	19:59	904223006.1	10.54	0.10		10.53	0.10			Standard
d18O_K108_061213_Rad@13a	1.69	2.06E-03	9.67E-03	1.53E+09	7.23E-02	3.14E+06	7.02E-02	20:05	900774762.8	26.39	0.09		26.38	0.09			Ki08
d18O_K108_061213_Rad@13b	1.69	2.06E-03	6.86E-03	1.53E+09	2.76E-02	3.14E+06	3.03E-02	20:10	901944427.4	26.49	0.07		26.48	0.07			Ki08
d18O_K108_061213_Rad@13c	1.68	2.06E-03	7.22E-03	1.52E+09	5.27E-02	3.14E+06	5.03E-02	20:16	905901309.0	26.70	0.07		26.69	0.07			Ki08
d18O_K108_061213_Rad@14	1.67	2.06E-03	8.18E-03	1.52E+09	8.04E-02	3.13E+06	8.10E-02	20:21	908367952.4	24.89	0.08		24.88	0.08			Ki08
d18O_K108_061213_Rad@15	1.68	2.06E-03	7.50E-03	1.53E+09	6.83E-02	3.15E+06	6.89E-02	20:27	911867589.2	24.96	0.07		24.95	0.07			Ki08
d18O_K108_061213_Rad@16	1.68	2.05E-03	9.10E-03	1.52E+09	1.15E-01	3.12E+06	1.14E-01	20:32	907143100.2	24.57	0.09		24.56	0.09			Ki08
d18O_K108_061213_Rad@17	1.66	2.05E-03	9.76E-03	1.49E+09	1.01E-01	3.06E+06	1.05E-01	20:38	895445071.7	24.00	0.10		23.99	0.10			Ki08
d18O_K108_061213_Rad@18	1.66	2.06E-03	6.93E-03	1.51E+09	9.39E-02	3.10E+06	9.18E-02	20:43	906469387.6	25.25	0.07		25.24	0.07			Ki08
d18O_K108_061213_Rad@19	1.66	2.05E-03	7.26E-03	1.50E+09	1.33E-01	3.08E+06	1.37E-01	20:49	904443728.6	24.69	0.07		24.68	0.07			Ki08
d18O_K108_061213_Rad@20	1.66	2.05E-03	1.05E-02	1.53E+09	1.28E-01	3.14E+06	1.28E-01	20:55	922089710.8	24.57	0.10		24.56	0.10			Ki08
d18O_NIST_K108_061213@13	1.66	2.03E-03	6.81E-03	1.52E+09	1.31E-01	3.08E+06	1.32E-01	21:00	919143671.6	10.36	0.07		10.34	0.07			Standard
d18O_NIST_K108_061213@14	1.66	2.03E-03	8.65E-03	1.51E+09	1.39E-01	3.06E+06	1.41E-01	21:06	909604945.1	10.17	0.09		10.15	0.09			Standard
d18O_NIST_K108_061213@15	1.66	2.03E-03	9.03E-03	1.50E+09	8.08E-02	3.05E+06	8.06E-02	21:11	909045049.1	10.44	0.09		10.43	0.09			Standard
d18O_NIST_K108_061213@16	1.65	2.03E-03	8.55E-03	1.50E+09	1.23E-01	3.05E+06	1.25E-01	21:17	909199694.1	10.71	0.08		10.69	0.08			Standard

Table A2 Continued.

SIMS ANALYSES						Mount: PRIM123			Standard: UNIL-Q1 (Paine)	Analyse: $\delta^{18}O$			Value= 9.81±0.14 (VSMOW, 2σ)				Date: 26.06.2014
	Beam	H'2/L'2 ($^{18}O/^{16}O$)		L'2 (^{18}O/Coeff)		H'2 (^{16}O/Coeff)		Time	Yield	Measurements (‰)		mean	Drift correction (‰)		Calibration (‰)		Comment
	nA	CPS	2SD	CPS	2SD	CPS	2SD		CPS/nA	$\delta^{18}O$	2SD int	2SD	$\delta^{18}O$	2SD	$\delta^{18}O_{VSMOW}$	2SD	
d18O_prim123_paine@48								17:54		6.69	0.17	6.59	6.66	0.17	9.94	0.20	Standard
d18O_prim123_paine@49								18:07		6.73	0.18	0.23	6.70	0.18	9.98	0.20	Standard
d18O_prim123_paine@50								18:12		6.76	0.18		6.73	0.18	10.02	0.20	Standard
d18O_prim123_paine@51								18:17		6.49	0.12		6.46	0.12	9.75	0.19	Standard
d18O_prim123_paine@52								18:21		6.54	0.21		6.51	0.21	9.80	0.21	Standard
d18O_prim123_paine@53								18:26		6.62	0.14		6.59	0.14	9.88	0.19	Standard
d18O_prim123_paine@54								18:31		6.55	0.16		6.52	0.16	9.81	0.20	Standard
d18O_prim123_paine@55								18:35		6.65	0.13		6.62	0.13	9.91	0.19	Standard
d18O_prim123_paine@56								18:40		6.54	0.16		6.51	0.16	9.79	0.20	Standard
d18O_prim123_paine@57								18:45		6.69	0.17		6.66	0.17	9.95	0.20	Standard
d18O_prim123_paine@58								18:50		6.43	0.17		6.40	0.17	9.68	0.20	Standard
d18O_prim123_paine@59								18:54		6.41	0.20		6.38	0.20	9.66	0.21	Standard
d18O_prim123_paine@60								18:59		6.52	0.17		6.50	0.17	9.78	0.20	Standard
d18O_prim123_r4c1@1								19:04		27.57	0.20	27.49	27.54	0.20	30.90	0.21	base Ki08C
d18O_prim123_r4c1@2								19:09		27.31	0.18	1.00	27.28	0.18	30.64	0.20	base Ki08C
d18O_prim123_r4c1@3								19:13		27.56	0.15		27.54	0.15	30.89	0.20	base Ki08C
d18O_prim123_r4c1@4								19:18		26.92	0.17		26.90	0.17	30.25	0.20	base Ki08C
d18O_prim123_r1c2@1								19:23		28.40	0.14		28.37	0.14	31.73	0.20	middle Ki08C
d18O_prim123_r1c2@2								19:27		27.69	0.14		27.67	0.14	31.02	0.20	middle Ki08C
d18O_prim123_r1c2@3								19:32		26.99	0.16		26.96	0.16	30.31	0.20	middle Ki08C
d18O_prim123_paine@61								19:37		6.47	0.17	6.53	6.44	0.17	9.73	0.20	Standard
d18O_prim123_paine@62								19:42		6.42	0.19	0.23	6.40	0.19	9.68	0.20	Standard
d18O_prim123_paine@63								19:46		6.53	0.14		6.51	0.14	9.79	0.19	Standard
d18O_prim123_paine@64								19:51		6.68	0.23		6.66	0.23	9.95	0.21	Standard
d18O_prim123_r1c2@4								19:56		27.68	0.20	28.08	27.66	0.20	31.01	0.21	middle Ki08C
d18O_prim123_r2c2@1								20:01		27.63	0.19	0.82	27.61	0.19	30.96	0.21	middle Ki08C
d18O_prim123_r2c2@2								20:05		27.97	0.22		27.94	0.22	31.30	0.21	middle Ki08C
d18O_prim123_r2c2@3								20:10		27.89	0.21		27.86	0.21	31.22	0.21	middle Ki08C
d18O_prim123_r2c2@4								20:15		27.83	0.16		27.81	0.16	31.16	0.20	middle Ki08C
d18O_prim123_r2c2@5								20:20		27.49	0.14		27.47	0.14	30.83	0.20	middle Ki08C
d18O_prim123_r2c2@6								20:24		28.14	0.11		28.12	0.11	31.48	0.19	middle Ki08C
d18O_prim123_r3c2@1								20:29		27.92	0.14		27.90	0.14	31.25	0.20	middle Ki08C
d18O_prim123_r3c2@2								20:34		27.98	0.16		27.96	0.16	31.31	0.20	middle Ki08C
d18O_prim123_r3c2@3								20:38		28.40	0.19		28.38	0.19	31.74	0.21	middle Ki08C
d18O_prim123_r3c2@4								20:43		28.36	0.18		28.34	0.18	31.70	0.20	middle Ki08C
d18O_prim123_r4c2@1								20:48		28.47	0.21		28.45	0.21	31.81	0.21	middle Ki08C
d18O_prim123_r4c2@2								20:53		28.43	0.15		28.41	0.15	31.77	0.20	middle Ki08C
d18O_prim123_r4c2@3								20:57		29.09	0.17		29.07	0.17	32.43	0.20	middle Ki08C
d18O_prim123_r4c2@4								21:02		27.92	0.23		27.90	0.23	31.25	0.22	middle Ki08C
d18O_prim123_paine@65								21:07		6.36	0.12	6.54	6.35	0.12	9.63	0.19	Standard
d18O_prim123_paine@66								21:12		6.67	0.14	0.56	6.65	0.14	9.94	0.19	Standard
d18O_prim123_paine@67								21:16		6.27	0.12		6.25	0.12	9.54	0.19	Standard
d18O_prim123_paine@68								21:21		6.87	0.17		6.86	0.17	10.14	0.20	Standard
d18O_prim123_r4c2@5								21:26		27.45	0.22	27.62	27.44	0.22	30.79	0.21	middle Ki08C
d18O_prim123_r4c2@6								21:31		27.34	0.17	0.92	27.32	0.17	30.68	0.20	middle Ki08C
d18O_prim123_r4c2@7								21:35		27.34	0.16		27.33	0.16	30.68	0.20	middle Ki08C
d18O_prim123_r4c2@8								21:40		27.70	0.16		27.69	0.16	31.04	0.20	middle Ki08C
d18O_prim123_r5c1@1								21:45		27.57	0.20		27.55	0.20	30.91	0.21	middle Ki08C
d18O_prim123_r5c1@2								21:49		27.61	0.18		27.60	0.18	30.95	0.20	middle Ki08C
d18O_prim123_r5c1@3								21:54		27.90	0.12		27.88	0.12	31.24	0.19	middle Ki08C
d18O_prim123_r5c1@4								21:59		27.18	0.18		27.17	0.18	30.52	0.21	middle Ki08C
d18O_prim123_r5c1@5								22:03		27.32	0.17		27.31	0.17	30.66	0.20	middle Ki08C
d18O_prim123_r5c1@6								22:08		28.88	0.14		28.87	0.14	32.22	0.20	middle Ki08C
d18O_prim123_r1c3@1								22:13		27.17	0.17		27.16	0.17	30.51	0.20	top Ki08C
d18O_prim123_r2c3@1								22:18		27.77	0.23		27.76	0.23	31.11	0.22	top Ki08C
d18O_prim123_r2c3@2								22:22		28.10	0.19		28.08	0.19	31.44	0.21	top Ki08C
d18O_prim123_r2c3@3								22:27		27.83	0.14		27.82	0.14	31.17	0.20	top Ki08C
d18O_prim123_r2c3@4								22:32		27.06	0.18		27.05	0.18	30.40	0.20	top Ki08C
d18O_prim123_paine@69								22:37		6.73	0.12	6.45	6.72	0.12	10.00	0.19	Standard
d18O_prim123_paine@70								22:41		6.53	0.20	0.60	6.52	0.20	9.81	0.20	Standard
d18O_prim123_paine@71								22:46		6.50	0.14		6.49	0.14	9.78	0.19	Standard
d18O_prim123_paine@72								22:51		6.02	0.19		6.01	0.19	9.30	0.20	Standard
d18O_prim123_r3c3@1								22:56		26.46	0.17	26.95	26.45	0.17	29.80	0.20	top Ki08C
d18O_prim123_r3c3@2								23:00		27.56	0.18	0.78	27.55	0.18	30.90	0.20	top Ki08C
d18O_prim123_r3c3@3								23:05		26.90	0.16		26.89	0.16	30.24	0.20	top Ki08C
d18O_prim123_r4c3@1								23:10		26.77	0.10		26.76	0.10	30.12	0.19	top Ki08C
d18O_prim123_r4c3@2								23:15		26.43	0.17		26.42	0.17	29.77	0.20	top Ki08C
d18O_prim123_r4c3@3								23:19		26.77	0.20		26.76	0.20	30.11	0.21	top Ki08C
d18O_prim123_r4c3@4								23:24		26.95	0.15		26.94	0.15	30.30	0.20	top Ki08C
d18O_prim123_r5c3@1								23:29		26.74	0.27		26.74	0.27	30.09	0.23	top Ki08C
d18O_prim123_r5c3@2								23:34		27.00	0.17		27.00	0.17	30.35	0.20	top Ki08C

Table A2 Continued.

SIMS ANALYSES						Mount: PRIM123			Standard: UNIL-Q1 (Paine)	Analyse: $\delta^{18}O$			Value= 9.81±0.14 (VSMOW, 2σ)				Date: 26.06.2014
	Beam	H'2/L'2 ($^{18}O/^{16}O$)		L'2 (^{18}O/Coeff)		H'2 (^{16}O/Coeff)		Time	Yield	Measurements (‰)		mean	Drift correction (‰)		Calibration (‰)		Comment
	nA	CPS	2SD	CPS	2SD	CPS	2SD		CPS/nA	$\delta^{18}O$	2SD int	2SD	$\delta^{18}O$	2SD	$\delta^{18}O_{VSMOW}$	2SD	
d18O_prim123_r5c3@3								23:38		26.50	0.17		26.49	0.17	29.84	0.20	top Ki08C
d18O_prim123_r1c4@1								23:43		26.91	0.10		26.90	0.10	30.25	0.19	Ki08C
d18O_prim123_r1c4@2								23:48		27.14	0.10		27.14	0.10	30.49	0.19	Ki08C
d18O_prim123_r1c4@3								23:53		27.84	0.18		27.84	0.18	31.19	0.21	Ki08C
d18O_prim123_r1c4@4								23:57		27.29	0.20		27.29	0.20	30.64	0.21	Ki08C
d18O_prim123_r1c4@5								0:02		26.97	0.15		26.97	0.15	30.32	0.20	Ki08C
d18O_prim123_paine@74								0:07		6.44	0.11	6.43	6.44	0.11	9.72	0.19	Standard
d18O_prim123_paine@75								0:12		6.43	0.13	0.03	6.43	0.13	9.71	0.19	Standard
d18O_prim123_paine@76								0:16		6.44	0.13		6.44	0.13	9.73	0.19	Standard
d18O_prim123_paine@77								0:21		6.41	0.10		6.40	0.10	9.69	0.19	Standard
d18O_prim123_r2c4@1								0:26		27.19	0.21	27.37	27.19	0.21	30.54	0.21	Ki08C
d18O_prim123_r2c4@2								0:31		26.99	0.15	1.16	26.99	0.15	30.34	0.20	Ki08C
d18O_prim123_r2c4@3								0:35		26.16	0.13		26.16	0.13	29.51	0.19	Ki08C
d18O_prim123_r3c4@1								0:40		28.58	0.15		28.58	0.15	31.93	0.20	Ki08C
d18O_prim123_r3c4@2								0:45		27.52	0.20		27.52	0.20	30.88	0.21	Ki08C
d18O_prim123_r3c4@3								0:50		28.44	0.19		28.44	0.19	31.79	0.21	Ki08C
d18O_prim123_r3c4@4								0:54		27.07	0.18		27.07	0.18	30.42	0.20	Ki08C
d18O_prim123_r3c4@5								0:59		27.23	0.19		27.23	0.19	30.58	0.21	Ki08C
d18O_prim123_r4c4@1								1:04		27.46	0.18		27.46	0.18	30.81	0.20	Ki08C
d18O_prim123_r4c4@2								1:08		27.05	0.16		27.05	0.16	30.40	0.20	Ki08C
d18O_prim123_r4c4@3								1:13		27.42	0.10		27.42	0.10	30.78	0.19	Ki08C
d18O_prim123_r4c4@4								1:18		27.56	0.11		27.56	0.11	30.91	0.19	Ki08C
d18O_prim123_r5c4@1								1:23		27.00	0.12		27.01	0.12	30.36	0.19	Ki08C
d18O_prim123_r5c4@2								1:27		27.59	0.15		27.59	0.15	30.94	0.20	Ki08C
d18O_prim123_r5c4@3								1:32		27.27	0.14		27.27	0.14	30.63	0.20	Ki08C
d18O_prim123_paine@78								1:37		6.77	0.15	6.64	6.77	0.15	10.06	0.19	Standard
d18O_prim123_paine@79								1:42		6.79	0.16	0.43	6.80	0.16	10.08	0.20	Standard
d18O_prim123_paine@80								1:46		6.33	0.24		6.33	0.24	9.61	0.22	Standard
d18O_prim123_paine@81								1:51		6.66	0.11		6.66	0.11	9.95	0.19	Standard
d18O_prim123_r1c5@1								1:56		26.73	0.17	27.10	26.73	0.17	30.08	0.20	Ki08C
d18O_prim123_r1c5@2								2:01		26.79	0.12	1.17	26.79	0.12	30.15	0.19	Ki08C
d18O_prim123_r1c5@3								2:05		26.88	0.16		26.88	0.16	30.23	0.20	Ki08C
d18O_prim123_r2c5@1								2:10		27.64	0.18		27.65	0.18	31.00	0.20	Ki08C
d18O_prim123_r2c5@2								2:15		27.28	0.14		27.29	0.14	30.64	0.20	Ki08C
d18O_prim123_r2c5@3								2:19		27.44	0.14		27.45	0.14	30.80	0.20	Ki08C
d18O_prim123_r3c5@1								2:24		25.41	0.16		25.42	0.16	28.77	0.20	Ki08C
d18O_prim123_r3c5@2								2:29		27.25	0.16		27.26	0.16	30.61	0.20	Ki08C
d18O_prim123_r3c5@3								2:34		27.28	0.14		27.28	0.14	30.64	0.20	Ki08C
d18O_prim123_r3c5@4								2:38		27.64	0.12		27.64	0.12	31.00	0.19	Ki08C
d18O_prim123_r3c5@5								2:43		27.27	0.17		27.28	0.17	30.63	0.20	Ki08C
d18O_prim123_r4c5@1								2:48		27.85	0.16		27.86	0.16	31.22	0.20	Ki08C
d18O_prim123_r4c5@2								2:53		27.40	0.15		27.41	0.15	30.76	0.20	Ki08C
d18O_prim123_r4c5@3								2:57		26.98	0.12		26.99	0.12	30.34	0.19	Ki08C
d18O_prim123_r4c5@4								3:02		26.65	0.12		26.66	0.12	30.01	0.19	Ki08C
d18O_prim123_paine@82								3:07		6.66	0.18	6.49	6.67	0.18	9.96	0.20	Standard
d18O_prim123_paine@83								3:12		6.09	0.18	0.54	6.10	0.18	9.39	0.20	Standard
d18O_prim123_paine@84								3:16		6.64	0.13		6.65	0.13	9.94	0.19	Standard
d18O_prim123_paine@85								3:21		6.57	0.14		6.58	0.14	9.87	0.19	Standard
d18O_prim123_r4c5@5								3:26		26.63	0.17	27.06	26.65	0.17	30.00	0.20	Ki08C
d18O_prim123_r4c5@6								3:31		27.53	0.21	0.77	27.55	0.21	30.90	0.21	Ki08C
d18O_prim123_r5c5@1								3:35		27.17	0.14		27.18	0.14	30.54	0.20	Ki08C
d18O_prim123_r5c5@2								3:40		26.89	0.16		26.90	0.16	30.26	0.20	Ki08C
d18O_prim123_r1c6@1								3:45		31.36	0.15	31.16	31.37	0.15	34.74	0.20	Pi01
d18O_prim123_r1c6@2								3:50		30.17	0.15	1.03	30.18	0.15	33.54	0.20	Pi01
d18O_prim123_r1c6@3								3:54		30.15	0.20		30.16	0.20	33.53	0.21	Pi01
d18O_prim123_r2c6@1								3:59		31.35	0.10		31.36	0.10	34.73	0.19	Pi01
d18O_prim123_r2c6@2								4:04		31.37	0.16		31.39	0.16	34.75	0.20	Pi01
d18O_prim123_r2c6@3								4:09		31.21	0.14		31.23	0.14	34.59	0.20	Pi01
d18O_prim123_r2c6@4								4:13		31.28	0.12		31.29	0.12	34.66	0.19	Pi01
d18O_prim123_r2c6@5								4:18		31.49	0.13		31.51	0.13	34.88	0.19	Pi01
d18O_prim123_r2c6@6								4:23		31.32	0.20		31.34	0.20	34.71	0.21	Pi01
d18O_prim123_r2c6@7								4:27		31.38	0.15		31.40	0.15	34.77	0.20	Pi01
d18O_prim123_r2c6@8								4:32		31.71	0.22		31.72	0.22	35.09	0.21	Pi01

Table A2 Continued.

	SIMS ANALYSES							Mount: PRIM123	Standard: UNIL-Q1 (Paine)	Analyse: $\delta^{18}O$			Value= 9.81±0.14 (VSMOW, 2σ)				Date: 26.06.2014
	Beam	H'2/L'2 ($^{18}O/^{16}O$)		L'2 (^{18}O/Coeff)		H'2 (^{16}O/Coeff)		Time	Yield	Measurements (‰)		mean	Drift correction (‰)		Calibration (‰)		Comment
	nA	CPS	2SD	CPS	2SD	CPS	2SD		CPS/nA	$\delta^{18}O$	2SD int	2SD	$\delta^{18}O$	2SD	$\delta^{18}O_{VSMOW}$	2SD	
d18O_prim123_paine@86								4:37		6.37	0.22	6.55	6.39	0.22	9.67	0.21	Standard
d18O_prim123_paine@87								4:42		6.64	0.12	0.28	6.66	0.12	9.95	0.19	Standard
d18O_prim123_paine@88								4:46		6.52	0.21		6.54	0.21	9.83	0.21	Standard
d18O_prim123_paine@89								4:51		6.67	0.19		6.69	0.19	9.98	0.20	Standard
d18O_prim123_r4c6@1								4:56		31.54	0.15	31.12	31.56	0.15	34.92	0.20	Pi01
d18O_prim123_r4c6@2								5:01		31.09	0.16	0.75	31.11	0.16	34.47	0.20	Pi01
d18O_prim123_r4c6@3								5:05		31.24	0.10		31.26	0.10	34.62	0.19	Pi01
d18O_prim123_r5c6@1								5:10		30.49	0.13		30.50	0.13	33.87	0.19	Pi01
d18O_prim123_r5c6@2								5:15		30.50	0.20		30.52	0.20	33.89	0.21	Pi01
d18O_prim123_r5c6@3								5:20		31.29	0.13		31.31	0.13	34.68	0.20	Pi01
d18O_prim123_r1c7@1								5:25		31.34	0.17		31.36	0.17	34.72	0.20	Pi01
d18O_prim123_r1c7@2								5:29		31.41	0.16		31.43	0.16	34.80	0.20	Pi01
d18O_prim123_r1c7@3								5:34		31.04	0.16		31.07	0.16	34.43	0.20	Pi01
d18O_prim123_r1c7@4								5:39		31.31	0.17		31.33	0.17	34.69	0.20	Pi01
d18O_prim123_r2c7@1								5:44		31.53	0.10		31.55	0.10	34.92	0.19	Pi01
d18O_prim123_r2c7@2								5:48		31.17	0.18		31.19	0.18	34.56	0.20	Pi01
d18O_prim123_r3c7@1								5:53		30.36	0.14		30.38	0.14	33.75	0.20	Pi01
d18O_prim123_r3c7@2								5:58		31.16	0.17		31.18	0.17	34.55	0.20	Pi01
d18O_prim123_r4c7@1								6:03		31.35	0.10		31.38	0.10	34.74	0.19	Pi01
d18O_prim123_paine@90								6:08		6.78	0.24	6.50	6.81	0.24	10.09	0.22	Standard
d18O_prim123_paine@91								6:12		6.21	0.15	0.51	6.23	0.15	9.52	0.20	Standard
d18O_prim123_paine@92								6:17		6.62	0.14		6.64	0.14	9.93	0.19	Standard
d18O_prim123_paine@93								6:22		6.38	0.14		6.41	0.14	9.69	0.19	Standard
d18O_prim123_r4c7@2								6:27		31.09	0.10	31.07	31.12	0.10	34.48	0.19	Pi01
d18O_prim123_r5c7@1								6:31		31.61	0.17	0.56	31.64	0.17	35.00	0.20	Pi01
d18O_prim123_r5c7@2								6:36		30.94	0.14		30.96	0.14	34.33	0.20	Pi01
d18O_prim123_r5c7@3								6:41		31.23	0.17		31.26	0.17	34.62	0.20	Pi01
d18O_prim123_r5c7@4								6:46		31.45	0.20		31.48	0.20	34.84	0.21	Pi01
d18O_prim123_r5c7@5								6:50		31.34	0.11		31.37	0.11	34.73	0.19	Pi01
d18O_prim123_r1c8@1								6:55		30.88	0.14		30.91	0.14	34.27	0.20	Ca01
d18O_prim123_r1c8@2								7:00		30.91	0.12		30.93	0.12	34.30	0.19	Ca01
d18O_prim123_r2c8@1								7:05		31.49	0.17		31.52	0.17	34.89	0.20	Ca01
d18O_prim123_r2c8@2								7:09		30.79	0.17		30.82	0.17	34.18	0.20	Ca01
d18O_prim123_r3c8@1								7:14		30.71	0.13		30.73	0.13	34.10	0.20	Ca01
d18O_prim123_r3c8@2								7:19		30.74	0.13		30.77	0.13	34.13	0.20	Ca01
d18O_prim123_r4c8@1								7:24		30.96	0.19		30.99	0.19	34.36	0.21	Ca01
d18O_prim123_r4c8@2								7:28		30.88	0.17		30.91	0.17	34.28	0.20	Ca01
d18O_prim123_r5c8@1								7:33		31.11	0.20		31.14	0.20	34.51	0.21	Ca01
d18O_prim123_r5c8@2								7:38		31.00	0.19		31.03	0.19	34.40	0.21	Ca01
d18O_prim123_paine@94								7:43		6.55	0.17	6.48	6.59	0.17	9.87	0.20	Standard
d18O_prim123_paine@95								7:48		6.45	0.19	0.12	6.48	0.19	9.77	0.20	Standard
d18O_prim123_paine@96								7:52		6.45	0.13		6.48	0.13	9.76	0.19	Standard

Table A2 Continued.

ppendix Table A2. Continued

SIMS ANALYSES								Mount: BR2		Standard: UNIL-Q1 (Paine)		Analyse: $\delta^{18}O$			Value= 9.81±0.14 (VSMOW, 2σ)			Date: 14.04.2015
	Beam	H'2/L'2 ($^{18}O/^{16}O$)		L'2 (^{18}O/Coeff)		H'2 (^{16}O/Coeff)		Time	Yield		Measurements (‰)		mean	Drift correction (‰)		Calibration (‰)		Comment
	nA	CPS	2SD	CPS	2SD	CPS	2SD		CPS/nA		$\delta^{18}O$	2SD int	2SD	$\delta^{18}O$	2SD	$\delta^{18}O_{VSMOW}$	2SD	
140515_br2_testpaine@1	1.97	2.0145E-03	1.2679E-02	1.4717E+09	5.2494E-02	2.9656E+06	4.3500E-02	17:20	7.4783E+08	7.4607E+08	4.66	0.25	4.65					Standard
140515_br2_testpaine@2	1.98	2.0140E-03	8.9695E-03	1.4819E+09	2.8681E-02	2.9847E+06	2.9597E-02	17:25	7.4953E+08	1.0993E+07	4.41	0.18	0.37					Standard
140515_br2_testpaine@3	1.98	2.0142E-03	1.1183E-02	1.4795E+09	3.8761E-02	2.9802E+06	4.2002E-02	17:29	7.4894E+08		4.47	0.22						Standard
140515_br2_testpaine@4	1.98	2.0149E-03	1.0001E-02	1.4609E+09	1.6068E-02	2.9437E+06	1.6269E-02	17:34	7.3853E+08		4.85	0.20						Standard
140515_br2_testpaine@5	1.98	2.0142E-03	1.4034E-02	1.4944E+09	2.1438E-01	3.0143E+06	2.3441E-01	17:39	7.5507E+08		4.46	0.28						Standard
140515_br2_testpaine@6	1.98	2.0147E-03	7.8538E-03	1.4653E+09	5.4533E-02	2.9519E+06	5.7382E-02	17:43	7.3950E+08		4.73	0.16						Standard
140515_br2_testpaine@7	1.98	2.0147E-03	1.1185E-02	1.4715E+09	4.6543E-02	2.9635E+06	5.4643E-02	17:48	7.4342E+08		4.74	0.22						Standard
140515_br2_testpaine@8	1.98	2.0150E-03	1.0887E-02	1.4758E+09	1.1557E-01	2.9738E+06	1.1759E-01	17:52	7.4569E+08		4.90	0.22						Standard
140515_br2_paine@1	1.97	2.0143E-03	8.9543E-03	1.4216E+09	7.9991E-02	2.8634E+06	7.8642E-02	19:00	7.2035E+08	7.2178E+08	4.54	0.18	4.45	4.54	0.18	9.96	0.27	Standard
140515_br2_paine@2	1.99	2.0142E-03	1.3856E-02	1.4200E+09	9.9809E-02	2.8583E+06	1.1641E-01	19:05	7.1375E+08	1.5227E+07	4.50	0.28	0.25	4.51	0.28	9.93	0.29	Standard
140515_br2_paine@3	1.99	2.0138E-03	6.9811E-03	1.4283E+09	3.9485E-02	2.8766E+06	3.8631E-02	19:09	7.1795E+08		4.31	0.14		4.31	0.14	9.73	0.27	Standard
140515_br2_paine@4	1.99	2.0137E-03	9.1124E-03	1.4290E+09	6.5486E-02	2.8777E+06	6.3412E-02	19:14	7.1803E+08		4.23	0.18		4.23	0.18	9.65	0.27	Standard
140515_br2_paine@5	1.99	2.0143E-03	8.7964E-03	1.4328E+09	3.4024E-02	2.8861E+06	3.8082E-02	19:18	7.2073E+08		4.53	0.18		4.54	0.18	9.95	0.27	Standard
140515_br2_paine@6	1.99	2.0144E-03	1.2133E-02	1.4436E+09	5.8303E-02	2.9079E+06	6.1019E-02	19:23	7.2413E+08		4.58	0.24		4.58	0.24	10.00	0.29	Standard
140515_br2_paine@7	2.00	2.0142E-03	1.0712E-02	1.4393E+09	2.7755E-02	2.8989E+06	3.1101E-02	19:28	7.2016E+08		4.51	0.21		4.51	0.21	9.93	0.28	Standard
140515_br2_paine@8	2.00	2.0141E-03	9.6234E-03	1.4760E+09	3.2841E-02	2.9728E+06	2.8371E-02	19:32	7.3914E+08		4.43	0.19		4.44	0.19	9.85	0.28	Standard
d18O_radio140515_Br2_gr1@1	2.00	2.0389E-03	1.5807E-02	1.4017E+09	6.0009E-02	2.8570E+06	4.0383E-02	19:37	7.0251E+08	7.0047E+08	16.82	0.32	15.58	16.82	0.32	22.31	0.31	Ki03s
d18O_radio140515_Br2_gr1@2	1.99	2.0401E-03	1.1066E-02	1.3951E+09	2.6177E-02	2.8463E+06	2.8260E-02	19:42	6.9982E+08	3.9415E+06	17.41	0.22	4.46	17.41	0.22	22.90	0.28	Ki03s
d18O_radio140515_Br2_gr1@3	1.99	2.0366E-03	9.9212E-03	1.3969E+09	3.0066E-02	2.8446E+06	3.4419E-02	19:46	7.0152E+08		15.67	0.20		15.67	0.20	21.15	0.28	Ki03s
d18O_radio140515_Br2_gr1@4	1.99	2.0301E-03	6.7530E-03	1.3913E+09	6.0588E-02	2.8247E+06	5.8691E-02	19:51	6.9802E+08		12.41	0.14		12.41	0.14	17.87	0.27	Ki03s
d18O_radio140515_Br2_gr2@1	2.00	2.0434E-03	1.2515E-02	1.3939E+09	3.5156E-02	2.8481E+06	3.2805E-02	19:55	6.9705E+08	6.9814E+08	19.06	0.25	18.44	19.06	0.25	24.55	0.29	Ki03s
d18O_radio140515_Br2_gr2@2	2.00	2.0401E-03	9.5465E-03	1.4051E+09	4.5668E-02	2.8666E+06	4.5191E-02	20:00	7.0281E+08	6.6714E+06	17.43	0.19	2.26	17.43	0.19	22.92	0.28	Ki03s
d18O_radio140515_Br2_gr2@3	2.00	2.0401E-03	1.0915E-02	1.3876E+09	3.4774E-02	2.8301E+06	2.9395E-02	20:05	6.9383E+08		17.41	0.22		17.41	0.22	22.90	0.28	Ki03s
d18O_radio140515_Br2_gr2@4	1.99	2.0418E-03	1.2076E-02	1.3929E+09	3.8936E-02	2.8446E+06	3.2173E-02	20:09	6.9964E+08		18.25	0.24		18.26	0.24	23.75	0.29	Ki03s
d18O_radio140515_Br2_gr2@5	1.99	2.0454E-03	1.0534E-02	1.3886E+09	3.1597E-02	2.8400E+06	3.1218E-02	20:14	6.9735E+08		20.05	0.21		20.05	0.21	25.55	0.28	Ki03s
140515_br2_paine@9	1.99	2.0142E-03	1.0504E-02	1.4825E+09	2.1759E-02	2.9862E+06	2.6957E-02	20:19	7.4444E+08	7.3844E+08	4.50	0.21	4.66	4.50	0.21	9.92	0.28	Standard
140515_br2_paine@10	2.00	2.0148E-03	1.4517E-02	1.4641E+09	4.3177E-02	2.9500E+06	4.1462E-02	20:23	7.3292E+08	1.2316E+07	4.80	0.29	0.30	4.80	0.29	10.22	0.30	Standard
140515_br2_paine@11	2.00	2.0143E-03	9.8040E-03	1.4658E+09	6.1377E-02	2.9528E+06	6.8370E-02	20:28	7.3335E+08		4.56	0.20		4.56	0.20	9.98	0.28	Standard
140515_br2_paine@12	1.99	2.0148E-03	1.2234E-02	1.4790E+09	3.6988E-02	2.9800E+06	4.3894E-02	20:32	7.4306E+08		4.77	0.24		4.78	0.24	10.19	0.29	Standard
d18O_radio140515_Br2_gr3@1	1.98	2.0471E-03	1.0873E-02	1.4265E+09	5.3185E-02	2.9205E+06	5.5674E-02	20:37	7.1934E+08	7.3124E+08	20.91	0.22	21.48	20.91	0.22	26.42	0.28	Ki22C1
d18O_radio140515_Br2_gr3@2	1.99	2.0485E-03	1.0795E-02	1.4613E+09	9.1119E-02	2.9933E+06	9.0378E-02	20:42	7.3557E+08	2.5396E+07	21.59	0.22	2.43	21.59	0.22	27.10	0.28	Ki22C1
d18O_radio140515_Br2_gr3@3	1.99	2.0520E-03	1.2653E-02	1.4484E+09	3.5080E-02	2.9722E+06	3.8923E-02	20:46	7.2778E+08		23.34	0.25		23.34	0.25	28.86	0.29	Ki22C1
d18O_radio140515_Br2_gr3@4	1.99	2.0470E-03	1.0114E-02	1.4856E+09	3.6346E-02	3.0400E+06	4.4932E-02	20:51	7.4644E+08		20.82	0.20		20.83	0.20	26.33	0.28	Ki22C1
d18O_radio140515_Br2_gr3@5	1.99	2.0434E-03	9.6476E-03	1.4038E+09	2.6716E-02	2.8682E+06	3.2176E-02	20:56	7.0582E+08		19.03	0.19		19.04	0.19	24.53	0.28	Ki22C1
d18O_radio140515_Br2_gr3@6	1.98	2.0490E-03	9.3152E-03	1.4458E+09	5.4291E-02	2.9627E+06	5.7843E-02	21:00	7.2875E+08		21.85	0.19		21.85	0.19	27.36	0.28	Ki22C1
d18O_radio140515_Br2_gr3@7	1.99	2.0507E-03	1.2197E-02	1.4703E+09	4.2753E-02	3.0152E+06	4.7936E-02	21:05	7.3772E+08		22.69	0.24		22.69	0.24	28.21	0.29	Ki22C1
d18O_radio140515_Br2_gr3@8	1.99	2.0481E-03	1.3244E-02	1.4837E+09	3.9313E-02	3.0387E+06	3.8180E-02	21:09	7.4454E+08		21.40	0.26		21.40	0.26	26.91	0.29	Ki22C1
d18O_radio140515_Br2_gr3@9	2.00	2.0487E-03	6.6624E-03	1.4671E+09	4.0567E-02	3.0057E+06	3.7622E-02	21:14	7.3516E+08		21.71	0.13		21.71	0.13	27.22	0.27	Ki22C1
140515_br2_paine@13	1.99	2.0142E-03	1.0027E-02	1.4674E+09	3.9020E-02	2.9559E+06	3.6676E-02	21:19	7.3604E+08	7.3321E+08	4.48	0.20	4.40	4.48	0.20	9.90	0.28	Standard
140515_br2_paine@14	1.99	2.0141E-03	9.3583E-03	1.4559E+09	5.8341E-02	2.9323E+06	6.0529E-02	21:23	7.3174E+08	3.9080E+06	4.46	0.19	0.18	4.46	0.19	9.88	0.27	Standard
140515_br2_paine@15	1.99	2.0139E-03	9.4521E-03	1.4584E+09	2.4628E-02	2.9378E+06	1.9779E-02	21:28	7.3295E+08		4.35	0.19		4.35	0.19	9.76	0.27	Standard
140515_br2_paine@16	1.99	2.0138E-03	1.3860E-02	1.4599E+09	2.7210E-02	2.9398E+06	3.2193E-02	21:33	7.3211E+08		4.30	0.28		4.30	0.28	9.72	0.29	Standard
d18O_radio140515_Br2_gr4@1	1.99	2.0424E-03	1.2517E-02	1.4415E+09	5.7240E-02	2.9441E+06	6.2154E-02	21:37	7.2258E+08	7.4529E+08	18.54	0.25	21.25	18.54	0.25	24.03	0.29	Ki22C2
d18O_radio140515_Br2_gr4@2	1.99	2.0478E-03	1.5479E-02	1.4899E+09	3.3808E-02	3.0516E+06	3.4507E-02	21:42	7.4771E+08	2.7189E+07	21.25	0.31	2.63	21.25	0.31	26.76	0.31	Ki22C2
d18O_radio140515_Br2_gr4@3	1.98	2.0427E-03	1.1041E-02	1.4480E+09	3.5966E-02	2.9575E+06	3.9393E-02	21:47	7.3067E+08		18.72	0.22		18.72	0.22	24.21	0.28	Ki22C2
d18O_radio140515_Br2_gr4@4	1.99	2.0482E-03	9.8935E-03	1.4368E+09	5.3914E-02	2.9430E+06	5.8898E-02	21:51	7.2217E+08		21.42	0.20		21.42	0.20	26.93	0.28	Ki22C2
d18O_radio140515_Br2_gr4@5	1.99	2.0491E-03	1.2985E-02	1.4888E+09	3.1612E-02	3.0508E+06	3.0725E-02	21:56	7.4641E+08		21.89	0.26		21.89	0.26	27.40	0.29	Ki22C2
d18O_radio140515_Br2_gr4@6	1.99	2.0485E-03	1.0735E-02	1.4898E+09	3.2229E-02	3.0522E+06	4.0204E-02	22:00	7.4800E+08		21.61	0.21		21.61	0.21	27.12	0.28	Ki22C2
d18O_radio140515_Br2_gr5@1	1.99	2.0470E-03	1.0590E-02	1.4803E+09	2.7127E-02	3.0301E+06	2.8287E-02	22:05	7.4394E+08		20.83	0.21		20.83	0.21	26.33	0.28	Ki21
d18O_radio140515_Br2_gr5@2	1.99	2.0503E-03	9.6154E-03	1.4873E+09	2.6907E-02	3.0497E+06	2.4176E-02	22:10	7.4825E+08		22.50	0.19		22.51	0.19	28.02	0.28	Ki21
d18O_radio140515_Br2_gr5@3	1.99	2.0486E-03	6.8234E-03	1.4823E+09	2.9963E-02	3.0364E+06	2.7771E-02	22:14	7.4346E+08		21.63	0.14		21.63	0.14	27.14	0.27	Ki21
d18O_radio140515_Br2_gr5@4	2.00	2.0476E-03	1.0200E-02	1.5054E+09	2.6344E-02	3.0815E+06	2.4642E-02	22:19	7.5447E+08		21.13	0.20		21.13	0.20	26.64	0.28	Ki21
d18O_radio140515_Br2_gr5@5	2.00	2.0502E-03	9.6912E-03	1.5205E+09	4.4074E-02	3.1181E+06	3.9582E-02	22:24	7.5917E+08		22.44	0.19		22.44	0.19	27.95	0.28	Ki21
d18O_radio140515_Br2_gr5@6	2.00	2.0484E-03	1.0873E-02	1.4908E+09	4.3648E-02	3.0540E+06	4.4622E-02	22:28	7.4683E+08		21.53	0.22		21.54	0.22	27.04	0.28	Ki21
d18O_radio140515_Br2_gr5@7	1.99	2.0520E-03	1.0148E-02	1.4613E+09	2.4649E-02	2.9989E+06	2.3251E-02	22:33	7.3343E+08		23.36	0.20		23.36	0.20	28.88	0.28	Ki21
d18O_radio140515_Br2_gr5@8	1.99	2.0461E-03	8.3618E-03	1.5487E+09	5.0461E-02	3.1687E+06	4.8005E-02	22:38	7.7670E+08		20.40	0.17		20.41	0.17	25.91	0.28	Ki21
d18O_radio140515_Br2_gr5@9	2.00	2.0505E-03	1.0648E-02	1.4919E+09	3.0944E-02	3.0594E+06	3.2686E-02	22:42	7.4714E+08		22.60	0.21		22.60	0.21	28.12	0.28	Ki21
d18O_radio140515_Br2_gr5@10	2.00	2.0456E-03	9.9916E-03	1.5073E+09	3.9431E-02	3.0832E+06	4.2336E-02	22:47	7.5363E+08		20.17	0.20		20.17	0.20	25.67	0.28	Ki21
140515_br2_paine@17	2.00	2.0142E-03	9.4454E-03	1.4595E+09	4.5298E-02	2.9399E+06	4.6275E-02	22:52	7.3113E+08	7.4063E+08	4.47	0.19	4.37	4.47	0.19	9.89	0.27	Standard
140515_br2_paine@18	2.00	2.0141E-03	9.0255E-03	1.4719E+09	5.6323E-02	2.9644E+06	5.5145E-02	22:56	7.3678E+08	1.6158E+07	4.42	0.18	0.17	4.42	0.18	9.84	0.27	Standard
140515_br2_paine@19	1.99	2.0138E-03	8.5434E-03	1.4885E+09	4.4780E-02	2.9977E+06	4.3428E-02	23:01	7.4647E+08		4.31	0.17		4.31	0.17	9.73	0.27	Standard
140515_br2_paine@20	2.00	2.0138E-03	1.2886E-02	1.4962E+09	2.2739E-02	3.0126E+06	2.7453E-02	23:05	7.4815E+08		4.29	0.26		4.29	0.26	9.71	0.29	Standard
d18O_radio140515_Br2_gr6@1	2.00	2.0578E-03	9.1688E-03	1.5231E+09	2.8598E-02	3.1342E+06	2.9968E-02	23:10	7.6110E+08		26.21	0.18	25.95	26.21	0.18	31.74	0.28	Ki15
d18O_radio140515_Br2_gr6@2	2.00	2.0572E-03	1.0059E-02	1.5107E+09	1.6305E-02	3.1076E+06	1.5332E-02	23:15	7.5710E+08		25.94	0.20	1.44	25.94	0.20	31.47	0.28	Ki15
d18O_radio140515_Br2_gr6@3	1.99	2.0548E-03	9.8617E-03	1.4837E+09	3.1167E-02	3.0499E+06	3.2894E-02	23:19	7.4520E+08		24.73	0.20		24.73	0.20	30.25	0.28	Ki15
d18O_radio140515_Br2_gr6@4	2.00	2.0585E-03	1.2934E-02	1.4987E+09	4.7440E-02	3.0842E+06	4.2849E-02	23:24	7.5051E+08		26.59	0.26		26.59	0.26	32.13	0.29	Ki15
d18O_radio140515_Br2_gr6@5	2.01	2.0581E-03	7.8919E-03	1.5086E+09	1.9408E-02	3.1051E+06	1.9347E-02	23:29	7.5195E+08		26.39	0.16		26.39	0.16	31.92	0.28	Ki15
d18O_radio140515_Br2_gr6@6	2.00	2.0577E-03	1.2480E-02	1.5266E+09	1.9646E-02	3.1414E+06	2.1926E-02	23:33	7.6190E+08		26.16	0.25		26.16	0.25	31.69	0.29	Ki15
d18O_radio140515_Br2_gr6@7	2.00	2.0584E-03	1.2653E-02	1.5127E+09	4.5715E-02	3.1138E+06	5.0727E-02	23:38	7.5671E+08		26.53	0.25		26.53	0.25	32.07	0.29	Ki15
d18O_radio140515_Br2_gr6@8	2.00	2.0580E-03	9.9670E-03	1.5252E+09	2.3034E-02	3.1389E+06	1.8790E-02	23:42	7.6176E+08		26.34	0.20		26.35	0.20	31.88	0.28	Ki15
d18O_radio140515_Br2_gr6@9	2.00	2.0545E-03	1.2870E-02	1.5223E+09	6.5557E-02	3.1276E+06	6.4638E-02	23:47	7.6111E+08		24.57	0.26		24.57	0.26	30.09	0.29	Ki15
d18O_radio140515_Br2_gr6@10	2.00	2.0575E-03	1.2083E-02	1.5043E+09	3.3333E-02	3.0952E+06	3.1344E-02	23:52	7.5226E+08		26.08	0.24		26.08	0.24	31.61	0.29	Ki15

Table A2 Continued.

SIMS ANALYSES								Mount: BR2		Standard: UNIL-Q1 (Paine)	Analyse: $\delta^{18}O$			Value= 9.81±0.14 (VSMOW, 2σ)				Date: 14.04.2015	
	Beam	H'2/L'2 ($^{18}O/^{16}O$)		L'2 (^{18}O/Coeff)		H'2 (^{16}O/Coeff)		Time	Yield	Measurements (‰)		mean	Drift correction (‰)		Calibration (‰)		Comment		
	nA	CPS	2SD	CPS	2SD	CPS	2SD		CPS/nA	$\delta^{18}O$	2SD int	2SD	$\delta^{18}O$	2SD	$\delta^{18}O_{VSMOW}$	2SD			
140515_br2_paine@25	2.00	2.0125E-03	8.2597E-03	1.5085E+09	1.0837E-02	3.0359E+06	1.3709E-02	23:56	7.5417E+08	3.65	0.17	4.18	3.65	0.17	9.06	0.27	Standard		
140515_br2_paine@26	2.00	2.0141E-03	1.3749E-02	1.4626E+09	4.3975E-02	2.9458E+06	5.4017E-02	0:01	7.3000E+08	4.42	0.27	0.76	4.42	0.27	9.84	0.29	Standard		
140515_br2_paine@27	2.00	2.0136E-03	9.5459E-03	1.4850E+09	2.2870E-02	2.9900E+06	2.2158E-02	0:06	7.4219E+08	4.17	0.19		4.17	0.19	9.58	0.28	Standard		
140515_br2_paine@28	2.00	2.0142E-03	1.1873E-02	1.4853E+09	3.8832E-02	2.9919E+06	3.9387E-02	0:10	7.4386E+08	4.49	0.24		4.49	0.24	9.91	0.28	Standard		
d18O_radio140515_Br2_gr7@1	2.00	2.0527E-03	1.5478E-02	1.5605E+09	6.3102E-02	3.2034E+06	6.7789E-02	0:15	7.8210E+08	23.68	0.31	23.75	23.68	0.31	29.20	0.31	Ki09		
d18O_radio140515_Br2_gr7@2	1.99	2.0532E-03	9.4119E-03	1.5769E+09	2.9077E-02	3.2385E+06	3.4585E-02	0:20	7.9252E+08	23.93	0.19	0.87	23.93	0.19	29.45	0.28	Ki09		
d18O_radio140515_Br2_gr7@3	1.99	2.0532E-03	7.8983E-03	1.5668E+09	2.2060E-02	3.2173E+06	2.2523E-02	0:24	7.8751E+08	23.95	0.16		23.95	0.16	29.48	0.27	Ki09		
d18O_radio140515_Br2_gr7@4	1.99	2.0530E-03	8.9644E-03	1.5539E+09	2.3064E-02	3.1902E+06	3.0209E-02	0:29	7.8061E+08	23.83	0.18		23.83	0.18	29.35	0.28	Ki09		
d18O_radio140515_Br2_gr7@5	2.00	2.0534E-03	9.2730E-03	1.5748E+09	1.7150E-02	3.2338E+06	1.7185E-02	0:34	7.8768E+08	24.02	0.19		24.02	0.19	29.54	0.28	Ki09		
d18O_radio140515_Br2_gr7@6	2.00	2.0536E-03	8.7920E-03	1.5326E+09	2.0553E-02	3.1470E+06	2.2563E-02	0:38	7.6632E+08	24.16	0.18		24.16	*0.18*	29.68	*0.28*	Ki09		
d18O_radio140515_Br2_gr7@7	2.00	2.0532E-03	9.2751E-03	1.5403E+09	1.3827E-02	3.1623E+06	1.5197E-02	0:43	7.7121E+08	23.95	0.19		23.95	0.19	29.47	0.28	Ki09		
d18O_radio140515_Br2_gr7@8	2.00	2.0507E-03	9.8689E-03	1.4999E+09	1.1862E-02	3.0759E+06	1.8338E-02	0:48	7.5146E+08	22.70	0.20		22.70	0.20	28.21	0.28	Ki09		
d18O_radio140515_Br2_gr7@9	2.00	2.0524E-03	8.3424E-03	1.5175E+09	2.3201E-02	3.1148E+06	2.6401E-02	0:52	7.6045E+08	23.53	0.17		23.53	0.17	29.05	0.28	Ki09		
140515_br2_paine@25	2.00	2.0125E-03	8.2597E-03	1.5085E+09	1.0837E-02	3.0359E+06	1.3709E-02	0:57	7.5417E+08	3.65	0.17	4.18	3.65	0.17	9.06	0.27	Standard		
140515_br2_paine@26	2.00	2.0141E-03	1.3749E-02	1.4626E+09	4.3975E-02	2.9458E+06	5.4017E-02	1:02	7.3000E+08	4.42	0.27	0.76	4.42	0.27	9.84	0.29	Standard		
140515_br2_paine@27	2.00	2.0136E-03	9.5459E-03	1.4850E+09	2.2870E-02	2.9900E+06	2.2158E-02	1:06	7.4219E+08	4.17	0.19		4.17	0.19	9.58	0.28	Standard		
140515_br2_paine@28	2.00	2.0142E-03	1.1873E-02	1.4853E+09	3.8832E-02	2.9919E+06	3.9387E-02	1:11	7.4386E+08	4.49	0.24		4.49	0.24	9.91	0.28	Standard		
d18O_radio140515_Br2_gr8@1	1.99	2.0544E-03	6.2092E-03	1.5709E+09	1.5287E-02	3.2268E+06	1.2770E-02	1:16	7.8745E+08	24.52	0.12	25.75	24.52	0.12	30.04	0.27	Ki4C		
d18O_radio140515_Br2_gr8@2	2.00	2.0547E-03	9.7278E-03	1.5733E+09	2.5268E-02	3.2329E+06	2.5208E-02	1:20	7.8586E+08	24.66	0.19	1.78	24.66	0.19	30.19	0.28	Ki4C		
d18O_radio140515_Br2_gr8@3	2.00	2.0553E-03	1.3332E-02	1.5736E+09	2.9982E-02	3.2349E+06	2.8401E-02	1:25	7.8719E+08	24.98	0.27		24.98	0.27	30.50	0.30	Ki4C		
d18O_radio140515_Br2_gr8@4	2.00	2.0570E-03	8.6687E-03	1.5576E+09	1.3254E-02	3.2038E+06	2.1054E-02	1:29	7.7850E+08	25.83	0.17		25.83	0.17	31.36	0.28	Ki4C		
d18O_radio140515_Br2_gr8@5	2.00	2.0593E-03	1.0546E-02	1.5500E+09	1.9507E-02	3.1927E+06	2.4540E-02	1:34	7.7653E+08	26.96	0.21		26.96	0.21	32.50	0.28	Ki4C		
d18O_radio140515_Br2_gr8@6	2.00	2.0566E-03	8.8795E-03	1.5845E+09	2.3793E-02	3.2583E+06	2.0756E-02	1:39	7.9390E+08	25.63	0.18		25.62	0.18	31.15	0.28	Ki4C		
d18O_radio140515_Br2_gr8@7	2.00	2.0575E-03	1.2316E-02	1.5632E+09	1.8248E-02	3.2163E+06	2.0853E-02	1:43	7.8180E+08	26.07	0.25		26.06	0.25	31.60	0.29	Ki4C		
d18O_radio140515_Br2_gr8@8	1.99	2.0579E-03	9.2151E-03	1.5582E+09	1.6052E-02	3.2062E+06	2.0276E-02	1:48	7.8111E+08	26.27	0.18		26.27	0.18	31.80	0.28	Ki4C		
d18O_radio140515_Br2_gr8@9	1.99	2.0590E-03	8.0311E-03	1.5713E+09	1.2521E-02	3.2353E+06	1.3137E-02	1:53	7.8934E+08	26.83	0.16		26.83	0.16	32.36	0.28	Ki4C		
140515_br2_paine@29	1.99	2.0136E-03	1.2263E-02	1.4803E+09	2.0893E-02	2.9809E+06	2.1863E-02	1:57	7.4350E+08	4.18	0.25	4.53	4.18	0.25	9.60	0.29	Standard		
140515_br2_paine@30	1.99	2.0141E-03	1.0785E-02	1.4852E+09	4.4082E-02	2.9915E+06	4.8745E-02	2:02	7.4540E+08	4.45	0.22	0.56	4.45	0.22	9.86	0.28	Standard		
140515_br2_paine@31	2.00	2.0145E-03	1.3614E-02	1.4826E+09	4.3489E-02	2.9873E+06	4.4552E-02	2:07	7.4126E+08	4.63	0.27		4.63	0.27	10.05	0.29	Standard		
140515_br2_paine@32	2.00	2.0149E-03	1.0551E-02	1.4837E+09	6.7282E-02	2.9893E+06	6.6640E-02	2:11	7.4147E+08	4.85	0.21		4.85	0.21	10.27	0.28	Standard		
d18O_radio140515_Br2_gr9@1	2.00	2.0571E-03	9.5420E-03	1.5571E+09	2.1809E-02	3.2037E+06	2.2612E-02	2:16	7.7975E+08	25.91	0.19	26.12	25.90	0.19	31.44	0.28	Ki44		
d18O_radio140515_Br2_gr9@2	2.00	2.0582E-03	1.0153E-02	1.5405E+09	2.4376E-02	3.1705E+06	2.6045E-02	2:21	7.7119E+08	26.42	0.20	0.87	26.41	0.20	31.95	0.28	Ki44		
d18O_radio140515_Br2_gr9@3	2.00	2.0583E-03	1.0939E-02	1.5424E+09	2.5690E-02	3.1745E+06	3.1688E-02	2:25	7.7176E+08	26.46	0.22		26.46	0.22	32.00	0.29	Ki44		
d18O_radio140515_Br2_gr9@4	2.01	2.0584E-03	1.1965E-02	1.5462E+09	2.0302E-02	3.1827E+06	2.3204E-02	2:30	7.6922E+08	26.53	0.24		26.52	0.24	32.06	0.29	Ki44		
d18O_radio140515_Br2_gr9@5	2.01	2.0557E-03	1.0936E-02	1.5377E+09	1.3379E-02	3.1608E+06	2.0601E-02	2:35	7.6648E+08	25.17	0.22		25.16	0.22	30.69	0.29	Ki44		
d18O_radio140515_Br2_gr9@6	2.00	2.0581E-03	9.5489E-03	1.5643E+09	2.2290E-02	3.2198E+06	2.0301E-02	2:39	7.8068E+08	26.38	0.19		26.38	0.19	31.91	0.28	Ki44		
d18O_radio140515_Br2_gr9@7	2.00	2.0579E-03	9.5134E-03	1.5516E+09	2.2132E-02	3.1932E+06	2.3971E-02	2:44	7.7517E+08	26.30	0.19		26.30	0.19	31.83	0.28	Ki44		
d18O_radio140515_Br2_gr9@8	2.01	2.0574E-03	9.4813E-03	1.5494E+09	2.5269E-02	3.1876E+06	2.1038E-02	2:48	7.7035E+08	26.04	0.19		26.03	0.19	31.57	0.28	Ki44		
d18O_radio140515_Br2_gr9@9	2.01	2.0571E-03	9.1190E-03	1.5578E+09	2.0742E-02	3.2046E+06	2.4767E-02	2:53	7.7403E+08	25.87	0.18		25.87	0.18	31.40	0.28	Ki44		
140515_br2_paine@33	2.01	2.0138E-03	1.0547E-02	1.4845E+09	3.9720E-02	2.9896E+06	4.3025E-02	2:58	7.3905E+08	4.29	0.21	4.48	4.29	0.21	9.70	0.28	Standard		
140515_br2_paine@34	2.00	2.0142E-03	8.1319E-03	1.4902E+09	5.5718E-02	3.0017E+06	5.7874E-02	3:02	7.4328E+08	4.49	0.16	0.27	4.49	0.16	9.91	0.27	Standard		
140515_br2_paine@35	2.01	2.0144E-03	1.0499E-02	1.4860E+09	5.5475E-02	2.9932E+06	5.9384E-02	3:07	7.4053E+08	4.60	0.21		4.59	0.21	10.01	0.28	Standard		
140515_br2_paine@36	2.01	2.0143E-03	1.2267E-02	1.4821E+09	2.6190E-02	2.9849E+06	3.3507E-02	3:12	7.3852E+08	4.56	0.25		4.55	0.25	9.97	0.29	Standard		
d18O_radio140515_Br2_gr10@1	2.01	2.0404E-03	1.4050E-02	1.5284E+09	2.5807E-02	3.1185E+06	2.3635E-02	3:16	7.6098E+08	17.55	0.28	19.42	17.55	0.28	23.04	0.30	Ki25up		
d18O_radio140515_Br2_gr10@2	2.01	2.0454E-03	9.1052E-03	1.5268E+09	3.1637E-02	3.1230E+06	3.3011E-02	3:21	7.5889E+08	20.06	0.18	4.97	20.06	0.18	25.56	0.28	Ki25up		
d18O_radio140515_Br2_gr10@3	2.01	2.0462E-03	1.2212E-02	1.5325E+09	1.6666E-02	3.1361E+06	1.5799E-02	3:26	7.6390E+08	20.46	0.24		20.46	0.24	25.96	0.29	Ki25up		
d18O_radio140515_Br2_gr10@4	2.01	2.0474E-03	8.5655E-03	1.5157E+09	1.9028E-02	3.1037E+06	1.9533E-02	3:30	7.5298E+08	21.06	0.17		21.05	0.17	26.56	0.28	Ki25up		
d18O_radio140515_Br2_gr10@5	2.02	2.0349E-03	1.5043E-02	1.4694E+09	2.8121E-02	2.9900E+06	3.7696E-02	3:35	7.2828E+08	14.79	0.30		14.79	0.30	20.26	0.30	Ki25up		
d18O_radio140515_Br2_gr10@6	2.02	2.0524E-03	1.3965E-02	1.5275E+09	1.9213E-02	3.1361E+06	3.1977E-02	3:40	7.5528E+08	23.54	0.28		23.54	0.28	29.06	0.30	Ki25up		
d18O_radio140515_Br2_gr10@7	2.02	2.0407E-03	1.5395E-02	1.5262E+09	3.1763E-02	3.1145E+06	3.4770E-02	3:44	7.5625E+08	17.70	0.31						Ki25up	Optical rejection	
d18O_radio140515_Br2_gr10@8	2.01	2.0445E-03	8.4551E-03	1.4997E+09	2.8287E-02	3.0655E+06	2.4565E-02	3:49	7.4628E+08	19.58	0.17		19.57	0.17	25.07	0.28	Ki25up		
d18O_radio140515_Br2_gr10@9	2.01	2.0453E-03	6.3718E-03	1.4969E+09	3.8126E-02	3.0627E+06	3.6583E-02	3:54	7.4372E+08	20.02	0.13		20.01	0.13	25.51	0.27	Ki25up		
140515_br2_paine@37	2.01	2.0142E-03	1.3017E-02	1.4842E+09	6.8412E-02	2.9895E+06	7.3530E-02	3:58	7.3850E+08	4.50	0.26	4.42	4.50	0.26	9.91	0.29	Standard		
140515_br2_paine@38	2.01	2.0139E-03	1.3526E-02	1.4713E+09	3.8917E-02	2.9631E+06	3.8115E-02	4:03	7.3090E+08	4.34	0.27	0.14	4.34	0.27	9.75	0.29	Standard		
140515_br2_paine@39	2.01	2.0140E-03	1.2609E-02	1.4901E+09	3.6778E-02	3.0011E+06	4.0231E-02	4:08	7.4089E+08	4.38	0.25		4.38	0.25	9.80	0.29	Standard		
140515_br2_paine@40	2.01	2.0141E-03	1.1093E-02	1.4844E+09	4.7458E-02	2.9895E+06	4.5383E-02	4:12	7.4027E+08	4.46	0.22		4.46	0.22	9.87	0.28	Standard		
d18O_radio140515_Br2_gr11@1	2.01	2.0542E-03	1.2385E-02	1.5052E+09	2.8608E-02	3.0917E+06	3.9070E-02	4:17	7.4808E+08	24.43	0.25	24.48	24.42	0.25	29.95	0.29	Ki35		
d18O_radio140515_Br2_gr11@2	2.01	2.0552E-03	1.3942E-02	1.4681E+09	5.0650E-02	3.0169E+06	4.9550E-02	4:22	7.2920E+08	24.94	0.28	0.84	24.94	0.28	30.47	0.30	Ki35		
d18O_radio140515_Br2_gr11@3	2.01	2.0540E-03	8.7273E-03	1.4545E+09	3.2119E-02	2.9878E+06	3.8597E-02	4:26	7.2296E+08	24.36	0.17		24.35	0.17	29.88	0.28	Ki35		
d18O_radio140515_Br2_gr11@4	2.01	2.0537E-03	9.8142E-03	1.4601E+09	4.9966E-02	2.9984E+06	5.2033E-02	4:31	7.2712E+08	24.21	0.20		24.20	0.20	29.72	0.28	Ki35		
d18O_radio140515_Br2_gr11@5	2.01	2.0535E-03	1.2990E-02	1.4505E+09	2.4116E-02	2.9791E+06	3.0135E-02	4:35	7.2247E+08	24.07	0.26		24.07	0.26	29.59	0.29	Ki35		
d18O_radio140515_Br2_gr11@6	2.02	2.0536E-03	7.0180E-03	1.4737E+09	3.1820E-02	3.0263E+06	3.4386E-02	4:40	7.2889E+08	24.14	0.14		24.13	0.14	29.65	0.27	Ki35		
d18O_radio140515_Br2_gr11@7	2.02	2.0541E-03	1.1239E-02	1.4644E+09	4.7109E-02	3.0079E+06	4.8573E-02	4:45	7.2516E+08	24.40	0.22		24.39	0.22	29.92	0.29	Ki35		
d18O_radio140515_Br2_gr11@8	2.01	2.0541E-03	8.9686E-03	1.4812E+09	4.3694E-02	3.0423E+06	4.4731E-02	4:49	7.3543E+08	24.38	0.18		24.38	0.18	29.90	0.28	Ki35		
d18O_radio140515_Br2_gr11@9	2.01	2.0561E-03	1.4276E-02	1.4918E+09	2.6651E-02	3.0668E+06	2.8144E-02	4:54	7.4118E+08	25.37	0.29		25.36	0.29	30.89	0.30	Ki35		

Table A2 Continued.

	SIMS ANALYSES							Mount: BR2	Standard: UNIL-Q1 (Paine)	Analyse: $\delta^{18}O$			Value= 9.81±0.14 (VSMOW, 2σ)				Date: 14.04.2015
	Beam	H'2/L'2 ($^{18}O/^{16}O$)		L'2 (^{18}O/Coeff)		H'2 (^{16}O/Coeff)		Time	Yield	Measurements (‰)		mean	Drift correction (‰)		Calibration (‰)		Comment
	nA	*CPS*	*2SD*	*CPS*	*2SD*	*CPS*	*2SD*		CPS/nA	$\delta^{18}O$	*2SD int*	*2SD*	$\delta^{18}O$	*2SD*	$\delta^{18}O_{VSMOW}$	*2SD*	
140515_br2_paine@41	2.01	2.0139E-03	1.2606E-02	1.4916E+09	4.4111E-02	3.0041E+06	4.8000E-02	4:59	7.4051E+08	4.36	0.25	4.49	4.36	0.25	9.77	0.29	Standard
140515_br2_paine@42	2.02	2.0143E-03	7.5291E-03	1.4967E+09	5.8138E-02	3.0150E+06	6.0334E-02	5:03	7.4260E+08	4.54	0.15	0.33	4.53	0.15	9.95	0.27	Standard
140515_br2_paine@43	2.01	2.0136E-03	9.7661E-03	1.4941E+09	4.9050E-02	3.0085E+06	5.0592E-02	5:08	7.4173E+08	4.19	0.20		4.19	0.20	9.60	0.28	Standard
140515_br2_paine@44	2.01	2.0143E-03	1.0264E-02	1.4966E+09	5.7832E-02	3.0146E+06	5.8963E-02	5:13	7.4592E+08	4.52	0.21		4.52	0.21	9.93	0.28	Standard
140515_br2_paine@45	2.00	2.0142E-03	7.4181E-03	1.4883E+09	4.0642E-02	2.9978E+06	3.7716E-02	5:17	7.4327E+08	4.47	0.15		4.47	0.15	9.88	0.27	Standard
140515_br2_paine@46	2.00	2.0146E-03	1.4133E-02	1.4684E+09	4.9321E-02	2.9581E+06	5.5404E-02	5:22	7.3316E+08	4.68	0.28		4.68	0.28	10.10	0.29	Standard
140515_br2_paine@47	2.01	2.0145E-03	1.0599E-02	1.4818E+09	3.0936E-02	2.9847E+06	3.8462E-02	5:27	7.3779E+08	4.62	0.21		4.62	0.21	10.03	0.28	Standard

Table A2 Continued.

SIMS ANALYSES								Mount: BR3		Standard: UNIL-Q1 (Paine)	Analyse: $\delta^{18}O$			Value= 9.81±0.14 (VSMOW, 2σ)			Date: 14.04.2015
	Beam	H'2/L'2 ($^{18}O/^{16}O$)		L'2 (^{18}O/Coeff)		H'2 (^{16}O/Coeff)		Time	Yield	Measurements (‰)		mean	Drift correction (‰)		Calibration (‰)		Comment
	nA	CPS	2SD	CPS	2SD	CPS	2SD		CPS/nA	$\delta^{18}O$	2SD int	2SD	$\delta^{18}O$	2SD	$\delta^{18}O_{VSMOW}$	2SD	
140515_paine@1	1.97	2.0144E-03	7.5961E-03	1.5674E+09	4.5188E-02	3.1576E+06	4.7680E-02	8:26	7.9525E+08	4.57	0.15	4.56					Standard
140515_paine@2	1.98	2.0144E-03	1.1085E-02	1.5684E+09	4.4887E-02	3.1594E+06	4.3534E-02	8:30	7.9230E+08	4.61	0.22	0.22					Standard
140515_paine@3	1.98	2.0143E-03	1.7491E-02	1.5658E+09	3.6993E-02	3.1536E+06	3.3730E-02	8:34	7.9111E+08	4.52	0.35						Standard
140515_paine@4	1.97	2.0144E-03	1.3015E-02	1.5672E+09	3.0677E-02	3.1570E+06	2.9677E-02	8:38	7.9393E+08	4.60	0.26						Standard
140515_paine@5	1.98	2.0146E-03	8.9310E-03	1.5757E+09	5.6550E-02	3.1744E+06	5.1997E-02	8:43	7.9705E+08	4.69	0.18						Standard
140515_paine@6	1.98	2.0145E-03	9.6261E-03	1.5755E+09	4.8705E-02	3.1737E+06	5.2459E-02	8:47	7.9685E+08	4.66	0.19						Standard
140515_paine@7	1.99	2.0143E-03	8.8205E-03	1.5768E+09	4.9378E-02	3.1769E+06	4.1567E-02	8:51	7.9319E+08	4.52	0.18						Standard
140515_paine@8	1.98	2.0143E-03	9.9692E-03	1.5862E+09	3.7202E-02	3.1966E+06	3.5316E-02	8:56	8.0007E+08	4.54	0.20						Standard
140515_paine@9	1.98	2.0144E-03	9.9843E-03	1.5842E+09	3.7976E-02	3.1905E+06	3.2924E-02	9:00	8.0168E+08	4.59	0.20						Standard
140515_paine@10	1.98	2.0138E-03	1.3169E-02	1.5779E+09	4.8894E-02	3.1779E+06	4.9305E-02	9:04	7.9656E+08	4.30	0.26						Standard
d18O_radio140515_Br3_paine@1	1.97	2.0140E-03	1.1224E-02	1.5759E+09	5.9807E-02	3.1736E+06	6.2564E-02	9:53	8.0139E+08	4.40	0.22	4.53	4.24	0.22	9.60	0.22	Standard
d18O_radio140515_Br3_paine@2	1.98	2.0143E-03	1.0981E-02	1.5662E+09	3.3991E-02	3.1551E+06	3.6386E-02	9:57	7.9171E+08	4.52	0.22	0.38	4.36	0.22	9.73	0.22	Standard
d18O_radio140515_Br3_paine@3	1.98	2.0141E-03	7.7322E-03	1.5873E+09	5.4908E-02	3.1968E+06	5.3109E-02	10:02	8.0101E+08	4.45	0.15		4.30	0.15	9.66	0.20	Standard
d18O_radio140515_Br3_paine@4	1.98	2.0141E-03	1.2153E-02	1.5929E+09	3.1149E-02	3.2075E+06	3.2102E-02	10:07	8.0286E+08	4.45	0.24		4.30	0.24	9.66	0.23	Standard
d18O_radio140515_Br3_paine@5	1.98	2.0138E-03	8.9721E-03	1.5955E+09	3.4362E-02	3.2129E+06	3.2311E-02	10:11	8.0717E+08	4.27	0.18		4.12	0.18	9.48	0.21	Standard
d18O_radio140515_Br3_paine@6	1.98	2.0149E-03	9.7544E-03	1.6038E+09	5.1111E-02	3.2313E+06	5.2090E-02	10:16	8.1085E+08	4.84	0.20		4.69	0.20	10.06	0.21	Standard
d18O_radio140515_Br3_paine@7	1.98	2.0143E-03	9.7689E-03	1.6063E+09	5.7908E-02	3.2352E+06	5.6644E-02	10:20	8.1205E+08	4.53	0.20		4.39	0.20	9.75	0.21	Standard
d18O_radio140515_Br3_paine@8	1.98	2.0148E-03	9.1141E-03	1.5897E+09	4.7397E-02	3.2030E+06	5.1057E-02	10:25	8.0370E+08	4.79	0.18		4.65	0.18	10.02	0.21	Standard
d18O_radio140515_Br3_gr1@1	1.98	2.0627E-03	7.0126E-03	1.5795E+09	5.2311E-02	3.2590E+06	4.2582E-02	10:30	7.9896E+08	28.65	0.14	28.62	28.52	0.14	34.01	0.21	So08
d18O_radio140515_Br3_gr1@2	1.98	2.0641E-03	7.9866E-03	1.5653E+09	4.5819E-02	3.2303E+06	5.5423E-02	10:34	7.9042E+08	29.37	0.16	0.82	29.24	0.16	34.74	0.21	So08
d18O_radio140515_Br3_gr1@3	1.98	2.0624E-03	1.0332E-02	1.5809E+09	6.1447E-02	3.2606E+06	6.6979E-02	10:39	7.9943E+08	28.52	0.21		28.40	0.21	33.89	0.22	So08
d18O_radio140515_Br3_gr1@4	1.98	2.0625E-03	8.8849E-03	1.5863E+09	6.2522E-02	3.2716E+06	6.1141E-02	10:43	8.0237E+08	28.58	0.18		28.46	0.18	33.95	0.21	So08
d18O_radio140515_Br3_gr1@5	1.98	2.0629E-03	9.1006E-03	1.5762E+09	4.4274E-02	3.2515E+06	4.6674E-02	10:48	7.9672E+08	28.78	0.18		28.66	0.18	34.15	0.21	So08
d18O_radio140515_Br3_gr1@6	1.98	2.0614E-03	8.5968E-03	1.5802E+09	4.9633E-02	3.2582E+06	4.3214E-02	10:53	7.9820E+08	28.03	0.17		27.92	0.17	33.40	0.21	So08
d18O_radio140515_Br3_gr1@7	1.98	2.0621E-03	1.0961E-02	1.5830E+09	7.0530E-02	3.2646E+06	7.1747E-02	10:57	7.9943E+08	28.39	0.22		28.27	0.22	33.76	0.22	So08
d18O_radio140515_Br3_gr2@1	1.98	2.0602E-03	1.4264E-02	1.5541E+09	6.5466E-02	3.2018E+06	6.7887E-02	11:02	7.8398E+08	27.43	0.29	23.91	27.32	0.29	32.80	0.24	So07
d18O_radio140515_Br3_gr2@2	1.98	2.0593E-03	6.8244E-03	2.1206E+09	1.7804E-01	4.3670E+06	1.7613E-01	11:06	1.0697E+09	26.96	0.14	17.03	26.85	0.14	32.34	0.21	So07
d18O_radio140515_Br3_gr2@3	1.97	2.0622E-03	1.1080E-02	1.5730E+09	5.4932E-02	3.2439E+06	5.7170E-02	11:11	7.9736E+08	28.42	0.22		28.32	0.22	33.81	0.22	So07
d18O_radio140515_Br3_gr2@4	1.98	2.0596E-03	8.7962E-03	1.9483E+09	1.5611E-01	4.0124E+06	1.5205E-01	11:16	9.8607E+08	27.13	0.18		27.03	0.18	32.52	0.21	So07
d18O_radio140515_Br3_gr2@5	1.97	2.0578E-03	9.0787E-03	2.0793E+09	2.1865E-01	4.2788E+06	2.1698E-01	11:20	1.0528E+09	26.24	0.18		26.15	0.18	31.62	0.21	So07
d18O_radio140515_Br3_gr2@6	1.98	2.0583E-03	1.0504E-02	2.0309E+09	1.0032E-01	4.1805E+06	9.5310E-02	11:25	1.0254E+09	26.50	0.21		26.41	0.21	31.89	0.22	So07
d18O_radio140515_Br3_paine@9	1.99	2.0146E-03	9.1072E-03	1.6168E+09	3.4022E-01	3.2569E+06	3.4274E-01	11:29	8.1431E+08	4.67	0.18	4.62	4.58	0.18	9.94	0.21	Standard
d18O_radio140515_Br3_paine@10	1.98	2.0141E-03	8.3437E-03	1.5959E+09	3.7470E-02	3.2144E+06	3.5425E-02	11:34	8.0641E+08	4.45	0.17	0.31	4.37	0.17	9.73	0.21	Standard
d18O_radio140515_Br3_paine@11	1.98	2.0148E-03	7.4845E-03	1.6019E+09	1.7570E-01	3.2270E+06	1.7641E-01	11:39	8.0951E+08	4.81	0.15		4.73	0.15	10.09	0.20	Standard
d18O_radio140515_Br3_paine@12	1.98	2.0143E-03	9.3439E-03	1.6060E+09	5.5825E-02	3.2352E+06	5.7138E-02	11:43	8.1024E+08	4.56	0.19		4.49	0.19	9.85	0.21	Standard
d18O_radio140515_Br3_gr3@1	1.99	2.0553E-03	1.2495E-02	1.5931E+09	6.6427E-02	3.2742E+06	6.3870E-02	11:48	8.0224E+08	24.99	0.25	24.22	24.92	0.25	30.39	0.23	Ki07c
d18O_radio140515_Br3_gr3@2	1.98	2.0566E-03	1.1755E-02	1.5917E+09	5.0107E-02	3.2735E+06	5.1802E-02	11:52	8.0351E+08	25.63	0.24	3.71	25.56	0.24	31.03	0.23	Ki07c
d18O_radio140515_Br3_gr3@3	1.99	2.0493E-03	1.2591E-02	1.5870E+09	4.7491E-02	3.2522E+06	4.5062E-02	11:57	7.9928E+08	22.00	0.25		21.93	0.25	27.39	0.23	Ki07c
d18O_radio140515_Br3_gr3@4	1.98	2.0545E-03	1.2088E-02	1.5900E+09	6.7878E-02	3.2666E+06	6.7430E-02	12:02	8.0328E+08	24.59	0.24		24.52	0.24	29.99	0.23	Ki07c
d18O_radio140515_Br3_gr3@5	1.98	2.0480E-03	1.0745E-02	1.5753E+09	5.7108E-02	3.2265E+06	6.2246E-02	12:06	7.9607E+08	21.34	0.21		21.28	0.21	26.73	0.22	Ki07c
d18O_radio140515_Br3_gr3@6	1.98	2.0547E-03	1.1412E-02	1.5763E+09	6.5060E-02	3.2388E+06	6.3635E-02	12:11	7.9586E+08	24.66	0.23		24.61	0.23	30.08	0.23	Ki07c
d18O_radio140515_Br3_gr4@1	1.98	2.0580E-03	1.0909E-02	1.5857E+09	3.7810E-02	3.2646E+06	4.8430E-02	12:15	8.0051E+08	26.33	0.22	23.38	26.28	0.22	31.76	0.22	Ki51top
d18O_radio140515_Br3_gr4@2	1.99	2.0589E-03	1.2698E-02	1.5931E+09	4.1088E-02	3.2808E+06	4.6143E-02	12:20	7.9876E+08	26.79	0.25	16.46	26.74	0.25	32.23	0.23	Ki51top
d18O_radio140515_Br3_gr4@3	1.99	2.0574E-03	7.9695E-03	1.5862E+09	3.2610E-02	3.2631E+06	3.3827E-02	12:25	7.9745E+08	26.06	0.16	19.04	26.01	0.16	31.49	0.21	Ki51top
d18O_radio140515_Br3_gr4@4	1.99	2.0589E-03	1.2118E-02	1.5862E+09	3.9742E-02	3.2659E+06	4.5912E-02	12:29	7.9824E+08	26.76	0.24		26.72	0.24	32.20	0.23	Ki51top
d18O_radio140515_Br3_gr4@5	1.98	2.0577E-03	1.0026E-02	1.5980E+09	9.6213E-02	3.2885E+06	9.6650E-02	12:34	8.0593E+08	26.19	0.20		26.16	0.20	31.63	0.22	Ki51top
d18O_radio140515_Br3_gr4@6	1.99	2.0589E-03	8.5302E-03	1.5845E+09	4.9684E-02	3.2627E+06	4.6286E-02	12:38	7.9640E+08	26.80	0.17		26.77	0.17	32.25	0.21	Ki51top
d18O_radio140515_Br3_paine@13	1.98	2.0147E-03	9.8334E-03	1.6005E+09	3.9950E-02	3.2252E+06	4.5947E-02	12:43	8.0644E+08	4.74	0.20	4.63	4.71	0.20	10.07	0.21	Standard
d18O_radio140515_Br3_paine@14	1.98	2.0147E-03	9.1502E-03	1.5807E+09	2.6666E-02	3.1846E+06	2.5008E-02	12:48	7.9706E+08	4.76	0.18	0.27	4.73	0.18	10.10	0.21	Standard
d18O_radio140515_Br3_paine@15	1.98	2.0144E-03	6.5430E-03	1.6096E+09	3.1934E-02	3.2421E+06	3.4734E-02	12:52	8.1466E+08	4.56	0.13		4.54	0.13	9.90	0.20	Standard
d18O_radio140515_Br3_paine@16	1.98	2.0142E-03	1.4387E-02	1.5927E+09	3.1478E-02	3.2082E+06	3.7717E-02	12:57	8.0328E+08	4.47	0.29		4.45	0.29	9.82	0.24	Standard
d18O_radio140515_Br3_gr5@1	1.98	2.0582E-03	1.1254E-02	1.5784E+09	3.9344E-02	3.2485E+06	4.1283E-02	13:01	7.9635E+08	26.44	0.23	25.38	26.42	0.23	31.90	0.22	Ki24down
d18O_radio140515_Br3_gr5@2	1.99	2.0562E-03	1.0787E-02	1.5973E+09	4.9794E-02	3.2841E+06	4.9763E-02	13:06	8.0217E+08	25.42	0.22	1.42	25.41	0.22	30.88	0.22	Ki24down
d18O_radio140515_Br3_gr5@3	1.99	2.0551E-03	1.0210E-02	1.5998E+09	7.6048E-02	3.2881E+06	7.8757E-02	13:11	8.0521E+08	24.90	0.20		24.89	0.20	30.36	0.22	Ki24down
d18O_radio140515_Br3_gr5@4	1.98	2.0545E-03	1.3236E-02	1.6002E+09	5.8976E-02	3.2879E+06	5.6577E-02	13:15	8.0751E+08	24.57	0.26		24.57	0.26	30.03	0.24	Ki24down
d18O_radio140515_Br3_gr5@5	1.99	2.0546E-03	8.5196E-03	1.5929E+09	4.2350E-02	3.2734E+06	3.5596E-02	13:20	8.0103E+08	24.64	0.17		24.64	0.17	30.11	0.21	Ki24down
d18O_radio140515_Br3_gr5@6	1.99	2.0569E-03	9.6288E-03	1.5969E+09	2.4274E-02	3.2845E+06	3.3297E-02	13:24	8.0269E+08	25.77	0.19		25.78	0.19	31.25	0.22	Ki24down
d18O_radio140515_Br3_gr6@1	2.00	2.0572E-03	6.2610E-03	1.6021E+09	5.0197E-02	3.2959E+06	4.9153E-02	13:29	8.0216E+08	25.94	0.13	23.21	25.95	0.13	31.42	0.20	Ki06c
d18O_radio140515_Br3_gr6@2	1.99	2.0560E-03	9.6086E-03	1.6066E+09	6.4770E-02	3.3030E+06	6.6236E-02	13:33	8.0621E+08	25.33	0.19	16.98	25.34	0.19	30.81	0.22	Ki06c
d18O_radio140515_Br3_gr6@3	2.00	2.0573E-03	1.1267E-02	1.6098E+09	6.2885E-02	3.3115E+06	6.0649E-02	13:38	8.0554E+08	26.00	0.23		26.01	0.23	31.49	0.22	Ki06c
d18O_radio140515_Br3_gr6@4	2.00	2.0607E-03	9.5554E-03	1.6162E+09	4.4613E-02	3.3306E+06	4.1091E-02	13:43	8.0839E+08	27.70	0.19		27.72	0.19	33.20	0.22	Ki06c
d18O_radio140515_Br3_gr6@5	2.00	2.0562E-03	8.3557E-03	1.6083E+09	6.0586E-02	3.3070E+06	6.2021E-02	13:47	8.0441E+08	25.43	0.17		25.45	0.17	30.93	0.21	Ki06c
d18O_radio140515_Br3_gr6@6	2.00	2.0613E-03	8.5896E-03	1.5995E+09	4.4099E-02	3.2968E+06	4.4749E-02	13:52	7.9837E+08	27.97	0.17		27.99	0.17	33.48	0.21	Ki06c
d18O_radio140515_Br3_paine@17	2.00	2.0134E-03	1.8619E-02	1.6222E+09	4.2488E-02	3.2663E+06	4.9269E-02	13:57	8.1061E+08	4.11	0.37	4.24	4.13	0.37	9.49	0.27	Standard
d18O_radio140515_Br3_paine@18	2.00	2.0137E-03	1.0385E-02	1.6176E+09	4.8985E-02	3.2577E+06	5.4165E-02	14:01	8.0984E+08	4.23	0.21	0.29	4.26	0.21	9.63	0.22	Standard
d18O_radio140515_Br3_paine@19	1.99	2.0136E-03	6.2335E-03	1.6170E+09	5.5978E-02	3.2561E+06	5.7822E-02	14:06	8.1186E+08	4.17	0.12		4.20	0.12	9.56	0.20	Standard
d18O_radio140515_Br3_paine@920	2.00	2.0141E-03	1.3886E-02	1.6159E+09	3.8743E-02	3.2554E+06	4.0580E-02	14:10	8.0885E+08	4.44	0.28		4.47	0.28	9.84	0.23	Standard

Table A2 Continued.

SIMS ANALYSES							Mount: BR3		Standard: UNIL-Q1 (Paine)		Analyse: $\delta^{18}O$			Value= 9.81±0.14 (VSMOW, 2σ)				Date: 14.04.2015
	Beam	H'2/L'2 ($^{18}O/^{16}O$)		L'2 (^{18}O/Coeff)		H'2 (^{16}O/Coeff)		Time	Yield		Measurements (‰)		mean	Drift correction (‰)		Calibration (‰)		Comment
	nA	*CPS*	*2SD*	*CPS*	*2SD*	*CPS*	*2SD*		CPS/nA		$\delta^{18}O$	*2SD int*	*2SD*	$\delta^{18}O$	*2SD*	$\delta^{18}O_{VSMOW}$	*2SD*	
d18O_radio140515_Br3_gr7@1	1.99	2.0579E-03	9.8242E-03	1.5945E+09	4.1556E-02	3.2810E+06	4.7304E-02	14:15	8.0094E+08	8.0172E+08	26.26	0.20	25.41	26.30	0.20	31.78	0.22	Ki58
d18O_radio140515_Br3_gr7@2	1.99	2.0567E-03	1.1881E-02	1.5875E+09	3.6403E-02	3.2662E+06	3.4088E-02	14:19	7.9653E+08	7.1286E+06	25.71	0.24	1.70	25.75	0.24	31.22	0.23	Ki58
d18O_radio140515_Br3_gr7@3	1.99	2.0543E-03	1.1860E-02	1.6034E+09	3.8438E-02	3.2939E+06	4.3818E-02	14:24	8.0563E+08		24.48	0.24		24.53	0.24	30.00	0.23	Ki58
d18O_radio140515_Br3_gr7@4	2.00	2.0580E-03	1.0815E-02	1.5997E+09	3.3992E-02	3.2919E+06	3.5435E-02	14:29	8.0115E+08		26.31	0.22		26.36	0.22	31.84	0.22	Ki58
d18O_radio140515_Br3_gr7@5	2.00	2.0565E-03	8.6944E-03	1.6091E+09	4.7579E-02	3.3093E+06	4.7838E-02	14:33	8.0595E+08		25.60	0.17		25.66	0.17	31.13	0.21	Ki58
d18O_radio140515_Br3_gr7@6	2.00	2.0562E-03	1.0563E-02	1.5966E+09	5.5373E-02	3.2832E+06	6.2954E-02	14:38	8.0013E+08		25.42	0.21		25.47	0.21	30.95	0.22	Ki58
d18O_radio140515_Br3_gr8@1	1.99	2.0535E-03	1.0402E-02	1.6009E+09	5.4207E-02	3.2874E+06	5.5081E-02	14:42	8.0487E+08	8.0602E+08	24.07	0.21	22.30	24.13	0.21	29.59	0.22	Ki02c
d18O_radio140515_Br3_gr8@2	1.99	2.0585E-03	9.4521E-03	1.6209E+09	5.2628E-02	3.3369E+06	5.0725E-02	14:47	8.1461E+08	9.0089E+06	26.59	0.19	16.02	26.65	0.19	32.13	0.22	Ki02c
d18O_radio140515_Br3_gr8@3	2.00	2.0554E-03	8.1359E-03	1.6080E+09	5.9228E-02	3.3054E+06	6.0502E-02	14:52	8.0398E+08		25.04	0.16		25.11	0.16	30.58	0.21	Ki02c
d18O_radio140515_Br3_gr8@4	2.00	2.0546E-03	7.3647E-03	1.6120E+09	3.1208E-02	3.3113E+06	2.5613E-02	14:56	8.0713E+08		24.64	0.15		24.71	*0.15*	30.18	*0.21*	Ki02c
d18O_radio140515_Br3_gr8@5	2.00	2.0554E-03	9.8535E-03	1.6028E+09	4.9655E-02	3.2946E+06	5.1795E-02	15:01	8.0277E+08		25.03	0.20		25.10	0.20	30.57	0.22	Ki02c
d18O_radio140515_Br3_gr8@6	2.00	2.0583E-03	1.0983E-02	1.6032E+09	5.6943E-02	3.2998E+06	5.8913E-02	15:05	8.0279E+08		26.47	0.22		26.54	0.22	32.02	0.22	Ki02c
d18O_radio140515_Br3_paine@21	1.99	2.0137E-03	1.1746E-02	1.6216E+09	4.8692E-02	3.2667E+06	5.8164E-02	15:10	8.1317E+08	8.0763E+08	4.25	0.23	4.31	4.33	0.23	9.69	0.22	Standard
d18O_radio140515_Br3_paine@22	1.99	2.0136E-03	1.4682E-02	1.6079E+09	5.4959E-02	3.2377E+06	5.7112E-02	15:15	8.0674E+08	8.4847E+06	4.19	0.29	0.23	4.27	0.29	9.63	0.24	Standard
d18O_radio140515_Br3_paine@23	1.99	2.0139E-03	1.4136E-02	1.6090E+09	5.4740E-02	3.2405E+06	6.1151E-02	15:19	8.0771E+08		4.34	0.28		4.43	0.28	9.79	0.24	Standard
d18O_radio140515_Br3_paine@24	2.00	2.0141E-03	1.0659E-02	1.6022E+09	3.9530E-02	3.2268E+06	4.0008E-02	15:24	8.0288E+08		4.45	0.21		4.54	0.21	9.91	0.22	Standard
d18O_radio140515_Br3_gr9@1	2.00	2.0566E-03	7.8349E-03	1.6039E+09	3.6382E-02	3.2987E+06	3.8441E-02	15:28	8.0379E+08	8.0457E+08	25.63	0.16	25.81	25.73	0.16	31.20	0.21	Ro01
d18O_radio140515_Br3_gr9@2	2.00	2.0559E-03	6.5617E-03	1.6152E+09	5.5207E-02	3.3206E+06	5.7953E-02	15:33	8.0843E+08	4.3833E+06	25.27	0.13	2.85	25.37	0.13	30.85	0.20	Ro01
d18O_radio140515_Br3_gr9@3	1.99	2.0529E-03	1.0474E-02	1.5949E+09	4.4644E-02	3.2741E+06	4.8635E-02	15:38	8.0251E+08		23.81	0.21		23.91	0.21	29.38	0.22	Ro01
d18O_radio140515_Br3_gr9@4	2.00	2.0568E-03	1.1236E-02	1.6064E+09	5.4170E-02	3.3040E+06	5.5845E-02	15:42	8.0469E+08		25.71	0.22		25.82	0.22	31.29	0.22	Ro01
d18O_radio140515_Br3_gr9@5	2.00	2.0570E-03	1.1767E-02	1.6041E+09	2.9637E-02	3.2993E+06	2.9767E-02	15:47	8.0266E+08		25.84	0.24		25.95	0.24	31.42	0.23	Ro01
d18O_radio140515_Br3_gr9@6	2.00	2.0569E-03	1.0355E-02	1.6144E+09	5.5648E-02	3.3209E+06	5.8142E-02	15:51	8.0532E+08		25.80	0.21		25.91	0.21	31.39	0.22	Ro01
d18O_radio140515_Br3_gr10@1	2.00	2.0626E-03	1.0964E-02	1.6014E+09	6.1221E-02	3.3039E+06	6.9828E-02	15:56	8.0096E+08	8.0458E+08	28.60	0.22	25.27	28.72	0.22	34.21	0.22	So09
d18O_radio140515_Br3_gr10@2	1.99	2.0621E-03	7.3478E-03	1.6060E+09	3.8774E-02	3.3115E+06	3.9660E-02	16:01	8.0563E+08	8.1086E+06	28.38	0.15	18.44	28.50	0.15	33.99	0.21	So09
d18O_radio140515_Br3_gr10@3	1.99	2.0635E-03	1.5496E-02	1.6192E+09	6.4650E-02	3.3411E+06	6.6010E-02	16:05	8.1212E+08		29.06	0.31		29.18	0.31	34.68	0.25	So09
d18O_radio140515_Br3_gr10@4	2.00	2.0629E-03	6.7772E-03	1.6034E+09	6.3745E-02	3.3077E+06	6.5363E-02	16:10	8.0192E+08		28.76	0.14		28.89	0.14	34.38	0.21	So09
d18O_radio140515_Br3_gr10@5	2.00	2.0620E-03	7.1795E-03	1.6086E+09	4.5577E-02	3.3171E+06	4.4597E-02	16:14	8.0428E+08		28.34	0.14		28.47	0.14	33.96	0.21	So09
d18O_radio140515_Br3_gr10@6	2.01	2.0641E-03	9.8248E-03	1.6107E+09	5.9519E-02	3.3247E+06	5.7385E-02	16:19	8.0260E+08		29.39	0.20		29.52	0.20	35.02	0.22	So09
d18O_radio140515_Br3_paine@25	2.00	2.0140E-03	1.0113E-02	1.6226E+09	3.3302E-02	3.2678E+06	2.7709E-02	16:24	8.1061E+08	8.1053E+08	4.38	0.20	4.32	4.52	0.20	9.88	0.21	Standard
d18O_radio140515_Br3_paine@26	2.00	2.0138E-03	7.3749E-03	1.6226E+09	6.7910E-02	3.2677E+06	6.5738E-02	16:28	8.1055E+08	4.1039E+06	4.29	0.15	0.21	4.43	0.15	9.79	0.20	Standard
d18O_radio140515_Br3_paine@27	2.01	2.0139E-03	7.8518E-03	1.6245E+09	6.8367E-02	3.2714E+06	6.5860E-02	16:33	8.0845E+08		4.36	0.16		4.51	0.16	9.87	0.21	Standard
d18O_radio140515_Br3_paine@28	2.00	2.0137E-03	9.6395E-03	1.6249E+09	5.7790E-02	3.2721E+06	5.6906E-02	16:37	8.1335E+08		4.24	0.19		4.39	0.19	9.75	0.21	Standard
d18O_radio140515_Br3_paine@29	2.00	2.0142E-03	1.5898E-02	1.6114E+09	5.7144E-02	3.2457E+06	5.6851E-02	16:42	8.0747E+08		4.48	0.32		4.63	0.32	9.99	0.25	Standard
d18O_radio140515_Br3_paine@30	2.00	2.0138E-03	1.0493E-02	1.6223E+09	3.9456E-02	3.2671E+06	3.7203E-02	16:47	8.1240E+08		4.31	0.21		4.46	0.21	9.82	0.22	Standard
d18O_radio140515_Br3_paine@31	2.00	2.0135E-03	1.6753E-02	1.6213E+09	7.1055E-02	3.2649E+06	7.3036E-02	16:52	8.1090E+08		4.15	0.34		4.31	0.34	9.67	0.25	Standard

Table A2 Continued.

	SIMS ANALYSES							Mount: BR4		Standard: UNIL-Q1 (Paine)		Analyse: $\delta^{18}O$		Value= 9.81±0.14 (VSMOW, 2σ)			Date: 15.04.2015
	Beam	H'2/L'2 ($^{18}O/^{16}O$)		L'2 (^{18}O/Coeff)		H'2 (^{16}O/Coeff)		Time	Yield	Measurements (‰)		mean	Drift correction (‰)		Calibration (‰)		Comment
	nA	CPS	2SD	CPS	2SD	CPS	2SD		CPS/nA	$\delta^{18}O$	2SD int	2SD	$\delta^{18}O$	2SD	$\delta^{18}O_{VSMOW}$	2SD	
painetest@1	2.03	2.0128E-03	6.6115E-03	1.6665E+09	6.0345E-02	3.3541E+06	6.1440E-02	16:53	8.2107E+08	3.78	0.13	3.87					Standard
painetest@2	2.04	2.0135E-03	9.9076E-03	1.6795E+09	5.8593E-02	3.3813E+06	5.9778E-02	16:57	8.2462E+08	4.12	0.20	0.18					Standard
painetest@3	2.04	2.0128E-03	8.5675E-03	1.6707E+09	6.0638E-02	3.3628E+06	6.1744E-02	17:02	8.1719E+08	3.81	0.17						Standard
painetest@4	2.04	2.0129E-03	1.2050E-02	1.6703E+09	5.1319E-02	3.3623E+06	5.1232E-02	17:06	8.1840E+08	3.85	0.24						Standard
painetest@5	2.04	2.0125E-03	1.0420E-02	1.6687E+09	6.8309E-02	3.3584E+06	6.7110E-02	17:11	8.1805E+08	3.65	0.21						Standard
painetest@6	2.04	2.0134E-03	1.1243E-02	1.6710E+09	5.9893E-02	3.3641E+06	6.4247E-02	17:15	8.2070E+08	4.08	0.22						Standard
painetest@7	2.04	2.0125E-03	1.0240E-02	1.6690E+09	6.4622E-02	3.3581E+06	5.6129E-02	17:20	8.1875E+08	3.66	0.20						Standard
painetest@8	2.04	2.0133E-03	1.3648E-02	1.6759E+09	6.2192E-02	3.3741E+06	5.9052E-02	17:24	8.2077E+08	4.03	0.27						Standard
d18O_radio140515_Br6_paine@1	2.01	2.0130E-03	1.2063E-02	1.6573E+09	5.7584E-02	3.3361E+06	5.8641E-02	18:13	8.2328E+08	3.87	0.24	3.81	3.82	0.24	9.80	0.19	Standard
d18O_radio140515_Br6_paine@2	2.03	2.0126E-03	1.3146E-02	1.6583E+09	6.7066E-02	3.3374E+06	7.2164E-02	18:18	8.1787E+08	3.69	0.26	0.21	3.63	0.26	9.62	0.20	Standard
d18O_radio140515_Br6_paine@3	2.03	2.0128E-03	1.0243E-02	1.6676E+09	6.4683E-02	3.3567E+06	6.5774E-02	18:22	8.2021E+08	3.77	0.20		3.72	0.20	9.70	0.18	Standard
d18O_radio140515_Br6_paine@4	2.04	2.0129E-03	1.0343E-02	1.6716E+09	5.6885E-02	3.3648E+06	5.7190E-02	18:27	8.1937E+08	3.85	0.21		3.80	0.21	9.78	0.18	Standard
d18O_radio140515_Br6_paine@5	2.04	2.0130E-03	7.0072E-03	1.6696E+09	6.0927E-02	3.3611E+06	5.7248E-02	18:31	8.1734E+08	3.89	0.14		3.84	0.14	9.82	0.16	Standard
d18O_radio140515_Br6_paine@6	2.04	2.0125E-03	7.9833E-03	1.6723E+09	6.7213E-02	3.3655E+06	6.8291E-02	18:36	8.1943E+08	3.63	0.16		3.58	0.16	9.56	0.17	Standard
d18O_radio140515_Br6_paine@7	2.04	2.0128E-03	6.2833E-03	1.6732E+09	5.9769E-02	3.3678E+06	5.9234E-02	18:40	8.2120E+08	3.81	0.13		3.75	0.13	9.74	0.16	Standard
d18O_radio140515_Br6_paine@8	2.04	2.0131E-03	9.3588E-03	1.6707E+09	7.2400E-02	3.3633E+06	7.4907E-02	18:44	8.1884E+08	3.95	0.19		3.90	0.19	9.89	0.17	Standard
d18O_radio150515_Br4_gr1@1	2.04	2.0126E-03	1.0713E-02	1.7466E+09	1.9396E-01	3.5153E+06	1.9457E-01	18:49	8.5588E+08	3.70	0.21	28.66					So28 Optical rejection
d18O_radio150515_Br4_gr1@2	2.05	2.0639E-03	1.0934E-02	1.6641E+09	7.8706E-02	3.4349E+06	7.9034E-02	18:53	8.1346E+08	29.30	0.22	1.31	29.25	0.22	35.38	0.19	So28
d18O_radio150515_Br4_gr1@3	2.05	2.0622E-03	1.0006E-02	1.6176E+09	6.9460E-02	3.3359E+06	6.8421E-02	18:58	7.9054E+08	28.44	0.20		28.39	0.20	34.52	0.18	So28
d18O_radio150515_Br4_gr1@4	2.04	2.0628E-03	1.1832E-02	1.6309E+09	8.6208E-02	3.3643E+06	9.0018E-02	19:02	8.0026E+08	28.72	0.24		28.68	0.24	34.81	0.19	So28
d18O_radio150515_Br4_gr1@5	2.03	2.0635E-03	8.7081E-03	1.6403E+09	6.8295E-02	3.3844E+06	7.1627E-02	19:07	8.0623E+08	29.06	0.17		29.02	0.17	35.15	0.17	So28
d18O_radio150515_Br4_gr1@6	2.03	2.0627E-03	8.6922E-03	1.6381E+09	9.4310E-02	3.3791E+06	9.5999E-02	19:11	8.0524E+08	28.66	0.17		28.62	0.17	34.75	0.17	So28
d18O_radio150515_Br4_gr1@7	2.03	2.0618E-03	9.7494E-03	1.6533E+09	8.1503E-02	3.4090E+06	8.0144E-02	19:16	8.1268E+08	28.24	0.19		28.20	0.19	34.33	0.18	So28
d18O_radio150515_Br4_gr1@8	2.04	2.0602E-03	6.5240E-03	1.6480E+09	1.0019E-01	3.3951E+06	9.8400E-02	19:20	8.0874E+08	27.41	0.13		27.36	0.13	33.49	0.16	So28
d18O_radio150515_Br4_gr1@9	2.04	2.0643E-03	9.9301E-03	1.6524E+09	7.3786E-02	3.4107E+06	7.8049E-02	19:25	8.0879E+08	29.46	0.20		29.42	0.20	35.56	0.18	So28
d18O_radio140515_Br6_paine@9	2.04	2.0131E-03	1.1790E-02	1.6703E+09	7.1457E-02	3.3626E+06	7.0241E-02	19:29	8.1938E+08	3.96	0.24	4.00	3.92	0.24	9.90	0.19	Standard
d18O_radio140515_Br6_paine@10	2.04	2.0132E-03	1.0369E-02	1.6724E+09	5.7800E-02	3.3666E+06	6.0129E-02	19:33	8.1831E+08	3.97	0.21	0.10	3.93	0.21	9.91	0.18	Standard
d18O_radio140515_Br6_paine@11	2.03	2.0132E-03	1.4134E-02	1.6672E+09	5.1836E-02	3.3566E+06	5.6460E-02	19:38	8.1961E+08	4.01	0.28		3.97	0.28	9.95	0.20	Standard
d18O_radio140515_Br6_paine@12	2.03	2.0134E-03	9.9310E-03	1.6697E+09	7.1045E-02	3.3601E+06	6.3874E-02	19:42	8.2351E+08	4.07	0.20		4.03	0.20	10.01	0.18	Standard
d18O_radio140515_Br6_gr2@1	2.03	2.0606E-03	7.5153E-03	1.6508E+09	8.5454E-02	3.4018E+06	8.6739E-02	19:47	8.1405E+08	27.64	0.15	26.58	27.60	0.15	33.73	0.17	So17
d18O_radio140515_Br6_gr2@2	2.03	2.0610E-03	1.3998E-02	1.6299E+09	8.7293E-02	3.3592E+06	8.9474E-02	19:51	8.0145E+08	27.84	0.28	5.24	27.80	0.28	33.93	0.21	So17
d18O_radio140515_Br6_gr2@3	2.04	2.0600E-03	1.1269E-02	1.6309E+09	7.3518E-02	3.3598E+06	7.9697E-02	19:56	8.0034E+08	27.35	0.23		27.32	0.23	33.44	0.19	So17
d18O_radio140515_Br6_gr2@4	2.03	2.0452E-03	1.0559E-02	1.6003E+09	7.5922E-02	3.2728E+06	7.5878E-02	20:00	7.8638E+08	19.94	0.21		19.91	0.21	25.99	0.18	So17
d18O_radio140515_Br6_gr2@5	2.03	2.0560E-03	9.8680E-03	1.6332E+09	4.9607E-02	3.3581E+06	5.0205E-02	20:05	8.0493E+08	25.34	0.20		25.30	0.20	31.42	0.18	So17
d18O_radio140515_Br6_gr2@6	2.04	2.0603E-03	6.6486E-03	1.6284E+09	7.6420E-02	3.3549E+06	7.7954E-02	20:09	7.9976E+08	27.50	0.13		27.46	0.13	33.59	0.16	So17
d18O_radio140515_Br6_gr2@7	2.03	2.0612E-03	8.4631E-03	1.6211E+09	6.7242E-02	3.3417E+06	6.8599E-02	20:13	7.9744E+08	27.92	0.17		27.88	0.17	34.01	0.17	So17
d18O_radio140515_Br6_gr2@8	2.04	2.0617E-03	1.2065E-02	1.6050E+09	8.3643E-02	3.3089E+06	8.4944E-02	20:18	7.8769E+08	28.16	0.24		28.13	0.24	34.26	0.19	So17
d18O_radio140515_Br6_gr2@9	2.03	2.0604E-03	8.5175E-03	1.6097E+09	7.1580E-02	3.3165E+06	7.1947E-02	20:22	7.9172E+08	27.53	0.17		27.49	0.17	33.62	0.17	So17
d18O_radio140515_Br6_paine@13	2.03	2.0133E-03	1.0406E-02	1.6731E+09	7.0130E-02	3.3688E+06	7.1789E-02	20:27	8.2422E+08	4.06	0.21	3.97	4.03	0.21	10.01	0.18	Standard
d18O_radio140515_Br6_paine@14	2.03	2.0131E-03	7.9494E-03	1.6718E+09	6.9382E-02	3.3652E+06	7.2143E-02	20:31	8.2281E+08	3.93	0.16	0.15	3.90	0.16	9.88	0.16	Standard
d18O_radio140515_Br6_paine@15	2.03	2.0132E-03	6.4113E-03	1.6791E+09	7.4820E-02	3.3805E+06	7.5146E-02	20:36	8.2753E+08	3.99	0.13		3.96	0.13	9.95	0.16	Standard
d18O_radio140515_Br6_paine@16	2.04	2.0130E-03	1.4092E-02	1.6802E+09	5.5541E-02	3.3812E+06	4.9147E-02	20:40	8.2420E+08	3.88	0.28		3.85	0.28	9.84	0.20	Standard
d18O_radio140515_Br6_gr3@1	2.04	2.0547E-03	7.2567E-03	1.6311E+09	6.4278E-02	3.3516E+06	6.9380E-02	20:45	8.0093E+08	24.71	0.15	25.36	24.68	0.15	30.79	0.16	Ki39
d18O_radio140515_Br6_gr3@2	2.04	2.0562E-03	6.0968E-03	1.6286E+09	6.4868E-02	3.3488E+06	6.6075E-02	20:49	7.9826E+08	25.42	0.12	1.06	25.39	0.12	31.51	0.16	Ki39
d18O_radio140515_Br6_gr3@3	2.03	2.0573E-03	1.2111E-02	1.6200E+09	6.7266E-02	3.3329E+06	7.1486E-02	20:54	7.9772E+08	25.99	0.24		25.96	0.24	32.08	0.19	Ki39
d18O_radio140515_Br6_gr3@4	2.03	2.0575E-03	9.4845E-03	1.6208E+09	6.9018E-02	3.3350E+06	6.4867E-02	20:58	7.9791E+08	26.07	0.19		26.04	0.19	32.16	0.18	Ki39
d18O_radio140515_Br6_gr3@5	2.03	2.0542E-03	8.2619E-03	1.6161E+09	8.7287E-02	3.3198E+06	8.3911E-02	21:02	7.9673E+08	24.44	0.17		24.41	0.17	30.52	0.17	Ki39
d18O_radio140515_Br6_gr3@6	2.04	2.0559E-03	6.9500E-03	1.6288E+09	8.6267E-02	3.3488E+06	8.5161E-02	21:07	7.9993E+08	25.30	0.14		25.27	0.14	31.39	0.16	Ki39
d18O_radio140515_Br6_gr3@7	2.04	2.0565E-03	1.3798E-02	1.6427E+09	8.7269E-02	3.3779E+06	8.7515E-02	21:11	8.0614E+08	25.59	0.28		25.57	0.28	31.69	0.20	Ki39
d18O_radio140515_Br6_gr3@8	2.04	2.0559E-03	7.5944E-03	1.6369E+09	8.8253E-02	3.3653E+06	8.9474E-02	21:16	8.0421E+08	25.26	0.15		25.24	0.15	31.35	0.17	Ki39
d18O_radio140515_Br6_gr3@9	2.04	2.0563E-03	6.9231E-03	1.6517E+09	7.3132E-02	3.3960E+06	7.2204E-02	21:20	8.1042E+08	25.46	0.14		25.44	0.14	31.55	0.16	Ki39
d18O_radio140515_Br6_paine@17	2.03	2.0128E-03	1.4981E-02	1.6804E+09	7.4403E-02	3.3827E+06	7.5310E-02	21:25	8.2612E+08	3.79	0.30	3.77	3.77	0.30	9.76	0.21	Standard
d18O_radio140515_Br6_paine@18	2.04	2.0126E-03	1.1448E-02	1.6748E+09	5.9975E-02	3.3706E+06	6.3258E-02	21:29	8.2182E+08	3.68	0.23	0.20	3.65	0.23	9.64	0.18	Standard
d18O_radio140515_Br6_paine@19	2.04	2.0130E-03	1.1013E-02	1.6734E+09	5.5880E-02	3.3686E+06	5.6228E-02	21:34	8.1936E+08	3.90	0.22		3.88	0.22	9.87	0.18	Standard
d18O_radio140515_Br6_paine@20	2.04	2.0126E-03	7.5113E-03	1.6755E+09	5.9092E-02	3.3724E+06	5.8587E-02	21:38	8.2245E+08	3.70	0.15		3.68	0.15	9.67	0.16	Standard
d18O_radio140515_Br6_gr4@1	2.03	2.0611E-03	1.2760E-02	1.6522E+09	5.9432E-02	3.4053E+06	6.0746E-02	21:43	8.1359E+08	27.88	0.26	28.16	27.86	0.26	33.99	0.20	So13
d18O_radio140515_Br6_gr4@2	2.03	2.0618E-03	9.3055E-03	1.6402E+09	6.9547E-02	3.3816E+06	7.1132E-02	21:47	8.0792E+08	28.24	0.19	0.80	28.22	0.19	34.36	0.18	So13
d18O_radio140515_Br6_gr4@3	2.03	2.0606E-03	1.1790E-02	1.6354E+09	6.7997E-02	3.3700E+06	6.9344E-02	21:51	8.0583E+08	27.63	0.24		27.62	0.24	33.74	0.19	So13
d18O_radio140515_Br6_gr4@4	2.03	2.0628E-03	8.8919E-03	1.6310E+09	7.5209E-02	3.3646E+06	7.2690E-02	21:56	8.0326E+08	28.71	0.18		28.69	0.18	34.83	0.17	So13
d18O_radio140515_Br6_gr4@5	2.03	2.0612E-03	6.5772E-03	1.6364E+09	7.3007E-02	3.3731E+06	7.0941E-02	22:00	8.0417E+08	27.92	0.13		27.91	0.13	34.04	0.16	So13
d18O_radio140515_Br6_gr4@6	2.03	2.0614E-03	1.3608E-02	1.6427E+09	7.5065E-02	3.3863E+06	7.8724E-02	22:05	8.0762E+08	28.02	0.27		28.00	0.27	34.13	0.20	So13
d18O_radio140515_Br6_gr4@7	2.04	2.0610E-03	1.0066E-02	1.6356E+09	8.0492E-02	3.3708E+06	7.9730E-02	22:09	8.0171E+08	27.85	0.20		27.83	0.20	33.96	0.18	So13
d18O_radio140515_Br6_gr4@8	2.04	2.0629E-03	6.0910E-03	1.6272E+09	5.9428E-02	3.3567E+06	5.8503E-02	22:14	7.9857E+08	28.78	0.12		28.77	0.12	34.90	0.16	So13
d18O_radio140515_Br6_gr4@9	2.04	2.0622E-03	1.0600E-02	1.6241E+09	6.3944E-02	3.3496E+06	6.3582E-02	22:18	7.9780E+08	28.41	0.21		28.40	0.21	34.53	0.18	So13
d18O_radio140515_Br6_paine@21	2.03	2.0134E-03	1.3811E-02	1.6781E+09	6.5189E-02	3.3787E+06	6.6906E-02	22:23	8.2643E+08	4.10	0.28	3.88	4.09	0.28	10.07	0.20	Standard
d18O_radio140515_Br6_paine@22	2.03	2.0126E-03	9.6559E-03	1.6764E+09	7.5909E-02	3.3740E+06	7.7536E-02	22:27	8.2428E+08	3.70	0.19	0.33	3.69	0.19	9.67	0.17	Standard
d18O_radio140515_Br6_paine@23	2.04	2.0130E-03	7.5023E-03	1.6745E+09	6.8699E-02	3.3710E+06	6.5879E-02	22:31	8.2069E+08	3.89	0.15		3.88	0.15	9.87	0.16	Standard
d18O_radio140515_Br6_paine@24	2.04	2.0129E-03	7.8080E-03	1.6712E+09	6.6718E-02	3.3627E+06	6.3211E-02	22:36	8.1830E+08	3.83	0.16		3.82	0.16	9.80	0.16	Standard

Table A2 Continued.

	SIMS ANALYSES					Mount: BR4			Standard: UNIL-Q1 (Paine)		Analyse: $\delta^{18}O$			Value= 9.81±0.14 (VSMOW, 2σ)				Date: 15.04.2015
	Beam	H'2/L'2 ($^{18}O/^{16}O$)		L'2 (^{18}O/Coeff)		H'2 (^{16}O/Coeff)		Time	Yield		Measurements (‰)		mean	Drift correction (‰)		Calibration (‰)		Comment
	nA	*CPS*	*2SD*	*CPS*	*2SD*	*CPS*	*2SD*		CPS/nA		$\delta^{18}O$	*2SD int*	*2SD*	$\delta^{18}O$	*2SD*	$\delta^{18}O_{VSMOW}$	*2SD*	
d18O_radio140515_Br6_gr5@1	2.04	2.0525E-03	9.9192E-03	1.6439E+09	4.7133E-02	3.3743E+06	4.4173E-02	22:40	8.0608E+08	8.0381E+08	23.59	0.20	22.46	23.58	0.20	29.68	0.18	Go 73
d18O_radio140515_Br6_gr5@2	2.03	2.0470E-03	8.9851E-03	1.6326E+09	7.0408E-02	3.3421E+06	7.3858E-02	22:45	8.0303E+08	8.0914E+06	20.87	0.18	1.98	20.86	0.18	26.95	0.17	Go 73
d18O_radio140515_Br6_gr5@3	2.03	2.0506E-03	6.7719E-03	1.6380E+09	5.2645E-02	3.3588E+06	5.4022E-02	22:49	8.0575E+08		22.62	0.14		22.61	0.14	28.71	0.16	Go 73
d18O_radio140515_Br6_gr5@4	2.03	2.0495E-03	7.5490E-03	1.6389E+09	6.0033E-02	3.3587E+06	6.3272E-02	22:54	8.0722E+08		22.11	0.15		22.10	0.15	28.20	0.17	Go 73
d18O_radio140515_Br6_gr5@5	2.04	2.0511E-03	8.9839E-03	1.6210E+09	5.8196E-02	3.3247E+06	6.0297E-02	22:58	7.9528E+08		22.87	0.18		22.86	0.18	28.96	0.17	Go 73
d18O_radio140515_Br6_gr5@6	2.04	2.0471E-03	8.6845E-03	1.6341E+09	5.6994E-02	3.3454E+06	5.7484E-02	23:03	8.0161E+08		20.88	0.17		20.88	0.17	26.96	0.17	Go 73
d18O_radio140515_Br6_gr5@7	2.04	2.0518E-03	9.3622E-03	1.6354E+09	6.1400E-02	3.3556E+06	6.3598E-02	23:07	8.0360E+08		23.24	0.19		23.23	0.19	29.33	0.17	Go 73
d18O_radio140515_Br6_gr5@8	2.04	2.0511E-03	1.0948E-02	1.6473E+09	4.6602E-02	3.3789E+06	4.6857E-02	23:11	8.0930E+08		22.90	0.22		22.90	0.22	29.00	0.18	Go 73
d18O_radio140515_Br6_gr5@9	2.03	2.0515E-03	1.1724E-02	1.6306E+09	6.6403E-02	3.3448E+06	6.8572E-02	23:16	8.0241E+08		23.09	0.23		23.09	0.23	29.19	0.19	Go 73
d18O_radio140515_Br6_paine@25	2.03	2.0128E-03	6.8165E-03	1.6575E+09	7.2023E-02	3.3361E+06	7.5977E-02	23:20	8.1572E+08	8.2451E+08	3.78	0.14	3.78	3.78	0.14	9.76	0.16	Standard
d18O_radio140515_Br6_paine@26	2.03	2.0131E-03	1.0038E-02	1.6657E+09	7.3176E-02	3.3532E+06	7.2728E-02	23:25	8.1998E+08	2.4027E+07	3.94	0.20	0.24	3.94	0.20	9.93	0.18	Standard
d18O_radio140515_Br6_paine@27	2.04	2.0126E-03	8.9633E-03	1.6692E+09	6.2025E-02	3.3593E+06	6.3903E-02	23:29	8.2007E+08		3.67	0.18		3.67	0.18	9.65	0.17	Standard
d18O_radio140515_Br6_paine@28	2.03	2.0127E-03	1.0576E-02	1.7129E+09	3.9317E-01	3.4476E+06	3.9562E-01	23:34	8.4227E+08		3.72	0.21		3.72	0.21	9.70	0.18	Standard
d18O_radio140515_Br6_gr6@1	2.08	2.0569E-03	8.6139E-03	1.6499E+09	6.1225E-02	3.3934E+06	6.0493E-02	23:38	7.9379E+08	8.1007E+08	25.76	0.17	25.56	25.76	0.17	31.88	0.17	Ki40
d18O_radio140515_Br6_gr6@2	2.03	2.0560E-03	1.1792E-02	1.6580E+09	7.2280E-02	3.4088E+06	7.1059E-02	23:43	8.1492E+08	2.0046E+07	25.35	0.24	1.22	25.35	0.24	31.46	0.19	Ki40
d18O_radio140515_Br6_gr6@3	2.03	2.0577E-03	7.7751E-03	1.6545E+09	6.3783E-02	3.4041E+06	6.7496E-02	23:47	8.1517E+08		26.16	0.16		26.16	0.16	32.28	0.17	Ki40
d18O_radio140515_Br6_gr6@4	2.03	2.0567E-03	1.1418E-02	1.6706E+09	6.6511E-02	3.4358E+06	6.2533E-02	23:52	8.2397E+08		25.67	0.23		25.68	0.23	31.79	0.19	Ki40
d18O_radio140515_Br6_gr6@5	2.06	2.0573E-03	1.0457E-02	1.6438E+09	6.2807E-02	3.3819E+06	6.0193E-02	23:56	7.9717E+08		26.00	0.21		26.00	0.21	32.12	0.18	Ki40
d18O_radio140515_Br6_gr6@6	2.04	2.0565E-03	1.3010E-02	1.6476E+09	4.0814E-02	3.3878E+06	3.7466E-02	0:01	8.0598E+08		25.59	0.26		25.59	0.26	31.71	0.20	Ki40
d18O_radio140515_Br6_gr6@7	2.04	2.0567E-03	9.9386E-03	1.6460E+09	6.9676E-02	3.3856E+06	6.7519E-02	0:05	8.0579E+08		25.67	0.20		25.68	0.20	31.79	0.18	Ki40
d18O_radio140515_Br6_gr6@8	2.04	2.0570E-03	7.2394E-03	1.6395E+09	4.4224E-02	3.3723E+06	4.4000E-02	0:09	8.0534E+08		25.82	0.14		25.82	0.14	31.94	0.16	Ki40
d18O_radio140515_Br6_gr6@9	2.03	2.0532E-03	1.2171E-02	1.6655E+09	5.7576E-02	3.4196E+06	5.9742E-02	0:14	8.2024E+08		23.94	0.24		23.95	0.24	30.06	0.19	Ki40
d18O_radio140515_Br6_gr6@10	2.04	2.0566E-03	8.1340E-03	1.6658E+09	5.2508E-02	3.4248E+06	4.6906E-02	0:18	8.1837E+08		25.64	0.16		25.64	0.16	31.76	0.17	Ki40
d18O_radio140515_Br6_paine@29	2.04	2.0131E-03	7.7599E-03	1.6811E+09	5.5309E-02	3.3841E+06	5.4268E-02	0:23	8.2469E+08	8.2486E+08	3.94	0.16	3.84	3.94	0.16	9.93	0.16	Standard
d18O_radio140515_Br6_paine@30	2.04	2.0129E-03	1.0935E-02	1.6801E+09	6.2244E-02	3.3819E+06	6.8602E-02	0:27	8.2455E+08	2.3284E+06	3.86	0.22	0.15	3.87	0.22	9.86	0.18	Standard
d18O_radio140515_Br6_paine@31	2.03	2.0128E-03	9.9995E-03	1.6744E+09	6.5245E-02	3.3701E+06	6.5109E-02	0:32	8.2371E+08		3.77	0.20		3.78	0.20	9.77	0.18	Standard
d18O_radio140515_Br6_paine@32	2.03	2.0128E-03	9.5395E-03	1.6800E+09	7.8006E-02	3.3813E+06	7.9009E-02	0:36	8.2648E+08		3.78	0.19		3.79	0.19	9.78	0.17	Standard
d18O_radio140515_Br6_gr7@1	2.04	2.0645E-03	1.0391E-02	1.6652E+09	5.3227E-02	3.4378E+06	5.5013E-02	0:41	8.1560E+08	8.2039E+08	29.59	0.21	29.14	29.60	0.21	35.74	0.18	So25
d18O_radio140515_Br6_gr7@2	2.04	2.0641E-03	1.2728E-02	1.6695E+09	7.1093E-02	3.4462E+06	7.4626E-02	0:45	8.1914E+08	8.1707E+06	29.35	0.25	0.65	29.36	0.25	35.50	0.20	So25
d18O_radio140515_Br6_gr7@3	2.04	2.0635E-03	9.8006E-03	1.6681E+09	5.8688E-02	3.4421E+06	5.9999E-02	0:50	8.1861E+08		29.08	0.20		29.09	0.20	35.23	0.18	So25
d18O_radio140515_Br6_gr7@4	2.03	2.0628E-03	9.4296E-03	1.6657E+09	6.9193E-02	3.4359E+06	7.0098E-02	0:54	8.1959E+08		28.73	0.19		28.74	0.19	34.88	0.18	So25
d18O_radio140515_Br6_gr7@5	2.03	2.0629E-03	1.3748E-02	1.6751E+09	6.8349E-02	3.4555E+06	6.3326E-02	0:59	8.2524E+08		28.77	0.27		28.78	0.27	34.91	0.20	So25
d18O_radio140515_Br6_gr7@6	2.03	2.0639E-03	8.3532E-03	1.6715E+09	5.6673E-02	3.4499E+06	5.5875E-02	1:03	8.2307E+08		29.29	0.17		29.31	0.17	35.45	0.17	So25
d18O_radio140515_Br6_gr7@7	2.03	2.0628E-03	9.0524E-03	1.6831E+09	7.0948E-02	3.4717E+06	7.0958E-02	1:08	8.2771E+08		28.74	0.18		28.76	0.18	34.89	0.17	So25
d18O_radio140515_Br6_gr7@8	2.03	2.0640E-03	9.1899E-03	1.6632E+09	6.0975E-02	3.4327E+06	6.1198E-02	1:12	8.1806E+08		29.35	0.18		29.36	0.18	35.50	0.17	So25
d18O_radio140515_Br6_gr7@9	2.04	2.0641E-03	1.0231E-02	1.6616E+09	6.7873E-02	3.4297E+06	6.8461E-02	1:16	8.1645E+08		29.39	0.20		29.41	0.20	35.55	0.18	So25
d18O_radio140515_Br6_paine@33	2.04	2.0129E-03	1.0114E-02	1.6741E+09	5.7104E-02	3.3695E+06	6.0851E-02	1:21	8.2187E+08	8.2496E+08	3.83	0.20	3.78	3.85	0.20	9.83	0.18	Standard
d18O_radio140515_Br6_paine@34	2.04	2.0126E-03	1.0055E-02	1.6809E+09	6.4429E-02	3.3831E+06	6.4582E-02	1:25	8.2545E+08	4.9991E+06	3.71	0.20	0.28	3.73	0.20	9.71	0.18	Standard
d18O_radio140515_Br6_paine@35	2.03	2.0125E-03	1.2008E-02	1.6772E+09	5.9848E-02	3.3751E+06	5.8759E-02	1:30	8.2459E+08		3.64	0.24		3.66	0.24	9.64	0.19	Standard
d18O_radio140515_Br6_paine@36	2.03	2.0131E-03	8.7266E-03	1.6816E+09	7.3801E-02	3.3852E+06	7.5762E-02	1:34	8.2793E+08		3.96	0.17		3.98	0.17	9.97	0.17	Standard
d18O_radio140515_Br6_g8@1	2.03	2.0560E-03	1.2459E-02	1.6640E+09	6.2323E-02	3.4211E+06	6.6347E-02	1:39	8.1857E+08	8.2294E+08	25.33	0.25	25.23	25.35	0.25	31.46	0.19	Ki41
d18O_radio140515_Br6_g8@2	2.03	2.0580E-03	7.8959E-03	1.6689E+09	5.6224E-02	3.4347E+06	5.5084E-02	1:43	8.2386E+08	1.1542E+07	26.35	0.16	1.54	26.37	0.16	32.49	0.17	Ki41
d18O_radio140515_Br6_g8@3	2.03	2.0557E-03	9.1606E-03	1.6804E+09	8.5850E-02	3.4545E+06	8.8395E-02	1:48	8.2970E+08		25.20	0.18		25.22	0.18	31.33	0.17	Ki41
d18O_radio140515_Br6_g8@4	2.03	2.0567E-03	7.7263E-03	1.6768E+09	5.8464E-02	3.4488E+06	6.0128E-02	1:52	8.2770E+08		25.70	0.15		25.72	0.15	31.84	0.17	Ki41
d18O_radio140515_Br6_g8@5	2.03	2.0529E-03	9.5368E-03	1.6730E+09	8.5429E-02	3.4343E+06	8.6683E-02	1:57	8.2287E+08		23.78	0.19		23.81	0.19	29.91	0.18	Ki41
d18O_radio140515_Br6_g8@6	2.03	2.0537E-03	9.0134E-03	1.6493E+09	5.2726E-02	3.3874E+06	5.6799E-02	2:01	8.1057E+08		24.21	0.18		24.23	0.18	30.34	0.17	Ki41
d18O_radio140515_Br6_g8@7	2.03	2.0556E-03	1.0172E-02	1.6617E+09	7.1631E-02	3.4159E+06	7.3094E-02	2:06	8.1781E+08		25.14	0.20		25.16	0.20	31.28	0.18	Ki41
d18O_radio140515_Br6_g8@8	2.03	2.0569E-03	9.4115E-03	1.6718E+09	6.9062E-02	3.4387E+06	6.7582E-02	2:10	8.2503E+08		25.76	0.19		25.79	0.19	31.90	0.18	Ki41
d18O_radio140515_Br6_g8@9	2.03	2.0553E-03	1.0145E-02	1.6761E+09	7.3415E-02	3.4447E+06	7.4823E-02	2:15	8.2712E+08		25.00	0.20		25.02	0.20	31.14	0.18	Ki41
d18O_radio140515_Br6_g8@10	2.03	2.0570E-03	9.6903E-03	1.6793E+09	6.9951E-02	3.4543E+06	7.4507E-02	2:19	8.2616E+08		25.82	0.19		25.85	0.19	31.96	0.18	Ki41
d18O_radio140515_Br6_paine@37	2.03	2.0129E-03	7.2914E-03	1.6884E+09	6.5959E-02	3.3986E+06	6.8471E-02	2:24	8.3076E+08	8.2501E+08	3.86	0.15	3.73	3.89	0.15	9.88	0.16	Standard
d18O_radio140515_Br6_paine@38	2.04	2.0123E-03	1.3103E-02	1.6781E+09	6.4507E-02	3.3772E+06	6.2111E-02	2:28	8.2319E+08	7.6752E+06	3.53	0.26	0.47	3.56	0.26	9.54	0.19	Standard
d18O_radio140515_Br6_paine@39	2.03	2.0132E-03	6.4785E-03	1.6724E+09	5.4989E-02	3.3671E+06	5.3187E-02	2:33	8.2285E+08		4.00	0.13		4.03	0.13	10.02	0.16	Standard
d18O_radio140515_Br6_paine@40	2.03	2.0123E-03	9.8918E-03	1.6701E+09	6.8308E-02	3.3608E+06	7.1730E-02	2:37	8.2324E+08		3.55	0.20		3.58	0.20	9.56	0.18	Standard
d18O_radio140515_Br6_gr9@1	2.03	2.0639E-03	1.1245E-02	1.6708E+09	5.6669E-02	3.4482E+06	5.7050E-02	2:42	8.2448E+08	8.2269E+08	29.25	0.22	29.06	29.28	0.22	35.42	0.19	So31
d18O_radio140515_Br6_gr9@2	2.04	2.0632E-03	9.6273E-03	1.6758E+09	6.5172E-02	3.4574E+06	6.5107E-02	2:46	8.2266E+08	6.9887E+06	28.92	0.19	0.56	28.95	0.19	35.09	0.18	So31
d18O_radio140515_Br6_gr9@3	2.03	2.0645E-03	7.6299E-03	1.6640E+09	4.9439E-02	3.4353E+06	5.2569E-02	2:50	8.1847E+08		29.59	0.15		29.62	0.15	35.76	0.17	So31
d18O_radio140515_Br6_gr9@4	2.03	2.0628E-03	1.0990E-02	1.6715E+09	8.1053E-02	3.4480E+06	8.2205E-02	2:55	8.2245E+08		28.70	0.22		28.74	0.22	34.87	0.19	So31
d18O_radio140515_Br6_gr9@5	2.03	2.0628E-03	1.2228E-02	1.6741E+09	7.3456E-02	3.4534E+06	7.4855E-02	2:59	8.2483E+08		28.73	0.24		28.77	0.24	34.90	0.19	So31
d18O_radio140515_Br6_gr9@6	2.03	2.0632E-03	9.5657E-03	1.6748E+09	7.6589E-02	3.4551E+06	8.1301E-02	3:04	8.2635E+08		28.92	0.19		28.96	0.19	35.10	0.18	So31
d18O_radio140515_Br6_gr9@7	2.03	2.0634E-03	9.1334E-03	1.6743E+09	7.8146E-02	3.4547E+06	7.9450E-02	3:08	8.2500E+08		29.02	0.18		29.06	0.18	35.19	0.17	So31
d18O_radio140515_Br6_gr9@8	2.03	2.0638E-03	7.7889E-03	1.6753E+09	7.4662E-02	3.4574E+06	7.7046E-02	3:13	8.2438E+08		29.24	0.16		29.28	0.16	35.42	0.17	So31
d18O_radio140515_Br6_gr9@9	2.04	2.0636E-03	1.1822E-02	1.6617E+09	6.4215E-02	3.4292E+06	6.5094E-02	3:17	8.1559E+08		29.15	0.24		29.19	0.24	35.32	0.19	So31

Table A2 Continued.

		SIMS ANALYSES						Mount: BR4	Standard: UNIL-Q1 (Paine)		Analyse: $\delta^{18}O$			Value= 9.81±0.14 (VSMOW, 2σ)				Date: 15.04.2015	
	Beam	H'2/L'2 ($^{18}O/^{16}O$)		L'2 (^{18}O/Coeff)		H'2 (^{16}O/Coeff)		Time	Yield		Measurements (‰)		mean	Drift correction (‰)		Calibration (‰)		*Comment*	
	nA	*CPS*	*2SD*	*CPS*	*2SD*	*CPS*	*2SD*		CPS/nA		$\delta^{18}O$	*2SD int*	*2SD*	$\delta^{18}O$	*2SD*	$\delta^{18}O_{VSMOW}$	*2SD*		
d18O_radio140515_Br6_paine@41	2.03	2.0128E-03	9.4529E-03	1.6693E+09	5.6510E-02	3.3603E+06	5.7901E-02	3:22	8.2374E+08	8.2356E+08	3.80	0.19	3.75	3.83	0.19	9.82	0.17	Standard	
d18O_radio140515_Br6_paine@42	2.02	2.0124E-03	1.1556E-02	1.6689E+09	6.9828E-02	3.3585E+06	6.9682E-02	3:26	8.2425E+08	1.0853E+06	3.58	0.23	0.26	3.62	0.23	9.60	0.18	Standard	
d18O_radio140515_Br6_paine@43	2.03	2.0130E-03	6.5448E-03	1.6689E+09	6.0907E-02	3.3597E+06	6.1402E-02	3:31	8.2310E+08		3.89	0.13		3.93	0.13	9.91	0.16	Standard	
d18O_radio140515_Br6_paine@44	2.03	2.0127E-03	1.1426E-02	1.6739E+09	5.5716E-02	3.3693E+06	5.4761E-02	3:35	8.2315E+08		3.73	0.23		3.77	0.23	9.76	0.18	Standard	
d18O_radio140515_Br6_gr10@1	2.03	2.0569E-03	1.2726E-02	1.6393E+09	7.8974E-02	3.3720E+06	8.2507E-02	3:40	8.0672E+08	8.1658E+08	25.80	0.25	17.93	25.84	0.25	31.96	0.20	So21	
d18O_radio140515_Br6_gr10@02	2.03	2.0560E-03	8.6852E-03	1.7008E+09	1.0990E-01	3.4968E+06	1.0932E-01	3:44	8.3935E+08	2.0905E+07	25.33	0.17	19.67	25.37	0.17	31.49	0.17	So21	
d18O_radio140515_Br6_gr10@03	2.04	2.0363E-03	1.4335E-02	1.6862E+09	6.6989E-02	3.4335E+06	6.7297E-02	3:49	8.2744E+08		15.52	0.29						So21	Optical rejection
d18O_radio140515_Br6_gr10@04	2.05	2.0605E-03	7.7522E-03	1.6728E+09	6.7246E-02	3.4468E+06	6.9840E-02	3:53	8.1767E+08		27.57	0.16		27.62	0.16	33.75	0.17	So21	
d18O_radio140515_Br6_gr10@05	2.04	2.0136E-03	8.8607E-03	1.6799E+09	6.1452E-02	3.3825E+06	5.9898E-02	3:58	8.2334E+08		4.19	0.18						So21	Optical rejection
d18O_radio140515_Br6_gr10@06	2.03	2.0128E-03	1.5543E-02	1.6625E+09	8.5399E-02	3.3463E+06	8.7025E-02	4:02	8.1888E+08		3.77	0.31						So21	Optical rejection
d18O_radio140515_Br6_gr10@07	2.03	2.0235E-03	9.8608E-03	1.6563E+09	1.5207E-01	3.3515E+06	1.5292E-01	4:07	8.1449E+08		9.10	0.20						So21	Optical rejection
d18O_radio140515_Br6_gr10@08	2.04	2.0558E-03	1.3207E-02	1.6496E+09	1.0729E-01	3.3911E+06	1.0481E-01	4:11	8.0846E+08		25.23	0.26		25.27	0.26	31.39	0.20	So21	
d18O_radio140515_Br6_gr10@09	2.04	2.0562E-03	9.9306E-03	1.6634E+09	1.0450E-01	3.4204E+06	1.0807E-01	4:16	8.1393E+08		25.45	0.20		25.50	0.20	31.62	0.18	So21	
d18O_radio140515_Br6_gr10@10	2.04	2.0593E-03	1.2063E-02	1.6390E+09	7.4060E-02	3.3751E+06	7.5852E-02	4:20	8.0425E+08		26.97	0.24		27.02	0.24	33.15	0.19	So21	
d18O_radio140515_Br6_gr10@11	2.03	2.0218E-03	1.4269E-02	1.6421E+09	6.7430E-02	3.3199E+06	7.0024E-02	4:25	8.0779E+08		8.27	0.29						So21	Optical rejection
d18O_radio140515_Br6_paine@45	2.03	2.0125E-03	1.0628E-02	1.6738E+09	5.6629E-02	3.3687E+06	5.6469E-02	4:29	8.2387E+08	8.2606E+08	3.62	0.21	3.73	3.67	0.21	9.65	0.18	Standard	
d18O_radio140515_Br6_paine@46	2.03	2.0127E-03	1.2121E-02	1.6810E+09	7.8859E-02	3.3833E+06	7.7703E-02	4:34	8.2699E+08	3.3265E+06	3.72	0.24	0.19	3.77	0.24	9.76	0.19	Standard	
d18O_radio140515_Br6_paine@47	2.04	2.0123E-03	9.1256E-03	1.6765E+09	6.7367E-02	3.3736E+06	7.0979E-02	4:38	8.2308E+08		3.55	0.18		3.60	0.18	9.58	0.17	Standard	
d18O_radio140515_Br6_paine@48	2.04	2.0128E-03	1.2353E-02	1.6848E+09	6.5180E-02	3.3916E+06	6.4496E-02	4:42	8.2769E+08		3.80	0.25		3.85	0.25	9.84	0.19	Standard	
d18O_radio140515_Br6_paine@49	2.04	2.0129E-03	9.3673E-03	1.6881E+09	5.5538E-02	3.3976E+06	5.5380E-02	4:47	8.2693E+08		3.82	0.19		3.87	0.19	9.86	0.17	Standard	
d18O_radio140515_Br6_paine@50	2.04	2.0127E-03	1.4054E-02	1.6846E+09	7.3290E-02	3.3906E+06	7.3790E-02	4:51	8.2614E+08		3.75	0.28		3.81	0.28	9.79	0.20	Standard	
d18O_radio140515_Br6_paine@51	2.04	2.0127E-03	1.3301E-02	1.6849E+09	5.3908E-02	3.3916E+06	5.3530E-02	4:56	8.2679E+08		3.74	0.27		3.80	0.27	9.79	0.20	Standard	
d18O_radio140515_Br6_paine@52	2.03	2.0128E-03	6.0676E-03	1.6806E+09	7.0343E-02	3.3830E+06	7.1467E-02	5:00	8.2699E+08		3.81	0.12		3.86	0.12	9.85	0.16	Standard	

Table A2 Continued.

SIMS ANALYSES						Mount: BR6			Standard: UNIL-Q1 (Paine)		Analyse: $\delta^{18}O$			Value= 9.81±0.14 (VSMOW, 2σ)				Date: 15.04.2015	
	Beam	H'2/L'2 ($^{18}O/^{16}O$)		L'2 (^{18}O/Coeff)		H'2 (^{16}O/Coeff)		Time	Yield		Measurements (‰)		mean	Drift correction (‰)		Calibration (‰)		Comment	
	nA	*CPS*	*2SD*	*CPS*	*2SD*	*CPS*	*2SD*		CPS/nA		$\delta^{18}O$	*2SD int*	*2SD*	$\delta^{18}O$	*2SD*	$\delta^{18}O_{VSMOW}$	*2SD*		
testpaine@1	2.05	2.0139E-03	1.7593E-02	1.4957E+09	4.6252E-02	3.0125E+06	4.5186E-02	8:15	7.2869E+08		4.36	0.35	4.24					Standard	
testpaine@2	2.06	2.0137E-03	1.2930E-02	1.4918E+09	6.7964E-02	3.0041E+06	6.1349E-02	8:20	7.2263E+08		4.23	0.26	0.32					Standard	
testpaine@3	2.06	2.0139E-03	9.5934E-03	1.5001E+09	2.9258E-02	3.0215E+06	3.6290E-02	8:24	7.2681E+08		4.32	0.19						Standard	
testpaine@4	2.07	2.0137E-03	1.4276E-02	1.5032E+09	8.1637E-02	3.0270E+06	8.1922E-02	8:29	7.2788E+08		4.24	0.29						Standard	
testpaine@5	2.07	2.0130E-03	1.0186E-02	1.5219E+09	2.1353E-02	3.0644E+06	2.8967E-02	8:34	7.3450E+08		3.88	0.20						Standard	
testpaine@6	2.07	2.0141E-03	1.2309E-02	1.5401E+09	7.0213E-02	3.1016E+06	6.7331E-02	8:38	7.4357E+08		4.42	0.25						Standard	
testpaine@7	2.08	2.0137E-03	1.7440E-02	1.5446E+09	6.4726E-02	3.1102E+06	6.3247E-02	8:43	7.4340E+08		4.23	0.35						Standard	
testpaine@8	2.07	2.0136E-03	8.3634E-03	1.5143E+09	4.3275E-02	3.0494E+06	4.2236E-02	8:48	7.3175E+08		4.21	0.17						Standard	
d18O_radio140515_Br6_paine@1	2.05	2.0132E-03	1.1915E-02	1.6203E+09	9.1067E-02	3.2616E+06	9.5347E-02	9:30	7.9053E+08		3.97	0.24	3.78	3.84	0.24	10.00	0.20	Standard	
d18O_radio140515_Br6_paine@2	2.06	2.0127E-03	6.1710E-03	1.6238E+09	9.9510E-02	3.2681E+06	1.0080E-01	9:34	7.8800E+08		3.72	0.12	0.32	3.59	0.12	9.75	0.17	Standard	
d18O_radio140515_Br6_paine@3	2.06	2.0129E-03	1.2560E-02	1.6247E+09	9.2470E-02	3.2704E+06	9.3494E-02	9:39	7.8716E+08		3.85	0.25		3.72	0.25	9.88	0.20	Standard	
d18O_radio140515_Br6_paine@4	2.07	2.0123E-03	1.0069E-02	1.6274E+09	8.0125E-02	3.2750E+06	8.4921E-02	9:43	7.8728E+08		3.56	0.20		3.44	0.20	9.59	0.19	Standard	
d18O_radio140515_Br6_paine@5	2.06	2.0126E-03	8.9395E-03	1.6332E+09	9.2634E-02	3.2870E+06	9.1676E-02	9:48	7.9116E+08		3.71	0.18		3.59	0.18	9.75	0.18	Standard	
d18O_radio140515_Br6_paine@6	2.07	2.0127E-03	9.3132E-03	1.6346E+09	8.9973E-02	3.2896E+06	8.8676E-02	9:53	7.9017E+08		3.73	0.19		3.61	0.19	9.77	0.18	Standard	
d18O_radio140515_Br6_paine@7	2.07	2.0133E-03	8.6549E-03	1.6374E+09	9.0309E-02	3.2965E+06	9.2172E-02	9:57	7.9178E+08		4.02	0.17		3.91	0.17	10.07	0.18	Standard	
d18O_radio140515_Br6_paine@8	2.07	2.0125E-03	7.0161E-03	1.6358E+09	9.4975E-02	3.2923E+06	9.4991E-02	10:02	7.8989E+08		3.65	0.14		3.55	0.14	9.70	0.17	Standard	
d18O_radio140515_Br6_gr1@1	2.06	2.0621E-03	8.9128E-03	1.6031E+09	8.4729E-02	3.3056E+06	8.8328E-02	10:07	7.7727E+08		28.38	0.18	28.45	28.27	0.18	34.58	0.18	So15	
d18O_radio140515_Br6_gr1@2	2.06	2.0629E-03	9.4579E-03	1.5975E+09	9.7854E-02	3.2958E+06	9.8009E-02	10:11	7.7719E+08		28.78	0.19	1.08	28.67	0.19	34.99	0.19	So15	
d18O_radio140515_Br6_gr1@3	2.06	2.0633E-03	9.9792E-03	1.6160E+09	1.0567E-01	3.3343E+06	1.0196E-01	10:16	7.8489E+08		28.97	0.20		28.87	0.20	35.18	0.19	So15	
d18O_radio140515_Br6_gr1@4	2.06	2.0608E-03	1.3238E-02	1.6160E+09	9.8559E-02	3.3302E+06	9.9441E-02	10:21	7.8478E+08		27.72	0.26		27.62	0.26	33.92	0.21	So15	
d18O_radio140515_Br6_gr1@5	2.06	2.0612E-03	1.0345E-02	1.6019E+09	1.0103E-01	3.3018E+06	1.0063E-01	10:25	7.7792E+08		27.91	0.21		27.81	0.21	34.12	0.19	So15	
d18O_radio140515_Br6_gr1@6	2.05	2.0632E-03	1.1117E-02	1.5966E+09	8.7404E-02	3.2938E+06	8.1651E-02	10:30	7.7715E+08		28.93	0.22		28.84	0.22	35.15	0.20	So15	
d18O_radio140515_Br6_gr2@1	2.05	1.9283E-03	1.9667E-01	5.4155E+07	5.1049E-02	1.0430E+05	1.7469E-01	10:35	2.6398E+07		-38.35	3.93	18.29					Ki48	
d18O_radio140515_Br6_gr2@2	2.05	2.0520E-03	1.0316E-02	1.5900E+09	1.0269E-01	3.2627E+06	1.0207E-01	10:40	7.7439E+08		23.36	0.21	1.84	23.27	0.21	29.55	0.19	Ki48	
d18O_radio140515_Br6_gr2@3	2.06	2.0556E-03	9.5755E-03	1.5935E+09	9.9016E-02	3.2755E+06	1.0056E-01	10:44	7.7274E+08		25.12	0.19		25.04	0.19	31.33	0.19	Ki48	
d18O_radio140515_Br6_gr2@4	2.06	2.0547E-03	9.0162E-03	1.5920E+09	1.0913E-01	3.2707E+06	1.1372E-01	10:49	7.7308E+08		24.69	0.18		24.61	0.18	30.90	0.18	Ki48	
d18O_radio140515_Br6_gr2@5	2.06	1.9352E-03	4.0611E-01	5.0912E+07	1.7019E-01	9.8523E+04	3.9726E-01	10:54	2.4774E+07		-34.91	8.12						Ki48	Yield rejection
d18O_radio140515_Br6_gr2@6	2.05	2.0241E-03	1.1963E-02	1.5707E+09	5.9758E-02	3.1791E+06	6.0775E-02	10:58	7.6585E+08		9.43	0.24						Ki48	Optical rejection
d18O_radio140515_Br6_paine@9	2.05	2.0130E-03	1.1705E-02	1.6333E+09	1.0300E-01	3.2879E+06	1.0464E-01	11:03	7.9709E+08		3.90	0.23	3.75	3.83	0.23	9.99	0.19	Standard	
d18O_radio140515_Br6_paine@10	2.06	2.0131E-03	8.1153E-03	1.6378E+09	9.3133E-02	3.2969E+06	9.9071E-02	11:08	7.9694E+08		3.92	0.16	0.36	3.85	0.16	10.01	0.18	Standard	
d18O_radio140515_Br6_paine@11	2.05	2.0124E-03	1.0659E-02	1.6314E+09	8.8680E-02	3.2832E+06	9.4583E-02	11:12	7.9539E+08		3.59	0.21		3.52	0.21	9.68	0.19	Standard	
d18O_radio140515_Br6_paine@12	2.04	2.0124E-03	1.2528E-02	1.6316E+09	9.2831E-02	3.2837E+06	1.0001E-01	11:17	7.9833E+08		3.60	0.25		3.54	0.25	9.70	0.20	Standard	
d18O_radio140515_Br6_gr3@1	2.04	2.0621E-03	1.0108E-02	1.5740E+09	8.4365E-02	3.2454E+06	8.4911E-02	11:22	7.7084E+08		28.36	0.20	27.76	28.30	0.20	34.61	0.19	So23	
d18O_radio140515_Br6_gr3@2	2.04	2.0610E-03	8.0251E-03	1.5743E+09	8.8386E-02	3.2446E+06	8.9124E-02	11:26	7.7198E+08		27.82	0.16	1.20	27.76	0.16	34.06	0.18	So23	
d18O_radio140515_Br6_gr3@3	2.04	2.0585E-03	9.9781E-03	1.5723E+09	9.3612E-02	3.2363E+06	9.5834E-02	11:31	7.7155E+08		26.60	0.20		26.55	0.20	32.85	0.19	So23	
d18O_radio140515_Br6_gr3@4	2.04	2.0615E-03	8.4235E-03	1.5705E+09	8.3251E-02	3.2377E+06	8.1275E-02	11:36	7.7032E+08		28.07	0.17		28.01	0.17	34.32	0.18	So23	
d18O_radio140515_Br6_gr3@5	2.04	2.0611E-03	8.1492E-03	1.5673E+09	1.0586E-01	3.2307E+06	1.1067E-01	11:40	7.6865E+08		27.89	0.16		27.84	0.16	34.15	0.18	So23	
d18O_radio140515_Br6_gr3@6	2.04	2.0610E-03	8.4231E-03	1.5701E+09	7.9481E-02	3.2359E+06	7.9874E-02	11:45	7.6865E+08		27.82	0.17		27.77	0.17	34.07	0.18	So23	
d18O_radio140515_Br6_gr4@1	2.04	2.0558E-03	1.2551E-02	1.5758E+09	9.5302E-02	3.2396E+06	9.9914E-02	11:50	7.7254E+08		25.22	0.25	25.05	25.18	0.25	31.47	0.20	Ki43s	
d18O_radio140515_Br6_gr4@2	2.04	2.0560E-03	7.1512E-03	1.5658E+09	8.3894E-02	3.2193E+06	8.2917E-02	11:54	7.6701E+08		25.32	0.14	0.86	25.28	0.14	31.57	0.17	Ki43s	
d18O_radio140515_Br6_gr4@3	2.04	2.0553E-03	1.1215E-02	1.5602E+09	6.9223E-02	3.2067E+06	6.9353E-02	11:59	7.6648E+08		25.00	0.22		24.96	0.22	31.25	0.20	Ki43s	
d18O_radio140515_Br6_gr4@4	2.03	2.0559E-03	1.0795E-02	1.5519E+09	9.8114E-02	3.1903E+06	9.8963E-02	12:04	7.6341E+08		25.26	0.22		25.23	0.22	31.52	0.19	Ki43s	
d18O_radio140515_Br6_gr4@5	2.03	2.0537E-03	9.1853E-03	1.5467E+09	8.2495E-02	3.1768E+06	8.5077E-02	12:08	7.6051E+08		24.21	0.18		24.17	0.18	30.46	0.18	Ki43s	
d18O_radio140515_Br6_gr4@6	2.04	2.0559E-03	9.6891E-03	1.5760E+09	1.0189E-01	3.2399E+06	1.0479E-01	12:13	7.7415E+08		25.30	0.19		25.27	0.19	31.56	0.19	Ki43s	
d18O_radio140515_Br6_paine@13	2.13	2.0128E-03	1.1931E-02	1.6354E+09	2.0230E-01	3.2913E+06	2.0002E-01	12:18	7.6771E+08		3.77	0.24	3.67	3.74	0.24	9.90	0.20	Standard	
d18O_radio140515_Br6_paine@14	2.04	2.0126E-03	1.2097E-02	1.6277E+09	1.1435E-01	3.2764E+06	1.1916E-01	12:23	7.9905E+08		3.67	0.24	0.17	3.65	0.24	9.80	0.20	Standard	
d18O_radio140515_Br6_paine@15	2.03	2.0125E-03	9.1071E-03	1.6208E+09	9.8747E-02	3.2621E+06	9.8133E-02	12:27	7.9714E+08		3.66	0.18		3.64	0.18	9.80	0.18	Standard	
d18O_radio140515_Br6_paine@16	2.03	2.0123E-03	1.5538E-02	1.6213E+09	9.5483E-02	3.2626E+06	9.4056E-02	12:32	7.9933E+08		3.56	0.31		3.54	0.31	9.70	0.22	Standard	
d18O_radio140515_Br6_gr5@1	2.03	2.0187E-03	1.4905E-02	1.4510E+09	4.1803E-01	2.9294E+06	4.0498E-01	12:37	7.1340E+08		6.74	0.30	14.20					Ki20	Optical rejection
d18O_radio140515_Br6_gr5@2	2.04	2.0319E-03	1.0360E-02	1.5447E+09	8.3110E-02	3.1390E+06	8.3679E-02	12:41	7.5638E+08		13.32	0.21	7.97	13.31	0.21	19.52	0.19	Ki20	
d18O_radio140515_Br6_gr5@3	2.04	2.0361E-03	1.3058E-02	1.5538E+09	7.7325E-02	3.1637E+06	7.1454E-02	12:46	7.6070E+08		15.39	0.26		15.38	0.26	21.61	0.21	Ki20	
d18O_radio140515_Br6_gr5@4	2.04	2.0364E-03	1.3753E-02	1.6184E+09	4.0052E-02	3.2966E+06	3.4498E-02	12:51	7.9139E+08		15.57	0.28		15.56	0.28	21.79	0.21	Ki20	
d18O_radio140515_Br6_gr5@5	2.04	2.0371E-03	1.1959E-02	1.5578E+09	9.5179E-02	3.1735E+06	9.0099E-02	12:55	7.6321E+08		15.92	0.24		15.91	0.24	22.14	0.20	Ki20	
d18O_radio140515_Br6_gr5@6	2.05	2.0419E-03	1.0489E-02	1.5766E+09	1.0723E-01	3.2191E+06	1.1302E-01	13:00	7.7060E+08		18.29	0.21		18.29	0.21	24.53	0.19	Ki20	
d18O_radio140515_Br6_gr6@1	2.05	2.0539E-03	8.7792E-03	2.1220E+09	2.0405E-01	4.3587E+06	1.9792E-01	13:05	1.0360E+09		24.31	0.18	24.35					So29	SEM rejection
d18O_radio140515_Br6_gr6@2	2.05	2.0537E-03	1.2637E-02	2.0202E+09	2.7549E-01	4.1489E+06	2.7047E-01	13:09	9.8587E+08		24.19	0.25	0.90					So29	SEM rejection
d18O_radio140515_Br6_gr6@3	2.04	2.0524E-03	1.1417E-02	2.1118E+09	2.2198E-01	4.3342E+06	2.1548E-01	13:14	1.0340E+09		23.56	0.23						So29	SEM rejection
d18O_radio140515_Br6_gr6@4	2.04	2.0546E-03	1.1355E-02	2.0779E+09	2.2026E-01	4.2691E+06	2.0921E-01	13:19	1.0188E+09		24.64	0.23						So29	SEM rejection
d18O_radio140515_Br6_gr6@5	2.04	2.0549E-03	1.0585E-02	2.1258E+09	2.0366E-01	4.3683E+06	2.0263E-01	13:23	1.0399E+09		24.80	0.21						So29	SEM rejection
d18O_radio140515_Br6_gr6@6	2.05	2.0546E-03	1.1793E-02	2.0132E+09	9.3889E-02	4.1364E+06	9.2734E-02	13:28	9.8238E+08		24.61	0.24						So29	SEM rejection
d18O_radio140515_Br6_paine@17	2.05	2.0124E-03	1.1103E-02	1.6330E+09	9.4529E-02	3.2862E+06	9.4052E-02	13:33	7.9782E+08		3.59	0.22	3.63	3.60	0.22	9.76	0.19	Standard	
d18O_radio140515_Br6_paine@18	2.04	2.0123E-03	9.5256E-03	1.6321E+09	8.2464E-02	3.2843E+06	8.1430E-02	13:37	7.9923E+08		3.55	0.19	0.15	3.57	0.19	9.73	0.18	Standard	
d18O_radio140515_Br6_paine@19	2.04	2.0127E-03	1.1824E-02	1.6369E+09	8.7225E-02	3.2945E+06	8.9616E-02	13:42	8.0045E+08		3.72	0.24		3.74	0.24	9.90	0.20	Standard	
d18O_radio140515_Br6_paine@20	2.05	2.0125E-03	9.8187E-03	1.6400E+09	9.8772E-02	3.3007E+06	1.0070E-01	13:47	7.9976E+08		3.65	0.20		3.67	0.20	9.83	0.18	Standard	
d18O_radio140515_Br6_gr7@1	2.05	2.0104E-03	1.2609E-02	1.5538E+09	4.3540E-02	3.1253E+06	3.1498E-02	13:52	7.5835E+08	5.0592E+08	2.61	0.25	-0.62					ki12s	Optical rejection
d18O_radio140515_Br6_gr7@2	2.05	2.0226E-03	1.0613E-02	1.4540E+09	1.1038E-01	2.9409E+06	1.0563E-01	13:56	7.0946E+08	5.6035E+08	8.69	0.21	15.52					ki12s	Optical rejection
d18O_radio140515_Br6_gr7@3	2.04	2.0167E-03	1.3620E-02	1.4269E+09	4.8856E-01	2.8775E+06	4.8737E-01	14:01	6.9926E+08		5.74	0.27						ki12s	Optical rejection
d18O_radio140515_Br6_gr7@4	2.03	1.9889E-03	4.5630E-02	3.4231E+08	4.9852E-01	6.8117E+05	5.3033E-01	14:06	1.6821E+08		-8.13	0.91						ki12s	Optical rejection
d18O_radio140515_Br6_gr7@5	2.04	1.9833E-03	4.6421E-02	2.8736E+08	2.9607E+00	5.6978E+05	2.9917E+00	14:10	1.4111E+08		-10.93	0.93						ki12s	Optical rejection
d18O_radio140515_Br6_gr7@6	2.04	2.0018E-03	1.3235E-02	1.1399E+09	5.5299E-01	2.2816E+06	5.4686E-01	14:15	5.5915E+08		-1.69	0.26						ki12s	Optical rejection

Table A2 Continued.

SIMS ANALYSES							Mount: BR6		Standard: UNIL-Q1 (Paine)		Analyse: $\delta^{18}O$			Value= 9.81±0.14 (VSMOW, 2σ)				Date: 15.04.2015
	Beam	H'2/L'2 ($^{18}O/^{16}O$)		L'2 (^{18}O/Coeff)		H'2 (^{16}O/Coeff)		Time	Yield		Measurements (‰)		mean	Drift correction (‰)		Calibration (‰)		Comment
	nA	*CPS*	*2SD*	*CPS*	*2SD*	*CPS*	*2SD*		CPS/nA		$\delta^{18}O$	*2SD int*	*2SD*	$\delta^{18}O$	*2SD*	$\delta^{18}O_{VSMOW}$	*2SD*	
d18O_radio140515_Br6_gr8@1	2.04	2.0627E-03	9.8599E-03	1.6296E+09	9.8020E-02	3.3613E+06	1.0131E-01	14:20	7.9940E+08	8.0161E+08	28.67	0.20	28.76	28.71	0.20	35.03	0.19	So26
d18O_radio140515_Br6_gr8@2	2.04	2.0623E-03	8.9823E-03	1.6240E+09	9.5548E-02	3.3491E+06	9.9399E-02	14:24	7.9640E+08	7.8550E+06	28.49	0.18	0.55	28.54	0.18	34.85	0.18	So26
d18O_radio140515_Br6_gr8@3	2.04	2.0624E-03	9.9467E-03	1.6371E+09	1.2179E-01	3.3763E+06	1.1920E-01	14:29	8.0410E+08		28.53	0.20		28.58	0.20	34.89	0.19	So26
d18O_radio140515_Br6_gr8@4	2.04	2.0638E-03	1.1112E-02	1.6444E+09	8.8016E-02	3.3938E+06	8.6612E-02	14:34	8.0772E+08		29.25	0.22		29.30	0.22	35.62	0.20	So26
d18O_radio140515_Br6_gr8@5	2.04	2.0629E-03	1.0914E-02	1.6333E+09	8.2686E-02	3.3693E+06	8.5715E-02	14:38	8.0036E+08		28.78	0.22		28.84	0.22	35.15	0.19	So26
d18O_radio140515_Br6_gr8@6	2.04	2.0630E-03	9.2247E-03	1.6370E+09	1.1487E-01	3.3774E+06	1.1415E-01	14:43	8.0167E+08		28.84	0.18		28.90	0.18	35.22	0.18	So26
d18O_radio140515_Br6_paine@21	2.04	2.0126E-03	9.5532E-03	1.6277E+09	9.1938E-02	3.2760E+06	8.9063E-02	14:48	7.9804E+08	7.9745E+08	3.71	0.19	3.57	3.77	0.19	9.93	0.18	Standard
d18O_radio140515_Br6_paine@22	2.04	2.0124E-03	1.0529E-02	1.6347E+09	1.0899E-01	3.2898E+06	1.0963E-01	14:52	8.0031E+08	5.3192E+06	3.60	0.21	0.37	3.67	0.21	9.83	0.19	Standard
d18O_radio140515_Br6_paine@23	2.06	2.0118E-03	9.4764E-03	1.6317E+09	8.6866E-02	3.2827E+06	8.3940E-02	14:57	7.9389E+08		3.30	0.19		3.37	0.19	9.53	0.18	Standard
d18O_radio140515_Br6_paine@24	2.05	2.0126E-03	6.1522E-03	1.6339E+09	8.7112E-02	3.2885E+06	8.7837E-02	15:02	7.9758E+08		3.68	0.12		3.75	0.12	9.91	0.17	Standard
d18O_radio140515_Br6_gr9@1	2.05	2.0624E-03	8.0225E-03	1.6290E+09	1.1587E-01	3.3600E+06	1.1590E-01	15:06	7.9511E+08	7.9483E+08	28.54	0.16	28.52	28.62	0.16	34.93	0.18	So12
d18O_radio140515_Br6_gr9@2	2.04	2.0629E-03	1.0816E-02	1.6147E+09	9.1531E-02	3.3311E+06	9.4773E-02	15:11	7.9120E+08	7.5465E+06	28.80	0.22	0.96	28.88	0.22	35.19	0.19	So12
d18O_radio140515_Br6_gr9@3	2.04	2.0606E-03	1.3828E-02	1.6191E+09	1.1003E-01	3.3361E+06	1.0808E-01	15:16	7.9519E+08		27.63	0.28		27.71	0.28	34.01	0.21	So12
d18O_radio140515_Br6_gr9@4	2.04	2.0627E-03	7.7437E-03	1.6132E+09	8.8812E-02	3.3275E+06	9.0414E-02	15:20	7.9173E+08		28.66	0.15		28.74	0.15	35.05	0.18	So12
d18O_radio140515_Br6_gr9@5	2.01	2.0634E-03	7.6818E-03	1.6122E+09	1.1141E-01	3.3268E+06	1.1283E-01	15:42	8.0173E+08		29.03	0.15		29.13	0.15	35.44	0.18	So12
d18O_radio140515_Br6_gr9@6	2.03	2.0623E-03	9.7393E-03	1.6116E+09	9.5404E-02	3.3238E+06	9.5948E-02	15:47	7.9402E+08		28.48	0.19		28.58	0.19	34.90	0.19	So12
d18O_radio140515_Br6_gr10@1	2.03	2.0467E-03	1.2809E-02	1.6129E+09	9.1036E-02	3.3010E+06	8.9046E-02	15:51	7.9351E+08	7.9023E+08	20.70	0.26	20.17	20.80	0.26	27.06	0.20	Go68
d18O_radio140515_Br6_gr10@2	2.04	2.0444E-03	9.4878E-03	1.6037E+09	1.0684E-01	3.2788E+06	1.0660E-01	15:56	7.8477E+08	1.0067E+07	19.53	0.19	1.13	19.63	0.19	25.89	0.18	Go68
d18O_radio140515_Br6_gr10@3	2.04	2.0453E-03	8.3673E-03	1.6034E+09	9.2715E-02	3.2792E+06	8.8639E-02	16:01	7.8609E+08		20.02	0.17		20.13	0.17	26.39	0.18	Go68
d18O_radio140515_Br6_gr10@4	2.04	2.0455E-03	1.2785E-02	1.6043E+09	1.0075E-01	3.2815E+06	9.8914E-02	16:06	7.8626E+08		20.10	0.26		20.21	0.26	26.47	0.20	Go68
d18O_radio140515_Br6_gr10@5	2.04	2.0447E-03	9.0250E-03	1.6268E+09	1.0585E-01	3.3263E+06	1.1124E-01	16:10	7.9553E+08		19.69	0.18		19.80	0.18	26.06	0.18	Go68
d18O_radio140515_Br6_gr10@6	2.05	2.0473E-03	8.3613E-03	1.6303E+09	9.2747E-02	3.3374E+06	9.5787E-02	16:15	7.9523E+08		20.98	0.17		21.09	0.17	27.36	0.18	Go68
d18O_radio140515_Br6_paine@25	2.05	2.0118E-03	1.0202E-02	1.6288E+09	8.3739E-02	3.2771E+06	8.4822E-02	16:20	7.9446E+08	7.9513E+08	3.30	0.20	3.49	3.42	0.20	9.57	0.19	Standard
d18O_radio140515_Br6_paine@26	2.04	2.0127E-03	8.2003E-03	1.6238E+09	1.0693E-01	3.2683E+06	1.0829E-01	16:24	7.9408E+08	2.3748E+06	3.75	0.16	0.37	3.87	0.16	10.03	0.18	Standard
d18O_radio140515_Br6_paine@27	2.04	2.0121E-03	7.8594E-03	1.6228E+09	1.0413E-01	3.2651E+06	1.0363E-01	16:29	7.9520E+08		3.45	0.16		3.57	0.16	9.73	0.17	Standard
d18O_radio140515_Br6_paine@28	2.05	2.0122E-03	8.3880E-03	1.6296E+09	9.4821E-02	3.2792E+06	9.4330E-02	16:34	7.9676E+08		3.49	0.17		3.62	0.17	9.77	0.18	Standard

Table A2 Continued.

SIMS ANALYSES						Mount: BR7			Standard: UNIL-Q1 (Paine)	Analyse: $\delta^{18}O$			Value= 9.81±0.14 (VSMOW, 2σ)				Date: 13.04.2015
	Beam	H'2/L'2 ($^{18}O/^{16}O$)		L'2 (^{18}O/Coeff)		H'2 (^{16}O/Coeff)		Time	Yield	Measurements (‰)		mean	Drift correction (‰)		Calibration (‰)		Comment
	nA	*CPS*	*2SD*	*CPS*	*2SD*	*CPS*	*2SD*		CPS/nA	$\delta^{18}O$	*2SD int*	*2SD*	$\delta^{18}O$	*2SD*	$\delta^{18}O_{VSMOW}$	*2SD*	
130415_paine@1	2.03	2.0156E-03	7.8906E-03	1.5494E+09	1.0101E-01	3.1228E+06	1.0130E-01	12:46	7.6258E+08	5.21	0.16	5.26					Standard
130415_paine@2	2.04	2.0151E-03	9.4127E-03	1.5814E+09	1.0882E-01	3.1871E+06	1.1154E-01	12:50	7.7628E+08	4.94	0.19	1.82					Standard
130415_paine@3	2.03	2.0157E-03	1.2454E-02	1.5910E+09	7.0947E-02	3.2071E+06	7.0409E-02	12:54	7.8302E+08	5.22	0.25						Standard
130415_paine@4	2.03	2.0158E-03	1.0970E-02	1.5925E+09	1.4901E-01	3.2098E+06	1.4968E-01	12:59	7.8491E+08	5.27	0.22						Standard
130415_paine@5	2.03	2.0166E-03	7.0652E-03	1.5157E+09	1.3474E-01	3.0567E+06	1.3233E-01	13:03	7.4605E+08	5.66	0.14						Standard
130415_paine@6	2.03	2.0162E-03	9.1504E-03	1.5383E+09	6.8801E-02	3.1019E+06	6.5965E-02	13:07	7.5718E+08	5.50	0.18						Standard
130415_paine@7	2.03	2.0167E-03	1.1013E-02	1.5199E+09	7.2171E-02	3.0650E+06	7.3476E-02	13:11	7.4896E+08	5.71	0.22						Standard
130415_paine@9	1.99	2.0170E-03	1.2067E-02	1.5135E+09	1.3627E-01	3.0527E+06	1.3241E-01	13:25	7.6155E+08	5.90	0.24						Standard
130415_paine@10	1.99	2.0167E-03	1.3572E-02	1.5321E+09	8.0729E-02	3.0897E+06	8.3999E-02	13:29	7.6895E+08	5.73	0.27						Standard
130415_paine@11	2.00	2.0163E-03	1.1614E-02	1.5304E+09	7.1198E-02	3.0857E+06	7.1665E-02	13:33	7.6621E+08	5.54	0.23						Standard
130415_paine@12	1.99	2.0171E-03	1.0455E-02	1.5319E+09	5.3360E-02	3.0889E+06	4.5523E-02	13:37	7.6908E+08	5.96	0.21						Standard
130415_paine@13	2.00	2.0174E-03	1.0641E-02	1.5045E+09	8.9284E-02	3.0350E+06	9.0106E-02	13:42	7.5318E+08	6.10	0.21						Standard
130415_paine@15	1.97	2.0180E-03	1.0980E-02	1.3095E+09	2.8252E-02	2.6426E+06	3.0618E-02	14:09	6.6623E+08	6.39	0.22						Standard
130415_paine@16	1.97	2.0184E-03	8.4364E-03	1.3326E+09	1.5886E-01	2.6898E+06	1.5578E-01	14:13	6.7607E+08	6.56	0.17						Standard
130415_paine@17	1.97	2.0179E-03	1.0718E-02	1.3416E+09	1.4828E-01	2.7075E+06	1.4874E-01	14:17	6.8276E+08	6.34	0.21						Standard
130415_paine@18	1.96	2.0188E-03	1.3141E-02	1.3274E+09	1.1918E-01	2.6798E+06	1.1447E-01	14:21	6.7566E+08	6.79	0.26						Standard
130415_paine@19	1.96	2.0183E-03	9.0536E-03	1.3304E+09	1.2245E-01	2.6852E+06	1.2228E-01	14:26	6.7741E+08	6.54	0.18						Standard
130415_paine@20	1.93	2.0162E-03	1.1624E-02	1.3349E+09	4.1606E-02	2.6910E+06	4.3800E-02	14:41	6.9288E+08	5.49	0.23						Standard
130415_paine@21	1.93	2.0165E-03	1.3010E-02	1.3168E+09	2.7791E-02	2.6554E+06	3.1095E-02	14:46	6.8206E+08	5.65	0.26						Standard
130415_paine@22	1.94	2.0157E-03	1.6604E-02	1.3108E+09	2.0965E-02	2.6420E+06	2.6607E-02	14:50	6.7723E+08	5.22	0.33						Standard
130415_paine@23	1.94	2.0155E-03	1.5079E-02	1.3108E+09	1.6958E-02	2.6417E+06	2.0658E-02	14:54	6.7525E+08	5.15	0.30						Standard
130415_paine@24	1.94	2.0163E-03	1.4509E-02	1.3067E+09	5.2514E-02	2.6348E+06	5.7951E-02	14:58	6.7459E+08	5.53	0.29						Standard
130415_paine@25	1.93	2.0159E-03	1.3068E-02	1.2995E+09	4.0062E-02	2.6194E+06	4.3406E-02	15:03	6.7227E+08	5.34	0.26						Standard
130415_paine@26	1.93	2.0163E-03	1.5462E-02	1.3004E+09	2.8943E-02	2.6217E+06	2.8061E-02	15:07	6.7435E+08	5.56	0.31						Standard
130415_paine@27	1.93	2.0158E-03	1.2187E-02	1.3057E+09	4.1994E-02	2.6318E+06	4.2313E-02	15:11	6.7624E+08	5.28	0.24						Standard
130415_paine@28	1.92	2.0133E-03	1.6687E-02	1.4918E+09	5.7281E-02	3.0034E+06	6.3561E-02	15:17	7.7561E+08	4.02	0.33						Standard
130415_paine@29	1.93	2.0129E-03	6.9970E-03	1.4888E+09	4.7319E-02	2.9972E+06	4.9858E-02	15:21	7.7006E+08	3.86	0.14						Standard
130415_paine@30	1.93	2.0130E-03	8.8625E-03	1.5390E+09	8.4649E-02	3.0979E+06	7.9960E-02	15:25	7.9794E+08	3.88	0.18						Standard
130415_paine@31	2.00	2.0128E-03	1.0751E-02	1.5583E+09	5.4511E-02	3.1365E+06	5.7148E-02	15:30	7.7771E+08	3.79	0.22						Standard
130415_paine@32	2.02	2.0126E-03	9.1744E-03	1.5627E+09	3.5377E-02	3.1450E+06	4.0030E-02	15:34	7.7182E+08	3.69	0.18						Standard
130415_paine@33	2.04	2.0130E-03	1.2464E-02	1.5871E+09	6.8061E-02	3.1965E+06	5.9685E-02	15:38	7.7830E+08	3.90	0.25						Standard
130415_paine@34	2.05	2.0132E-03	1.2983E-02	1.5984E+09	6.4136E-02	3.2175E+06	6.8171E-02	15:42	7.8004E+08	3.97	0.26						Standard
130415_paine@35	2.04	2.0129E-03	9.9295E-03	1.6026E+09	4.8911E-02	3.2261E+06	5.3946E-02	15:47	7.8405E+08	3.83	0.20						Standard
130415_Br7_paine@1	2.04	2.0127E-03	1.0806E-02	1.5596E+09	7.6244E-02	3.1391E+06	7.7670E-02	16:56	7.6634E+08	3.76	0.22	3.96	3.71	0.22	9.64	0.20	Standard
130415_Br7_paine@2	2.04	2.0133E-03	1.4296E-02	1.5709E+09	4.3052E-02	3.1629E+06	5.0097E-02	17:00	7.6842E+08	4.04	0.29	0.37	3.99	0.29	9.92	0.22	Standard
130415_Br7_paine@3	2.05	2.0128E-03	1.0913E-02	1.5752E+09	3.8583E-02	3.1702E+06	3.1134E-02	17:04	7.6663E+08	3.79	0.22		3.74	0.22	9.67	0.20	Standard
130415_Br7_paine@4	2.05	2.0132E-03	1.1310E-02	1.5816E+09	3.4133E-02	3.1854E+06	3.2646E-02	17:08	7.6993E+08	4.01	0.23		3.96	0.23	9.89	0.20	Standard
130415_Br7_paine@5	2.06	2.0127E-03	1.3649E-02	1.5863E+09	3.4680E-02	3.1927E+06	3.6680E-02	17:13	7.6956E+08	3.72	0.27		3.67	0.27	9.60	0.22	Standard
130415_Br7_paine@6	2.06	2.0129E-03	1.2716E-02	1.5639E+09	4.3366E-02	3.1476E+06	3.6962E-02	17:17	7.6098E+08	3.84	0.25		3.80	0.25	9.72	0.21	Standard
130415_Br7_paine@7	2.06	2.0138E-03	1.2409E-02	1.5734E+09	3.7702E-02	3.1684E+06	3.5322E-02	17:21	7.6457E+08	4.30	0.25		4.26	0.25	10.18	0.21	Standard
130415_Br7_paine@8	2.06	2.0131E-03	6.2288E-03	1.5904E+09	2.8036E-01	3.2015E+06	2.7970E-01	17:26	7.7191E+08	3.92	0.12		3.87	0.12	9.80	0.18	Standard
130415_Br7_paine@9	2.06	2.0134E-03	1.2815E-02	1.5918E+09	4.2764E-02	3.2048E+06	5.1509E-02	17:30	7.7332E+08	4.08	0.26		4.04	0.26	9.96	0.21	Standard
130415_Br7_paine@10	2.06	2.0135E-03	7.8612E-03	1.6008E+09	2.3403E-01	3.2232E+06	2.2951E-01	17:34	7.7731E+08	4.14	0.16		4.09	0.16	10.02	0.19	Standard
130415_Br7_gr11@1	2.06	2.0296E-03	1.4368E-02	1.9304E+09	2.3080E-01	3.9185E+06	2.3554E-01	17:38	9.3679E+08	12.18	0.29	13.80	12.14	0.29	18.12	0.22	Go74
130415_Br7_gr11@2	2.05	2.0326E-03	1.1081E-02	1.9359E+09	9.5799E-02	3.9350E+06	9.4847E-02	17:43	9.4235E+08	13.67	0.22	1.50	13.62	0.22	19.61	0.21	Go74
130415_Br7_gr11@3	2.05	2.0344E-03	1.1562E-02	1.9158E+09	9.3487E-02	3.8994E+06	8.4114E-02	17:47	9.3509E+08	14.54	0.23		14.50	0.23	20.49	0.21	Go74
130415_Br7_gr11@4	2.05	2.0321E-03	6.3894E-03	1.9441E+09	1.7510E-01	3.9509E+06	1.7558E-01	17:51	9.4681E+08	13.42	0.13		13.38	0.13	19.36	0.18	Go74
130415_Br7_gr11@5	2.06	2.0317E-03	7.5554E-03	1.8609E+09	1.5122E-01	3.7808E+06	1.4849E-01	17:56	9.0356E+08	13.22	0.15		13.18	0.15	19.16	0.19	Go74
130415_Br7_gr11@6	2.06	2.0334E-03	7.0346E-03	1.8874E+09	9.0756E-02	3.8380E+06	9.3422E-02	18:00	9.1553E+08	14.08	0.14		14.04	0.14	20.03	0.19	Go74
130415_Br7_gr11@7	2.06	2.0343E-03	9.5619E-03	1.8607E+09	3.6216E-02	3.7852E+06	4.0130E-02	18:04	9.0457E+08	14.50	0.19		14.46	0.19	20.45	0.20	Go74
130415_Br7_gr11@8	2.05	2.0332E-03	5.6310E-03	1.9362E+09	2.4568E-01	3.9369E+06	2.4437E-01	18:09	9.4401E+08	13.94	0.11		13.90	0.11	19.89	0.18	Go74
130415_Br7_gr11@9	2.05	2.0347E-03	1.0881E-02	1.8324E+09	1.1271E-01	3.7288E+06	1.1570E-01	18:13	8.9261E+08	14.70	0.22		14.66	0.22	20.65	0.20	Go74
130415_Br7_gr11@10	2.05	2.0328E-03	8.3452E-03	1.9256E+09	1.6175E-01	3.9144E+06	1.6020E-01	18:17	9.3808E+08	13.75	0.17		13.71	0.17	19.70	0.19	Go74
130415_Br7_paine@11	2.05	2.0133E-03	1.4886E-02	1.6115E+09	3.3702E-02	3.2445E+06	4.1020E-02	18:22	7.8505E+08	4.03	0.30	4.03	3.99	0.30	9.92	0.23	Standard
130415_Br7_paine@12	2.06	2.0137E-03	9.0543E-03	1.6097E+09	4.1832E-02	3.2420E+06	4.0076E-02	18:26	7.8187E+08	4.22	0.18	0.23	4.18	0.18	10.11	0.19	Standard
130415_Br7_paine@13	2.06	2.0132E-03	7.8793E-03	1.6044E+09	3.9902E-02	3.2291E+06	4.9710E-02	18:30	7.7830E+08	3.99	0.16		3.96	0.16	9.89	0.19	Standard
130415_Br7_paine@14	2.05	2.0132E-03	1.0807E-02	1.5991E+09	4.4087E-02	3.2192E+06	4.6435E-02	18:35	7.7905E+08	4.01	0.22		3.98	0.22	9.90	0.20	Standard
130415_Br7_paine@15	2.04	2.0130E-03	1.3452E-02	1.5957E+09	3.1639E-02	3.2119E+06	4.1065E-02	18:39	7.8059E+08	3.91	0.27		3.87	0.27	9.80	0.22	Standard
130415_Br7_gr5@1	2.05	2.0549E-03	1.4851E-02	1.5525E+09	5.4170E-02	3.1915E+06	6.9134E-02	18:43	7.5786E+08	24.78	0.30		24.74	0.30	30.79	0.23	Ki34s
130415_Br7_gr1@1	2.05	2.0534E-03	1.1258E-02	1.5689E+09	8.0312E-02	3.2216E+06	7.9699E-02	18:48	7.6619E+08	24.04	0.23	24.57	24.01	0.23	30.05	0.21	Ki08c
130415_Br7_gr1@2	2.06	2.0545E-03	8.9694E-03	1.5899E+09	4.7702E-02	3.2663E+06	4.8381E-02	18:52	7.7362E+08	24.56	0.18	2.03	24.53	0.18	30.58	0.20	Ki08c
130415_Br7_gr1@3	2.06	2.0587E-03	1.0989E-02	1.5780E+09	3.6569E-02	3.2486E+06	3.9260E-02	18:56	7.6675E+08	26.69	0.22		26.66	0.22	32.72	0.21	Ki08c
130415_Br7_gr1@4	2.06	2.0518E-03	1.1445E-02	1.5609E+09	8.7924E-02	3.2027E+06	8.2422E-02	19:01	7.5735E+08	23.24	0.23		23.21	0.23	29.25	0.21	Ki08c
130415_Br7_gr1@5	2.05	2.0551E-03	1.5309E-02	1.5641E+09	4.3248E-02	3.2153E+06	4.1565E-02	19:05	7.6201E+08	24.90	0.31		24.87	0.31	30.92	0.23	Ki08c
130415_Br7_gr1@6	2.05	2.0519E-03	1.0145E-02	1.5665E+09	5.9554E-02	3.2146E+06	6.4200E-02	19:09	7.6297E+08	23.28	0.20		23.25	0.20	29.30	0.20	Ki08c
130415_Br7_gr1@7	2.05	2.0547E-03	9.3874E-03	1.5573E+09	2.2510E-02	3.1999E+06	2.6416E-02	19:13	7.6043E+08	24.68	0.19		24.65	0.19	30.70	0.20	Ki08c
130415_Br7_gr1@8	2.05	2.0560E-03	1.0537E-02	1.5596E+09	4.0982E-02	3.2056E+06	4.8363E-02	19:18	7.5937E+08	25.33	0.21		25.30	0.21	31.35	0.20	Ki08c
130415_Br7_gr1@9	2.06	2.0551E-03	1.0745E-02	1.5483E+09	2.6274E-02	3.1819E+06	2.8286E-02	19:22	7.5075E+08	24.88	0.21		24.85	0.21	30.90	0.21	Ki08c
130415_Br7_gr1@10	2.06	2.0535E-03	1.3231E-02	1.5592E+09	6.6022E-02	3.2017E+06	6.7189E-02	19:26	7.5617E+08	24.07	0.26		24.04	0.26	30.08	0.22	Ki08c

Table A2 Continued.

SIMS ANALYSES								Mount: BR7		Analyse: $\delta^{18}O$				Value= 9.81±0.14 (VSMOW, 2σ)				Date: 13.04.2015	
130415_Br7_paine@16	2.06	2.0133E-03	9.9864E-03	1.6134E+09	6.4524E-02	3.2482E+06	6.1102E-02	19:31	7.8493E+08	4.02	0.20	3.88		3.99	0.20	9.92	0.20	Standard	
130415_Br7_paine@17	2.06	2.0129E-03	6.1700E-03	1.6248E+09	5.2735E-02	3.2706E+06	5.2544E-02	19:35	7.8979E+08	3.84	0.12		0.17	3.81	0.12	9.74	0.18	Standard	
130415_Br7_paine@18	2.06	2.0129E-03	1.4825E-02	1.6259E+09	4.7767E-02	3.2728E+06	4.5556E-02	19:39	7.8890E+08	3.86	0.30			3.83	0.30	9.76	0.23	Standard	
130415_Br7_paine@19	2.06	2.0129E-03	9.5201E-03	1.6287E+09	5.5131E-02	3.2785E+06	6.2063E-02	19:43	7.9131E+08	3.85	0.19			3.82	0.19	9.75	0.20	Standard	
130415_Br7_paine@20	2.06	2.0128E-03	6.1613E-03	1.6290E+09	5.5855E-02	3.2789E+06	5.5126E-02	19:48	7.8930E+08	3.81	0.12			3.79	0.12	9.71	0.18	Standard	
130415_Br7_gr2@1	2.07	2.0577E-03	9.5340E-03	1.5811E+09	3.7022E-02	3.2535E+06	3.6536E-02	19:52	7.6516E+08	26.16	0.19	25.38		26.14	0.19	32.20	0.20	Ki42	
130415_Br7_gr2@2	2.06	2.0557E-03	9.1871E-03	1.5577E+09	4.7364E-02	3.2019E+06	4.7538E-02	19:56	7.5686E+08	25.17	0.18		0.95	25.15	0.18	31.20	0.20	Ki42	
130415_Br7_gr2@3	2.06	2.0546E-03	1.2620E-02	1.5505E+09	7.3477E-02	3.1856E+06	7.6874E-02	20:01	7.5302E+08	24.64	0.25			24.61	0.25	30.66	0.22	Ki42	
130415_Br7_gr2@4	2.06	2.0551E-03	9.0504E-03	1.5706E+09	9.0269E-02	3.2275E+06	8.6779E-02	20:05	7.6412E+08	24.91	0.18			24.89	0.18	30.94	0.20	Ki42	
130415_Br7_gr2@5	2.06	2.0550E-03	1.0185E-02	1.5665E+09	4.0353E-02	3.2192E+06	4.3887E-02	20:09	7.5909E+08	24.85	0.20			24.83	0.20	30.88	0.20	Ki42	
130415_Br7_gr2@6	2.07	2.0570E-03	9.2942E-03	1.5488E+09	5.0414E-02	3.1858E+06	5.3561E-02	20:13	7.4882E+08	25.82	0.19			25.79	0.19	31.85	0.20	Ki42	
130415_Br7_gr2@7	2.06	2.0563E-03	9.3062E-03	1.5546E+09	5.4166E-02	3.1955E+06	4.6993E-02	20:18	7.5352E+08	25.48	0.19			25.46	0.19	31.51	0.20	Ki42	
130415_Br7_gr2@8	2.07	2.0564E-03	7.7441E-03	1.5436E+09	3.0539E-02	3.1743E+06	2.9880E-02	20:22	7.4667E+08	25.53	0.15			25.51	0.15	31.57	0.19	Ki42	
130415_Br7_gr2@9	2.06	2.0567E-03	1.0821E-02	1.5721E+09	7.9637E-02	3.2348E+06	7.1863E-02	20:26	7.6231E+08	25.69	0.22			25.67	0.22	31.73	0.21	Ki42	
130415_Br7_gr2@10	2.07	2.0564E-03	7.8830E-03	1.5536E+09	6.1468E-02	3.1946E+06	6.7371E-02	20:31	7.5230E+08	25.52	0.16			25.50	0.16	31.56	0.19	Ki42	
130415_Br7_paine@21	2.06	2.0135E-03	8.2644E-03	1.6395E+09	2.9975E-02	3.3004E+06	3.9715E-02	20:35	7.9542E+08	4.14	0.17	3.82		4.12	0.17	10.05	0.19	Standard	
130415_Br7_paine@22	2.07	2.0127E-03	1.0541E-02	1.6386E+09	6.2560E-02	3.2978E+06	6.3786E-02	20:39	7.9236E+08	3.72	0.21		0.41	3.70	0.21	9.62	0.20	Standard	
130415_Br7_paine@23	2.07	2.0130E-03	1.0813E-02	1.6413E+09	4.8296E-02	3.3039E+06	5.0713E-02	20:43	7.9121E+08	3.89	0.22			3.87	0.22	9.80	0.20	Standard	
130415_Br7_paine@24	2.07	2.0126E-03	7.8604E-03	1.6408E+09	4.0344E-02	3.3023E+06	3.9668E-02	20:48	7.9402E+08	3.71	0.16			3.70	0.16	9.62	0.19	Standard	
130415_Br7_paine@25	2.07	2.0125E-03	9.1706E-03	1.6240E+09	3.9576E-02	3.2685E+06	3.9593E-02	20:52	7.8483E+08	3.63	0.18			3.61	0.18	9.54	0.19	Standard	
130415_Br7_gr3@1	2.06	2.0537E-03	9.9265E-03	1.5711E+09	4.7466E-02	3.2263E+06	4.8092E-02	20:56	7.6296E+08	24.21	0.20	24.42		24.19	0.20	30.24	0.20	Ki03c	
130415_Br7_gr3@2	2.07	2.0550E-03	9.3157E-03	1.5448E+09	6.5358E-02	3.1743E+06	6.3441E-02	21:01	7.4770E+08	24.83	0.19		1.36	24.81	0.19	30.87	0.20	Ki03c	
130415_Br7_gr3@3	2.07	2.0543E-03	6.2825E-03	1.5344E+09	4.1491E-02	3.1516E+06	4.5539E-02	21:05	7.4098E+08	24.47	0.13			24.45	0.13	30.50	0.19	Ki03c	
130415_Br7_gr3@4	2.07	2.0560E-03	1.0020E-02	1.5543E+09	5.0174E-02	3.1956E+06	5.1811E-02	21:09	7.5043E+08	25.33	0.20			25.32	0.20	31.37	0.20	Ki03c	
130415_Br7_gr3@5	2.07	2.0534E-03	1.6693E-02	1.5466E+09	2.4248E-02	3.1764E+06	2.9871E-02	21:13	7.4871E+08	24.06	0.33			24.04	0.33	30.09	0.24	Ki03c	
130415_Br7_gr3@6	2.06	2.0539E-03	8.9509E-03	1.5508E+09	6.4003E-02	3.1855E+06	6.5277E-02	21:18	7.5303E+08	24.28	0.18			24.26	0.18	30.31	0.20	Ki03c	
130415_Br7_gr3@7	2.06	2.0561E-03	1.2948E-02	1.5577E+09	3.7181E-02	3.2035E+06	3.7255E-02	21:22	7.5509E+08	25.36	0.26			25.35	0.26	31.40	0.22	Ki03c	
130415_Br7_gr3@8	2.07	2.0527E-03	1.1367E-02	1.5531E+09	5.4693E-02	3.1880E+06	5.8873E-02	21:26	7.5171E+08	23.66	0.23			23.65	0.23	29.70	0.21	Ki03c	
130415_Br7_gr3@9	2.07	2.0548E-03	8.4085E-03	1.5557E+09	2.3984E-02	3.1966E+06	2.3769E-02	21:31	7.5168E+08	24.74	0.17			24.73	0.17	30.78	0.19	Ki03c	
130415_Br7_gr3@10	2.07	2.0518E-03	6.2550E-03	1.5495E+09	2.4479E-02	3.1792E+06	2.5309E-02	21:35	7.4879E+08	23.23	0.13			23.22	0.13	29.26	0.18	Ki03c	
130415_Br7_paine@26	2.06	2.0133E-03	1.0319E-02	1.6243E+09	5.5448E-02	3.2699E+06	5.8223E-02	21:39	7.8960E+08	4.03	0.21	3.83		4.02	0.21	9.94	0.20	Standard	
130415_Br7_paine@27	2.05	2.0126E-03	7.6468E-03	1.6159E+09	5.8938E-02	3.2525E+06	6.0901E-02	21:44	7.8657E+08	3.70	0.15		0.25	3.69	0.15	9.62	0.19	Standard	
130415_Br7_paine@28	2.06	2.0127E-03	1.1305E-02	1.6212E+09	5.3563E-02	3.2639E+06	4.5590E-02	21:48	7.8877E+08	3.76	0.23			3.75	0.23	9.68	0.20	Standard	
130415_Br7_paine@29	2.06	2.0130E-03	9.3745E-03	1.6257E+09	7.3638E-02	3.2723E+06	7.0757E-02	21:52	7.8898E+08	3.88	0.19			3.87	0.19	9.80	0.19	Standard	
130415_Br7_paine@30	2.06	2.0128E-03	1.1083E-02	1.6261E+09	4.9226E-02	3.2729E+06	4.8042E-02	21:56	7.8905E+08	3.79	0.22			3.78	0.22	9.71	0.20	Standard	
130415_Br7_gr4@1	2.06	2.0418E-03	1.2718E-02	1.5370E+09	3.6428E-02	3.1383E+06	3.6716E-02	22:01	7.4791E+08	18.27	0.25	19.85		18.26	0.25	24.27	0.22	Ki57	
130415_Br7_gr4@2	2.06	2.0468E-03	1.1904E-02	1.5337E+09	4.1215E-02	3.1393E+06	4.5267E-02	22:05	7.4490E+08	20.75	0.24		6.32	20.75	0.24	26.78	0.21	Ki57	
130415_Br7_gr4@3	2.06	2.0298E-03	1.6670E-02	1.5830E+09	9.4649E-02	3.2132E+06	9.4160E-02	22:09	7.6971E+08	12.27	0.33							Ki57	Optical rejection
130415_Br7_gr4@4	2.06	2.0482E-03	8.9288E-03	1.5427E+09	3.2754E-02	3.1595E+06	3.1420E-02	22:14	7.4833E+08	21.43	0.18			21.42	0.18	27.45	0.20	Ki57	
130415_Br7_gr4@5	2.07	2.0455E-03	1.0884E-02	1.5673E+09	4.2129E-02	3.2057E+06	4.7898E-02	22:18	7.5758E+08	20.11	0.22			20.10	0.22	26.13	0.21	Ki57	
130415_Br7_gr4@6	2.06	2.0524E-03	8.9179E-03	1.5764E+09	4.1225E-02	3.2345E+06	4.7880E-02	22:22	7.6548E+08	23.52	0.18			23.52	0.18	29.56	0.20	Ki57	
130415_Br7_gr4@7	2.07	2.0494E-03	9.4479E-03	1.5644E+09	6.2714E-02	3.2064E+06	5.8429E-02	22:27	7.5622E+08	22.06	0.19			22.05	0.19	28.09	0.20	Ki57	
130415_Br7_gr4@8	2.06	2.0426E-03	1.1356E-02	1.5558E+09	5.7892E-02	3.1778E+06	6.1339E-02	22:31	7.5380E+08	18.63	0.23			18.63	0.23	24.64	0.21	Ki57	
130415_Br7_gr4@9	2.07	2.0500E-03	1.3074E-02	1.5618E+09	3.3990E-02	3.2016E+06	3.8277E-02	22:35	7.5467E+08	22.33	0.26			22.33	0.26	28.36	0.22	Ki57	
130415_Br7_gr4@10	2.07	2.0436E-03	9.3365E-03	1.5385E+09	3.3097E-02	3.1439E+06	3.1000E-02	22:39	7.4468E+08	19.15	0.19			19.15	0.19	25.16	0.20	Ki57	
130415_Br7_paine@31	2.06	2.0127E-03	1.2704E-02	1.6355E+09	4.3566E-02	3.2923E+06	4.0634E-02	22:44	7.9246E+08	3.73	0.25	3.91		3.73	0.25	9.65	0.21	Standard	
130415_Br7_paine@32	2.06	2.0131E-03	6.1475E-03	1.6364E+09	4.8020E-02	3.2939E+06	4.7674E-02	22:48	7.9332E+08	3.94	0.12		0.28	3.94	0.12	9.87	0.18	Standard	
130415_Br7_paine@33	2.06	2.0132E-03	1.3488E-02	1.6398E+09	4.4770E-02	3.3013E+06	4.8020E-02	22:52	7.9605E+08	4.00	0.27			4.01	0.27	9.93	0.22	Standard	
130415_Br7_paine@34	2.06	2.0134E-03	1.0335E-02	1.6373E+09	5.2963E-02	3.2961E+06	5.3691E-02	22:57	7.9440E+08	4.07	0.21			4.07	0.21	10.00	0.20	Standard	
130415_Br7_paine@35	2.06	2.0128E-03	1.1630E-02	1.6344E+09	5.1662E-02	3.2886E+06	4.9216E-02	23:01	7.9251E+08	3.81	0.23			3.81	0.23	9.74	0.21	Standard	
130415_Br7_gr6@1	2.06	2.0409E-03	6.2150E-03	1.5784E+09	3.1588E-02	3.2216E+06	3.3336E-02	23:05	7.6522E+08	17.82	0.12	18.89		17.82	0.12	23.83	0.18	Ki34s	
130415_Br7_gr6@2	2.06	2.0478E-03	1.0634E-02	1.5464E+09	4.5610E-02	3.1664E+06	4.5263E-02	23:10	7.5072E+08	21.26	0.21		6.36	21.26	0.21	27.29	0.20	Ki34s	
130415_Br7_gr6@3	2.05	2.0443E-03	1.4171E-02	1.5584E+09	3.6849E-02	3.1850E+06	4.8582E-02	23:14	7.6028E+08	19.48	0.28			19.48	0.28	25.50	0.23	Ki34s	
130415_Br7_gr6@4	2.05	2.0453E-03	1.0290E-02	1.5412E+09	5.5255E-02	3.1520E+06	5.9955E-02	23:18	7.5074E+08	19.98	0.21			19.98	0.21	26.00	0.20	Ki34s	
130415_Br7_gr6@5	2.06	2.0491E-03	1.4270E-02	1.5255E+09	5.5228E-02	3.1260E+06	5.4152E-02	23:23	7.4195E+08	21.91	0.29			21.91	0.29	27.94	0.23	Ki34s	
130415_Br7_gr6@6	2.06	2.0275E-03	1.2054E-02	1.5431E+09	5.5999E-02	3.1297E+06	4.4519E-02	23:27	7.4904E+08	11.12	0.24							Ki34s	Optical rejection
130415_Br7_gr6@7	2.06	2.0420E-03	1.2947E-02	1.5812E+09	3.1247E-02	3.2287E+06	3.3753E-02	23:31	7.6575E+08	18.33	0.26			18.34	0.26	24.35	0.22	Ki34s	
130415_Br7_gr6@8	2.06	2.0459E-03	9.3083E-03	1.5531E+09	3.6190E-02	3.1769E+06	4.5820E-02	23:35	7.5285E+08	20.28	0.19			20.29	0.19	26.31	0.20	Ki34s	
130415_Br7_gr6@9	2.06	2.0450E-03	9.8072E-03	1.5632E+09	2.0241E-01	3.1965E+06	2.0242E-01	23:40	7.5951E+08	19.87	0.20			19.88	0.20	25.90	0.20	Ki34s	
130415_Br7_paine@36	2.06	2.0132E-03	1.0386E-02	1.6526E+09	2.1380E-01	3.3269E+06	2.1489E-01	23:44	8.0411E+08	3.97	0.21	3.87		3.97	0.21	9.90	0.20	Standard	
130415_Br7_paine@37	2.06	2.0127E-03	6.7732E-03	1.6447E+09	5.8738E-02	3.3106E+06	6.1652E-02	23:48	7.9692E+08	3.74	0.14		0.27	3.75	0.14	9.68	0.18	Standard	
130415_Br7_paine@38	2.17	2.0129E-03	8.1895E-03	1.6499E+09	2.1244E-01	3.3163E+06	1.6864E-01	23:53	7.5996E+08	3.82	0.16			3.83	0.16	9.76	0.19	Standard	
130415_Br7_paine@39	2.07	2.0133E-03	1.1682E-02	1.6326E+09	7.2361E-02	3.2867E+06	7.6305E-02	23:57	7.8849E+08	4.06	0.23			4.07	0.23	10.00	0.21	Standard	
130415_Br7_paine@40	2.07	2.0128E-03	7.6518E-03	1.6279E+09	6.6299E-02	3.2764E+06	6.5476E-02	0:01	7.8583E+08	3.78	0.15			3.79	0.15	9.72	0.19	Standard	

Table A2 Continued.

		SIMS ANALYSES					Mount: BR7				Analyse: $\delta^{18}O$			Value= 9.81±0.14 (VSMOW, 2σ)				Date: 13.04.2015
130415_Br7_gr7@1	2.07	2.0413E-03	8.8205E-03	1.5661E+09	5.8303E-02	3.1966E+06	5.6438E-02	0:06	7.5792E+08	18.02	0.18	17.96	18.03	0.18	24.04	0.19		Pe01
130415_Br7_gr7@2	2.06	2.0410E-03	1.0961E-02	1.5958E+09	6.4633E-02	3.2569E+06	6.6764E-02	0:10	7.7412E+08	17.84	0.22	0.34	17.85	0.22	23.86	0.21		Pe01
130415_Br7_gr7@3	2.07	2.0412E-03	9.8403E-03	1.5723E+09	4.5831E-02	3.2091E+06	5.1200E-02	0:14	7.5918E+08	17.95	0.20		17.96	0.20	23.97	0.20		Pe01
130415_Br7_gr7@4	2.07	2.0412E-03	1.1121E-02	1.5746E+09	4.8306E-02	3.2144E+06	5.3019E-02	0:18	7.6133E+08	17.96	0.22		17.98	0.22	23.99	0.21		Pe01
130415_Br7_gr7@5	2.07	2.0406E-03	1.2653E-02	1.5985E+09	4.8293E-02	3.2618E+06	5.1178E-02	0:23	7.7276E+08	17.64	0.25		17.66	0.25	23.67	0.22		Pe01
130415_Br7_gr7@6	2.07	2.0415E-03	9.3514E-03	1.6024E+09	4.4068E-02	3.2716E+06	4.4293E-02	0:27	7.7561E+08	18.12	0.19		18.14	0.19	24.15	0.20		Pe01
130415_Br7_gr7@7	2.07	2.0408E-03	1.0383E-02	1.6000E+09	6.6089E-02	3.2653E+06	6.7677E-02	0:31	7.7443E+08	17.76	0.21		17.78	0.21	23.79	0.20		Pe01
130415_Br7_gr7@8	2.06	2.0415E-03	1.1854E-02	1.6001E+09	5.6244E-02	3.2655E+06	6.4100E-02	0:36	7.7765E+08	18.13	0.24		18.14	0.24	24.15	0.21		Pe01
130415_Br7_gr7@9	2.06	2.0414E-03	1.0626E-02	1.6122E+09	4.0327E-02	3.2912E+06	4.1317E-02	0:40	7.8135E+08	18.05	0.21		18.06	0.21	24.07	0.20		Pe01
130415_Br7_gr7@10	2.08	2.0416E-03	1.1729E-02	1.6019E+09	4.0470E-02	3.2706E+06	4.0700E-02	0:44	7.7115E+08	18.15	0.23		18.16	0.23	24.18	0.21		Pe01
130415_Br7_paine@41	2.07	2.0128E-03	1.3816E-02	1.6287E+09	5.9794E-02	3.2783E+06	6.2528E-02	0:49	7.8652E+08	3.78	0.28	3.77	3.80	0.28	9.73	0.22		Standard
130415_Br7_paine@42	2.07	2.0126E-03	7.5271E-03	1.6392E+09	4.5352E-02	3.2993E+06	4.7950E-02	0:53	7.9292E+08	3.71	0.15	0.19	3.72	0.15	9.65	0.19		Standard
130415_Br7_paine@43	2.07	2.0128E-03	9.2617E-03	1.6376E+09	5.8778E-02	3.2960E+06	5.9020E-02	0:57	7.9138E+08	3.79	0.19		3.81	0.19	9.74	0.19		Standard
130415_Br7_paine@44	2.07	2.0130E-03	9.7547E-03	1.6455E+09	3.9894E-02	3.3121E+06	3.7300E-02	1:01	7.9671E+08	3.91	0.20		3.93	0.20	9.86	0.20		Standard
130415_Br7_paine@45	2.07	2.0126E-03	8.6098E-03	1.6485E+09	6.6983E-02	3.3179E+06	6.9927E-02	1:06	7.9613E+08	3.67	0.17		3.69	0.17	9.61	0.19		Standard
130415_Br7_gr8@1	2.06	2.0532E-03	8.5815E-03	1.6223E+09	4.9841E-02	3.3308E+06	5.3542E-02	1:10	7.8637E+08	23.92	0.17	24.14	23.94	0.17	29.98	0.19		Ki32
130415_Br7_gr8@2	2.06	2.0541E-03	1.1149E-02	1.6078E+09	5.2423E-02	3.3033E+06	4.6199E-02	1:14	7.8098E+08	24.36	0.22	1.85	24.39	0.22	30.43	0.21		Ki32
130415_Br7_gr8@3	2.06	2.0520E-03	7.9640E-03	1.6277E+09	3.8489E-02	3.3393E+06	4.3619E-02	1:19	7.8876E+08	23.35	0.16		23.37	0.16	29.41	0.19		Ki32
130415_Br7_gr8@4	2.07	2.0543E-03	1.0085E-02	1.6220E+09	2.5417E-02	3.3322E+06	2.4774E-02	1:23	7.8536E+08	24.48	0.20		24.50	0.20	30.55	0.20		Ki32
130415_Br7_gr8@5	2.07	2.0506E-03	1.2488E-02	1.6669E+09	7.7570E-02	3.4182E+06	7.7270E-02	1:27	8.0500E+08	22.63	0.25		22.65	0.25	28.69	0.22		Ki32
130415_Br7_gr8@6	2.07	2.0531E-03	9.1190E-03	1.6428E+09	5.5861E-02	3.3731E+06	5.4879E-02	1:32	7.9195E+08	23.89	0.18		23.92	0.18	29.96	0.20		Ki32
130415_Br7_gr8@7	2.07	2.0541E-03	1.1963E-02	1.6495E+09	4.1713E-02	3.3881E+06	4.4912E-02	1:36	7.9814E+08	24.37	0.24		24.39	0.24	30.44	0.21		Ki32
130415_Br7_gr8@8	2.07	2.0578E-03	1.0719E-02	1.6624E+09	4.3636E-02	3.4206E+06	4.5450E-02	1:40	8.0384E+08	26.21	0.21		26.24	0.21	32.30	0.21		Ki32
130415_Br7_gr8@9	2.07	2.0530E-03	1.0507E-02	1.6278E+09	5.7073E-02	3.3430E+06	5.3047E-02	1:45	7.8554E+08	23.84	0.21		23.87	0.21	29.92	0.20		Ki32
130415_Br7_gr8@10	2.07	2.0541E-03	1.2091E-02	1.6262E+09	2.8954E-02	3.3406E+06	2.7718E-02	1:49	7.8523E+08	24.37	0.24		24.40	0.24	30.45	0.21		Ki32
130415_Br7_paine@46	2.07	2.0131E-03	1.2332E-02	1.6530E+09	5.8693E-02	3.3280E+06	5.7706E-02	1:53	7.9834E+08	3.94	0.25	3.98	3.97	0.25	9.89	0.21		Standard
130415_Br7_paine@47	2.07	2.0131E-03	1.1541E-02	1.6508E+09	5.7534E-02	3.3235E+06	5.9458E-02	1:58	7.9616E+08	3.95	0.23	0.19	3.97	0.23	9.90	0.21		Standard
130415_Br7_paine@48	2.08	2.0135E-03	1.3465E-02	1.6573E+09	6.4496E-02	3.3366E+06	7.0916E-02	2:02	7.9825E+08	4.12	0.27		4.15	0.27	10.08	0.22		Standard
130415_Br7_paine@49	2.08	2.0133E-03	7.7254E-03	1.6574E+09	4.1213E-02	3.3368E+06	4.0021E-02	2:06	7.9871E+08	4.04	0.15		4.07	0.15	10.00	0.19		Standard
130415_Br7_paine@50	2.07	2.0130E-03	1.2734E-02	1.6527E+09	4.0470E-02	3.3269E+06	4.2480E-02	2:10	7.9723E+08	3.88	0.25		3.91	0.25	9.84	0.21		Standard
130415_Br7_gr9@1	2.06	2.0564E-03	1.1235E-02	1.6054E+09	5.6043E-02	3.3015E+06	5.2745E-02	2:15	7.7760E+08	25.54	0.22	26.49	25.57	0.22	31.63	0.21		ki46
130415_Br7_gr9@2	2.07	2.0538E-03	9.3720E-03	1.5845E+09	2.4793E-02	3.2544E+06	2.5093E-02	2:19	7.6501E+08	24.24	0.19	3.14	24.27	0.19	30.32	0.20		ki46
130415_Br7_gr9@3	2.07	2.0580E-03	1.0464E-02	1.6183E+09	5.8910E-02	3.3305E+06	5.7868E-02	2:23	7.8278E+08	26.34	0.21		26.37	0.21	32.43	0.20		ki46
130415_Br7_gr9@4	2.07	2.0582E-03	7.5584E-03	1.6106E+09	4.7902E-02	3.3150E+06	4.9974E-02	2:28	7.7664E+08	26.41	0.15		26.45	0.15	32.51	0.19		ki46
130415_Br7_gr9@5	2.08	2.0626E-03	1.1232E-02	1.6063E+09	4.5119E-02	3.3132E+06	4.6286E-02	2:32	7.7397E+08	28.64	0.22		28.67	0.22	34.75	0.21		ki46
130415_Br7_gr9@6	2.08	2.0580E-03	6.8604E-03	1.5841E+09	2.9735E-02	3.2602E+06	3.0569E-02	2:36	7.6223E+08	26.32	0.14		26.35	0.14	32.41	0.19		ki46
130415_Br7_gr9@7	2.07	2.0581E-03	8.7777E-03	1.6002E+09	4.0477E-02	3.2936E+06	4.2022E-02	2:41	7.7308E+08	26.37	0.18		26.41	0.18	32.47	0.20		ki46
130415_Br7_gr9@8	2.06	2.0556E-03	1.1961E-02	1.5942E+09	3.3051E-02	3.2762E+06	4.3569E-02	2:45	7.7219E+08	25.11	0.24		25.15	0.24	31.20	0.21		ki46
130415_Br7_gr9@9	2.07	2.0579E-03	9.9090E-03	1.6120E+09	4.3813E-02	3.3174E+06	4.5560E-02	2:49	7.7981E+08	26.29	0.20		26.32	0.20	32.38	0.20		ki46
130415_Br7_gr9@10	2.07	2.0645E-03	9.0001E-03	1.6200E+09	3.7845E-02	3.3436E+06	4.1604E-02	2:54	7.8237E+08	29.58	0.18		29.62	0.18	35.70	0.20		ki46
130415_Br7_paine@51	2.06	2.0125E-03	1.1195E-02	1.6448E+09	4.5930E-02	3.3101E+06	4.4786E-02	2:58	7.9722E+08	3.66	0.22	3.88	3.69	0.22	9.62	0.20		Standard
130415_Br7_paine@52	2.07	2.0127E-03	1.1705E-02	1.6522E+09	4.8040E-02	3.3257E+06	4.9590E-02	3:02	7.9950E+08	3.72	0.23	0.41	3.76	0.23	9.69	0.21		Standard
130415_Br7_paine@53	2.07	2.0135E-03	9.2992E-03	1.6541E+09	4.6044E-02	3.3297E+06	4.1375E-02	3:07	8.0069E+08	4.12	0.19		4.16	0.19	10.09	0.19		Standard
130415_Br7_paine@54	2.07	2.0129E-03	7.9538E-03	1.6585E+09	5.4004E-02	3.3396E+06	4.9118E-02	3:11	8.0312E+08	3.84	0.16		3.87	0.16	9.80	0.19		Standard
130415_Br7_paine@55	2.07	2.0133E-03	6.1137E-03	1.6545E+09	4.8793E-02	3.3311E+06	5.0242E-02	3:15	7.9990E+08	4.05	0.12		4.09	0.12	10.02	0.18		Standard
130415_Br7_gr10@1	2.07	2.0510E-03	1.0000E-02	1.6475E+09	5.5959E-02	3.3790E+06	5.7198E-02	3:20	7.9631E+08	22.83	0.20	24.82	22.87	0.20	28.91	0.20		Ki01
130415_Br7_gr10@2	2.07	2.0542E-03	9.2442E-03	1.6333E+09	4.1036E-02	3.3560E+06	3.8015E-02	3:24	7.8940E+08	24.44	0.18	2.75	24.48	0.18	30.53	0.20		Ki01
130415_Br7_gr10@3	2.07	2.0543E-03	6.6651E-03	1.6308E+09	4.7081E-02	3.3505E+06	4.9811E-02	3:28	7.8900E+08	24.50	0.13		24.54	0.13	30.59	0.19		Ki01
130415_Br7_gr10@4	2.07	2.0557E-03	6.4748E-03	1.6357E+09	4.9818E-02	3.3625E+06	4.8193E-02	3:33	7.9026E+08	25.19	0.13		25.23	0.13	31.29	0.19		Ki01
130415_Br7_gr10@5	2.07	2.0559E-03	1.2957E-02	1.6463E+09	6.8035E-02	3.3844E+06	6.9672E-02	3:37	7.9599E+08	25.29	0.26		25.33	0.26	31.38	0.22		Ki01
130415_Br7_gr10@6	2.07	2.0551E-03	1.2335E-02	1.6492E+09	4.5291E-02	3.3881E+06	5.5411E-02	3:41	7.9534E+08	24.88	0.25		24.92	0.25	30.97	0.21		Ki01
130415_Br7_gr10@7	2.07	2.0617E-03	8.6618E-03	1.6357E+09	5.3595E-02	3.3723E+06	5.3639E-02	3:46	7.9131E+08	28.19	0.17		28.23	0.17	34.30	0.20		Ki01
130415_Br7_gr10@8	2.07	2.0540E-03	1.1271E-02	1.6328E+09	5.5840E-02	3.3539E+06	6.0428E-02	3:50	7.8762E+08	24.36	0.23		24.40	0.23	30.45	0.21		Ki01
130415_Br7_gr10@9	2.07	2.0531E-03	1.0015E-02	1.6296E+09	4.5858E-02	3.3447E+06	5.5887E-02	3:54	7.8910E+08	23.87	0.20		23.92	0.20	29.96	0.20		Ki01
130415_Br7_gr10@10	2.07	2.0546E-03	1.0142E-02	1.6624E+09	7.1304E-02	3.4159E+06	7.5395E-02	3:59	8.0425E+08	24.63	0.20		24.67	0.20	30.72	0.20		Ki01
130415_Br7_paine@56	2.07	2.0132E-03	1.3634E-02	1.6603E+09	4.6575E-02	3.3425E+06	4.7470E-02	4:03	8.0166E+08	4.01	0.27	3.86	4.06	0.27	9.99	0.22		Standard
130415_Br7_paine@57	2.07	2.0128E-03	1.2699E-02	1.6424E+09	5.0568E-02	3.3058E+06	5.7074E-02	4:07	7.9180E+08	3.79	0.25	0.39	3.83	0.25	9.76	0.21		Standard
130415_Br7_paine@58	2.07	2.0132E-03	1.2540E-02	1.6405E+09	4.5179E-02	3.3017E+06	4.9661E-02	4:12	7.9153E+08	4.01	0.25		4.06	0.25	9.99	0.21		Standard
130415_Br7_paine@59	2.07	2.0135E-03	1.2256E-02	1.6461E+09	5.1195E-02	3.3145E+06	5.4455E-02	4:16	7.9400E+08	4.12	0.25		4.17	0.25	10.10	0.21		Standard
130415_Br7_paine@60	2.07	2.0130E-03	8.9796E-03	1.6371E+09	2.9047E-02	3.2954E+06	3.1532E-02	4:20	7.9010E+08	3.87	0.18		3.92	0.18	9.85	0.19		Standard
130415_Br7_paine@61	2.07	2.0129E-03	1.0915E-02	1.6307E+09	5.8448E-02	3.2828E+06	5.7201E-02	4:25	7.8927E+08	3.86	0.22		3.91	0.22	9.84	0.20		Standard
130415_Br7_paine@62	2.07	2.0126E-03	6.7828E-03	1.6309E+09	4.9124E-02	3.2829E+06	5.0105E-02	4:29	7.8616E+08	3.70	0.14		3.75	0.14	9.68	0.18		Standard
130415_Br7_paine@63	2.07	2.0122E-03	9.6890E-03	1.6269E+09	2.7193E-02	3.2740E+06	3.2466E-02	4:33	7.8647E+08	3.50	0.19		3.55	0.19	9.48	0.20		Standard

SIMS を用いた中生代放散虫岩の酸素同位体分析

Maximilien BÔLE・池田　昌之・Peter O. BAUMGARTNER・堀　利栄・
Anne-Sophie BOUVIER・Duje KUKOČ

要　旨

化石殻の炭酸カルシウムの酸素同位体比（$\delta^{18}O$）を用いた古海洋研究が広く用いられているが，珪質化石殻については分析の制約や同位体分別の不確定性等のため，古海洋研究への適用例は限られている．本論では，二次イオン質量分析計（SIMS）によって測定した日本，イタリア，スイス，ルーマニアの中生代チャートに含まれる放散虫化石 $\delta^{18}O$ 変動の古海洋指標としての有用性について報告する．53 試料 507 点の測定の結果，放散虫殻 $\delta^{18}O$ は 19.8 ～ 35.3 ‰で，現世及び新生代の放散虫殻の値と調和的であり，標準試料 UNIL-Q1 の繰り返し測定誤差 0.3 ‰以上に 1 チャート試料中の $\delta^{18}O$ 変化がみられる．このことから，続成作用（セグリゲーション）の影響による均一化は完全ではなく，初生的な値が保存されている可能性を支持する．さらに，予察的な放散虫化石の $\delta^{18}O$ 記録は低解像度にもかかわらず，1,000 万年スケールではコノドントのアパタイトや低 Mg 炭酸塩殻に確認される前期－中期三畳紀の正のシフトや後期三畳紀の安定した高い値と調和的であるが，前期ジュラ紀のパンサラッサ海遠洋域における放散虫化石 $\delta^{18}O$ の約 8 ‰の負のシフトはテチス海沿岸域の低 Mg 炭酸塩殻には確認されない．さらに高解像度で他指標と比較することで，放散虫化石の $\delta^{18}O$ 記録の古海洋学的意義をより深く理解できると期待される．

Bulletin of the Geological Survey of Japan, vol. 71 (4), p. 395–437, 2020

Note and Comment

Radiolarian research by the Geological Survey of Japan, AIST, with bibliographic lists from 1950 to 2019

ITO Tsuyoshi[1,*], NAKAE Satoshi[1] and ITAKI Takuya[1]

ITO Tsuyoshi, NAKAE Satoshi and ITAKI Takuya (2020) Radiolarian research by the Geological Survey of Japan, AIST, with bibliographic lists from 1950 to 2019. *Bulletin of the Geological Survey of Japan*, vol. 71(4), p. 395–437, 7 figs, 6 tables, 1 appendix.

Abstract: The Geological Survey of Japan (GSJ), established in 1882, marked its 135th anniversary in 2017 and has issued numerous publications, such as geologic maps, research articles and newsletters, during its history. This article compiles previous GSJ publications related to radiolarian research for future reference. In the GSJ publications from 1950 to 2019, the term of RADIOLARIA in Japanese appears in 252 Geological Maps of the Quadrangle Series (1:50,000), in 21 Geological Maps of the Quadrangle Series (1:200,000), in 75 articles of the Bulletin of the Geological Survey of Japan, in 14 items in Chishitsu News, in 21 items in GSJ Chishitsu News and in seven articles in the Cruise Report. The GSJ publications related to radiolarian research increased during the 1980s, which is consistent with the commonly called Radiolarian Revolution.

Keywords: radiolaria, bibliography, compilation, Paleozoic, Mesozoic, Cenozoic, Japan

1. Introduction

The Geological Survey of Japan (GSJ), a Japanese public organization for geological survey, was established in 1882 under the Ministry of Agriculture and Commerce. In 2001, the National Institute of Advanced Industrial Science and Technology (AIST) was extensively restructured as an independent administrative agency to integrate 15 research institutes, including GSJ.

Since its establishment, GSJ has aimed to make geological maps of Japan and has published many geological maps on several scales (Fig. 1) (Kato *et al.*, 2011). In 1890, GSJ published a geological map of the Japanese Islands (1:3,000,000) for the first time (Fig. 2A). Geologic maps of the Japanese Islands have been often renewed. The most recently published geological map of the Japanese Islands (1:1,000,000) was published in 1992 as the 3rd Edition (Fig. 2B). Twenty quadrangular areas (1:500,000) cover the Japanese Islands (Fig. 3).

GSJ began publishing Geological Maps of the Quadrangle Series (1:50,000) in the 1950s and continued the publication thereafter (e.g. Saito, 2009; Miyazaki, 2018). Radiolarians are important index fossils used to make the geologic maps of the series, some of which contain descriptions of radiolarians. In addition to the geological maps, GSJ has issued various publications, such as the Bulletin of the Geological Survey of Japan and GSJ Chishitsu News. Some of these publications also contain radiolarian information.

GSJ has also conducted marine surveys since the 1970s (e.g. Arai *et al.*, 2013). Some of their survey results have been presented via GSJ publications, such as in the Cruise Report. Description of radiolarians are included in many of these publications because they are marine protozoa that are generally included in ocean deposits around the Japanese Islands.

Geological Maps of the Quadrangle Series (1:50,000), the Bulletin of the Geological Survey of Japan, GSJ Chishitsu News and Chishitsu News can be downloaded as portable document format (PDF) files from the website of GSJ (Appendix). All documents are OCRed; thus, we searched the documents for the term RADIOLARIA in Japanese (=“放散虫”). The Cruise Report was also downloaded as a PDF file from the website; however, the files are not OCRed.

Here, we present a brief history of radiolarian research by GSJ via the compilation of previous publications. This paper aims to provide bibliographic lists related to radiolarians for future reference.

[1] AIST, Geological Survey of Japan, Research Institute of Geology and Geoinformation

[*] Corresponding author: ITO, T., Central 7, 1-1-1 Higashi, Tsukuba, Ibaraki 305-8567, Japan. Email: ito-t@aist.go.jp

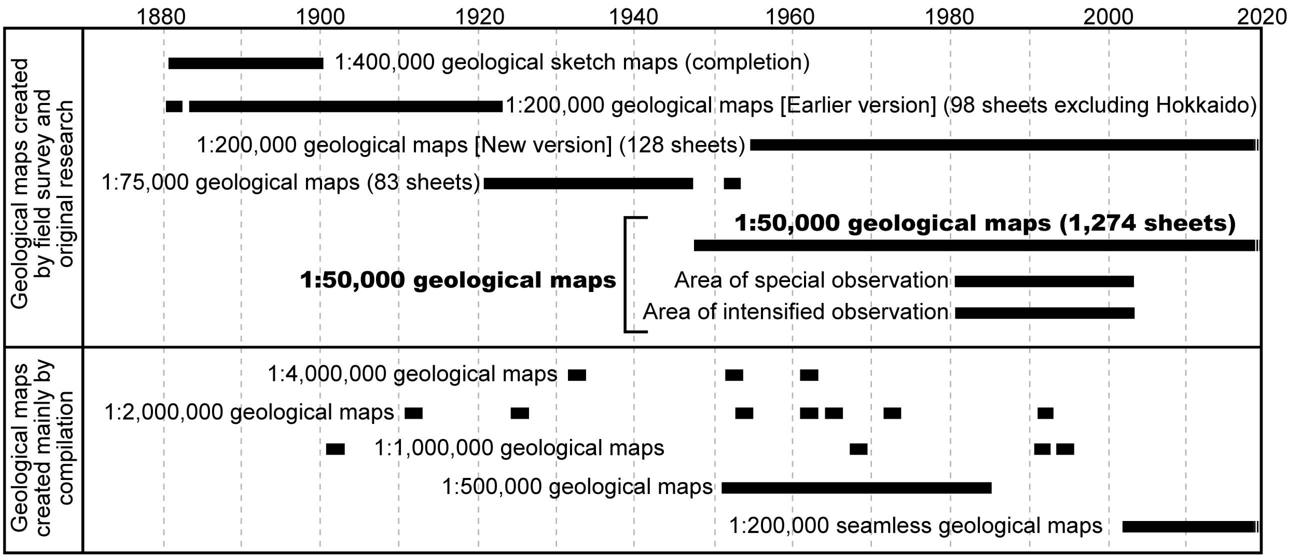

Fig. 1 History of the creation of geological maps by GSJ (modified from Kato *et al.*, 2011).

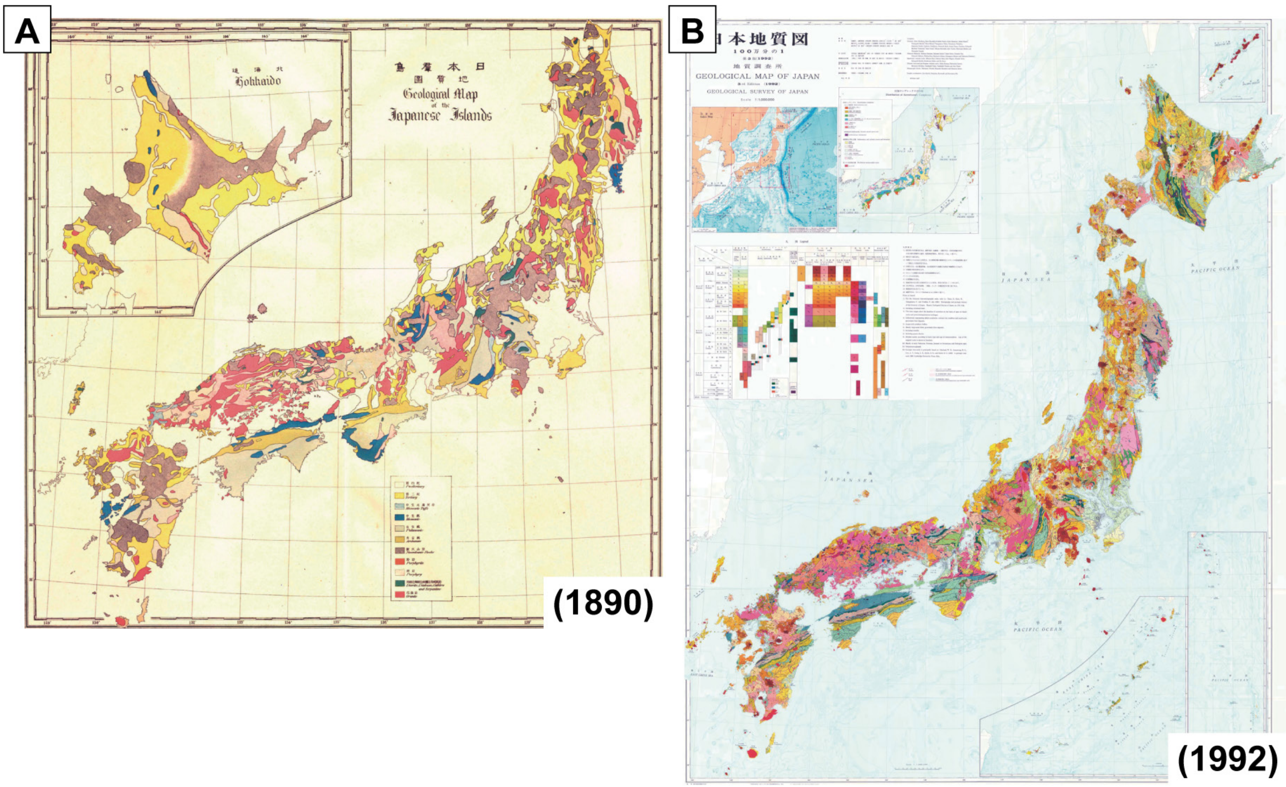

Fig. 2 Geological maps of GSJ. A: First published geological map of the Japanese Islands (1:3,000,000) by GSJ in 1890, as drawn by T. Harada (reprints from Kato *et al.*, 2011); B: Most recently published geological map of the Japanese Islands (1:1,000,000, 3rd Edition) by GSJ in 1992.

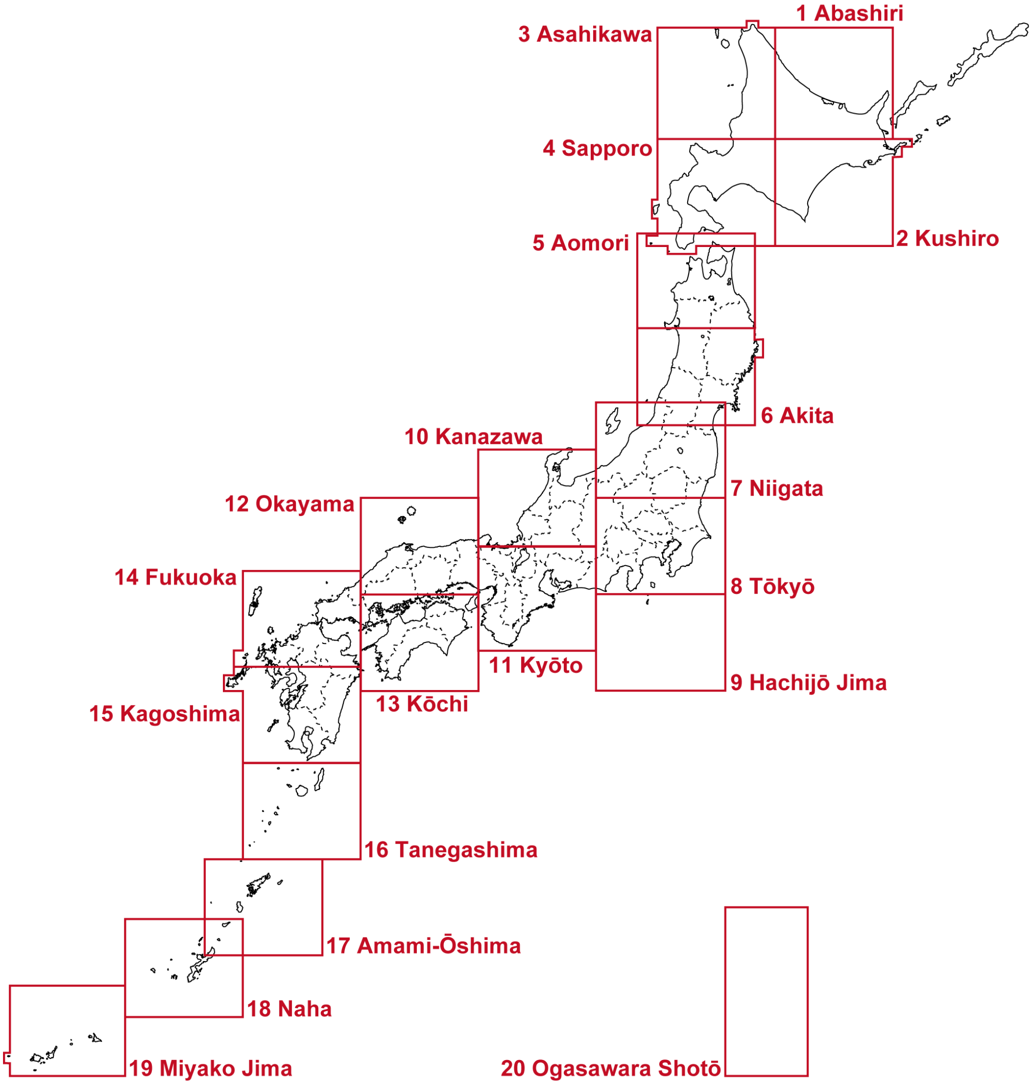

Fig. 3 Japanese Islands with quadrangular areas of 1:500,000.

2. Notable descriptions of radiolarian research in GSJ publications

2. 1 Geological Maps of the Quadrangle Series (1:50,000)

The Geological Maps of the Quadrangle Series (1:50,000) have been published since the 1950s (Fig. 1). Between 1951 and 2019, over 700 geological maps in the series have been published. Among them, 252 geological maps contain descriptions of radiolaria (Table 1).

Until the early 1970s, radiolaria were not an important index fossil because they could not be extracted from hard rocks. Pessagno and Newport (1972) discovered a radiolarian extraction method by using hydrofluoric acid (HF). Since their discovery, radiolarian studies have rapidly progressed (e.g. Ichikawa, 1982; Yao *et al.*, 2001; O'Dogherty *et al.*, 2009; Danelian *et al.*, 2017). High-resolution biochlonology based on microfossils (radiolaria and conodont) prompted the overturn of previously believed scenarios for geologic history of the Japanese Islands (e.g. Sakai *et al.*, 1982; Nakaseko *et al.*, 1983; Ichikawa *et al.*, 1985; Ichikawa, 1990; Isozaki and Maruyama, 1991; Yao and Mizutani, 1993; Isozaki *et al.*, 2010; Agematsu-Watanabe and Kamata, 2018). This research progress and the revision of the geologic history are commonly referred to as the Radiolarian Revolution (e.g. Ishigaki and Yao, 1982; Nakaseko, 1984; Sato, 1989; Suzuki and Aita, 2011; Matsuoka and Ito, 2017). Likewise, the GSJ Publications related to radiolarian research also increased in the early 1980s (Fig. 4). Among the geological maps from 1981 to 2019 that include radiolarian descriptions, approximately half present an occurrence list and/or an image of radiolarians in addition to the text.

Meanwhile, even before the 1970s, radiolarian had been described in some geologic maps. In the 1950s, S. Igi had shown an occurrence species list of radiolarians (identified by K. Ichikawa) from chert of the Hidaka Group in the

Table 1 Bibliographic list from the Geological Maps of the Quadrangle Series (1:50,000) that include radiolarian descriptions.
+: Appearance from its district. -: Appearance from adjacent district(s).

No.	District		Author(s)	Year	Text	Occurrence list	Illustrations			Radiolarian age									
	English	Japanese					SEM	Etched surface	Thin section	Silurian	Devonian	Carboniferous	Permian	Triassic	Jurassic	Cretaceous	Paleogene	Neogene	Quaternary
1	**Abashiri**	**網走**																	
9	Kamiokoppe	上興部	Hasegawa K. *et al.*	1969	+														
10	Okoppe	興部	Hasegawa K. and Uozumi	1975	+														
14	Takinoue	滝上	Matsunami	2002	+	+										+	+		
15	Kamishokotsu	上渚滑	Matsunami *et al.*	2002	-											-	-		
23	Maruseppu-Hokubu	丸瀬布北部	Yahata *et al.*	1988	+	+									+	+	+		
24	Engaru	遠軽	Tajika and Yahata	1991	+				+						+	+	+		
26, 27	Abashiri	網走	Kawakami G. *et al.*	2018	-										-	-			
47	Kitami	北見	Ishida and Sawamura	1968	+														
58	Honki	本岐	Yamaguchi and Sawamura	1965	+														
2	**Kushiro**	**釧路**																	
2	Tokachigawajōryū	十勝川上流	Sakō and Hasegawa	1957	+														
5	Rikubetsu	陸別	Mitani *et al.*	1960	+														
19	Ashorobuto	足寄太	Mitani *et al.*	1958	+														
32	Honbetsu	本別	Mitani *et al.*	1959	+														
33	Kamicharo	上茶路	Sato S. *et al.*	1961	+														
53	Nukanai	糠内	Yamaguchi and Satoh	1989	+														
56	Idonnappudake	イドンナップ岳	Suzuki M. *et al.*	1961a	+														
59	Chūrui	忠類	Yamaguchi *et al.*	2003	+														
65	Mitsuishi	三石	Wada *et al.*	1992	-											-			
66	Nishicha	西舎	Sakai and Kanie	1986	+	+										+			
69	Urakawa	浦河	Kanie and Sakai	2002	+											+			
72	Erimo-Misaki	襟裳岬	Igi and Kakimi	1956	+	+													
3	**Asahikawa**	**旭川**																	
16	Kamisarufutsu	上猿払	Tanaka K.	1960	+														
20	Pinneshiri	敏音知	Igi	1959	+														
25	Hatsuura	初浦	Hata	1961	+														

Table 1 Continued.

No.	District		Author(s)	Year	Text	Occurrence list	Illustrations			Radiolarian age									
	English	Japanese					SEM	Etched surface	Thin section	Silurian	Devonian	Carboniferous	Permian	Triassic	Jurassic	Cretaceous	Paleogene	Neogene	Quaternary
35	Soeushinai	添牛内	Hashimoto *et al.*	1965	+														
39	Horokanai	幌加内	Igi *et al.*	1958	+	+													
40	Kenbuchi	剣淵	Matsushita *et al.*	1977	+														
41	Rumoi	留萌	Tsushima and Yamaguchi	1954	+														
42	Ebishima	恵比島	Watanabe and Yaoshida	1995	+														
44	Pippu	比布	Suzuki J.	1957	+														
48	Fukagawa	深川	Suzuki J.	1953	+														
49	Asahikawa	旭川	Suzuki J.	1955	+														
54	Biei	美栄	Suzuki M. *et al.*	1961b	+														
4	**Sapporo**	**札幌**																	
7	Shimofurano	下富良野	Hashimoto	1955	+														
15	Ikushumbetsu-Dake	幾春別岳	Yoshida T. and Kambe	1955	+														
16	Yamabe	山部	Hashimoto	1953	+														
23	Yūbari	夕張	Sasa *et al.*	1964	+														
24	Ōyubari	大夕張	Nagao *et al.*	1954	+														
25	Ishikarikanayama	石狩金山	Osanai *et al.*	1958	+														
32	Oiwake	追分	Matsuno and Hata	1960	+														
33	Momijiyama	紅葉山	Takahashi Koh. *et al.*	2002	+											+	+		
34	Hidaka	日高	Takahashi Koh. and Suzuki	1986	+														
35, 46	Harauta and Karibayama	原歌及び狩場山	Yamagishi and Kurosawa	1987	-									-	-	-			
41	Tarumaizan	樽前山	Doi	1957	+														
45	Iwachishi	岩知志	Takahashi Koh. and Suzuki	1978	+														
47	Ohbirayama	大平山	Kurosawa *et al.*	1993	+	+	+							+	+	+			
52	Shiraoi	白老	Doi	1953	+														
55	Tomikawa	富川	Imai and Sumi	1957	+														
56	Biu	比宇	Yoshida T. *et al.*	1959	+														

Table 1 Continued.

No.	District: English	District: Japanese	Author(s)	Year	Text	Occurrence list	Illustrations: SEM	Illustrations: Etched surface	Illustrations: Thin section	Radiolarian age: Silurian	Devonian	Carboniferous	Permian	Triassic	Jurassic	Cretaceous	Paleogene	Neogene	Quaternary
64, 65, 71, 72	Okushiritō Hokubu and Nambu	奥尻島北部及び南部	Hata *et al.*	1982	+													+	
73	Kumaishi	熊石	Hata	1975	+														
87	Esan	恵山	Fujiwara and Kōnoya	1969	+														
92	Matsumae	松前	Hata *et al.*	1990	+										-	-		+	
5	**Aomori**	**青森**																	
4	Shiriyazaki	尻屋崎	Tsushima and Takizawa	1977	+														
5	Ichinohe	一戸	Tuzino *et al.*	2018	+				+						+				
10	Kodomari	小泊	Tsushima and Uemura	1959	+														
11	Kanita	蟹田	Uemura *et al.*	1959	+														
20	Ajigasawa	鯵ヶ沢	Hirayama J. and Uemura	1985	+														
22	Aomori-Seibu	青森西部	Nagamori *et al.*	2013	+													+	
26	Fukaura	深浦	Moritani	1968	+														
35	Nakahama	中浜	Ōzawa *et al.*	1983	+														
38	Towada ko	十和田湖	Kudo *et al.*	2019	+										-				
43	Noshiro	能代	Ōzawa *et al.*	1984	+														
49	Rikuchū-Ōno	陸中大野	Yoshida T. *et al.*	1987	+														
51	Ugo-Hamada	羽後浜田	Ōzawa *et al.*	1985	+	+												+	
52	Moritake	森岳	Ōzawa *et al.*	1985	+														
6	**Akita**	**秋田**																	
1, 2	Toga and Funakawa	戸賀及び船川	Kano K. *et al.*	2011	+													+	
3	Gojōme	五城目	Hase and Hirayama	1970	+														
4	Aniai, 2nd Edition	阿仁合(第2版)	Kano K. *et al.*	2012	+													+	
11	Akita	秋田	Huzioka *et al.*	1977	+														
12	Taiheizan	大平山	Ōzawa *et al.*	1981	+														
19	Ugo-Wada	羽後和田	Huzioka *et al.*	1976	+													+	
20	Kariwano	刈和野	Tsuchiya and Yoshikawa	1994	+	+												+	

Table 1 Continued.

No.	District		Author(s)	Year	Text	Occurrence list	Illustrations			Radiolarian age									
	English	Japanese					SEM	Etched surface	Thin section	Silurian	Devonian	Carboniferous	Permian	Triassic	Jurassic	Cretaceous	Paleogene	Neogene	Quaternary
24	Hayachine San	早池峰山	Kawamura *et al.*	2013	+		+		+		+	-		+	+				
26	Miyako	宮古	Yoshida T. and Katada	1984	+														
28	Honjō	本荘	Ōzawa *et al.*	1977	+														
35, 36	Otsuchi and Karodake	大槌・霞露岳	Yoshida T. and Katada	1964	+														
37	Kisakata	象潟	Ōzawa *et al.*	1982	+														
38	Yashima	矢島	Ōzawa *et al.*	1988	+	+												+	
39	Asamai	浅舞	Ōzawa *et al.*	1979a	+														
46, 47	Chōkaisan and Fukura	鳥海山及び吹浦	Nakano and Tsuchiya	1992	+	+												+	
48	Yuzawa	湯沢	Ōzawa *et al.*	1979b	+														
55	Sakata	酒田	Ikebe *et al.*	1979	+	+												+	
56	Ōsawa	大沢	Tsuchiya	1989	+													+	
64	Tsuruoka	鶴岡	Tsuchiya *et al.*	1984	+	+												+	
65	Kiyokawa	清川	Ōzawa *et al.*	1986	+	+												+	
79	Toyona	登米	Takizawa *et al.*	1990	+		+		+						+				
98	Sendai	仙台	Kitamura *et al.*	1986	+														
7	**Niigata**	**新潟**																	
11	Iidesan	飯豊山	Takahashi Yut. *et al.*	1996	-										-				
12	Tamaniwa	玉庭	Yanagisawa and Yamamoto	1998	-										-	-			
16	Kakuda	角田	Fujita *et al.*	1988	-														
25	Sōmanakamura	相馬中村	Yanagisawa *et al.*	1996	+											+			
26	Izumozaki	出雲崎	Kobayashi *et al.*	1993	+													+	
27	Sanjō	三条	Kobayashi *et al.*	2002	+													+	
27	Kamo	加茂	Kudo *et al.*	2011	+	+							+	+	+				
31	Kitakata	喜多方	Yamamoto *et al.*	2005	+													+	
35, 36	Haramachi and Ōmika	原町及び大甕	Kubo *et al.*	1990	+											-			
37	Kashiwazaki	柏崎	Kobayashi *et al.*	1995	+													+	
38	Nagaoka	長岡	Kobayashi *et al.*	1991	-														

Table 1 Continued.

No.	District: English	District: Japanese	Author(s)	Year	Text	Occurrence list	Illustrations: SEM	Illustrations: Etched surface	Illustrations: Thin section	Radiolarian age: Silurian	Devonian	Carboniferous	Permian	Triassic	Jurassic	Cretaceous	Paleogene	Neogene	Quaternary
41	Miyashita	宮下	Yamamoto and Komazawa	2004	+													+	
42	Wakamatsu	若松	Yamamoto and Yoshioka	1992	+										+	+			
46	Namie and Iwaki-Tomioka	浪江及び磐城富岡	Kubo *et al.*	1994	+													+	
50	Ojiya	小千谷	Yanagisawa *et al.*	1986	-										-				
51	Suhara	須原	Takahashi Yut. *et al.*	2004	+	+			+				+	+	+				
54	Tajima	田島	Yamamoto	1999	+										+				
58, 59	Kawamae and Ide	川前及び井出	Kubo *et al.*	2002	+													+	
63	Tōkamachi	十日町	Yanagisawa *et al.*	1985	+										+				
64	Hakkaisan	八海山	Chihara and Komatsu	1992	-										-				
70	Takanuki	竹貫	Kano H. *et al.*	1973	+														
71, 58, 59	Taira and Kawamae (incl. Ide)	平・川前（付井出）	Iwao and Matsui	1961	+														
103	Utsunomiya	宇都宮	Yoshikawa *et al.*	2010	-									-	-				
8	**Tōkyō**	**東京**																	
7	Tochigi	栃木	Fujimoto	1961	+														
11	Nakaminato	那珂湊	Sakamoto *et al.*	1972	+														
27	Yorii	寄居	Makimoto and Takeuchi	1992	+	+	+						+	+	+				
34	Takatō	高遠	Makimoto *et al.*	1996	+								-		-	+			
37	Mitsumine	三峰	Hara *et al.*	2010	+	+			+				+	+	+	+			
45	Ichinose	市野瀬	Kawachi *et al.*	1983	-														
49	Itsukaichi	五日市	Sakai	1987	+	+							+	+	+	+	+	+	
50	Ōme	青梅	Ueki and Sakai	2007	+								+	+	+	+			
59	Kofu	甲府	Katada	1956	+														
62	Hachiōji	八王子	Ueki *et al.*	2013	+											+	-		
69	Minobu	身延	Ozaki and Sugiyama	2018	+	+									-	-	-	-	
79	Nanbu	南部	Sugiyama Y. and Matsuda	2014	+	+										+	+	+	

Table 1 Continued.

No.	District		Author(s)	Year	Text	Occurrence list	Illustrations			Radiolarian age									
	English	Japanese					SEM	Etched surface	Thin section	Silurian	Devonian	Carboniferous	Permian	Triassic	Jurassic	Cretaceous	Paleogene	Neogene	Quaternary
84	Yokosuka	横須賀	Eto *et al.*	1998	+													+	
85	Futtsu	富津	Nakajima and Watanabe	2005	+													+	
87	Kazusa-Ohara	上総大原	Utsunomiya and Ooi	2019	+														+
89	Shimizu	清水	Sugiyama Y. and Shimokawa	1990	+	+											+	+	
94	Nago	那古	Suzuki Y. *et al.*	1990	+														
95	Kamogawa	鴨川	Nakajima *et al.*	1981	+														
98	Shizuoka	静岡	Sugiyama Y. *et al.*	1982	+													+	
102	Tateyama	館山	Kawakami S. and Shishikura	2006	+													+	
10	**Kanazawa**	**金沢**																	
3, 4, 6, 7	Suzumisaki, Noto-iida and Hōryūzan	珠洲岬, 能登飯田及び宝立山	Yoshikawa *et al.*	2002	+													+	
14	Itoigawa	糸魚川	Nagamori *et al.*	2018	-								-						
15, 16	Ōchigata and Abugashima	邑知潟･虻ガ島	Imai and Sakamoto	1966	+														
18	Tomari	泊	Takeuchi M. *et al.*	2017	-								-						
19	Kotaki	小滝	Nagamori *et al.*	2010	+				+				+						
23	Uozu	魚津	Sumi and Nozawa	1973	+														
25	Shiroumadake	白馬岳	Nakano *et al.*	2002	+								+						
28	Yatsuo	八尾	Sakamoto and Nozawa	1960	+													+	
31	Ōmachi	大町	Kato *et al.*	1989	+		+						+	+					
37	Yaigatake	槍ヶ岳	Harayama *et al.*	1991	+								+	+	+				
45	Kamikōchi	上高地	Harayama	1990	+	+	+			+	+			+	+				
47	Fukui	福井	Kano K. *et al.*	2007	+														
52	Takayama	高山	Yamada *et al.*	1985	+	+							+	+	+				
53	Norikuradake	乗鞍岳	Nakano *et al.*	1995	+	+			+				+	+	+				
58	Arashimadake	荒島岳	Kawai *et al.*	1957	+														

Table 1 Continued.

No.	District		Author(s)	Year	Text	Occurrence list	Illustrations			Radiolarian age									
	English	Japanese					SEM	Etched surface	Thin section	Silurian	Devonian	Carboniferous	Permian	Triassic	Jurassic	Cretaceous	Paleogene	Neogene	Quaternary
60	Hagiwara	萩原	Kawada *et al.*	1988	+	+								+	+				
61	Ontakesan	御岳山	Yamada and Kobayashi	1988	+				+					-	-				
62	Kiso-Fukushima	木曽福島	Takeuchi M. *et al.*	1998	+									-	+				
63	Ina	伊那	Katada and Isomi	1962	+														
66, 67	Imajō and Takenami	今庄及び竹波	Nakae *et al.*	2013	+	+							+	+	+				
68	Kanmuri Yama	冠山	Nakae *et al.*	2015	+	+			+				+	+	+				
69	Neo	根尾	Kawai	1964	-														
70	Hachiman	八幡	Wakita	1984	+	+	+						+	+	+				
71	Gero	下呂	Wakita and Koido	1994	+	+								+	+	+			
76	Tangoyura	丹後由良	Hirokawa and Kuroda	1958	+														
78	Nishizu	西津	Nakae *et al.*	2002	+	+			+				+	+	+				
79	Tsuruga	敦賀	Kurimoto *et al.*	1999	+	+	+		+				+		+				
80	Yokoyama	横山	Saito and Sawada	2000	+	+	+		+				+	+	+				
81	Tanigumi	谷汲	Wakita	1991	+	+							+	+	+	+			
82	Mino	美濃	Wakita	1995	+	+								-	+	-			
83	Kanayama	金山	Mizutani and Koido	1992	+	+								+	+				
11	**Kyōto**	**京都**																	
2	Maizuru	舞鶴	Igi *et al.*	1961	+														
3	Obama	小浜	Hirokawa *et al.*	1957	+														
4	Kumagawa	熊川	Nakae and Yoshioka	1998	+	+	+		+				+	+	+				
5	Chikubu Shima	竹生島	Nakae *et al.*	2001	+		+		+						+				
8	Gifu	岐阜	Yoshida F. and Wakita	1999	+	+							+	+	+				
13	Fukuchiyama	福知山	Kurimoto and Makimoto	1990	+	+	+						+	+	+				
14	Ayabe	綾部	Kimura *et al.*	1989	+	+							+	-	+				
15	Yotsuya	四ツ谷	Kimura *et al.*	1994	+	+			+				-	+	+				
16	Kitakomatsu	北小松	Kimura *et al.*	2001	+	+	+						-	-	+				
20	Nagoya-Hokubu	名古屋北部	Sakamoto *et al.*	1984	+		+								+				

Table 1 Continued.

No.	District		Author(s)	Year	Text	Occurrence list	Illustrations			Radiolarian age									
	English	Japanese					SEM	Etched surface	Thin section	Silurian	Devonian	Carboniferous	Permian	Triassic	Jurassic	Cretaceous	Paleogene	Neogene	Quaternary
25	Sasayama	篠山	Kurimoto *et al.*	1993	+		+		+				+	+	+				
26	Sonobe	園部	Imoto *et al.*	1991	+								+	+	+				
27	Kyōto-Seihokubu	京都西北部	Imoto *et al.*	1989	+			+	+				+	+	+				
28	Kyōto-Tōhokubu	京都東北部	Kimura *et al.*	1998	+	+	+						+	+	+				
29	Ōmi-hachiman	近江八幡	Yoshida F. *et al.*	2003	+														
30	Gozaishoyama	御在所山	Harayama *et al.*	1989	+	+							+	+	+				
31	Kuwana	桑名	Yoshida F. *et al.*	1991	+	+	+						-	-	+				
38	Hirone	広根	Matsuura *et al.*	1995	+								-	-	+				
39	Kyōto-Seinambu	京都西南部	Miyachi *et al.*	2005	+	+	+						+	+	+				
40	Kyōto-Tōnambu	京都東南部	Wakita *et al.*	2013	+	+	+						+	+	+				
41	Minakuchi	水口	Nakano *et al.*	2003	+				+										
49	Kōbe	神戸	Huzita and Kasama	1983	-														
50	Ōsaka-Seihokubu	大阪西北部	Huzita and Kasama	1982	+														
54	Tsu-Seibu	津西部	Yoshida F. *et al.*	1995	+														
58, 70	Toyohashi and Tahara	豊橋及び田原	Nakashima *et al.*	2008	+	+	+		+				+	+	+				
59	Hamamatsu	浜松	Isomi and Inoue	1972	+														
60, 71	Mitsuke and Kakezuka	見付・掛塚	Makiyama and Sakamoto	1957	+														
62	Ōsaka-Seinambu	大阪西南部	Huzita and Maeda	1985	-														
69	Iragomisaki	伊良湖岬	Nakashima *et al.*	2010	+	+	+		+				+	+	+				
73	Kishiwada	岸和田	Itihara *et al.*	1986	+														
79	Toba	鳥羽	Uchino *et al.*	2017	+	+			+		+		+	+	+	+			
81	Kokawa	粉河	Makimoto *et al.*	2004	+										-	+			
82	Koyasan	高野山	Hirayama K. and Kambe	1959	+														
83	Sanjōgatake	山上ヶ岳	Shiida *et al.*	1989	+	+			+					+	+	+			
88	Kainan	海南	Hirayama K. and Tanaka	1956a	+														
89	Todorogi	動木	Hirayama K. and Tanaka	1956b	+														
96	Ryūjin	龍神	Tokuoka *et al.*	1981	+												+		

Table 1 Continued.

No.	District: English	District: Japanese	Author(s)	Year	Text	Occurrence list	Illustrations: SEM	Illustrations: Etched surface	Illustrations: Thin section	Radiolarian age: Silurian	Devonian	Carboniferous	Permian	Triassic	Jurassic	Cretaceous	Paleogene	Neogene	Quaternary
106	Esumi	江住	Tateishi *et al.*	1979	+														
12	**Okayama**	**岡山**																	
2	Urago	浦郷	Tiba *et al.*	2000	+														
11, 21	Tottorihokubu and Tottorinambu	鳥取北部及び鳥取南部	Murayama *et al.*	1963	+														
16	Imaichi	今市	Kano K. *et al.*	1998	+														
17	Matsue	松江	Kano K. *et al.*	1994	+														
25, 26	Iwami-Ōda and Ōura	石見大田及び大浦	Kano K. *et al.*	1998	+									+	+				
32	Chizu	智頭	Yamada	1966	+				+										
36, 37	Yunotsu and Gōtsu	温泉津及び江津	Kano K. *et al.*	2001	-								-						
46	Yamasaki	山崎	Yamamoto *et al.*	2002	+	+	+						-	+	+				
47	Ikuno	生野	Yoshikawa *et al.*	2005	+	+			+				+	+	+				
50	Akana	赤名	Matsuura	1990	+														
58	Tatsuno	龍野	Yamamoto *et al.*	2000	+	+	+						+	+	+				
59	Hōjō	北条	Ozaki *et al.*	1995	+	+	+						+	+	+				
13	**Kōchi**	**高知**																	
1	Tsuta	津田	Takahashi Yuh. *et al.*	1989	+								+		-				
2	Hiroshima	広島	Takahashi Yuh.	1991	-								-		-				
3	Kaitaichi	海田市	Takagi and Mizuno	1999	-										-				
11	Sumoto	洲本	Takahashi Yut. *et al.*	1992	+											+			
12	Ōtake	大竹	Higashimoto *et al.*	1986	+	+	+						+	+	+				
13	Itsuku Shima	厳島	Matsuura *et al.*	1999	-										-				
24	Iwakuni	岩国	Higashimoto *et al.*	1983	-										-				
25, 26	Kurahashi Jima and Hashira Jima	倉橋島及び柱島	Matsuura	1998	-									-	-				
30	Kan-onji	観音寺	Noda *et al.*	2017	+											+			
40	Niihama	新居浜	Aoya *et al.*	2013	+											+			

Table 1 Continued.

No.	District		Author(s)	Year	Text	Occurrence list	Illustrations			Radiolarian age									
	English	Japanese					SEM	Etched surface	Thin section	Silurian	Devonian	Carboniferous	Permian	Triassic	Jurassic	Cretaceous	Paleogene	Neogene	Quaternary
52	Hibihara	日比原	Aoya and Yokoyama	2009	+				+					-	-				
53	Motoyama	本山	Endo and Yokoyama	2019	+								+		-				
55	Kitagawa	北川	Hara *et al.*	2014	+				+				+		+	+			
59	Ōzu	大洲	Banno *et al.*	2010	+										+				
77	Uwajima	宇和島	Teraoka *et al*.	1986	+	+							+	+	+	+			
87	Tsurumisaki	鶴御崎	Okumura and Teraoka	1988	+	+										+			
88, 89	Iyokashima and Sukumo	伊予鹿島及び宿毛	Tanaka K.	1980	+	+										+	+		
14	**Fukuoka**	**福岡**																	
34	Kokura	小倉	Nakae *et al.*	1998	+	+			+				+						
68	Sasebo	佐世保	Matsui *et al.*	1989	+														
77	Saganoseki	佐賀関	Miyazaki and Yoshioka	1994	+								+						
87	Inukai	犬飼	Teraoka *et al.*	1992	+	+	+							+	+				
88	Usuki	臼杵	Kambe and Teraoka	1968	-								-						
15	**Kagoshima**	**鹿児島**																	
24	Miemachi	三重町	Sakai *et al.*	1993	+	+	+						+	+	+	+			
25	Saiki	佐伯	Teraoka *et al.*	1990	+	+								-	+	+			
34	Kumata	熊田	Okumura *et al.*	1998	+	+									+	+			
35	Kamae	蒲江	Okumura *et al.*	1985	+	+										+	+		
41	Tomochi	砥用	Saito *et al.*	2005	+	+	+		+	+	+		+	+	+				
44	Nobeoka	延岡	Okumura *et al.*	2010	-											-	-		
51	Shiibamura	椎葉村	Saito *et al.*	1996	+	+	+								+	+	+		
59	Murasho	村所	Hara *et al.*	2009	+	+	+		+							-	+	+	
60	Osuzuyama	尾鈴山	Kimura *et al.*	1991	+	+											+		
68, 69	Tsuma and Takanabe	妻及び高鍋	Endo and Suzuki	1986	+												+		
90	Sueyoshi	末吉	Saito *et al.*	1994	+	+	+									+	+		
100	Kaimon Dake	開聞岳	Kawanabe and Sakaguchi	2005	-											-			

Table 1 Continued.

No.	District: English	District: Japanese	Author(s)	Year	Text	Occurrence list	Illustrations: SEM	Illustrations: Etched surface	Illustrations: Thin section	Radiolarian age: Silurian	Devonian	Carboniferous	Permian	Triassic	Jurassic	Cretaceous	Paleogene	Neogene	Quaternary
17	**Amami-Ōshima**	**奄美大島**																	
6	Yuwan	湯湾	Takeuchi M.	1993	+	+							+	+	+	+			
13	Iheya Jima and Izena Jima	伊平屋島及び伊是名島	Ujiié	2000	+	+							+	+	+				
18	**Naha**	**那覇**																	
13, 14	Naha and Okinawashi-Nambu	那覇及び沖縄市南部	Ujiié and Kaneko	2006	+										+				
15, 16	Itoman and Kudaka Jima	糸満及び久高島	Kaneko and Ujiié	2006	+										+				
20	**Ogasawara Shotō**	**小笠原諸島**																	
2	Chichijima Rettō	父島列島	Umino and Nakano	2007	+	+											+		
3	Hahajima Rettō	母島列島	Umino *et al.*	2016	-														

Erimo-Misaki district (Igi and Kakimi, 1956) and from chert of the Sorachi Group in the Horokanai district (Igi *et al.*, 1958). They regarded the Hidaka and Sorachi groups as pre-Cretaceous and Upper Jurassic, respectively.

Mid-Mesozoic accretionary complexes are widely exposed in the Japanese Islands and generally contain Permian, Triassic and Jurassic radiolarians (e.g. Kojima *et al.*, 2016). Because of their importance for age determination to draw the geological maps, their occurrences have been reported by several maps in most areas (Fig. 5).

Yamada (1966) presented a thin section photograph of radiolarian remains within phyllite of the Sangun metamorphic rocks in the Chizu district (Fig. 6A), which was the first illustration of radiolarians in the geological maps of the series. Sakamoto *et al.* (1984) presented Jurassic radiolarians (Fig. 6B) from siliceous rocks in the Nagoya-Hokubu district. This was the first radiolarian description with scanning electron microscopy (SEM) images in the geological maps of the series.

2. 2 Geological Maps of the Quadrangle Series (1:200,000)

The Geological Maps of the Quadrangle Series (1:200,000) have been published since the 1880s (Fig. 1). Since the 1950s, new version of the series has been published. However, the series published before 2000 contains the geological map only but not the explanation text. The explanation text of 21 geological maps contain descriptions of radiolaria (Table 2).

Radiolarian images are not generally shown in the series because of a space constraint. Saito *et al.* (2007b) showed Eocene radiolarian images reprinted from Saito *et al.* (2007a).

2. 3 Bulletin of the Geological Survey of Japan

The Bulletin of the Geological Survey of Japan is an open access monthly–bimonthly journal that has been published since 1950. Research achievements by primarily GSJ's researchers have been published in this journal.

Among the 709 issues of this journal from 1950 to 2019, 75 articles contain descriptions of radiolarians (Table 3). Article including radiolarian description increased in the early 1980s (Fig. 4) as in the case of the Geological Maps of the Quadrangle Series (1:50,000).

Some articles contain abundant radiolarian images (e.g. Hori, 2004b, c, d; Motoyama *et al.*, 2010; Nakae, 2013a, b; Kurimoto *et al.*, 2015). Radiolarian images have covered some volumes of the Bulletin of the Geological Survey of Japan (e.g. vol. 55, no. 9/10; vol. 68, no. 2; vol. 70, no. 1/2). Sugiyama and Saito (1994) described two new species, i.e. *Podocyrtis* (*Lampterium*) *mirabilis* Sugiyama and Saito and *Lophocyrtis*? *cavifundus* Sugiyama and Saito from the Paleogene in the Sueyoshi district. Kamikuri (2019b) described new species, *Lychnocanoma californica* Kamikuri, from the upper Miocene in the eastern North Pacific.

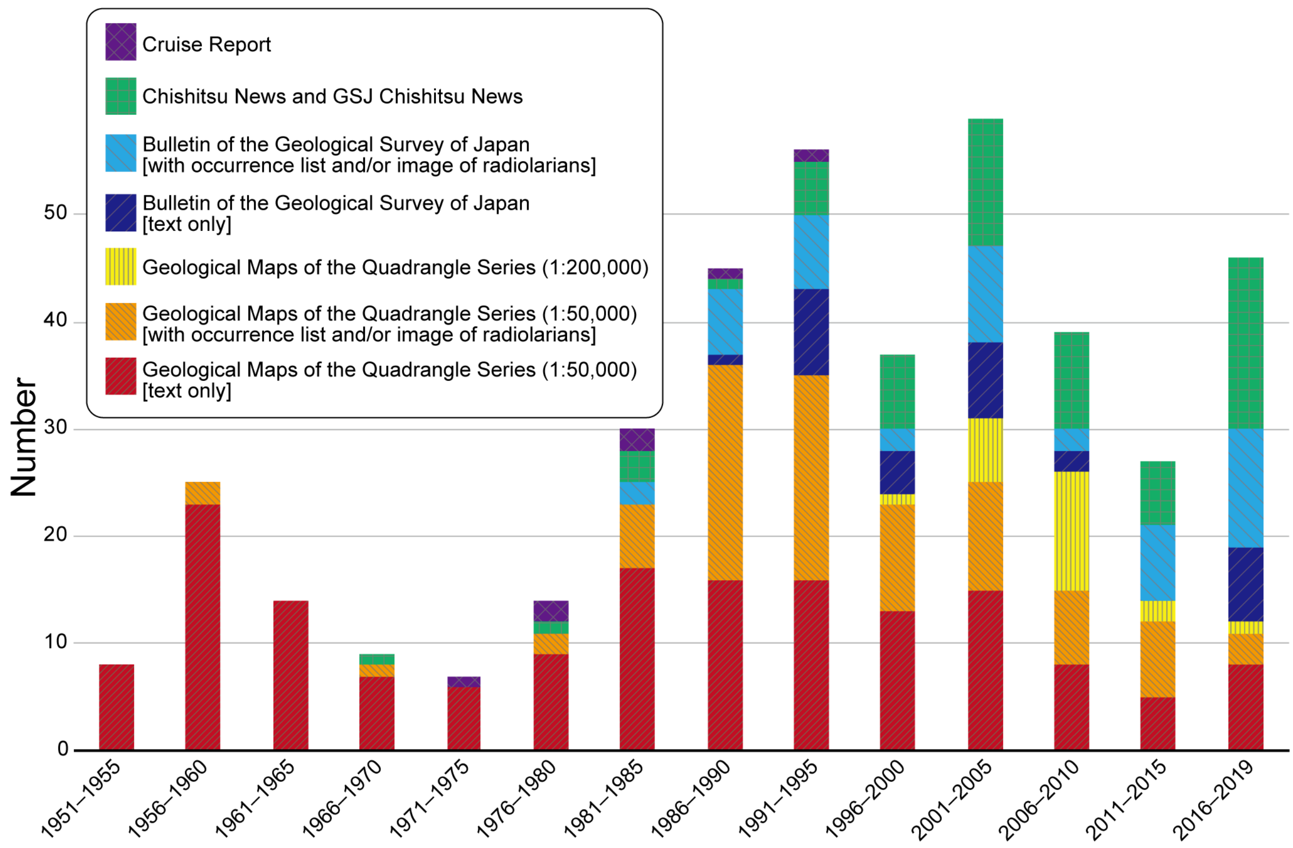

Fig. 4 Quinquennial number of GSJ publications that contain the term RADIOLARIA in Japanese (=“放散虫”).

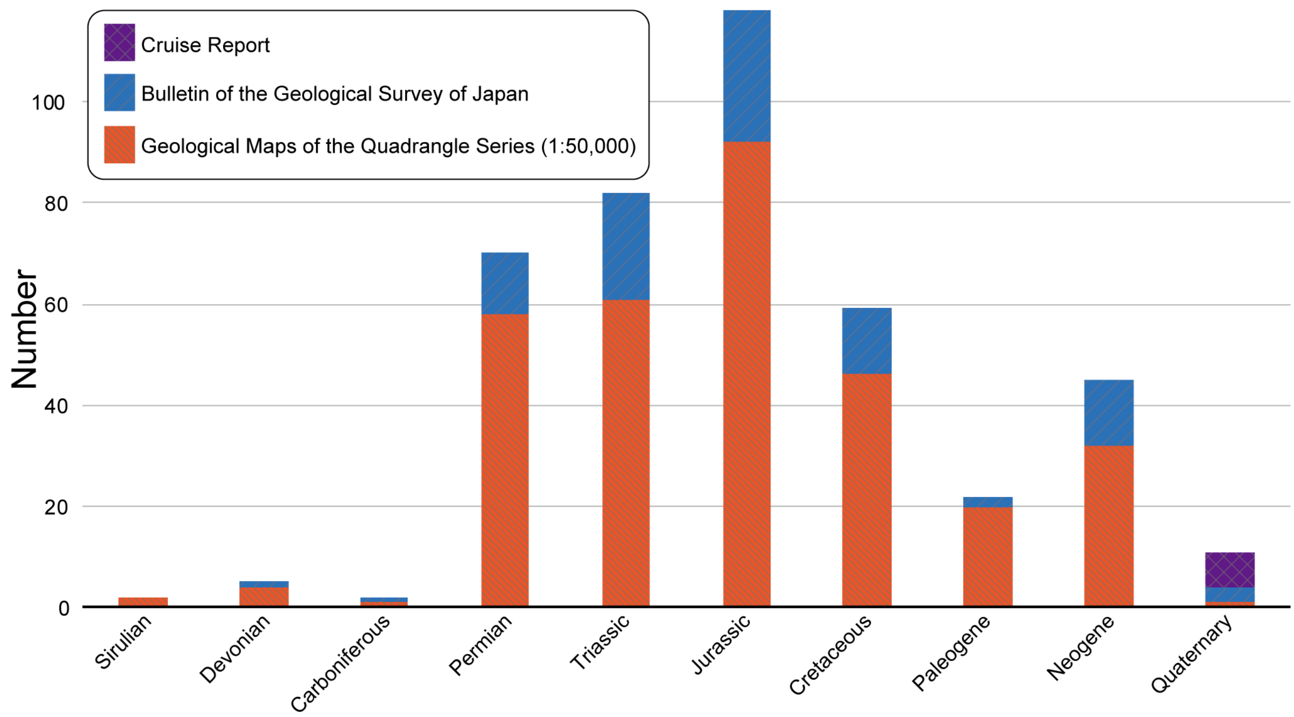

Fig. 5 Age distribution of radiolarian descriptions in GSJ publications.

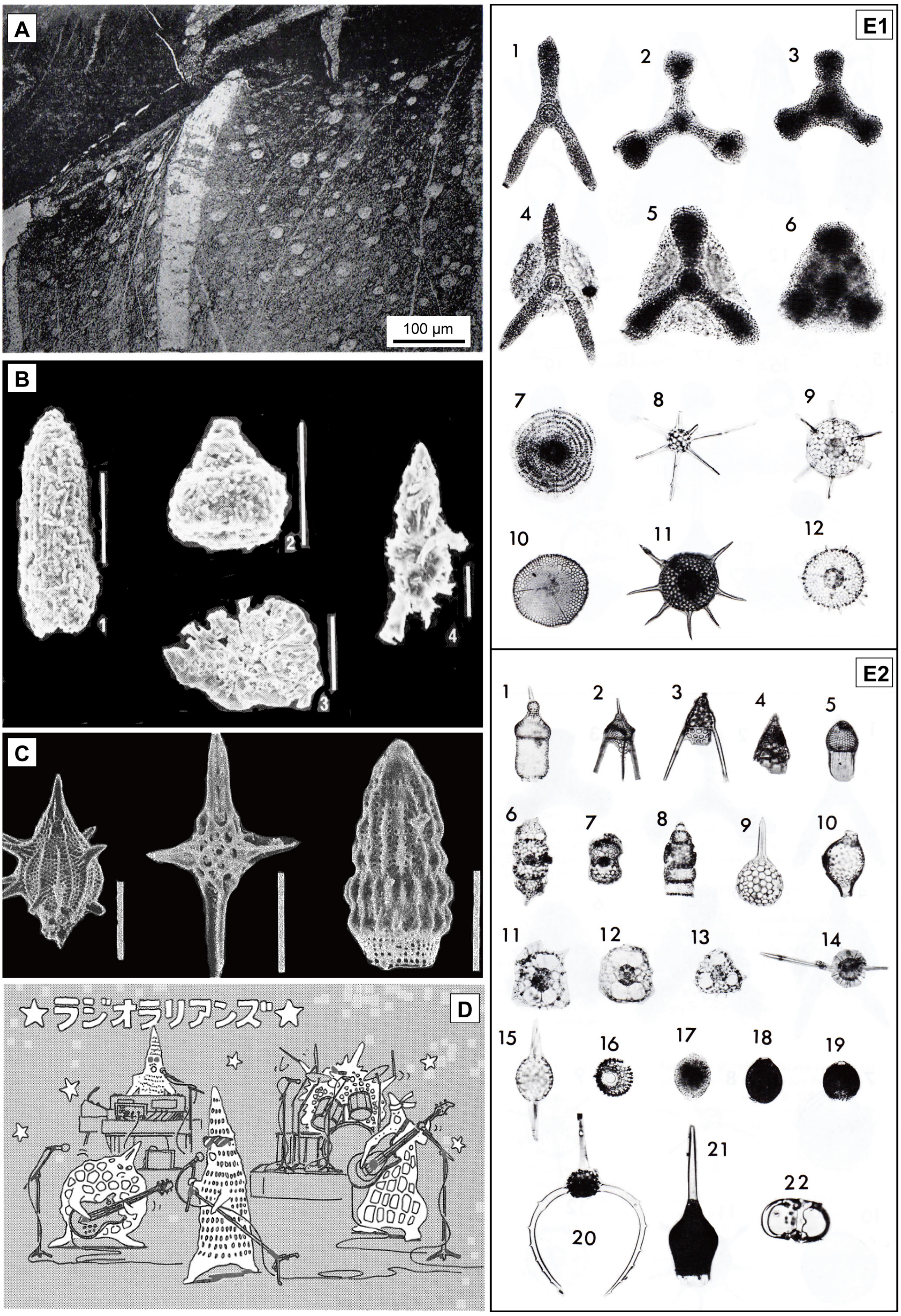

Fig. 6 Notable figures of radiolarian research by GSJ. A: First photograph of radiolarians within phyllite (thin section) in the Geological Maps of the Quadrangle Series (1:50,000) (reprints from Yamada, 1966). B: First SEM images of radiolarians in Geological Maps of the Quadrangle Series (1:50,000) (reprints from Sakamoto *et al.*, 1984). C: First SEM images of radiolarians in GSJ publications (Chishitsu News) (reprints from Sakai *et al.*, 1982). D: Illustrations of cartoon radiolarians shown in Chishitsu News (reprints from Wakita and Kawamura, 1985). E: Possible first images of radiolarian individuals in GSJ publications (Cruise Report) (reprints from Arita and Mizuno, 1977).

Table 2 Bibliographic list from the Geological Maps of the Quadrangle Series (1:200,000) that include radiolarian descriptions.

District		Author(s)	Year
English	Japanese		
Ichinoseki	一関	Takeuchi K. *et al.*	2005
Ise	伊勢	Nishioka *et al.*	2010
Ishigaki Jima	石垣島	Nakae *et al.*	2009
Kaimon Dake and a part of Kuro Shima	開聞岳及び黒島の一部	Kawanabe *et al.*	2004
Kōfu	甲府	Ozaki *et al.*	2002
Kubokawa	窪川	Hara *et al.*	2006
Mito (2nd Edition)	水戸(第2版)	Yoshioka *et al.*	2001
Nakatsu	中津	Ishizuka *et al.*	2009
Niigata (2nd Edition)	新潟(第2版)	Takahashi Yut. *et al.*	2010
Ōita (2nd Edition)	大分(第2版)	Hoshizumi *et al.*	2015
Okayama and Marugame	岡山及丸亀	Matsuura *et al.*	2002
Shirakawa	白河	Kubo *et al.*	2007
Shizuoka and Omae Zaki (2nd Edition)	静岡及び御前崎(第2版)	Sugiyama *et al.*	2010
Toyohashi and Irago Misaki	豊橋及び伊良湖岬	Makimoto *et al.*	2004
Urakawa	浦河	Sakai *et al.*	2000
Wajima (2nd Edition)	輪島(第2版)	Ozaki *et al.*	2019
Yaku Shima	屋久島	Saito *et al.*	2007b
Yamaguchi and Mishima	山口及び見島	Matsuura *et al.*	2007
Yatsushiro and a part of Nomo Zaki	八代及び野母崎の一部	Saito *et al.*	2010
Yokosuka (2nd Edition)	横須賀(第2版)	Takeuchi K. *et al.*	2015
Yoron Jima and Naha	与論島及び那覇	Nakae *et al.*	2010

2. 4 Chishitsu News and GSJ Chishitsu News

Chishitsu News and GSJ Chishitsu News are monthly newsletters published by GSJ. Chishitsu News was published from 1953 to 2011. From 2011 and onward, GSJ Chishitsu News has been published as a successor to Chishitsu News.

In total, 14 and 21 articles containing radiolarian descriptions were published in Chishitsu News and GSJ Chishitsu News, respectively (Tables 4, 5). Fukuda and Natori (1977) showed a transmitted photomicrograph of Neogene radiolaria reprinted from Nakaseko and Sugano (1973). This was possibly the first isolated radiolarian images presented in the GSJ publications. Sakai *et al.* (1982) introduced a micropaleontological study on conodont and radiolaria and described their significance in Chishitsu News at the dawn of the Radiolarian Revolution. They also showed SEM images (Fig. 6C), which were the first SEM images published in the GSJ publications. Wakita and Kawamura (1985) wrote an essay about radiolarians, which included some SEM images, thin section and cartoons (Fig. 6D).

Since 1997, the Geological Museum owned by GSJ has displayed radiolarian exhibits, such as panels and models (Toshimitsu and Saito, 1997). The Geological Museum also made a poster showing radiolarians with reconstructed oceanic plate stratigraphy in Jurassic accretionary complexes (Fig. 7). Special exhibitions related to radiolarians have often been displayed in the museum (e.g. Shibahara *et al.*, 2012; Ito *et al.*, 2017).

2. 5 Cruise Report

GSJ had published the Cruise Report from 1972 to 1997. Twenty-four issues of the Cruise Report were published during this time period. Among them, seven articles contain descriptions of radiolarians (Table 6).

Arita and Mizuno (1977) showed photomicrographs of living radiolarians from the central–eastern part of the Central Pacific Basin (Fig. 6E). These were possibly one of the first isolated radiolarian images in the GSJ publications like Fukuda and Natori (1977).

Acknowledgments: Dr. UCHINO Takayuki (Geological Survey of Japan, AIST) has carefully reviewed the manuscript and has provided constructive comments. Dr. Toshimitsu Seiichi (Geological Survey of Japan, AIST) provided a reprinted poster of "Reconstructed Oceanic Plate Stratigraphy in Jurassic accretionary complexes and radiolarian fossils in Japan" made by the Geological Museum of GSJ.

Table 3 Bibliographic list from the Bulletin of the Geological Survey of Japan that include radiolarian descriptions.

Author(s)	Bibliography				Text	Occurrence list	Images			Radiolarian age								
	Year	Vol.	No.	Pages			SEM	Transmitted	Thin section	Devonian	Carboniferous	Permian	Triassic	Jurassic	Cretaceous	Paleogene	Neogene	Quaternary
Hara and Hara	2019	70	1/2	117–123	+		+								+			
Hara *et al.*	2012	63	11/12	301–308	+		+		+						+			
Hattori	1993	44	7	455–469	+													
Hori N.	2004a	55	9/10	271–285	+							+	+	+				
	2004b	55	9/10	287–301	+	+	+					+						
	2004c	55	9/10	303–334	+	+	+						+					
	2004d	55	9/10	335–388	+	+	+							+				
	2005	56	1/2	37–83	+	+	+					+	+	+				
Hori N. *et al.*	2002	53	9/10	689–724	+	+	+							+				
Hori R. S.	1993	44	9	555–570	+		+							+				
Imoto and Saijyo	1993	44	9	547–554	+							+	+					
Ishiga and Yamakita	1993	44	7	419–423	+													
Ishiga *et al.*	1993	44	12	721–726	+													
Ito	2019a	70	1/2	225–247	+	+	+	+	+			+	+	+				
Kakuwa	1993	44	9	533–546	+													
Kametaka *et al.*	2005	56	7/8	237–243	+		+		+			+						
Kamikuri	2019a	70	1/2	137–161	+	+		+									+	
	2019b	70	1/2	163–194	+	+		+									+	
Kashiwagi and Kurimoto	2003	54	7/8	279–293	+	+	+						+	+				
Kimura	1997	48	6	313–337	+													
Kimura and Nakae	1993	44	12	727–743	+	+	+		+					+				
Kojima *et al.*	1994	45	2	63–97	+	+	+						+	+	+			
Kojima and Saito	2000	51	4	143–165	+		+						+	+				
Kurimoto	1987	38	2	69–80	+	+	+						+	+				
	1989	40	2	55–63	+	+	+					+		+				
	1994a	45	5	235–255	+	+	+	+							+			
Kurimoto and Kuwahara	1991	42	2	69–73	+	+	+						+	+				
Kurimoto *et al.*	2015	66	3/4	41–79	+	+	+								+			
Matsuzaki and Itaki	2019	70	1/2	195–209	+	+		+									+	
Mizutani	2019	70	1/2	261–265	+													
Motoyama	2019	70	1/2	125–136	+												+	+
Motoyama and Itaki	2019	70	1/2	1–4	+													
Motoyama and Maruyama	2019	46	7	333–374	+	+	+	+									+	
Motoyama *et al.*	2010	61	3/4	87–103	+	+		+								+	+	+
Musashino	1993	44	12	699–705	+													
Muto *et al.*	2019	70	1/2	43–89	+								+					
Nakae	1993	44	7	471–481	+													
	2000	51	4	113–128	+	+	+		+					+				
	2001	52	6/7	245–252	+	+	+					+						
	2002	53	1	51–59	+	+	+						+	+				
	2006	57	1/2	29–50	+				+									
	2011	62	11/12	441–453	+	+	+					+						
	2012	63	9/10	269–281	+	+						+						
	2013a	64	3/4	85–112	+	+	+						+	+				
	2013b	64	5/6	151–190	+	+	+						+	+				
	2016	67	3	81–100	+	+	+		+					+				

Table 3 Continued.

Author(s)	Bibliography Year	Vol.	No.	Pages	Text	Occurrence list	Images SEM	Transmitted	Thin section	Radiolarian age Devonian	Carboniferous	Permian	Triassic	Jurassic	Cretaceous	Paleogene	Neogene	Quaternary
Nakae and Kurihara	2017	68	2	57–86	+	+	+		+						+			
Nakato *et al.*	2005	56	5/6	225–236	+													+
Noda and Kurihara	2016	67	4	119–131	+	+	+								+			
Saito	1993	44	9	571–596	+	+	+					+	+	+				
Suto *et al.*	2005	56	11/12	375–409	+												+	
Sugiyama K. and Saito	1994	45	7	383–404	+	+	+	+								+		
Takahashi M. *et al.*	1999	50	3	225–243	+												+	
Takemura	2019	70	1/2	267–272	+													
Takeuchi M. and Takizawa	1991	42	9	439–472	+													
Teraoka and Kurimoto	1986	37	8	417–453	+	+	+	+							+			
Tominaga *et al.*	2019	70	3	299–314	+							+		+	+			
Tuzino	2010	61	3/4	125–136	+													
Uchino	2010	61	9/10	365–381	+													
	2017a	68	2	23–24	+													
Uchino and Hori	2011	62	3/4	191–196	+		+		+				+					
Uchino and Ishida	2017	68	2	25–39	+	+	+							+				
Uchino and Kurihara	2019	70	1/2	109–115	+		+		+	+	+							
Wakita	1983	34	7	329–342	+	+	+						+	+	+			
	1988a	39	6	367–421	+	+	+		+				+	+	+			
	1988b	39	11	675–757	+								+	+	+			
Wakita and Isomi	1986	37	6	325–333	+		+						+	+				
Wakita and Okamura	1982	33	4	161–185	+		+						+	+	+			
Yanagisawa	1999	50	3	167–213	+												+	
	2003a	54	1/2	1–13	+												+	
Yanagisawa *et al.*	1989	40	8	405–467	+	+		+									+	
	2003a	54	1/2	29–47	+												+	
	2003b	54	11/12	351–364	+												+	
Yao	2019	70	1/2	246–260	+													
Yoshii *et al.*	1997	48	10	567–584	+													

Table 4 Bibliographic list from Chishitsu News that include radiolarian descriptions.

Author(s)	Bibliography			Contents	Images	Age
	Year	No.	Pages			
Endo and Sarashina	2007	632	41–45	Structure and function of proteins		
Fukuda and Natori	1977	273	32–43	Report on international congress about the Neogene in the Pacific	Transmitted photomicrograph	Neogene
Hara *et al.*	2005	611	49–59	Geology of Lao		
Kanie	2007	633	22–30	Cenozoic stratigraphy of the Ryukyu Arc		
Kanie	1998	532	59–61	Mollusks research in museum		
Kano K. *et al.*	2003	584	48–49	Outline of the Geological map of Japan (1:2,000,000)		
Kashiwagi *et al.*	2004	604	15–22	Geology of Mongolia	SEM images	Devonian?
	2005	605	55–60	Geology of Mongolia		
Katada *et al.*	1970	186	48–51	Thin section of limestone and chert	Thin section	
Kishimoto	1991	437	41–55	Mineral resources in China		
Kurimoto	1994b	482	21–30	Radiolarian biostratigraphy and the Geological maps of Quadrangle Series, 1:50,000	Sketches; SEM images	Mainly Permian to Jurassic
Matsuura *et al.*	1996	498	22–24	Outline of the Geological map of the Hirone district (Quadrangle Series, 1:50,000)		
Nakajima	1986	387	6–15	Geology around Himalayan		
Nakano *et al.*	2005	612	53–57	Outline of the Geological map of the Minakuchi district (Quadrangle Series, 1:50,000)		
Nohara *et al.*	1983	343	9–21	Research on deep sea mineral resource	Transmitted photomicrograph	Quaternary
Saito	1997	514	14–22	Research progress of the Jurassic accretionary complex of Japan		
Saito and Nishioka	1995	487	63–66	Outreach with using geological maps		
Saito and Ozaki	2000	548	59–61	Outreach with using geological maps		
Saito *et al.*	1997	514	7–13	Exhibition of the Geological Museum		
	2006	619	56–60	Outline of the Geological map of the Tomochi district (Quadrangle Series, 1:50,000)		
	2008	647	52–60	Outline of the Geological map of the Yakushima (1:200,000)	SEM images	Jurassic
Sakai *et al.*	1982	337	166–167	Research progress of radiolaria and conodont	SEM images	Jurassic
Sato T.	1991a	438	13–25	Research progress of Paleozoic–Mesozoic in Japan		
	1991b	440	19–33	Research progress of Paleozoic–Mesozoic in Japan		
Shinbo	2006	624	42–47	Observation of foraminifera in beach sands		
Takechi	2010	666	48–52	Fossil in Okayama Prefecture	Thin section	

Table 4 Continued.

Author(s)	Bibliography			Contents	Images	Age
	Year	No.	Pages			
Tanaka Y.	2007	634	29–34	Biogenic particles including radiolarian one		
Takahashi Koz.	2002	576	37–43	Diatom and radiolarian (including Phaeodarian)	SEM images	Recent
Takahashi Yut.	1996	506	7–14	Geology of the Iide Mountains		
	2005	607	57–62	Outline of the Geological map of the Suhara district (Quadrangle Series, 1:50,000)		
Teraoka	2004	599	40–48	Geology of Shimanto accretionary complex		
Tokuhashi	2008	645	26–52	Report on excursion of 17th International Sedimentology Congress 2006, Fukuoka		
Toshimitsu and Saito	1997	514	frontispiece	Exhibition of the Geological Museum	Hand-size model	Mainly Mesozoic
Wakita	2001	567	52–66	Geology of Indonesia		
	2002a	574	53–67	Geology of Indonesia		
	2002b	576	44–59	Geology of Indonesia		
Wakita and Kawamura	1985	376	60–66	Research progress of radiolaria	SEM images; Thin section; Cartoon	Devonian–recent
Yamada	2009	660	32–47	Geological map compiled by T. Harada		
	2011	679	8–22	Geological map compiled by T. Kochibe and others		
Yoshida F.	2003	592	61–63	Photographs of Shirasaki coast		

Table 5 Bibliographic list from GSJ Chishitsu News that include radiolarian descriptions.

Author(s)	Bibliography				Contents	Images	Age
	Year	Vol.	No.	Pages			
Hara and Ito	2018	7	11	259–261	International training course in the Kanto Mountains including field excursion and observation on radiolarian fossil	SEM images	Permian
Itaki	2019	8	5	125–127	Artificial intelligence technology for accurate identification and sampling of radiolarians	Transmitted photomicrograph	Quaternary
Ito	2017a	6	5	166–174	Author's radiolarian research in China		
	2017b	6	5	175–178	Chinese signage of words of sedimentology including "radiolarian ooze"		
	2017c	6	11	373–376	Chinese signage of words of paleontology including "radiolarian"		
	2017d	6	11	377–380	Chinese local name based on scientific name with examples of Permian radiolarians		
	2019b	8	7	175–180	Report on the 5th International Palaeontological Congress, with observation of samples of Deflandre (1952)	Transmitted photomicrograph	Carboniferous
Kano K.	2013	2	8	235–238	Outline of the Geological map of the Aniai district, 2nd Edition (Quadrangle Series, 1:50,000)		
Kato	2012	1	10	293–309	Excursion in the Chichibu area including "radiolarian slate" noted by K. Hosaka		
Kawabata	2016	5	8	263–265	Introduction of new staffs of the Geological Survey of Japan in 2016		
Nakashima *et al.*	2015	4	8	230–234	Lecture of Cenozoic stratigraphy in Japan		
Ozaki	2019	8	2	31–40	Outline of the Geological map of the Minobu district (Quadrangle Series, 1:50,000)		
Takahashi M.	2017	6	5	149–157	Discussion on tectonic boundary between Northeast and Southwest Japan		
Takahashi Yut. *et al.*	2018	7	11	303–308	International training course in the Abukuma Mountains		
Toshimitsu *et al.*	2019	8	12	322–335	Chronological timetable of the Geological Museum		
Tuzino *et al.*	2019	8	10	261–272	Exhibition of rocks (inc. radiolarian chert) in the Geological Museum		
Uchino	2015	4	3	69–74	Origin of "Shiraishi" in the "Shikinen Sengu ceremony" at Ise Jingu		
	2017b	6	9	283–288	Vegetation on chert in the Toba District		
	2018	7	4	91–101	Outline of the Geological map of the Toba district (Quadrangle Series, 1:50,000)		
Uchino and Kawamura	2014	3	11	329–333	Outline of the Geological map of the Hayachine San district (Quadrangle Series, 1:50,000)		
Utsunomiya	2018	7	9	223–226	Report on the 16th International Nannoplankton Association Meeting		

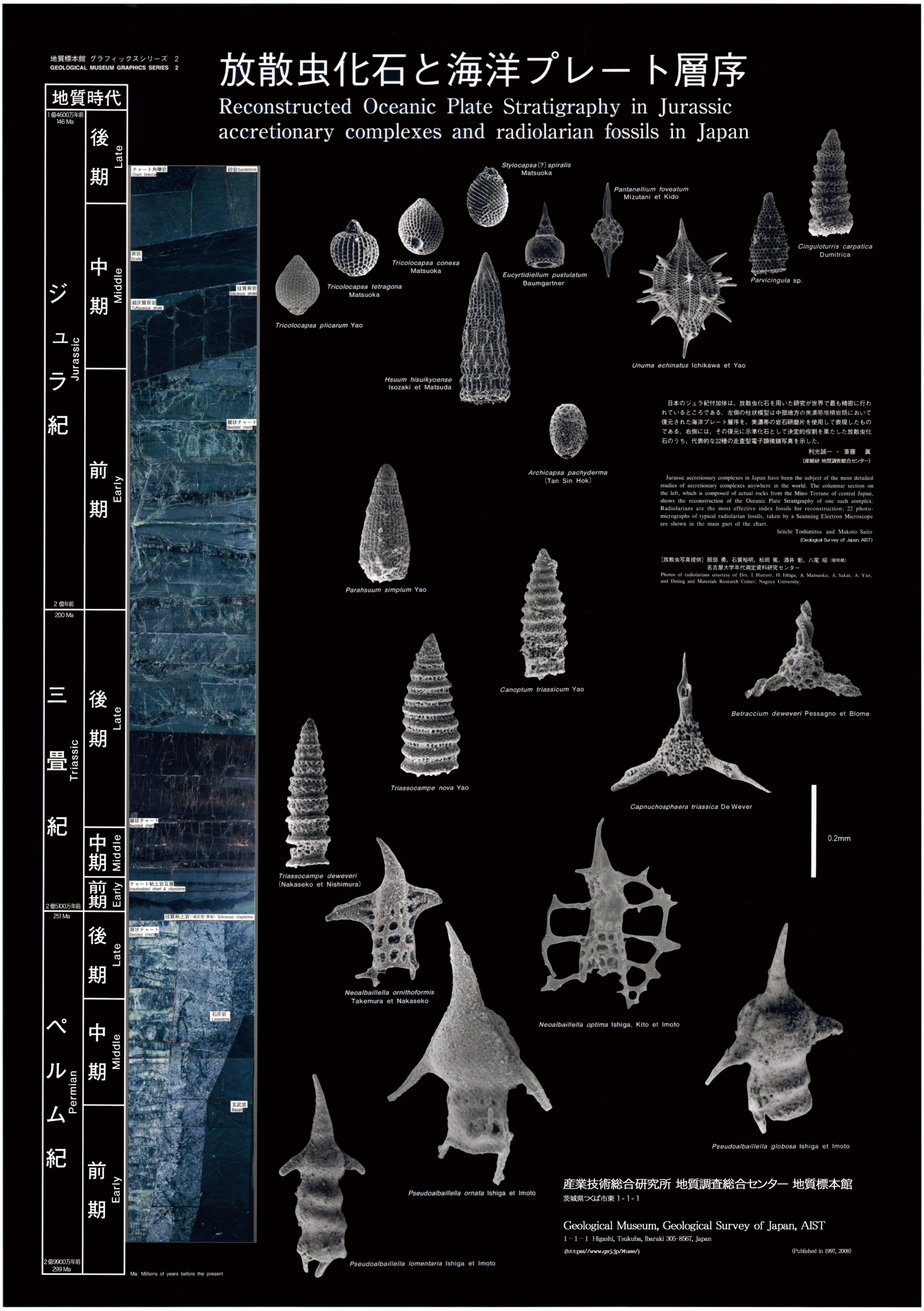

Fig. 7 Reprinted poster of “Reconstructed Oceanic Plate Stratigraphy in Jurassic accretionary complexes and radiolarian fossils in Japan” made by the Geological Museum of GSJ.

Table 6 Bibliographic list from the Cruise Report that include radiolarian descriptions.

Author(s)	Bibliography			Ocean area	Occurrence list	Images	Age
	Year	No.	Pages				
Arita and Mizuno	1977	8	301–308	Central Pacific		Transmitted photomicrograph	Quaternary
Hasegawa S. *et al.*	1976	7	80–85	Southern Kurile Trench and Slope			Quaternary
Inoue *et al.*	1972	1	20–33	Northwest Pacific			Quaternary
Nishimura	1984	20	67–89	Magellan Trough		Smear slide	Quaternary
	1986	21	56–83	Central Pacific		Transmitted photomicrograph; SEM image	Quaternary
Nishimura and Ikehara	1992	22	85–96	Central Pacific	+		Quaternary
Takayangi *et al.*	1982	18	301–308	Wake-Tahiti Transect in the Central Pacific	+		Quaternary

References

Agematsu-Watanabe, S. and Kamata, Y. (2018) Recent progress in Paleozoic–Mesozoic microfossil research in deep-sea sediments of Japanese accretionary complexes: current status and future direction on study of radiolarians and conodonts. *The Journal of the Geological Society of Japan,* **124**, 951–965. (in Japanese with English abstract).

Akazawa, K. (1993) Stratigraphy of the Permian–Triassic transition and the Paleozoic/Mesozoic boundary. *Bulletin of the Geological Survey of Japan*, **44**, 425–445. (in Japanese with English abstract).

Aoya, M., Noda, A., Mizuno, K., Mizukami, T., Miyachi, Y., Matsuura, H., Endo, S., Toshimitsu, S. and Aoki, M. (2013) *Geology of the Niihama district*. Quadrangle Series, 1:50,000, Geological Survey of Japan, AIST, 181p. (in Japanese with English abstract).

Aoya, M. and Yokoyama, S. (2009) *Geology of the Hibihara district.* Quadrangle Series, 1:50,000, Geological Survey of Japan, AIST, 75p. (in Japanese with English abstract).

Arai, K., Shimoda, G. and Ikehara, K. (2013) Marine geological mapping project in the Okinawa area — Geoinformation for the development of submarine mineral resources—. *Synthesiology – English Edition*, **6**, 158–165.

Arita, M. and Mizuno, A. (1977) Results of preliminary study on some microfossils. *Cruise Report*, no. 8 (Deep Sea Mineral Resources Investigation in the Central-Eastern Part of Central Pacific Basin, January–March 1976 (GH76-1 Cruise)), 131–135.

Banno, Y., Mizuno, K. and Miyazaki, K. (2010) *Geology of the Ōzu district*. Quadrangle Series, 1:50,000, Geological Survey of Japan, AIST, 58p. (in Japanese with English abstract).

Chihara, K. and Komatsu, M. (1992) *Geology of the Hakkaisan district*. With geological Sheet Map at 1:50,000, Geological Survey of Japan, 107p. (in Japanese with English abstract).

Danelian, T., Aitchison, J. C., Noble, P., Caridroit, M., Suzuki, N. and O'Dogherty, L. (2017) Historical insights on nearly 130 years of research on Paleozoic radiolarians. *Geodiversitas*, **39**, 351–361.

Deflandre, G. (1952) *Albaillella* nov. gen., radiolaire fossile du Carbonifère inférieur, type d'une lignée aberrante éteinte. *Comptes Rendus hebdomadaires des Séances de l'Académie des Sciences (Paris), Série D: Sciences naturelles*, **234**, 872–874.

Doi, S. (1953) *Explanatory text of the Geological Map of Japan, scale 1:50,000, "Shiraoi"*. Geological Survey of Japan, 130p. (in Japanese with English abstract).

Doi, S. (1957) *Explanatory text of the Geological Map of Japan, scale 1:50,000, "Tarumaizan"*. Geological Survey of Japan, 130p. (in Japanese with English abstract).

Endo, H. and Suzuki, Y. (1986) *Geology of the Tsuma and Takanabe district*. With Geological Sheet Map at 1:50,000, Geological Survey of Japan, 105p. (in Japanese with English abstract).

Endo, K. and Sarashina, I. (2007) Structure and function of skeletal matrix proteins. *Chishitsu News*, no. 632, 41–45. (in Japanese).

Endo, S. and Yokoyama, S. (2019) *Geology of the Motoyama district.* Quadrangle Series, 1:50,000, Geological Survey of Japan, AIST, 100p. (in Japanese with English abstract).

Eto, T., Yazaki, K., Urabe, A. and Isobe, I. (1998) *Geology of the Yokosuka district*. With Geological Sheet Map at 1:50,000, Geological Survey of Japan, 128p. (in Japanese with English abstract).

Fujimoto, H. (1961) *Explanatory text of the Geological Map of Japan, scale 1:50,000, "Tochigi"*. Geological Survey of Japan, 62p. (in Japanese with English

abstract).
Fujita, Y., Kano, H., Takizawa, F. and Yashima, R. (1988) *Geology of the Kakuda district*. With Geological Sheet Map at 1:50,000, Geological Survey of Japan, 99p. (in Japanese with English abstract).
Fujiwara, T. and Kōnoya, M. (1969) *Explanatory text of the Geological Map of Japan, scale 1:50,000, "Esan"*. Geological Survey of Japan, 57p. (in Japanese with English abstract).
Fukuda, O. and Natori, H. (1977) Upper Cenozoic in the Pacific area, Part 2: Report on the 1st international congress about the Neogene in the Pacific. *Chishitsu News*, no. 273, 32–43. (in Japanese).
Hara, H. and Hara, K. (2019) Radiolarians from chert of the Cretaceous Shimanto accretionary complex in the Umaji district, Kochi Prefecture, Southwest Japan. *Bulletin of the Geological Survey of Japan*, **70**, 117–123. (in Japanese with English abstract)
Hara, H., Hara, K. and Kurihara, T. (2012) Cretaceous radiolarians from the Shimanto accretionary complex in the Kitagawa district, Tokushima Prefecture, Southwest Japan. *Bulletin of the Geological Survey of Japan*, **63**, 301–308. (in Japanese with English abstract).
Hara, H. and Ito, T. (2018) Report of GSJ International Training Course 2018: One day field excursion of the Chichibu Jurassic accretionary complex in the Kanto Mountains, and observation of radiolarian fossils. *GSJ Chishitsu News*, **7**, 259–261. (in Japanese).
Hara, H., Kimura, K. and Naito, K. (2009) *Geology of the Murasho district*. Quadrangle Series, 1:50,000, Geological Survey of Japan, AIST, 56p. (in Japanese with English abstract).
Hara, H., Ueki, T., Okamura, Y., Ohno, T., Komazawa, M., Kishimoto, K. and Joushima, M. (2006) *Geological Map of Japan 1:200,000 Kubokawa Quadrangle*. Geological Survey of Japan, AIST, 8p. (in Japanese with English abstract).
Hara, H., Ueki, T. and Tsujino, Y. (2014) *Geology of the Kitagawa district*. Quadrangle Series, 1:50,000, Geological Survey of Japan, AIST, 72p. (in Japanese with English abstract).
Hara, H., Ueno, H., Tsunoda, K., Hisada, K., Shimizu, M., Takeuchi, K. and Ozaki, M. (2010) *Geology of the Mitsumine district*. Quadrangle Series, 1:50,000, Geological Survey of Japan, AIST, 110p. (in Japanese with English abstract).
Hara, H., Ueno, H., Kamata, Y., Ichise, M. and Hisada, K. (2005) Micro-continental collision tectonics in Lao PDR: Healing geological survey near the Mekong River-. *Chishitsu News*, no. 611, 49–59. (in Japanese).
Harayama, S. (1990) *Geology of the Kamikōchi district*. With Geological Sheet Map at 1:50,000, Geological Survey of Japan, 175p. (in Japanese with English abstract).
Harayama, S., Miyamura, M., Yoshida, F., Mimura, K. and Kurimoto, C. (1989) *Geology of the Goshozaiyama district*. With Geological Sheet Map at 1:50,000, Geological Survey of Japan, 145p. (in Japanese with English abstract).
Harayama, S., Takeuchi, M., Nakano, S., Sato, T. and Takizawa, F. (1991) *Geology of the Yarigatake district*. With Geological Sheet Map at 1:50,000, Geological Survey of Japan, 190p. (in Japanese with English abstract).
Hase, H. and Hirayama, J. (1970) *Geology of the Gojōme district*. With Geological Sheet Map at 1:50,000, Geological Survey of Japan, 46p. (in Japanese with English abstract).
Hasegawa, S., Sakai, T., Okamura, M. and Takayama, T. (1976) Age assignment of the siltstone fragments dredged. *Cruise Report*, no. 7 (Geological Investigation of Japan and Southern Kurile Trench and Slope Areas, GH76-2 Cruise, April–June 1976), 80–85.
Hasegawa, K. and Uozumi, S. (1975) *Explanatory text of the Geological Map of Japan, scale 1:50,000, "Okoppe"*. Geological Survey of Hokkaido, 23p. (in Japanese with English abstract).
Hasegawa, K., Nagao, S., Kawachi, S. and Yoshida, M. (1969) *Explanatory text of the Geological Map of Japan, scale 1:50,000, "Kamiokoppe"*. Hokkaido Development Agency, 25p. (in Japanese with English abstract).
Hashimoto, W. (1953) *Explanatory text of the Geological Map of Japan, scale 1:50,000, "Yamabe"*. Hokkaido Development Agency, 82p. (in Japanese with English abstract).
Hashimoto, W. (1955) *Explanatory text of the Geological Map of Japan, scale 1:50,000, "Shimofurano"*. Hokkaido Development Agency, 71p. (in Japanese with English abstract).
Hashimoto, W., Nagao, S. and Kano, S. (1965) *Explanatory text of the Geological Map of Japan, scale 1:50,000, "Soeushinai"*. Hokkaido Development Agency, 92p. (in Japanese with English abstract).
Hata, M. (1961) *Explanatory text of the Geological Map of Japan, scale 1:50,000, "Hatsuura"*. Geological Survey of Japan, 60p. (in Japanese with English abstract).
Hata, M. (1975) *Geology of the Kumaishi district*. Quadrangle Series, scale 1:50,000, Geological Survey of Japan, 34p. (in Japanese with English abstract).
Hata, M., Minoura, N., Onuma, K. and Kato, M. (1990) *Geology of the Matsumae district*. With Geological Sheet Map at 1:50,000, Geological Survey of Japan, 98p. (in Japanese with English abstract).
Hata, M., Segawa, S. and Yajima, J. (1982) *Geology of the Okushiritō Hokubu and Nambu district*. Quadrangle Series, scale 1:50,000, Geological Survey of Japan, 83p. (in Japanese with English abstract).
Hattori, I. (1993) Internal texture of white chert in the Nanjo Massif, Fukui Prefecture, Central Japan and its diagenetic modification. *Bulletin of the Geological Survey of Japan*, **44**, 455–469. (in Japanese with

English abstract).
Higashimoto, S., Nureki, T., Hara, I., Tsukuda, E. and Nakajima, T. (1983) *Geology of the Iwakuni district*. Quadrangle Series, scale 1:50,000, Geological Survey of Japan, 79p. (in Japanese with English abstract).
Higashimoto, S., Takahashi, Y., Makimoto, H., Wakita, K. and Tsukuda, E. (1986) *Geology of the Ōtake district.* With Geological Sheet Map at 1:50,000, Geological Survey of Japan, 70p. (in Japanese with English abstract).
Hirayama, J. and Uemura, F. (1985) *Geology of the Ajigasawa district.* With Geological Sheet Map at 1:50,000, Geological Survey of Japan, 86p. (in Japanese with English abstract).
Hirayama, K. and Kambe, N. (1959) *Explanatory text of the Geological Map of Japan, scale 1:50,000, "Koyasan"*. Geological Survey of Japan, 41p. (in Japanese with English abstract).
Hirayama, K. and Tanaka, K. (1956a) *Explanatory text of the Geological Map of Japan, scale 1:50,000, "Todorogi"*. Geological Survey of Japan, 37p. (in Japanese with English abstract).
Hirayama, K. and Tanaka, K. (1956b) *Explanatory text of the Geological Map of Japan, scale 1:50,000, "Kainan"*. Geological Survey of Japan, 62p. (in Japanese with English abstract).
Hirokawa, O. and Kuroda, K. (1958) *Explanatory text of the Geological Map of Japan, scale 1:50,000, "Tangoyura"*. Geological Survey of Japan, 23p. (in Japanese with English abstract).
Hirokawa, O., Isomi, H. and Kuroda, K. (1957) *Explanatory text of the Geological Map of Japan, scale 1:50,000, "Obama"*. Geological Survey of Japan, 31p. (in Japanese with English abstract).
Hori, N. (2004a) Oceanic plate stratigraphy of the accretionary complex of the Chichibu Belt in the Toyohashi district, Aichi Prefecture, Southwest Japan. *Bulletin of the Geological Survey of Japan*, **55**, 271–285. (in Japanese with English abstract).
Hori, N. (2004b) Permian radiolarians from chert of the Chichibu Belt in the Toyohashi district, Aichi Prefecture, Southwest Japan. *Bulletin of the Geological Survey of Japan*, **55**, 287–301. (in Japanese with English abstract).
Hori, N. (2004c) Triassic radiolarians from chert of the Chichibu Belt in the Toyohashi district, Aichi Prefecture, Southwest Japan. *Bulletin of the Geological Survey of Japan*, **55**, 303–334. (in Japanese with English abstract).
Hori, N. (2004d) Jurassic radiolarians from chert and clastic rocks of the Chichibu Belt in the Toyohashi district, Aichi Prefecture, Southwest Japan. *Bulletin of the Geological Survey of Japan*, **55**, 335–388. (in Japanese with English abstract).
Hori, N. (2005) Paleozoic and Mesozoic radiolarians from the Chichibu Belt in the Iragomisaki district, Atsumi Peninsula, Aichi Prefecture, Southwest Japan. *Bulletin of the Geological Survey of Japan*, **56**, 37–83. (in Japanese with English abstract).
Hori, N., Saito, M. and Toshimitsu, S. (2002) Late Jurassic radiolarian fauna from the Ikenohara Formation of the Kurosegawa Belt in the Toyo–Izumi area, Kumamoto Prefecture, Kyushu, Japan. *Bulletin of the Geological Survey of Japan*, **53**, 689–724.
Hori, R. S. (1993) Toarcian Oceanic Event in deep-sea sediments. *Bulletin of the Geological Survey of Japan*, **44**, 555–570. (in Japanese with English abstract).
Hoshizumi, H., Saito, M., Mizuno, K., Miyazaki, K., Toshimitsu, S., Matsumoto, A., Ohno, T. and Miyakawa, A. (2015) *Geological Map of Japan 1:200,000 Ōita (2nd Edition) Quadrangle*. Geological Survey of Japan, AIST, 8p. (in Japanese with English abstract).
Huzioka, K., Ozawa, A., Takayama, T. and Ikebe, Y. (1977) *Geology of the Akita district*. Quadrangle Series, scale 1:50,000, Geological Survey of Japan, 75p. (in Japanese with English abstract).
Huzioka, K., Ozawa, A. and Ikebe, Y. (1976) G*eology of the Ugo-wada district*. Quadrangle Series, scale 1:50,000, Geological Survey of Japan, 65p. (in Japanese with English abstract).
Huzita, K. and Kasama, T. (1982) *Geology of the Ōsaka-Seihokubu district*. Quadrangle Series, scale 1:50,000, Geological Survey of Japan, 112p. (in Japanese with English abstract).
Huzita, K. and Kasama, T. (1983) *Geology of the Kōbe district*. Quadrangle Series, scale 1:50,000, Geological Survey of Japan, 115p. (in Japanese with English abstract).
Huzita, K. and Maeda, Y. (1985) *Geology of the Ōsaka-Seinambu district*. Quadrangle Series, scale 1:50,000, Geological Survey of Japan, 103p. (in Japanese with English abstract).
Ichikawa, K. (1982) History of Paleontology on Mesozoic and Paleozoic radiolarians in Japan. *News of Osaka Micropalaeontologists (NOM)*, *Special Volume*, no. 5, 1–9. (in Japanese with English abstract).
Ichikawa, K. (1990) Pre-Cretaceous terranes of Japan. *In* Ichikawa, K., Mizutani, S., Hara, I., Hada, S. and Yao, A. ed., *Pre-Cretaceous terranes of Japan*, Publication of IGCP Project No. 224: Pre-Jurassic Evolution of Eastern Asia, Nippon Insatsu Shuppan Co. Ltd., Osaka, 1–12.
Ichikawa, K., Hada, S. and Yao, A. (1985) Recent problems of Paleozoic–Mesozoic microbiostratigraphy and Mesozoic geohistory of Southwest Japan. *The Memoirs of the Geological Society of Japan*, no. 25, 1–18. (in Japanese with English abstract).
Igi, S. (1959) *Explanatory text of the Geological Map of Japan, scale 1:50,000, "Pinneshiri"*. Geological Survey of Japan, 41p. (in Japanese with English abstract).
Igi, S. and Kakimi, T. (1956) *Explanatory text of the Geological Map of Japan, scale 1:50,000, "Erimo-*

Misaki". Geological Survey of Japan, 22p. (in Japanese with English abstract).

Igi, S., Kuroda, K. and Hattori, H. (1961) *Explanatory text of the Geological Map of Japan, scale 1:50,000, "Maizuru"*. Geological Survey of Japan, 50p. (in Japanese with English abstract).

Igi, S., Tanaka, K., Hata, M. and Satō, H. (1958) *Explanatory text of the Geological Map of Japan, scale 1:50,000, "Horokanai"*. Geological Survey of Japan, 55p. (in Japanese with English abstract).

Igi, S. and Wadatsumi, K. (1980) *Geology of the Kamigori District.* Quadrangle Series, 1:50,000, Geological Survey of Japan, 74p. (in Japanese with English abstract).

Ikebe, Y., Ōzawa, A. and Inoue, H. (1979) *Geology of the Sakata district*. Quadrangle Series, scale 1:50,000, Geological Survey of Japan, 42p. (in Japanese with English abstract).

Imai, I., Sakamoto, T. and Nozawa, T. (1966) *Geology of the Ōchigata and Abugashima district*. Quadrangle Series, scale 1:50,000, Geological Survey of Japan, 67p. (in Japanese with English abstract).

Imai, S. and Sumi, Y. (1957) *Explanatory text of the Geological Map of Japan, scale 1:50,000, "Tomikawa"*. Hokkaido Development Agency, 52p. (in Japanese with English abstract).

Imoto, N., Matsuura, H., Musashino, M., Shimizu, D. and Ishida, S. (1991) *Geology of the Sonobe district.* With Geological Sheet Map at 1:50,000, Geological Survey of Japan, 68p. (in Japanese with English abstract).

Imoto, N. and Saijyo, Y. (1993) Constituents of Permian and Triassic Bedded Cherts in the Tamba Belt. *Bulletin of the Geological Survey of Japan*, **44**, 547–554. (in Japanese with English abstract).

Imoto, N., Shimizu, D., Musashino, M. and Ishida, S. (1989) *Geology of the Kyōto-Seihokubu district.* With Geological Sheet Map at 1:50,000, Geological Survey of Japan, 84p. (in Japanese with English abstract).

Ishida, M. and Sawamura, K. (1968) *Geology of the Kitami district*. Quadrangle Series, scale 1:50,000, Geological Survey of Japan, 36p. (in Japanese with English abstract).

Ishida, N. (2019) Summer surface water polycystine radiolarians in the eastern margin of the Japan Sea. *Bulletin of the Geological Survey of Japan*, **70**, 101–108.

Inoue, E., Suzuki, T., Matsumoto, E. and Yuasa, M. (1972) Deep sea sediments. *Cruise Report*, no. 1 (Deep Sea Mineral Resources Investigations in Northwest Pacific, November–December 1972), 20–33.

Ishiga, H., Ishida, K., Sampei, Y., Musashino, M., Yamakita, S., Kajiwara, Y. and Morikiyo, T. (1993) Oceanic pollution at the Permian–Triassic boundary in pelagic condition from carbon and sulfur stable isotopic excursion, Southwest Japan. *Bulletin of the Geological Survey of Japan*, **44**, 721–726.

Ishiga, H. and Yamakita, S. (1993) Permian/Triassic boundary in pelagic sediments, Southwest Japan —an introduction—. *Bulletin of the Geological Survey of Japan*, **44**, 419–423. (in Japanese with English abstract).

Ishigaki, S. and Yao, A. (1982) Radiolarian revolution: A dialogue between radiolarian researcher and teacher*. *Education of Earth Science and Movement for Science**, 11, 93–102. (in Japanese).

Ishizuka, Y., Ozaki, M., Hoshizumi, H., Matsuura, H., Miyazaki, K., Nawa, K., Sanematsu, K. and Komazawa, M. (2009) *Geological Map of Japan 1:200,000 Nakatsu Quadrangle*. Geological Survey of Japan, AIST, 8p. (in Japanese with English abstract).

Isomi, H. and Inoue, M. (1972) *Geology of the Hamamatsu district.* Quadrangle Series, scale 1:50,000, Geological Survey of Japan, 35p. (in Japanese with English abstract).

Isozaki, Y. and Maruyama, S. (1991) Studies on orogeny based on plate tectonics in Japan and new geotectonics subdivision of the Japanese Islands. *Journal of Geography (Chigaku Zasshi),* **100**, 697–761. (in Japanese with English abstract).

Isozaki, Y., Aoki, K., Nakama, T. and Yanai, S. (2010) New insight into a subduction-related orogen: A reappraisal of the geotectonic framework and evolution of the Japanese Islands. *Gondwana Research*, **18**, 82–105.

Itaki, T. (2019) New technology utilizing artificial intelligence has been established for accurate identification and sampling of microfossils -Enabling high-speed automatic analysis of geological strata-. *GSJ Chishitsu News*, **8**, 125–127. (in Japanese).

Itihara, M., Ichikawa, K. and Yamada, N. (1986) *Geology of the Kishiwada district.* With Geological Sheet Map at 1:50,000, Geological Survey of Japan, 148p. (in Japanese with English abstract).

Ito, T. (2017a) Introduction of China University of Geosciences, Wuhan. *GSJ Chishitsu News*, **6**, 166–174. (in Japanese).

Ito, T. (2017b) Geological terms in Chinese: Part 4 Sedimentology. *GSJ Chishitsu News*, **6**, 175–178. (in Japanese).

Ito, T. (2017c) Geological terms in Chinese: Part 7 Paleontology. *GSJ Chishitsu News,* **6**, 373–376. (in Japanese).

Ito, T. (2017d) Geological terms in Chinese: Part 8 Chinese local name based on scientific name. *GSJ Chishitsu News*, **6**, 377–380. (in Japanese).

Ito, T. (2019a) A report of Permian, Triassic, and Jurassic radiolarian occurrences from the Ashio terrane in the Hachioji Hills, eastern Gunma Prefecture, central Japan. *Bulletin of the Geological Survey of Japan*, **70**, 225–247.

Ito, T. (2019b) Report of the Hirokawa Research Fund in the 2018 fiscal year: the 5th International Palaeontological Congress and preliminary arrangements of cooperative research about improvements of radiolarian bio-stratigraphy of the Permian (Paleozoic), with the observation of G. Deflandre's radiolarian samples. *GSJ Chishitsu News*, **8**, 175–180. (in Japanese).

Ito, T., Kurihara, T., Hakoiwa, H., Ibaraki, Y. and Matsuoka, A. (2017) Discovery of the oldest fossil in Niigata Prefecture of central Japan from the Kotaki area, Itoigawa: A report on collaboration research of Itoigawa City, Niigata University, and Geological Survey of Japan, AIST. *Bulletin of the Itoigawa City Museums*, no. 4, 23–31 (in Japanese with English abstract).

Iwao, S. and Matsui, H. (1961) *Explanatory text of the Geological Map of Japan, scale 1:50,000, "Taira and Kawamae (incl. Ide)"*. Geological Survey of Japan, 103p. (in Japanese with English abstract).

Kakuwa, Y. (1993) Sedimentary petrographical study on bedded cherts of the Northern Chichibu Belt in eastern Shikoku— with special reference to the P/T boundary—. *Bulletin of the Geological Survey of Japan*, **44**, 533–546. (in Japanese with English abstract).

Kambe, N. and Teraoka, Y. (1968) *Geology of the Usuki district*. Quadrangle Series, scale 1:50,000, Geological Survey of Japan, 63p. (in Japanese with English abstract).

Kametaka, M., Nakae, S. and Kameda, K. (2005) Early Permian radiolarians from siliceous mudstone in the Rikuchu-Seki District, North Kitakami Terrane. *Bulletin of the Geological Survey of Japan*, **56**, 237–243. (in Japanese with English abstract).

Kamikuri, S. (2019a) Radiolarian assemblages from the lower to middle Miocene at IODP Site U1335 in the eastern equatorial Pacific. *Bulletin of the Geological Survey of Japan*, **70**, 137–161.

Kamikuri, S. (2019b) Middle to late Miocene radiolarians from ODP Site 1021 in the eastern North Pacific. *Bulletin of the Geological Survey of Japan*, **70**, 163–194.

Kaneko, N. (2007) Cenozoic stratigraphy in the Okinawa Island and Ryukyu Arc. *Chishitsu News*, no. 633, 22–30. (in Japanese).

Kaneko, N. and Ujiié, H. (2006) *Geology of the Itoman and Kudaka Jima district*. Quadrangle Series, 1:50,000, Geological Survey of Japan, AIST, 47p. (in Japanese with English abstract).

Kanie, Y. (1998) Paleontological and geological studies on the bathyal molluscs in the museum, focused from global to local. *Chishitsu News*, no. 532, 58–61. (in Japanese).

Kanie, Y. and Sakai, A. (2002) *Geology of the Urakawa district*. Quadrangle Series, 1:50,000, Geological Survey of Japan, AIST, 43p. (in Japanese with English abstract).

Kano, H., Kuroda, Y., Uruno, K., Nureki, T., Kanisawa, S., Maruyama, T., Umemura, H., Mitsukawa, H., Seto, N., Ohira, Y., Sato, S. and Isshiki, N. (1973) *Geology of the Takanuki district.* Quadrangle Series, scale 1:50,000, Geological Survey of Japan, 109p. (in Japanese with English abstract).

Kano, K. (2013) New development in Green Tuff research: the 2nd edition of quadrangle map 1:50,000, Aniai. *GSJ Chishitsu News*, 2, 235–238. (in Japanese).

Kano, K., Kurimoto, C., Iwaya, T., Hoshizono, H., Matsuura, H., Makimoto, H. and Miyazaki, J. (2003) Introduction of the "Geological Map of Japan 1:2,000,000, 5th Edition". *Chishitsu News*, no. 584, 48–49. (in Japanese).

Kano, K., Matsuura, H., Sawada, Y. and Takeuchi, K. (1998) *Geology of the Iwami-Ōda and Ōura district.* With Geological Sheet Map at 1:50,000, Geological Survey of Japan, 118p. (in Japanese with English abstract).

Kano, K., Ohguchi, T., Ishikawa, Y., Yanai, K., Fujimoto, Y., Uemura, K., Ogasawara, K. and Komazawa, M. (2012) *Geology of the Aniai district*, *2nd Edition*. Quadrangle Series, 1:50,000, Geological Survey of Japan, AIST, 59p. (in Japanese with English abstract).

Kano, K., Ohguchi, T., Yanagisawa, Y., Awata, Y., Kobayashi, N., Sato, Y., Hayashi, S., Kitazato, H., Ogasawara, K. and Komazawa, M. (2011) *Geology of the Toga and Funakawa district*. Quadrangle Series, 1:50,000, Geological Survey of Japan, AIST, 127p. (in Japanese with English abstract).

Kano, K., Takarada, S., Makimoto, H., Tsuchiya, N. and Bunno, M. (2001) *Geology of the Yunotsu and Gōtsu district*. With Geological Sheet Map at 1:50,000, Geological Survey of Japan, 129p. (in Japanese with English abstract).

Kano, K., Takeuchi, K. and Matsuura, H. (1991) *Geology of the Imaichi district*. With Geological Sheet Map at 1:50,000, Geological Survey of Japan, 79p. (in Japanese with English abstract).

Kano, K., Yamamoto, H. and Nakagawa, T. (2007) *Geology of the Fukui district*. Quadrangle Series, 1:50,000, Geological Survey of Japan, AIST, 68p. (in Japanese with English abstract).

Kano, K., Yamauchi, S., Takayasu, K., Matsuura, H. and Bunno. M. (1994) *Geology of the Matsue district.* With Geological Sheet Map at 1:50,000, Geological Survey of Japan, 126p. (in Japanese with English abstract).

Kashiwagi, K. and Kurimoto, C. (2003) Reexamination of radiolarian biochronology of the Shimizu Formation (Northern Chichibu Belt) in the Shimizu-Misato area, western Kii Peninsula, Southwest Japan. *Bulletin of the Geological Survey of Japan*, **54**, 279–293.

Kashiwagi, K., Tsukada, K., Kurihara, T., Niwa, M. and Tokiwa, T. (2005) Geological expedition to Mongolia (part 2): Geology and Geological field survey in Mongolia. *Chishitsu News*, no. 605, 55–60. (in Japanese).

Kashiwagi, K., Tsukada, K. and Takahashi, Y. (2004) Geological expedition to Mongolia (part 1): East Eurasian Geological Seminar 2003 and Paleozoic radiolarians. *Chishitsu News*, no. 604, 15–22. (in

Japanese).
Katada, M. (1956) *Explanatory text of the Geological Map of Japan, scale 1:50,000, "Kofu"*. Geological Survey of Japan, 27p. (in Japanese with English abstract).
Katada, M., Fujinuki, T. and Masai, Y. (1970) Rocks under microscope part 4: Limestone and chert of the Paleozoic strata*. *Chishitsu News*, no. 186, 48–51. (in Japanese).
Katada, M. and Isomi, H. (1962) *Explanatory text of the Geological Map of Japan, scale 1:50,000, "Ina"*. Geological Survey of Japan, 28p. (in Japanese with English abstract).
Kato, H. (2012) Geological Excursions to the Chichibu area, central Japan, which Kenji Miyazawa and Kanai Hosaka participated. *GSJ Chishitsu News*, **1**, 293–309. (in Japanese).
Kato, H., Sato, M., Mimura, K. and Takizawa, F. (1989) *Geology of the Ōmachi district.* With Geological Sheet Map at 1:50,000, Geological Survey of Japan, 102p. (in Japanese with English abstract).
Kato, H., Wakita, K., Sugawara, Y., Miyano, S. and Miyazaki, K. (2011) *History of geological maps in Japan*. Open-File Report of Geological Survey of Japan, no. 535, Geological Survey of Japan, AIST, 21p.
Kawabata, D. (2016) Report on an instruction course of new staffs of the Geological Survey of Japan in 2016*. *GSJ Chishitsu News*, **5**, 263–265. (in Japanese).
Kawachi, Y., Yuasa, M. and Katada, M. (1983) *Geology of the Ichinose district.* Quadrangle Series, scale 1:50,000, Geological Survey of Japan, 70p. (in Japanese with English abstract).
Kawada, K., Isomi, H. and Sugiyama, Y. (1988) *Geology of the Hagiwara district*. With Geological Sheet Map at 1:50,000, Geological Survey of Japan, 82p. (in Japanese with English abstract).
Kawai, M. (1964) *Explanatory text of the Geological Map of Japan, scale 1:50,000, "Neo"*. Geological Survey of Japan, 66p. (in Japanese with English abstract).
Kawai, M., Hirayama, K. and Yamada, N. (1957) *Explanatory text of the Geological Map of Japan, scale 1:50,000, "Arashimadake"*. Geological Survey of Japan, 110p. (in Japanese with English abstract).
Kawakami, G., Horise, W., Hasegawa, T., Hayashi, K. and Watanabe, M. (2018) *Geology of the Abashiri district.* Quadrangle Series, 1:50,000, Geological Survey of Japan, AIST, 66p. (in Japanese with English abstract).
Kawakami, S. and Shishikura, M. (2006) *Geology of the Tateyama district*. Quadrangle Series, 1:50,000, Geological Survey of Japan, AIST, 82p. (in Japanese with English abstract).
Kawamura, T., Uchino, T., Kawamura, M., Yoshida, K., Nakagawa, M. and Nagata, H. (2013) *Geology of the Hayachine San district*. Quadrangle Series, 1:50,000, Geological Survey of Japan, AIST, 101p. (in Japanese with English abstract).
Kawanabe, Y. and Sakaguchi, K. (2005) *Geology of the Kaimon Dake district.* Quadrangle Series, 1:50,000, Geological Survey of Japan, AIST, 82p. (in Japanese with English abstract).
Kawanabe, Y., Sakaguchi, K., Saito, M., Komazawa, M. and Yamazaki, T. (2004) *Geological Map of Japan 1:200,000 Kaimon Dake Quadrangle with a part of Kuro Shima Quadrangle.* Geological Survey of Japan, AIST, 8p. (in Japanese with English abstract).
Kawatani, A., Sashida, K., Agematsu, S. and Kohno, N. (2019) Radiolarian fossils from the Miocene Tsurushi Formation distributed in Sado Island, Niigata Prefecture, Japan. *Bulletin of the Geological Survey of Japan*, **70**, 91–99. (in Japanese with English abstract)
Kimura, K. (1994) Accretionary prism geology and revision of geological map of Japan (scale 1:1,000,000). *Chishitsu News*, no. 482, 14–20. (in Japanese).
Kimura, K. (1997) Offscraping, underplating and out-of-sequence thrusting Process of an accretionary prism: On-land example from the Mino–Tamba Belt, central Japan. *Bulletin of the Geological Survey of Japan*, **48**, 313–337.
Kimura, K., Iwaya, T., Mimura, K., Sato, Y., Sato, T., Suzuki, Y. and Sakamaki, Y. (1991) *Geology of the Osuzuyama district*. With Geological Sheet Map at 1:50,000, Geological Survey of Japan, 137p. (in Japanese with English abstract).
Kimura, K., Makimoto, H. and Yoshioka, T. (1989) *Geology of the Ayabe district*. With Geological Sheet Map at 1:50,000, Geological Survey of Japan, 104p. (in Japanese with English abstract).
Kimura, K. and Nakae, S. (1993) Occurrence of siliceous claystone and associated greenstones in the Mino–Tamba Belt. *Bulletin of the Geological Survey of Japan,* **44**, 727–743. (in Japanese with English abstract).
Kimura, K., Nakae, S. and Takahashi, Y. (1994) *Geology of the Yotsuya district*. With Geological Sheet Map at 1:50,000, Geological Survey of Japan, 52p. (in Japanese with English abstract).
Kimura, K., Yoshioka, T., Imoto, N., Tanaka, S., Musashino, M. and Takahashi, Y. (1998) *Geology of the Kyōto-Tōhokubu district.* With Geological Sheet Map at 1:50,000, Geological Survey of Japan, 89p. (in Japanese with English abstract).
Kimura, K., Yoshioka, T., Nakano, S. and Matsuoka, A. (2001) *Geology of the Kitakomatsu district*. With Geological Sheet Map at 1:50,000, Geological Survey of Japan, 102p. (in Japanese with English abstract).
Kishimoto, F. (1991) Mineral resources of People's Republic of China (6) -their good points and weak points-. *Chishitsu News*, no. 437, 41–55. (in Japanese).
Kitamura, N., Ishii, T., Sangawa, A. and Nakagawa, H. (1986) *Geology of the Sendai district.* With Geological Sheet Map at 1:50,000, Geological Survey of Japan, 134p. (in Japanese with English abstract).
Kobayashi, I., Tateishi, M. and Komatsubara, T. (2002) *Geology of the Sanjō district*. Quadrangle Series,

1:50,000, Geological Survey of Japan, AIST, 98p. (in Japanese with English abstract).
Kobayashi, I., Tateishi, M. and Uemura, T. (1993) *Geology of the Izumozaki district*. With Geological Sheet Map at 1:50,000, Geological Survey of Japan, 91p. (in Japanese with English abstract).
Kobayashi, I., Tateishi, M., Yoshioka, T. and Shimizu, M. (1991) *Geology of the Nagaoka district*. With Geological Sheet Map at 1:50,000, Geological Survey of Japan, 132p. (in Japanese with English abstract).
Kobayashi, I., Tateishi, M., Yoshimura, T. Ueda, T. and Kato, H. (1995) *Geology of the Kashiwazaki district.* With Geological Sheet Map at 1:50,000, Geological Survey of Japan, 102p. (in Japanese with English abstract).
Kojima, S., Hayasaka, Y., Hiroi, Y., Matsuoka, A., Sano, H., Sugamori, Y., Suzuki, N., Takemura, S., Tsujimori, T. and Uchino, T. (2016) Pre-Cretaceous accretionary complexes. *In* Moreno, T., Wallis, S., Kojima, T. and Gibbons, W. eds., *The Geology of Japan*, Geological Society, London, 61–100.
Kojima, S., Naka, T., Kimura, K., Mengal, J. M., Siddiqui, M. R. H. and Bakht, M. S. (1994) Mesozoic radiolarians from the Bagh Complex in the Muslim Bagh area, Pakistan: Their significance in reconstructing the geologic history of ophiolites along the Neo-Tethys suture zone. *Bulletin of the Geological Survey of Japan*, **45**, 63–97.
Kojima, S. and Saito, M. (2000) Triassic and Jurassic radiolarians from the Tokuyama area, Mino terrane, central Japan. *Bulletin of the Geological Survey of Japan*, **51**, 143–165.
Kubo, K., Yanagisawa, Y., Toshimitsu, S., Banno, Y., Kaneko, N., Yoshioka, T. and Takagi, T. (2002) *Geology of the Kawamae and Ide district*. Quadrangle Series, 1:50,000, Geological Survey of Japan, AIST, 136p. (in Japanese with English abstract).
Kubo, K., Yanagisawa, Y., Yamamoto, T., Nakae, S., Takahashi, Y., Toshimitsu, S., Banno, Y., Miyachi, Y., Takahashi, M., Komazawa, M. and Ohno, T. (2007) *Geological Map of Japan 1:200,000 Shirakawa Quadrangle*. Geological Survey of Japan, AIST, 8p. (in Japanese with English abstract).
Kubo, K., Yanagisawa, Y., Yoshioka, T. and Takahashi, Y. (1994) *Geology of the Namie and Iwaki-Tomioka district*. With Geological Sheet Map at 1:50,000, Geological Survey of Japan, 104p. (in Japanese with English abstract).
Kubo, K., Yanagisawa, Y., Yoshioka, T., Yamamoto, T. and Takizawa, F. (1990) *Geology of the Haramachi and Ōmika district*. Quadrangle Series, scale 1:50,000, Geological Survey of Japan, 155p. (in Japanese with English abstract).
Kudo, T., Uchino, T., Komatsubara, T., Takahashi, Y. and Yanagisawa, Y. (2011) *Geology of the Kamo district.* Quadrangle Series, 1:50,000, Geological Survey of Japan, AIST, 162p. (in Japanese with English abstract).
Kudo, T., Uchino, T. and Hamasaki, S. (2019) *Geology of the Towada Ko district*. Quadrangle Series, 1:50,000, Geological Survey of Japan, AIST, 192p. (in Japanese with English abstract).
Kurimoto, C. (1987) Triassic and Jurassic radiolarians from the southwestern part of the Mino Terrane, central Japan. *Bulletin of the Geological Survey of Japan*, **38**, 69–80. (in Japanese with English abstract).
Kurimoto, C. (1989) Microfossils from the Gozaishoyama district in the southwestern part of the Mino Terrane, central Japan. *Bulletin of the Geological Survey of Japan*, **40**, 55–63. (in Japanese with English abstract).
Kurimoto, C. (1994a) Geology of the Kudoyama area in the western Kii Peninsula, Southwest Japan, with reference to disappearance of the Chichibu terrane. *Bulletin of the Geological Survey of Japan*, **45**, 235–255.
Kurimoto, C. (1994b) Radiolarian biostratigraphy and geological sheet maps at 1:50,000. *Chishitsu News*, no. 482, 21–30. (in Japanese).
Kurimoto, C. and Kuwahara, K. (1991) Radiolarians from the Ojigahata area of Shiga Prefecture, southwestern part of the Mino Terrane. *Bulletin of the Geological Survey of Japan*, **42**, 63–73. (in Japanese with English abstract).
Kurimoto, C., Kimura, K. and Takeuchi, M. (2015) Geology and radiolarian fossils of the Upper Cretaceous Hanazono Formation in the Koyasan area, northwestern part of Kii Peninsula, Southwest Japan. *Bulletin of the Geological Survey of Japan*, **66**, 41–79. (in Japanese with English abstract).
Kurimoto, C. and Makimoto, H. (1990) *Geology of the Fukuchiyama district*. With Geological Sheet Map at 1:50,000, Geological Survey of Japan, 97p. (in Japanese with English abstract).
Kurimoto, C., Matsuura, H. and Yoshikawa, T. (1993) *Geology of the Sasayama district*. With Geological Sheet Map at 1:50,000, Geological Survey of Japan, 93p. (in Japanese with English abstract).
Kurimoto, C., Naito, K., Sugiyama, Y. and Nakae, S. (1999) *Geology of the Tsuruga district*. With Geological Sheet Map at 1:50,000, Geological Survey of Japan, 73p. (in Japanese with English abstract).
Kurosawa, K., Tajika, J., Yahata, M. and Yamagishi, H. (1993) *Explanatory text of the Geological Map of Japan, scale 1:50,000, "Ohbirayama"*. Geological Survey of Hokkaido, 79p. (in Japanese with English abstract).
Makimoto, H., Miyata, T., Mizuno, K. and Sangawa, A. (2004) *Geology of the Kokawa district*. Quadrangle Series, 1:50,000, Geological Survey of Japan, AIST, 89p. (in Japanese with English abstract).
Makimoto, H., Takagi, H., Miyachi, Y. Nakano, S., Kato, H. and Yoshioka, T. (1996) *Geology of the Takatō district*. With Geological Sheet Map at 1:50,000, Geological Survey of Japan, 114p. (in Japanese with

English abstract).
Makimoto, H. and Takeuchi, K. (1992) *Geology of the Yorii district*. With Geological Sheet Map at 1:50,000, Geological Survey of Japan, 136p. (in Japanese with English abstract).
Makimoto, H., Yamada, N., Mizuno, K., Takada, A., Komazawa, M. and Sudo, T. (2004) *Geological Map of Japan 1:200,000 Toyohashi and Irago Misaki Quadrangle*. Geological Survey of Japan, AIST, 8p. (in Japanese with English abstract).
Makiyama, J. and Sakamoto, T. (1957) *Explanatory text of the Geological Map of Japan, scale 1:50,000, "Mitsuke and Kakezuka"*. Geological Survey of Japan, 43p. (in Japanese with English abstract).
Matsui, K., Furukawa, T. nd Sawamura, K. (1989) *Geology of the Sasebo district.* With Geological Sheet Map at 1:50,000, Geological Survey of Japan, 92p. (in Japanese with English abstract).
Matsunami, T. (2002) *Explanatory text of the Geological Map of Japan, scale 1:50,000, "Takinoue"*. Geological Survey of Hokkaido, 37p. (in Japanese with English abstract).
Matsunami, T., Yahata, M. and Matsushita, K. (2002) *Explanatory text of the Geological Map of Japan, scale 1:50,000, "Kamishokotsu"*. Geological Survey of Hokkaido, 54p. (in Japanese with English abstract).
Matsuno, K. and Hata, M. (1960) *Explanatory text of the Geological Map of Japan, scale 1:50,000, "Oiwake"*. Hokkaido Development Agency, 34p. (in Japanese with English abstract).
Matsuoka, A. and Ito, T. (2017) Editorial: Progress in radiolarian research during the last two decades. *Science Reports of Niigata University (Geology)*, no. 32 (supplement), i–iv.
Matsushita, K., Terashima, K. and Osanai, H. (1977) *Explanatory text of the Geological Map of Japan, scale 1:50,000, "Kenbuchi"*. Geological Survey of Hokkaido, 30p. (in Japanese with English abstract).
Matsuura, H. (1990) *Geology of the Akana district*. With Geological Sheet Map at 1:50,000, Geological Survey of Japan, 73p. (in Japanese with English abstract).
Matsuura, H. (1998) *Geology of the Kurahashi Jima and Hashira Jima district*. With Geological Sheet Map at 1:50,000, Geological Survey of Japan, 53p. (in Japanese with English abstract).
Matsuura, H., Bunno, M. and Tsukuda, E. (1999) *Geology of the Itsukushima district.* With Geological Sheet Map at 1:50,000, Geological Survey of Japan, 37p. (in Japanese with English abstract).
Matsuura, H., Kurimoto, C., Sangawa, A. and Bunno, M. (1995) *Geology of the Hirone district.* With Geological Sheet Map at 1:50,000, Geological Survey of Japan, 110p. (in Japanese with English abstract).
Matsuura, H., Kurimoto, C., Sangawa, A. and Bunno, M. (1996) Geology of the Hirone district (Quadrangle Series, 1:50,000)*. *Chishitsu News*, no. 498, 22–24. (in Japanese).
Matsuura, H., Kurimoto, C., Yoshida, F., Saito, Y., Makimoto, H., Toshimitsu, S., Iwaya, T., Komazawa, M. and Hiroshima, T. (2002) *Geological Map of Japan 1:200,000 Okayama and Marugame Quadrangle*. Geological Survey of Japan, AIST, 8p. (in Japanese with English abstract).
Matsuura, H., Ozaki, M., Wakita, K., Makimoto, H., Mizuno, K., Kametaka, M., Sudo, T., Morijiri, R. and Komazawa, M. (2007) *Geological Map of Japan 1:200,000 Yamaguchi and Mishima Quadrangle*. Geological Survey of Japan, AIST, 8p. (in Japanese with English abstract).
Matsuzaki, K. M. and Itaki, T. (2019) Late Miocene polycystine radiolarians of the Japan Sea (IODP Exp. 346 Site U1425). *Bulletin of the Geological Survey of Japan*, **70**, 195–209.
Mitani, K., Fujiwara, T. and Ishiyama, S. (1960) *Explanatory text of the Geological Map of Japan, scale 1:50,000, "Rikubetsu"*. Hokkaido Development Agency, 42p. (in Japanese with English abstract).
Mitani, K., Hashimoto, W., Yoshida, T. and Oda, Y. (1959) *Explanatory text of the Geological Map of Japan, scale 1:50,000, "Honbetsu".* Hokkaido Development Agency, 66p. (in Japanese with English abstract).
Mitani, K., Osanai, H. and Hashimoto, W. (1958) *Explanatory text of the Geological Map of Japan, scale 1:50,000, "Ashorobuto"*. Hokkaido Development Agency, 66p. (in Japanese with English abstract).
Miyachi, Y., Kusunoki, T., Musashino, M., Tainosho, Y. and Imoto, N. (2005) *Geology of the Kyōto-Seinambu district.* Quadrangle Series, 1:50,000, Geological Survey of Japan, AIST, 90p. (in Japanese with English abstract).
Miyamura, M. (1982) The geosynclinals sediments of the Permian Period in the western part of the Mino Zone, especially on the non-calcareous facies. *Bulletin of the Geological Survey of Japan*, **32**, 23–32. (in Japanese with English abstract).
Miyazaki, K. (2018) 1:50,000 quadrangle geological mapping project in Japan —Overall and individual scenarios of mapping project—. *Synthesiology*, **11**, 55–68. (in Japanese with English abstract).
Miyazaki, K. and Yoshioka, T. (1994) *Geology of the Saganoseki distric*t. With Geological Sheet Map at 1:50,000, Geological Survey of Japan, 40p. (in Japanese with English abstract).
Mizutani, S. (2019) Personal history of my study on radiolarian biostratigraphy. *Bulletin of the Geological Survey of Japan*, **70**, 261–265. (in Japanese with English abstract)
Mizutani, S. and Koido, Y. (1992) *Geology of the Kanayama district*. With Geological Sheet Map at 1:50,000, Geological Survey of Japan, 111p. (in Japanese with English abstract).
Moritani, T. (1968) *Geology of the Fukaura district.* Quadrangle Series, scale 1:50,000, Geological Survey of Japan, 57p. (in Japanese with English abstract).

Motoyama, A. (2019) A review of Neogene radiolarian biostratigraphy in Japan during the last two decades. *Bulletin of the Geological Survey of Japan*, **70**, 125–136. (in Japanese with English abstract)

Motoyama, A. and Itaki, T. (2019) Special issue on micropaleontological study: Scientific results from the joint meeting of Micropaleontological Reference Center Meeting 2016 and 13th Radiolarian Symposium. *Bulletin of the Geological Survey of Japan*, **70**, 1–4. (in Japanese with English abstract).

Motoyama, I., Kamikuri, S., TuZino, T., Kawamura, K. and Miwa, T. (2010) Radiolarians from rock samples recovered from the Kushiro submarine canyon. *Bulletin of the Geological Survey of Japan*, **61**, 87–103. (in Japanese with English abstract).

Murayama, M., Isshiki, N. and Sakamoto, T. (1963) *Explanatory text of the Geological Map of Japan, scale 1:50,000, "Tottorihokubu and Tottorinambu"*. Geological Survey of Japan, 66p. (in Japanese with English abstract).

Motoyama, A. and Maruyama, T. (1995) Neogene stratigraphy, radiolarians and diatoms of the central western part of the Tsugaru Peninsula, northern Honshu, Japan. *Bulletin of the Geological Survey of Japan*, **46**, 333–374. (in Japanese with English abstract)

Musashino, M. (1993) Chemical composition of the "Toishi-type" siliceous shale —Part 1—. *Bulletin of the Geological Survey of Japan*, **44**, 699–705. (in Japanese with English abstract).

Muto, S., Takahashi, S., Yamakita, S., Soda, K. and Onoue, T. (2019) Conodont-based age calibration of the Middle Triassic Anisian radiolarian biozones in pelagic deep-sea bedded chert. *Bulletin of the Geological Survey of Japan*, **70**, 43–89.

Nagamori, H., Furukawa, R., Takeuchi, M. and Nakazawa, T. (2018) *Geology of the Itoigawa district.* Quadrangle Series, 1:50,000, Geological Survey of Japan, AIST, 75p. (in Japanese with English abstract).

Nagamori, H., Takarada, S. and Azuma, T. (2013) *Geology of the Aomori-Seibu district*. Quadrangle Series, 1:50,000, Geological Survey of Japan, AIST, 67p. (in Japanese with English abstract).

Nagamori, H., Takeuchi, M., Furukawa, R., Nakazawa, T. and Nakano, S. (2010) *Geology of the Kotaki district*. Quadrangle Series, 1:50,000, Geological Survey of Japan, AIST, 130p. (in Japanese with English abstract).

Nagao, S., Osanai, H. and Sakō, S. (1954) *Explanatory text of the Geological Map of Japan, scale 1:50,000, "Ōyubari"*. Hokkaido Development Agency, 121p. (in Japanese with English abstract).

Nakae, S. (1993) The Permo–Triassic boundary as a decollement zone within pelagic siliceous sediments, with reference to Jurassic accretion of the Tamba Terrane, SW Japan. *Bulletin of the Geological Survey of Japan*, **44**, 471–481. (in Japanese with English abstract).

Nakae, S. (2000) Three kinds of Middle to Late Jurassic pelitic rocks from the Ashio Terrane at the Daigo district in the Yamizo Mountains, central Japan. *Bulletin of the Geological Survey of Japan*, **51**, 113–128. (in Japanese with English abstract).

Nakae, S. (2001) Permian radiolarians from cherts of the Tamba Terrane in the Nishizu district, Fukui, Southwest Japan. *Bulletin of the Geological Survey of Japan*, **52**, 245–252.

Nakae, S. (2002) Triassic and Jurassic radiolarians from the Tamba Terrane in the Nishizu district, Fukui, Southwest Japan. *Bulletin of the Geological Survey of Japan*, **53**, 51–59.

Nakae, S. (2006) Stratigraphy and structure of the Jurassic accretionary complex in the Daigo district, northern Ibaraki and eastern Tochigi Prefectures, central Japan. *Bulletin of the Geological Survey of Japan*, **57**, 29–50.

Nakae, S. (2011) Middle and Late Permian radiolarians from the Nanjo Mountains, Fukui Prefecture, Southwest Japan. *Bulletin of the Geological Survey of Japan*, **62**, 441–453.

Nakae, S. (2012) Geology of the Permian Higashimata Complex in the Nanjō Mountains, Fukui Prefecture, Southwest Japan. *Bulletin of the Geological Survey of Japan*, **63**, 269–281.

Nakae, S. (2013a) Triassic to Middle Jurassic radiolarians from pelagic cherts in the Nanjō Mountains, Southwest Japan —Part 1. Imajō district. *Bulletin of the Geological Survey of Japan*, **64**, 85-112.

Nakae, S. (2013b) Triassic to Middle Jurassic radiolarians from pelagic cherts in the Nanjō Mountains, Southwest Japan —Part 2. Kanmuri Yama district. *Bulletin of the Geological Survey of Japan*, **64**, 151-190.

Nakae, S. (2016) Jurassic radiolarians from the Ichinohe–Kunohe area (Iwate Prefecture) in the North Kitakami Belt, Japan. *Bulletin of the Geological Survey of Japan*, **67**, 81–100.

Nakae, S., Kaneko, N., Miyazaki, K., Ohno, T. and Komazawa, M. (2010) *Geological Map of Japan 1:200,000 Yoron Jima and Naha Quadrangle*. Geological Survey of Japan, AIST, 8p. (in Japanese with English abstract).

Nakae, S., Komatsubara, T. and Naito, K. (2002) *Geology of the Nishizu district.* Quadrangle Series, 1:50,000, Geological Survey of Japan, AIST, 90p. (in Japanese with English abstract).

Nakae, S., Komatsubara, T., Takahashi, Y. and Yoshikawa, T. (2013) *Geology of the Imajō and Takenami district.* Quadrangle Series, 1:50,000, Geological Survey of Japan, AIST, 110p. (in Japanese with English abstract).

Nakae, S., Komatsubara, T. and Yoshikawa, T. (2015) *Geology of the Kanmuri Yama district.* Quadrangle Series, 1:50,000, Geological Survey of Japan, AIST, 107p. (in Japanese with English abstract).

Nakae, S. and Kurihara, T. (2017) Preliminary report on the radiolarian age of the Upper Cretaceous Matoya Group (Shimanto belt) in the Toba District, Mie Prefecture, Southwest Japan. *Bulletin of the Geological Survey of Japan*, **68**, 57–86.

Nakae, S., Nagamori, H., Miyazaki, K. and Komazawa, M. (2009) *Geological Map of Japan 1:200,000 Ishigaki Jima Quadrangle*. Geological Survey of Japan, AIST, 8p. (in Japanese with English abstract).

Nakae, S., Ozaki, M., Ota, M., Yabumoto, Y., Matsuura, H. and Tomita, S. (1998) *Geology of the Kokura district.* With Geological Sheet Map at 1:50,000, Geological Survey of Japan, 126p. (in Japanese with English abstract).

Nakae, S. and Yoshioka, T. (1998) *Geology of the Kumagawa district.* With Geological Sheet Map at 1:50,000, Geological Survey of Japan, 71p. (in Japanese with English abstract).

Nakae, S., Yoshioka, T. and Naito, K. (2001) *Geology of the Chikubu Shima district.* With Geological Sheet Map at 1:50,000, Geological Survey of Japan, 71p. (in Japanese with English abstract).

Nakajima, T. (1986) Sea in Himalayan and its disappearance, Part 2*. *Chishitsu News*, no. 387, 6–15. (in Japanese).

Nakajima, T., Makimoto, H., Hirayama, J. and Tokuhashi, S. (1981) *Geology of the Kamogawa district.* Quadrangle Series, scale 1:50,000, Geological Survey of Japan, 114p. (in Japanese with English abstract).

Nakajima, T. and Watanabe, M. (2005) *Geology of the Futtsu district.* Quadrangle Series, 1:50,000, Geological Survey of Japan, AIST, 102p. (in Japanese with English abstract).

Nakano, S., Kawabe, T., Harayama, S., Mizuno, K., Takagi, T., Komura, R. and Kimura, K. (2003) *Geology of the Minakuchi district.* Quadrangle Series, 1:50,000, Geological Survey of Japan, AIST, 83p. (in Japanese with English abstract).

Nakano, S., Kawabe, T., Harayama, S., Mizuno, K., Takagi, T., Komura, R. and Kimura, K. (2005) Introduction to a new published 1:50,000 Quadrangle Series, Geology of the Minakuchi district -Mt. Tanakami-yama and Shigaraki Town, called the Konan Alps and well- known as a pottery town-. *Chishitsu News*, no. 612, 53–57. (in Japanese).

Nakano, S., Otsuka, T., Adachi, M., Harayama, S. and Yoshioka, T. (1995) *Geology of the Norikuradake district.* With Geological Sheet Map at 1:50,000, Geological Survey of Japan, 139p. (in Japanese with English abstract).

Nakano, S., Takeuchi, M., Yoshikawa, T., Nagamori, H., Kariya, Y., Okumura, K. and Taguchi, Y. (2002) *Geology of the Shiroumadake district.* Quadrangle Series, 1:50,000, Geological Survey of Japan, AIST, 105p. (in Japanese with English abstract).

Nakano, S. and Tsuchiya, N. (1992) *Geology of the Chōkaisan and Fukura district.* With Geological Sheet Map at 1:50,000, Geological Survey of Japan, 138p. (in Japanese with English abstract).

Nakaseko, K. (1984) An essential role of radiolarian fossils in biostratigraphy. *Journal of Geography (Chigaku Zasshi)*, **93**, 96–102. (in Japanese).

Nakaseko, K., Mizutani, S. and Yao, A. (1983) Radiolarian fossils and the Mesozoic of the Japanese Islands*. *Kagaku*, **53**, 177–183. (in Japanese with English abstract).

Nakaseko, K. and Sugano, K. (1977) Neogene radiolarian zonation in Japan. *The Memoirs of the Geological Society of Japan*, no. 8, 23–33. (in Japanese).

Nakashima, R., Hori, N., Miyazaki, K. and Nishioka, Y. (2008) *Geology of the Toyohashi and Tahara district.* Quadrangle Series, 1:50,000, Geological Survey of Japan, AIST, 113p. (in Japanese with English abstract).

Nakashima, R., Hori, N., Miyazaki, K. and Nishioka, Y. (2010) *Geology of the Iragomisaki district.* Quadrangle Series, 1:50,000, Geological Survey of Japan, AIST, 69p. (in Japanese with English abstract).

Nakashima, R., Tanaka, Y., Utsunomiya, M., Fujiwara, O., Kaneko, N. and Nishida, K. (2015) Report on lecture entitled "Advancement on the Cenozoic stratigraphy in Japan —Microbiostratigraphy and Geology—. *GSJ Chishitsu News*, **4**, 230–234. (in Japanese).

Nakato, A., Motoyama, I. and Kawahata, H. (2005) Seasonal and latitudinal changes of radiolarian sinking population in sediment trap samples from the central North Pacific. *Bulletin of the Geological Survey of Japan*, **56**, 225–236. (in Japanese with English abstract).

Nishimura, A. (1984) Deep-sea sediments in the GH80-5 area in the northern vicinity of the Magellan Trough. *Cruise Report*, no. 20 (Marine Geology, Geophysics, and Manganese Nodules in the Northern Vicinity of the Magellan Trough, August–October 1980 (GH80-5 Cruise)), 67–89.

Nishimura, A. (1986) Deep-Sea sediments in the Central Equatorial Pacific (GH81-4 area). *Cruise Report*, no. 21 (Marine Geology, Geophysics, and Manganese Nodules around Deep-sea Hills in the Central Pacific Basin, August – October 1981 (GH81-4 Cruise)), 56–83.

Nishimura, A. and Ikehara, K. (1992) Deep-sea sediments in the southern part of the Central Pacific Basin (GH82-4 area). *Cruise Report*, no. 22 (Marine Geology, Geophysics and Manganese Nodule Deposits in the Southern Part of the Central Pacific Basin, August–October 1982 (Hakurei-Maru Cruise GH82-4)), 56–83.

Nishioka, Y., Nakae, S., Takeuchi, K., Banno, Y., Mizuno, K., Ozaki, M., Nakashima, R., Sanematsu, K., Nawa, K. and Komazawa, M. (2010) *Geological Map of Japan 1:200,000 Ise Quadrangle*. Geological Survey of Japan, AIST, 8p. (in Japanese with English abstract).

Noda, A. and Kurihara, T. (2016) Late Cretaceous radiolarian assemblages obtained from the Izumi

Group in the Kan-onji district, eastern Shikoku, Japan. *Bulletin of the Geological Survey of Japan*, **67**, 119–131. (in Japanese with English abstract).

Noda, A., Ueki, T., Kawabata, H., Matsuura, H. and Aoya, M. (2017) *Geology of the Kan-onji district.* Quadrangle Series, 1:50,000, Geological Survey of Japan, AIST, 96p. (in Japanese with English abstract).

Nohara, M., Nishimura, A., Usui, A., Tanahashi, M., Yamazaki, T., Ikehara, K., Watanabe, K. and Moritani, T. (1983) Geological research on mineral resource in deep-sea: Research voyage in 1982, GH82-4*. *Chishitsu News*, no. 343, 9–21. (in Japanese).

O'Dogherty, L., De Wever, P. and Gorican, Š. (2009) Historical perspective: 140 years of Mesozoic radiolarian taxonomy. Geodiversitas, 31, 357–369.

Okumura, K., Sakai, A., Takahashi, M., Miyazaki, K. and Hoshizumi, H. (1998) *Geology of the Kumata district*. With Geological Sheet Map at 1:50,000, Geological Survey of Japan, 100p. (in Japanese with English abstract).

Okumura, K. and Teraoka, Y. (1988) *Geology of the Tsurumisaki district*. With Geological Sheet Map at 1:50,000, Geological Survey of Japan, 36p. (in Japanese with English abstract).

Okumura, K., Teraoka, Y., Imai, I., Hoshizumi, H., Ono, K. and Shishido, A. (2010) *Geology of the Nobeoka district*. Quadrangle Series, 1:50,000, Geological Survey of Japan, AIST, 50p. (in Japanese with English abstract).

Okumura, K., Teraoka, Y. and Sugiyama, Y. (1985) *Geology of the Kamae district.* With Geological Sheet Map at 1:50,000, Geological Survey of Japan, 58p. (in Japanese with English abstract).

Osanai, H., Nagao, S., Mitani, K., Hasegawa, K. and Hashimoto, W. (1958) *Explanatory text of the Geological Map of Japan, scale 1:50,000, "Ishikarikanayama"*. Hokkaido Development Agency, 80p. (in Japanese with English abstract).

Ozaki, M. (2019) Introduction of the Geological map of the Minobu District (Quadrangle Series, 1:50,000). *GSJ Chishitsu News*, **8**, 31–40. (in Japanese).

Ozaki, M., Inoue, T., Takagi, T., Komazawa, M. and Okuma, S. (2019) *Geological Map of Japan 1:200,000 Wajima (2nd Edition) Quadrangle.* Geological Survey of Japan, AIST, 8p. (in Japanese with English abstract).

Ozaki, M., Kurimoto, C. and Harayama, S. (1995) *Geology of the Hōjō district*. With Geological Sheet Map at 1:50,000, Geological Survey of Japan, 101p. (in Japanese with English abstract).

Ozaki, M., Makimoto, H., Sugiyama, Y., Mimura, K., Sakai, A., Kubo, K., Kato, H., Komazawa, M., Hiroshima, T. and Sudo, S. (2002) *Geological Map of Japan 1:200,000 Kōfu Quadrangle*. Geological Survey of Japan, AIST, 8p. (in Japanese with English abstract).

Ozaki, M. and Sugiyama, Y. (2018) *Geology of the Minobu district*. Quadrangle Series, 1:50,000, Geological Survey of Japan, AIST, 169p. (in Japanese with English abstract).

Ōzawa, A., Ikebe, Y., Arakawa, Y., Tsuchiya, N., Satoh, H. and Kakimi, T. (1982) *Geology of the Kisakata district.* With Geological Sheet Map at 1:50,000, Geological Survey of Japan, 73p. (in Japanese with English abstract).

Ōzawa, A., Ikebe, Y., Hirayama, J., Awata, Y. and Takayasu, T. (1984) *Geology of the Noshiro district*. Quadrangle Series, scale 1:50,000, Geological Survey of Japan, 91p. (in Japanese with English abstract).

Ōzawa, A., Kano, H., Maruyama, T., Tsuchiya, N., Itō, M., Hirayama, J. and Shinada, S. (1981) *Geology of the Taiheizan district*. With Geological Sheet Map at 1:50,000, Geological Survey of Japan, 69p. (in Japanese with English abstract).

Ōzawa, A., Katahira, T., Nakano, S., Tsuchiya, N. and Awata, Y. (1988) *Geology of the Yashima district.* With Geological Sheet Map at 1:50,000, Geological Survey of Japan, 87p. (in Japanese with English abstract).

Ōzawa, A., Katahira, T. and Tsuchiya, N. (1986) *Geology of the Kiyokawa district*. With Geological Sheet Map at 1:50,000, Geological Survey of Japan, 61p. (in Japanese with English abstract).

Ōzawa, A., Kujiraoka, A. and Awata, Y. (1985) *Geology of the Ugo-Hamada district*. With Geological Sheet Map at 1:50,000, Geological Survey of Japan, 57p. (in Japanese with English abstract).

Ōzawa, A., Kujiraoka, A., Awata, Y., Takayasu, T. and Hirayama, J. (1985) *Geology of the Moritake district.* Quadrangle Series, scale 1:50,000, Geological Survey of Japan, 69p. (in Japanese with English abstract).

Ōzawa, A., Ohguchi, T. and Takayasu, T. (1979a) *Geology of the Asamai district.* With Geological Sheet Map at 1:50,000, Geological Survey of Japan, 53p. (in Japanese with English abstract).

Ōzawa, A., Ohguchi, T. and Takayasu, T. (1979b) *Geology of the Yuzawa district.* Quadrangle Series, scale 1:50,000, Geological Survey of Japan, 67p. (in Japanese with English abstract).

Ōzawa, A., Takayasu, A., Ikebe, Y., Huzioka, K. (1977) *Geology of the Honjō district*. Quadrangle Series, scale 1:50,000, Geological Survey of Japan, 54p. (in Japanese with English abstract).

Ōzawa, A., Tsuchiya, N. and Sumi, K. (1983) *Geology of the Nakahama district*. Quadrangle Series, scale 1:50,000, Geological Survey of Japan, 69p. (in Japanese with English abstract).

Pessagno, E. A. and Newport, J. N. (1972) A technique for extracting Radiolaria from radiolarian cherts. *Micropaleontology*, **18**, 231–234.

Saito, M. (1993) Geologic significance of the "Toishi-type" shale in the evolution of the Jurassic melanges in the Kuze area, western Mino Terrane, central Japan. *Bulletin of the Geological Survey of Japan*,

44, 571–596. (in Japanese with English abstract).
Saito, M. (1997) Progress of researches on Jurassic accretionary complexes in Japan. *Chishitsu News*, no. 514, 14–22. (in Japanese).
Saito, M. (2010) The advanced geological researches and fundamental national land information — Development process of the geological map of Japan—. *Synthesiology – English Edition*, **3**, 13–25.
Saito, M., Geshi, N., Ogasawara, M., Nagamori, H. and Komazawa, M. (2008) World Heritage Yakushima in a viewpoint of Sightseeing Geology: New publication of Geological Map of Japan, 1:200,000 Yakushima. *Chishitsu News*, no. 647, 52–60. (in Japanese).
Saito, M., Kawakami, S. and Ogasawara, M. (2007a) Establishment of stratigraphic framework of the Shimanto accretionary complex in Yakushima Island, Japan, based on newly found Eocene radiolarian fossils. *The Journal of the Geological Society of Japan*, **113**, 266–269. (in Japanese with English abstract).
Saito, M., Kimura, K., Naito, K. and Sakai, A. (1996) *Geology of the Shiibamura district.* With Geological Sheet Map at 1:50,000, Geological Survey of Japan, 133p. (in Japanese with English abstract).
Saito, M., Miyazaki, K., Toshimitsu, S. and Hoshizumi, H. (2005) *Geology of the Tomochi district.* Quadrangle Series, 1:50,000, Geological Survey of Japan, AIST, 218p. (in Japanese with English abstract).
Saito, M., Miyazaki, K., Toshimitsu, S. and Hoshizumi, H. (2006) Geological map of Japan 1: 50,000, "Tomochi", the geologic epitome of Japan shown by 149 legends. *Chishitsu News*, no. 619, 56–60. (in Japanese).
Saito, M. and Nishioka, Y. (1995) The exhibitation of the geological sheet maps published in fiscal 1993. *Chishitsu News*, no. 487, 63–66. (in Japanese).
Saito, M., Ogasawara, M., Nagamori, H., Geshi, N. and Komazawa, M. (2007b) *Geological Map of Japan 1:200,000 Yaku Shima Quadrangle*. Geological Survey of Japan, AIST, 8p. (in Japanese with English abstract).
Saito, M. and Ozaki, M. (2000) Do you know the geology where you live? *Chishitsu News*, no. 548, 59–61. (in Japanese).
Saito, M., Sato, Y. and Yokoyama, S. (1994) *Geology of the Sueyoshi district.* With Geological Sheet Map at 1:50,000, Geological Survey of Japan, 111p. (in Japanese with English abstract).
Saito, M. and Sawada, Y. (2000) *Geology of the Yokoyama district*. With Geological Sheet Map at 1:50,000, Geological Survey of Japan, 126p. (in Japanese with English abstract).
Saito, M., Takarada, S., Toshimitsu, S., Mizuno, K., Miyazaki, K., Hoshizumi, H., Hamasaki, S., Sakaguchi, K., Ohno, T. and Murata, Y. (2010) *Geological Map of Japan 1:200,000 Yatsushiro Quadrangle with a part of Nomo Zaki Quadrangle*. Geological Survey of Japan, AIST, 8p. (in Japanese with English abstract).
Saito, M., Toshimitsu, S., Sugiyama, K., Takeuchi, M., Kurimoto, C. and Nakae, S. (1997) New exhibition, "Jurassic accretionary complexes and radiolarian biostratigraphy in Japan" at the Geological Museum, Geological Survey of Japan. *Chishitsu News*, no. 514, 7–13. (in Japanese).
Sakai, A. (1987) *Geology of the Itsukaichi district*. With Geological Sheet Map at 1:50,000, Geological Survey of Japan, 75p. (in Japanese with English abstract).
Sakai, A. and Kanie, Y. (1986) *Geology of the Nishicha district*. With Geological Sheet Map at 1:50,000, Geological Survey of Japan, 92p. (in Japanese with English abstract).
Sakai, A., Nakagawa, M., Takahashi, Y., Komazawa, M. and Hiroshima, T. (2000) *Geological Map of Japan 1:200,000 Urakawa Quadrangle.* Geological Survey of Japan, 8p. (in Japanese with English abstract).
Sakai, A., Teraoka, Y., Miyazaki, K., Hoshizumi, H. and Sakamaki, Y. (1993) *Geology of the Miemachi district*. With Geological Sheet Map at 1:50,000, Geological Survey of Japan, 115p. (in Japanese with English abstract).
Sakai, A., Wakita, K., Yoshida, T. and Aoki, C. (1982) Micropaleontological research on conodont and radiolaria*. *Chishitsu News*, no. 337, 166–167. (in Japanese).
Sakamoto, T., Kuwahara, T., Itoigawa, J., Takada, Y., Wakita, K. and Onoe, T. (1984) *Geology of the Nagoya-Hokubu district.* Quadrangle Series, scale 1:50,000, Geological Survey of Japan, 64p. (in Japanese with English abstract).
Sakamoto, T. and Nozawa, T. (1960) *Explanatory text of the Geological Map of Japan, scale 1:50,000, "Yatsuo"*. Geological Survey of Japan, 69p. (in Japanese with English abstract).
Sakamoto, T., Tanaka, K., Soya, T., Noma, T. and Matsuno, K. (1972) *Geology of the Nakaminato district*. Quadrangle Series, scale 1:50,000, Geological Survey of Japan, 94p. (in Japanese with English abstract).
Sakō, S. and Hasegawa, K. (1957) *Explanatory text of the Geological Map of Japan, scale 1:50,000, "Tokachigawajōryū"*. Hokkaido Development Agency, 38p. (in Japanese with English abstract).
Sasa, Y., Tanaka, K. and Hata, M. (1964) *Explanatory text of the Geological Map of Japan, scale 1:50,000, "Yūbari"*. Hokkaido Development Agency, 184. (in Japanese with English abstract).
Sato, S., Nagahama, H. and Yoshida, T. (1961) *Explanatory text of the Geological Map of Japan, scale 1:50,000, "Kamicharo"*. Hokkaido Development Agency, 60p. (in Japanese with English abstract).
Sato, T. (1989) Radiolarian Revolution in the study of Japanese Paleozoic–Mesozoic. *Journal of the Japan Society of Engineering Geology*, **30**, 153–162. (in Japanese).

Sato, T. (1991a) Metamorphosis of Japanese Mesozoic-Paleozoic. *Chishitsu News*, no. 438, 13–25. (in Japanese).

Sato, T. (1991b) Metamorphosis of Japanese Mesozoic-Paleozoic (2). *Chishitsu News*, no. 440, 19–33. (in Japanese).

Shibahara, A., Itaki, T. and Watanabe, M. (2012) Investigation of the Earth by Microfossils: Microfossil and Geological Survey*. *GSJ Research Books**, no. 565. (in Japanese). https://www.gsj.jp/data/openfile/no0565/gsj_openfile_565.pdf (Accessed:2020-05-24)

Shiida, I., Suwa, K., Umeda, K. and Hoshino, M. (1989) *Geology of the Sanjōgatake district.* With Geological Sheet Map at 1:50,000, Geological Survey of Japan, 100p. (in Japanese with English abstract).

Shinbo, K. (2006) Plenty of Foraminifers are found in Beach Sands. *Chishitsu News*, no. 624, 42–47. (in Japanese).

Sugiyama, K. and Saito, M. (1994) Paleogene radiolarians from the Hyuga and Nichinan Groups in the Sueyoshi district, southeastern Kyushu, Japan. *Bulletin of the Geological Survey of Japan*, **45**, 383–404.

Sugiyama, Y. and Matsuda, T. (2014) *Geology of the Nanbu district*. Quadrangle Series, 1:50,000, Geological Survey of Japan, AIST, 134p. (in Japanese with English abstract).

Sugiyama, Y., Mizuno, K., Kano, K., Muramatsu, T., Matsuda, T., Ishizuka, O., Oikawa, T., Takada, A., Arai, K., Okamura, Y., Sanematsu, K., Takahashi, M., Oyama, Y. and Komazawa, M. (2010) *Geological Map of Japan 1:200,000 Shizuoka and Omae Zaki (2nd Edition) Quadrangle.* Geological Survey of Japan, AIST, 8p. (in Japanese with English abstract).

Sugiyama, Y. and Shimokawa, K. (1990) *Geology of the Shimizu district*. With Geological Sheet Map at 1:50,000, Geological Survey of Japan, 103p. (in Japanese with English abstract).

Sugiyama, Y., Shimokawa, K., Sakamoto, T. and Hata, M. (1982) *Geology of the Shizuoka district*. Quadrangle Series, scale 1:50,000, Geological Survey of Japan, 86p. (in Japanese with English abstract).

Sumi, Y. and Nozawa, T. (1973) *Geology of the Uozu district*. Quadrangle Series, scale 1:50,000, Geological Survey of Japan, 104p. (in Japanese with English abstract).

Suto, I., Yanagisawa, Y. and Ogasawara, K. (2005) Tertiary geology and chronostratigraphy of the Joban area and its environs, northeastern Japan. *Bulletin of the Geological Survey of Japan*, **56**, 375–409. (in Japanese with English abstract).

Suzuki, J. (1953) *Explanatory text of the Geological Map of Japan, scale 1:50,000, "Fukagawa"*. Hokkaido Development Agency, 44p. (in Japanese with English abstract).

Suzuki, J. (1955) *Explanatory text of the Geological Map of Japan, scale 1:50,000, "Asahikawa"*. Hokkaido Development Agency, 32p. (in Japanese with English abstract).

Suzuki, J. (1957) *Explanatory text of the Geological Map of Japan, scale 1:50,000, "Pippu"*. Hokkaido Development Agency, 27p. (in Japanese with English abstract).

Suzuki, M., Osanai, H., Matsui, K. and Watanabe, J. (1961a) *Geology of the Idonnappudake district.* Quadrangle Series, scale 1:50,000, Geological Survey of Japan, 64p. (in Japanese with English abstract).

Suzuki, M., Watanabe, J. and Kasugai, A. (1961b) *Geology of the Biei district*. Quadrangle Series, scale 1:50,000, Geological Survey of Japan, 32p. (in Japanese with English abstract).

Suzuki, N. and Aita, Y. (2011) Radiolaria: achievements and unresolved issues: taxonomy and cytology. *Plankton and Benthos Research*, **6**, 69–91.

Suzuki, Y., Kodama, K. and Mitsunashi, T. (1990) *Geology of the Nago district.* Quadrangle Series, scale 1:50,000, Geological Survey of Japan, 48p. (in Japanese with English abstract).

Tajika, J. and Yahata, M. (1991) *Explanatory text of the Geological Map of Japan, scale 1:50,000, "Engaru".* Geological Survey of Hokkaido, 104p. (in Japanese with English abstract).

Takagi, T. and Mizuno, K. (1999) *Geology of the Kaitaichi district.* With Geological Sheet Map at 1:50,000, Geological Survey of Japan, 49p. (in Japanese with English abstract).

Takahashi, Koh. and Suzuki, M. (1978) *Explanatory text of the Geological Map of Japan, scale 1:50,000, "Iwachishi".* Geological Survey of Hokkaido, 46p. (in Japanese with English abstract).

Takahashi, Koh. and Suzuki, M. (1986) *Explanatory text of the Geological Map of Japan, scale 1:50,000, "Hidaka"*. Geological Survey of Hokkaido, 44p. (in Japanese with English abstract).

Takahashi, Koh., Taniguchi, H., Watanabe, J. and Ishimaru, S. (2002) *Explanatory text of the Geological Map of Japan, scale 1:50,000, "Momojiyama"*. Geological Survey of Hokkaido, 116p. (in Japanese with English abstract).

Takahashi, Koz. (2002) Diatoms and Radiolaria. *Chishitsu News*, no. 576, 37–43. (in Japanese).

Takahashi, M. (2017) Geological problem for the tectonic boundary between Northeast and Southwest Japan – Displacement of volcanic front-. *GSJ Chishitsu News*, **6**, 149–157. (in Japanese).

Takahashi, M. Mita, I., Watanabe, M. and Motoyama, I. (1999) Integrated stratigraphy of the Middle Miocene marine sequence in the Boso Peninsula, central Japan a review. *Bulletin of the Geological Survey of Japan*, **50**, 225–243.

Takahashi, Yuh. (1991) *Geology of the Hiroshima district.* With Geological Sheet Map at 1:50,000, Geological Survey of Japan, 41p. (in Japanese with English abstract).

Takahashi, Yuh., Makimoto, H., Wakita, K. and Sakai, A.

(1989) *Geology of the Tsuta district.* With Geological Sheet Map at 1:50,000, Geological Survey of Japan, 56p. (in Japanese with English abstract).

Takahashi, Yut. (1996) Geology of the Iide mountain range. *Chishitsu News*, no. 506, 7–14. (in Japanese).

Takahashi, Yut., Miyazaki, K., Mikoshiba, M., Nakamura, Y., Banno, Y., Sato, D. and Wakita, K. (2018) Report of GSJ International Training Course 2018: Geological excursion in the Abukuma Mountains and practical works in laboratories (petrography, XRF and EPMA). *GSJ Chishitsu News*, **7**, 303–308. (in Japanese).

Takahashi, Yut., Sangawa, A., Mizuno, K. and Hattori, H. (1992) *Geology of the Sumoto district.* With Geological Sheet Map at 1:50,000, Geological Survey of Japan, 107p. (in Japanese with English abstract).

Takahashi, Yut., Toyoshima, T., Shimura, T., Hara, H., Takeuchi, K., Sakai, A. and Nakano, S. (2004) *Geology of the Suhara district*. Quadrangle Series, 1:50,000, Geological Survey of Japan, AIST, 80p. (in Japanese with English abstract).

Takahashi, Yut., Toyoshima, T., Shimura, T., Hara, H., Takeuchi, K., Sakai, A. and Nakano, S. (2005) Geological Map of Japan 1:50,000, Suhara. *Chishitsu News*, no. 607, 57–62. (in Japanese).

Takahashi, Yut., Yamamoto, T. and Yanagisawa, Y. (1996) *Geology of the Iidesan district.* With Geological Sheet Map at 1:50,000, Geological Survey of Japan, 52p. (in Japanese with English abstract).

Takahashi, Yut., Yanagisawa, Y., Yamamoto, T., Urabe, A., Uchino, T., Kudo, T., Takagi, T. and Komazawa, M. (2010) *Geological Map of Japan 1:200,000 Niigata (2nd Edition) Quadrangle.* Geological Survey of Japan, AIST, 8p. (in Japanese with English abstract).

Takayanagi, Y., Sakai, T., Oda, M. and Hasegawa, S. (1982) Micropaleontology of piston cores, Wake to Tahiti. *Cruise Report*, no. 18 (Regional Data of Marine Geology, Geophysics, and Manganese Nodules: the Wake-Tahiti Transect in the Central Pacific, January–March 1980 (GH80-1 Cruise)), 238–263.

Takechi, Y. (2010) Fossils from Okayama Prefecture, Japan. *Chishitsu News*, no. 666, 48–52. (in Japanese).

Takemura, A. (2019) Historical review of NOM (News of Osaka Micropaleontologists), Japanese Radiolarian Symposium and InterRad Meeting. *Bulletin of the Geological Survey of Japan*, **70**, 267–272. (in Japanese with English abstract)

Takeuchi, K., Oikawa, T., Saito, M., Ishizuka, O., Sanematsu, K. and Komazawa, M. (2015) *Geological Map of Japan 1:200,000 Yokosuka (2nd Edition) Quadrangle.* Geological Survey of Japan, AIST, 8p. (in Japanese with English abstract).

Takeuchi, M. (1993) *Geology of the Yuwan district.* With Geological Sheet Map at 1:50,000, Geological Survey of Japan, 69p. (in Japanese with English abstract).

Takeuchi, M., Furukawa, R., Nagamori, H. and Oikawa, T. (2017) *Geology of the Tomari district.* Quadrangle Series, 1:50,000, Geological Survey of Japan, AIST, 121p. (in Japanese with English abstract).

Takeuchi, M., Kano, K., Ujiie-Mikoshiba, M., Nakagawa, M. and Komazawa, M. (2005) *Geological Map of Japan 1:200,000 Ichinoseki Quadrangle*. Geological Survey of Japan, AIST, 8p. (in Japanese with English abstract).

Takeuchi, M., Nakano, S., Harayama, S. and Otsuka, T. (1998) *Geology of the Kiso-Fukushima district.* With Geological Sheet Map at 1:50,000, Geological Survey of Japan, 94p. (in Japanese with English abstract).

Takeuchi, M. and Takizawa, F. (1991) Sedimentary environment and provenance analysis of the Tetori Group in the Yakushi Dake area, Hida Mountainland. *Bulletin of the Geological Survey of Japan*, **42**, 439–472. (in Japanese with English abstract)

Takizawa, F., Kamada, K., Sakai, A. and Kubo, K. (1990) *Geology of the Toyoma district*. With Geological Sheet Map at 1:50,000, Geological Survey of Japan, 126p. (in Japanese with English abstract).

Tanaka, K. (1960) *Explanatory text of the Geological Map of Japan, scale 1:50,000, "Kamisarufutsu".* Geological Survey of Japan, 65p. (in Japanese with English abstract).

Tanaka, K. (1980) *Explanatory text of the Geological Map of Japan, scale 1:50,000, "Iyokashima and Sukumo".* Geological Survey of Japan, 58p. (in Japanese with English abstract).

Tanaka, Y. (2007) Biogenic particles in sea area around Ryukyu Arc. *Chishitsu News*, no. 634, 29–34. (in Japanese).

Tateishi, M., Bessho, T., Harata, T., Hisatomi, K., Inouchi, Y., Ishigami, T., Kumon, F., Nakaya, S., Sakamoto, T., Suzuki, H. and Tokuoka, T. (1979) *Geology of the Esumi district.* Quadrangle Series, scale 1:50,000, Geological Survey of Japan, 71p. (in Japanese with English abstract).

Teraoka, Y. (2004) Shimanto Supergroup in Kyushu, Southwest Japan. *Chishitsu News*, no. 599, 40–48. (in Japanese).

Teraoka, Y., Ikeda, Y. and Kashima, N. (1986) *Geology of the Uwajima district.* Quadrangle Series, scale 1:50,000, Geological Survey of Japan, 91p. (in Japanese with English abstract).

Teraoka, Y. and Kurimoto, C. (1986) Cretaceous stratigraphy of the Shimanto Terrane in the Uwajima area, west Shikoku, southwest Japan, with reference to the stratigraphic distribution of mega- and radiolarian fossils. *Bulletin of the Geological Survey of Japan*, **37**, 417–453. (in Japanese with English abstract).

Teraoka, Y., Miyazaki, K., Hoshizumi, H., Yoshioka, T., Sakai, A. and Ono, K. (1992) *Geology of the Inukai district*. Quadrangle Series, scale 1:50,000, Geological Survey of Japan, 129p. (in Japanese with English abstract).

Teraoka, Y., Okumura, K., Murata, A. and Hoshizumi, H. (1990) *Geology of the Saiki district.* With Geological Sheet Map at 1:50,000, Geological Survey of Japan,

78p. (in Japanese with English abstract).
Tiba, T., Kaneko, N. and Kano, K. (2000) *Geology of the Urago district*. With Geological Sheet Map at 1:50,000, Geological Survey of Japan, 74p. (in Japanese with English abstract).
Tokuhashi, S. (2008) Report on the geologic excursion at Tsushima Islands from Sep. 3 to Sep. 5, 2006, conducted as a field excursion FE-B11 of ISC 2006, Fukuoka, Japan. *Chishitsu News*, no. 645, 26–52. (in Japanese).
Tokuoka, T., Harata, T., Inouchi, Y., Ishigami, T., Kimura, K., Kumon, F., Nakajō, K., Nakaya, S., Sakamoto, T., Suzuki, H. and Taniguchi, J. (1981) *Geology of the Ryūjin district.* Quadrangle Series, scale 1:50,000, Geological Survey of Japan, 72p. (in Japanese with English abstract).
Tominaga, K., Hara, H. and Tokiwa, T. (2019) Zircon U–Pb ages of the Kashiwagi Unit of the accretionary complex in the Northern Chichibu Belt, Kanto Mountains, central Japan. *Bulletin of the Geological Survey of Japan*, **70**, 299–314. (in Japanese with English abstract).
Toshimitsu, S., Fujiwara, O. and Morita, S. (2019) A chronological table of the Geological Museum, GSJ, from 2001 to 2019. *GSJ Chishitsu News*, **8**, 322–335. (in Japanese).
Toshimitsu, S. and Saito, M. (1997) New exhibition of the Geological Museum: Formation of accretionary prism and radiolarian fossils*. *Chishitsu News*, no. 514, frontispiece. (in Japanese).
Tsuchiya, N. (1989) *Geology of the Ōsawa district.* Quadrangle Series, scale 1:50,000, Geological Survey of Japan, 85p. (in Japanese with English abstract).
Tsuchiya, N., Ōzawa, A. and Ikebe, Y. (1984) *Geology of the Tsuruoka district.* Quadrangle Series, scale 1:50,000, Geological Survey of Japan, 77p. (in Japanese with English abstract).
Tsuchiya, N. and Yoshioka, T. (1994) *Geology of the Kariwano district.* Quadrangle Series, scale 1:50,000, Geological Survey of Japan, 72p. (in Japanese with English abstract).
Tsushima, K. and Takizawa, F. (1977) *Explanatory text of the Geological Map of Japan, scale 1:50,000, "Shiriyazaki"*. Geological Survey of Japan, 32p. (in Japanese with English abstract).
Tsushima, K. and Uemura, F. (1959) *Explanatory text of the Geological Map of Japan, scale 1:50,000, "Kodomari"*. Geological Survey of Japan, 32p. (in Japanese with English abstract).
Tsushima, K. and Yamaguchi, S. (1954) *Explanatory text of the Geological Map of Japan, scale 1:50,000, "Rumoi"*. Geological Survey of Japan, 16p. (in Japanese with English abstract).
Tuzino, T. (2010) Dive report of "Shinkai 6500" at a middle part of upper reaches of the Kushiro Submarine Canyon, off Tokachi, Hokkaido, Japan. *Bulletin of the Geological Survey of Japan*, **61**, 125–136. (in Japanese with English abstract).
Uchino, T., Asakawa, N., Tsuneki, T. and Kawamura, T. (2019) New exihibtion of touchable rocks in Geological Museum. *GSJ Chishitsu News*, **8**, 261–272. (in Japanese).
Tuzino, T., Kudo, T., Nakae, S., Kondo, R., Nishioka, Y. and Ueki, T. (2018) *Geology of the Ichinohe district.* Quadrangle Series, 1:50,000, Geological Survey of Japan, AIST, 161p. (in Japanese with English abstract).
Uchino, T. (2010) Geologic map and lithology of the Early Jurassic accretionary complex of the Ashio Terrane in the Kamo district (western part of the Kambara Mountains), Niigata Prefecture, Southwest Japan. *Bulletin of the Geological Survey of Japan*, **61**, 365–381. (in Japanese with English abstract).
Uchino, T. (2015) Origin of "Shiraishi" (white rounded pebble and cobble) used in the "Oshiraishi-mochi event" held prior to the "Shikinen Sengu ceremony" at Ise Jingu (the Grand Shrine of Ise). *GSJ Chishitsu News*, **4**, 69–74. (in Japanese).
Uchino, T. (2017a) Special issue on the depositional ages from the Toba District (Quadrangle series 1:50,000). *Bulletin of the Geological Survey of Japan*, **68**, 23–24. (in Japanese).
Uchino, T. (2017b) Pteridophyte (Pyrrosia lingua) selecting chert as a habitat –an example in the Toba district, Mie Prefecture–. *GSJ Chishitsu News*, **6**, 283–288. (in Japanese).
Uchino, T. (2018) Introduction of the geological map of the Toba District (quadrangle series, 1:50,000) and explanation of its geologic structure. *GSJ Chishitsu News*, **7**, 91–101. (in Japanese).
Uchino, T. and Hori, R. S. (2011) Late Triassic radiolarians from siliceous mudstone of the Ashio Terrane in the Kamo district (Quadrangle series 1:50,000), Niigata Prefecture, Japan. *Bulletin of the Geological Survey of Japan*, **62**, 191–196. (in Japanese with English abstract).
Uchino, T. and Ishida, N. (2017) Middle and Late Jurassic radiolarian fossils from mudstone in the Southern Chichibu Belt in the Toba District (Quadrangle series 1:50,000), Shima Peninsula, Mie Prefecture, Southwest Japan. *Bulletin of the Geological Survey of Japan*, **68**, 25–39. (in Japanese with English abstract).
Uchino, T. and Kawamura, T. (2014) Introduction of new quadrangle geological map, 1:50,000 Hayachine San. *GSJ Chishitsu News*, **3**, 329–333. (in Japanese).
Uchino, T. and Kurihara, T. (2019) Middle Devonian–early Carboniferous radiolarian fossils extracted from the conglomerate in the Nedamo Complex, Nedamo Terrane, Northeast Japan. *Bulletin of the Geological Survey of Japan*, **70**, 109–115. (in Japanese with English abstract).
Uchino, T., Nakae, S. and Nakashima, R. (2017) *Geology of the Toba district*. Quadrangle Series, 1:50,000, Geological Survey of Japan, AIST, 141p. (in Japanese

with English abstract).
Ueki, T., Hara, H. and Ozaki, M. (2013) *Geology of the Hachiōji district.* Quadrangle Series, 1:50,000, Geological Survey of Japan, AIST, 137p. (in Japanese with English abstract).
Ueki T. and Sakai, A. (2007) *Geology of the Ōme district.* Quadrangle Series, 1:50,000, Geological Survey of Japan, AIST, 189p. (in Japanese with English abstract).
Uemura, F., Tsushima, K. and Saitō, M. (1959) *Explanatory text of the Geological Map of Japan, scale 1:50,000, "Kanita"*. Geological Survey of Japan, 30p. (in Japanese with English abstract).
Ujiié, H. (2000) *Geology of the Iheya Jima and Izena Jima district*. With Geological Sheet Map at 1:50,000, Geological Survey of Japan, 25p. (in Japanese with English abstract).
Ujiié, H. and Kaneko, N. (2006) *Geology of the Naha and Okinawashi-Nambu district*. Quadrangle Series, 1:50,000, Geological Survey of Japan, AIST, 48p. (in Japanese with English abstract).
Umino, S., Ishizuka, O. and Kanayama, K. (2016) *Geology of the Hahajima Rettō District*. Quadrangle Series, 1:50,000, Geological Survey of Japan, AIST, 46p. (in Japanese with English abstract).
Umino, S. and Nakano, S (2007) *Geology of the Chichijima Rettō district*. Quadrangle Series, 1:50,000, Geological Survey of Japan, AIST, 71p. (in Japanese with English abstract).
Ustunomiya, M. (2018) Report of the 16th International Nannoplankton Association Meeting and preliminary arrangements of cooperative research about improvements of calcareous nannofossil biostratigraphy. *GSJ Chishitsu News*, **7**, 223–226. (in Japanese).
Utsunomiya, M. and Ooi, S (2019) *Geology of the Kazusa-Ohara district*. Quadrangle Series, 1:50,000, Geological Survey of Japan, AIST, 127p. (in Japanese with English abstract).
Wada, N., Takahashi, K. and Watanabe, J. (1992) *Explanatory text of the Geological Map of Japan, scale 1:50,000, "Mitsuishi"*. Geological Survey of Hokkaido, 73p. (in Japanese with English abstract).
Wakita, K. (1983) Allochthonous blocks and submarine slide deposits in the Jurassic formation southwest of Gujo-hachiman, Gifu Prefecture, central Japan. *Bulletin of the Geological Survey of Japan*, **34**, 329–342. (in Japanese with English abstract).
Wakita, K. (1984) *Geology of the Hachiman district.* With Geological Sheet Map at 1:50,000, Geological Survey of Japan, 89p. (in Japanese with English abstract).
Wakita, K. (1988a) Early Cretaceous mélange in the Hida–Kanayama area, central Japan. *Bulletin of the Geological Survey of Japan*, **39**, 367–421.
Wakita, K. (1988b) Origin of chaotically mixed rock bodies in the Early Jurassic to Early Cretaceous sedimentary complex of the Mino terrane, central Japan. *Bulletin of the Geological Survey of Japan*, **39**, 675–757.
Wakita, K. (1991) *Geology of the Tanigumi district.* With Geological Sheet Map at 1:50,000, Geological Survey of Japan, 53p. (in Japanese with English abstract).
Wakita, K. (1995) *Geology of the Mino district.* With Geological Sheet Map at 1:50,000, Geological Survey of Japan, 36p. (in Japanese with English abstract).
Wakita, K. (2001) Oh! My sweet Karangsambung -A geological trip Cretaceous accretionary complex in central Java, Indonesia. *Chishitsu News*, no. 567, 52–66. (in Japanese).
Wakita, K. (2002a) Secrets of lost diamonds A geological trip Cretaceous accretionary complex in south Kalimantan, Indonesia. *Chishitsu News*, no. 574, 53–67. (in Japanese).
Wakita, K. (2002b) Hard kiss of mosquito on the equator -A geological trip Cretaceous accretionary complex in west Kalimantan, Indonesia. *Chishitsu News*, no. 576, 44–59. (in Japanese).
Wakita, K., Igawa, T., Takarada, S. and Fusejima, Y. (2008) Creation of seamless geological map of Japan at the scale of 1:200,000 and its distribution through the web —For maximum accessibility and utilization of geological information—. *Synthesiology – English Edition*, **1**, 73–84.
Wakita, K. and Isomi, H. (1986) Discovery of Triassic and Jurassic radiolarians from the Sakamoto-toge area, Gifu Prefecture and its significance. *Bulletin of the Geological Survey of Japan*, **37**, 325–333. (in Japanese with English abstract).
Wakita, K. and Kawamura, Y. (1985) Going on the top of the hit "chert"*. *Chishitsu News*, no. 376, 60–66. (in Japanese).
Wakita, K. and Koido, Y. (1994) *Geology of the Gero district*. With Geological Sheet Map at 1:50,000, Geological Survey of Japan, 79p. (in Japanese with English abstract).
Wakita, K. and Okamura, Y. (1982) Mesozoic sedimentary rocks containing allochthonous blocks, Gujo-hachiman, Gifu Prefecture, central Japan. *Bulletin of the Geological Survey of Japan*, **33**, 161–185. (in Japanese with English abstract).
Wakita, K., Takeuchi, K., Mizuno, K., Komatsubara, T., Nakano, S., Takemura, K. and Taguchi, Y. (2013) *Geology of the Kyōto-Tōnambu district*. Quadrangle Series, 1:50,000, Geological Survey of Japan, AIST, 124p. (in Japanese with English abstract).
Watanabe, M. and Yoshida, F. (1995) *Geology of the Ebishima district*. With Geological Sheet Map at 1:50,000, Geological Survey of Japan, 61p. (in Japanese with English abstract).
Yahata, M., Tajika, J. and Kurosawa, K. (1988) *Explanatory text of the Geological Map of Japan, scale 1:50,000, "Maruseppu-Hokubu"*. Geological Survey of Hokkaido, 110p. (in Japanese with English abstract).
Yamada, N. (1966) *Explanatory text of the Geological*

Map of Japan, scale 1:50,000, "Chizu". Geological Survey of Japan, 69p. (in Japanese with English abstract).

Yamada, N. (2009) Reconnaissance Geological Map, Division II (*Tobu*) compiled by Toyokitsi Harada -Review of the Reconnaissance Geological Map Series of Japan, part 2-. *Chishitsu News*, no. 660, 32–47. (in Japanese).

Yamada, N. (2011) Reconnaissance Geological Map, Division IV (*Seibu*) T. Kochibe *et al.* (1894) -Review of the Reconnaissance Geological Map Series of Japan, part 4-. *Chishitsu News*, no. 679, 8–22. (in Japanese).

Yamada, N., Adachi, M., Kajita, S., Hirayama, S., Yamazaki, H. and Bunno, H. (1985) *Geology of the Takayama district*. Quadrangle Series, scale 1:50,000, Geological Survey of Japan, 111p. (in Japanese with English abstract).

Yamada, N. and Kobayashi, T. (1988) *Geology of the Ontakesan district*. With Geological Sheet Map at 1:50,000, Geological Survey of Japan, 136p. (in Japanese with English abstract).

Yamagishi, H. and Kurosawa, K. (1987) *Explanatory text of the Geological Map of Japan, scale 1:50,000, "Harauta and Karibayama"*. Geological Survey of Hokkaido, 36p. (in Japanese with English abstract).

Yamaguchi, S. and Satoh, H. (1989) *Geology of the Nukanai district*. With Geological Sheet Map at 1:50,000, Geological Survey of Japan, 78p. (in Japanese with English abstract).

Yamaguchi, S., Satoh, H. and Matsui, M. (2003) *Geology of the Chūrui district*. Quadrangle Series, 1:50,000, Geological Survey of Japan, AIST, 68p. (in Japanese with English abstract).

Yamaguchi, S. and Sawamura, K. (1965) *Explanatory text of the Geological Map of Japan, scale 1:50,000, "Honki"*. Geological Survey of Hokkaido, 42p. (in Japanese with English abstract).

Yamamoto, T. (1999) *Geology of the Tajima district*. With Geological Sheet Map at 1:50,000, Geological Survey of Japan, 85p. (in Japanese with English abstract).

Yamamoto, T. and Komazawa, M. (2004) *Geology of the Miyashita district*. Quadrangle Series, 1:50,000, Geological Survey of Japan, AIST, 71p. (in Japanese with English abstract).

Yamamoto, T., Kurimoto, C. and Yoshioka, T. (2000) *Geology of the Tatsuno district*. With Geological Sheet Map at 1:50,000, Geological Survey of Japan, 66p. (in Japanese with English abstract).

Yamamoto, T., Kurimoto, C. and Yoshioka, T. (2002) *Geology of the Yamasaki district.* Quadrangle Series, 1:50,000, Geological Survey of Japan, AIST, 48p. (in Japanese with English abstract).

Yamamoto, T. and Yoshioka, T. (1992) *Geology of the Wakamatsu district*. With Geological Sheet Map at 1:50,000, Geological Survey of Japan, 73p. (in Japanese with English abstract).

Yamamoto, T., Yoshioka, T., Makino, M. and Sumita, T. (2005) *Geology of the Kitakata district.* Quadrangle Series, 1:50,000, Geological Survey of Japan, AIST, 63p. (in Japanese with English abstract).

Yanagisawa, Y. (1999) Diatom biostratigraphy of the Miocene sequence in the Suzu area, Noto Peninsula, Ishikawa Prefecture, central Japan. *Bulletin of the Geological Survey of Japan*, **50**, 167–213. (in Japanese with English abstract).

Yanagisawa, Y. (2003a) Miocene diatoms of the upper part of the Arakawa Group distributed in the Karasuyama area, Tochigi Prefecture, central Japan (part 1): Diatom biostratigraphy. *Bulletin of the Geological Survey of Japan*, **54**, 1–13. (in Japanese with English abstract).

Yanagisawa, Y. (2003b) Miocene diatoms of the upper part of the Arakawa Group distributed in the Karasuyama area, Tochigi Prefecture, central Japan (part 2): Paleobathymetric change. *Bulletin of the Geological Survey of Japan*, **54**, 15–27. (in Japanese with English abstract).

Yanagisawa, Y., Chihara, K., Suzuki, Y., Uemura, T., Kodama, K. and Kato, H. (1985) *Geology of the Tōkamachi district*. Quadrangle Series, scale 1:50,000, Geological Survey of Japan, 104p. (in Japanese with English abstract).

Yanagisawa, Y., Kobayashi, I., Takeuchi, K., Tateishi, M., Chihara, K. and Kato, H. (1986) *Geology of the Ojiya district*. Quadrangle Series, scale 1:50,000, Geological Survey of Japan, 177p. (in Japanese with English abstract).

Yanagisawa, Y., Nakamura, K., Suzuki, Y., Sawamura, K., Yoshida, F., Tanaka, Y., Honda, Y. and Tanahashi, M. (1989) Tertiary biostratigraphy and subsurface geology of the Futaba district, Joban Coalfield, northeast Japan. *Bulletin of the Geological Survey of Japan*, **40**, 405–467. (in Japanese with English abstract).

Yanagisawa, Y., Takahashi, T., Nagahashi, Y., Yoshida, T. and Kurokawa, K. (2003) Tephra beds of the Pliocene Dainenji Formation distributed in the Pacific side of Fukushima Prefecture, northeastern Japan (part 1): Chronostratigraphy. *Bulletin of the Geological Survey of Japan*, **54**, 351–364. (in Japanese with English abstract).

Yanagisawa, Y., Yamaguchi, T., Hayashi, H. and Takahashi, M. (2003) Marine diatom biostratigraphy and paleoenvironment of the upper Miocene Kubota Formation in the Higashi-tanagura area, Fukushima Prefecture, northeastern Japan. *Bulletin of the Geological Survey of Japan*, **54**, 29–47. (in Japanese with English abstract).

Yanagisawa, Y. and Yamamoto, T. (1998) *Geology of the Tamaniwa district*. Quadrangle Series, scale 1:50,000, Geological Survey of Japan, 94p. (in Japanese with English abstract).

Yanagisawa, Y., Yamamoto, T., Banno, Y., Tazawa, J., Yoshioka, T., Kubo, K. and Takizawa, F. (1996) *Geology of the Sōmanakamura district*. Quadrangle Series, scale 1:50,000, Geological Survey of Japan, 144p. (in Japanese with English abstract).

Yao, A. (2019) Development of Paleozoic - Mesozoic radiolarian research in the latter half of the 20th century in Japan. *Bulletin of the Geological Survey of Japan*, **70**, 249–260. (in Japanese with English abstract).

Yao, A. and Mizutani, S. (1993) Research on radiolarian fossils and re-examination of Paleozoic–Mesozoic stratigraphy in Japan. *In* Geological Society of Japan, ed., *Hundred Years of Geology in Japan: Centennial Volume of the Geological Society of Japan*, Soubun Printing Co. Ltd., 131–137. (in Japanese).

Yao, A., Mizutani, S. and Kuwahara, K. (2001) Trend of Japanese radiolarian research from a view point of radiolarian database. *News of Osaka Micropalaeontologists (NOM)*, *Special Volume*, no. 12, 375–383. (in Japanese with English abstract).

Yoshida, F. (2003) Giant limestone olistolith at Shirasaki coast in Yura-cho, Kii Peninsula -photo-essay on geoscience-. *Chishitsu News*, no. 592, 61–63. (in Japanese).

Yoshida, F., Kurimoto, C. and Miyamura, M. (1991) *Geology of the Kuwana district*. With Geological Sheet Map at 1:50,000, Geological Survey of Japan, 154p. (in Japanese with English abstract).

Yoshida, F., Nishioka, Y., Kimura, K. and Nagamori, H. (2003) *Geology of the Ōmi-hachiman district.* Quadrangle Series, 1:50,000, Geological Survey of Japan, AIST, 72p. (in Japanese with English abstract).

Yoshida, F., Takahashi, Y. and Nishioka, Y. (1995) *Geology of the Tsu-Seibu district*. With Geological Sheet Map at 1:50,000, Geological Survey of Japan, 136p. (in Japanese with English abstract).

Yoshida, F. and Wakita, K. (1999) *Geology of the Gifu district.* With Geological Sheet Map at 1:50,000, Geological Survey of Japan, 71p. (in Japanese with English abstract).

Yoshida, T. and Kambe, N. (1955) *Explanatory text of the Geological Map of Japan, scale 1:50,000, "Ikushumbetsu-Dake"*. Hokkaido Development Agency, 31p. (in Japanese with English abstract).

Yoshida, T. and Katada, M. (1964) *Explanatory text of the Geological Map of Japan, scale 1:50,000, "Otsuchi and Karodake"*. Geological Survey of Japan, 30p. (in Japanese with English abstract).

Yoshida, T. and Katada, M. (1984) *Geology of the Miyako district.* Quadrangle Series, scale 1:50,000, Geological Survey of Japan, 44p. (in Japanese with English abstract).

Yoshida, T., Matsuno, K., Satoh, H. and Yamaguchi, S. (1959) *Explanatory text of the Geological Map of Japan, scale 1:50,000, "Biu"*. Hokkaido Development Agency, 47p. (in Japanese with English abstract).

Yoshida, T., Yoshii, M., Katada, M., Tanaka, K., Sakamoto, T. and Satoh, H. (1987) *Geology of the Rikuchū-Ōno district.* With Geological Sheet Map at 1:50,000, Geological Survey of Japan, 70p. (in Japanese with English abstract).

Yoshii, M., Goto, H. and Katada, M. (1997) Major and trace elements of the Paleozoic–Mesozoic chert in the North Kitakami Mountains, Northeast Japan. *Bulletin of the Geological Survey of Japan*, **48**, 567–584. (in Japanese with English abstract).

Yoshikawa, T., Kano, K., Yanagisawa, Y., Komazawa, M., Joshima, M. and Kikawa, E. (2002) *Geology of the Suzumisaki, Noto-iida and Hōryūzan district*. Quadrangle Series, 1:50,000, Geological Survey of Japan, AIST, 76p. (in Japanese with English abstract).

Yoshikawa, T., Kurimoto, C. and Aoki, M. (2005) *Geology of the Ikuno district*. Quadrangle Series, 1:50,000, Geological Survey of Japan, AIST, 48p. (in Japanese with English abstract).

Yoshikawa, T., Yamamoto, T. and Nakae, S. (2010) *Geology of the Ustunomiya district*. Quadrangle Series, 1:50,000, Geological Survey of Japan, AIST, 79p. (in Japanese with English abstract).

Yoshioka, T., Takizawa, F., Takahashi, M., Miyazaki, K., Banno, Y., Yanagisawa, Y., Takahashi, Y., Kubo, K., Seki, Y., Komazawa, M. and Hiroshima, T. (2001) *Geological Map of Japan 1:200,000 Mito (2nd Edition) Quadrangle.* Geological Survey of Japan, 8p. (in Japanese with English abstract).

* Translated by the authors

Recieved January 9, 2019
Accepted March 12, 2020
Published on-line June 12, 2020

Appendix: How to access and download the publications mentioned in this article

A1. Geological Map of the Quadrangle Series (1:50,000 and 1:200,000)

Access the web page (https://gbank.gsj.jp/datastore/download.php?lang=en) and do as follows. The numbers correspond to the numbers in the circles in Fig. A1.
1: Enter or copy-paste a district name.
2: Click the “search” button.
3: Select the check box that you need.
4: Click the “download” button.

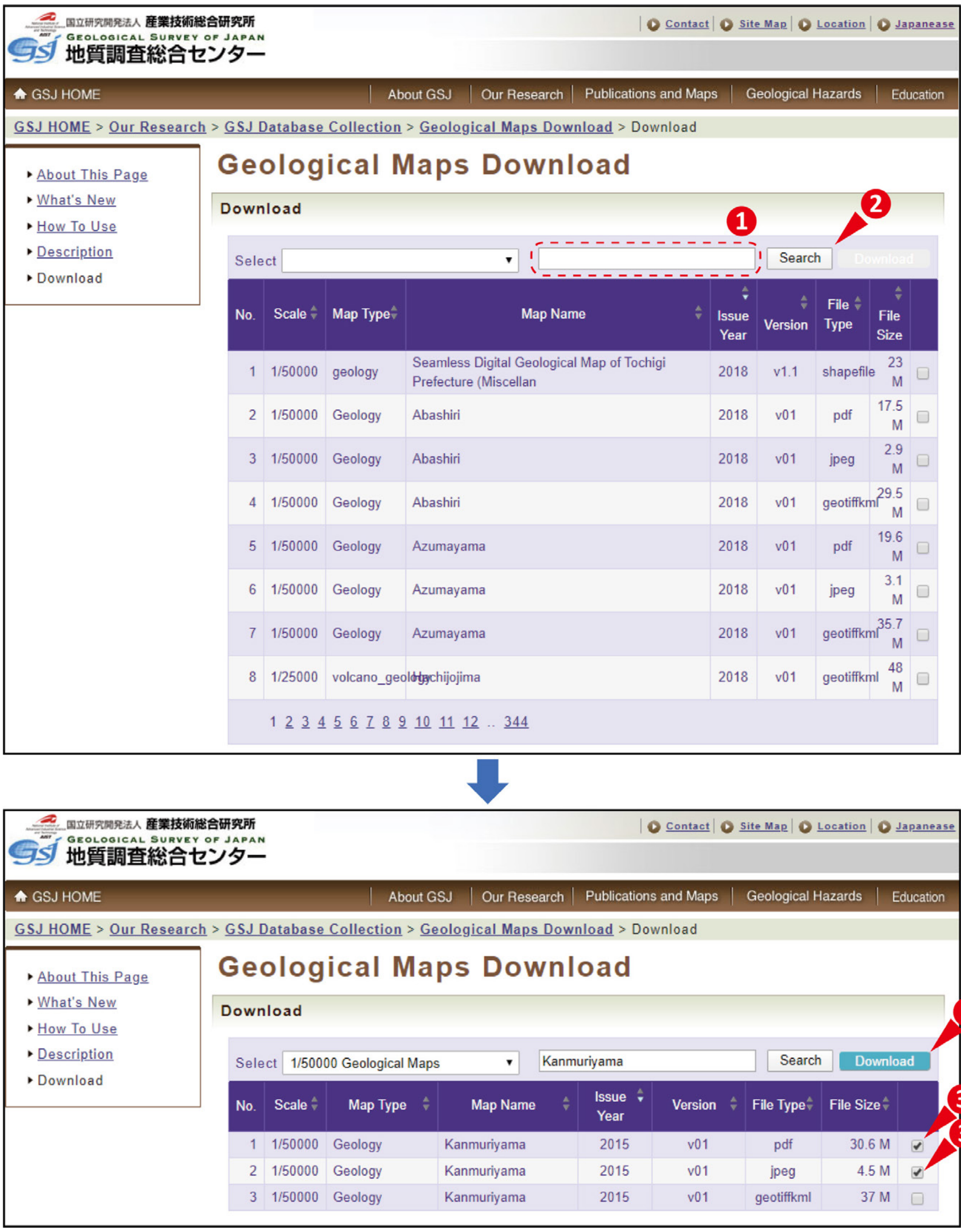

Fig. A1 Image captures of the webpage for search and download of geological maps from GSJ.

A2. Bulletin of the Geological Survey of Japan (1950 to 2011, vol. 52, no. 2/3)

Access the web page (https://www.gsj.jp/en/publications/bull-gsj/index.html) and download the article of interest.

A3. Bulletin of the Geological Survey of Japan (2011, vol. 52, no. 4/5 to present)

Access the web page (https://www.gsj.jp/en/publications/bulletin/index.html) and download the article of interest.

A4. Chishitsu News [Japanese only]

Access the web page (https://www.gsj.jp/publications/pub/chishitsunews/news-contents.html) and download the article of interest.

A5. GSJ Chishitsu News [Japanese only]

Access the web page (https://www.gsj.jp/publications/gcn/gcn.html) and download the article of interest.

A6. Cruise Report

Access the web page (https://www.gsj.jp/en/publications/cruise-rep/index.html) and download the article of interest.

地質調査総合センターにおける放散虫研究の歴史及び 1950 年～ 2019 年（昭和 25 年～令和元年）の関連出版物目録

伊藤　剛・中江　訓・板木　拓也

要　旨

1882 年（明治 15 年）に設立された地質調査所（現 産業技術総合研究所地質調査総合センター）は，2017 年に創立 135 周年を迎えた．その歴史の中で，地質図，論文，ニュース誌など，数多くの出版物を刊行してきた．本論では，これらの出版物の中で放散虫に関係するものを纏めた．1950 年（昭和 25 年）から 2019 年（令和元年）の間の出版物の中で，「放散虫」という単語は，5 万分の 1 地質図幅では 252 編，20 万分の 1 地質図幅では 21 編，地質調査所月間報告及び地質調査研究報告では 75 編，地質ニュースでは 14 編，GSJ 地質ニュースでは 21 編，Cruise Report では 7 編の論文・記事で記述されている．放散虫研究にかかわる出版物の数は 1980 年代に増加しており，これはいわゆる放散虫革命と同時期である．

地質調査総合センター研究資料集

695	20 世紀初頭の震源データ　－主に台湾周辺地域－　–G-EVER アジア太平洋地域地震火山ハザード情報システムデータ　6/7–	石川 有三
696	深部調査井 WD-1 のコア試料写真	佐々木 宗建・佐脇 貴幸・阪口 圭一
697	火山灰カタログ２： 2-1. 草津白根山（本白根山）2018 年噴火噴出物 2-2. 御嶽山 2014 年噴火噴出物 2-3. 雲仙岳（普賢岳）1990 年～ 1995 年噴火噴出物 2-4. 三宅島 2000 年噴火噴出物	松本 恵子･下司 信夫･島村 哲也･岩橋 くるみ
698	瀬戸地区の窯業地下資源調査試錐柱状図集	須藤 定久・高木 哲一
699	支笏・洞爺・濁川・大山火山の大規模噴火の前駆活動と噴火推移	金田 泰明･後藤 義瑛･西野 佑紀･宝田 晋治・下司 信夫
700	大規模火砕噴火推移時系列データ集　その１	下司 信夫・池上 郁彦・西原　歩
701	ベントナイトなどのメチレンブルー吸着量の測定方法の JIS 規格（JIS Z 2451）の解説書の補足	三好 陽子･鈴木 正哉･森本 和也･渡邊 保貴・宮腰 久美子・高木 哲一
702	新規富士火山降下火砕物の層序、平均最大粒径、最小体積及び化学組成	山元 孝広･中野　俊･石塚 吉浩･高田　亮
703	火山灰カタログ 3：阿蘇山（中岳）2014 年～ 2016 年噴火噴出物	松本 恵子・大槻 静香・下司 信夫
704	産総研地下水等総合観測点の孔井における孔壁画像資料	木口　努･松本 則夫･北川 有一･重松 紀生･板場 智史･塚本　斉･佐藤　努
705	Modified GOTIC2：地下での観測における海洋潮汐荷重効果を推定するソフトウェア	上垣内 修・松本 則夫・弘瀬 冬樹
706	霧島火山新燃岳 2008 年噴火噴出物の分布	下司 信夫・宝田 晋治

地質調査総合センターの最新出版物

5 万分の 1 地質図幅	明智・角館・馬路	
20 万分の 1 地質図幅	高知（第 2 版）・輪島（第 2 版）・広尾（第 2 版）	
200 万分の 1 地質編集図	No. 4	日本地質図（第 5 版）
	No. 11	日本の火山（第 3 版）
特殊地質図	No. 12	富士火山地質図（第 2 版）
	No. 33	日本周辺海域鉱物資源分布図（第 2 版）
	No. 41	栃木県シームレス地質図
海洋地質図	No. 90	沖縄島南部周辺海域海洋地質図（1:20 万）
火山地質図	No. 20	八丈島火山地質図（1:2.5 万）
水文環境図	No. 6	山形盆地（第 2 版）
	No. 10	勇払平野
	No. 11	大阪平野
空中磁気図	No. 47	富士火山地域高分解能空中磁気異常図
	No. 48	仙台平野南部沿岸地域高分解能空中磁気異常図
重力図	No. 33	金沢地域重力図（ブーゲー異常）
	S3	甲府地域重力構造図（ブーゲー異常）
海外地球科学図	アジア鉱物資源図（1:500 万）	
	東アジア地域地震火山災害情報図（1:1000 万）	
海陸シームレス地質図	S-6	海陸シームレス地質情報集「房総半島東部沿岸域」
燃料資源図	FR-3	燃料資源地質図「関東地方」
土壌評価図	E-7	表層土壌評価基本図「高知県地域」
数値地質図	G-16	20 万分の 1 日本シームレス地質図　DVD 版
	G-17	九州地質ガイド
	V-3	口永良部島火山地質データベース
	G20-1	20 万分の 1 数値地質図幅集「北海道北部」第 2 版
	G20-2	20 万分の 1 数値地質図幅集「北海道南部」第 2 版
その他	中部地方の地球化学図	
	海と陸の地球化学図	
	関東の地球化学図	
	日本列島及びその周辺の熱データベース	

事務局
国立研究開発法人 産業技術総合研究所
地質調査総合センター
地質情報基盤センター　出版室
https://www.gsj.jp/inquiries.html

Secretariat Office
National Institute of Advanced Industrial Science and Technology
Geological Survey of Japan
Geoinformation Service Center Publication Office
https://www.gsj.jp/en/

地質調査研究報告 第71巻 第4号
令和2年11月13日　発行

国立研究開発法人 産業技術総合研究所
地質調査総合センター

〒305-8567
茨城県つくば市東1-1-1 中央第7

Bulletin of the Geological Survey of Japan
Vol. 71 No. 4 Issue November 13, 2020

Geological Survey of Japan, AIST

AIST Tsukuba Central 7, 1-1-1, Higashi,
Tsukuba, Ibaraki 305-8567 Japan

AIST16-G68699-71-4

Online ISSN : 2186-490X
Print ISSN : 1346-4272

BULLETIN
OF THE
GEOLOGICAL SURVEY OF JAPAN

Vol. 71 No. 4 2020

CONTENTS

Special Issue:
Scientific results from InterRad XV in Niigata 2017 (Proceedings)

GSJ Bulletin special issue: Scientific results from InterRad XV in Niigata 2017 (Proceedings)
NAKAE Satoshi and UCHINO Takayuki 235

Radiolarian-inspired art design: Simplification and identification
ITO Tsuyoshi, MORIA, YOKOYAMA Hayato, ISHIWATA Sayaka and MATSUOKA Atsushi 239

Early Oxfordian radiolarians from the ammonite-bearing Fludergraben section (Northern Calcareous Alps, Austria)
SUZUKI Hisashi and GAWLICK Hans-Jürgen 243

Middle Jurassic radiolarians from the ammonite bearing Toyora Group, Yamaguchi Prefecture, Southwest Japan
NISHIZONO Yukihisa and YONEMITSU Isao 281

Radiolarian age of Triassic striped chert within the Jurassic accretionary complex of the Ashio terrane in the Ashikaga area, Tochigi Prefecture, central Japan
ITO Tsuyoshi 297

Late Jurassic radiolarians from mudstone near the U–Pb-dated sandstone of the North Kitakami Belt in the northeastern Shimokita Peninsula, Tohoku, Japan
UCHINO Takayuki and SUZUKI Noritoshi 313

SIMS analysis of Si isotope for radiolarian test in Mesozoic bedded chert, Inuyama, central Japan
Maximilien BÔLE, IKEDA Masayuki, Peter O. BAUMGARTNER, HORI S. Rie and Anne-Sophie BOUVIER 331

Oxygen isotope analysis of Mesozoic radiolarites using SIMS
Maximilien BÔLE, IKEDA Masayuki, Peter O. BAUMGARTNER, HORI S. Rie, Anne-Sophie BOUVIER and Duje KUKOČ 355

Radiolarian research by the Geological Survey of Japan, AIST, with bibliographic lists from 1950 to 2019
ITO Tsuyoshi, NAKAE Satoshi and ITAKI Takuya 395

地　調　研　報
Bull. Geol. Surv. Japan
Vol. 71, No. 4, 2020

Geological Survey of Japan, AIST